

INFLUENCE OF CHARGE AND ITS DISTRIBUTION ON
BIOLOGICAL APPLICATIONS OF *BIS*-TRIARYLBORANES
AND
PRELIMINARY INVESTIGATIONS ON H₂O₂-CLEAVABLE ARYL
BORONATE ESTERS

Dissertation zur Erlangung des naturwissenschaftlichen Doktorgrades der
Julius-Maximilians-Universität Würzburg

vorgelegt von
Sarina Maria Berger
aus Augsburg

Würzburg, 2021



Eingereicht bei der Fakultät für Chemie und Pharmazie am

24.06.2021

Gutachter der schriftlichen Arbeit

1. Gutachter: Prof. Dr. Dr. h.c. Todd B. Marder

2. Gutachter: Prof. Dr. Ulrich Schatzschneider

Prüfer des öffentlichen Promotionskolloquiums

1. Prüfer: Prof. Dr. Dr. h.c. Todd B. Marder

2. Prüfer: Prof. Dr. Ulrich Schatzschneider

3. Prüfer: Prof. Dr. Dr. Lorenz Meinel

Datum des öffentlichen Promotionskolloquiums

Doktorurkunde ausgehändigt am

Bled defsch scho sei, Mädle, bloß net of da Koopf gfalla.

Old country lore of my grandma

Die Experimente zur vorliegenden Arbeit wurden zwischen Juli 2018 und Februar 2021 am Institut für Anorganische Chemie der Julius-Maximilians-Universität Würzburg unter der Aufsicht von Prof. Dr. Dr. h. c. Todd B. Marder durchgeführt.

The experiments for the present thesis were done between July 2018 and February 2021 at the Institut für Anorganische Chemie at the Julius-Maximilians-Universität Würzburg under supervision of Prof. Dr. Dr. h. c. Todd B. Marder.

ACKNOWLEDGMENT

I want to thank **Prof. Dr. Dr. h. c. Todd B. Marder** for giving me the chance to work on my PhD thesis in his group, to visit our collaboration partners in Croatia and to present my results at several conferences. It was an amazing experience to meet all these people! I also want to thank you for treating us as your family and for giving me the freedom to grow as a person and to find my way in chemistry while showing me what science can look like.

I want to thank **Prof. Dr. Dr. Lorenz Meinel** and his team for the chance to take a look into the completely new field of pharmaceutical chemistry. A special thanks goes out to **Martina Raschig** for sharing your experiences and knowledge in this field with me, for hanging in there with me in all these countless meetings talking about the same things over and over again and for the great evenings watching and discussing 'The Taste'.

Thank you, **Prof. Dr. Ivo Piantanida** from the Institut Ruđer Bošković in Zagreb for hosting me in Croatia, showing me the city and introducing me to the new world of biomacromolecules and their interactions with other molecules. Thank you, **Dr. Lidija-Marija Tumir**, for sharing your DNAPore with me. A special thanks goes to **Dr. Željka Ban, Ivona Krošl, Iva Orehovec, Iva Zonjić**, and **Dr. Dijana Pavlović Saftić** for sharing your knowledge and time in and after the lab with me although every one of you had a lot to organize during these days before Christmas! Seeing advent and pre-Christmas season in a completely new country was an amazing experience. All of you are great and I am glad, I met you!

Thank you, **Michael Moos** from the working group of **Prof. Dr. Christoph Lambert** for booking measurement time for me. Thank you, **Arthur Turkin, David Mims**, and **Chantal Roger** for showing me the differences between our old and your new FLS system.

Thank you, **Dr. Ivo Krummenacher** from the working group of **Prof. Dr. Holger Braunschweig** for recording the CV spectra with me within an incredibly short amount of time. I think, I have never worked as fast as I did during these two days! Thank you for your help discussing the results and proof-reading them.

Thank you, **Dr. Alexandra Friedrich** and **Johannes Krebs**, for being so incredibly patient with my tiny little crystals! I am glad, I did not have to bother you more often asking if the crystals are suitable for measurement. Thank you, **Dr. Rüdiger Bertermann, Marie-Luise Schäfer**, and **Laura Wolz** for your countless service NMR measurements, especially the low- and high-temperature studies. Thank you, **Sabine Timmenroth** and **Liselotte Michels** for the elemental analyses. Thank you, **Gertrud Wunderling** for keeping our kitchen in good shape all the time! Thank you, **Alfred Schertzer** for doing all those tiny

little things. Without you, nothing in the building would work. Thank you, **Manfred Reinhart, Wolfgang Obert, Alois Ruf, Berthold Fertig, and Bernhard Werner** for your expertise in each of your fields which helped very much in turning our ideas into reality.

A large thank you goes to **Maria Eckhardt, Uschi Rüppel, and Cornelia Walter** for your organizational skills, help with paperwork, always listening to every problem and help solving them! I would have been lost without your patience!

I want to thank **Dr. Jörn Nitsch, Dr. Stefanie Griesbeck, Dr. Florian Rauch, and Dr. Matthias Fergner** for helping with photophysical problems, especially when the FLS system did what it wanted but not what it was supposed to do. Thank you, **Hildegard Holzinger** for ordering everything I needed to do my chemistry. Thank you, **Dr. Stephan Wagner** for your expertise in HRMS measurements, ordering new instruments, and repairing the GC-MS systems. Some investigations in this thesis would not have been possible without your help! Thank you very, very much, **Christoph Mahler** and **Sabine Lorenzen** for all these countless discussions about non-chemistry topics and your enormous knowledge and experience in HRMS measurements and chemical methods. Knowing, that I can always ask you for help and advice was extremely reassuring! Thank you, **Sabine** for sharing your trainees with me from time to time! Without you conscientiously educating them, it would not have been possible that **Ann-Katrin Richard** finds the calculation error me and my students had made for a long time. Thank you both very much!

A special thanks goes to **Dr. Stefanie Griesbeck, Dr. Florian Rauch, Dr. Julia Merz, and Dr. Matthias Fergner** for sharing your knowledge and experience with me. Thank you, **Flo, Matze, and Julia** for proof-reading and discussions. Thank you, **Steffi** and **Flo** for taking me as I am, introducing me to this working group, teaching me the rules of triarylborane chemistry and that both of you believed in me before I was able to see what I have learned during my Bachelor's and Master's studies! I would not have been able to come so far without you! Thank you, **Robert Ricker, Johannes Krebs, Flo, and Julia**: without you, it would not have been the same being in the ACII! Similarly, supervising biology students would not have been the same without the help of **Jan Maier**.

I want to thank my interns **Jessica Rühle, Felix Full, Johannes Schwarzmann, Alexandra Phillipps, and Marco Weber** for all your work! Without your help and patience, it would have taken me much longer to reach the end. I know that I asked for much from time to time, but I was only able to do so because I knew that you could do it! I am very grateful for everything you did! Thank you, **Wen Jun Ng** for your help during your employment.

Thank you **Wiebke Daul**, **Alexandra Phillipps**, and **Wen Jun Ng** for working on your Master's Theses under my supervision. Only your work gave me the chance to focus on my chemistry!

A very important thank you goes to the whole AK Marder family, especially **Steffi**, **Flo R.**, **Julia**, **Jan**, **Jiang**, **Xiaocui**, **Wenbo** and everybody else, who organized and participated in the countless days in the old and new building when we cooked, discussed, talked, went hiking, had brunch or just enjoyed a beer or Radler discussing about everything. I really missed these times during the past 1.5 years...

A special thank you goes to the AK Boardgame members **Johannes**, **Robert**, and **Jan** for all of those evenings and nights diving into and exploring completely different worlds. I did not expect that simply playing boardgames gives the chance to leave everything else behind. I also want to thank all our 'guest players' who enjoyed participating at our board game evenings, especially **Tom Parsons**. I really loved these nights! Without one of these nights, I think, the new building would have been flooded. Thank you very much for your patience, help, stamina, and creativity that night! I think, I will never ever again be so happy to have forgotten my keys somewhere!

Apart from my scientific family, I want to thank everybody who accompanied my last 9 years in Würzburg: my present and former basketball teammates and coaches, especially **Heidi**, **Charlie**, and **Pia**. Meeting you every week, working my ass off on the court, winning and losing together with you gave me the strength to work my way through all of the ups and downs at work, too! I want to thank all my flat mates for having an open ear and telling stories from worlds far apart from chemistry in the evening when cooking or eating together. I will never forget any one of you! A special thanks goes to **Prathiba** for stumbling into my life! You opened my horizon to so much more than just English language, Indian cooking, and scientific work. I am not sure if I would be where I am without you. I want to thank my friends at home, especially **Mäggy** and **Sabse** for always being there! Although we do not meet regularly, I know, that I can always count on you! Thank you very much! A special thanks goes to those strangers called fellow students who became friends. Without especially you, **Mira**, **Alena**, **Jasmin**, and **Robin**, studying would not have been the same! Thank you for taking me as I am! I am glad we never lost sight of each other. I will never forget our parties, picnicks, cooking evenings, and evenings playing computer games! Although we will scatter in the next months, I hope we will never lose each other!

I want to thank my **parents** for not listening to an elementary teacher and letting me do my Abitur. Without you and your support, I would not be the person I am standing right here right now! Thank you, **Fabian** and **Jonas** for being my brothers. We might not always

have the same opinion, but I know that, no matter which problems we might have had before, I can always count on you! Knowing that you as my family are always right behind me, helping whenever needed, gives me the strength to discover unknown lands.

Last but not least I want to thank **Jan** from the bottom of my heart for being this incredible, amazing, and fascinating person. You are this one person I never knew I would search for and yet we have found each other. The last two years would not have been the same without you! Knowing that I have you right next to me makes the future less scary but rather interesting to discover. I love you!

LIST OF PUBLICATIONS

Publication	Position
<p><i>Synthetic Approaches to Triarylboranes from 1885 to 2020</i>, S. M. Berger, M. Ferger, T. B. Marder, <i>Chem. Eur. J.</i> 2021, 27, 7043-7058.</p> <p>This paper is slightly modified and reproduced in this dissertation with permission from Wiley-VCH. It is published under a creative common license and does not require further permission statements.</p>	Chapter 2
<p><i>Synthesis of Highly Functionalizable Symmetrically and Unsymmetrically Substituted Triarylboranes from Bench-Stable Boron Precursors</i>, M. Ferger, S. M. Berger, F. Rauch, M. Schönitz, J. Rühle, J. Krebs, A. Friedrich, T. B. Marder, <i>Chem. Eur. J.</i> 2021, 27, 9094– 9101. DOI: 10.1002/chem.202100632</p> <p>The parts of this paper done by S. M. Berger are reproduced in this dissertation in a modified form with permission from Wiley-VCH. The paper is published under a creative common license and does not require further permission statements.</p>	Chapter 3
<p><i>Applications of Triarylborane Materials in Cell Imaging and Sensing of Bio-relevant Molecules such as DNA, RNA, and Proteins</i>, S. M. Berger, T. B. Marder, <i>Mater. Horiz.</i> 2021, DOI: 10.1039/D1MH00696G.</p> <p>This paper is slightly modified and reproduced in this dissertation with permission from The Royal Society of Chemistry.</p>	Chapter 5
<p><i>Bithiophene-Cored, mono-, bis-, and tris-(Trimethylammonium)-Substituted, bis-Triarylborane Chromophores: Effect of the Number and Position of Charges on Cell Imaging and DNA/RNA Sensing</i>, S. M. Berger, J. Rühle, J. Schwarzmann, A. Phillipps, A.-K. Richard, M. Ferger, I. Krummenacher, L.-M. Tumir, Ž. Ban, I. Crnolatac, D. Majhen, I. Barišić, I. Piantanida, D. Schleier, S. Griesbeck, A. Friedrich, H. Braunschweig, T. B. Marder, <i>submitted article</i>.</p>	Chapters 3, 4 & 6

LIST OF ABBREVIATIONS

A	acceptor or arginine or ampere
A549 cell	adenocarcinomic human alveolar basal epithelial cell
abs	absorption
Ac	acetate
AF647	alexa fluor 647
AIE	aggregation induced emission
APCI	atmospheric-pressure chemical ionization
Ar	aryl
ASAP	atmospheric solids analysis probe
ATP	adenosine triphosphate
Bu	butyl
BINAP	2,2'- <i>bis</i> -1,1'-binaphthyl
bipy	2,2'-bipyridine
BNCT	boron-neutron capture therapy
BODIPY	4-bora-3 α ,4 α -diazas-indacene cored compound
B-PAH	boron-containing poly-aromatic hydrocarbon
Bpin	pinacol boronic ester, pinacolato-borane
B ₂ pin ₂	<i>bis</i> -pinacolato diboron
BSA	bovine serum albumin
c	concentration
c ₀	concentration at the beginning of the experiment
C	cytosine
cal	calories, 1 cal = 4.184 J
CD	circular dichroism
C _{nc}	no cytotoxicity up to this concentration
COD	cyclooctadiene
coe	cyclooctene
C _{incub}	concentration of triarylboron compound used for incubation
C _{incub} ^{cd}	concentration of commercial dye used for incubation
cRGD	cyclic arginine, glycine, and aspartic acid
CT	charge transfer
ctDNA	calf thymus DNA
CV	cyclic voltammetry or cyclic voltammogram
cyclen	1,4,7,10-tetrazacyclododecane
d	doublet or day(s)

D	donor or aspartic acid
DAPI	4',6-diamidino-2-phenylindole
dba	(1 <i>E</i> ,4 <i>E</i>)-1,5-diphenylpenta-1,4-dien-3-one
dd	doublet of doublet
ddd	doublet of doublet of doublet
DFT	density functional theory
DMEM	Dulbecco's Modified Eagle Medium
DMF	<i>N,N</i> -dimethylformamide
DMSO	dimethyl sulfoxide
DNA	deoxyribonucleic acid
DNApore	cylindrical shaped formation of six intertwined DNA threads forming a pore in the middle
DNBS	2,4-dinitrobenzenesulfonyl
dppf	1,1'- <i>bis</i> -(diphenylphosphino)ferrocene
ds	double stranded
dtbpy	4,4'- <i>di-tert</i> -butyl-2,2'-dipyridyl
duryl	1,2,4,5-tetramethylphenyl
E	energy
$E_{1/2}^{ox}$	oxidation potential
$E_{1/2}^{red}$	reduction potential
EEA1	early endosome antigen 1
ESI	electrospray ionization
eV	electronvolt, 1 eV = $1.602176634 \times 10^{-19}$ J
exc	excitation
F	Farad, 1F = $1s^4 A^2 m^{-2} kg^{-1}$
Fc	ferrocenyl
Fc ⁺	ferrocenium
FBS	fetal bovine serum
fl	fluorescence
FLIM	fluorescence lifetime microscopy
FLP	Frustrated Lewis pair
G	guanine or glycine
GGT	γ -glutamyltranspeptidase
GM	Göppert-Mayer, 1 GM = $10^{-50} \text{ cm}^4 \text{ s photon}^{-1}$
GM130	golgin subfamily A member 2
<i>h</i>	Planck's constant
h	hour(s)

HEK 293T cell	human embryonic kidney cell
HeLa cell	human cervical cancer cell
HepG2 cell	human liver carcinoma cell
HLCT	hybrid localized charge transfer
HOMO	highest occupied molecular orbital
HPLC	high performance liquid chromatography
HRMS	high resolution mass spectrometry
HUVEC-1 cell	human umbilical vein endothelial cell
Hz	Hertz, s^{-1}
$h\nu$	irradiation with light
i	<i>iso</i>
ICD	induced circular dichroism
IMes	1,3- <i>bis</i> -(2,4,6-trimethylphenyl)-1,3-dihydro-2H-imidazol-2-ylidene
IR	infrared
irrev.	irreversible
ISC	intersystem crossing
J	joule, $1 \text{ J} = 1 \text{ kg m}^2 \text{ s}^{-2}$
k	kilo, 10^3
k_B	Boltzmann's constant
k_c	equilibrium constant at T_c
k_{nr}	non-radiative decay rate constant
k_r	radiative decay rate constant
LAMP-1	lysosome membrane protein 1
LDA	lithium diisopropylamine
LE	locally excited
LIFDI	liquid injection field desorption/ionization
$\log K_s$	binding constant for interaction with biopolymer(s)
LTG	LysoTracker™ Green
LTR	LysoTracker™ Red
LUMO	lowest unoccupied molecular orbital
m	multiplet or mili, 10^{-3}
M	molarity, $1 \text{ M} = 1 \text{ mol L}^{-1}$ or mega, 10^6
MAO	monoamine oxidase
max	maximum
MCF-7 cell	human breast cancer cell
MeCN	acetonitrile

Mes	mesityl, 1,3,5-trimethylphenyl
min	minute(s)
MTDF	MitoTracker™ DeepRed FM
MTRC	MitroTracker™ Red CMXRos
<i>n</i>	<i>normal</i>
n	nano, 10 ⁻⁹
NBS	<i>N</i> -bromosuccinimide
<i>n</i> BuLi	<i>n</i> -butyl lithium
NCS	<i>N</i> -chlorosuccinimide
NMR	nuclear magnetic resonance
NIH/3T3 cell	mouse fibroblast cell
NIR	near infrared
N. R.	no data reported
<i>o</i>	<i>ortho</i> -position
OD	optical density
OLED	organic light emitting diode
ox	oxidation
<i>p</i>	<i>para</i> -position
p	piko, 10 ⁻¹²
pApU	ds poly rA – poly rU
PBS	phosphate-buffered saline
PDT	photodynamic therapy
PET	positron emission tomography
Ph	phenyl
POS-1 cell	osteosarcoma tumor cell
ppm	parts per million
r	ration between compound and biopolymer
R	ideal gas constant or arginine
red	reduction
RNA	ribonucleic acid
R _r	Pearson value
s	singlet or second(s)
SCE	standard calomel electrode
SERS	surface enhanced Raman scattering
SHE	standard hydrogen electrode
SKOV-3 cell	ovarian tumor cell

SPhos	2-dicyclohexylphosphino-2',6'-dimethoxybiphenyl
ss	single stranded
<i>t</i>	<i>tert</i>
T	thymine or temperature
T _c	coalescence temperature
<i>t</i> -BuLi	<i>tert</i> -butyl lithium
TD-DFT	time-dependent density-functional theory
Tf	triflate
THF	tetrahydrofuran
t _{incub}	incubation time for triarylboron compound
t _{incub} ^{cd}	incubation time for commercial dye
Tip	tri <i>is</i> opropylphenyl
T _m	thermal denaturation temperature
TMSCI	trimethylsilyl chloride
TPEF	two-photon excited fluorescence
Turbor-Grignard	<i>iso</i> -propyl magnesium chloride lithium chloride, <i>i</i> PrMgCl·LiCl
U	uracil
U87MG cell	human primary glioblastoma
UV	ultra-violet
V	volt, 1 V = 1 kg m ² s ⁻³ A ⁻¹
W	watt, 1 W = 1 kg m ² s ⁻³
WI38 cell	diploid human fibroblast cell derived from lung tissue of a 3-month-gestation female fetus
Xantphos	(9,9-dimethyl-9H-xanthene-4,5-diyl)- <i>bis</i> -(diphenylphosphane)
xylyl	dimethylphenyl
¹ O ₂	singlet oxygen
³ O ₂	triplet oxygen
Å	Angstrom, 1 Å = 100 pm
<i>α</i>	<i>alpha</i> -position
<i>β</i>	<i>beta</i> -position
ΔE _{calc}	calculated bandgap
ΔE _{CV}	electrochemical bandgap
ΔE _{opt}	optical bandgap
ΔG [‡]	rotational barrier
ΔT _m	difference between two T _m

$\Delta\nu$	peak separation in Hz at the low temperature limit
ε	molar extinction coefficient
ε_r	dielectric constant
λ	wavelength
Λ	orbital overlap parameter
μ	mikro, 10^{-6}
σ_2	two-photon absorption cross section
τ	lifetime
τ_0	natural lifetime
Φ_f	fluorescence quantum yield
Φ_Δ	singlet oxygen sensitizing quantum yield
χ^2	Durbin-Watson factor

ANNOTATION

The author is aware that the dipole moment of charged compounds is defined relative to its origin. Thus, it is not an observable quantity. However, herein, the term dipole moment will be used to describe the distribution of the electron density over the molecules for convenience.

TABLE OF CONTENTS

1	Introduction	3
2	Synthetic Approaches to Triarylboranes from 1885 to 2020	11
2.1	Introduction	11
2.2	Synthesis of Symmetrically-Substituted Triarylboranes	12
2.2.1	Boron Trichloride, Tribromide and Boronic Esters as Boron Sources	12
2.2.2	Boron Trifluoride as the Boron Source	14
2.2.3	Metal-Boron Exchange Reactions for the Synthesis of Triarylboranes	19
2.2.4	Potassium Aryltrifluoroborates as Boron Sources	23
2.2.5	Direct Dimesitylborylation	26
2.3	Synthesis of Unsymmetrically-Substituted Triarylboranes	27
2.3.1	Boronic Esters as Boron Sources	27
2.3.2	Borane Dimethyl Sulfide as the Boron Source	30
2.3.3	Boron Trifluoride as the Boron Source	30
2.3.4	Boron Tribromide as the Boron Source	31
2.4	Summary and Outlook	32
3	The Basis of This Work – An Unsymmetrically-Substituted, Amine-Containing Triarylborane	35
3.1	Introduction	35
3.2	Results and Discussions	36
3.2.1	Synthesis	36
3.2.2	Crystal Structures and Rotational Barriers	39
3.2.3	Photophysical Properties	43
3.2.3.1	Neutral Triarylboranes	43
3.2.3.2	Cationic Triarylboranes	47
3.2.4	Electrochemical Properties	50
3.2.5	HOMO-LUMO Gaps	53
3.2.6	Singlet Oxygen Sensitization	54
3.3	Conclusions	57
4	Synthesis and Selected Properties of Bithiophene-Cored, <i>Mono-</i> , <i>Bis-</i> , and <i>Tris-</i> (Trimethylammonium)-Substituted, <i>Bis</i> -Triarylborane Chromophores	61
4.1	Introduction	61
4.2	Results and Discussion	62
4.2.1	Synthesis	62
4.2.2	Solubility in Water	65
4.2.3	Photophysical Properties	66
4.2.3.1	Neutral bis-Triarylboranes	66

4.2.3.2	Cationic bis-Triarylboranes	73
4.2.4	Electrochemical Properties	79
4.2.4.1	Neutral bis-Triarylboranes.....	79
4.2.4.2	Cationic bis-Triarylboranes	82
4.2.5	HOMO-LUMO Gaps.....	85
4.2.6	Singlet Oxygen Sensitization	87
4.3	Conclusions	89
5	Applications of Triarylborane Materials in Cell Imaging and Sensing of Bio-relevant Molecules such as DNA, RNA, and Proteins.....	95
5.1	Introduction.....	95
5.2	Triarylborane-Loaded Nanogels.....	97
5.3	Neutral Triarylboranes	98
5.4	Cationic Triarylboranes.....	102
5.5	Discussion	105
5.6	Summary and Outlook	108
6	Interaction of Bithiophene-Cored, <i>Mono-</i> , <i>Bis-</i> , and <i>Tris-</i> (Trimethylammonium)-Substituted, <i>Bis</i> -Triarylborane Chromophores with DNAs, RNA, and Cells	113
6.1	Introduction.....	113
6.2	Results and Discussion.....	114
6.2.1	Physico-Chemical Properties in Buffered Solution	114
6.2.2	Interaction with DNA and RNA at pH 7.....	115
6.2.2.1	Thermal Melting Experiments	115
6.2.2.2	Fluorimetric Titrations	116
6.2.2.3	Circular Dichroism Experiments.....	118
6.2.3	Interaction with DNAs at pH 8.....	119
6.2.3.1	Thermal Melting Experiments	119
6.2.3.2	Fluorimetric Titrations	120
6.2.3.3	Circular Dichroism Experiments.....	122
6.2.4	Interaction with Cells.....	123
6.2.4.1	MTT Assay	124
6.2.4.2	Emission Bleaching and Photoinduced Cell Damage.....	125
6.2.4.3	Co-localization Studies	128
6.3	Conclusions	131
7	Proof-of-Concept Investigations of H ₂ O ₂ -Cleavable Aryl Boronate Esters and Subsequent Formation of Coumarin.....	135
7.1	Introduction.....	135
7.2	Results and Discussion.....	138
7.2.1	Synthesis.....	138

7.2.2	Solubility in Water and PBS Buffer	139
7.2.3	Photophysical Properties.....	141
7.2.4	Cleavage experiments	144
7.3	Conclusions	154
8	Summary / Zusammenfassung.....	157
8.1	Summary	157
8.1.1	Chapter 1	157
8.1.2	Chapter 2.....	157
8.1.3	Chapter 3.....	159
8.1.4	Chapter 4.....	161
8.1.5	Chapter 5.....	163
8.1.6	Chapter 6.....	163
8.1.7	Chapter 7	165
8.2	Zusammenfassung.....	167
8.2.1	Kapitel 1	167
8.2.2	Kapitel 2.....	167
8.2.3	Kapitel 3.....	169
8.2.4	Kapitel 4.....	171
8.2.5	Kapitel 5.....	173
8.2.6	Kapitel 6.....	174
8.2.7	Kapitel 7.....	176
9	Experimental	181
9.1	General Experimental Details.....	181
9.2	Synthesis	188
9.2.1	Chapter 3.....	189
9.2.2	Chapter 4.....	196
9.2.3	Chapter 6.....	213
9.2.4	Chapter 7	214
10	References	221
11	Appendix	235
11.1	Cyclic Voltammograms.....	235
11.1.1	Chapter 3.....	236
11.1.1.1	Neutral Triarylboranes.....	236
11.1.1.2	Cationic Triarylboranes	239
11.1.2	Chapter 4.....	241
11.1.2.1	Neutral bis-Triarylboranes	241
11.1.2.2	Cationic bis-Triarylboranes.....	247

11.2	Singlet Oxygen Sensitization	251
11.3	Studies in Buffered Solutions	253
11.3.1	Chapter 6.....	253
11.3.1.1	Physico-Chemical Properties of Cat¹⁺-Cat³⁺ in Buffered Solution....	253
11.3.1.1.1	Solubility in Sodium Cacodylate at pH 7	253
11.3.1.1.2	Stability of UV/Vis Spectra	253
11.3.1.1.3	Fluorimetric Spectra.....	258
11.3.1.2	Interaction of Cat¹⁺-Cat³⁺ with ctDNA, and pApU at pH 7	262
11.3.1.2.1	Thermal Melting Experiments	262
11.3.1.2.2	Fluorimetric Titrations	264
11.3.1.2.3	Circular Dichroism Experiments.....	268
11.3.1.3	Interaction of Cat¹⁺-Cat⁴⁺ with ctDNA, and DNApore at pH 8	270
11.3.1.3.1	Thermal Melting Experiments	270
11.3.1.3.2	Fluorimetric Titrations	272
11.3.1.3.3	Circular Dichroism Experiments.....	276
11.3.1.1	Cell Studies	281
11.3.1.1.1	Photoinduced Cell Damage	281
11.4	NMR Spectra	287
11.4.1	Chapter 3.....	287
11.4.2	Chapter 4.....	298
11.4.3	Chapter 7.....	322
11.5	HRMS Spectra.....	327
11.5.1	Chapter 7.....	327
11.6	Crystal Structures	330
11.6.1	Chapter 3.....	330
11.7	TD-DFT Calculations	331
11.7.1	Chapter 3.....	331
11.7.2	Chapter 4.....	341
11.7.2.1	Sulfur Atoms of Bithiophene on Same Side	341
11.7.2.2	Sulfur Atoms of Bithiophene on Opposite Sides.....	357
11.8	XYZ Coordinates	377
11.8.1	Chapter 3.....	377
11.8.2	Chapter 4.....	381
11.8.2.1	Sulfur Atoms of Bithiophene on Same Side	381
11.8.2.2	Sulfur Atoms of Bithiophene on Opposite Sides.....	393
11.9	Declaration of Authorship.....	409
11.9.1	Chapter 2.....	409

11.9.2	Chapter 5	411
11.10	Affidavit / Eidesstattliche Erklärung	413
11.10.1	Affidavit	413
11.10.2	Eidesstattliche Erklärung	413
11.11	List of Compounds.....	414
11.11.1	Chapter 3	414
11.11.2	Chapters 4 and 6.....	415
11.11.3	Chapter 7	416

CHAPTER 1

INTRODUCTION

1 Introduction

Three-coordinate organoboron compounds adopt a trigonal-planar structure in which the remaining, unoccupied p-orbital of the boron center (pink, Figure 1.1A) is perpendicular to the BC_3 plane (green, Figure 1.1A). This empty p-orbital makes these compounds strong π -acceptors. Thus, they can be used as the accepting moiety in donor-acceptor (D-A) compounds which are, in general, highly efficient light absorbing and emitting compounds. This property is needed in several applications such as photovoltaics, light-emitting devices (e.g. OLEDs) or biological imaging and sensing. Due to the inherent electron-deficiency, organoboron compounds can also be used in electronic devices as, e.g., electron-transport layers. However, for most of these potential applications, air- and moisture stable compounds are required. Thus, the Lewis acidity and tendency for hydrolysis must be inhibited.

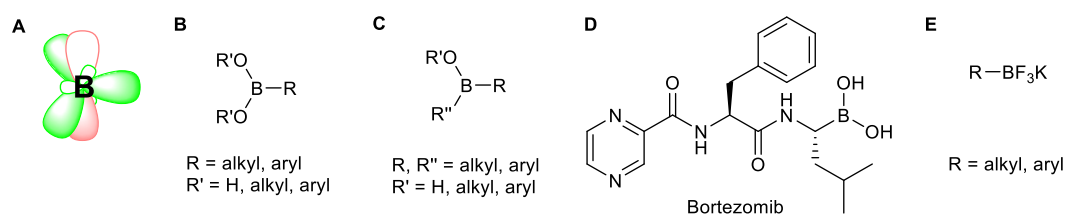


Figure 1.1: **A)** Electronic structure of three-coordinate boron. **B)** General structure of boronic acids and esters. **C)** General structure of borinic acids and esters. **D)** Structure of Bortezomib.^[1] **E)** General structure of potassium aryl trifluoroborates.

Two strategies for such stabilization employ steric or electronic factors. An example of the latter is the direct binding of oxygen atoms to the boron. The resulting compounds are called boronic acids and esters ($RB(OR)_2$; Figure 1.1B) or borinic acids and esters ($R_2B(OR)$; Figure 1.1C). An example of a potential application of such compounds is Bortezomib (Figure 1.1D), which is used in the treatment of blood cancer,^[1] although many boronic acids and esters were found to be mutagenic^[2] according to the Ames assay.^[3-4] Boronic acids and esters are of current interest as they are cleaved in the presence of H_2O_2 .^[5-8] A relationship between higher cellular concentrations of H_2O_2 and diseases such as diabetes, neurodegenerative disorders, and cancer was found.^[9] Hence, boronic esters are being investigated for potential applications in H_2O_2 sensing and drug delivery. An example of such a system was investigated during this thesis research and is presented in Chapter 7. The work described in this chapter continues the preliminary studies reported in the Master's Thesis of Wiebke Daul, which was carried out under the supervision of Sarina M. Berger.^[10] Thus, some of these results are repeated for completeness and are cited herein.

Another possibility to obtain air- and moisture-stable, organoboron compounds, is the population of the empty p-orbital by binding a fourth atom such as oxygen, nitrogen or fluorine. The resulting four-coordinate compounds are negatively charged salts, called borates, which are tetrahedral. Potassium aryl trifluoroborates (Figure 1.1E) have found wide application in organic synthesis mainly with the loss of the boron motif in cross-coupling reactions.^[11-12] However, as Chapter 2 summarizes, previous work by different groups demonstrates that potassium aryl trifluoroborates can also be used as starting materials for the synthesis of triarylboranes. In this dissertation, triarylboranes bearing one or two different types of aromatic systems are called symmetrically-substituted. When there are three different arenes around the boron, the resulting compound is called an unsymmetrically-substituted triarylborane. A systematic synthetic approach to such compounds starting from potassium aryl trifluoroborates is presented in Chapter 3 and the dissertation of Matthias Ferger.^[13]

In triarylboranes, the empty p-orbital of the boron center is protected from nucleophilic attack mainly *via* sterical shielding (Figure 1.2A),^[14] electronic stabilization (Figure 1.2B),^[15] or planarization (Figure 1.2C).^[16] The stabilization in the latter case results from the fact that the boron center cannot change its conformation to tetrahedral upon binding to another atom. For compound **1.2** (Figure 1.2B),^[15] stabilization results, to a certain extent, from weak interactions with fluorine lone pairs, but predominantly from steric shielding.

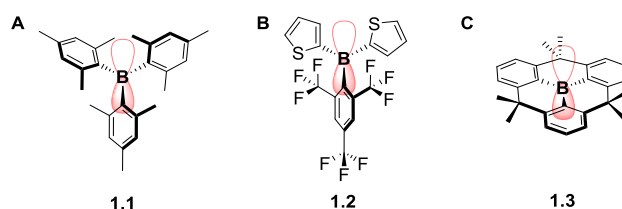


Figure 1.2: Stabilization of the empty p-orbital in three-coordinate organoboron compounds by **A)** steric constraint;^[14] **B)** fluorinated groups in *ortho* position;^[15] **C)** planarization.^[16]

The use of sterically demanding aryl groups was first discovered in 1957 (Figure 1.2A).^[14] Typically, substituents such as mesityl (1,3,5-trimethylphenyl; Mes) or triisopropylphenyl (Tip), are used, resulting in a propeller-like structure.^[17] Such sterically stabilized triarylboranes have found many potential applications,^[18-25] especially as optoelectronics,^[26-28] sensors for anions or small molecules,^[29-34] and as bioimaging agents^[8, 32, 35-49] due to the ease of their modification and their unique photophysical and electrochemical properties. For the latter potential applications, triarylboranes also have to be water-soluble. This can be achieved by incorporation into water-soluble polymers,

by attaching solubilizing groups containing either oxygen or nitrogen, which are able to undergo hydrogen bonding with water, or by introduction of anionic or cationic moieties. A detailed insight into these strategies, the reported structures, and their use in biological applications is presented in Chapter 5.

However, in 2009, Gabbaï and coworkers reported derivatives of trimesitylborane bearing one, two or three trimethylammonium groups in positions *para* to the boron center instead of methyl groups,^[50] and at least two trimethylammonium groups are required to achieve water-solubility. This concept was used by Marder and coworkers to synthesize a bithiophene-bridged, *bis*-triarylborane with four cationic charges (**Cat⁴⁺**; Figure 1.3).^[43] This compound is not only water-soluble in concentrations of up to 1.0 mM, but also enters cells and stains different cell organelles therein,^[43] most likely due to protein binding.^[51] The same group reported additional tetra-cationic compounds in which the bithiophene bridge was exchanged by other, (hetero)aromatic systems.^[44, 46, 52-53] All of these compounds are water-soluble and water-stable if they contain at least five *ortho*-methyl groups or other groups with similar steric demand, such as *e.g.* anthracene.^[44] In addition, the localization of these compounds in cells was monitored not only by fluorescence spectroscopy but also by Raman spectroscopy in the case of **1.4f-1.4i**.

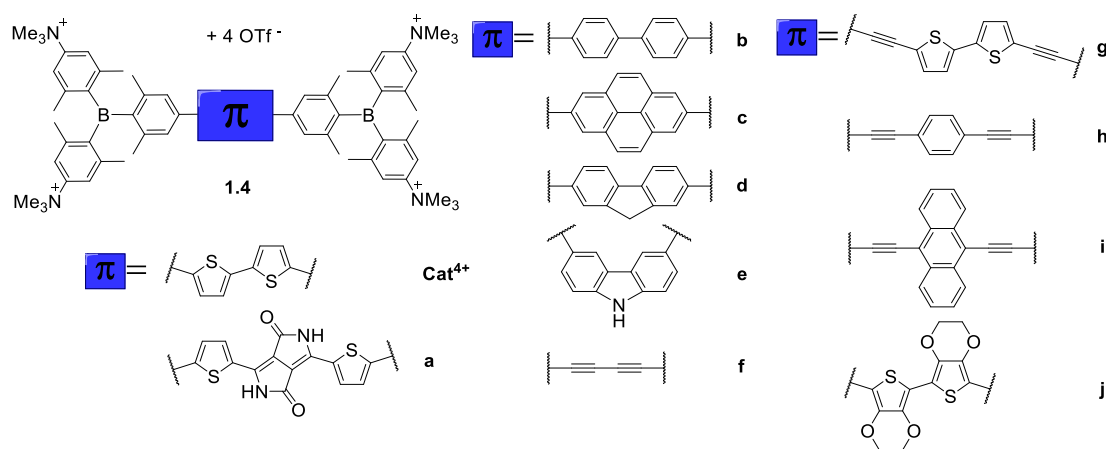


Figure 1.3: Overview of water-stable, tetra-cationic, *bis*-triarylborane-substituted chromophores by Marder and coworkers.^[13, 43, 46, 52-53]

From co-localization studies, most of the compounds **1.4a-1.4f** were shown to localize at similar places in different cell lines, mainly in lysosomes. Thus, these studies show that the bridging unit of such *bis*-triarylborane chromophores has only a minor influence on their intra-cellular localization. However, the influence of the number and distribution of the cationic charges on these compounds remained uninvestigated. This issue was first examined in the Master's Thesis of Domenic Schleier, who aimed to synthesize selectively charged compounds by selective methylation of the neutral precursor **Neut4** using methyl

triflate.^[54] The isolation of selectively charged compounds similar to **Neut2Cat**²⁺ and **Neut2Cat(i)**²⁺ (Figure 1.4A) using this approach was not possible as: a) stoichiometric amounts of methylation agent yielded mixtures of differently charged compounds; and b) the two di-cationic compounds **Neut2Cat**²⁺ and **Neut2Cat(i)**²⁺ cannot be separated by various techniques including high performance liquid chromatography (HPLC). Thus, in the Master's Thesis of Sarina M. Berger, the aim of synthesizing selectively charged compounds was approached *via* the synthesis of compounds **Neut1-Neut4** that can only be methylated at the desired positions, hence leading to **Cat**¹⁺-**Cat**³⁺ (Figure 1.4B).^[55]

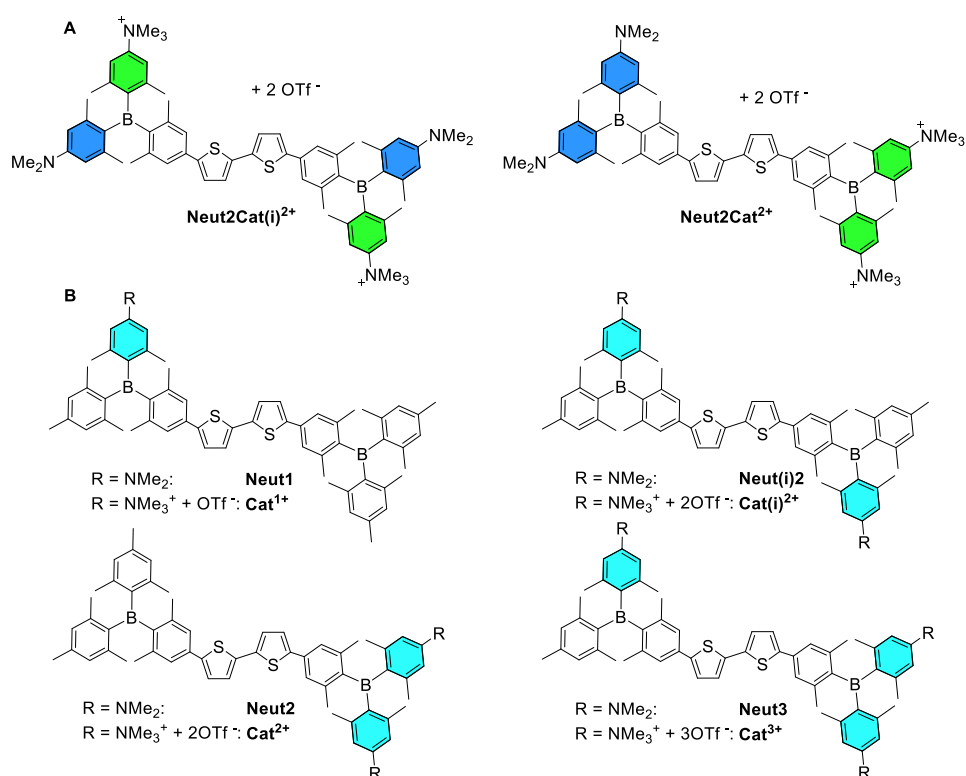


Figure 1.4: **A**) Structures of **Neut2Cat**²⁺ and **Neut2Cat(i)**²⁺ which Schleier attempted to synthesize.^[54] **B**) Target compounds of this work and the Master's Thesis of Sarina M. Berger.^[55]

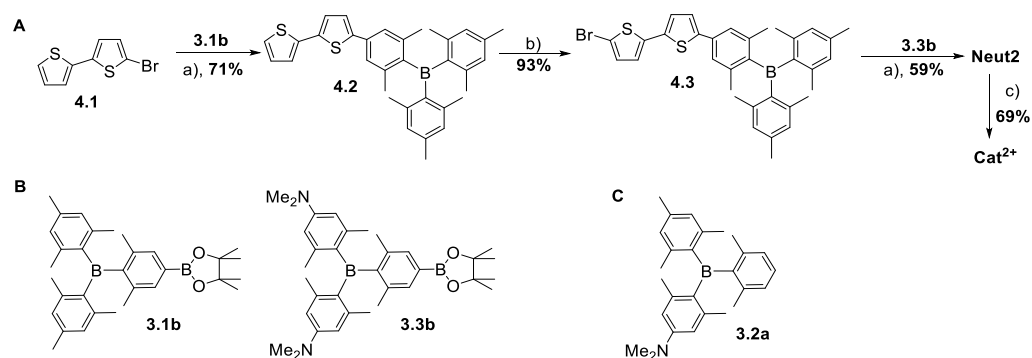


Figure 1.5: **A)** Synthetic route to **Cat**²⁺: a) Pd₂(dba)₃·CHCl₃, SPhos, KOH, toluene/water 2:1, 85 °C, 2d; b) NBS, DMF, 0 °C, 15 min then r.t., 2 h; c) MeOTf, CH₂Cl₂, r.t., 2 d.^[55] **B)** Structures of borylated triarylboranes **3.1b** and **3.3b**. **C)** Structure of the new, unsymmetrically substituted triarylborane **3.2a**.

In course of Sarina M. Berger's Master's Thesis, only the synthesis of **Cat**²⁺ was achieved by sequential Suzuki-Miyaura cross-coupling reactions (Figure 1.5A) using the two known borylated triarylboranes **3.1b** and **3.3b** (Figure 1.5B).^[43, 54, 56] For the synthesis of the remaining compounds, following the same synthetic strategy, triarylborane **3.2a** (Figure 1.5C), bearing three different aromatic systems, is required. Throughout this dissertation, such compounds are called 'unsymmetrically-substituted triarylboranes'. As shown in Chapter 2 of this thesis, a synthetic route to such triarylboranes was not widely accessible at the beginning of the Master's Thesis or this dissertation. Thus, development of such a methodology were initiated in 2018^[55] and continued in the present thesis. For completeness, some of the previous results are cited herein. However, the final isolation of **3.2a** (Chapter 3) and compounds **Cat**¹⁺, **Cat(i)**²⁺ and **Cat**³⁺ (Chapter 4) was achieved during this dissertation research. After successful synthesis, the water-solubility, photophysical and electrochemical properties, and singlet oxygen sensitization efficiencies of the triarylboranes and *bis*-triarylboranes (Chapters 3 and 4) and the interaction of the latter with DNA and RNA in aqueous environments and cells (Chapter 6) was investigated.

CHAPTER 2

SYNTHETIC APPROACHES TO TRIARYLBORANES FROM 1885 TO 2020

2 Synthetic Approaches to Triarylboranes from 1885 to 2020

The following chapter is slightly modified and reproduced from *Chem. Eur. J.* **2021**, *27*, 7043-7058^[57] with permission from Wiley-VCH.

2.1 Introduction

Within the last few decades, compounds containing three-coordinate boron motifs have found increasing applicability in various fields including optoelectronics,^[26-28] selective sensors for anions^[29, 31, 34] or small molecules,^[32-33] and bioimaging agents^[43-46, 48, 51] due to the empty p-orbital at the boron center. Whereas numerous compounds and their potential applications have been reviewed by several groups,^[8, 18-25] synthetic methodology for the preparation of triarylboranes has been reviewed only rarely. In 1956, a summary by Lappert, *et al.* gave a very general overview of the syntheses of many different types of organoboron compounds.^[58] Very recently, Melen and coworkers summarized synthetic pathways to halogenated triarylboranes as well as their use in catalysis and frustrated Lewis pair (FLP) chemistry.^[59] This review presents developments in the synthesis of triarylboranes since their first report in 1885.^[60]

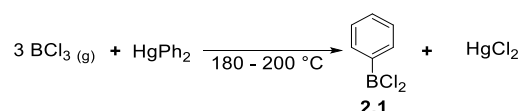
In theory, it is possible to synthesize 3-fold symmetric triarylboranes bearing one type of aromatic system (BAr_3) as well as those containing two or three different aromatic systems ($\text{BAr}_2\text{Ar}'$ or $\text{BArAr}'\text{Ar}''$). Furthermore, their synthesis should be possible from all known boron trihalides. Recently, the synthesis of triarylboranes from potassium aryltrifluoroborates^[61-65] and boronic esters^[66] was reported. Dibenzoboroles^[67] or boron-containing poly-aromatic hydrocarbons (B-PAHs)^[68-70] are not discussed herein as both topics have been reviewed recently.

This review is divided into sections based on symmetrically- (BAr_3 , $\text{BAr}_2\text{Ar}'$) and unsymmetrically-substituted ($\text{BArAr}'\text{Ar}''$) triarylboranes depending on the starting material used as the boron source. In this context, the term unsymmetrically-substituted triarylboranes means that the boron center is bound to three different aromatic systems. Symmetrically-substituted triarylboranes bear one or two different types of aromatic groups as indicated in parentheses (*vide infra*) and, thus, have either (exact or approximate) 3-fold or 2-fold symmetry, respectively.

2.2 Synthesis of Symmetrically-Substituted Triarylboranes

2.2.1 Boron Trichloride, Tribromide and Boronic Esters as Boron Sources

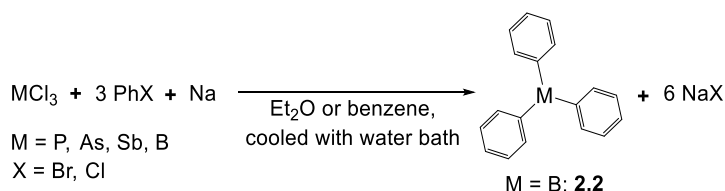
In 1880, Michaelis and coworkers began to investigate arylboranes to determine the valency of boron, which was, at the time, debated to be three or five.^[71] They reacted gaseous BCl_3 with diphenylmercury at elevated temperatures in a sealed tube and observed the formation of dichlorophenylborane **2.1** and HgCl_2 (Scheme 2.1). Compound **1** was isolated *via* distillation and was characterized by elemental analysis and conclusive follow-up chemistry.



Scheme 2.1: Synthesis of dichlorophenylborane **2.1** from BCl_3 .^[71]

After addition of different aqueous solutions, they obtained phenylboronic acid, the respective ethyl ester and the sodium, calcium and silver salts of the acid, as well as their *p*-tolyl analogues.^[72] On an interesting side note, phenylboronic acid, as well as its sodium salt, were also investigated for their antiseptic behavior, and were consumed by humans on a gram scale without causing any considerable complaints.^[72] In 2015,^[2] a series of boronic acids and esters were tested using the Ames assay,^[3-4] and most of them were found to be mutagenic. Thus, this class of compounds should be treated with appropriate care and due testing should be performed prior to use in humans, although several boronic acids or related compounds have been approved for use as drugs.^[2]

In a different approach, Michaelis and coworkers developed a procedure to generate triphenyl derivatives of various main group elements (M), namely phosphorus, arsenic, antimony, and boron.^[73-74] The respective MCl_3 compound was reacted with a phenylhalide and elemental sodium at low temperature to generate the corresponding triphenyl compound according to Scheme 2.2.

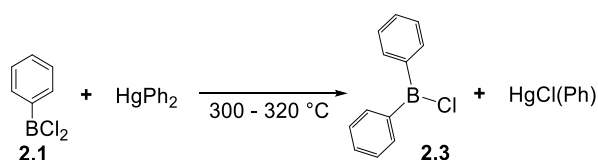


Scheme 2.2: Synthesis of triphenyl derivatives of main group elements.^[60, 73-74]

In 1885, Michaelis and coworkers mentioned that, *via* this general route, a small amount of triphenylborane **2.2** was obtained, but it was not discussed further.^[60] To the best of the

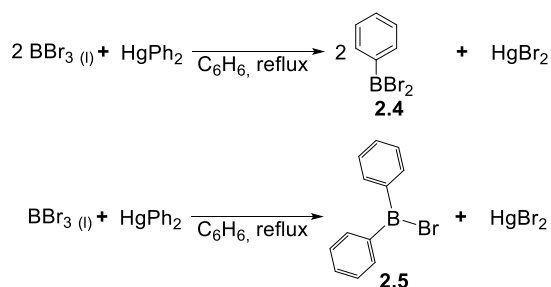
authors' knowledge, this was the first literature report of the synthesis of a triarylborane. Four years later, the synthesis of **2.2** was improved by reacting dichlorophenylborane **2.1** with chlorobenzene and sodium.^[75] This time, compound **2.2** was characterized by elemental analysis and the appearance of a green flame characteristic of boron^[76] when burning the compound.

In 1889, Gattermann and coworkers reported a convenient method for the synthesis of BCl_3 .^[77] Thus, access to the starting material was facilitated. Therefore, Michaelis *et al.* synthesized more dichloroarylboranes and their respective boronic acids, namely the *o*-tolyl, α -naphthyl, β -naphthyl, *p*-methoxyphenyl, *o*-methoxyphenyl and *p*-ethoxyphenyl derivatives.^[78] For the latter three compounds, the reaction proceeded smoothly at room temperature. Furthermore, chlorodiphenylborane **2.3** and its borinic acid derivative were reported and characterized. Compound **2.3** was formed by reacting dichlorophenylborane with diphenylmercury at ca. 300 °C in a sealed tube (Scheme 2.3). It was noted that triphenylborane **2.2** was not obtained this way.



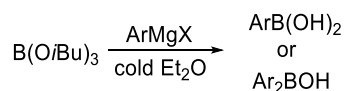
Scheme 2.3: Synthesis of chlorodiphenylborane **2.3** under harsh conditions.^[78]

In 1901, Michaelis and coworkers reported an improved method for the synthesis of mono- and diarylboranes in which they replaced gaseous BCl_3 with liquid and, thus, easier to handle BBr_3 as the boron source.^[79] For this purpose, they developed a convenient and large-scale synthesis of BBr_3 from elemental boron and bromine. BBr_3 was then reacted with diphenylmercury in dry benzene. The reaction was performed in a flask with a reflux condenser at 80 °C. Depending on the stoichiometry, dibromophenylborane **2.4** and bromodiphenylborane **2.5** were synthesized and isolated *via* distillation. Some derivatives, namely dibromo-*p*-tolylborane, dibromo-2,4-dimethylphenylborane, and dibromo-2,4,5-trimethylphenylborane were synthesized and characterized, accordingly. The respective boronic and borinic acids were obtained and characterized after hydrolysis. Again, it was mentioned that, despite extensive studies in this direction, triphenylborane could not be isolated. They assumed that triphenylborane had been formed, but complete separation from diphenyl impurities could not be achieved.



Scheme 2.4: Synthesis of mono- and diarylboranes, starting from BBr_3 .^[79]

Another difficulty of arylborane syntheses were the often laborious and multi-step syntheses of the required diarylmercury compounds. With the discovery of the Grignard reagent in 1900, a powerful tool for the transfer of aryl groups became available.^[80] The first to utilize this in arylborane chemistry, were Khotinsky and Melamed.^[81] They reacted various alkylborate esters with an aryl Grignard reagent in a cold Et_2O solution. The best results were obtained for the *iso*-butylborate ester. Furthermore, Khotinsky and Melamed characterized the phenylboronic *iso*-butyl ester and the *m*-tolylboronic *iso*-butyl ester, as well as the respective boronic acids after saponification. In an attempt to attach two arenes to the boron using Grignard reagents, Strecker reacted an excess of phenyl magnesiumbromide with BCl_3 , but obtained only phenylboronic acid after aqueous work up.^[82] A more extensive study of the reactions of aryl Grignard reagents with the *iso*-butylborate ester was carried out by König and Scharrnbeck in 1915. The results were reported in 1930.^[83] They characterized several novel arylboronic acids and diarylborinic acids which were synthesized according to Scheme 2.5 and isolated after aqueous work-up indicating that the organometallic reagent used was too unreactive to form the corresponding triarylborane. More than 70 years later, it was demonstrated by several groups that triarylboranes can also be synthesized using boronic esters as starting materials and more reactive organometallic reagents (*vide infra*).^[2, 36, 84-88]

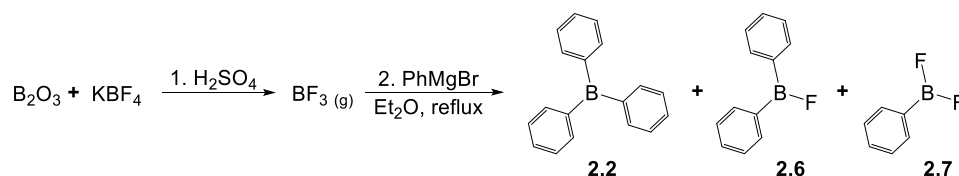


Scheme 2.5: Synthesis of boronic acids and borinic acids, starting from *iso*-butylborate ester.^[83]

2.2.2 Boron Trifluoride as the Boron Source

Despite reports of the synthesis of triphenylborane,^[60, 75] reproducible synthetic access was only available for mono- and diarylboranes in the beginning of the 20th century. This changed with the studies of Krause, who made use of the synthesis of gaseous boron

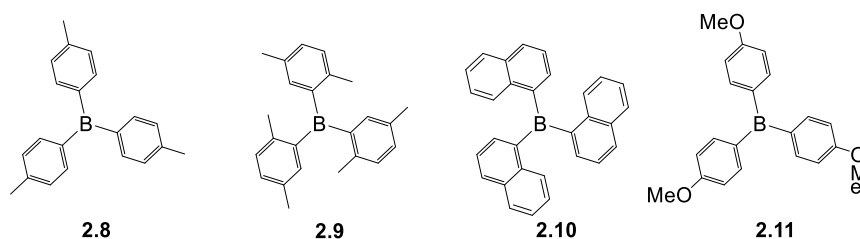
trifluoride (BF_3) from boric anhydride (B_2O_3), sulfuric acid (H_2SO_4) and potassium tetrafluoroborate (KBF_4), reported by Schiff *et al.*^[89] In 1921, Krause and coworkers used gaseous BF_3 in combination with Grignard reagents to yield trialkylboranes as well as alkylboronic acids.^[90] Subsequently, Krause *et al.* applied this method for the synthesis of triphenylborane **2.2**.^[91]



Scheme 2.6: Synthesis of the first reported triarylborane **2.2** according to Krause *et al.*^[91]

They isolated BPh_3 **2.2** by distillation of the crude reaction mixture in ca. 50% yield. The product crystallized easily, but it was also mentioned that **2.2** decomposes in air. Furthermore, Krause and coworkers observed the formation of phenyldifluoroborane **2.6** as well as diphenylfluoroborane **2.7**, but isolation of these two compounds was not possible by distillation. This indicates that the reactivity of the Grignard reagent is insufficient to generate only BPh_3 , as byproducts **2.6** and **2.7** were observed. However, with BPh_3 **2.2** in hand, the group investigated its reactivity with neat sodium^[92] and the other alkali metals potassium, lithium, rubidium and cesium.^[93] Krause and coworkers observed the formation of intensely colored solutions as well as the formation of, mostly, yellow crystals. Both solutions and solids were reported to be highly air sensitive, as the solutions turned colorless when exposed to air. The colorless solution was converted into the colored solution again if neat metal was still present in the solution. After Krause and coworkers had isolated the reaction product of BPh_3 **2.2** with neat sodium,^[93] they titrated the reaction product under a nitrogen atmosphere with elemental iodine which regenerated BPh_3 and sodium iodide. In the same study, the synthesis of tri-*p*-tolylborane **2.8** was mentioned. Its final synthesis and full characterization were reported two years later.^[94] Again, the reactivity of **2.8** with sodium and potassium was investigated as well as its reaction with nitrogenous bases such as ammonia, pyridine, and piperidine. The reaction of **2.8** with neat sodium was described to be the same as for **2.2**. During the reactions of **2.8** with nitrogenous bases, the group observed a temperature increase of the reaction mixture as well as the formation of crystalline and more air-stable products, which were assigned to be addition products of the nitrogenous bases with **2.8**. This assumption was confirmed by elemental analysis of the reaction products. In 1930, Krause and coworkers also reported the synthesis of tri-*p*-xylylborane **2.9** and tri- α -naphthylborane **2.10**, which were investigated similarly to the previous compounds **2.2** and **2.8**.^[95] For the isolation of

2.9 and **2.10**, the work up was slightly modified. Thus, to quench the remaining Grignard reagent, water was added, and the resulting crude mixture was distilled with exclusion of air, as none of the previously synthesized triarylboranes are stable to air.

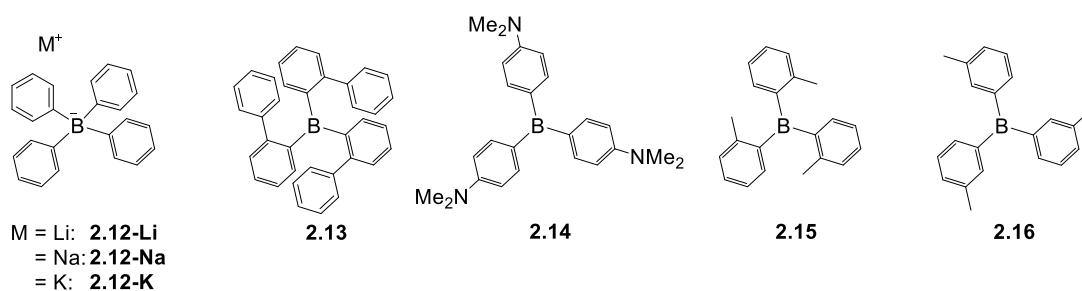


Scheme 2.7: Structures of compounds **2.8-2.11**.^[94-96]

Nevertheless, what they refer to as an “oxidation process” of compound **2.10** starts only after two weeks in air. Furthermore, Krause *et al.* reported that solutions of **2.10** in benzene, chloroform, tetrachloromethane, carbon disulfide, and diethyl ether show a light blueish fluorescence that was more clearly visible with a quartz lamp. They did not provide any further information regarding what kind of lamp or which wavelength they used for excitation. Furthermore, the observed fluorescence was not investigated in detail. In 1931, the same group reported another triarylborane, namely tri-*p*-anisylborane **2.11**, which was found to be as air-sensitive as triphenylborane **2.2**.^[96] In addition, Krause *et al.* had to change their work up once again, as they could not isolate **2.11** in pure form from the crude reaction mixture. Therefore, they reacted a crude mixture of **2.11** with gaseous ammonia to form the corresponding tetra-coordinate Lewis acid-base adduct, which was then purified and subsequently reacted with sulfuric acid with exclusion of air to yield compound **2.11**. Similarly, 20 years later, the same group described the formation of BPh₃ upon heating different tetraarylborate salts to at least 200°C.^[97] Tetraarylborates are used on rare occasions to this day as valuable, alternative precursors to triarylboranes.^[98-100]

Based on this work, Brown *et al.* re-synthesized tri- α -naphthylborane **2.10** as a reference Lewis acid to estimate the Lewis base strength of primary, secondary, and tertiary amines,^[101] having slightly modified the synthesis of the triarylborane. To make the synthesis safer, Brown and coworkers used boron trifluoride etherate (BF₃·OEt₂) instead of gaseous boron trifluoride. Furthermore, they found that the triarylborane they synthesized was stable to air for more than one year. As this finding was in contrast with the reports of Krause *et al.*,^[95] Brown *et al.* had a closer look into the geometry of the compound. They assigned the discrepancy between their and the earlier results to the existence of two possible rotational conformers, i.e., steric hindrance resulted in restricted rotation around the B-C bonds.

In 1947, Wittig *et al.* investigated the possible application of triphenylborane **2** as a catalyst for the lithiation of hydrocarbons.^[102] Instead of successful catalysis of the reaction, they found the formation of a stable complex which was later identified as lithium tetraphenylborate **2.12-Li**.^[103] Further investigations of such compounds, especially the reaction of sodium tetraphenylborate **2.12-Na** with various mono-cationic elements in aqueous solution, led to the discovery of an almost insoluble complex **2.12-K** formed after addition of potassium salts. Later on, compound **2.12-Na** became commercially available as Kalignost[®] for the quantitative analysis of potassium in aqueous solution.^[104]

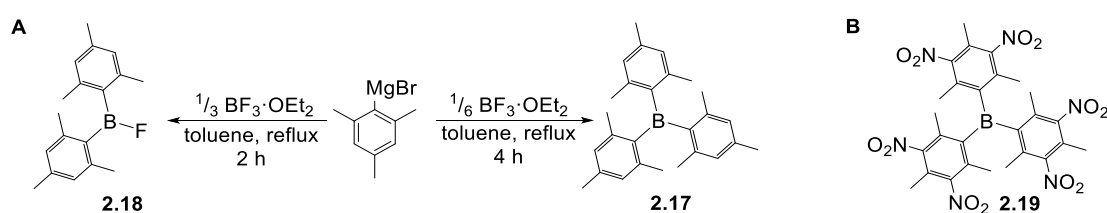


Scheme 2.8: Structures of compounds **2.12-2.16**.^[103-104]

Wittig and coworkers found that triarylboranes such as **2** can also be synthesized from the corresponding, more reactive lithiated species instead of the Grignard reagent.^[103] As long as it was possible to synthesize the desired compounds from Grignard reagents and BF₃ etherate, they did so. However, for tri-(*o*-diphenyl)- **2.13** and tri-(4-(*N,N*-dimethylamino)phenyl)borane **2.14**, Wittig *et al.* used the corresponding aryllithium reagent.^[104] Nevertheless, the synthesis of **2.14** was still challenging, as the amine formed complexes with excess BF₃. Furthermore, this group reported a yellowish fluorescence from **2.14** in the solid state as well as a blue fluorescence in acetone upon irradiation with UV light. Compounds **2.15** and **2.16** were described as having a yellowish-white fluorescence upon UV-irradiation. None of these observations were further explained or investigated by Wittig *et al.* Very recently, Marder and coworkers reported that a sample of pure **2.16** showed only blue fluorescence, with no phosphorescence being observed at room temperature.^[105]

In 1956, Lappert summarized the preparation, chemical and physical properties, reactivities, etc. of almost all organoboranes that had been synthesized up to that date.^[58] In this summary, several methods to synthesize monohaloboranes as well as unsymmetrically-substituted diaryl borinic esters were described. However, almost none of these syntheses were utilized for the formation of triarylboranes, especially not for the formation of boranes bearing three different aromatic systems.

One year later, Brown *et al.* reported the synthesis of the sterically-demanding trimesitylborane **2.17** from the corresponding Grignard reagent and BF_3 etherate.^[14] The group heated the reagents in toluene under reflux for 4 h which they described as forcing conditions. If the reaction was stopped after 2 h, only fluorodimesitylborane **2.18** was isolated showing once again that the formation of triarylboranes from Grignard reagents is possible but requires heat to achieve completion due to the lower reactivity of arylmagnesium reagents compared to, e.g., aryllithium reagents. Furthermore, Brown and coworkers examined the reactivity of **2.17** with amines as well as its decomposition with water and oxygen. It was found that **2.17** was less reactive than tri- α -naphthyl- **2.10** or triphenylborane **2.2** due to its greater steric hindrance.

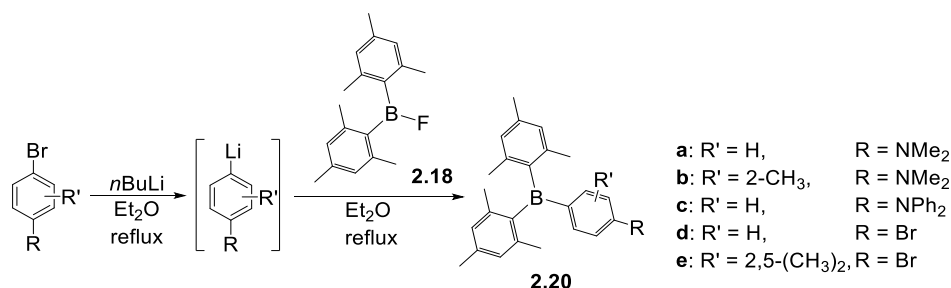


Scheme 2.9: **A)** Reaction sequences for the synthesis of compounds **2.17** and **2.18**.^[14] **B)** Structure of compound **2.19**.^[106]

Subsequently, the syntheses of compounds **2.17** and **2.18** were further improved by Hawkins *et al.*^[106] who changed the solvent for the formation of the Grignard reagent from diethyl ether to THF according to a general procedure reported by Ramsden *et al.*^[107] This change resulted in a shorter reaction time for the formation of the Grignard reagent as well as an increased yield. In addition, this led to the isolation of fluorodimesitylborane **2.18** in 96% yield. Due to its steric hinderance, the reaction of excess mesityl Grignard reagent with BF_3 etherate at 55 °C stops at the fluorodimesitylborane stage as long as the reaction time is shorter than 2 h. Furthermore, Hawkins and coworkers were able to nitrate **2.17** to yield compound **2.19**.

In 1967, at Eastman Kodak, Grisdale and coworkers began to investigate the photophysical reactions of tetraarylborates and triarylboranes in solution.^[108] They again found trimesitylborane **2.17** to be more stable than triphenylborane **2.2**. To investigate further the influence of different substituents on the stability of triarylboranes, Grisdale *et al.* had a closer look at the influence of the *para*-substituent in various dimesitylphenylboranes.^[109] To synthesize a variety of these new triarylboranes **2.20**, this group was the first to combine the methods previously developed by different groups. First, Grisdale and coworkers isolated fluorodimesitylborane **2.18** as reported by Brown.^[14] This fluoroborane was then added to a lithiated species prepared from the corresponding

halogenated aromatics yielding **2.20a-e** in 40 - 90%, as Wittig *et al.* had found lithium reagents to be suitable to react with boronhalides.^[103] This reaction sequence reflects the different reactivities of Grignard and organolithium reagents. Grisdale *et al.* also conducted one of the first systematic investigations of the photophysical properties of the new triarylboranes in various solvents, observing emission solvatochromism, suggesting the stabilization of charge transfer excited states in polar solvents.

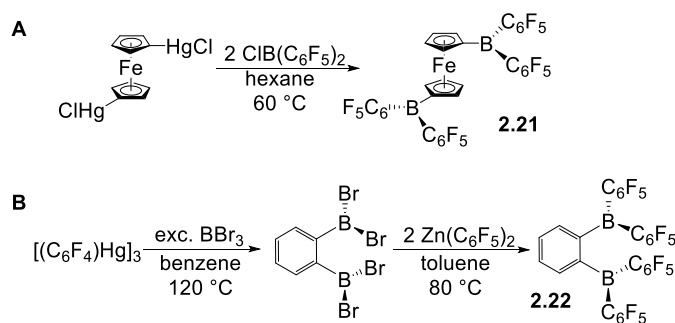


Scheme 2.10: Synthetic route to symmetrically-substituted triarylboranes **2.20a-e** reported by Grisdale *et al.*^[109]

2.2.3 Metal-Boron Exchange Reactions for the Synthesis of Triarylboranes

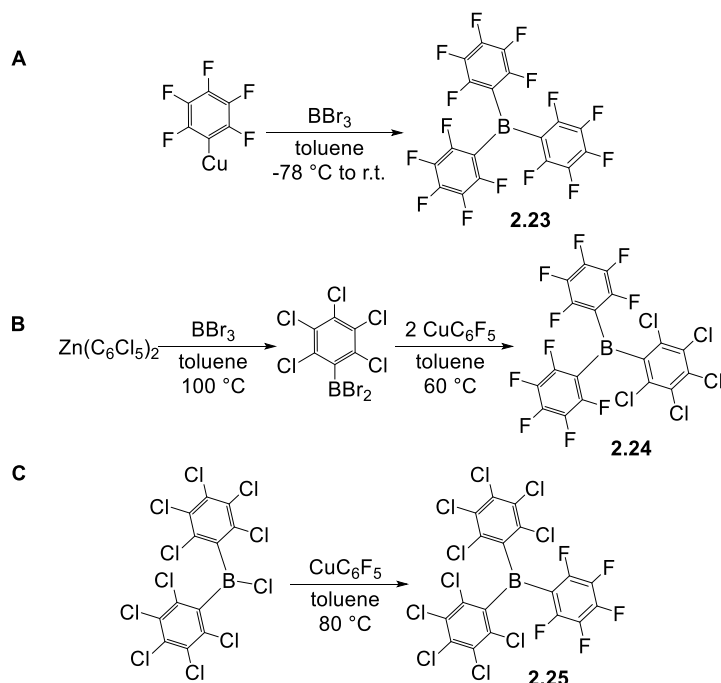
To date, the most widely used method for the synthesis of triarylboranes is the procedure developed by Grisdale and coworkers (Scheme 2.10)^[109] i.e., reaction of BF₃ with either Grignard reagents or lithium reagents as discovered by Krause *et al.*^[91] and Wittig *et al.*,^[103] respectively. However, mercury, zinc, copper, silicon, and tin reagents have also been employed in the synthesis of triarylboranes with different reactivities, solvent compatibilities, stabilities, and accessibilities of these organometallic reagents. Furthermore, while mercury and tin reagents are not widely used currently due to their toxicities, other safety aspects may dominate the choice of organometallic reagent, depending on the organic group to be transferred.

Arylmercury compounds were the first ArM reagents to be used for the synthesis of arylboranes (*vide supra*), but apart from a few reports on arylboronic acid syntheses,^[110-111] they have generally been replaced by Grignard or organolithium reagents. However, in 2001, Piers and coworkers obtained the diborylated ferrocene compound **2.21** by reacting 1,1'-Fc(HgCl)₂ with ClB(C₆F₅)₂ (Scheme 2.11A).^[112] The same group made use of Hg-B exchange to generate the diborylated compound **2.22**, which was then converted into a triarylborane *via* Zn-B exchange (Scheme 2.11B).^[113] A year before, they reported Zn(C₆F₅)₂ as a potential C₆F₅ transfer agent, which reacted with BCl₃ to generate inseparable mixtures of mono-, di- and triarylboranes.^[114]



Scheme 2.11: **A**) Hg-B exchange reaction by Piers and coworkers.^[112] **B**) Sequential Hg-B and Zn-B exchange reaction by Piers, Collins, Marder and coworkers.^[113]

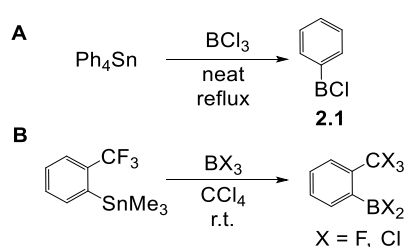
In 2003, Jäkle *et al.* demonstrated the applicability of arylcopper reagents in Cu-B exchange reactions.^[115] Using mesitylcopper, a maximum of two arenes were attached even when the reaction with BX_3 ($X = Cl, Br$) was heated to 100 °C, or when dichlorophenylborane **2.1** was used as the starting material to decrease the steric demand around the boron. Reaction of C_6F_5Cu with BX_3 at room temperature gave $B(C_6F_5)_3$ **2.23** irrespective of stoichiometry (Scheme 2.12A). Pentafluorophenylcopper was also employed by Ashley, O'Hare and coworkers as an aryl transfer reagent for the synthesis of triarylboranes **2.24** and **2.25** (Scheme 2.12B, C) and, in one case, they made use of a Zn-B exchange to form the dibromoarylboration precursor (Scheme 2.12B).^[116]



Scheme 2.12: Triarylborane formation using CuC_6F_5 as an aryl transfer reagent by Jäkle and coworkers and O'Hare and coworkers, respectively.^[115-116]

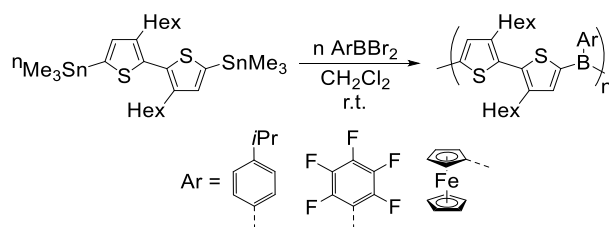
Later, Jäkle and coworkers demonstrated that 2,4,6-tri-*iso*-propylphenylcopper (CuTip) could also be employed in Cu-B exchange reactions. Thus, CuTip was reacted with sterically unhindered bromodiarylboranes to add the third arene to the boron center,^[117-118] and these triarylborane precursors were used in the formation of organoborane macrocycles and borazine oligomers.

Apart from Grignard and lithium reagents, the most widely used substrates for exchange reactions with boron are organosilanes and organotin reagents. Aryltin reagents were used in Sn-B exchange reactions in the 1960s. In a first approach by Burch *et al.*, the phenyl groups of SnPh₄ were transferred to BCl₃ to give compound **2.1**.^[119] Reaction of SnPh₄ with BCl₃ in CH₂Cl₂ transferred one of the four phenyl rings from tin to boron. Without the use of solvent, and under reflux conditions, all four rings were transferred (Scheme 2.13A). In 1970, a more selective method was reported by Chivers, who synthesized *ortho*-substituted *mono*-arylboranes from the corresponding *mono*-aryltrimethylsilanes according to Scheme 2.13B.^[120] Halogen exchange between BCl₃ and the *ortho*-trifluoromethylgroup was observed.



Scheme 2.13: Formation of *mono*-arylboranes *via* Sn-B exchange by Burch *et al.* and Chivers, respectively.^[119-120]

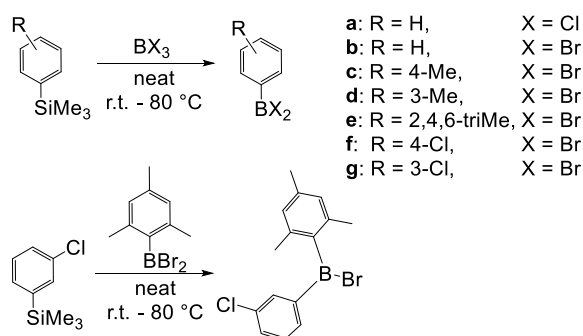
In 2005, Jäkle and coworkers reported the synthesis of triarylborane-containing polymers *via* Sn-B exchange,^[121] reacting a distannylated bithiophene precursor with different dibromoarylboranes to obtain the respective polymers (Scheme 2.14).



Scheme 2.14: Formation of triarylborane-containing polymers *via* Sn-B exchange.^[121]

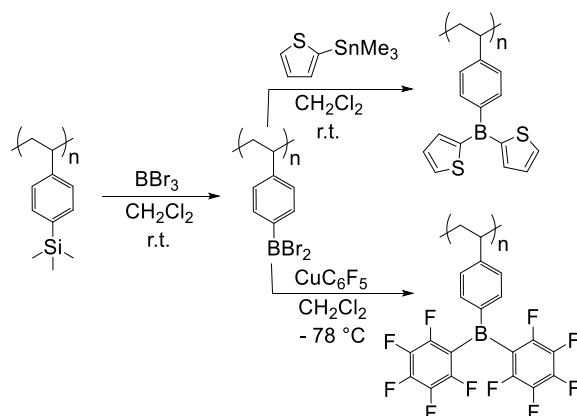
Based on this procedure, many different triarylborane-containing polymers and triarylborane model compounds were synthesized.^[122-123]

In 1986, Haubold and coworkers reported the synthesis of several mono- and diarylboranes *via* Si-B exchange.^[124] The exchange reaction was tolerant to some functional groups, and even an unsymmetrically-substituted ArAr'BBr compound was generated (Scheme 2.15). Starting from BBr₃, 35% of triphenylborane **2.2** was formed under harsh reaction conditions, whereas starting from BCl₃ gave the *mono*-arylboranes exclusively.



Scheme 2.15: Si-B exchange reactions reported by Haubold and coworkers.^[124]

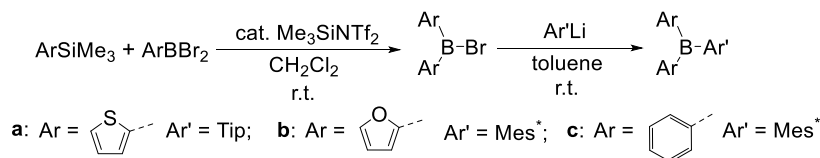
Further studies as well as potential applications were reported one year later by Kaufmann *et al.*^[125-126] and Snieckus *et al.*^[127] Jäkle and coworkers reported an efficient method for the introduction of a triarylborane moiety into the side chain of polystyrene.^[128-129] The first step involved Si-B exchange and, in the next step, the triarylborane was formed *via* Sn-B and Cu-B exchanges, respectively (Scheme 2.16).



Scheme 2.16: Si-B exchange reaction followed by Sn-B or Cu-B exchange for triarylborane formation by Jäkle and coworkers.^[128-129]

More recently, Helten and coworkers improved the Si-B exchange reaction significantly by employing a catalytic amount of Me₃SiNTf,^[130] synthesizing three triarylboranes *via* Si-B exchange and subsequent Li-B exchange reactions (Scheme 2.17). Helten and coworkers employed this method for the synthesis of triarylborane-containing

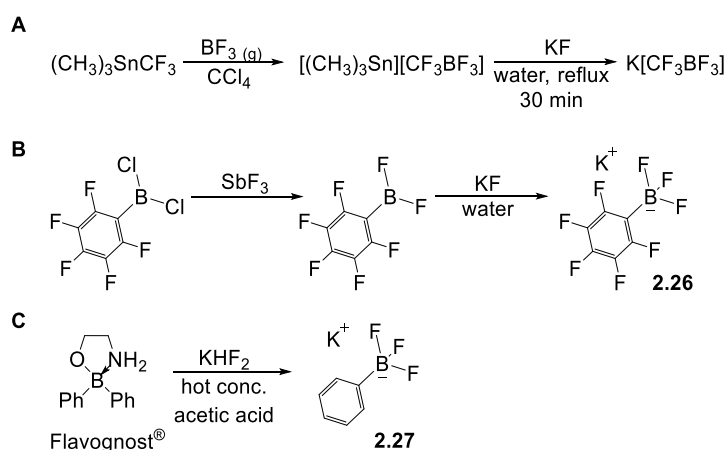
macromolecules and polymers. In each case, the third arene was attached to the boron using an aryl lithium reagent.^[131-132]



Scheme 2.17: Catalyzed Si-B exchange followed by Li-B exchange for triarylborane formation.^[130]

2.2.4 Potassium Aryltrifluoroborates as Boron Sources

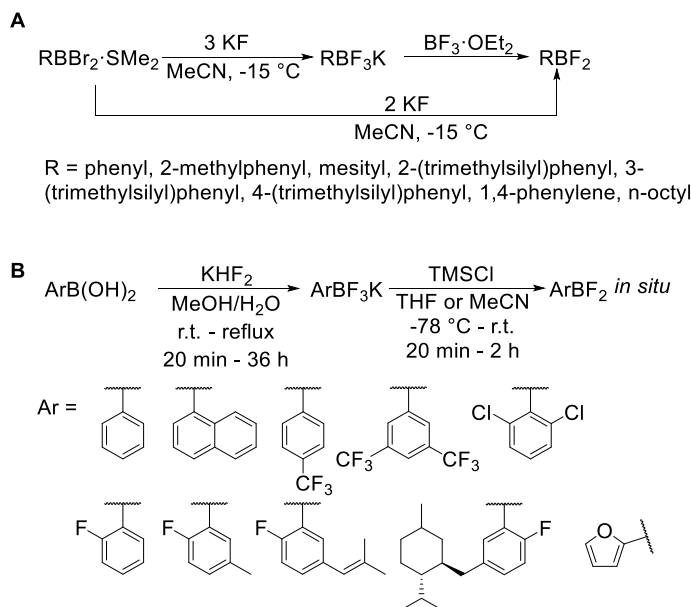
Potassium aryltrifluoroborates (ArBF₃K salts) have been known since 1960.^[133] Chambers *et al.* reported the synthesis of potassium (trifluoromethyl-)trifluoroborate from a boiling, aqueous solution of trimethyltin (trifluoromethyl-)trifluoroborate and potassium fluoride (Scheme 2.18A). In 1963, Stafford reported the synthesis of a potassium vinyltrifluoroborate that was isolated in a similar way to that previously described by Chambers.^[134] Two years later, Chambers reported the synthesis of an aromatic potassium trifluoroborate **2.26** which was obtained from reaction of (pentafluorophenyl)difluoroborane and potassium fluoride (Scheme 2.18B).^[135] In 1967, Thierig and Umland reported the synthesis of potassium phenyltrifluoroborate **2.27** from Flavognost[®] and potassium bifluoride (Scheme 2.18C).^[136]



Scheme 2.18: Synthetic pathways to potassium trifluoroborates by Chambers, Stafford, and Thierig, respectively.^[133-136]

About 20 years later, Kaufmann and coworkers made use of the solubility of potassium fluoride in acetonitrile to convert RBBr₂ compounds into their RBF₂ analogues or the

corresponding potassium trifluoroborates (Scheme 2.19A).^[137] They also found $\text{BF}_3 \cdot \text{OEt}_2$ to be a suitable reagent to convert the latter salts *in situ* into RBF_2 compounds.

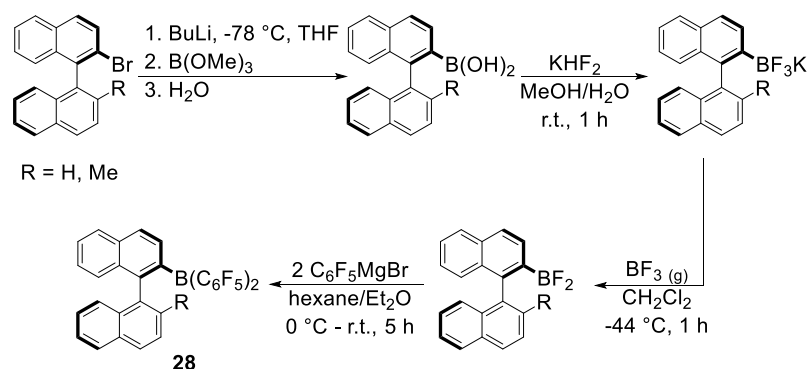


Scheme 2.19: **A**) Conversion of aryldibromoboranes to potassium aryltrifluoroborates or aryl difluoroboranes.^[137] **B**) A convenient route to potassium aryltrifluoroborates and their activation reactions.^[138]

Another way to activate potassium aryltrifluoroborates was reported by Vedejs in 1995,^[138] who showed that potassium aryltrifluoroborates can be activated *in situ* to form aryl difluoroboranes by addition of trimethylsilyl chloride (TMSCl). Furthermore, they provided a convenient route to potassium aryltrifluoroborates from the corresponding boronic acids and potassium bifluoride, KHF_2 (Scheme 2.19B).

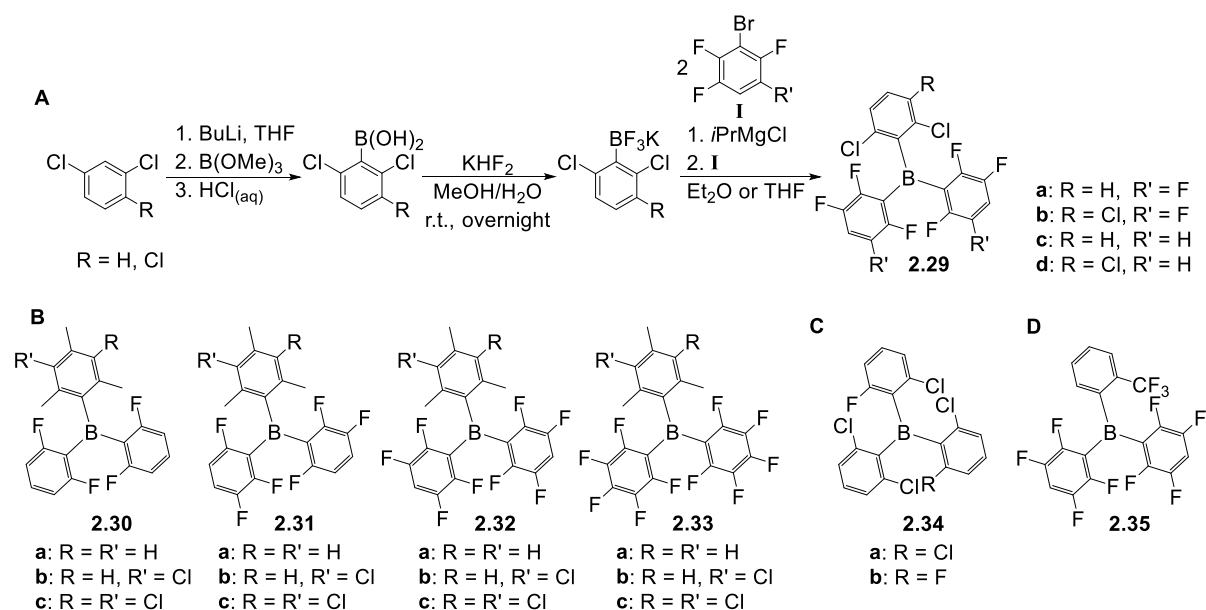
To date, BF_3K salts are mostly employed in reactions in which the boron motif is lost, e.g. in coupling reactions.^[139] However, such compounds can also be used as the boron source for the syntheses of triarylboranes.

In 2004, Morrison *et al.* were the first to synthesize triarylboranes **2.28** from potassium aryltrifluoroborate reagents which were activated with BF_3 etherate and then reacted with the Grignard reagent $\text{C}_6\text{F}_5\text{MgBr}$ (Scheme 2.20).^[61]



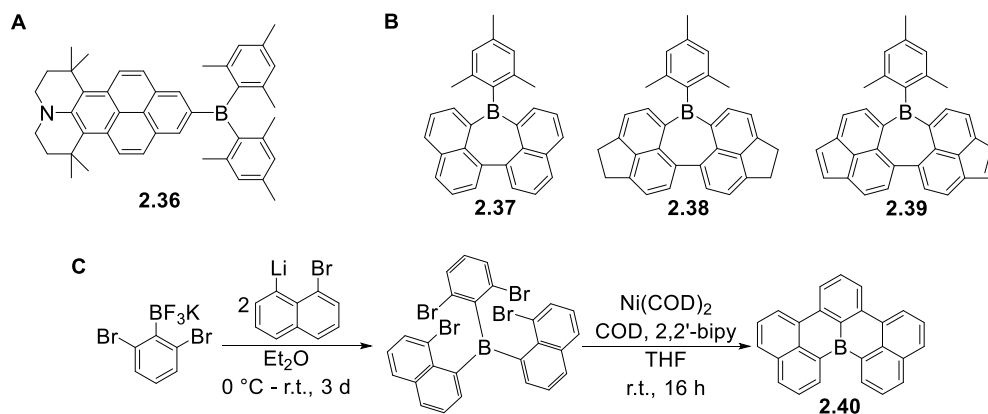
Scheme 2.20: First reported synthesis of triarylboranes from potassium aryltrifluoroborates.^[61]

Since then, a few other groups reported the synthesis of triarylboranes from these bench-stable boron precursors. Especially for applications in frustrated Lewis pairs, this approach was used for the synthesis of triarylboranes bearing aromatic systems in which multiple fluoro- and chloro-substituents are desired. Soós and coworkers^[62, 140-141] and Hoshimoto *et al.*^[142] synthesized triarylboranes **2.29-2.35** from potassium aryltrifluoroborates and Grignard reagents without prior activation of the BF_3K salt. The Grignard reagents in these cases were each prepared from the corresponding brominated precursor in combination with the so called 'Turbo-Grignard' *iso*-propyl magnesium chloride lithium chloride ($i\text{PrMgCl}\cdot\text{LiCl}$) as summarized in Scheme 2.21A. A very similar strategy, without the use of the Turbo-Grignard, was used by Marder and coworkers to synthesize a push-pull system with a pyrene core **2.36** (Scheme 2.22A).^[64]



Scheme 2.21: **A)** General reaction sequence for the synthesis of multi-halogenated triarylboranes.^[62] **B),**^[140] **C),**^[141] **D)**^[142] Structures of compounds **2.29-2.35** synthesized according to Scheme 2.21A.

In contrast, Wagner and coworkers synthesized triarylboranes as precursors to polycyclic aromatic hydrocarbons^[63] or quadruply annulated borepins.^[143] In both cases, the required triarylboranes were synthesized from potassium aryltrifluoroborates which were reacted with various aryl lithium reagents yielding compounds **2.37-2.40** (Scheme 2.22B, C).

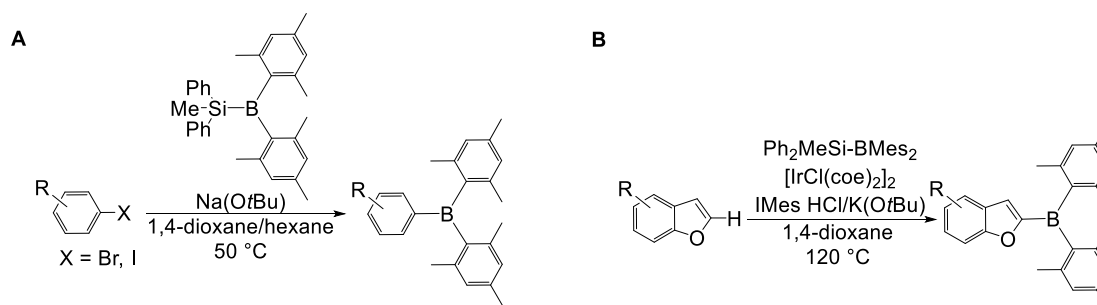


Scheme 2.22: **A)** Structure of compound **2.36**.^[64] **B)** Structures of compounds **2.37-2.39**.^[143] **C)** Synthetic route to planarized triarylboranes.^[63]

2.2.5 Direct Dimesitylborylation

Ito and coworkers reported the direct dimesitylborylation of various aryl halides^[144] by reaction of (diphenylmethylsilyl)dimesitylborene with aryl halides in the presence of a base

(Scheme 2.23A). The halide was replaced by boron or silicon in a ratio of ca. 9 to 1. Furthermore, the reaction was tolerant to several functional groups, and the resulting triarylboranes were isolated in moderate to good yields. In 2019, the same group reported an iridium-catalyzed C–H dimesitylborylation of benzofuran using a silyldimesitylborane reagent (Scheme 2.23B),^[145] preparing several derivatives and isolating the triarylboranes in moderate to good yields. Under optimized conditions, they reported the formation of the silylated side product in ca. 29% yield.



Scheme 2.23: **A)** Dimesitylborylation of aryl halides.^[144] **B)** Dimesitylborylation of benzofuran derivatives.^[145]

2.3 Synthesis of Unsymmetrically-Substituted Triarylboranes

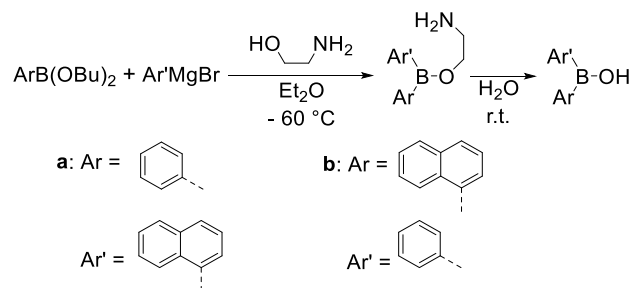
Thus far, the syntheses of symmetrically-substituted BAr_3 and BAr_2Ar' triarylboranes was summarized. The synthesis of unsymmetrically-substituted $BArAr'Ar''$ triarylboranes bearing three different aromatic rings bound to the boron center can be achieved by different routes, most of which use the same approaches used for the syntheses of symmetrically-substituted triarylboranes. However, other routes employed symmetrically-substituted triarylboranes as precursors.

One of the first unsymmetrically-substituted triarylboranes was reported in 1971 by Grisdale *et al.* at Eastman Kodak.^[146] As mentioned above, this group investigated the photolysis of triarylboranes and tetraarylborates. During these studies, they observed an organoboron compound, formed after irradiation of potassium dimesityldiphenylborate, which contained three different aromatic systems bound to the boron center.

2.3.1 Boronic Esters as Boron Sources

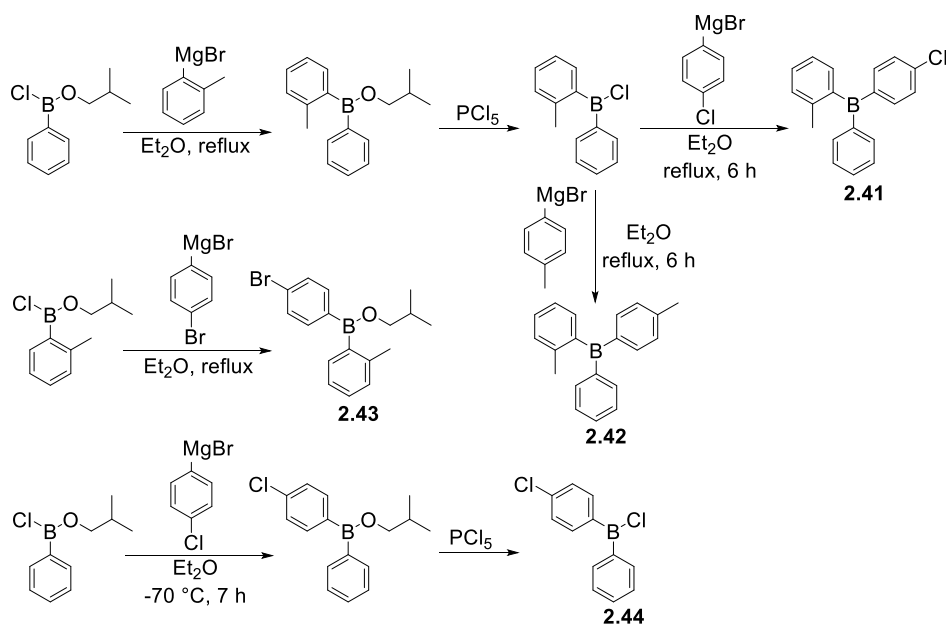
In 1955, Letsinger and coworkers reported the synthesis of the first unsymmetrically-substituted borinic acid starting from a boronic ester.^[147] They reacted phenylboronic acid butyl ester with α -naphthylmagnesium bromide and isolated the borinic acid as its β -aminoethyl ester,

which was readily hydrolyzed to the borinic acid (Scheme 2.24). They also demonstrated that the synthesis works when the aryl starting materials are switched to α -naphthylboronic acid butyl ester and phenylmagnesium bromide, respectively, but the product was not used for the synthesis of a BArAr'Ar'' triarylborane.



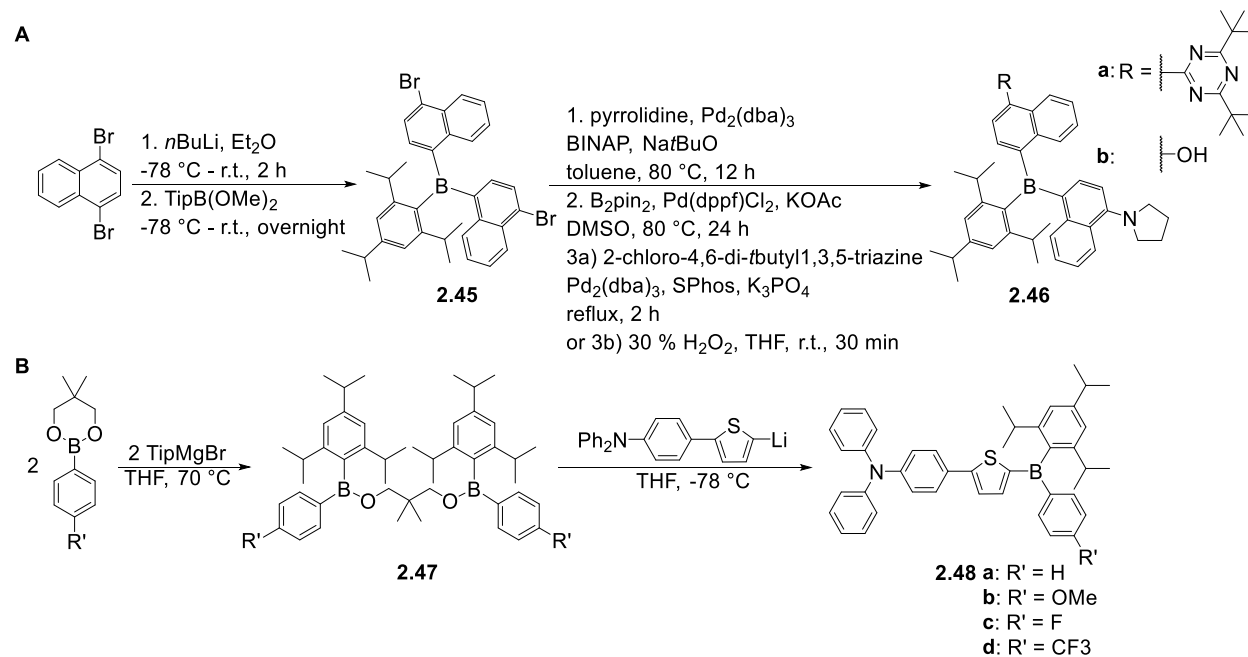
Scheme 2.24: Synthesis of an unsymmetrical borinic acid by Letsinger and coworkers.^[147]

In 1958, Mikhailov *et al.* reported the sequential synthesis of unsymmetrically-substituted triarylboranes^[148] (Scheme 2.25) starting from an *iso*-butyl borinic ester wherein the boron atom is additionally bound to one phenyl and one chlorine atom, respectively. In the first step, the chlorine atom was substituted by an *o*-tolyl group introduced from a Grignard reagent. In the second step, the *iso*-butyl substituent was converted to a chloride *via* reaction with PCl_5 . The chlorine atom was subsequently substituted by other arenes introduced from Grignard reagents yielding two different unsymmetrically-substituted triarylboranes (**2.41** and **2.42**). Mikhailov and coworkers reported the synthesis of two other borinic acids (**2.43** and **2.44**) but their conversion to unsymmetrically-substituted triarylboranes was not described.



Scheme 2.25: Syntheses of unsymmetrically-substituted triarylboranes **2.41** and **2.42**.^[148]

Recently, Liu *et al.*^[32, 39] synthesized the unsymmetrically-substituted triarylboranes **2.46a, b** from $\text{BAr}_2\text{Ar}'$ **2.45**. Compound **2.45** was synthesized from the boronic ester $\text{TipB}(\text{OMe})_2$ (Tip = Tri-*iso*-propyl), which was obtained from reaction of trimethoxyborane ($\text{B}(\text{OMe})_3$) with 2,4,6-tri-*iso*-propylphenyl magnesium bromide (TipMgBr).^[149] This boronic ester was then converted to the symmetrically-substituted triarylborane **2.45** by reaction with a lithiated species (Scheme 2.26A). Stepwise substitution of the bromides then yielded the unsymmetrically-substituted triarylboranes **2.46a, b** (Scheme 2.26A).

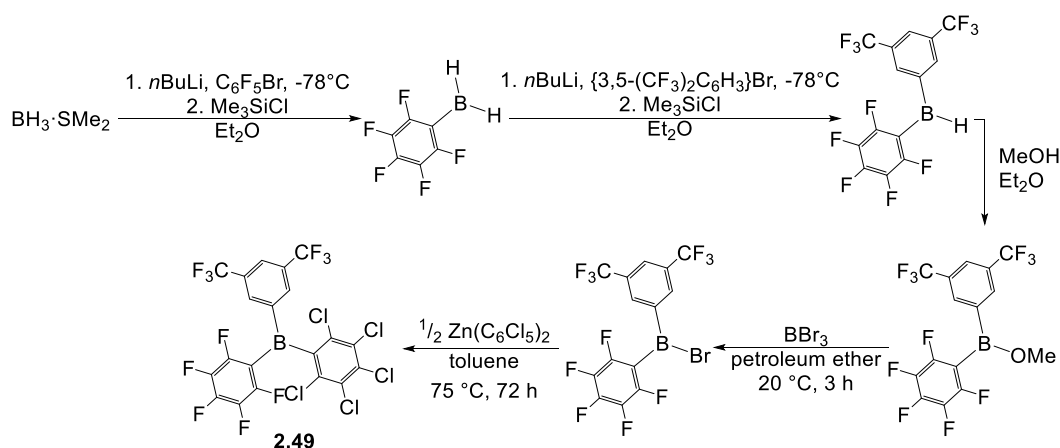


Scheme 2.26: **A**) Synthesis of unsymmetrically-substituted triarylborane **2.46** from a symmetrically-substituted precursor.^[32, 39] **B**) Synthesis of unsymmetrically-substituted triarylboranes **2.48a-d** from a boronic ester.^[66]

Yamaguchi and coworkers reported the synthesis of a series of unsymmetrically-substituted triarylboranes **2.48a-d** from a boronic ester precursor (Scheme 2.26B).^[66] This was then converted with TipMgBr to a dimeric intermediate **2.47**, which was cleaved by the addition of a lithiated species yielding compounds **2.48a-d** (Scheme 2.26B). In the same paper, Yamaguchi and coworkers reported the synthesis of a derivative of compound **2.48** bearing *tert*-butyl groups instead of the *iso*-propyl groups but it was not possible to synthesize **2.48e** according to Scheme 2.26B. Therefore, they used a different approach starting from boron tribromide (*vide infra*, Scheme 2.30B).

2.3.2 Borane Dimethyl Sulfide as the Boron Source

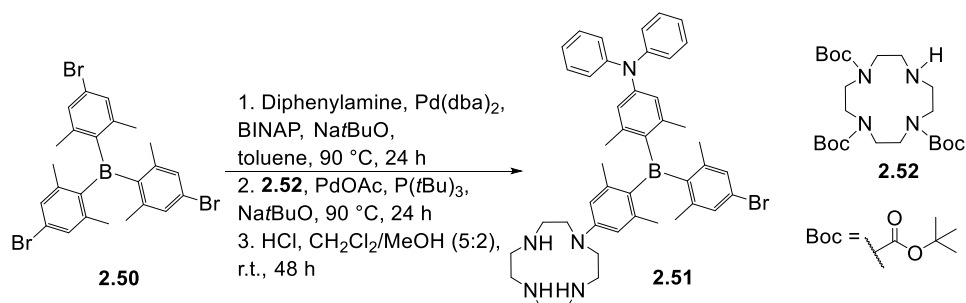
In 2016, Blagg *et al.* reported the synthesis of the ‘first 1:1:1 hetero-tri(aryl)borane’, by their own account.^[150] In terms of investigating the Lewis acidity of such ‘hetero-tri(aryl)boranes’, they substituted the hydrogen atoms of a borane dimethyl sulfide complex stepwise with arenes (Scheme 2.27). The first aromatic groups were introduced using aryl lithium reagents. The resulting intermediate was converted to a borinic ester with methanol and was then activated with BBr_3 for reaction with an organozinc reagent yielding the unsymmetrically-substituted triarylborane **2.49**.



Scheme 2.27: Synthesis of unsymmetrically-substituted triarylborane **2.49** from borane dimethyl sulfide.^[150]

2.3.3 Boron Trifluoride as the Boron Source

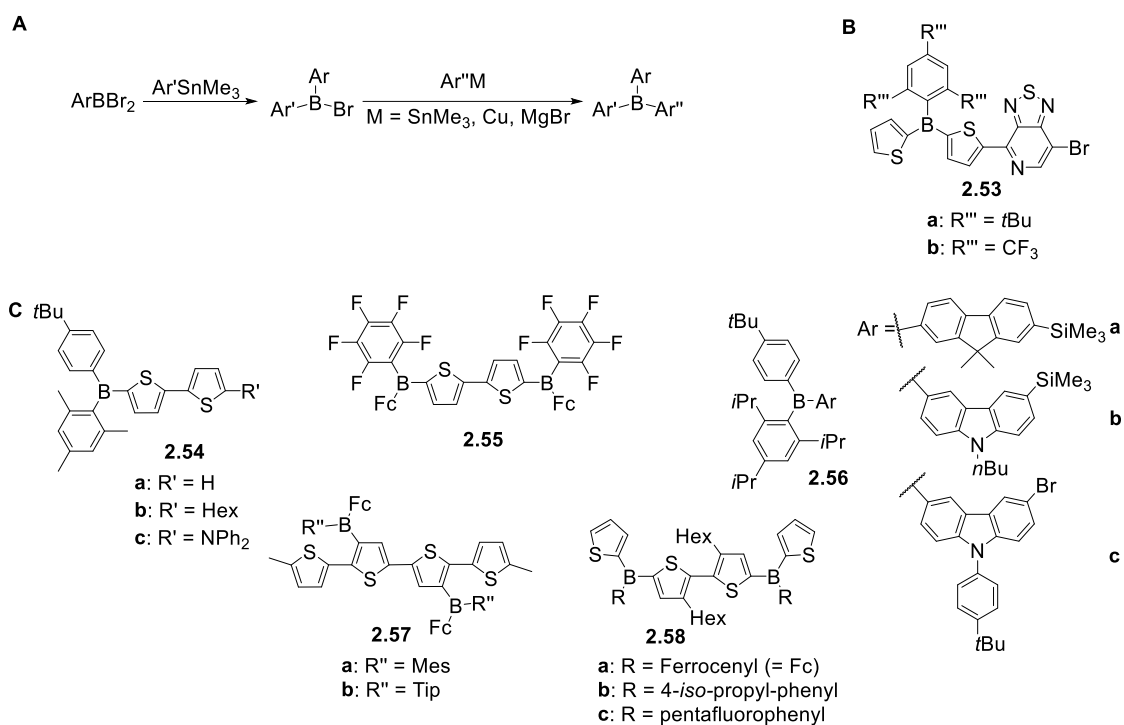
Liu *et al.* used the symmetrically-substituted compound **2.50**, which was prepared from $\text{BF}_3\cdot\text{OEt}_2$ and the respective aryl lithium reagent, to prepare unsymmetrically-substituted triarylborane **2.51** via sequential cross-coupling reactions.^[40]



Scheme 2.28: Synthesis of unsymmetrically-substituted triarylborane **2.51** by stepwise modification of a symmetrically-substituted precursor.^[40]

2.3.4 Boron Tribromide as the Boron Source

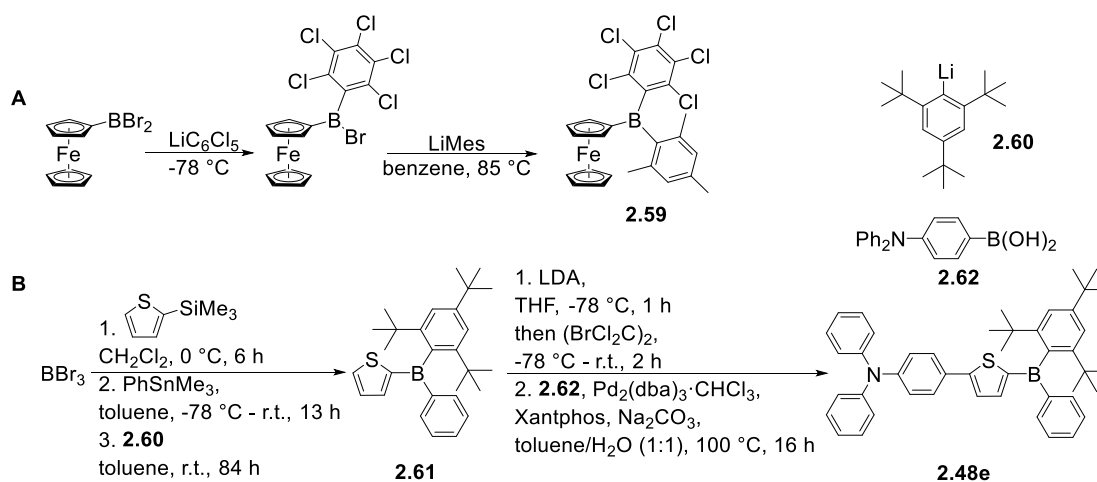
In 2005, Jäkle and coworkers reported the synthesis of different unsymmetrically-substituted triarylboranes as reference compounds for their polymers.^[121] Both monomeric and polymeric boron-containing systems were synthesized from aryldibromoboranes and organotin reagents (*vide supra*, Scheme 2.14; *vide infra*, Scheme 2.29). They subsequently used this strategy for similar applications with slight modifications of the synthetic procedure, the third aryl group being added *via* a tin,^[121] a copper^[151-153] or a Grignard reagent^[154] (Scheme 2.29).



Scheme 2.29: **A)** Synthetic route to unsymmetrically-substituted triarylboranes developed by Jäkle and coworkers.^[121] **B)** Structure of compound **2.53**.^[155] **C)** Compounds **2.54-2.58** synthesized according to Scheme 2.29A.^[121, 151-155]

The same group then reported the synthesis of an unsymmetrically-substituted triarylborane **2.53** (Scheme 2.29B) *via* stoichiometric Stille coupling of a symmetric precursor^[155] which had been obtained from boron tribromide and an excess of a tin reagent.^[15]

In 2014, Kelly *et al.* reported the synthesis of a ferrocene-containing triarylborane bearing three different aromatic systems by stepwise reaction of dibromoferrocenylborane with two different aryl lithium reagents (Scheme 2.30A).^[156]



Scheme 2.30: **A**) Synthesis of unsymmetrically-substituted triarylborane **2.59** by Kelly *et al.*^[156] **B**) Synthesis of sterically more demanding, unsymmetrically-substituted triarylborane **2.48e** by Yamaguchi and coworkers.^[66]

As shown in Scheme 2.26B, Yamaguchi and coworkers reported a route to unsymmetrically-substituted triarylboranes from boronic esters^[66] but for **2.48e**, the route was not successful as the incorporated arene was sterically too demanding. Therefore, they used a route established by Jäkle and coworkers: after a boron-silicon exchange at the thiophene, the ArBBr_2 system was reacted with a tin reagent followed by 2,4,6-tri-*tert*-butylphenyllithium to give **2.48e** (Scheme 2.30B).

2.4 Summary and Outlook

Over the years, the synthetic approaches to triarylboranes presented herein have led to the generation of countless compounds containing triarylborane motifs. Initially, examination of their properties was limited to their reactivity with other metals or as Lewis acids. Some of the early reaction sequences, such as those developed by Krause *et al.* and Grisdale *et al.*, are still used. Today, the applications of these compounds are no longer limited to their reactivity. The photophysical and electronic properties of triarylboranes and compounds containing this structural motif remain under increasingly active investigation as such properties lead to numerous applications, *e.g.* in OLEDs,^[27] optoelectronics,^[25-26, 28] sensors for anions^[29, 31, 34] or small molecules,^[32-33] catalysts for *e.g.* hydrogenation or amination of carbonyls^[62, 140-141] or bioimaging agents.^[8, 43-44, 46, 48] With the further exploration of more general routes to unsymmetrically-substituted triarylboranes, the applicability of these compounds can be expected to continue to increase as this structural motif provides the possibility for fine tuning of the photophysical and electronic properties of the resulting small molecules and, therefore, also of potential macromolecules and polymers.

CHAPTER 3

THE BASIS OF THIS WORK – AN UNSYMMETRICALLY-SUBSTITUTED, AMINE-CONTAINING TRIARYLBORANE

3 The Basis of This Work – An Unsymmetrically-Substituted, Amine-Containing Triarylborane

The synthesis and the crystal structures of **3.2a** and **3.2b** are published in *Chem. Eur. J.* **2021**, *27*, 9094-9101.^[157] The results are reproduced in a slightly modified form with the permission of Wiley VCH. The syntheses of **3.1a** and **3.1b** were reported previously,^[54] but the synthesis and the resulting yields were improved significantly in the course of this work.

3.1 Introduction

The development of a synthetic route to the unsymmetrically-substituted triarylboranes **3.2a**, bearing one mesitylene, one *ortho*-xylene, and one *N,N*,2,6-tetramethylaniline, is described together with its crystal structure, rotational barriers around the B–C bonds, photophysical and electrochemical properties, singlet oxygen sensitizing efficiency, and follow-up reactions. To examine the influence of different numbers of dimethylamino- or trimethylammonium groups on these properties, the triarylboranes **3.3a**^[43], **3.3c**,^[56] and **3.1a**^[54] (Figure 3.1A) were accordingly investigated herein. In previous studies, the isolation of only trace amounts of **3.2a** was reported from the reaction of 4-(*N,N*-dimethylamino)-2,6-dimethylphenyllithium and freshly isolated fluoroborane **3.6**, which was obtained from the reaction of potassium 2,6-dimethylphenyltrifluoroborate and mesityl magnesiumbromide (Figure 3.1B).^[55]

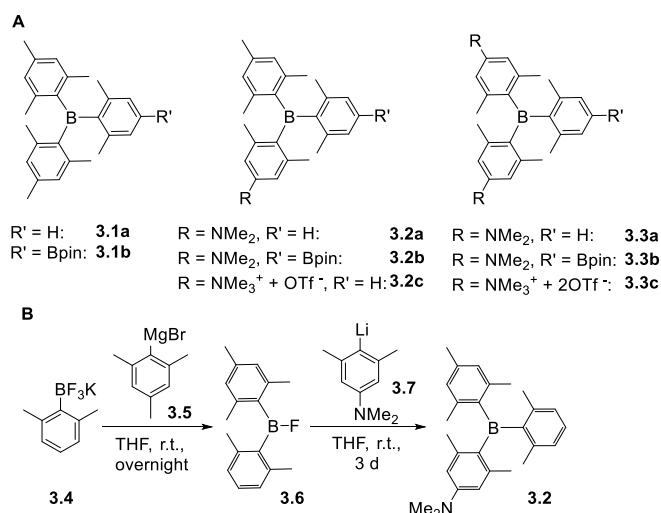


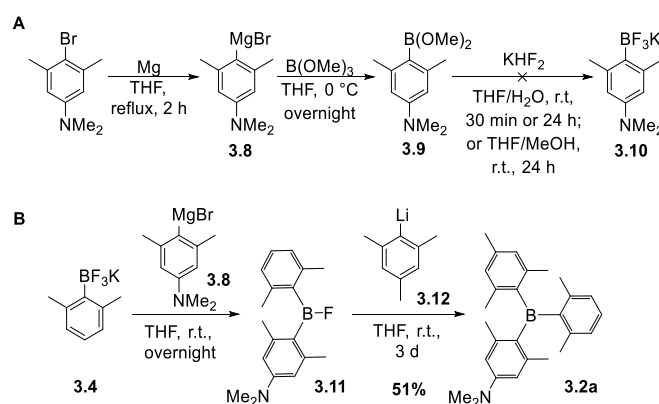
Figure 3.1: **A)** Structures of compounds **3.1-3.3**. **B)** Initial approach to **3.2**.^[55]

3.2 Results and Discussions

3.2.1 Synthesis

Influenced by the early syntheses of triarylboranes reported by Krause *et al.*^[91] and Brown *et al.*,^[14] the reaction temperature for the last step depicted in Figure 3.1B was increased to 70 °C giving **3.2a** in 5% isolated yield.

Ferger *et al.* showed that enhancement of the positive inductive (+I) effect of substituents in positions *para* to the boron atom of potassium aryltrifluoroborates increases the isolated yield of unsymmetrically-substituted triarylboranes.^[13, 157] Thus, as an alternative to **3.4**, synthesis of the more electron-rich potassium aryl trifluoroborate **3.10** was attempted *via* reaction of 4-*N,N*-dimethylamino-2,6-dimethylphenyl magnesium bromide **3.8** with trimethoxyborane and subsequent fluorination of the resulting boronic acid with potassium bifluoride (Scheme 3.1A). Complete formation of **3.8** was confirmed by GC-MS, while its conversion to **3.9** was confirmed by ¹¹B NMR spectroscopy. However, fluorination at room temperature with KHF₂ in a 2:1 mixture of THF and water for 30 min or 24 h gave *N,N*,3,5-tetramethylaniline and trace amounts of the desired compound **3.10**. Exchanging water for methanol gave only *N,N*,3,5-tetramethylaniline after stirring at room temperature for 24 h. Thus, it was not possible to isolate **3.10** due to proteoborylation of **3.9**.

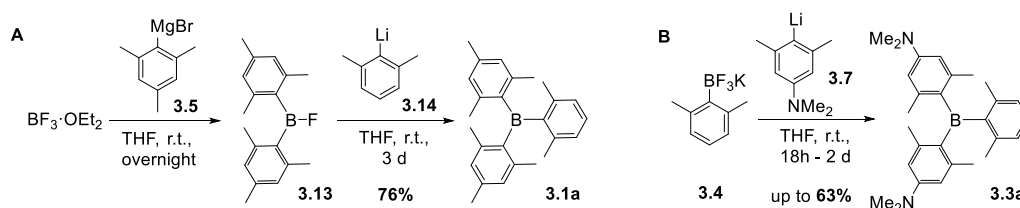


Scheme 3.1: **A)** Attempted synthesis of **3.10**. **B)** Optimized reaction sequence for **3.2a**.

Hence, a Grignard reagent was prepared of 4-bromo-*N,N*,3,5-tetramethylaniline and magnesium and was reacted with **3.4** to give fluoroborane **3.11** *in situ*, which was confirmed by ¹¹B NMR spectroscopy. Subsequent addition of mesityl lithium (**3.12**) gave **3.2a** in 10% yield. When changing the one-pot approach to a sequential reaction by separation of **3.11** from purely inorganic salts, the yield of **3.2a** increased to 51% (Scheme 3.1B). Similar yields of 47% and 30% were obtained for the sequential synthesis when the reaction time of the last step was decreased from 3 d to 18 h and when **3.4** was activated with trimethylsilyl chloride (TMSCl) prior to the first step, respectively. Usually, addition of

the latter is known to increase the reactivity of potassium aryltrifluoroborates,^[138] but, in this case, no increased reactivity was observed.

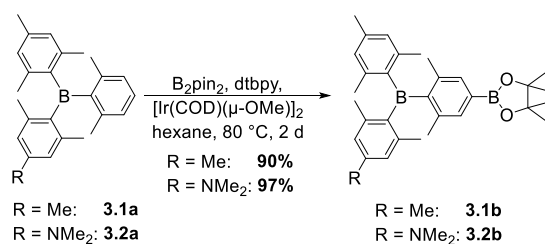
Using the basic approach developed by Gridale and co-workers,^[108] **3.1a** was synthesized from mesityl magnesium bromide **3.5**, boron trifluoride etherate ($\text{BF}_3 \cdot \text{OEt}_2$), and dimethylphenyl lithium **3.14**. Isolation of fluoroborane **3.13** and subsequent reaction with **3.14** gave the triarylborane **3.1a** in 76% yield over two steps (Scheme 3.2A). Previously, Schleier reported a yield of 25% who used Et_2O instead of THF for the second step.^[54]



Scheme 3.2: **A)** Synthetic route to **3.1a**. **B)** One pot synthesis of **3.3a**.

The synthesis of **3.3a** was reported in the literature with a yield of 33% over two steps.^[43] This yield was improved to up to 63% in a one-pot synthesis using potassium 2,6-dimethylphenyltrifluoroborate **3.4** and 4-(*N,N*-dimethylamino)-2,6-dimethylphenyl lithium **3.7** (Scheme 3.2B). The latter was isolated from reaction of *n*-butyl lithium and 4-bromo-3,5,*N,N*-tetramethylaniline in diethyl ether according to a literature procedure.^[50] For similar syntheses, it was observed that activation of the potassium salt with trimethylsilyl chloride prior to reaction with lithium reagents improves the yield.^[13, 157] This was not observed for the synthesis of **3.3a**, potentially due to the already increased reactivity of **3.7** compared to non-donor-substituted aryl lithium reagents.

To make **3.1a** and **3.3a** applicable in Suzuki-Miyaura cross-coupling reactions, a pinacolato-borane (Bpin) group was introduced *via* iridium catalyzed C–H borylation at the xylene moiety at the position *para* to the boron center.^[158-159] Hence, **3.3b** was synthesized according to the literature procedure.^[43-44, 46] Using similar reaction conditions (Scheme 3.3), **3.2a** was borylated giving **3.2b** in 97% yield and, for **3.1b**, the yield was increased from 66%^[54] to 90%.



Scheme 3.3: Borylation of triarylboranes **3.1a** and **3.2a**.

Methylation of **3.3a** with methyl triflate in dichloromethane gave **3.3c**.^[56] Similarly, from a reaction of **3.2a** and methyltriflate in dichloromethane, **3.2c** was obtained in 89% yield by precipitation upon addition of hexane. Despite washing **3.2c** multiple times with pure hexane, it was not possible to remove ca. 0.5% of **3.2a**, as shown in Figure 3.2, ¹H NMR spectra measured at 500 MHz in very high concentrations. Thus, the results of the photophysical and electrochemical measurements of **3.2c** and **3.3c** should be treated with caution.

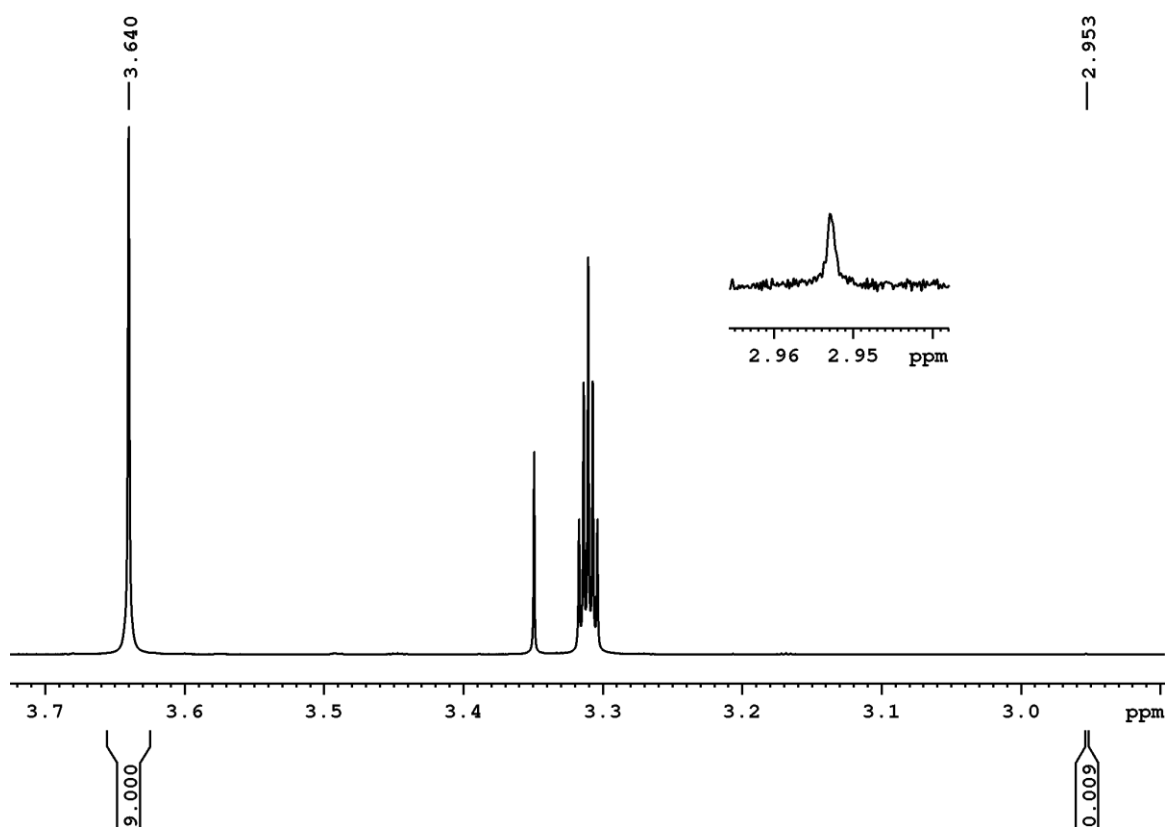


Figure 3.2: Enlarged extract of the 500 MHz ¹H NMR spectrum of **3.2c** in CD₃OD measured at room temperature.

3.2.2 Crystal Structures and Rotational Barriers

Crystals suitable for single crystal X-ray diffraction of **3.2a** were obtained from saturated CH_2Cl_2 solutions at $-20\text{ }^\circ\text{C}$ and of **3.2b** from slow evaporation of saturated 1:1 hexane/ethyl acetate solutions at room temperature. The bond lengths and torsion angles obtained are summarized in Table 3.1. The sum of the C–B–C angles in the BC_3 plane is 360° for both triarylboranes and both adopt a propeller-like structure.

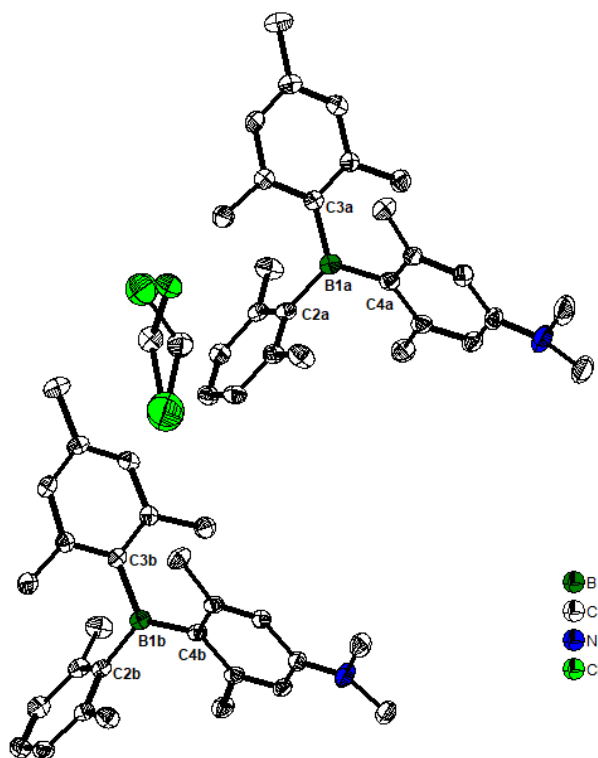


Figure 3.3: Molecular structure of **3.2a** in the solid state at 100 K. Atomic displacement ellipsoids are drawn at the 50% probability level and hydrogen atoms are omitted for clarity. There are two crystallographically independent molecules in the unit cell.

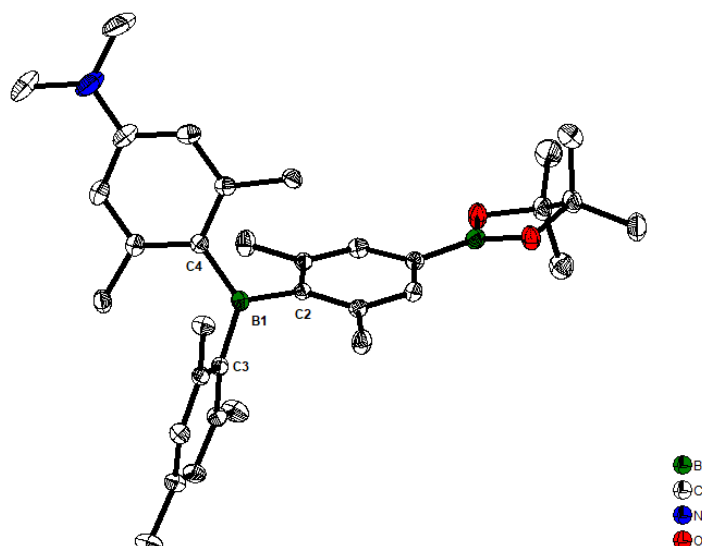


Figure 3.4: Molecular structure of **3.2b** in the solid state at 296 K. Atomic displacement ellipsoids are drawn at the 50% probability level and hydrogen atoms are omitted for clarity.

Table 3.1: Selected bond lengths and angles of **3.2a**, **3.2b**, **3.1a**,^[54] **3.3a**,^[43] and **3.3b**^[43] determined by single-crystal X-ray diffractions.

		3.2a	3.1a ^[54]	3.3a ^[43]	3.2b	3.3b ^[43]
Bond Length [Å]	B1a–C3a	1.574(3)	1.573(8)	-	1.577(2)	-
	B1b–C3b	1.594(3)				
	B1a–C2a	1.586(3)	1.586(8)	1.595(3)	1.589(2)	1.592(2)
	B1b–C2b	1.587(3)				
	B1a–C4a	1.570(3)	-	1.573(2)	1.568(2)	1.571(2)
	B1b–C4b	1.562(3)				1.567(2)
Torsion Angle [°]	^NMes – BC₃	48.00(5) 41.12(6)	-	53.0(1)	43.23(5)	42.4(1) 45.8(1)
	Mes – BC₃	50.80(6) 57.17(7)	51.8(8) 51.3(9)	-	52.94(6)	-
	xylyl – BC₃	52.67(5) 55.66(5)	47.2(8)	56.7(1)	55.65(6)	58.9(1)

For **3.2a**, the B–C bond lengths are 1.574(3) Å, 1.586(3) Å, and 1.570(3) Å for the mesityl, 2,6-dimethylphenyl, and 4-(*N,N*-dimethylamino)-2,6-dimethylphenyl groups, respectively. These values are very similar to those in **3.2b**, **3.1a**,^[54] **3.3a**,^[43] **3.3b**,^[43] the triduryl compound **3.15** (1.589(3) Å, 1.583(5) Å; Figure 3.5A)^[160] and BMe₃ (**2.17**; 1.580(4) Å, 1.573(4) Å; 1.579(2) Å; Figure 3.5B).^[161-162]

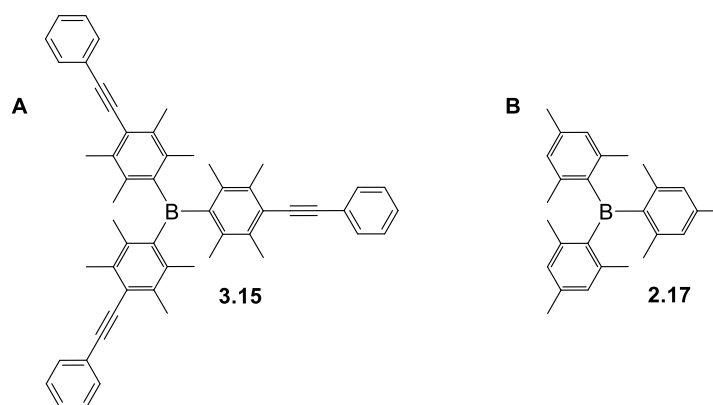


Figure 3.5: Previously reported compounds **3.15**^[160] and **2.17**.^[161-162]

Due to the steric constraints around the boron center, rotation around the B–C bonds is hindered. In the late 1960s and early 1970s, possible rotation mechanisms in BMe_3 were investigated in detail by Mislow and coworkers using ^1H NMR spectroscopy.^[161, 163-164] They concluded that a two-ring flip mechanism is most likely, wherein two aromatic systems rotate in the same direction around their B–C bonds, while the third ring rotates in the opposite direction. Furthermore, *via* temperature-dependent ^1H NMR spectroscopy they determined the rotational barrier to be ca. 11-16 kcal/mol and that it increases with increasing numbers of substituents *ortho* to the boron center.^[161] Similar results were obtained by Wang and co-workers^[165] and by Griesbeck *et al.*^[44] In the latter study, an increase of the rotational barrier of dimethylamino-substituted *bis*-triarylborane chromophores from 11.0 kcal/mol and 13.9 kcal/mol to 15.5 kcal/mol and 15.3 kcal/mol, respectively, upon methylation of the four dimethylamino groups was reported.

In the room temperature ^1H NMR spectra of **3.2a** and **3.2b**, one broad and two sharp signals were observed at ca. 2 ppm for the *ortho* methyl groups (Figure 3.6A, B). In contrast, for **3.2c**, six sharp signals were found in this region (Figure 3.6C).

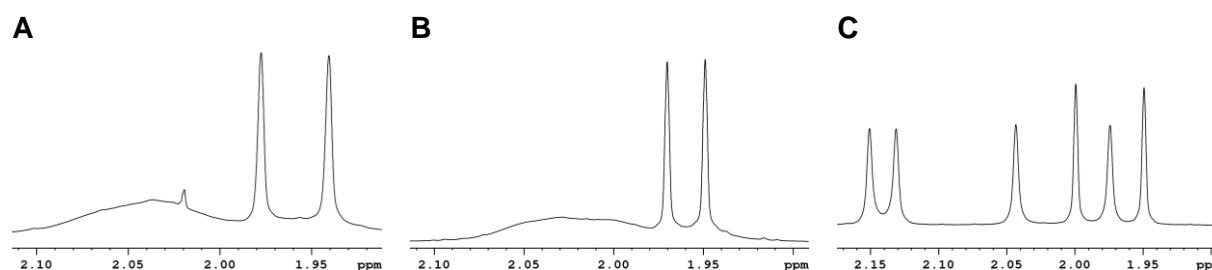


Figure 3.6: 500 MHz ^1H NMR spectra of **A) 3.2b**, **B) 3.2a**, and **C) 3.2c** at ca. 2 ppm recorded in CD_2Cl_2 at room temperature.

The rotational barriers ΔG^\ddagger of **3.2a** and **3.2c** were calculated for each aromatic system from temperature-dependent ^1H NMR spectroscopy using the Eyring equation (Equation 3.2) with k_c being the equilibrium constant at the coalescence temperature T_c , $\Delta\nu$ being the peak separation in Hz at the low temperature limit, the ideal gas constant R , Boltzmann's constant k_B , and Planck's constant h .

$$\text{Equation 3.1: } k_c = \frac{\pi}{\sqrt{2}} |\Delta\nu| = 2.22 |\Delta\nu|$$

$$\text{Equation 3.2: } \Delta G^\ddagger = RT_c \ln\left(\frac{k_B T_c}{h k_c}\right)$$

The resulting values are summarized in Table 3.2. ^1H NMR spectra below room temperature (25 °C) were recorded in CD_2Cl_2 and at higher temperatures in $\text{C}_2\text{D}_2\text{Cl}_4$.

Table 3.2: Rotational barriers ΔG^\ddagger of **3.2a** and **3.2c** determined for each aromatic system in the aromatic (7.5 ppm-6.3 ppm) and aliphatic (2.2 ppm-1.9 ppm) regions from temperature dependent ^1H NMR spectra and the Eyring equation.

Aromatic system	3.2a		3.2c	
	Aromatic	Aliphatic	Aromatic	Aliphatic
4-(<i>N,N</i> -Dimethylamino-)/				
4-Trimethylammonium- 2,6-dimethylphenyl	[a]	13.9 kcal/mol	16.5 kcal/mol	16.0 kcal/mol
2,6-Dimethylphenyl	14.3 kcal/mol	15.2 kcal/mol	16.7 kcal/mol	16.4 kcal/mol
Mesityl	14.2 kcal/mol	15.0 kcal/mol	17.7 kcal/mol	17.1 kcal/mol

[a] Cannot be determined as corresponding ^1H NMR signal does not split until -90 °C.

The minor differences obtained between the values obtained from the aliphatic and aromatic regions are within the error of the measurement. In **3.2a**, the rotational barrier of the 4-*N,N*-dimethylamino-2,6-dimethylphenyl group is slightly lower than those of the 2,6-dimethylphenyl and mesityl groups, with values of ca. 14-15 kcal/mol. In contrast, in **3.2c**, the mesityl rotational barrier is slightly higher than those of the other two aromatic systems. However, for **3.2c**, all three values are increased by ca. 2 kcal/mol compared to **3.2a**, which is in accordance with the trend observed by Griesbeck *et al.*^[44]

3.2.3 Photophysical Properties

3.2.3.1 Neutral Triarylboranes

The photophysical properties of **3.1a**, **3.2a**, **3.3a**, **3.2c**, and **3.3c** were investigated in solvents of different polarity to examine the influence of increasing numbers of dimethylamino- and trimethylammonium groups, respectively. The absorption and emission spectra and the corresponding data for the neutral compounds **3.1a**, **3.2a**, and **3.3a** are summarized in Figure 3.7 and Table 3.3. Hexane (dielectric constant: $\epsilon_r = 1.9 \text{ F m}^{-1}$), toluene ($\epsilon_r = 2.4 \text{ F m}^{-1}$), Et₂O ($\epsilon_r = 4.3 \text{ F m}^{-1}$), CH₂Cl₂ ($\epsilon_r = 9.1 \text{ F m}^{-1}$), and acetonitrile ($\epsilon_r = 38 \text{ F m}^{-1}$) were chosen as solvents.^[166]

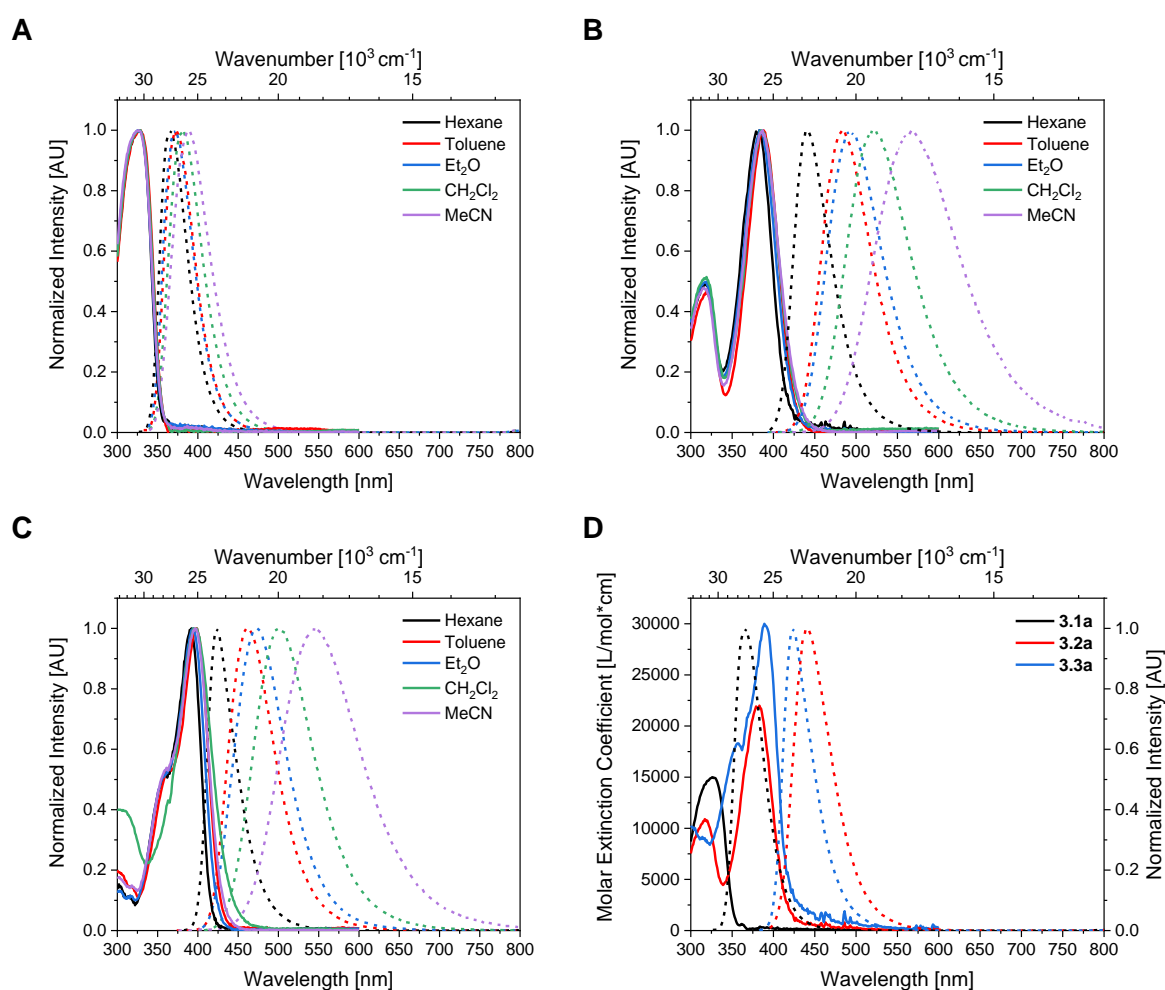


Figure 3.7: Absorption (solid lines) and emission (dotted lines; excitation at λ_{max}^{abs}) spectra of **A) 3.1a** **B) 3.2a** and **C) 3.3a** in solvents of different polarity; **D) Absorption (solid lines) and emission (dotted lines; excitation at λ_{max}^{abs}) spectra of 3.1a, 3.2a, and 3.3a in hexane.**

The absorption spectra of these compounds show no solvatochromic behavior while the emission spectra show positive solvatochromism. When comparing **3.1a**, **3.2a**, and **3.3a** in the same solvent, the shape of their absorption and emission spectra are similar (Figure 3.7D), while the molar extinction coefficient increases almost linearly with increasing

number of dimethylamino groups from 15 000 L mol⁻¹ cm⁻¹ over 22 000 L mol⁻¹ cm⁻¹ to 30 000 L mol⁻¹ cm⁻¹. The solvatochromic behavior is more pronounced for the amine-substituted compounds **3.2a** and **3.3a** than for **3.1a** because of significant charge-transfer from the dimethylamino donor groups.

Table 3.3: Photophysical data of **3.1a**, **3.2a**, and **3.3a** in solvents of different polarity.

	λ_{max}^{abs} [nm]	λ_{max}^{fl} [nm]	Apparent Stokes shift [cm ⁻¹]	τ [ns]	Φ_f	ϵ [10 ³ L mol ⁻¹ cm ⁻¹]	τ_0 [ns]	k_{nr} [10 ⁹ s ⁻¹]	k_f [10 ⁹ s ⁻¹]	
3.1a	Hexane	326	367	3 400	1.48	0.10	15	14.8	0.61	0.07
	Toluene	326	374	3 900	1.40	0.06	15	23.3	0.67	0.04
	Et ₂ O	325	371	3 800	1.50	0.08	-	18.7	0.61	0.05
	CH ₂ Cl ₂	326	381	4 400	1.40	0.07	-	20.0	0.66	0.05
	MeCN	326	388	4 900	1.56	0.07	-	22.3	0.60	0.04
3.2a	Hexane	383	440	3 400	5.17	0.34	22	15.2	0.13	0.07
	Toluene	388	486	5 200	8.53	0.48	-	17.8	0.06	0.06
	Et ₂ O	383	492	5 800	10.2	0.48	-	21.3	0.05	0.05
	CH ₂ Cl ₂	385	520	6 700	15.4	0.58	-	26.5	0.03	0.04
	MeCN	387	567	8 200	11.5	0.25	-	45.9	0.07	0.02
3.3a	Hexane	390	424	2 100	1.55	0.13	30	11.9	0.56	0.08
	Toluene	398	462	3 500	3.32	0.25	27	13.3	0.23	0.08
	Et ₂ O	394	474	4 300	5.24	0.24	-	21.8	0.14	0.05
	CH ₂ Cl ₂	397	501	5 200	12.0	0.41	-	29.3	0.05	0.03
	MeCN	395	546	7 000	9.50	0.28	-	33.9	0.08	0.03

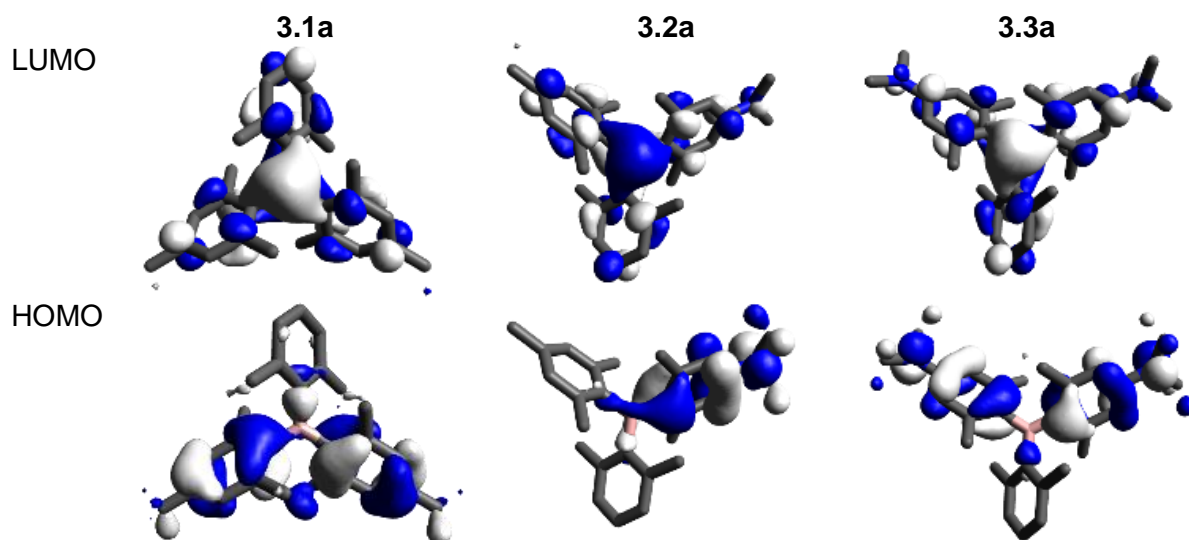


Figure 3.8: HOMOs and LUMOs of **3.1a**, **3.2a**, and **3.3a** from DFT calculations (B3LYP, 6-31G(d,p), gas phase).

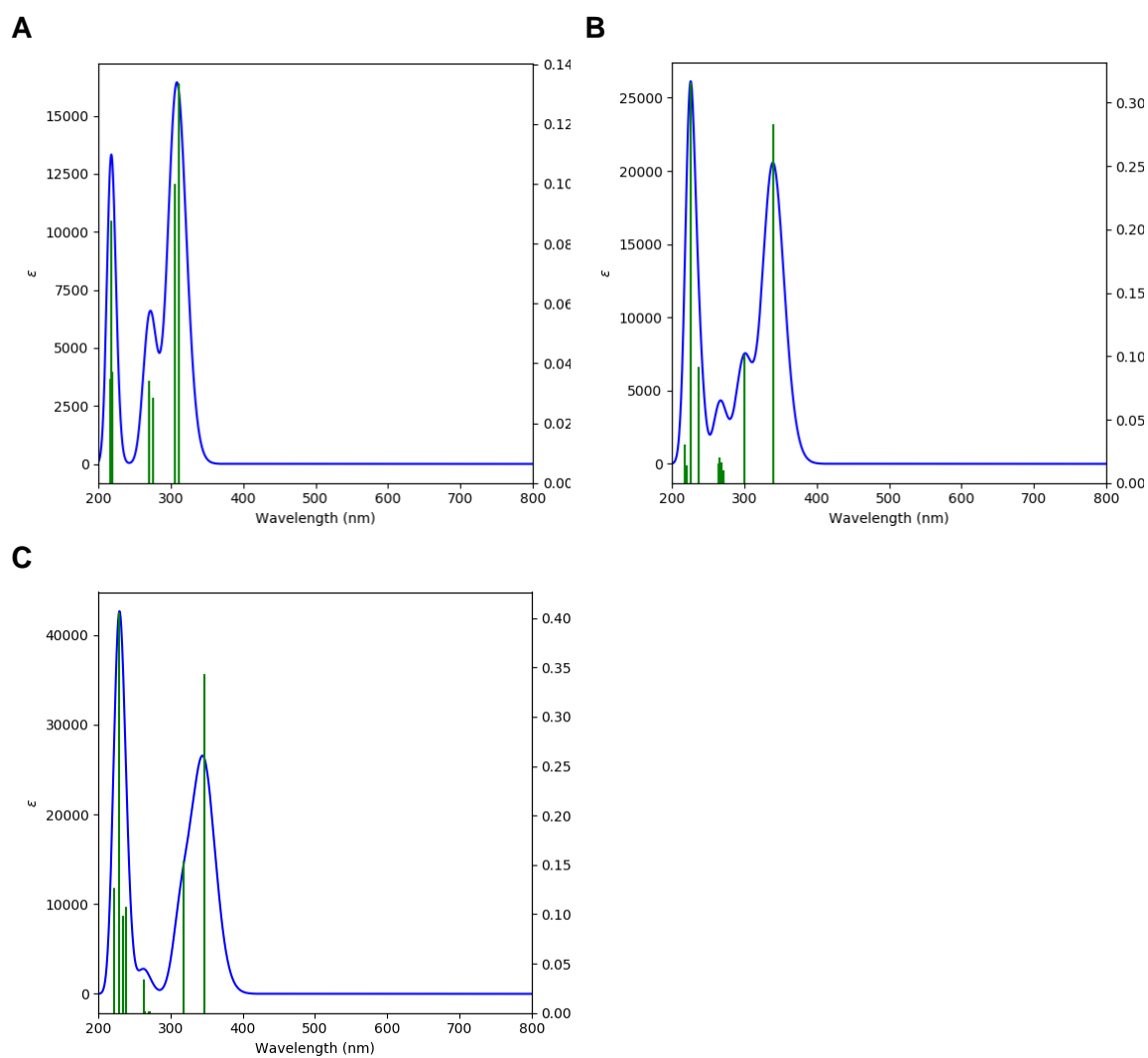


Figure 3.9: Calculated absorption spectra (CAM-B3LYP 6-31G(d,p), gas phase) of **A) 3.1a**, **B) 3.2a**, and **C) 3.3a**.

For all three triarylboranes, TD-DFT calculations identified the transition between the HOMO and LUMO to be the main transition of lowest energy. The LUMO of each triarylborane is located at the boron center and the HOMO is located at the most electron-rich aromatic systems, which are mesityl for **3.1a** and 4-(*N,N*-dimethylamino)-2,6-dimethylphenyl for **3.2a** and **3.3a** (Figure 3.8). When there is more than one electron-rich aromatic system, the HOMO is distributed equally over both. The calculated absorption spectra (Figure 3.9) of each neutral triarylborane fit the corresponding experimental spectra very well considering that the calculations were performed in the gas phase and the experiments in solution.

From the calculations, the orbital overlap parameter Λ was obtained, which is defined as $\Lambda = \frac{\sum_{i,a} c_{i,a}^2 \langle \varphi_a || \varphi_i \rangle}{\sum_{i,a} c_{i,a}^2}$ with φ_a and φ_i representing the occupied and unoccupied one-electron wavefunctions, respectively, $|\langle \varphi_a || \varphi_a \rangle|$ representing the norm of the one-electron wavefunction centroid and $c_{i,a}$ representing the weight of the one-electron excitation. Λ takes values between 0 and 1, with 0 corresponding to no spatial overlap and 1 to complete overlap between the orbitals participating in the respective transition.^[167] As Λ is 0.58, 0.49, and 0.52 for **3.1a**, **3.2a**, and **3.3a**, respectively, localized orbitals are suggested for each compound which indicates increasing charge-transfer (CT) character of the transitions in the order **3.1a** < **3.3a** < **3.2a**.^[167] As the apparent Stokes shifts increase in the same order, it is suggested that the introduction of a second dimethylamino group does not further increase the CT character of the transition.

The quantum yield is the largest for **3.2a** and the smallest for **3.1a** in all solvents examined. The fluorescence lifetimes of **3.1a** do not change with solvent polarity whereas for **3.2a** and **3.3a** the lifetimes increase with increasing solvent polarity but decrease in acetonitrile. This indicates more polarized excited states of **3.2a** and **3.3a** compared to **3.1a** which are better stabilized in more polar solvents (CH_2Cl_2) than in non-polar solvents (hexane). The natural lifetime (τ_0) of **3.2a** and **3.3a** increases, thus, the non-radiative rate constant (k_{nr}) decreases with increasing solvent polarity, as does the radiative rate constant (k_r) (Table 3.3). Such behavior was previously observed for a similar donor-acceptor compound containing carbazole as donor and dimesitylborane as acceptor.^[168] This is often not the case for very strong CT systems, and tuning of the relative donor and acceptor strength is required to obtain high Φ_f values in polar solvents.^[169]

3.2.3.2 Cationic Triarylboranes

The absorption and emission spectra and the corresponding data of the cationic compounds **3.2c**, and **3.3c** are summarized in Figure 3.10 and Table 3.4, respectively. Ethanol ($\epsilon_r = 25 \text{ F m}^{-1}$), acetonitrile ($\epsilon_r = 38 \text{ F m}^{-1}$), and water ($\epsilon_r = 80 \text{ F m}^{-1}$) were chosen as solvents.^[166] As both compounds do not dissolve well in pure water, concentrated acetonitrile solutions were diluted with water to less than 1% acetonitrile.

The absorption spectra of **3.2c** (Figure 3.10A) and **3.3c** (Figure 3.10B) do not show any solvatochromism. The low-energy transition bands at ca. 400 nm result from minor impurities of the neutral compounds **3.2a** and **3.3a** as discussed above. The emission spectra of both compounds display a small, positive solvatochromism, which is more pronounced for **3.2c** than for **3.3c**. In the latter, two strong electron-donating functionalities are replaced with strong electron-withdrawing trimethylammonium groups upon methylation while the first retains the mesityl group as a weaker electron-donor. Thus, the boron centers in **3.2c** and **3.3c** are expected to be more electron-deficient than in the neutral analogues **3.2a** and **3.3a**. TD-DFT calculations demonstrate that the HOMO to LUMO transitions are the transitions of lowest energy. The LUMOs remain at the boron moiety with some contribution of the trimethylammonium moiety for **3.2c**, while the HOMOs are localized at the more electron-rich mesityl and 2,6-dimethylphenyl moieties (Figure 3.11). For **3.3c**, the contribution of the trimethylammonium moieties to the LUMO is distributed over two aromatic systems. The calculated absorption spectra (Figure 3.12) of both cationic triarylboranes fit the experimental spectra well considering that the calculations were performed in the gas phase without ion-ion interactions while experiments were conducted in solutions.

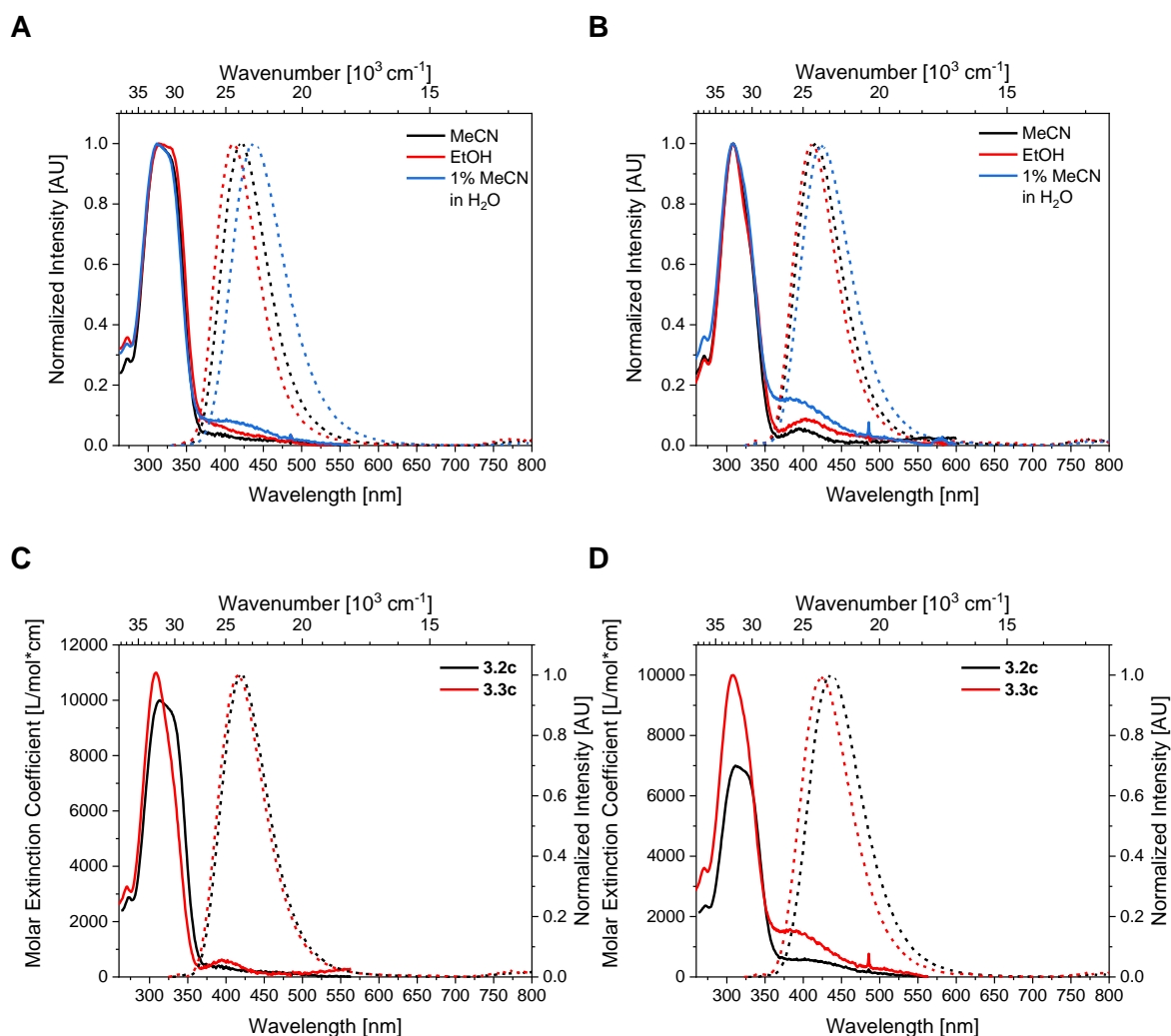
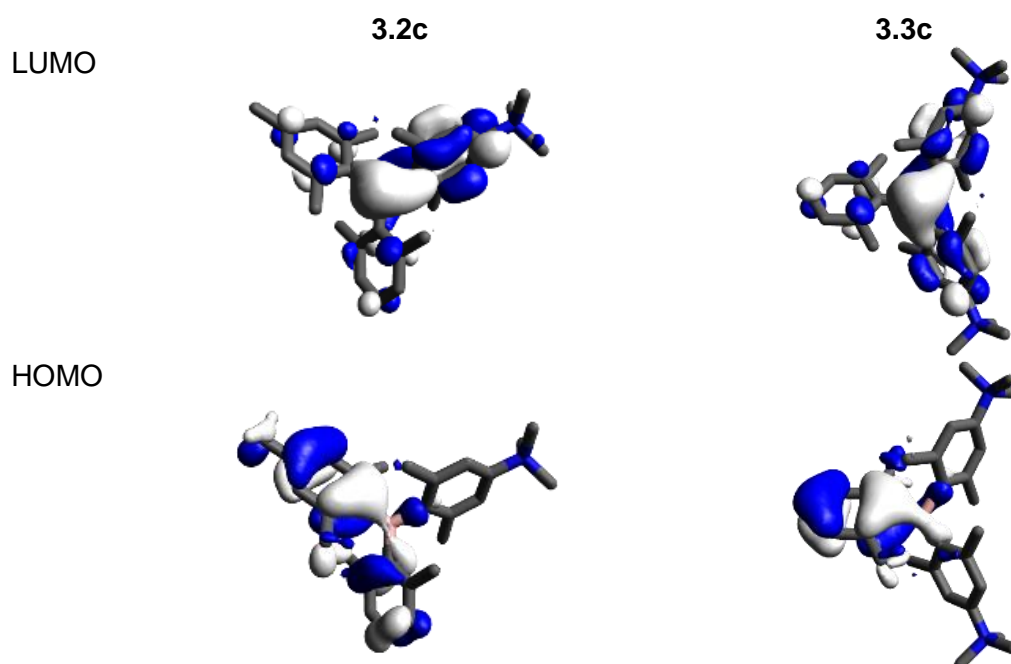


Figure 3.10: Absorption (solid lines) and emission (dotted lines; excitation at λ_{max}^{abs}) spectra of **A)** **3.2c** and **B)** **3.3c** in solvents of different polarity; Absorption (solid lines) and emission (dotted lines; excitation at λ_{max}^{abs}) spectra of **3.2c** and **3.3c** in **C)** ethanol and **D)** 1% acetonitrile in water.

The molar extinction coefficients of both cationic triarylboranes are slightly lower in an aqueous environment compared to pure acetonitrile while the absorption and emission spectra of **3.2c** and **3.3c** are at very similar positions and have almost identical shapes in the same solvents (Figure 3.10C, Figure 3.10D). The fluorescence quantum yields (ca. 0.10) are very similar for both compounds in all solvents, only for **3.2c** in aqueous solution does this increase to 0.19. The fluorescence lifetimes of both compounds increase with increasing solvent polarity, thus reflecting polarized excited states. Similarly to the neutral triarylboranes, the natural lifetimes increase with increasing solvent polarity while the radiative and non-radiative decay constants decrease (Table 3.4).

Table 3.4: Photophysical data of **3.2c** and **3.3c** in ethanol, acetonitrile, and 1% acetonitrile in water.

	λ_{max}^{abs} [nm]	λ_{max}^{fl} [nm]	Apparent Stokes shift [cm ⁻¹]	τ [ns]	Φ_f	ϵ [10 ³ L mol ⁻¹ cm ⁻¹]	τ_0 [ns]	k_{nr} [10 ⁹ s ⁻¹]	k_r [10 ⁹ s ⁻¹]	
3.2c	EtOH	315	410	7 400	2.39	0.08	-	29.9	0.38	0.03
	MeCN	314	420	8 000	3.37	0.11	10	30.6	0.26	0.03
	1% MeCN in H ₂ O	313	437	9 100	7.49	0.19	7	39.4	0.11	0.02
3.3c	EtOH	308	412	8 200	3.76	0.09	-	41.8	0.24	0.02
	MeCN	309	416	8 300	4.40	0.10	11	44.0	0.20	0.02
	1% MeCN in H ₂ O	308	425	8 900	6.65	0.11	10	60.4	0.13	0.02

Figure 3.11: HOMOs and LUMOs of **3.2c** and **3.3c** received from DFT calculations (B3LYP, 6-31G(d,p), gas phase).

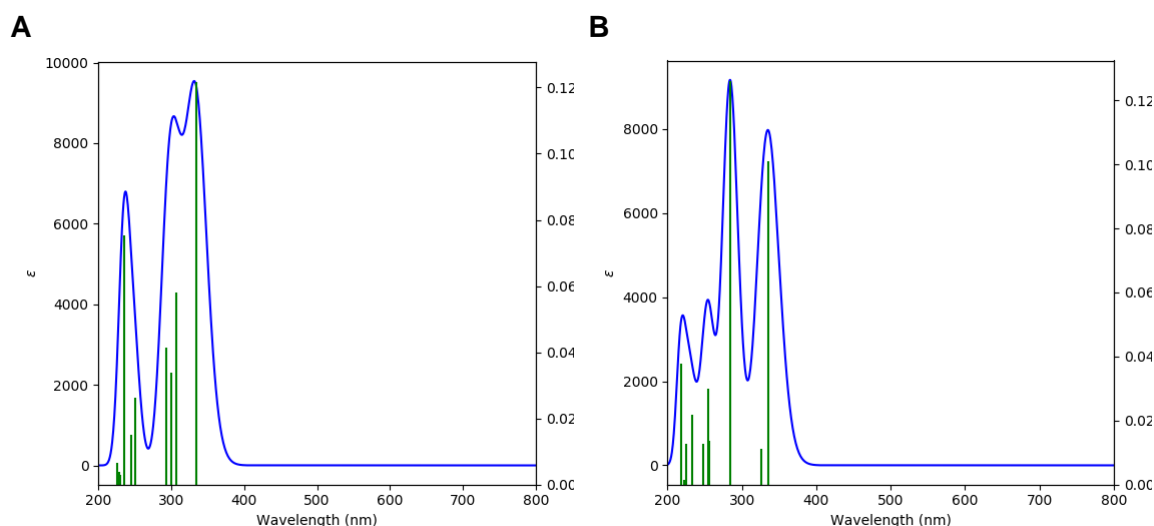


Figure 3.12: Calculated absorption spectra (CAM-B3LYP 6-31G(d,p), gas phase) of **A) 3.2c** and **B) 3.3c**.

In summary, the absorption and emission spectra of the triarylboranes shift bathochromically in the order **3.3c** < **3.2c** < **3.1a** < **3.2a** < **3.3a**, which correlates well with the electron density at the boron center induced by electron-withdrawing and electron-donating moieties. For the neutral triarylboranes, the molar extinction coefficients increase almost linearly by ca. 7 000 L mol⁻¹ cm⁻¹ per dimethylamino group. In contrast, for the trimethylammonium-substituted triarylboranes **3.2c** and **3.3c**, the molar extinction coefficient does not change significantly with the number of electron-withdrawing moieties.

3.2.4 Electrochemical Properties

The electrochemical properties of the neutral (Figure 3.13A-C) and cationic (Figure 3.13D) triarylboranes were examined in THF and acetonitrile, respectively, with [*n*Bu₄N][PF₆] as the electrolyte and a scan rate of 250 mV s⁻¹. The cyclic voltammograms of **3.3c** were reported before.^[170] Each measurement is referenced to the Fc/Fc⁺ ion couple and the results are summarized in Table 3.5. No oxidation potentials are expected to be observed for **3.1a**, **3.2c** and **3.3c**, within the electrochemical windows of the solvents used. In the case of **3.2c** and **3.3c**, ¹H NMR and absorption spectra confirmed minor impurities caused by non- or partially methylated starting material which results in minor oxidation waves in the corresponding cyclic voltammograms.

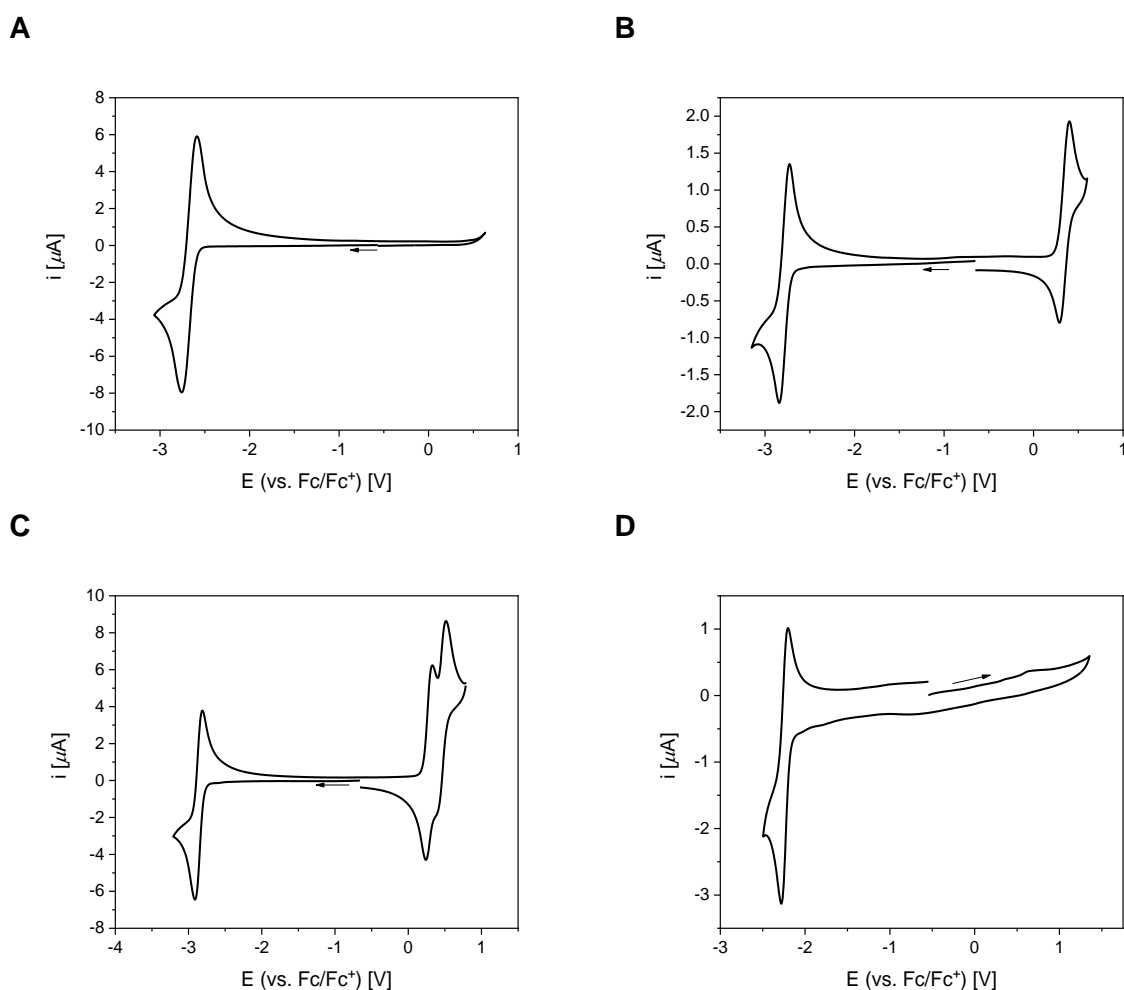


Figure 3.13: Cyclic voltammogram of **A) 3.1a**, **B) 3.2a**, and **C) 3.3a** in THF. **D)** Cyclic voltammogram of **3.2c** in MeCN.

Table 3.5: Reduction and oxidation potentials of **3.1a**, **3.2a**, and **3.3a** determined in THF, and of **3.2c** and **3.3c** determined in MeCN and referenced to the Fc/Fc⁺ redox couple.

	$E_{1/2}(\text{red})$ [V]	$E_{1/2}(\text{ox1})$ [V]	$E_{1/2}(\text{ox2})$ [V]
3.1a	-2.67	-	-
3.2a	-2.78	0.34	-
3.3a	-2.86	0.28	0.51 (irrev.)
3.2c	-2.24	-	-
3.3c ^[170]	-2.02	-	-

For **3.1a**, **3.2a**, and **3.3a**, one partially reversible 1e⁻ reduction potential was found at -2.67 V, -2.78 V, and -2.86 V (Table 3.5), respectively, resulting from the reduction of the boron center. These values decrease by ca. 0.1 V with each additional dimethylamino

group. In the case of **3.2a**, one $1e^-$ oxidation potential at 0.34 V was found. For **3.3a**, two oxidation potentials were found at 0.28 V and 0.51 V, the second being irreversible. For **3.2c**, one partially reversible $1e^-$ reduction potential at -2.24 V was observed which increases by 0.22 V upon addition of a second trimethylammonium group in **3.3c**. In summary, the reduction potentials decrease with increasing electron density at the boron center in the order **3.3c** > **3.2c** > **3.1a** > **3.2a** > **3.3a** due to the more pronounced electron-donating effect of the amino-group NMe_2 compared to the methyl group, and to the electron-withdrawing effect of the NMe_3^+ groups. Thus, the HOMO and LUMO energies calculated according to Equation 3.3 and Equation 3.4, respectively, decrease upon methylation of the amine (Table 3.6).

Table 3.6: HOMO and LUMO energies of **3.1a**, **3.2a**, **3.2c**, **3.3a**, and **3.3c** determined from cyclic voltammograms calculated according to Equation 3.3 and Equation 3.4.

	3.3c	3.2c	3.1a	3.2a	3.3a
E(HOMO) [eV]	-6.55	-6.28	-6.08	-5.60	-5.54
E(LUMO) [eV]	-3.08	-2.86	-2.59	-2.48	-2.40

$$\text{Equation 3.3: } E(\text{HOMO}) = \text{solvent correction} - E_{1/2}^{\text{ox}}$$

$$\text{Equation 3.4: } E(\text{LUMO}) = \text{solvent correction} - E_{1/2}^{\text{red}}$$

The solvent corrections are defined as -5.16 eV for CH_2Cl_2 , -5.10 eV for MeCN, and -5.26 eV for THF. These values result from the summary of different influences such as the different oxidation potentials of the Fc/Fc^+ couple in different solvents when measured against the standard calomel electrode (SCE; $E(Fc/Fc^+, CH_2Cl_2, [NBu_4][PF_6]) = 0.46$ eV; $E(Fc/Fc^+, MeCN, [NBu_4][PF_6]) = 0.40$ eV; $E(Fc/Fc^+, THF, [NBu_4][PF_6]) = 0.56$ eV),^[171] the referencing of these values against the standard hydrogen electrode (SHE; +4.46 eV),^[172] and finally, the referencing to the absolute value of the SHE (0.244 eV).^[173] As a result, the HOMO and LUMO energies in the gas phase can be calculated from experimental results.^[174]

Whenever no oxidation potential was detectable, the HOMO was calculated using the onset potential of the absorption according to Equation 3.5.

$$\text{Equation 3.5: } E(\text{HOMO}) = E(\text{LUMO}) - E(\text{onset absorption})$$

Thus, for **3.1a**, **3.2c**, and **3.3c**, the same values for the optical (ΔE_{opt}) and electrochemical bandgap (ΔE_{CV}) are obtained (*vide infra*).

Very similar energy values were reported by Gabbai and coworkers^[50] who examined the reduction potentials of triarylboranes **3.16a-c** and BMe_3 (**2.17**; Figure 3.14) in THF and acetonitrile using a glassy carbon electrode, 0.1 M $[\text{Bu}_4\text{N}][\text{PF}_6]$ as electrolyte and the Fc/Fc^+ couple as internal standard (Table 3.7). They reported a stepwise decrease of the reduction potential from the neutral triarylborane **2.17** to the *tri*-cationic derivative **3.16c** by 0.26 eV in acetonitrile and of 0.36 eV in THF with increasing number of trimethylammonium groups. Herein, this trend was confirmed, but the distinct values are lower most likely due to the slightly decreased electron density at the boron center of **3.1a**, **3.2c**, and **3.3c** resulting from the (partial) substitution of the mesityl group(s) of **2.17**, **3.16a**, and **3.16b** with less electron-rich 2,6-dimethylphenyl groups.

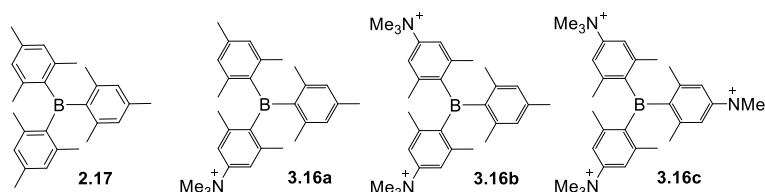


Figure 3.14: BMe_3 (**2.17**) and compounds **3.16a-c** reported by Gabbai and coworkers.^[50]

Table 3.7: Reduction potentials of **3.16a-c** and **2.17** determined by Gabbai and coworkers.^[50]

	$E_{1/2}$ (red) in MeCN [V]	$E_{1/2}$ (red) in THF [V]
2.17	-2.57	-2.9
3.16a	-2.33	-2.55
3.16b	-2.09	-2.19
3.16c	-1.86 (irrev.)	insoluble

3.2.5 HOMO-LUMO Gaps

HOMO-LUMO gaps were obtained from DFT calculations (ΔE_{calc}), absorption spectra (ΔE_{opt})^[175] and cyclic voltammograms (ΔE_{CV})^[171-174] according to literature known procedures. As shown in Equation 3.5, the onset energy of the absorption spectrum was used for the calculation of ΔE_{CV} in case no oxidation potential was obtained. The results are summarized in Table 3.8.

Table 3.8: Comparison of HOMO-LUMO gap energies obtained from DFT calculations (B3LYP, 6-31G(d,p), gas phase; ΔE_{calc}), absorption (ΔE_{opt}) and CV (ΔE_{CV}) measurements.

	ΔE_{calc} [eV]	ΔE_{opt} [eV]	ΔE_{CV} [eV]
3.1a	4.34	3.49	
3.2a	3.66	2.92	3.12
3.3a	3.63	2.92	3.14
3.2c	3.87	3.42	
3.3c	3.72	3.47	

The values of ΔE_{opt} and ΔE_{CV} are very similar and decrease with increasing electron-density at the boron center. The same trend can be observed for ΔE_{calc} although these gas phase values are generally ca. 0.7 eV higher than the experimental values. Nonetheless, comparison of the values in Table 3.8 show that the DFT calculations predict the trend in the HOMO-LUMO gaps well even for the cationic compounds although the triflate ion was not included in the calculations.

3.2.6 Singlet Oxygen Sensitization

Thus far, singlet oxygen sensitization by triarylboranes is rare, and typically attributed to moieties other than the boron center. Merz *et al.*^[65] observed a singlet oxygen sensitizing efficiency of 0.6 for a tetra-(di-(4-methoxyphenyl)amino)-substituted perylene (**3.17a**), but not for the tetra-(dimesitylboryl)-substituted analogue **3.17b** (Figure 3.15A).

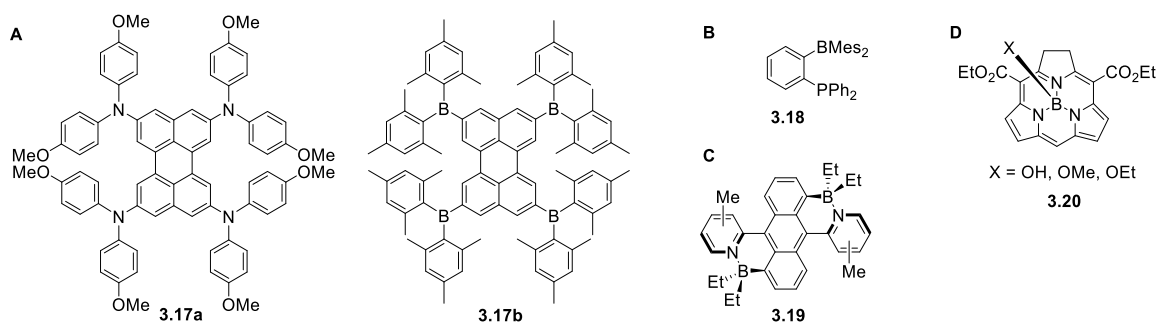


Figure 3.15: Singlet oxygen sensitizing compounds **3.17**,^[65] **3.18**,^[176] **3.19**,^[177] and **3.20**.^[178]

Porcel *et al.* reported the interaction of the triarylborane-phosphine compound **3.18** with $^1\text{O}_2$ but this interaction was attributed to the phosphine substituent and not to the boron.^[176] Similarly, other groups attributed the sensitization of **3.19**^[177] and **3.20**^[178] to the attached polycyclic aromatic hydrocarbon (PAH) and porphyrin motifs, respectively, rather than to the boranes.

Very recently, triarylboranes have been reported to be phosphorescent in the solid state, even at room temperature, which demonstrates the population of their triplet states.^[105] Efficiently populated triplet states can also be used for the sensitization of singlet oxygen in solution and, thus, might be good candidates for biological applications such as photodynamic therapy (PDT) in, e. g., photoinduced treatment of cancer cells.^[179] Hence, the ability to sensitize singlet oxygen in O₂-saturated acetonitrile solutions was investigated for **3.1a**, **3.2c**, and **3.3c**, and referenced to that obtained from a solution of the known ¹O₂ sensitizer perinaphthenone.^[180] The signal-to-noise ratio of all recorded spectra is low due to the small radiative rate constant ($k_r = 0.45 \text{ s}^{-1}$) of singlet oxygen in acetonitrile.^[181] Therefore, all values given have an estimated error of ± 0.1 .

From these spectra, **3.1a**, **3.2c**, and **3.3c** are found to sensitize singlet oxygen with an efficiency (Φ_Δ) of 0.3, 0.5, and 0.6, respectively (Figure 3.16). Thus, their sensitizing ability increases with increasing number of trimethylammonium substituents (Table 3.9). The corresponding fluorescence quantum yields in acetonitrile decrease in the same order from 0.34 to 0.11 and 0.10. Thus, the sum of singlet oxygen efficiencies Φ_Δ and fluorescence quantum yields Φ_f for these compounds is ca. 0.6-0.7 (Table 3.9). Hence, 30-40% of the excited states decay by processes other than fluorescence or ISC, assuming that the efficiency of ¹O₂ sensitization by the triplet states is 100%.

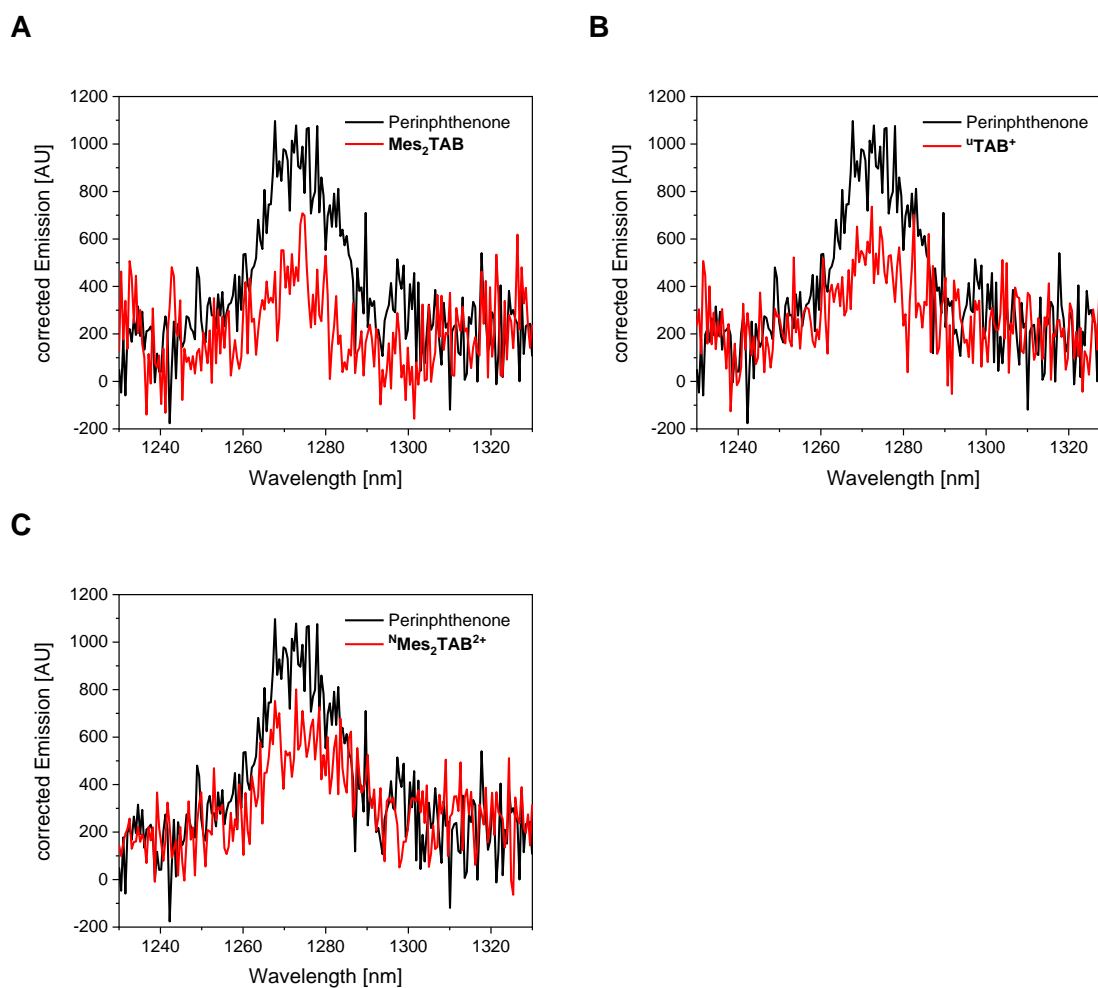


Figure 3.16: Emission spectra of **A) 3.1a**, **B) 3.2c**, and **C) 3.3c** relative to perinaphthenone determined in acetonitrile.

Table 3.9: Singlet oxygen sensitizing quantum yields (Φ_{Δ}) of **3.1a**, **3.2c**, and **3.3c** in relation to perinaphthenone and fluorescence quantum yields (Φ_f) determined in acetonitrile.

	Φ_{Δ}	Φ_f
3.1a	0.3	0.34
3.2c	0.5	0.11
3.3c	0.6	0.10

3.3 Conclusions

A synthetic route to an unsymmetrically-substituted triarylborane bearing three different aromatic systems, namely mesityl, 2,6-dimethylphenyl, and 4-(*N,N*-dimethylamino)-2,6-dimethylphenyl was developed. It is shown that the order of introduction as well as the choice of organo-metalate significantly influences the isolated yield of triarylborane **3.2a**. Crystal structures of **3.2a** and **3.2b** were analyzed, revealing the expected propeller-like structures and typical B–C bond lengths and angles. Investigation of the rotational barriers of **3.2a** and **3.2c** show an increase by 2 kcal/mol upon methylation, which is in accordance with the literature.^[44]

Investigation of the photophysical properties shows that substitution of the methyl groups of **3.1a** with dimethylamino groups results in more pronounced solvatochromic behavior of the emission, which is typical for charge-transfer compounds. The CT character of the transitions was confirmed by TD-DFT calculations. However, these effects are lost when the dimethylamino moieties are methylated leading to trimethylammonium groups. The absorption and emission maxima are found to shift bathochromically with increasing strength and number of donor substituents in the order **3.3c** < **3.2c** < **3.1a** < **3.2a** < **3.3a**. The molar extinction coefficients of the neutral triarylboranes increase by ca. 7 000 L mol⁻¹ cm⁻¹ per amino substituent, but are similar for both charged compounds. The influence of the second amino group on the photophysical properties is generally smaller than that of the first.

From cyclic voltammograms, the reduction potentials are found to decrease with increasing electron density at the boron center in the order **3.3c** > **3.2c** > **3.1a** > **3.2a** > **3.3a** due to the increasing electron density at the boron center.

In acetonitrile solutions, **3.1a**, **3.2c**, and **3.3c** are shown to sensitize singlet oxygen. The efficiency increases with increasing number of trimethylammonium groups in the order **3.1a** < **3.2c** < **3.3c** from 0.3 to 0.6.

These investigations show that, using the methodology reported herein, new molecules can be designed whose photophysical and electrochemical properties can be fine-tuned by the choice of the aromatic systems. After borylation, such compounds can be incorporated by, e.g., Suzuki-Miyaura cross-coupling reactions, into larger systems with very similar properties as shown in the following Chapter 4.

CHAPTER 4

SYNTHESIS AND SELECTED PROPERTIES OF
BITHIOPHENE-CORED, *MONO*-, *BIS*-, AND *TRIS*-
(TRIMETHYLAMMONIUM)-SUBSTITUTED, *BIS*-
TRIARYLBORANE CHROMOPHORES

4 Synthesis and Selected Properties of Bithiophene-Cored, *Mono*-, *Bis*-, and *Tris*-(Trimethylammonium)-Substituted, *Bis*-Triarylborane Chromophores

The synthesis of **Cat**²⁺ and preliminary investigations of its photophysical properties were reported in the Master's Thesis of Sarina M. Berger.^[55] The synthesis is shown here for completeness. The previously reported photophysical properties and water-solubility are corrected herein.

4.1 Introduction

Griesbeck *et al.* reported the synthesis and the photophysical properties of the neutral, bithiophene-bridged *bis*-triarylborane **Neut4** and its *tetra*-cationic analogue **Cat**⁴⁺ (Figure 4.1).^[43, 56] Subsequently, the influence of different bridging units on the stability of such compounds^[44] and of other bridges on the photophysical properties and potential biological applications were reported.^[46, 52-53] A more detailed summary of the previous results is given in Chapter 1. However, the influence of different numbers and distributions of the charge on the properties of such *bis*-triarylboranes remained uninvestigated. Thus, the aim of this work was to synthesize the selectively dimethylamino- (**Neut1**, **Neut2**, **Neut(i)2**, **Neut3**) and trimethylammonium-substituted compounds (**Cat**¹⁺, **Cat**²⁺, **Cat(i)**²⁺, **Cat**³⁺; Figure 4.1) and to investigate their influence on selected properties such as water-solubility, singlet oxygen sensitizing efficiency, HOMO-LUMO gaps, photophysics, and electrochemistry.

To provide a solid foundation for discussion, the incompletely reported properties of **Neut0**^[54] were re-investigated herein. For completeness, the synthesis of **Cat**²⁺, previously reported in the Master's Thesis of Sarina M. Berger,^[55] is shown again and the previously reported photophysical properties are corrected as they resulted from dispersed particles rather than dissolved molecules.

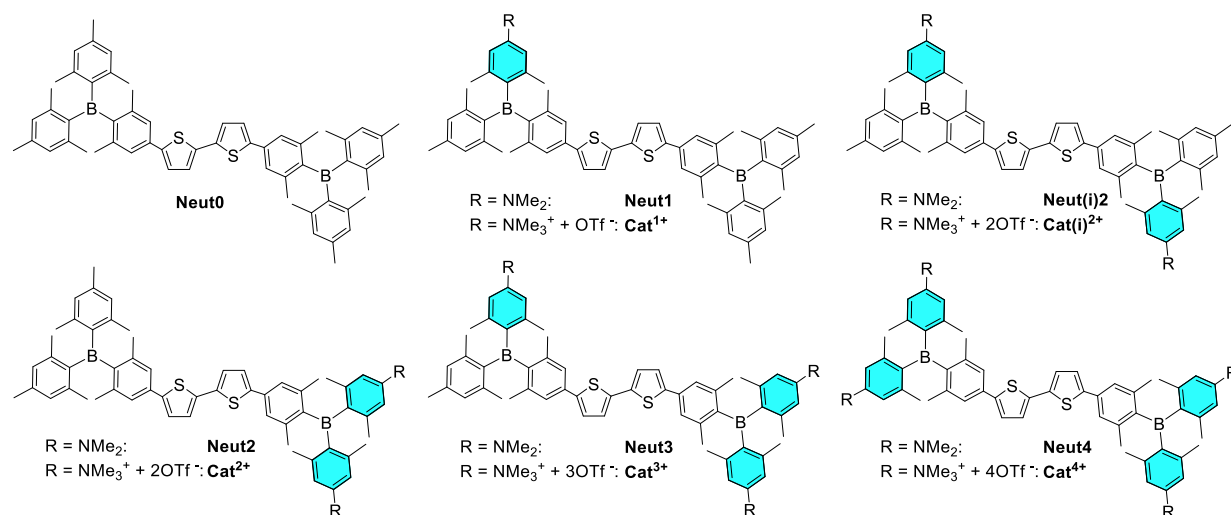


Figure 4.1: Structures of the compounds discussed herein.

4.2 Results and Discussion

4.2.1 Synthesis

The synthesis of **Cat**²⁺ was reported previously (Figure 4.2A)^[55] by an approach similar to the Suzuki-Miyaura-type cross-coupling strategy demonstrated by Griesbeck *et al.*^[43-44, 46, 56] In that reaction sequence, 5-bromo-2,2'-bithiophene is first reacted with **3.1b** (Figure 4.2B) under Suzuki-Miyaura cross-coupling conditions using Pd₂(dba)₃·CHCl₃ (dba = (1*E*,4*E*)-1,5-diphenylpenta-1,4-dien-3-one) as the pre-catalyst, 2-dicyclohexylphosphino-2',6'-dimethoxybiphenyl (SPhos) as the ligand, and potassium hydroxide as the base in a 2:1 mixture of toluene and water giving **4.2** in 71% yield. The 5'-position of the bithiophene of **4.2** was then brominated using *N*-bromosuccinimide (NBS) in DMF in 93% yield. In the next step, **4.3** was used in a second Suzuki-Miyaura cross-coupling reaction with **3.3b** under the same conditions giving **Neut2** in 59% yield. Finally, this compound was methylated using methyl triflate in dichloromethane solution yielding **Cat**²⁺ in 69%.

Using the same conditions for Suzuki-Miyaura cross-coupling, the non-amino-substituted *bis*-triarylborane **Neut0** was synthesized from 5,5'-dibromo-2,2'-bithiophene **4.4** and **3.1b**.^[54] Analogously, after successful synthesis of the borylated triarylborane **3.2b** (Figure 4.2B; Chapter 3), **Neut(i)2** was synthesized from **4.4** and **3.2b** in 53% yield (Figure 4.2C).

The previously reported compound **4.3**^[55] was reacted with **3.2b** under the Suzuki-Miyaura cross-coupling reaction conditions described above giving **Neut1** in 43% yield (Figure 4.2D).

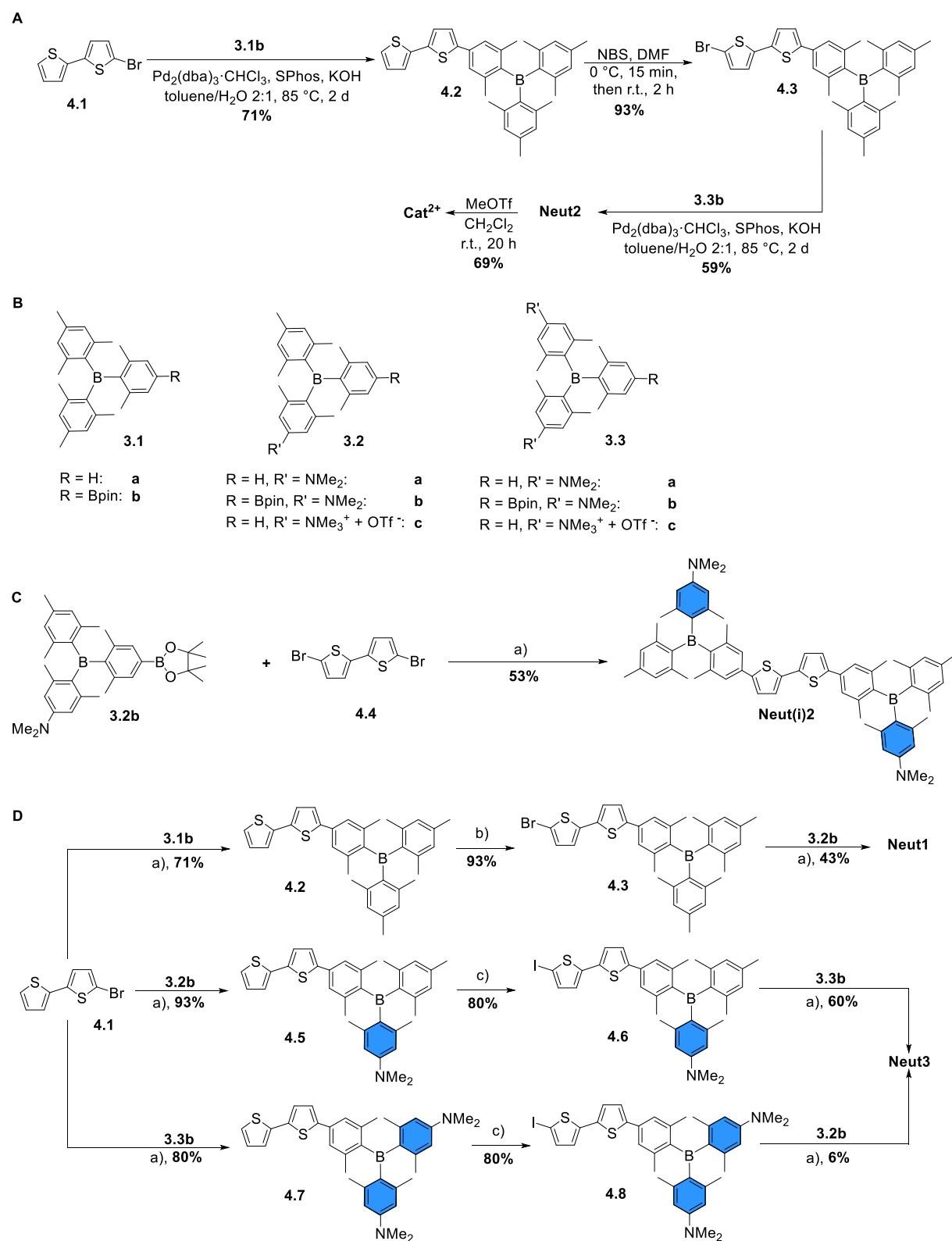


Figure 4.2: **A**) Synthesis of **Cat²⁺** reported previously.^[55] **B**) Molecular structures of **3.1-3.3**. **C**) Synthesis of **Neut(i)2**. **D**) Synthesis of **Neut1** and **Neut3**; a) Pd₂(dba)₃·CHCl₃, SPhos, KOH, toluene/water 2:1, 85 °C, 2d; b) NBS, DMF, 0 °C, 15 min then r.t., 2 h; c) nBuLi, THF, -78 °C, 1.5 h, then I₂, -78 °C → r.t., 18 h.

For the synthesis of **Neut3**, 5-bromo-2,2'-bithiophene **4.1** was reacted with **3.2b** and **3.3b** giving **4.5** and **4.7** in 93% and 80% yields, respectively (Figure 4.2D). These compounds were halogenated at the 5'-position of the bithiophene moiety to react in a second Suzuki-Miyaura cross-coupling reaction. It was found previously that bromination of **4.7** with NBS in DMF leads to selective bromination of one of the protons in position *ortho* to the dimethylamino moiety due to the stronger electron-donating effect of nitrogen compared to sulfur.^[55] Thus, inactivation of the dimethylamino groups was attempted by protonation with HCl prior to the reaction with NBS. This resulted in incomplete conversion and inseparable mixtures of multiply brominated and chlorinated compounds as indicated by HRMS. Similar results were obtained when using *N*-chlorosuccinimide (NCS) instead of NBS. Hence, the halogenation strategy was changed. Upon addition of iodine to mixtures of *n*BuLi and **4.5** or **4.7** in THF under an argon atmosphere, inseparable mixtures of **4.6** or **4.8** with their respective starting materials were obtained as indicated by ¹H NMR spectroscopy and HRMS. As only the iodinated compounds can react with borylated triarylboranes in Suzuki-Miyaura cross-coupling reactions, the mixtures of **4.5** and **4.6** or **4.7** and **4.8**, containing ca. 80% iodinated compounds, were used after minor purifications for the synthesis of **Neut3**, which was obtained in 6% and 60% yield, respectively (Figure 4.2D).

With **Neut1**, **Neut(i)2**, and **Neut3** in hand, methylation of the amino functionality using methyl triflate in dichloromethane gave the corresponding cationic compounds **Cat¹⁺**, **Cat(i)²⁺**, and **Cat³⁺** in 88%, 49%, and 57% yields, respectively. Thus, together with the previously reported compounds **Neut0**,^[54] **Cat²⁺**,^[55] **Cat⁴⁺**,^[43, 56] and the neutral precursors of the latter two, the influence of different numbers of dimethylamino- and trimethylammonium groups on water-solubility, singlet oxygen sensitizing efficiency, HOMO-LUMO gaps, and the photophysical and electrochemical properties were investigated.

4.2.2 Solubility in Water

In 2018, **Cat**²⁺ was reported to be soluble in pure water at concentrations suitable for photophysical measurements (10^{-5} mol L⁻¹) but the reported absorption spectrum clearly shows that aggregation or precipitation must have taken place as absorption was detected between 200 nm and 1100 nm although the compound and its solutions were reported to be yellow.^[55] Thus, the determination of the molar extinction coefficient of **Cat**¹⁺, **Cat**²⁺, **Cat(i)**²⁺, and **Cat**³⁺ in pure water was attempted. Hence, solutions with concentrations of ca. 3×10^{-6} mol L⁻¹ were shaken for 3 d in the dark leading to a colorless solution of **Cat**¹⁺ and slightly yellowish solutions of **Cat**²⁺, **Cat(i)**²⁺, and **Cat**³⁺. Each solution became colorless upon filtration (Nylon, 45 μ m) indicating that the color of the solutions resulted from dispersed but undissolved particles. This was confirmed by measuring the very weak absorbance of the filtered solutions at ca. 410 nm (Figure 4.3).

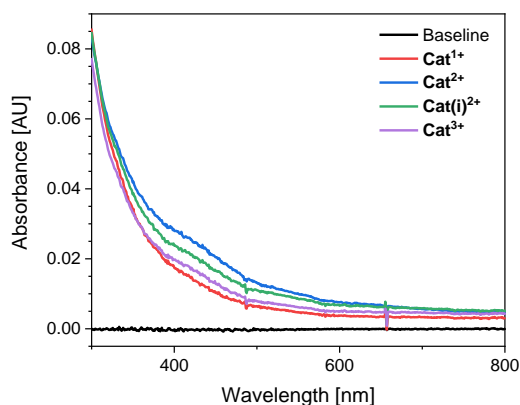


Figure 4.3: Absorption spectra of filtered solutions of **Cat**¹⁺, **Cat**²⁺, **Cat(i)**²⁺, and **Cat**³⁺ in pure water.

Thus, the selectively charged *bis*-triarylboranes **Cat**¹⁺, **Cat**²⁺, **Cat(i)**²⁺, and **Cat**³⁺ are insoluble in pure water, but concentrated solutions in acetonitrile can be diluted with water until the solution contains $\leq 1\%$ acetonitrile.

4.2.3 Photophysical Properties

4.2.3.1 Neutral *bis*-Triarylboranes

The absorption and emission spectra and the corresponding data of **Neut0**, **Neut1**, **Neut2**,^[55] **Neut(i)2**, **Neut3**, and **Neut4**^[56] are summarized in Figure 4.5A-E and Table 4.2, respectively. Hexane (dielectric constant: $\epsilon_r = 1.9 \text{ F m}^{-1}$), toluene ($\epsilon_r = 2.4 \text{ F m}^{-1}$), diethyl ether (Et_2O ; $\epsilon_r = 4.3 \text{ F m}^{-1}$), and CH_2Cl_2 ($\epsilon_r = 9.1 \text{ F m}^{-1}$) were chosen as solvents.^[166]

The absorption of the non-amino-substituted compound **Neut0** does not show solvatochromic behavior while its emission slightly shifts bathochromically by 587 cm^{-1} with increasing solvent polarity from hexane to CH_2Cl_2 . The fluorescence lifetimes, quantum yields, natural lifetime τ_0 , the radiative (k_r) and non-radiative rate constants (k_{nr}) do not change significantly with solvent polarity (Table 4.3). Thus, the absorption and emission processes of **Neut0** can be considered to result from locally excited states rather than charge-transfer processes. This was confirmed by DFT calculations giving a Λ value of 0.69 which is an indication of locally excited states.^[167] According to TD-DFT calculations, the transition of lowest energy is from HOMO to LUMO. The resulting calculated absorption spectra (Figure 4.4) fit the experimental results very well when considering that the calculations were performed in the gas phase while the experiments were done in solution. The HOMO of **Neut0** is located at the π -bonding orbitals of the xylene-bithiophene-xylene bridge while the LUMO is expanded from the empty p-orbital of one boron center over the antibonding π -orbitals of the bridge to the empty p-orbital of the second boron center (Table 4.1). Hence, the transitions in **Neut0** are of π - π^* nature and are localized at the conjugated bridge connecting the two boron centers. For the other four compounds **Neut1**, **Neut2**, **Neut(i)2**, and **Neut3**, Λ was calculated to be 0.68, 0.66, 0.70, and 0.70, respectively. The transitions of lowest energy are also from HOMO to LUMO, and the corresponding HOMOs and LUMOs are mainly located at the π -bridges while the LUMOs of **Neut1**, **Neut2** and **Neut3** are more pronounced at the more electron-deficient boron centers of the **3.1a** and **3.2a** moieties, respectively (Table 4.1). These results were obtained irrespective of the orientation of the sulfur atoms of the bithiophene bridge (pointing in the same or opposite directions). As in the solid state of similar compounds^[43, 53] the sulfur points in opposite directions, which was also shown to be energetically favorable by potential energy surface calculations,^[51] only this conformation is depicted in Table 4.1. In summary, the transitions of lowest energy in **Neut0**, **Neut1**, **Neut2**, **Neut(i)2**, **Neut3**, and **Neut4** are calculated to be of π - π^* nature despite the presence of one to three strong electron-donating dimethylamino groups (Table 4.1).

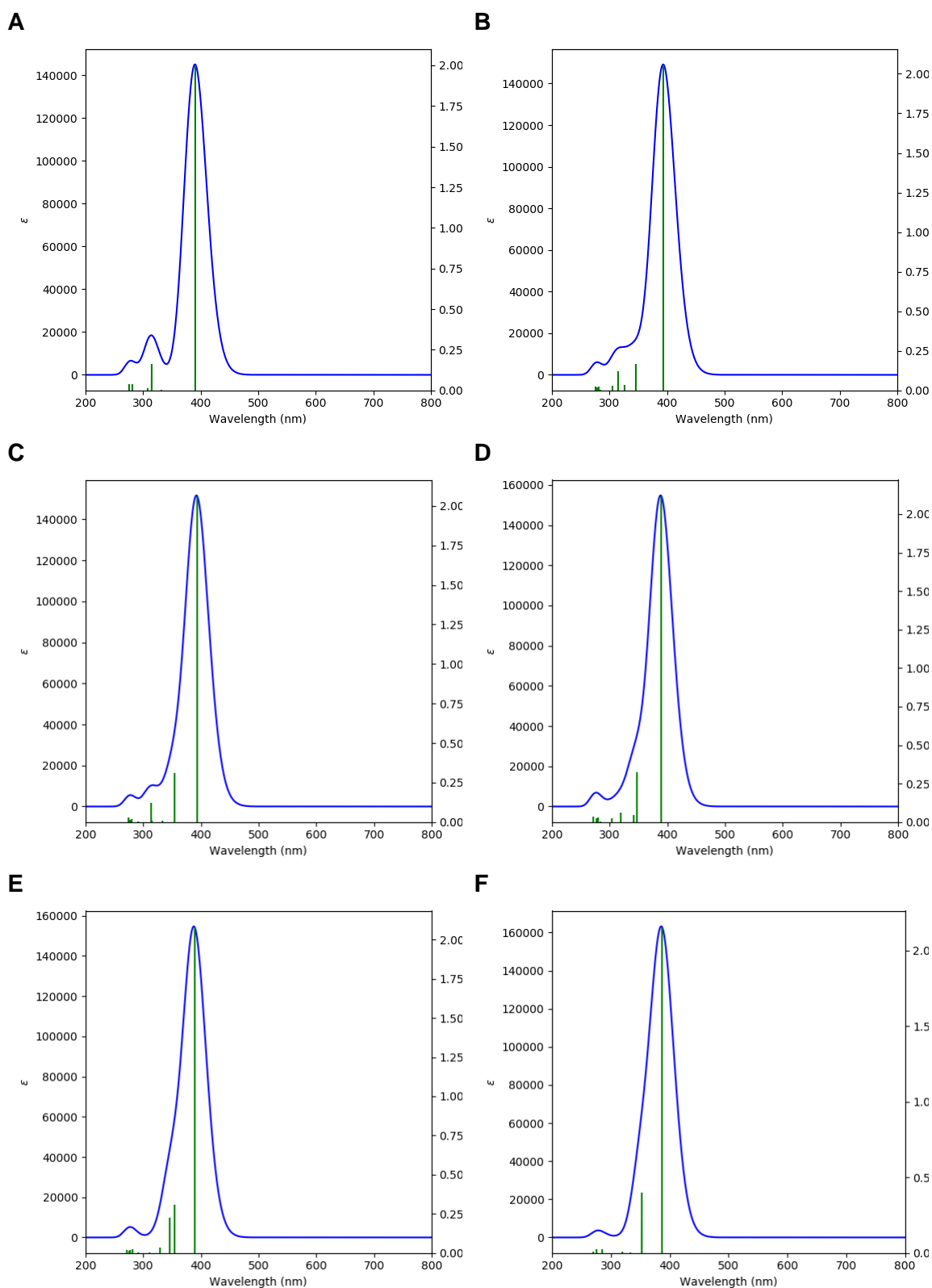


Figure 4.4: Calculated absorption spectra (CAM-B3LYP 6-31G(d,p), gas phase) of **A) Neut0**, **B) Neut1**, **C) Neut2**, **D) Neut(i)2**, **E) Neut3**, and **F) Neut4**.

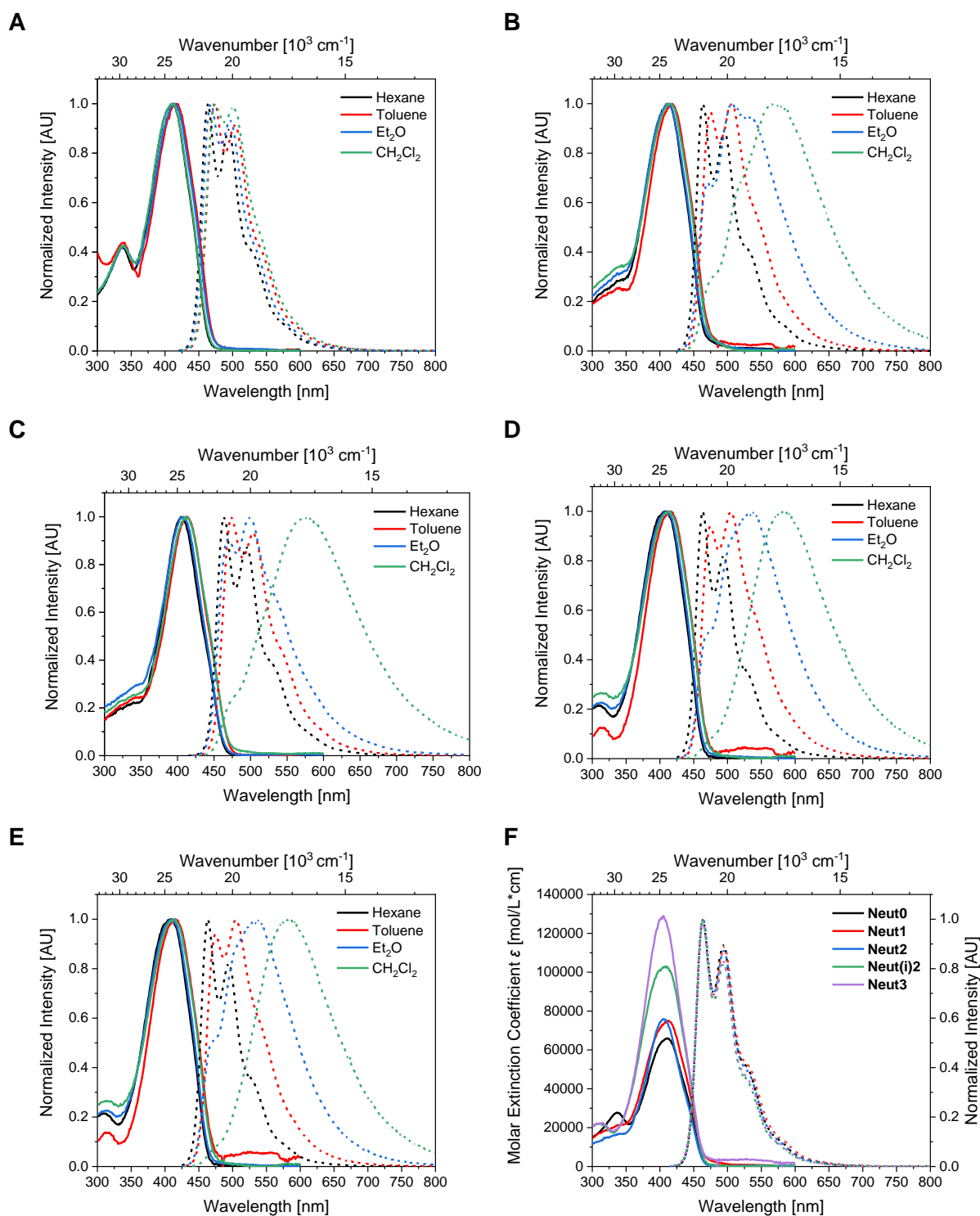


Figure 4.5: Absorption (solid lines) and emission (dotted lines; excitation at λ_{max}^{abs}) spectra of **A) Neut0**; **B) Neut1**; **C) Neut2**,^[55] **D) Neut(i)2**; **E) Neut3** in solvents of different polarity. **F) Absorption** (solid lines) and emission (dotted lines; excitation at λ_{max}^{abs}) spectra of **Neut0**, **Neut1**, **Neut2**, **Neut(i)2**, and **Neut3** in hexane.

Table 4.1: HOMO and LUMO of **Neut0**, **Neut1**, **Neut2**, **Neut(i)2**, **Neut3**, and **Neut4** obtained from DFT-calculations (B3LYP, 6-31G(d,p), gas phase).

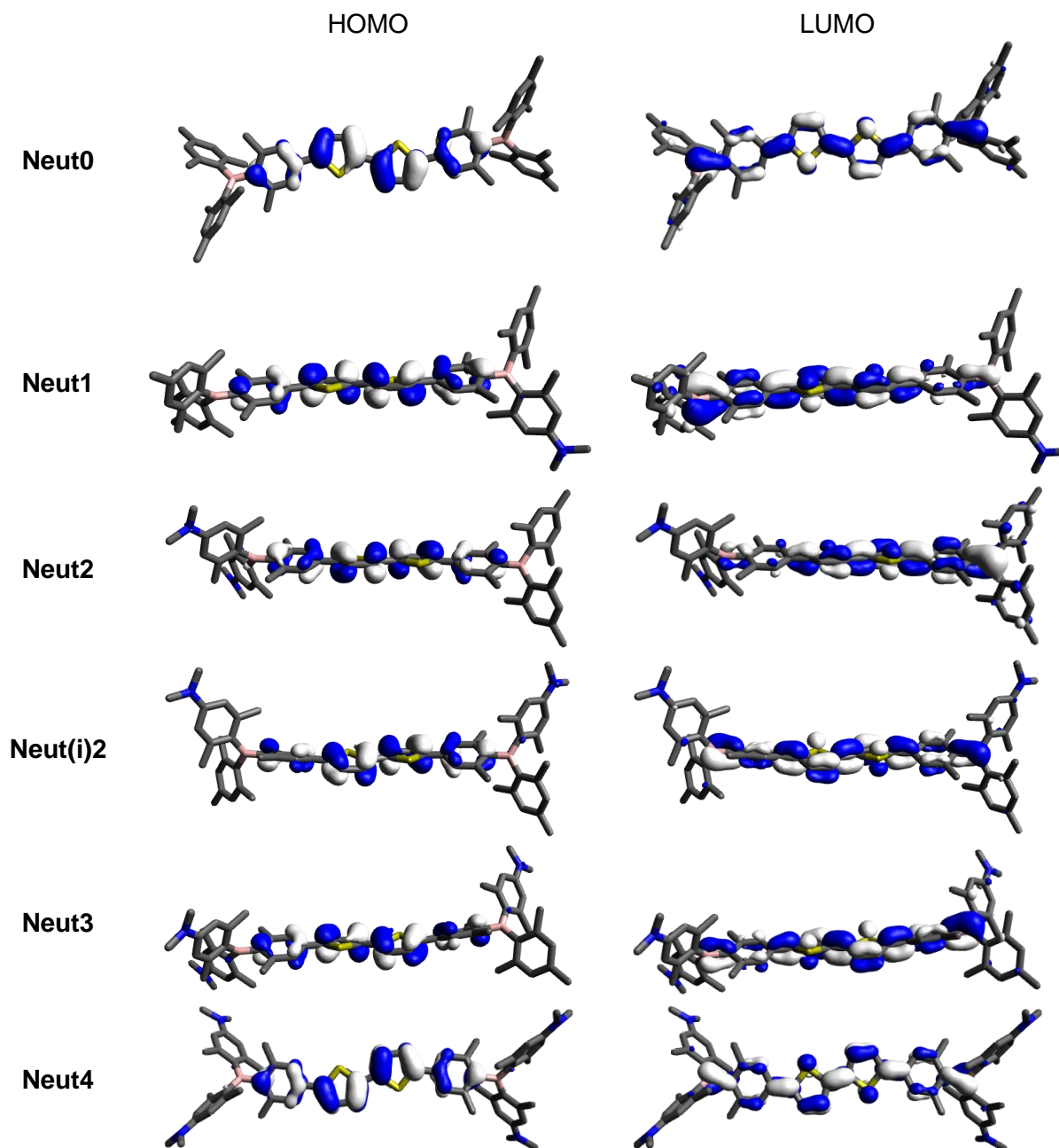


Table 4.2: Photophysical data of **Neut0**, **Neut1**, **Neut2**, **Neut(i)2**, **Neut3**, and **Neut4**.

	Solvent	λ_{max}^{abs} [nm]	λ_{max}^{fl} [nm]	Apparent Stokes shift [cm ⁻¹]	τ [ns]	Φ_f	ϵ [10 ³ L mol ⁻¹ cm ⁻¹]
Neut0	Hexane	410	464	2 800	0.52	0.31	66
	Toluene	416	474	2 900	0.56	0.35	52
	Et ₂ O	410	470	3 100	0.58	0.33	-
	CH ₂ Cl ₂	414	477	3 200	0.55	0.31	-
Neut1	Hexane	412	464	2 700	0.54	0.38	75
	Toluene	418	507	4 200	0.33 (13%) 1.61 (87%)	0.36	-
	Et ₂ O	412	507	4 500	0.61 (19%) 4.35 (81%)	0.33	-
	CH ₂ Cl ₂	416	568	6 400	0.69 (21%) 4.67 (79%)	0.21	-
Neut2 ^[55]	Hexane	405	464	3 100	0.54	0.32	76
	Toluene	412	474	3 200	0.89	0.33	-
	Et ₂ O	408	499	4 400	2.57	0.33	-
	CH ₂ Cl ₂	411	576	7 000	3.92	0.13	-
Neut(i)2	Hexane	408	464	2 900	0.54	0.39	103
	Toluene	416	505	4 200	0.47 (8%) 2.11 (92%)	0.38	-
	Et ₂ O	410	534	5 700	5.15	0.37	-
	CH ₂ Cl ₂	413	583	7 100	4.96	0.20	-
Neut3	Hexane	404	463	3 100	0.52	0.39	129
	Toluene	411	504	4 500	1.60	0.38	-
	Et ₂ O	406	530	5 800	4.58	0.35	-
	CH ₂ Cl ₂	413	583	7 100	4.77	0.20	-
Neut4 ^[56]	Hexane	403	462	3 200	0.53	0.31	133
	Toluene	410	472	3 200	-	-	-
	Et ₂ O	407	501	4 600	-	-	-
	CH ₂ Cl ₂	410	572	6 900	-	-	-

The emission spectra of **Neut1**, **Neut2**, **Neut(i)2**, and **Neut3** display positive solvatochromism, which increases with the number of dimethylamino groups and thus reflects the increasing electron-donating effect of the latter. In addition, the fine structure of the emission spectra of **Neut1**, **Neut2**, **Neut(i)2**, and **Neut3** is lost with increasing solvent polarity. The fluorescence quantum yield slightly decreases with increasing solvent polarity and is drastically lowered in CH₂Cl₂, the solvent with the highest polarity tested. Similar findings were reported for donor-acceptor compounds designed to increase the efficiency of blue light emitting OLEDs.^[182-184] From Lippert-Mataga plots containing at least 10 solvents, Ma, Yang, and coworkers obtained not only one linear correlation between the (apparent) Stokes shift and the solvents of low polarity, but a second correlation for solvents of high polarity. In combination with extensive DFT- and TD-DFT calculations, they showed that the experimental results can be explained by a combination of a locally excited (LE) and a CT state in the ground state. The solvent used for the measurement stabilizes the excited states differently and, thus, leads to a dependence of the localization of low-lying HOMOs and higher LUMOs from the polarity of the solvent. Ma, Yang, and coworkers call this phenomenon hybrid localized charge transfer (HLCT). As very similar data were obtained for **Neut1**, **Neut2**, **Neut(i)2**, and **Neut3**, HLCT character of their transitions can be assumed as well.

The natural lifetime τ_0 of **Neut1**, **Neut2**, **Neut(i)2**, and **Neut3** tends to increase with increasing solvent polarity while k_r and k_{nr} tend to decrease (Table 4.3), which was observed for the *mono*-triarylboranes as well (Chapter 3). In contrast, the same values do not change significantly for **Neut0**.

The molar extinction coefficient in hexane increases in the order **Neut0** < **Neut1** \approx **Neut2** < **Neut(i)2** < **Neut3** < **Neut4**^[56] from 66 000 L mol⁻¹ cm⁻¹ over 75 000 L mol⁻¹ cm⁻¹, 76 000 L mol⁻¹ cm⁻¹, 103 000 L mol⁻¹ cm⁻¹, and 129 000 L mol⁻¹ cm⁻¹ to 133 000 L mol⁻¹ cm⁻¹ but no linear correlation with the number of dimethylamino groups is observed. When comparing the absorption and emission spectra of **Neut0**, **Neut1**, **Neut2**, **Neut(i)2**, and **Neut3** in hexane, very similar shape and location is found for the respective spectra (Figure 4.5F), but the molar extinction coefficient increases non-linearly with increasing number of dimethylamino groups.

Table 4.3: Natural lifetimes (τ_0) and the radiative and non-radiative rate constants (k_r , k_{nr}) of **Neut0**, **Neut1**, **Neut2**, **Neut(i)2**, **Neut3**, and **Neut4** in solvents of different polarity.

	Solvent	τ_0 [ns]	k_{nr} [10^9 s $^{-1}$]	k_r [10^9 s $^{-1}$]
Neut0	Hexane	1.68	1.33	0.60
	Toluene	1.60	1.16	0.62
	Et ₂ O	1.76	1.16	0.57
	CH ₂ Cl ₂	1.77	1.25	0.56
Neut1	Hexane	1.42	1.15	0.70
	Toluene	[a]	[a]	[a]
	Et ₂ O	[a]	[a]	[a]
	CH ₂ Cl ₂	[a]	[a]	[a]
Neut2 ^[55]	Hexane	1.69	1.26	0.59
	Toluene	2.70	0.75	0.37
	Et ₂ O	7.79	0.26	0.19
	CH ₂ Cl ₂	30.1	0.22	0.03
Neut(i)2	Hexane	1.38	1.13	0.72
	Toluene	[a]	[a]	[a]
	Et ₂ O	13.9	0.12	0.07
	CH ₂ Cl ₂	24.8	0.16	0.04
Neut3	Hexane	1.33	1.17	0.75
	Toluene	4.21	0.39	0.24
	Et ₂ O	13.1	0.14	0.08
	CH ₂ Cl ₂	21.7	0.16	0.05
Neut4 ^[56]	Hexane	1.71	-	-

[a] Not determined due to multiple fluorescence lifetimes.

4.2.3.2 Cationic *bis*-Triarylboranes

The absorption and emission spectra and the corresponding data of the cationic compounds **Cat**¹⁺-**Cat**³⁺ are summarized in Figure 4.6A-D and Table 4.4, respectively. As solvents, ethanol (dielectric constant: $\epsilon_r = 25 \text{ F m}^{-1}$), acetonitrile ($\epsilon_r = 38 \text{ F m}^{-1}$), and dilutions of 1% acetonitrile in water were chosen, with pure water having a ϵ_r of 80 F m^{-1} .^[166]

The absorption spectra of **Cat**¹⁺, **Cat**²⁺, **Cat(i)**²⁺, and **Cat**³⁺ show no solvatochromic behavior, while for the emission spectra small bathochromic shifts of ca. 520 cm^{-1} , 1060 cm^{-1} , 229 cm^{-1} , and 316 cm^{-1} are observed, respectively, upon increasing the solvent polarity from ethanol to $\leq 1\%$ acetonitrile in water. Thus, the transition processes are not of charge-transfer character. In contrast the orbital overlap parameter Λ , which is obtained from DFT calculations (B3LYP, 6-31G(d,p), gas phase), has values of 0.36, 0.30, and 0.35 for **Cat**¹⁺, **Cat**²⁺, and **Cat**³⁺, respectively. Hence, the corresponding transitions, calculated by TD-DFT calculations (CAM-B3LYP 6-31G(d,p), gas phase), are of charge transfer character. In addition, the calculations indicate the transitions of lowest energy to be from HOMO to LUMO, with the HOMO being located at the bithiophene bridge and the LUMO being located at the most electron-deficient boron moieties **3.2c** and **3.3c** for **Cat**¹⁺, and **Cat**²⁺, **Cat**³⁺, respectively (Table 4.5).

In contrast, the Λ value of **Cat(i)**²⁺ (0.53) is similar to the values obtained for the neutral compounds and, thus, suggests π - π^* nature of the transition. This is due to **Cat(i)**²⁺ having the same electron-deficient triarylborane motif **3.2c** at both sides of the bithiophene bridge. Similar results were reported for **Cat**⁴⁺.^[43] As a result, the calculated absorption spectrum of **Cat(i)**²⁺ (Figure 4.7C) fits the experimental spectrum well, while the corresponding spectra of **Cat**¹⁺, **Cat**²⁺, and **Cat**³⁺ do not fit each other well. Most likely, this is because the counterions of the cationic compounds and the resulting ion-ion interactions were not considered during the calculations. Thus, the resulting values have to be treated with caution and only qualitative statements can be made.

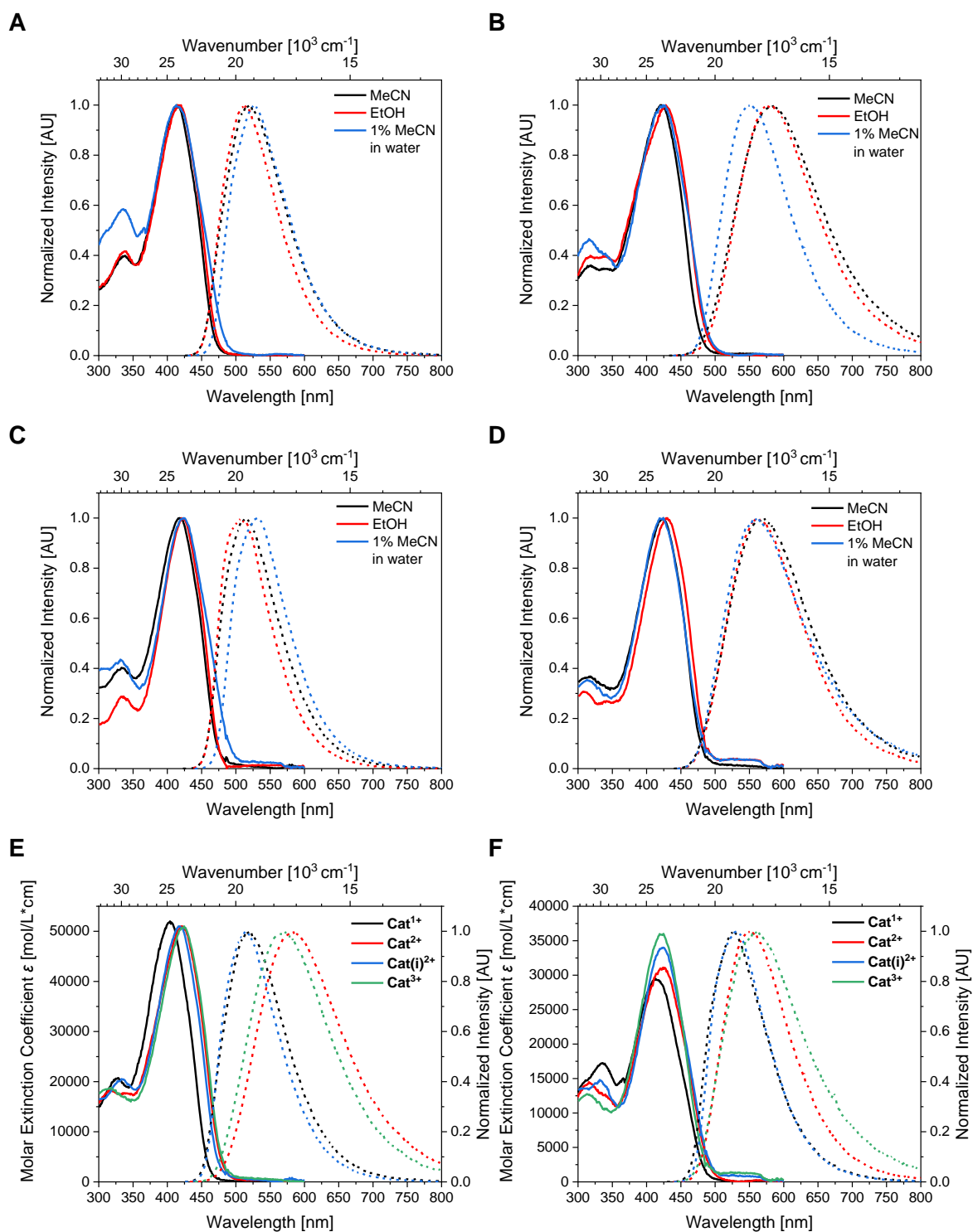
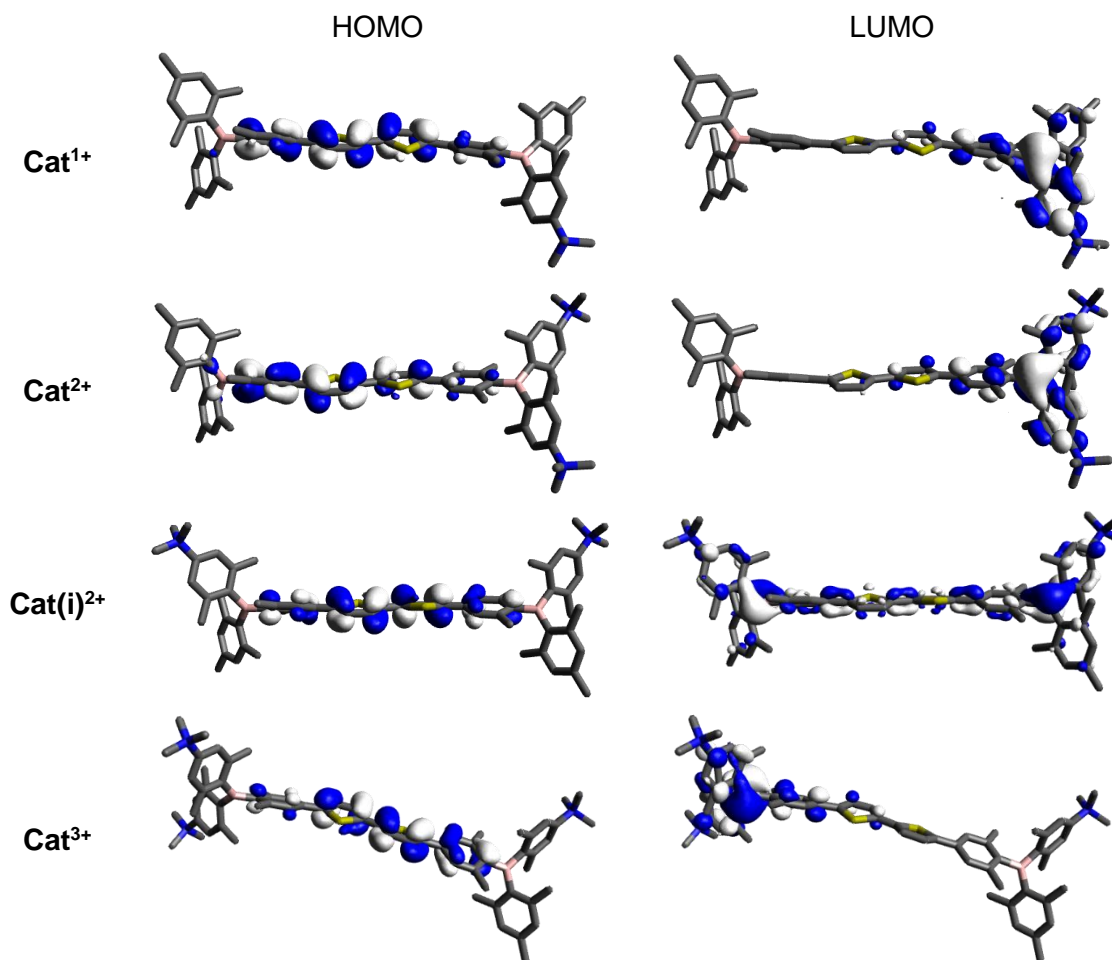


Figure 4.6: Absorption (solid lines) and emission (dotted lines; excitation at λ_{max}^{abs}) spectra of **A**) Cat^{1+} ; **B**) Cat^{2+} ; **C**) $\text{Cat}^{(i)2+}$; **D**) Cat^{3+} ; in solvents of different polarity. Absorption (solid lines) and emission (dotted lines; excitation at λ_{max}^{abs}) spectra of Cat^{1+} , Cat^{2+} , $\text{Cat}^{(i)2+}$, and Cat^{3+} in **E**) acetonitrile and **F**) 1% acetonitrile in water.

Table 4.4: Photophysical data of **Cat**¹⁺, **Cat**²⁺, **Cat(i)**²⁺, **Cat**³⁺, and **Cat**⁴⁺.

	Solvent	λ_{max}^{abs} [nm]	λ_{max}^{fl} [nm]	Apparent Stokes shift [cm ⁻¹]	τ [ns]	Φ_f	ϵ [10 ³ L mol ⁻¹ cm ⁻¹]
Cat ¹⁺	EtOH	417	513	4 500	0.70	0.28	-
	MeCN	414	519	4 900	0.82	0.34	52
	1% MeCN in water	415	527	5 100	0.54 (89%) 1.93 (11%)	0.07	29
Cat ²⁺	EtOH	428	582	6 200	3.09	0.49	-
	MeCN	420	584	6 700	2.98	0.48	51
	1% MeCN in water	424	550	5 400	0.76 (52%) 2.74 (48%)	0.15	31
Cat(i) ²⁺	EtOH	423	509	4 000	0.70	0.35	-
	MeCN	418	515	4 500	0.75	0.35	51
	1% MeCN in water	424	530	4 700	0.63 (89%) 1.79 (11%)	0.15	34
Cat ³⁺	EtOH	431	564	5 500	0.92 (16%) 2.44 (84%)	0.46	-
	MeCN	424	568	6 000	2.41	0.46	51
	1% MeCN in water	423	558	5 700	0.24 (80%) 1.98 (20%)	0.08	36
Cat ⁴⁺ [43]	EtOH	435	545	4 600	-	0.50	-
	MeCN	428	554	5 300	1.9	0.41	51
	water	425	570	6 000	-	0.10	-

Table 4.5: HOMO and LUMO orbitals of **Cat**¹⁺, **Cat**²⁺, **Cat(i)**²⁺, and **Cat**³⁺ obtained from DFT-calculations (B3LYP, 6-31G(d,p), gas phase).



The fluorescent quantum yields of **Cat**¹⁺, **Cat**²⁺, **Cat(i)**²⁺, **Cat**³⁺, and **Cat**⁴⁺ are very similar in ethanol and acetonitrile but significantly lower in aqueous solution. The fluorescence lifetime was found to be biexponential in aqueous solution for **Cat**¹⁺, **Cat**²⁺, **Cat(i)**²⁺, **Cat**³⁺, while no value was reported for **Cat**⁴⁺.^[43] For **Cat**³⁺, in ethanol a biexponential lifetime was found. Thus, no natural lifetimes or radiative and non-radiative rate constants (Table 4.6) were calculated for these solvents and compounds.

The absorption spectra of **Cat**¹⁺, **Cat**²⁺, **Cat(i)**²⁺, and **Cat**³⁺ in acetonitrile (Figure 4.6E) have the same shape and similar wavelengths. In addition, the molar extinction coefficient is almost the same for **Cat**¹⁺, **Cat**²⁺, **Cat(i)**²⁺, **Cat**³⁺, and **Cat**⁴⁺, being ca. 51 000 L mol⁻¹ cm⁻¹. Thus, different numbers of trimethylammonium groups in such *bis*-triarylborane chromophores barely influence the absorption spectra or the molar extinction coefficient. The emission spectra are found to shift bathochromically in the order **Cat(i)**²⁺ ≈ **Cat**¹⁺ << **Cat**⁴⁺ < **Cat**³⁺ < **Cat**²⁺ upon changing the solvent from ethanol to water. This order is not dependent on the number of trimethylammonium groups but on the increasing

dipole moment of the *bis*-triarylboranes, which results from the uneven distribution of electron-deficient and electron-rich boron centers over the molecule. It must be noted that the dipole moment of charged compounds is defined relative to its origin. Thus, it is not an observable quantity.^[185-186] However, the term dipole moment will be used herein to describe the distribution of the electron density over the molecules for convenience. A similar but slightly modified order ($\text{Cat}^{1+} \approx \text{Cat}(\text{i})^{2+} < \text{Cat}^{2+} < \text{Cat}^{3+} < \text{Cat}^{4+}$) is observed for the bathochromic shift (ca. $1\,400\text{ cm}^{-1}$) of the emission spectra of Cat^{1+} , Cat^{2+} , $\text{Cat}(\text{i})^{2+}$, Cat^{3+} , and Cat^{4+} in aqueous solution, with respect to each other. The shape of the absorption and emission spectra in this solvent is very similar for all four compounds. The absorption maxima do not shift significantly while the molar extinction coefficient increases with increasing number of trimethylammonium groups in the order $\text{Cat}^{1+} < \text{Cat}^{2+} < \text{Cat}(\text{i})^{2+} < \text{Cat}^{3+}$ being 29 000, 31 000 L, 34 000, and 36 000 $\text{L mol}^{-1}\text{ cm}^{-1}$, respectively.

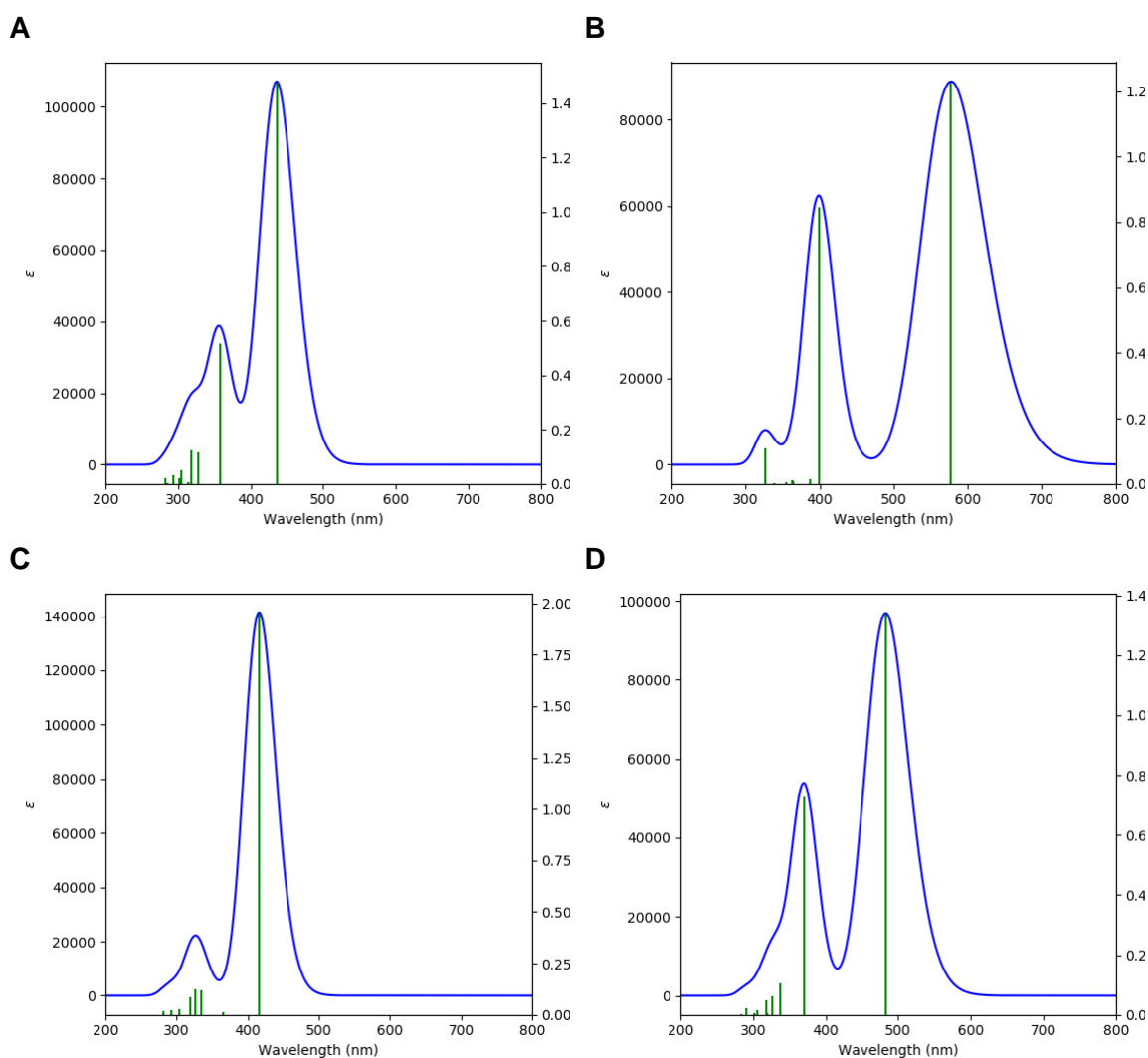


Figure 4.7: Calculated absorption spectra (CAM-B3LYP 6-31G(d,p), gas phase) of **A) Cat^{1+} , B) Cat^{2+} , C) $\text{Cat}(\text{i})^{2+}$, D) Cat^{3+} .**

Table 4.6: Natural lifetimes (τ_0) and the radiative and non-radiative rate constants (k_r , k_{nr}) of **Cat¹⁺**, **Cat²⁺**, **Cat(i)²⁺**, **Cat³⁺**, and **Cat⁴⁺** in solvents of different polarity.

	Solvent	τ_0 [ns]	k_{nr} [10^9 s ⁻¹]	k_r [10^9 s ⁻¹]
Cat¹⁺	Ethanol	2.50	1.03	0.40
	Acetonitrile	2.41	0.80	0.41
	1% MeCN in water	[a]	[a]	[a]
Cat²⁺	Ethanol	6.33	0.16	0.16
	Acetonitrile	6.21	0.17	0.16
	1% MeCN in water	[a]	[a]	[a]
Cat(i)²⁺	Ethanol	2.00	0.93	0.50
	Acetonitrile	2.14	0.87	0.47
	1% MeCN in water	[a]	[a]	[a]
Cat³⁺	Ethanol	[a]	[a]	[a]
	Acetonitrile	5.24	3.83	0.33
	1% MeCN in water	[a]	[a]	[a]
Cat⁴⁺ [43]	Acetonitrile	4.6	0.31	0.21

[a] Not determined due to multiple fluorescence lifetimes.

4.2.4 Electrochemical Properties

4.2.4.1 Neutral *bis*-Triarylboranes

Cyclic voltammograms of the neutral *bis*-triarylboranes **Neut0**, **Neut1**, **Neut2**, **Neut(i)2**, **Neut3**, and **Neut4** were recorded in THF with [*n*Bu₄N][PF₆] as the electrolyte and with a scan rate of 250 mV s⁻¹ to examine the influence of different numbers of dimethylamino groups on their reduction and oxidation potentials. THF (ca. -3.5 V to +0.6 V)^[187] was chosen as the solvent due to the lower solubility of **Neut0**, **Neut1**, **Neut2**, **Neut(i)2**, **Neut3**, and **Neut4** in acetonitrile and the positively shifted CV window of the latter (ca. -3 V to +1.5 V).^[188] The spectra are shown in Figure 4.8 and the resulting potentials are summarized in Table 4.7.

The cyclic voltammograms show one irreversible reduction potential at -2.95 V, -3.03 V, -2.96 V, -3.09 V, -3.11 V, and -3.03 V and one reversible reduction at -2.31 V, -2.34 V, -2.33 V, -2.39 V, -2.40 V, and -2.40 V for **Neut0**, **Neut1**, **Neut2**, **Neut(i)2**, **Neut3**, and **Neut4**, respectively. Peak-to-peak splitting analyses in comparison with the internal standard Fc/Fc⁺ showed each reversible process to be a one electron process. As the reduction potentials of **Neut0**, **Neut1**, **Neut2**, **Neut(i)2**, **Neut3**, and **Neut4** are very similar, the reduction of a boron atom in such neutral *bis*-triarylboranes is independent of the number or distribution of dimethylamino groups. For **Neut1**, **Neut2**, **Neut(i)2**, **Neut3**, and **Neut4**, an irreversible 1e⁻ oxidation potential at 0.39 V, 0.32 V, 0.34 V, 0.40 V, and 0.32 V was observed, while for **Neut0**, no oxidation was observed within the solvent window. For **Neut3**, a second irreversible oxidation potential was found at 0.49 V. Each oxidation potential can be interpreted as the removal of one electron from the non-bonding orbital of one nitrogen atom. Thus, the voltage required for reversible oxidation are very similar for these five *bis*-triarylboranes. The oxidation of the bithiophene moiety was not observed for any of the compounds as higher voltages would have been required which would have oxidized THF as well.^[187]

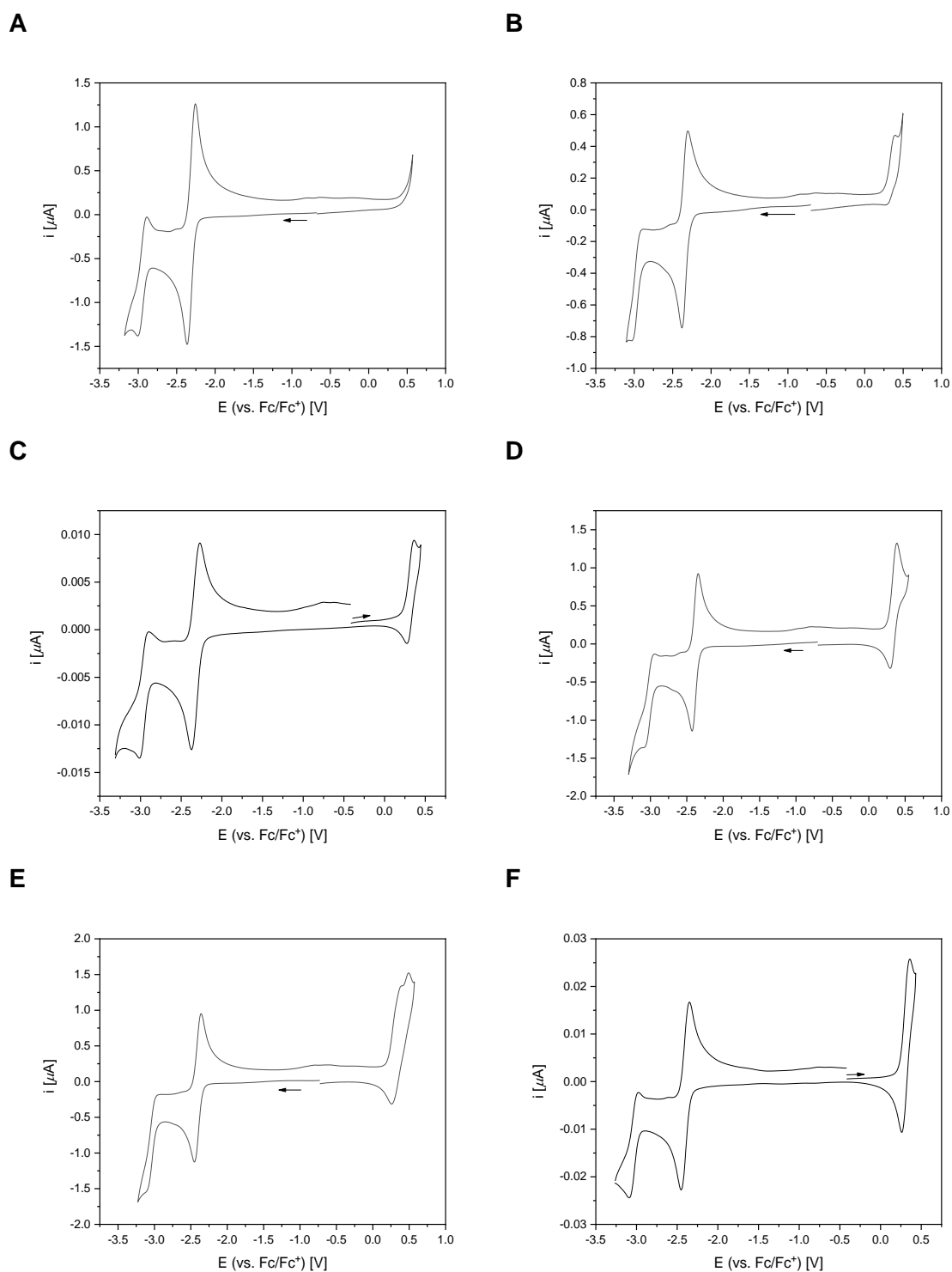


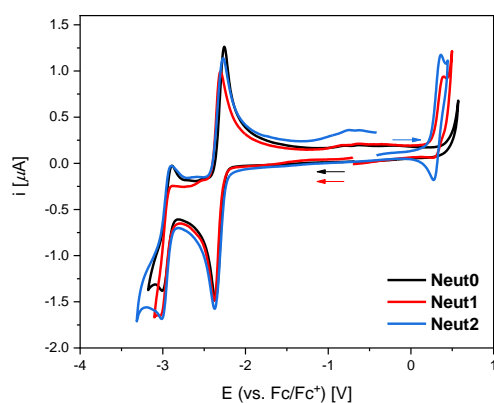
Figure 4.8: Cyclic voltammograms of **A) Neut0**, **B) Neut1**, **C) Neut2**, **D) Neut(i)2**, **E) Neut3**, and **F) Neut4** measured in THF vs. Fc/Fc⁺ (scan rate: 250 mV s⁻¹).

Table 4.7: Electrochemical potentials of **Neut0**, **Neut1**, **Neut2**, **Neut(i)2**, **Neut3**, **Neut4**, **3.1a**, **3.2a**, and **3.3a** determined in THF.

	$E_{1/2}$ (red1) [V]	$E_{1/2}$ (red2) [V]	$E_{1/2}$ (ox1) [V]	$E_{1/2}$ (ox2) [V]
Neut0	-2.31	-2.95 (irrev.)		
Neut1	-2.34	-3.03 (irrev.)	0.39 (irrev.)	
Neut2	-2.33	-2.96 (irrev.)	0.32 (irrev.)	
Neut(i)2	-2.39	-3.09 (irrev.)	0.34 (irrev.)	
Neut3	-2.40	-3.11 (irrev.)	0.40 (irrev.)	0.49 (irrev.)
Neut4	-2.40	-3.03 (irrev.)	0.32 (irrev.)	
3.1a	-2.67			
3.2a	-2.78		0.34	
3.3a	-2.86		0.28	0.51 (irrev.)

Comparison of the reduction potentials of **Neut0**, **Neut1**, **Neut2**, **Neut(i)2**, **Neut3**, and **Neut4** and the *mono*-triarylboranes **3.1a**, **3.2a**, and **3.3a** (Table 4.7; Chapter 3) reveals an increase of the potential of the latter upon connection *via* a bithiophene bridge. Hence, the electron density at the boron center of such *bis*-triarylboranes is lower than in the *mono*-triarylboranes while the oxidation potentials of the amines is barely influenced.

A



B

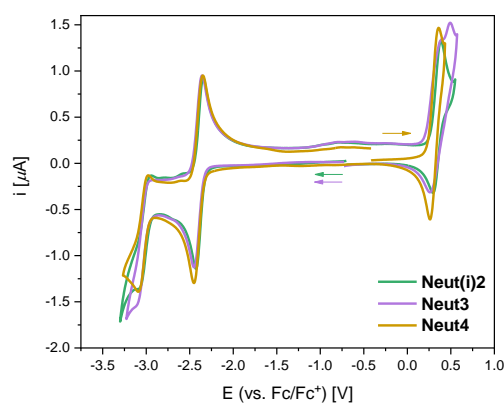


Figure 4.9: Comparison of cyclic voltammograms of **A) Neut0**, **Neut1**, **Neut2**, and **B) Neut(i)2**, **Neut3**, **Neut4** measured in THF vs. Fc/Fc^+ (scan rate: 250 mV s^{-1}).

Comparison of the CV spectra of **Neut0**, **Neut1**, and **Neut2** (Figure 4.9A) reveals almost identical shapes and positions of the reduction waves while the amplitude of the oxidation waves increases with increasing number of dimethylamino groups. In contrast, the shape

and position of **Neut(i)2**, **Neut3**, and **Neut4** (Figure 4.9B) is almost identical for reduction and oxidation.

4.2.4.2 Cationic *bis*-Triarylboranes

Cyclic voltammograms of the cationic *bis*-triarylboranes **Cat**¹⁺, **Cat**²⁺, **Cat(i)**²⁺, and **Cat**³⁺ were recorded in acetonitrile with [nBu₄N][PF₆] as the electrolyte and a scan rate of 250 mV s⁻¹ to examine the influence of different numbers of trimethylammonium groups on the reduction and oxidation potentials. Acetonitrile was chosen as the solvent as the cationic compounds are insoluble in THF. The spectra are shown in Figure 4.10 and the resulting potentials are summarized in Table 4.8.

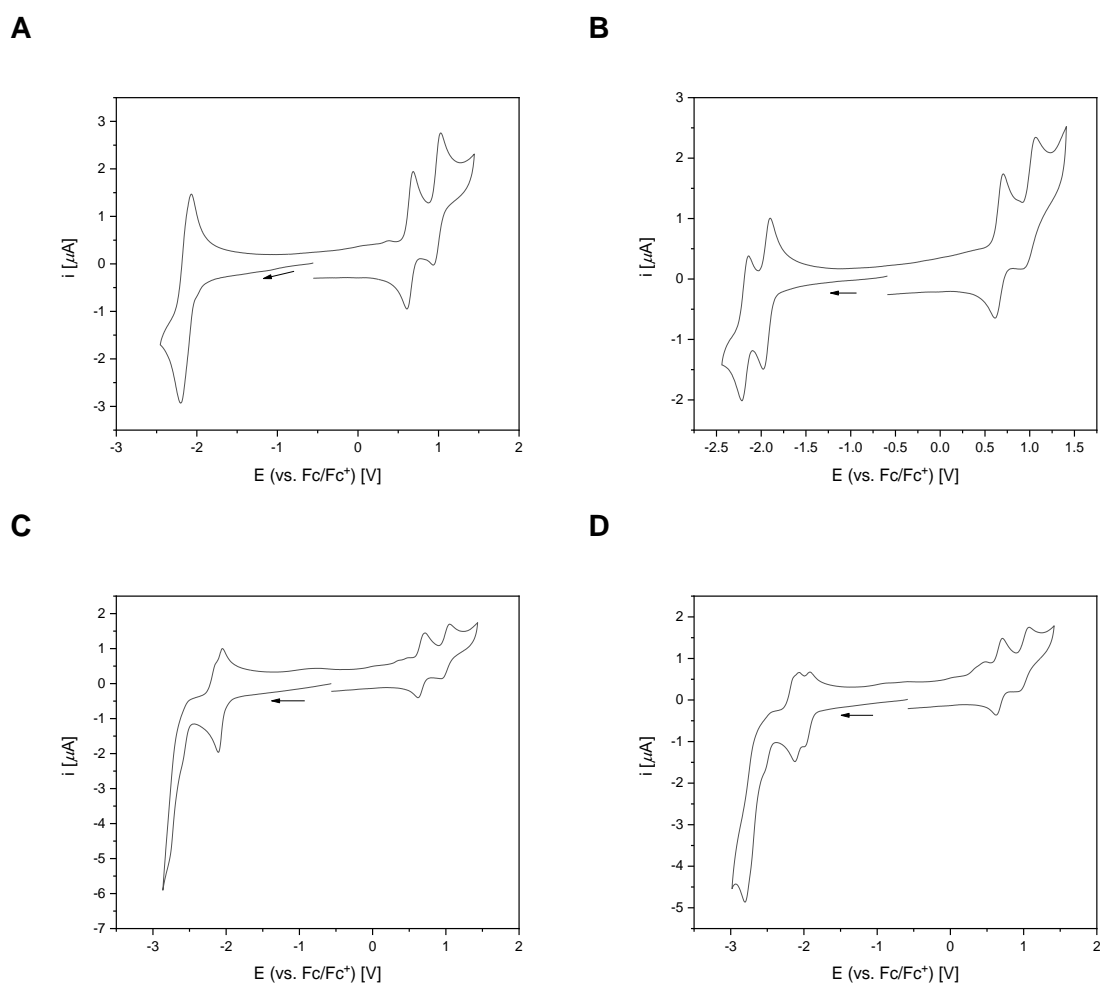


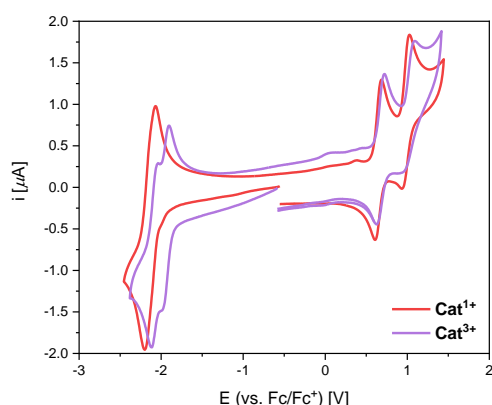
Figure 4.10: Cyclic voltammograms of **A) Cat**¹⁺, **B) Cat**²⁺, **C) Cat(i)**²⁺, and **D) Cat**³⁺ measured in MeCN vs. Fc/Fc⁺ (scan rate: 250 mV s⁻¹).

Table 4.8: Electrochemical potentials of **Cat**¹⁺-**Cat**⁴⁺ determined in MeCN.

MeCN	$E_{1/2}$ (red1) [V]	$E_{1/2}$ (red2) [V]	$E_{1/2}$ (red3) [V]	$E_{1/2}$ (ox1) [V]	$E_{1/2}$ (ox2) [V]
Cat ¹⁺	-2.13			0.64	0.98
Cat ²⁺	-1.94	-2.18		0.66	0.99
Cat(i) ²⁺	-2.07	-2.76 (irrev.)		0.66	0.98
Cat ³⁺	-1.94	-2.07	-2.80 (irrev.)	0.67	1.01
Cat ⁴⁺ ^[13]	-1.93	-2.78 (irrev.)		0.68	1.10
3.2c	-2.24				
3.3c ^[170]	-2.02				

For the cationic *bis*-triarylboranes **Cat**¹⁺, **Cat**²⁺, **Cat(i)**²⁺, and **Cat**³⁺, two reversible 1e⁻ oxidation potentials at 0.64 V, 0.66 V, 0.66 V, 0.67 V and at 0.98 V, 0.99 V, 0.98 V, 1.01 V were obtained, respectively. These oxidation potentials are higher than those observed for the neutral compounds and reflect the oxidation of the bithiophene moiety. For the same compounds, a reversible 1e⁻ reduction potential was found at -2.13 V, -1.94 V, -2.07 V, and -1.94 V, respectively. For **Cat**²⁺ and **Cat**³⁺, a second reversible reduction potential at -2.18 V and -2.07 V was determined, while the second reduction potential of **Cat(i)**²⁺ and the third of **Cat**³⁺ at -2.76 V and -2.80 V, respectively, were found to be irreversible. These values are ca. 0.3-0.5 V higher than those of the corresponding neutral compounds.

A



B

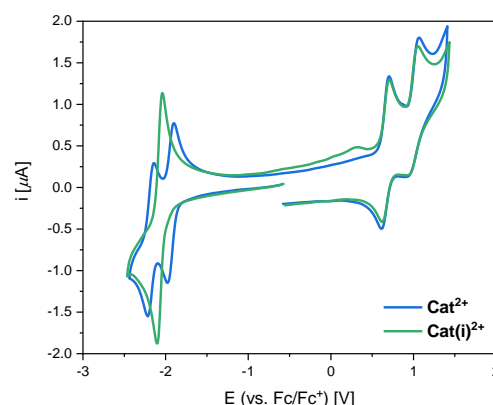


Figure 4.11: Comparison of cyclic voltammograms of **A) Cat**¹⁺ and **Cat**³⁺ and **B) Cat**²⁺ and **Cat(i)**²⁺ measured in MeCN vs. Fc/Fc⁺.

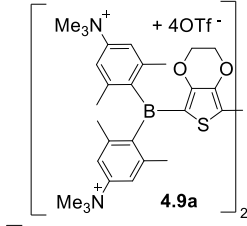
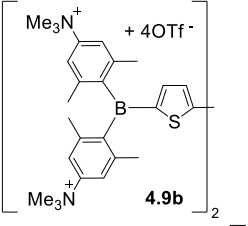
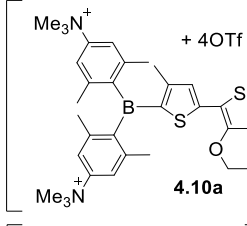
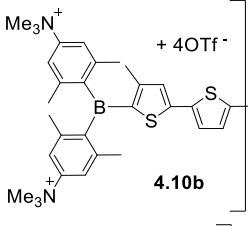
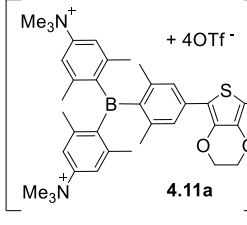
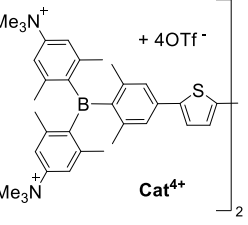
Comparison of the oxidation potentials of all cationic compounds (Figure 4.11) reveals the same shape and location for all four compounds. In contrast, the reduction wave of **Cat(i)**²⁺ is sharp while that of **Cat**¹⁺ is slightly broader and for **Cat**²⁺ and **Cat**³⁺, two reduction waves

are observed. When comparing the location of the corresponding reduction potentials, the same value of -2.07 V is found for **Cat(i)**²⁺ and for **Cat**³⁺. Thus, this value likely reflects the reduction of the **3.2c** moiety present in both systems. Hence, the second reduction potential of **Cat**³⁺ at -1.94 V for the **3.3c** moiety is expected to be found for **Cat**²⁺ as well. Indeed, **Cat**²⁺ has one reduction potential at -1.94 V and a second at -2.18 V which might be the reduction potentials of **3.3c** and **3.1a**, respectively. Assuming the reduction potentials of **3.1a** and **3.2c** bound to a bithiophene bridge are -2.18 V and -2.07 V, respectively, **Cat**¹⁺ is expected to display a split reduction wave with potentials at these values, but only one reduction potential of -2.13 V is found. However, the difference between the expected values is 0.11 V and the width of all recorded waves is 0.1 V. Thus, the expected splitting of **Cat**¹⁺ cannot be resolved with the experimental settings and leads to a broadening of the reduction wave of **Cat**¹⁺ instead. It was not possible to improve the resolution of this wave by pulse voltammetry experiments (Figure 11.12D).

In summary, reduction potentials of -2.18 V, -2.07 V, and -1.94 V were found for the triarylborane motifs **3.1a**, **3.2c**, and **3.3c** bound to a bithiophene moiety while values of -2.67 V (in THF), -2.24 V, and -2.02 V^[170] were found for the *mono*-triarylboranes, respectively. Comparison of these values reveals an increase of the reduction potential upon connecting two triarylboranes *via* a bithiophene bridge, thus indicating a lower electron-density at the boron centers of the *bis*-triarylboranes compared to the *mono*-triarylboranes.

Very recently, the electrochemical data of **Cat**⁴⁺ were reported to be very similar to the values expected from the measurements of the selectively charged compounds investigated herein (Table 4.8).^[13] Thus, the present study shows that different numbers of trimethylammonium groups or their distribution over a *bis*-triarylborane chromophore do not significantly influence the reduction potentials as they are predominantly influenced by the electronic situation at the boron center. If this situation is changed, the reduction potentials of *bis*-triarylboranes increase by ca. 0.45 V when replacing the xylene moiety of **Cat**⁴⁺ by an unsubstituted thiophene moiety in **4.9b**, as demonstrated by Ferger (Table 4.9).^[13]

Table 4.9: Compounds and corresponding reduction potentials reported by Ferger.^[13]

$E_{1/2}(\text{red1})$ [V]		$E_{1/2}(\text{red1})$ [V]	
	-1.59		-1.46
	-1.78		-1.71
	-1.97		-1.92

4.2.5 HOMO-LUMO Gaps

Analogously to the investigation of the HOMO-LUMO gaps of *mono*-triarylboranes shown in Chapter 3, the HOMO-LUMO gaps of the neutral and cationic triarylboranes **Neut0**, **Neut1**, **Neut2**, **Neut(i)2**, **Neut3**, and **Neut4** and **Cat¹⁺**, **Cat²⁺**, **Cat(i)²⁺**, **Cat³⁺**, and **Cat⁴⁺** were examined by DFT calculations (ΔE_{calc}), absorption spectra (ΔE_{opt})^[175] and cyclic voltammograms (ΔE_{CV})^[171-174] according to literature procedures. As shown in Equation 3.5, the onset energy of the absorption spectrum was used for the calculation of ΔE_{CV} in case no oxidation potential was obtained. The results are summarized in Table 4.10.

The HOMO-LUMO gap of **Neut0**, **Neut1**, **Neut2**, **Neut(i)2**, **Neut3**, and **Neut4** determined from absorption or CV spectra is very similar for all compounds and do not show any significant changes while ΔE_{calc} is slightly higher than the experimental values. The experimental values obtained for **Cat¹⁺**, **Cat²⁺**, **Cat(i)²⁺**, **Cat³⁺**, and **Cat⁴⁺** are very similar to each other and to the values obtained for the neutral compounds but the calculated HOMO-LUMO gaps are significantly lower, especially for **Cat²⁺** and **Cat³⁺**. Most likely, this results from underestimated ion-ion interactions which take place in solutions but were not taken into account during the calculations as only the cationic compound without its anionic counterion was included. Thus, ΔE_{calc} of **Cat¹⁺**, **Cat²⁺**, **Cat(i)²⁺**, and **Cat³⁺** must be treated with caution.

Table 4.10: Comparison of HOMO-LUMO gap energies obtained from DFT calculations (ΔE_{calc} ; B3LYP, 6-31G(d,p), gas phase), absorption (ΔE_{opt}) and CV (ΔE_{CV}) measurements.

	ΔE_{calc} [eV]	ΔE_{opt} [eV]	ΔE_{CV} [eV]
Neut0	3.01	2.65	
Neut1	2.99	2.65	2.73
Neut2	2.99	2.67	2.65
Neut(i)2	3.07	2.66	2.73
Neut3	3.07	2.66	2.80
Neut4	3.10	- [a]	2.72
Cat¹⁺	2.09	2.62	2.77
Cat²⁺	1.32	2.56	2.60
Cat(i)²⁺	2.58	2.58	2.73
Cat³⁺	1.83	2.56	2.61
Cat⁴⁺	- [b]	2.55 [c]	2.60
3.1a	4.34	3.49	
3.2a	3.66	2.92	3.12
3.3a	3.63	2.92	3.14
3.2c	3.87	3.42	
3.3c	3.72	3.47	

[a] No data were reported for this compound.^[43] [b] Different basis set was used for calculations in the literature.^[43] [c] Calculated from absorption spectra reported in the literature.^[43]

In summary, no dependency of the HOMO-LUMO gap of such *bis*-triarylborane compounds on the number or distribution of dimethylamino- and trimethylammonium groups over the chromophore was found. However, in comparison with the values of the HOMO-LUMO gaps found for the *mono*-triarylboranes, a significant decrease of the gap by ca. 0.3 – 0.9 eV is observed.

4.2.6 Singlet Oxygen Sensitization

The singlet oxygen sensitization efficiency Φ_{Δ} of **Cat**¹⁺, **Cat**²⁺, **Cat(i)**²⁺, and **Cat**³⁺ was determined by fluorescence spectroscopy between ca. 1230 nm and 1330 nm in acetonitrile solutions relative to perinaphthenone (Figure 4.12), which is known to sensitize singlet oxygen with an efficiency of 1.^[180] The signal-to-noise ratio of all recorded spectra is limited due to the small radiative rate constant ($k_r = 0.45 \text{ s}^{-1}$) of singlet oxygen in acetonitrile.^[181] Therefore, all values given have an estimated error of ± 0.1 .

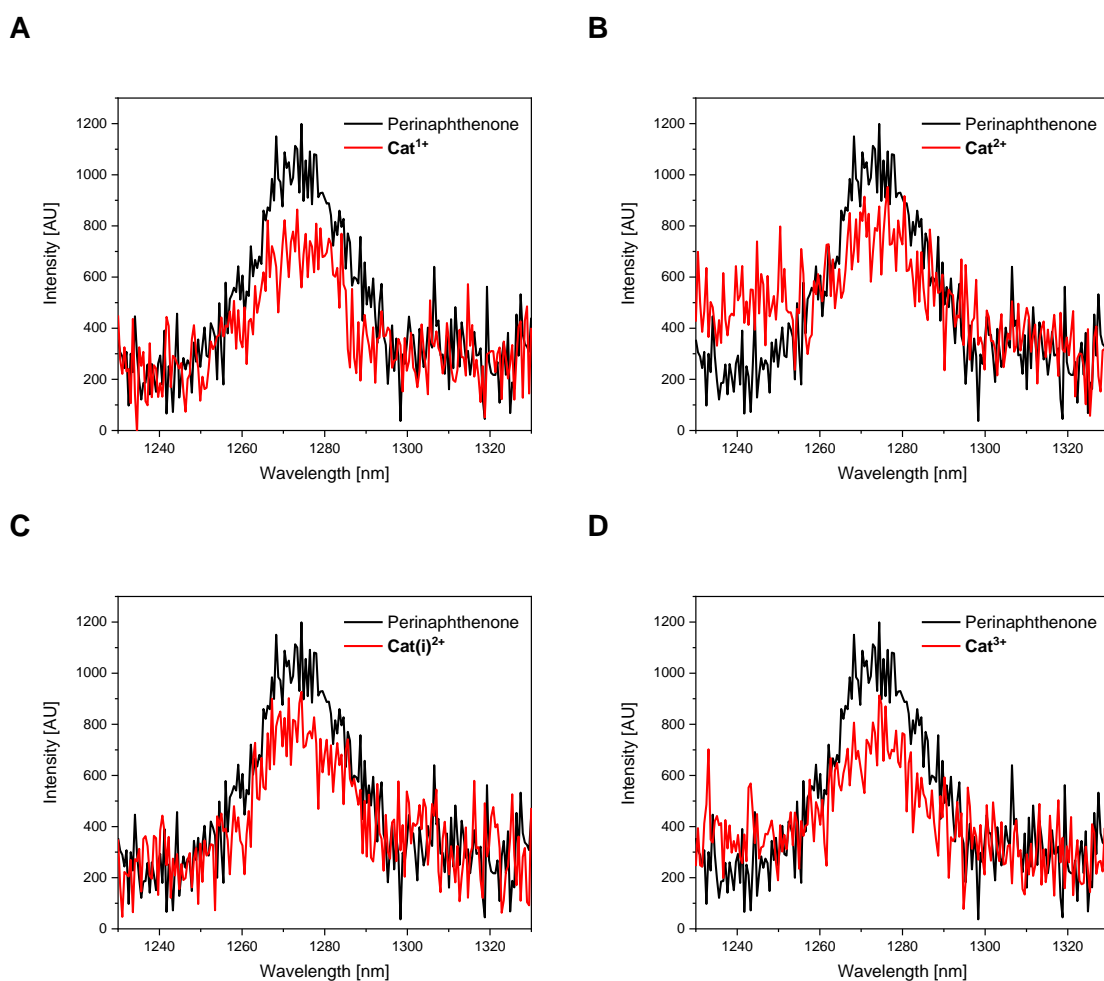


Figure 4.12: Emission spectra of **A) Cat**¹⁺, **B) Cat**²⁺, **C) Cat(i)**²⁺, and **D) Cat**³⁺ relative to perinaphthenone determined in acetonitrile.

From these measurements, singlet oxygen sensitization efficiencies of 0.6, 0.8, 0.7, and 0.6 was determined for **Cat**¹⁺, **Cat**²⁺, **Cat(i)**²⁺, and **Cat**³⁺, respectively (Table 4.11). As the emission spectrum of **Cat**²⁺ tails into the region monitored (Figure 11.16 and between 1230 and 1260 nm in Figure 4.12B), the corresponding efficiency is overestimated. In the case of **Cat**³⁺, an insignificant tailing of the emission spectrum is observed (Figure 11.16 and between 1230 and 1260 nm in Figure 4.12D), which can be considered minor, taking the general error of the measurement into account. Thus, Φ_{Δ} is assumed to be ca. 0.6 for

Cat¹⁺, **Cat²⁺**, **Cat(i)²⁺**, and **Cat³⁺**. The same value was reported very recently for **Cat⁴⁺**.^[13] Hence, the singlet oxygen sensitization efficiency for bithiophene bridged, *bis*-triarylborane chromophores does not change significantly with the number or distribution of trimethylammonium groups. In contrast, the efficiency obtained for the *mono*-triarylboranes **3.1a**, **3.2c**, and **3.3c** (Chapter 3) increases from 0.3 to 0.5 and 0.6 with increasing number of trimethylammonium groups while the corresponding fluorescence quantum yields (Φ_f) decrease from 0.34 to 0.11 and 0.10, respectively. Thus, 30-40% of the excited states of the *mono*-triarylboranes decay by processes other than fluorescence or inter system crossing (ISC). This is not observed for **Cat¹⁺**, **Cat²⁺**, **Cat(i)²⁺**, **Cat³⁺**, and **Cat⁴⁺** for which $\Phi_\Delta = 0.6$ and $\Phi_f \approx 0.4$ (Table 4.11). Hence, it is suggested that 40% of the excited singlet states of these *bis*-triarylboranes decay *via* fluorescence while the remaining 60% undergo ISC to a dark triplet state from which interaction with ³O₂ results in the formation of ¹O₂.

Table 4.11: Singlet oxygen sensitization efficiencies relative to perinaphthenone and fluorescence quantum yields of **Cat¹⁺**, **Cat²⁺**, **Cat(i)²⁺**, **Cat³⁺**, and **Cat⁴⁺** in acetonitrile.

	Φ_Δ	Φ_f
Cat¹⁺	0.6	0.34
Cat²⁺	0.8 ^[a]	0.48
Cat(i)²⁺	0.7	0.35
Cat³⁺	0.6 ^[a]	0.46
Cat⁴⁺	0.6 ^[13]	0.41 ^[43]

[a] Values obtained from singlet oxygen sensitizing measurements overestimate the actual value of the respective compound due to tailing of the respective emission spectrum of the compound between 1230 nm and 1330 nm.

As outlined in Chapter 3, singlet oxygen sensitization was rarely reported for (tri)arylborane compounds or the efficiency was attributed to other moieties such as phosphine, polycyclic hydrocarbon (PAH), or porphyrin.^[176-178] For thiophene containing compounds **4.12a** and **4.13a** (Figure 4.13), singlet oxygen sensitization efficiencies of 0.14^[189] and 0.63^[190] were reported, respectively. The efficiency of **4.12a** was reported to increase to 0.54 upon introduction of arsenic to the backbone of the polymer (**4.12b**) due to the heavy atom effect and the resulting improvement of ISC.^[189] The same explanation was used for the lower efficiency of **4.13b** compared to **4.13a** due to missing bromine.^[190] The fluorescence quantum yield of **4.13a** was reported to be 0.03 in CH₂Cl₂ which indicates a less efficient radiative decay of the excited states than observed for **Cat¹⁺**, **Cat²⁺**, **Cat(i)²⁺**, **Cat³⁺**, and

Cat⁴⁺. Thus, the cationic *bis*-triarylboranes reported herein are highly efficient singlet oxygen sensitizing compounds which might be interesting for anti-proliferate applications.

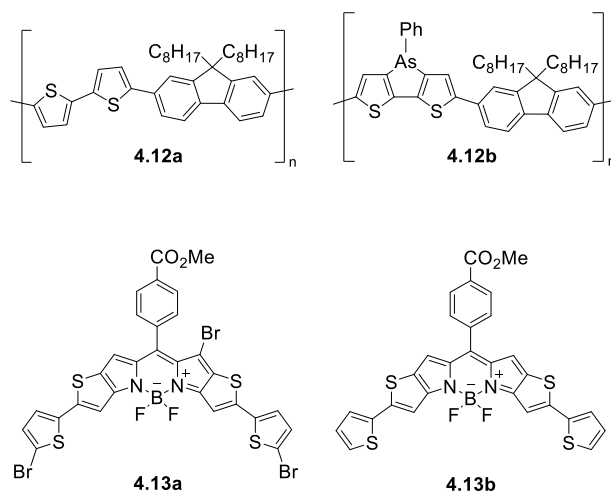


Figure 4.13: Molecular structures of **4.12**^[190] and **4.13**.^[189]

4.3 Conclusions

To examine the influence of different numbers and distributions of dimethylamino- and trimethylammonium groups on selected properties of bithiophene-bridged *bis*-triarylboranes, **Neut1**, **Neut2**, **Neut(i)2**, and **Neut3** and the resulting cationic compounds **Cat¹⁺**, **Cat²⁺**, **Cat(i)²⁺**, and **Cat³⁺** were synthesized. For the synthesis of the unsymmetrically-substituted precursors **Neut1**, **Neut2**, and **Neut3**, different halogenation strategies of intermediates **4.2**, **4.5**, and **4.7** had to be pursued due to the amine substituent. Thus, **4.5** and **4.7** were halogenated *via* lithiation and subsequent addition of I₂ whereas **4.2** was brominated with NBS. The selectively charged compounds **Cat¹⁺**, **Cat²⁺**, **Cat(i)²⁺**, and **Cat³⁺** were obtained in good to excellent yields of ca. 50-90%.

The absorption spectra of **Neut0**, **Neut1**, **Neut2**, **Neut(i)2**, **Neut3**, and **Neut4**^[56] display no solvatochromism and are very similar for the different compounds dissolved in the same solvent. In contrast, the corresponding emission spectra shift bathochromically with increasing solvent polarity. The apparent Stokes shift increases with increasing number of dimethylamino groups. The same is true for the molar extinction coefficient, which increases non-linearly from 66 000 L mol⁻¹ cm⁻¹ to 133 000 L mol⁻¹ cm⁻¹ in the order **Neut0** < **Neut1** < **Neut2** < **Neut(i)2** < **Neut3** < **Neut4**. TD-DFT calculations demonstrated the transition of lowest energy to be of π-π* nature with the HOMOs and LUMOs involved being located at the bridging unit between the two boron centers and the LUMO being extended to the most electron-deficient boron center.

For **Cat**¹⁺, **Cat**²⁺, **Cat(i)**²⁺, **Cat**³⁺, and **Cat**⁴⁺, the absorption spectra display no solvatochromism and the emission spectra only weak solvatochromic behavior. When comparing the emission spectra of **Cat**¹⁺, **Cat**²⁺, **Cat(i)**²⁺, **Cat**³⁺, and **Cat**⁴⁺ dissolved in the same solvent, a bathochromic shift with increasing dipole moment of the *bis*-triarylboranes is observed but the order is slightly different in acetonitrile (**Cat(i)**²⁺ \approx **Cat**¹⁺ \ll **Cat**⁴⁺ [43] $<$ **Cat**³⁺ $<$ **Cat**²⁺) and aqueous solutions (**Cat**¹⁺ \approx **Cat(i)**²⁺ $<$ **Cat**²⁺ $<$ **Cat**³⁺ $<$ **Cat**⁴⁺ [43]). Similarly to what was observed for the *mono*-triarylboranes, the molar extinction coefficient is almost independent of the number of trimethylammonium groups in acetonitrile solutions but increases slightly by ca. 2 000 L mol⁻¹ cm⁻¹ with increasing number of cationic charges in aqueous solution.

Hence, the number and distribution of trimethylamino- or trimethylammonium groups in *bis*-triarylborane chromophores influence the photophysical properties. In contrast, the singlet oxygen sensitizing efficiency of the cationic *bis*-triarylboranes is ca. 0.6, irrespective of the number or distribution of the trimethylammonium groups. In combination with their quantum yields of ca. 0.4, the excited states of **Cat**¹⁺, **Cat**²⁺, **Cat(i)**²⁺, and **Cat**³⁺ are demonstrated to decay highly efficiently by a combination of fluorescence and singlet oxygen sensitization.

For each of the neutral *bis*-triarylboranes, one reversible and one irreversible reduction potential was found, which are very similar to each other and, thus, are independent of the number of dimethylamino groups. In addition, for compounds containing a dimethylamino group, at least one irreversible oxidation was found. Comparing these values with the potentials obtained for the *mono*-triarylboranes **3.1a**, **3.2a**, and **3.3a**, an increase by ca. 0.3-0.5 V is observed. The same phenomenon is observed when comparing the values of **3.2c** and **3.3c** with the reduction potentials of **Cat**¹⁺, **Cat**²⁺, **Cat(i)**²⁺, and **Cat**³⁺ from which distinct values for each triarylborane moiety were obtained. In combination with literature values it is shown that the electronic situation of each boron center influences the reduction potential of cationic *bis*-triarylboranes more than number or distribution of trimethylammonium groups.

The HOMO-LUMO gaps obtained from absorption spectra and CV spectra are very similar for all neutral and cationic *bis*-triarylboranes examined. While for **Neut0**, **Neut1**, **Neut2**, **Neut(i)2**, **Neut3**, and **Neut4**, the calculated HOMO-LUMO gaps resemble the experimental values, for the cationic compounds, the calculated values must be treated with caution as ion-ion interactions were not taken into account. However, the HOMO-LUMO gap of bithiophene-bridged, *bis*-triarylborane compounds is shown to be independent of the number or distribution of dimethylamino- or trimethylammonium groups

over the chromophore and increases by ca. 0.3-0.9 eV compared to the *mono*-triarylboranes.

Although **Cat**¹⁺, **Cat**²⁺, **Cat(i)**²⁺, and **Cat**³⁺ are not soluble in pure water, concentrated acetonitrile solutions thereof can be diluted with water until the solution contains ≤1% acetonitrile. By exchanging acetonitrile with DMSO, the interactions of **Cat**¹⁺, **Cat**²⁺, **Cat(i)**²⁺, and **Cat**³⁺ with cells or with biomacromolecules, such as DNA and RNA, was investigated in aqueous solutions, as summarized in Chapter 6. The cationic *bis*-triarylboranes might be applicable as light-induced anti-proliferative drugs due to their high singlet oxygen sensitization efficiencies.

CHAPTER 5

APPLICATIONS OF TRIARYLBORANE MATERIALS IN
CELL IMAGING AND SENSING OF BIO-RELEVANT
MOLECULES SUCH AS DNA, RNA, AND PROTEINS

5 Applications of Triarylborane Materials in Cell Imaging and Sensing of Bio-relevant Molecules such as DNA, RNA, and Proteins

The following chapter is slightly modified and reproduced from *Mater. Horiz.* **2021**^[191] with permission from The Royal Society of Chemistry.

5.1 Introduction

For more than 100 years, many different types of organoboron compounds have been synthesized and their potential for applications in various fields^[18-19, 21] such as anion sensors,^[29-30, 34, 192-193] light emitting layers in organic light-emitting devices (OLEDs)^[27, 194] and electron conducting layers in organic solar cells has been clearly demonstrated.^[26, 28, 195] Some types of organoboron compounds, especially boronic acids, have also been investigated for biological applications such as bioimaging agents,^[32, 35-49, 51-52, 196] or anti-cancer drugs.^[197-198] However, for applications as anion sensors and bioimaging and sensing agents, organoboron compounds must be air- and moisture-stable. Therefore, their empty boron p-orbital in 3-coordinate boron compounds, which makes them good Lewis acids and susceptible to B–C bond hydrolysis, has to be stabilized. In addition, these compounds should be highly luminescent so that their localization in tissues or in specific cell organelles can be visualized by, *e. g.*, confocal fluorescence microscopy for imaging purposes. For sensing, upon interaction with the molecule to be detected, a change in emission is required. This can include a quenching of the emission, known as a ‘turn-off’ sensor, or a significant change in the emission wavelength. If compounds which are not inherently emissive are used, they should respond to a biological trigger resulting in a luminescence signal, which is known as a ‘turn-on’ sensor. In addition, it is useful to employ compounds which have large two-photon absorption cross-sections (σ_2) which allow the use of lower energy near infrared (NIR) excitation. As biological systems are relatively transparent in the NIR region of the spectrum, such systems provide deeper tissue penetration and lower background emission from biomolecules. This approach also provides a higher degree of 3D spatial resolution as the simultaneous absorption of two lower energy photons is proportional to the square of the excitation light intensity, which in turn is proportional to the square of the distance from the focal plane.

Several strategies have been developed to stabilize boron compounds for applications in aqueous media. One possibility is to bind a Lewis base to the empty p-orbital which results in 4-coordinate boron-containing compounds, for example, boranophosphates (**5.1**, Figure 5.1), 4-bora-3 α ,4 α -diazas-indacene cored compounds (BODIPYs, **5.2**) or amine-boranes (**5.3**). Boranophosphates have been synthesized as mimics of nucleotides, DNA, and RNA

and their biological activity has been investigated as summarized by Shaw *et al.*^[197] Furthermore, some derivatives of amine-boranes have shown potential application as anticancer agents.^[198] In addition to the possible applications of BODIPYs in OLEDs,^[194, 199-201] their biological applicability has been investigated more recently, especially as compounds for positron emission tomography (PET),^[202] as fluorescence indicators^[203] and, more generally, in medical diagnostics and treatment.^[204-205]

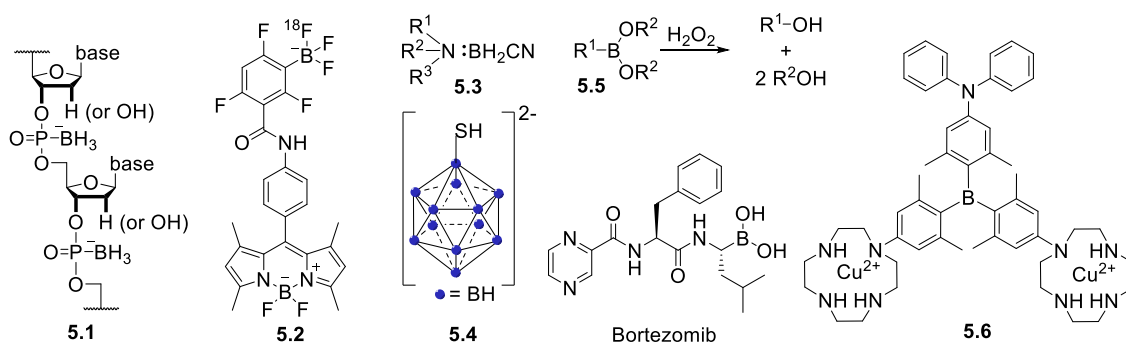


Figure 5.1: Exemplary structures of boranophosphates (**5.1**),^[197] BODIPYs (**5.2**),^[202] amine-boranes (**5.3**),^[198] boron clusters (**5.4**),^[206] boronic acids and esters (**5.5**) and their reaction with hydrogen peroxide (H₂O₂),^[1] and triarylboranes (**5.6**)^[21] investigated for their potential in biological applications.

Another set of air- and moisture-stable boron compounds are polyhedral clusters (**5.4**). For more than 30 years, different clusters have been attached to various natural compounds such as nucleosides, peptides, antibodies, etc., for applications of the resulting compounds in boron-neutron capture therapy (BNCT) for cancer treatment.^[206-209]

However, for 3-coordinate organoboron compounds, the empty p-orbital of the boron center can be stabilized, e.g., by using π -electron-donating atoms such as oxygen in boronic acids and esters (**5.5**). One of the most prominent examples of boronic acids in biological applications is Bortezomib (Figure 5.1), sold as Valcade[®] since 2003 for the treatment of different types of cancer.^[1] Other compounds containing a boronic ester motif are of current interest as they react with hydrogen peroxide (H₂O₂) to yield the corresponding alcohol (Figure 5.1)^[5-8] which might be useful for the treatment of diabetes, neurodegenerative disorders, or cancer.^[9]

Triarylboranes (**5.6**) can be stabilized by sterically demanding aryl groups such as 2,6-xylyl, mesityl or tri-*iso*-propylphenyl (Tip),^[29, 35, 38, 40, 42-44, 46, 49-50, 52, 210-211] which shield the empty p-orbital from nucleophilic attack by, e.g., water. This general approach was used

for all triarylboranes presented in the following sections. Attaching 2,6-xylyl, pyrenyl, 9-anthracenyl, or similar sterically-demanding substituents can yield compounds which are not only air- and moisture-stable but also water-soluble by incorporation of water-insoluble triarylboranes into water-soluble polymers or attachment of hydrophilic moieties such as biomolecules or cationic moieties. Selected examples of such triarylboranes which were investigated in cells were mentioned in reviews,^[212-214] but the subject has not yet been summarized. As this is a very young and promising field which may lead to applications of triarylboranes in bioimaging (or maybe even cancer treatment), we summarize and discuss results that have been obtained to date and provide a perspective on directions this field might take.

5.2 Triarylborane-Loaded Nanogels

Triarylboranes that are not water-soluble can be incorporated into polymeric structures by either covalent bonding between the triarylborane and the polymer (**5.7**, Figure 5.2) or by hydrophilic and hydrophobic interactions between the host (polymer) and the guest (triarylborane; **5.8**, **5.9**, **5.10**), which leads to water-soluble and cell permeable structures. Yang and co-workers, in cooperation with Hu, S. Li, Y. Li, Zhu, Zhang, and Shen, showed that this approach can lead to cell permeable polymers which stain the cytoplasm and give a fluorometric response to biothiols (**5.8**),^[36] to changes of temperature (**5.7**)^[37] or pH (**5.10-OH**),^[32] and to H₂O₂ (**5.10**),^[32] depending on the structure of the triarylborane. Furthermore, they showed that such nanogels are non-toxic to mouse fibroblast (NIH/3T3) cells up to concentrations of 0.4 µg/mL.

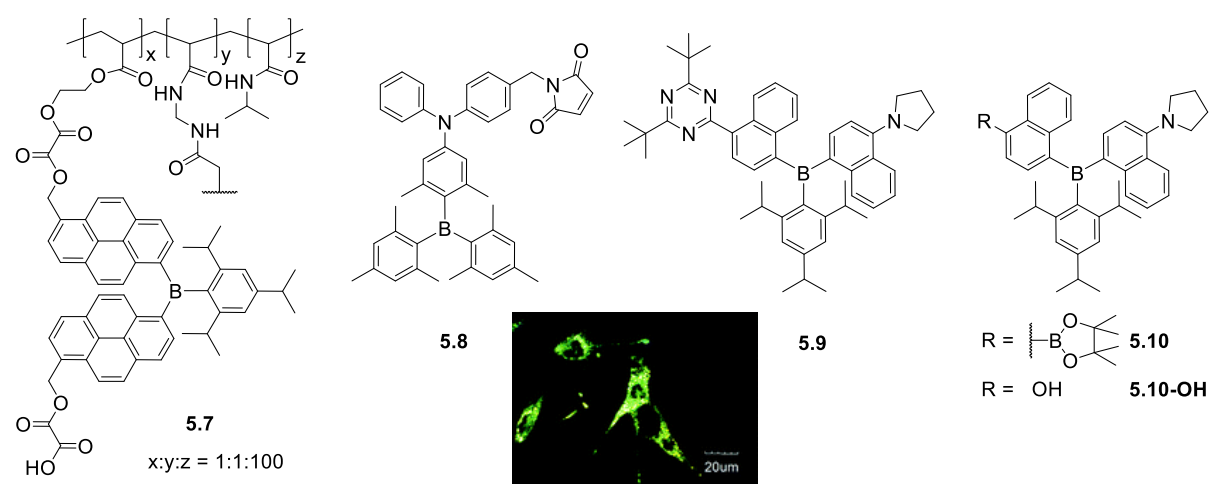


Figure 5.2: Molecular structures of compounds **5.7**,^[37] **5.8**,^[36] **5.9**,^[39] and **5.10**.^[32] Coloured picture depicts localization of NG-10 in NIH/3T3 cells. Picture is reproduced from ref. 32

with permission from the Centre National de la Recherche Scientifique (CNRS) and The Royal Society of Chemistry.

Triarylborane **5.8** bears a maleimide functionality which reacts selectively with biothiols, namely cysteine, homocysteine and glutathione, resulting in a turn-on fluorescence response within 10, 30 or 120 min, respectively.^[36] To monitor temperature changes inside NIH/3T3 cells, compound **5.7** consists of a triarylborane motif covalently bound to a polymeric backbone which changes its structure from coiled to globular upon increasing temperature.^[37] To obtain a stronger fluorometric response, **5.7** was mixed with the commercially available chromophore Nile red, which leads to a nanogel with a reversible color change in the stained cells from red at 25 °C to greenish at 37 °C. Donor- π -acceptor compound **5.9** was incorporated into a polymeric structure to provide a fluorometric response to changes of polarity (solvatochromism) and viscosity inside cells.^[39] Although the triarylborane itself was reported to show aggregation induced emission (AIE), inside the cell no differences in fluorescence were observed. However, from the staining pattern obtained, the authors concluded that, inside NIH/3T3 cells, the water-insoluble triarylborane **5.9** leaves the nanogel and aggregates in the cytoplasm, which leads to bright dots. Furthermore, they assumed that **5.9** enters the cell nucleus as single molecules. Similar behavior was reported for **NG-5.10**, a nanogel loaded with compound **5.10**, which gives a fluorometric response to H₂O₂ due to cleavage of its boronic ester moiety (Figure 5.2),^[32] and subsequent formation of a C–O bond yielding **NG-5.10-OH**, which changes the emission color from yellow to blue. In turn, **NG-5.10-OH** was shown to respond to cellular pH.

5.3 Neutral Triarylboranes

Another way to obtain triarylboranes which are water-soluble at concentrations required for biological applications is by attaching hydrophilic groups such as secondary amines or amides. The groups of Thilagar and Yang showed that specifically designed triarylboranes can stain different parts of cells selectively depending on the nature of their periphery. Thus, Thilagar and co-workers prepared a thiophenol sensor (**5.11a** and **5.11b**) by attaching a 2,4-dinitrobenzenesulfonyl (DNBS) moiety to a triarylborane resulting in a turn-on fluorescence sensor for thiophenol in human cervical cancer (HeLa) cells (Figure 5.3A).^[41] Compounds **5.11a** and **5.12a** were reported to have low cytotoxicity.

Yang, Zhu, Zhang, Liu, Leng, Xu, Fu, Li, Li and co-workers reported a series of cyclen-substituted triarylboranes (**5.13a-d**, **5.13a+3M²⁺**, **5.13b+2M²⁺**) that sense H₂S (**5.13b+2Cu²⁺**),^[38] RNA (**5.13b+2Zn²⁺**),^[48] **5.13b**)^[40] or monoamine oxidase (MAO) at the

surface of mitochondria (**5.13b**)^[196] in, e.g., human breast cancer (MCF-7) and human liver carcinoma (HepG2) cells. Compound **5.13b** was reported to enter NIH/3T3 cells within 5 min and to stain the cytoplasm and nucleoli, the latter most likely due to RNA binding which was indicated by co-localization experiments with SYTO™ RNaselect™.^[40] Low cytotoxicity was reported for the water-soluble compound **5.13b**.^[196] With an incubation time of over 1 h, **5.13a** and **5.13c** give rise to weak fluorescence in NIH/3T3 cells, but the staining pattern was not investigated further.^[38] The same compounds **5.13a-13d** were reported by Leng, Liu and co-workers for the selective sensing of monoamine oxidases (MAOs).^[196] In this more recent study, the low cytotoxicity of **5.13b** as well as its ability to enter cells was confirmed, whereas the staining pattern reported in NIH/3T3 cells was not. Complexation of **5.13b** with Cu²⁺ gives **5.13b+2Cu²⁺**, which enters NIH/3T3 cells, is non-cytotoxic, and stains the cytoplasm and the mitochondria as indicated by co-localization experiments with MTDf.^[38] It was proposed that the latter results most likely from the presence of H₂S in the mitochondria. Using Zn²⁺ instead of Cu²⁺ gives **5.13b+2Zn²⁺** which enters NIH/3T3 cells within 30 min and stains the nucleolus, the cell membrane, lysosomes, mitochondria, and the endoplasmic reticulum,^[48] as indicated by extensive co-localization studies. Localization in the nucleoli, cell membrane, and endoplasmic reticulum of NIH/3T3 cells was attributed to the ability of **5.13b+2Zn²⁺** to bind to RNA in the cell nucleus and to localize in hydrophobic regions of the cells. A similar staining pattern was reported for the compound in HeLa cells whereas slightly different staining patterns were observed in HepG2 cells, which Yang and co-workers attributed to higher viscosity and therefore slower distribution of **5.13b+2Zn²⁺** in the latter cell line. The compound is non-cytotoxic to any of the cell lines tested.

With a series of piperazine-modified triarylboranes (**5.14**, **5.15**, **5.16** and **5.17a-d**), Yang, Zhu, Zhang, Liu and co-workers showed that biomolecules such as cyclic pentapeptides, namely cRGD, can be attached to the triarylborane core (**5.16**, **5.17a-d**). These compounds are able to enter the cell nucleus (**5.15**)^[42] and to differentiate between healthy cells and cancer cells by binding to integrin $\alpha_v\beta_3$ (**5.16**)^[47] or by reacting with γ -glutamyltranspeptidase (GGT; **5.17b**).^[49] In aqueous solution, **5.14** and **5.15** were found to bind RNA preferentially over DNA.^[42] Without reporting the cytotoxicity of these compounds, NIH/3T3 cells were incubated with **5.14** and **5.15** and staining of the cytoplasm and the nucleoli was observed, the latter indicated by co-localization experiments with SYTO™ RNaselect™. For **5.15**, staining of the nuclear matrix, the nuclear membrane and the nuclear pore was indicated by confocal microscopy. From fluorescence lifetime microscopy (FLIM) measurements, Yang, Zhu, Zhang and co-workers concluded that the polarity in the centre of the nucleolus is lower than at its border. However, in

another report by Zhang, Liu, Yang and co-workers, no specific binding to the nucleoli, the nuclear membrane or matrix was mentioned for **5.15**.^[47]

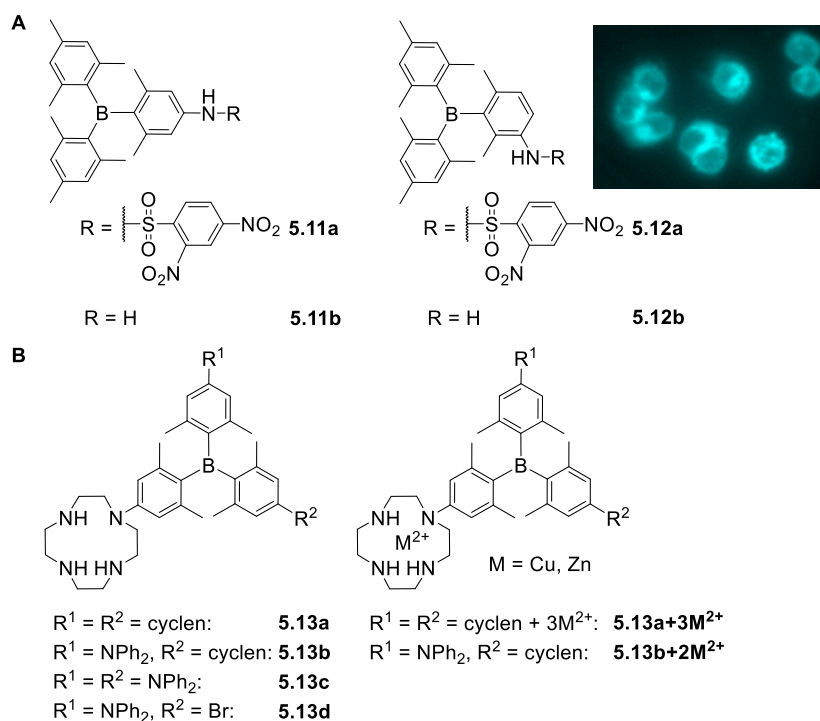


Figure 5.3: **A)** Structures of compounds **5.11** and **5.12** reported by Thilagar and co-workers. The colored picture shows the turn-on fluorescence sensing of thiophenol in HeLa cells. The picture is reprinted with permission from ref. 41. © 2018 American Chemical Society.^[41] **B)** Cyclen-substituted triarylboranes **5.13a-d**, **5.13a+3M²⁺**, **5.13b+2M²⁺** ($M = \text{Zn, Cu}$) reported by Yang and co-workers.^[38, 40, 48, 196]

Triarylborane **5.16** (Figure 5.4) was designed to distinguish tumor cells from healthy cells by not staining the latter ones as they do not overexpress integrin $\alpha_V\beta_3$.^[47] This was demonstrated by selective staining of human umbilical vein endothelial (HUVEC-1) and human primary glioblastoma (U87MG) cells over NIH/3T3 cells and pre-incubation studies with free cRGD. In contrast, all three cell lines were stained by the unmodified triarylborane **5.15**. As no cytotoxicity of compound **5.16** was observed, *in vivo* tests to image a tumor selectively in mice showed that the triarylborane stains the tumor within 60 min and exhibits bright fluorescence for another 30 min.

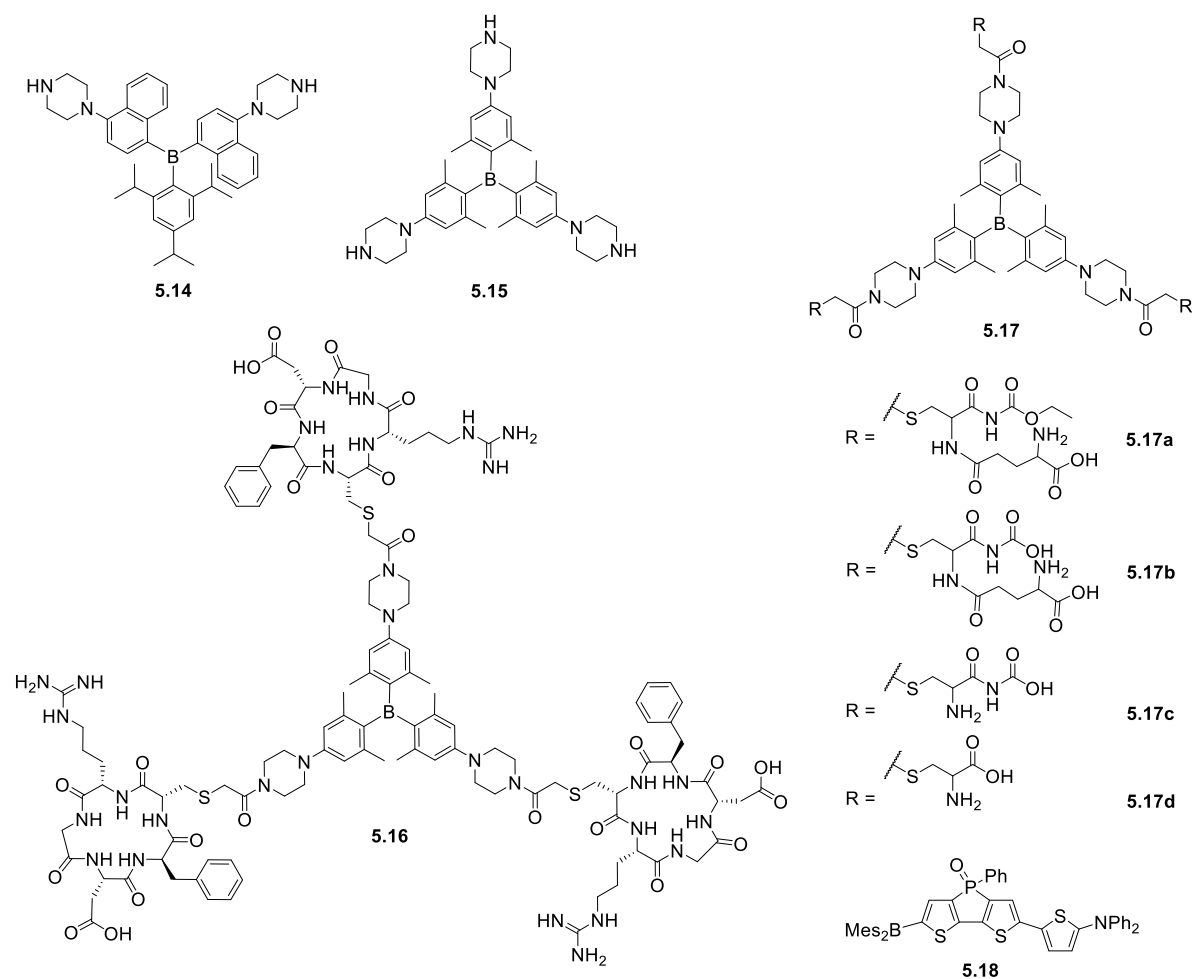


Figure 5.4: Piperazine-substituted triarylboranes **5.14**, **5.15**, **5.16** and **5.17a-d** reported by Yang and co-workers.^[42, 47, 49]

To obtain a fluorescent probe for the detection of GGT, **5.15** was modified with a peptide yielding **5.17b** (Figure 5.4), which can be hydrolyzed by GGT in two steps leading to **5.17c** and **5.15**, and enhancement of the fluorescence was observed.^[49] Compound **5.17b** does not enter HUVEC or NIH/3T3 cells but does enter ovarian tumor (SKOV-3) cells due to the presence of GGT. After 60 min of incubation with **5.17b**, an increasing fluorescence signal of a SKOV-3 tumor in mice was observed and, after 90 min, the tumor was clearly detectable.

Very recently, Yamaguchi and co-workers reported that the neutral, NIR-emissive D-A-A compound **5.18** (Figure 5.4) can be injected in DMSO solution or in 18% DMSO in PBS with 1.6% BSA, respectively, to observe blood vessels in Japanese medaka larvae by confocal microscopy and in mice brains by two-photon excitation microscopy.^[215]

5.4 Cationic Triarylboranes

The attachment of cationic groups to a sterically-stabilized boron core can lead to water-soluble triarylboranes. The groups of Yang, in cooperation with S. Li and Y. Li, as well as of Marder, in cooperation with Blanchard-Desce, Meinel, Yamaguchi, Lambert, and Piantanida, showed that triarylborane (**5.19**, Figure 5.5) and *bis*-triarylborane chromophores (**5.20-5.21**) equipped with cationic charges are all soluble in aqueous environments and cell permeable, as long as they are stable in water, and almost non-cytotoxic. The specifically designed triarylborane **5.19** selectively stains adenosine triphosphate (ATP) at the surface of mitochondria.^[35, 216] To the best of our knowledge, this was the first triarylborane applied in a cellular environment. Compound **5.19** bears two di(*1H*-imidazol-1-yl)methane dicationic groups, which account for its water-solubility, resulting in a detector that is selective for intracellular ATP, non-cytotoxic and stains cytoplasm and mitochondria. This was demonstrated by co-localization experiments in NIH/3T3 cells, as was binding to the mitochondria due to ATP production by mitochondrial oxidative phosphorylation in eukaryotic cells, by pre-incubation experiments and FLIM measurements.

Marder and co-workers reported a series of tetracationic *bis*-triarylborane chromophores that selectively stain lysosomes (**5.20b-f**, **5.21a-c**, **5.23**, Figure 5.5),^[44-46] localize in protein environments in cells (**5.19a**),^[43, 51] the endoplasmic reticulum (**5.20g**)^[52] or lysosomes and mitochondria simultaneously (**5.22**).^[45] However, none of these compounds bears a motif that is structurally related to a biomolecule or known to direct the compound to a specific organelle inside the cell. Blanchard-Desce, Meinel, and Marder and co-workers reported the bithiophene bridged compound **5.20a** to be water-soluble, cell permeable, non-cytotoxic to NIH/3T3, human embryonic kidney (HEK 293T) and HepG2-16 cells, and its absorption and emission spectra showed it to be more stable than the commercially available dye MitroTracker™ Red CMXRos (MTRC).^[43] From one- and two-photon excited fluorescence spectroscopy of **5.20a** in fixed osteosarcoma tumor (POS-1) cells and extensive RNA-, DNA-, and protein-binding studies performed in cooperation with Piantanida and co-workers,^[51] a hypsochromic shift of the emission maximum of **5.20a** in the cell compared to its emission spectrum in aqueous solutions was assigned to its binding to proteins in the cell. Thus, studying the interactions of the organoboranes with DNAs, RNAs and proteins in buffered solutions increased the information content of the cell imaging experiments. A series of related *bis*-triarylborane chromophores (**5.21a-c**) showed that significant steric hindrance is required to yield water-stability which is only provided by **5.21c** of this series and the previously reported compound **5.20a**.^[44]

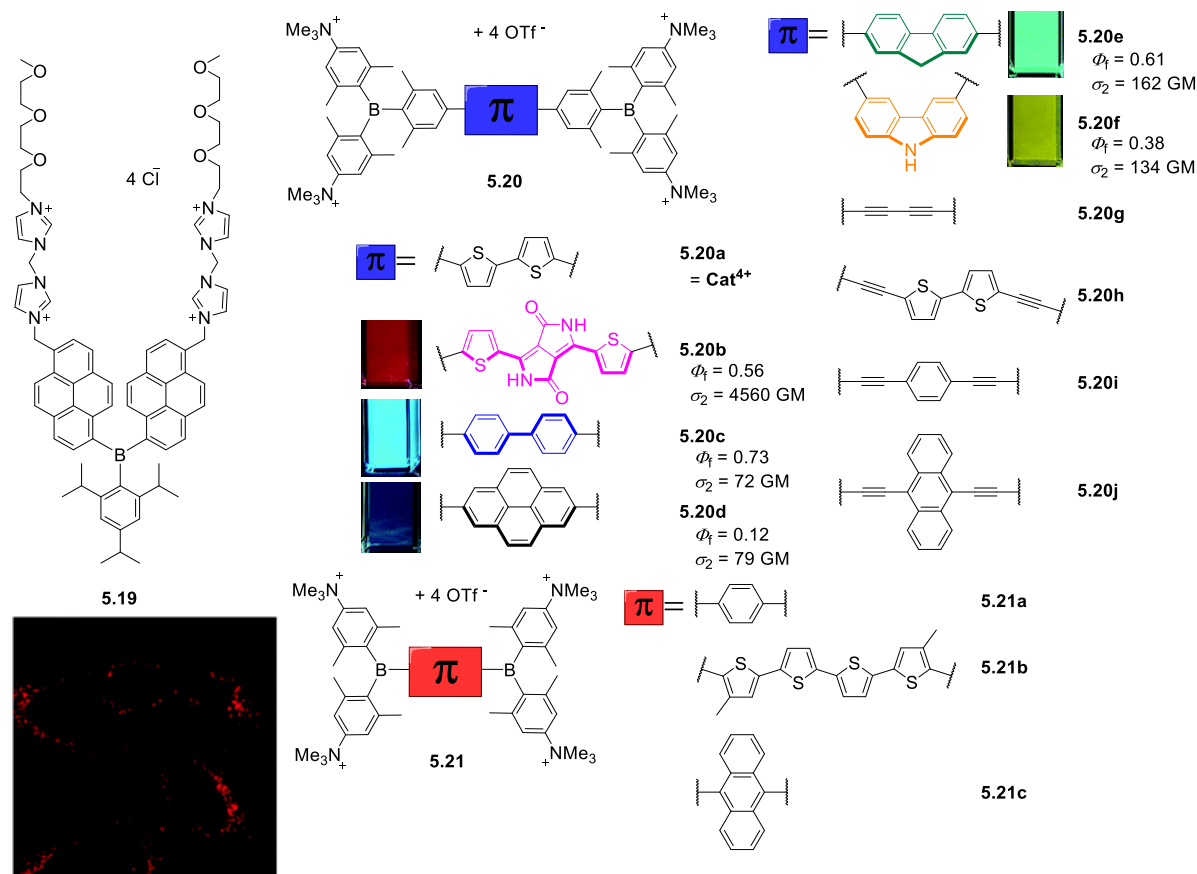


Figure 5.5: Molecular structures of **5.19**^[35, 216] of Yang, S. Li, Y. Li and co-workers and **5.20a-j**,^[43, 46, 52-53] **5.21a-c**^[44] of Marder, Blanchard-Desce, Meinel, Yamaguchi, Lambert, Piantanida and co-workers. The small pictures show the emission of the compounds under UV irradiation in cuvettes when dissolved in acetonitrile. The fluorescence microscope image shows a high degree of localization in the lysosomes of HeLa cells stained with **5.20b**. Colored images are reproduced from ref. 46 with permission of The Royal Society of Chemistry.

Compound **5.21c** showed no cytotoxicity, was cell-permeable within 1 h and localizes to a high degree at lysosomes as indicated by co-localization experiments. Subsequently, compounds **5.20b-f** were synthesized to examine the effect of the bridging unit on the photophysical properties, cell viability, cell permeability and localization in the cells (Figure 5.5).^[46] These five *bis*-triarylboranes were cell permeable, non-toxic to HeLa cells and their localization at lysosomes was demonstrated by co-localization experiments with different LysoTrackers™. Compound **5.20b** was shown to be taken up by the cell *via* the endocytosis pathway and has very good photostability, as 95% of the initial fluorescence intensity remained after irradiation for 12 min. Additionally, of the compounds in this series **5.20b** exhibits particularly red-shifted absorption and fluorescence spectra and an exceptionally high two-photon absorption cross-section of 4560 GM at 740 nm (Figure

5.5). Another compound (**5.20g**) related to this series was reported to be non-cytotoxic to HeLa and HEK cells and the staining pattern obtained suggests binding to the endoplasmic reticulum, but co-localization experiments have not yet been reported.^[52] In addition, the interaction of **5.20g** with DNAs, RNAs, and proteins was investigated in buffered solutions *via* fluorimetry, surface-enhanced Raman scattering (SERS) and Raman spectroscopy revealing strong quenching of the emission and enhancement of Raman signals upon binding. Very recently, this series was extended by three more alkyne-substituted *bis*-triarylboranes (**5.20h-j**) which are also efficient dual fluorescence and Raman chromophores to detect DNA and RNA at very low concentrations in aqueous buffered solutions, strongly dependent on the bridging unit.^[53]

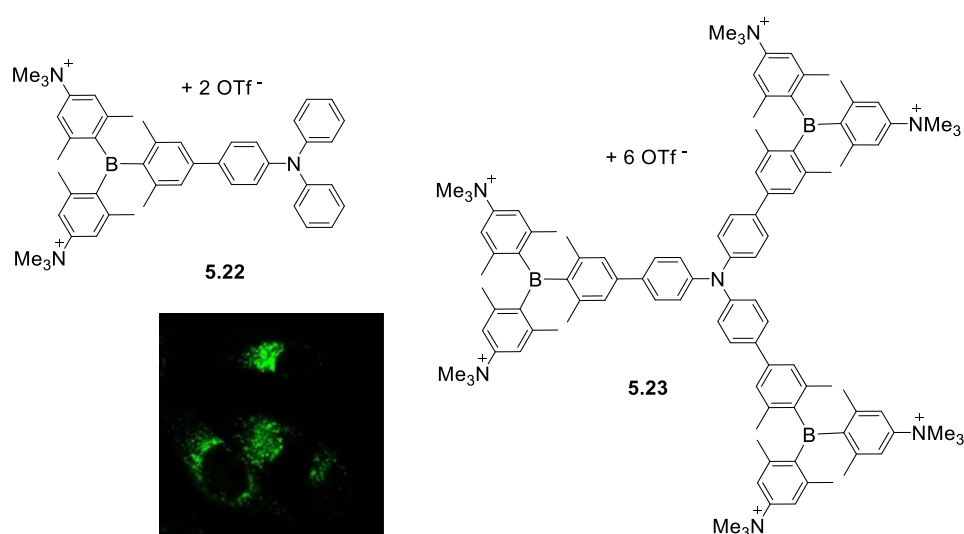


Figure 5.6: Molecular structures of compound **5.22** and **5.23** by Marder, Yamaguchi, Lambert and co-workers.^[45] The colored picture displays the localization of **5.23** in lysosomes of HeLa cells and is reproduced from ref. 45 with the permission of Wiley VCH.

Related dipolar and octopolar donor- π -acceptor compounds **5.22** and **5.23**, respectively, (Figure 5.6) were shown to be soluble in water in the presence of 0.5% DMSO, non-cytotoxic to HeLa cells and cell permeable.^[45] Co-localization experiments of **5.23** with LysoTracker™ Red (LTR) showed a high selectivity of this compound for accumulation in lysosomes. In contrast, **5.22** stains both lysosomes and mitochondria. The accumulation of both compounds can be monitored by two-photon excited fluorescence (TPEF) microscopy which provides deeper tissue penetration via NIR excitation in the ‘biologically transparent window’ and increases the 3D resolution of the images. Due to its higher two-photon brightness, lower toxicity, and higher selectivity for lysosomes, **5.23** is found to be a better candidate for bioimaging applications than **5.22**.

5.5 Discussion

A summary of the results obtained for staining of cell organelles with triarylboranes shows significant differences in the methods applied and the results obtained. For example, concentrations which cause cytotoxic effects vary drastically, even for very similar compounds (Table 5.1). Compounds **5.20d** and **5.20e** show no cytotoxic effects to HeLa cells up to concentrations of 5 μM whereas **5.20b-c** and **5.20f** are non-cytotoxic up to concentrations of 10 μM and **5.20g** was reported to be non-cytotoxic up to concentrations of 100 μM . Surprisingly, the only difference between those molecules is the π -bridge connecting the two triarylborane moieties. Therefore, it might be concluded that, in the case of *bis*-triarylborane chromophores (**5.20**), the toxicity mainly results from various bridging units which was also shown to influence the mode of binding between these compounds and DNA, RNA or proteins in buffered solutions.^[51-53]

In addition, the concentrations employed and incubation times are very different for the triarylboranes and commercially available dyes (Table 5.1). For example, staining of NIH/3T3 cells with **5.13b+2Cu²⁺** was reported after 5 min at concentrations of 10 μM whereas the commercial dye MTFD was used at a concentration of 0.1 μM with an incubation time of 30 min.^[38] Thus, for the commercial dye, longer incubation times are required while the concentration used is lowered by 99%. Similarly, NIH/3T3 cells were incubated with **5.13b+2Zn²⁺** at 10 μM concentrations for 30 min while the concentrations used for the commercial dyes were as low as 5 μM for DiD and 75 nM for LTR DND-99.^[48] Commercial dyes are used at lower concentrations but take longer to enter cells.

In some cases, the data for the same compound, varies drastically, as described for **5.13b** (Table 5.1). On one hand, this compound was reported to stain NIH/3T3 cells at concentrations of 10 μM within 35 min,^[40] but was also reported to stain the same cell line within 10 min using only 2 μM concentrations.^[196]

Cytotoxicity tests for some of the compounds which have been applied to several cell lines, such as **5.13b**, **5.14**, **5.15**, and **5.17b**, and Pearson values (R_r , a measure of the degree of overlap of the images) for co-localization studies with **5.13b**, **5.13b+2Zn²⁺**, **5.14**, **5.15**, **5.16**, and **5.20a** have not been reported. Without cytotoxicity studies, it is not known whether the concentrations used for imaging experiments effect the viability of the cell line or, for compounds used in *in vivo* experiments such as **5.17b**, maybe even the animal. Interestingly, for **5.13b+2Zn²⁺**, R_r values are given for some co-localization experiments but not others (Table 5.1).^[48] Without these correlation values, the degree of localization in specific cell organelles is not known.

Table 5.1: Summary of cell experiments done with all triarylboranes mentioned in this review. c_{nc} = no cytotoxicity up to this concentration; c_{incub} = concentration of triarylboron compound used for incubation; t_{incub} = incubation time for triarylboron compound; c_{incub}^{cd} = concentration of commercial dye used for incubation; t_{incub}^{cd} = incubation time for commercial dye; N.R. = no data reported. - = not investigated. MTFD = MitoTracker™ DeepRed FM; LTR = LysoTracker™ Red; MTRC = MitroTracker™ Red CMXRos; LTG = LysoTracker™ Green.

Section	Compound	Cell line	c_{nc}	c_{incub} [μ M]	t_{incub} [h]	Dye for co-localization	c_{incub}^{cd} [μ M]	t_{incub}^{cd} [min]	R_r
5.2	5.7 [37]	NIH/3T3	0.4 μ g/mL [a]	-	-	-	-	-	-
	5.8 [36]	NIH/3T3	1.0 μ M	0.40	0.5	-	-	-	-
	5.9 [39]	NIH/3T3	0.4 μ g/mL [a]	N.R.	0.5	-	-	-	-
	5.NG-10 [32]	NIH/3T3	0.4 μ g/mL [a]	10	0.5	-	-	-	-
5.3	5.11a [41]	HeLa	15 μ M	10	0.5	-	-	-	-
	5.12a [41]	HeLa	15 μ M	10	0.5	-	-	-	-
	5.13a [40]	NIH/3T3	-	N.R.	1	-	-	-	-
		NIH/3T3 [40]	-	10	0.58	SYTO™ RNA-select™	5	35	N.R.
		NIH/3T3 [40]	-	N.R.	0.08	-	-	-	-
	5.13b	NIH/3T3 [196]	low toxicity [b]	2	0.17	MTDF	0.1	30	N.R.
		MCF-7 [196]	low toxicity [b]	2	0.17	MTDF	0.1	30	N.R.
		HepG2 [196]	low toxicity [b]	2	0.17	MTDF	0.1	30	N.R.
	5.13b+2 Cu²⁺ [38]	NIH/3T3	40 μ M	10	0.08	MTDF	0.1	30	0.87
	5.13a+3 Zn²⁺ [48]	NIH/3T3	50 μ M	N.R.	1	-	-	-	-
5.13a+3 Zn²⁺ [48]	HeLa	50 μ M	-	-	-	-	-	-	
	HepG2	50 μ M	-	-	-	-	-	-	
5.13b+2 Zn²⁺ [48]	NIH/3T3	50 μ M	10	0.5	SYTO™ RNA-select™	0.5	20	N.R.	
					DiD	5	30	N.R.	

Table 5.1: To be continued.

					LTR DND-99	0.075	30	0.77	
		NIH/3T3	50 μ M	10	0.5	MDRF	0.5	45	0.85
	5.13b+2					ER-tracker TM Red	1	30	0.91
	Zn²⁺ [48]	HeLa	50 μ M	N.R.	N.R.	-	-	-	-
		HepG2	50 μ M	N.R.	N.R.	-	-	-	-
	5.14 [42]	NIH/3T3	-	10	0.5	SYTO TM RNA-select TM	5	30	N.R.
		NIH/3T3 [42]	-	10	0.5	SYTO TM RNA-select TM	5	30	N.R.
		NIH/3T3 [47]	-	1	0.25	-	-	-	-
5.3	5.15	HUVEC-1 [47]	-	1	0.25	-	-	-	-
		U87MG [47]	-	1	0.25	-	-	-	-
		NIH/3T3 [49]	-	? [c]	0.08	-	-	-	-
		NIH/3T3	5 μ M	1	0.25	-	-	-	-
	5.16 [47]	HUVEC-1	5 μ M	1	0.25	-	-	-	-
		U87MG	5 μ M	1	0.25	DiD red	5	20	N.R.
	5.17b [49]	NIH/3T3	-	10	1	-	-	-	-
		HUVEC	-	10	1	-	-	-	-
	5.17b [49]	SKOV-3	-	1	1	-	-	-	-
	5.17c [49]	NIH/3T3	-	? [c]	0.5	-	-	-	-
	5.19 [35, 216]	NIH/3T3	4 μ M	1	0.5	MTDF	0.1	30	0.86
		NIH/3T3	10 μ M	10	0.75	MTRC	0.125	45	N.R.
	5.20a [43]	HEK293T	10 μ M	-	-	-	-	-	-
		HepG2-16	10 μ M	-	-	-	-	-	-
5.4		POS-1	-	0.3	8	-	-	-	-
	5.20b [46]	HeLa	10 μ M	0.5	2	LTG	0.1	20	0.81
	5.20c [46]	HeLa	10 μ M	0.5	2	LTR	0.1	20	0.80
	5.20d [46]	HeLa	5 μ M	0.5	2	LTR	0.1	20	0.73
	5.20e [46]	HeLa	5 μ M	0.5	2	LTR	0.1	20	0.75
	5.20f [46]	HeLa	10 μ M	0.5	2	LTR	0.1	20	0.83

Table 5.1: To be continued.

	5.20g ^[52]	HeLa	100 μ M	1	2	-	-	-	-
		HEK	100 μ M	-	-	-	-	-	-
5.4	5.21c ^[44]	HeLa	5 μ M	5	1	LTR	0.1	20	0.86
	5.22 ^[45]	HeLa	1 μ M	0.5	2	LTR	0.1	20	0.48
						MTDR	0.05	20	0.42
5.23 ^[45]	HeLa	1 μ M	0.5	2	LTR	0.1	20	0.81	

[a] Concentration used for cytotoxicity was reported in this unit by Hu, S. Li, Y. Li, Zhu, Zhang, and Shen, Yang and co-workers.^[32, 37, 39] [b] No specific values were given in the text, and the supporting information was not accessible.^[196] [c] Exact numbers were reported in the supporting information which was not accessible online.^[49]

Given the observed differences in cytotoxicity, concentrations and incubation times, it would be useful for comparisons for there to be a standardized procedure for testing such new compounds. Standards exist for the characterization of new compounds as their structure and purity are analysed by NMR and IR spectroscopy, mass spectrometry, X-ray diffraction, and elemental analysis with standard reporting protocols. In the field of organic photovoltaic and OLEDs, standardized methods exist for data collection and analysis to determine whether the respective absorbing or emitting layer improved the performance of the resulting device. Such standardization is currently missing for chemists who want to examine the biological applicability of their triarylborane chromophores. Standardized protocols could include the use of at least one standard cell line by all research groups, together with uniform incubation times and concentrations. This would allow better comparison of the results obtained for different compounds by various groups. In addition, examination of the cytotoxicity of the chromophores to the standardized cell line prior to any in vivo experiments is highly recommended.

5.6 Summary and Outlook

Triarylborane chromophores can respond to various changes in the cellular environment, e.g., temperature, pH or to small molecules or biopolymers such as DNA, RNA, and proteins. They are often cell permeable and non-cytotoxic to various cell lines such as NIH/3T3, HEK, and HeLa cells, can localize in a variety of cell organelles, and can bind selectively to various DNAs, RNAs, and/or proteins. In addition, most of the compounds reported show one- and two-photon excited fluorescence and are more photostable than

some commercial dyes, *e.g.*, MitoTracker™ or SYTO™ RNaselect™, and some can be used as dual fluorescence and Raman/SERS chromophores. Careful design of the compounds and collaboration among synthetic chemists, experts in pharmaceutical chemistry, biochemistry, and bioimaging are important to move this field forward. Development of standardized protocols will also be helpful.

CHAPTER 6

INTERACTION OF BITHIOPHENE-CORED, *MONO*-, *BIS*-,
AND *TRIS*-(TRIMETHYLAMMONIUM)-SUBSTITUTED, *BIS*-
TRIARYLBORANE CHROMOPHORES WITH DNAs, RNA,
AND CELLS

6 Interaction of Bithiophene-Cored, *Mono*-, *Bis*-, and *Tris*-(Trimethylammonium)-Substituted, *Bis*-Triarylborane Chromophores with DNAs, RNA, and Cells

6.1 Introduction

In 2016, **Cat⁴⁺** was reported to be water-soluble, cell permeable and non-cytotoxic to NIH/3T3, HEK 293T, and HEPG2-16 cells up to concentrations of 10 $\mu\text{mol L}^{-1}$. Inside of fixed POS-1 cells, the mitochondria are stained, and the emission detected is hypsochromically shifted compared to the emission of **Cat⁴⁺** in water. Due to the shift, localization of **Cat⁴⁺** in a less polar environment compared to water was assumed.^[43] A few years later, the same compound was reported to bind to double-stranded (ds) DNA, ds-RNA, single-stranded (ss) RNA, and to bovine serum albumin (BSA) in buffered solutions with a hypsochromic shift of the emission spectrum when bound to the latter.^[51] These results suggest that the binding reported in fixed POS-1 cells occurs in a protein-like environment. A series of similar tetra-cationic *bis*-triarylboranes (**5.20b-f**; Chapter 5) was reported to stain the lysosomes of HeLa cells selectively.^[44, 46] In another series of alkyne-modified compounds (**5.20h-j**; Chapter 5), strong interactions with DNAs and RNAs were demonstrated.^[53] As a consequence of these previous studies, the influence of different charges on the interaction of **Cat¹⁺**, **Cat²⁺**, **Cat(i)²⁺**, and **Cat³⁺** with RNA and different DNAs was investigated in buffered solution of different pH. Lastly, the behavior of these selectively charged *bis*-triarylboranes was examined in different cell lines.

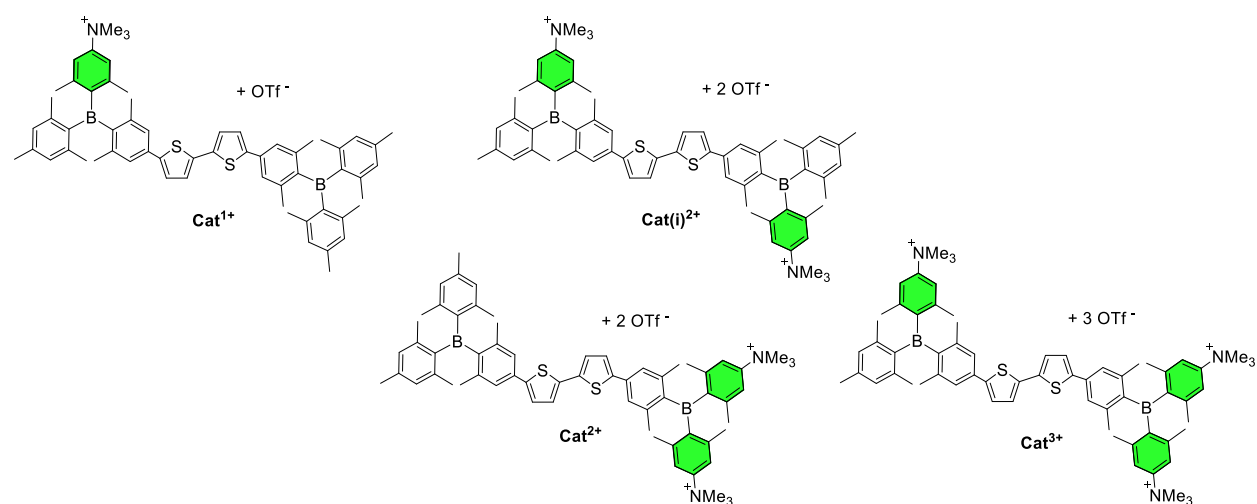


Figure 6.1: Compounds **Cat¹⁺**, **Cat²⁺**, **Cat(i)²⁺**, and **Cat³⁺**.

6.2 Results and Discussion

Changes of the fluorescence of **Cat**¹⁺, **Cat**²⁺, **Cat(i)**²⁺, and **Cat**³⁺ upon addition of increasing amounts of DNA or RNA were studied at pH 7 and/or pH 8. In combination with the results of thermal denaturation and circular dichroism (CD) experiments of the polynucleotides, which are known to be unique for the respective molecule, conclusions about the mode of interaction (intercalation, major or minor groove binding, or external binding) can be drawn.^[217-220]

Due to the limited solubility of **Cat**¹⁺, **Cat**²⁺, **Cat(i)**²⁺, and **Cat**³⁺ in pure water (Chapter 4), stock solutions in DMSO were prepared for the following biological studies and diluted with aqueous sodium cacodylate buffer (pH 7, *I* = 0.05 M) or aqueous potassium chloride buffer (pH 8; 15 mmol L⁻¹ Tris-HCl, 300 mmol L⁻¹ KCl) as indicated. Prior to any biological studies, the influence of different concentrations of **Cat**¹⁺, **Cat**²⁺, **Cat(i)**²⁺, and **Cat**³⁺, temperature, or pH on the absorption and emission spectra of the respective compounds was investigated.

6.2.1 Physico-Chemical Properties in Buffered Solution

The absorption spectra (Figure 11.18-Figure 11.21) and molar extinction coefficients obtained in sodium cacodylate buffer at pH 7 are very similar to the values obtained from aqueous solutions containing ≤1% acetonitrile as summarized in Table 6.1. Upon heating, the absorption of **Cat**¹⁺, **Cat**²⁺, **Cat(i)**²⁺, and **Cat**³⁺ decreases in intensity. The intensity is not completely restored after cooling to room temperature. These effects are large for **Cat**¹⁺ (ca. 30%) and small for **Cat**²⁺, **Cat(i)**²⁺, and **Cat**³⁺ (ca. 5%; Figure 11.18C-Figure 11.21C).

Table 6.1: Absorption maxima and molar extinction coefficient of **Cat**¹⁺, **Cat**²⁺, **Cat(i)**²⁺, and **Cat**³⁺ determined in 1% MeCN in water and DMSO in sodium cacodylate.

	DMSO in sodium cacodylate buffer		1% MeCN in water	
	λ_{max}^{abs} [nm]	ϵ [L mol ⁻¹ cm ⁻¹]	λ_{max}^{abs} [nm]	ϵ [L mol ⁻¹ cm ⁻¹]
Cat ¹⁺	414	33 300 ±600	415	29 500 ±1 200
Cat ²⁺	422	37 700 ±900	424	31 100 ±300
Cat(i) ²⁺	417	30 800 ±200	424	34 000 ±1 500
Cat ³⁺	421	30 900 ±700	423	36 000 ±900

The emission spectra of **Cat**¹⁺, **Cat**²⁺, **Cat(i)**²⁺, and **Cat**³⁺ in buffered solutions are similar to those recorded in aqueous solutions containing $\leq 1\%$ acetonitrile (Chapter 4) and their intensity increases linearly with increasing concentration of the compounds. Upon heating, the emission of **Cat**¹⁺, **Cat**²⁺, and **Cat**³⁺ is quenched by ca. 40-50% while the emission of **Cat(i)**²⁺ increases by ca. 15%. After cooling to room temperature, the intensities of the emission of **Cat**²⁺ and **Cat**³⁺ were restored, while the intensities of **Cat**¹⁺ and **Cat(i)**²⁺ remained at a lower level and a higher level (Figure 11.22-Figure 11.25), respectively. Thus, changes observed during the subsequent measurements have to be larger than those indicated here to be caused by the interaction with DNA or RNA.

6.2.2 Interaction with DNA and RNA at pH 7

To examine the interaction of **Cat**¹⁺, **Cat**²⁺, **Cat(i)**²⁺, and **Cat**³⁺ with biological macromolecules at pH 7, naturally occurring calf thymus (ct-) DNA and the ds-polymer poly rA – poly rU (pApU) were chosen as examples for DNA and RNA having B-helical and A-helical structures, respectively. The most relevant difference between the latter two structures is the size of their major and minor grooves, which is increased for the A-helix compared to the B-helix. Thus, bulky small molecules (small in comparison with biomacromolecules such as DNAs, RNAs, or proteins), such as **Cat**¹⁺, **Cat**²⁺, **Cat(i)**²⁺, and **Cat**³⁺, might fit better into the grooves of A-helical structures, which would result in increased interactions between the *bis*-triarylboranes and pApU compared to ct-DNA.

6.2.2.1 Thermal Melting Experiments

The characteristic change of the absorption at 260 nm of ctDNA and pApU upon increasing temperature allows the determination of their specific denaturation temperatures in sodium cacodylate buffered solutions.^[218] In the presence of up to 30 mol% **Cat**¹⁺, no change of the melting point was observed. In contrast, the melting temperature of ctDNA increased by 12, 4, and 3 °C in the presence of 30 mol% **Cat**²⁺, **Cat(i)**²⁺, and **Cat**³⁺, respectively. For pApU, an increase by 11, 13, and 6 °C was obtained in the presence of 30 mol% **Cat**²⁺, **Cat(i)**²⁺, and **Cat**³⁺, respectively (Figure 6.2, Table 6.2). Thus, these measurements suggest that each of the *bis*-triarylborane interacts with ctDNA and pApU at pH 7 except for **Cat**¹⁺. From increasing denaturation temperatures, stabilization of the secondary structure of the DNA or RNA can be assumed.^[218] The stabilizing effect of **Cat**²⁺ and **Cat(i)**²⁺ increases with increasing concentration of the compounds. For ctDNA, no such influence was observed in the presence of **Cat**³⁺.

When comparing the changes of the melting temperatures of ctDNA and pApU at pH 7 in the presence of **Cat**²⁺, **Cat(i)**²⁺, and **Cat**³⁺ with the values reported for **Cat**⁴⁺,^[51] greater influence of the *tetra*-cationic compound at lower concentrations was observed. Thus, stronger binding of **Cat**⁴⁺ compared to **Cat**¹⁺, **Cat**²⁺, **Cat(i)**²⁺, and **Cat**³⁺ is indicated.

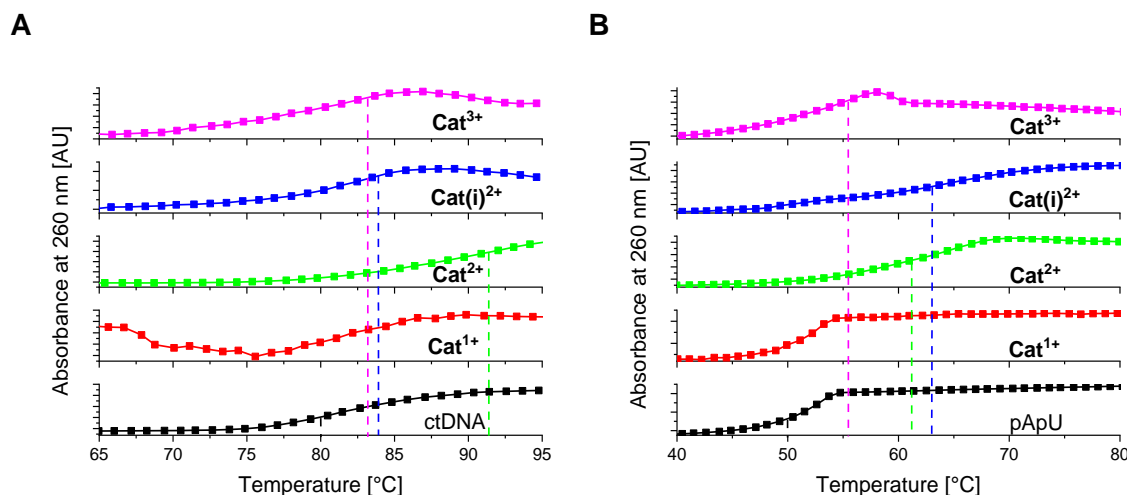


Figure 6.2: Thermal denaturation curves of **A**) ctDNA ($c(\text{ctDNA}) = 2.26 \times 10^{-5} \text{ mol L}^{-1}$, $r_{[\text{bis-triarylboranes}]/[\text{ctDNA}]} = 0.3$) and **B**) pApU ($c(\text{pApU}) = 2.49 \times 10^{-5} \text{ mol L}^{-1}$; ratio $r_{[\text{compound}]/[\text{pApU}]} = 0.3$) at pH 7 upon addition of *bis*-triarylboranes. Error in ΔT_m values: $\pm 0.5 \text{ }^\circ\text{C}$. The colored vertical lines are added to chart the changes of the melting temperatures.

Table 6.2: Summary of ΔT_m values of studied polynucleotides upon addition of **Cat**¹⁺, **Cat**²⁺, **Cat(i)**²⁺, **Cat**³⁺, and **Cat**⁴⁺ at pH 7.

	Cat ¹⁺			Cat ²⁺			Cat(i) ²⁺			Cat ³⁺			Cat ⁴⁺ [51]
	0.1	0.2	0.3	0.1	0.2	0.3	0.1	0.2	0.3	0.1	0.2	0.3	
ctDNA ^[b] [$^\circ\text{C}$]	0	0	0	0	5.9	11.8	1.7	2.9	3.8	3.6	3.5	3.2	7.3
pApU ^[b] [$^\circ\text{C}$]	0	0	0	0	2.0	11.1	1.3	13.0	13.0	0.6	6.0	5.5	9.5

[a] $r = [\text{compound}]/[\text{polynucleotide}]$; [b] Error of $\Delta T_m = \pm 0.5^\circ\text{C}$.

6.2.2.2 Fluorimetric Titrations

As demonstrated in Chapter 4, the *bis*-triarylboranes **Cat**¹⁺, **Cat**²⁺, **Cat(i)**²⁺, and **Cat**³⁺ are highly emissive fluorophores with characteristic excitation and emission wavelengths (Figure 4.5, Figure 4.6). Changes of the respective emission in the presence of increasing concentrations of ctDNA and pApU were investigated in sodium cacodylate buffered solution (Figure 11.30-Figure 11.37) and normalized to the emission of the single

compound (Figure 6.3). From the slope of the compensating curve, binding constants were calculated using the Scatchard equation^[221] and the von Hippel formalism^[222] (Table 6.3).

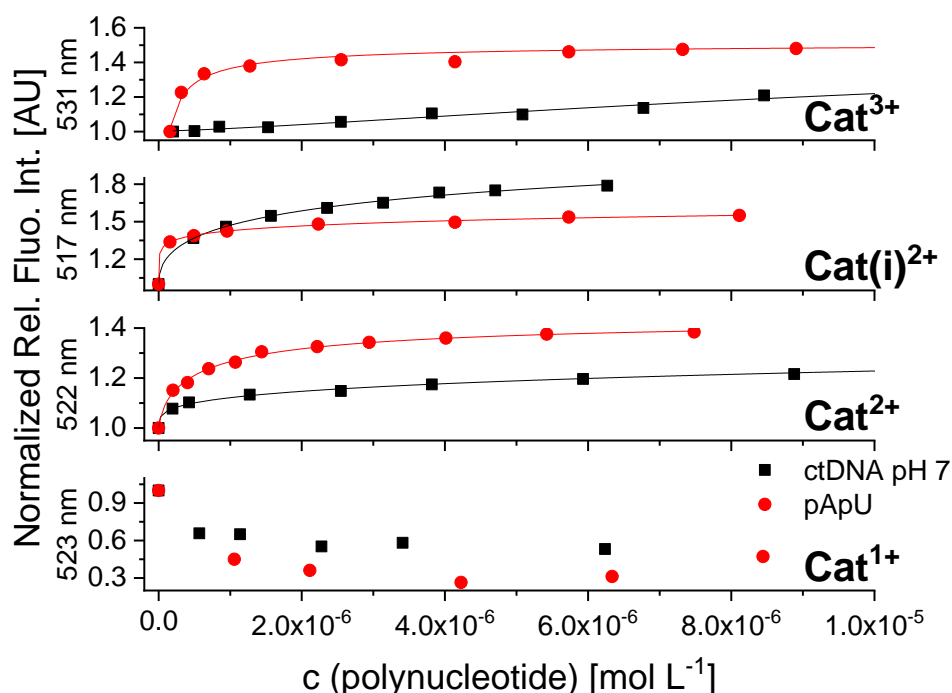


Figure 6.3: Normalized fluorimetric titration of **Cat**¹⁺ ($\lambda_{\text{exc}} = 414$ nm), **Cat**²⁺ ($\lambda_{\text{exc}} = 422$ nm), **Cat(i)**²⁺ ($\lambda_{\text{exc}} = 417$ nm), **Cat**³⁺ ($\lambda_{\text{exc}} = 421$ nm) with ctDNA and pApU at pH 7 using $c(\text{compounds}) = 1 \times 10^{-7}$ mol L⁻¹.

Table 6.3: Binding constants^[a] (log K_s) of **Cat**¹⁺, **Cat**²⁺, **Cat(i)**²⁺, **Cat**³⁺, and **Cat**⁴⁺ with polynucleotides calculated from fluorimetric titrations according to literature procedures.^[221-222]

	Cat ¹⁺	Cat ²⁺	Cat(i) ²⁺	Cat ³⁺	Cat ⁴⁺ [51]
ctDNA	^[b]	6.4	6.9	6.5	7.0
pApU	^[b]	7.0	7.8	7.5	~7

[a] Analyses of titration data by means of the Scatchard equation^[221] with von Hippel formalism^[222] gave values of the ratio $r = [\text{bound compound}]/[\text{polynucleotide}] = 0.2 - 0.3$; for easier comparison, all log K_s values were re-calculated for fixed $r = 0.25$ (ds-polynucleotides). Correlation coefficients were > 0.99 for all calculated K_s values. [b] Negligible emission change.

Upon addition of ctDNA or pApU to a solution of **Cat**¹⁺ in sodium cacodylate buffered solutions, no significant change of the emission was observed. Thus, no significant

interaction between the *mono*-cation and the polynucleotides is apparent. In contrast, the emission of **Cat**²⁺, **Cat(i)**²⁺, and **Cat**³⁺ increases with increasing amount of polynucleotides with binding constants similar to those reported for **Cat**⁴⁺.^[51] These experiments indicate similarly strong interactions between polynucleotides and trimethylammonium-substituted *bis*-triarylboranes irrespective of the number or distribution of the latter, as long as the number is larger than 1.

6.2.2.3 Circular Dichroism Experiments

Due to their helical structure, polynucleotides are chiral molecules while **Cat**¹⁺, **Cat**²⁺, **Cat(i)**²⁺, and **Cat**³⁺ are not. Thus, the former display unique circular dichroism (CD) spectra due to their secondary structure.^[223] By monitoring the CD spectra of the polynucleotides upon addition of the cationic *bis*-triarylboranes, useful information about the modes of interaction between these molecules can be gained.^[220, 224]

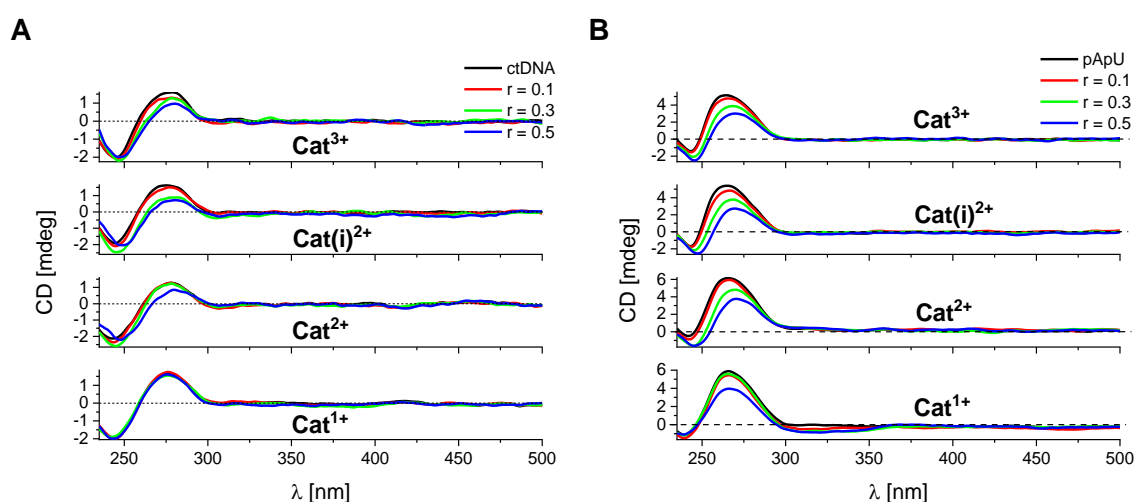


Figure 6.4: CD titration of **A**) ctDNA ($c = 2 \times 10^{-5} \text{ mol L}^{-1}$) and **B**) pApU ($c = 2.5 \times 10^{-5} \text{ mol L}^{-1}$) with **Cat**¹⁺, **Cat**²⁺, **Cat(i)**²⁺, and **Cat**³⁺ at molar ratios $r_{[\text{dye}]/[\text{polynucleotide}]} = 0.1 - 0.5$ at pH 7.

Upon addition of **Cat**¹⁺ to ctDNA or pApU, no significant change of the CD spectra was observed while for **Cat**²⁺, **Cat(i)**²⁺, and **Cat**³⁺, the intensity of the CD spectra between 230 nm and 300 nm (Figure 6.4) decreased slightly. This can be attributed to an unwinding of the double helix of the polynucleotides upon insertion of the *bis*-triarylboranes. In contrast to the previously reported *tetra*-cationic compound **Cat**⁴⁺,^[51] no ICD bands were observed at 400-500 nm. Thus, **Cat**²⁺, **Cat(i)**²⁺, and **Cat**³⁺ might be oriented non-uniformly with respect to the chiral axis of the polynucleotide. From the present data, it was not possible to derive direct structural information about the orientation of the *bis*-triarylboranes inside the DNA/RNA binding site. Nevertheless, in analogy to the previous

binding studies,^[51-53] groove binding of **Cat**²⁺, **Cat(i)**²⁺, and **Cat**³⁺ can be presumed. In accordance with thermal denaturation and fluorimetric titration experiments, no binding was detected for **Cat**¹⁺.

6.2.3 Interaction with DNAs at pH 8

The interaction of **Cat**¹⁺, **Cat**²⁺, **Cat(i)**²⁺, and **Cat**³⁺ with ctDNA and DNApore was investigated in potassium chloride solutions (15 mmol L⁻¹ Tris-HCl, 300 mmol L⁻¹ KCl) at pH 8. DNApore describes a tubular biomacromolecule consisting of six oligonucleotides which form a cavity in the middle providing space for cationic bis-triarylboranes as demonstrated in Figure 6.5B. The exact structure of DNApore and its decomposition are summarized in Figure 6.5A and Table 9.1.

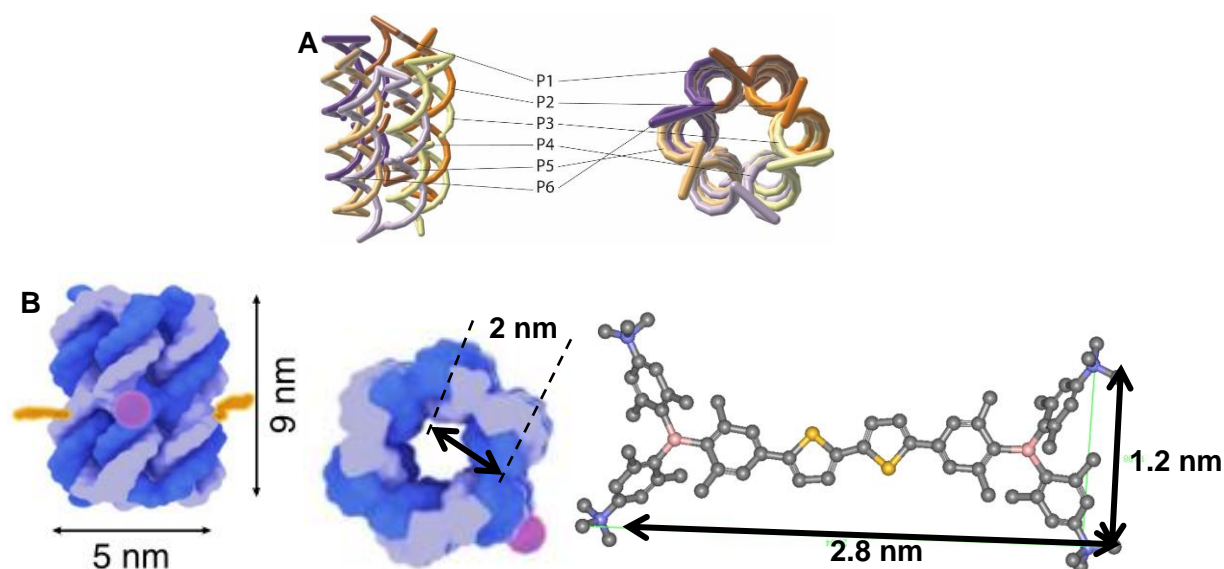


Figure 6.5: **A)** Schematic presentation of DNApore. The composition of oligonucleotides P1-P6 is given in (Figure 9.1; Table 9.1). **B)** Schematic depiction showing that **Cat**⁴⁺ and the analogues **Cat**¹⁺, **Cat**²⁺, **Cat(i)**²⁺, and **Cat**³⁺ (width ca. 1.2 nm) fit into the cavity of the DNApore (width ca. 2 nm).

6.2.3.1 Thermal Melting Experiments

The thermal denaturation temperatures of ctDNA in potassium chloride buffer at pH 8 (15 mmol L⁻¹ Tris-HCl, 300 mmol L⁻¹ KCl) was investigated. Under the same conditions, the denaturation of DNApore was found to be slightly biphasic, most likely due to the presence of two different conformers. Upon addition of **Cat**¹⁺, **Cat**²⁺, **Cat(i)**²⁺, and **Cat**³⁺, (Table 6.4, Figure 6.6A) the melting temperature of ctDNA increases by 0.7, 8.7, 5.5, and 3.5 °C, respectively. In the case of DNApore, the biphasic nature of the transition was

increased in the presence of **Cat**¹⁺, **Cat(i)**²⁺, and **Cat**⁴⁺. For all compounds, both transitions were stabilized, and the stabilizing effect was found to increase with increasing number of cationic charges in the order **Cat**¹⁺ < **Cat**²⁺ ≈ **Cat(i)**²⁺ < **Cat**³⁺ < **Cat**⁴⁺.

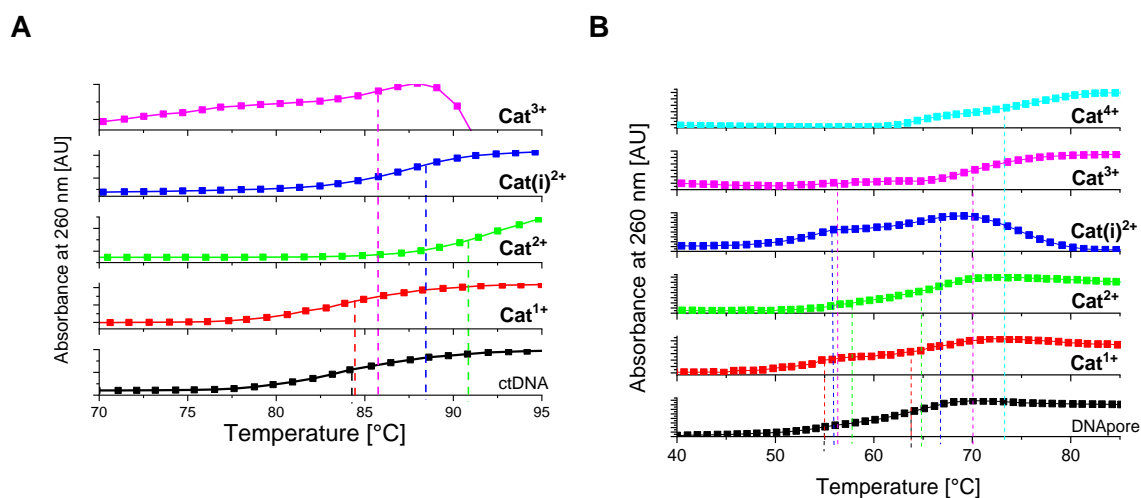


Figure 6.6: Thermal denaturation curves of **A)** ctDNA ($c(\text{ctDNA}) = 2.26 \times 10^{-5} \text{ mol L}^{-1}$, $r_{[\text{bis-triarylboranes}]/[\text{ctDNA}]} = 0.2$) and **B)** DNApore ($c(\text{DNApore}) = 2 \times 10^{-5} \text{ mol L}^{-1}$; ratio $r_{[\text{compound}]/[\text{DNApore}]} = 0.25$) at pH 8 upon addition of bis-triarylboranes. Error in ΔT_m values: $\pm 0.5 \text{ }^\circ\text{C}$. The colored vertical lines are added to chart the changes of the melting temperatures.

Table 6.4: Summary of ΔT_m values^[a] [$^\circ\text{C}$] of studied polynucleotides upon addition of **Cat**¹⁺, **Cat**²⁺, **Cat(i)**²⁺, **Cat**³⁺, and **Cat**⁴⁺ at pH 8.

r ^[b]	Cat ¹⁺	Cat ²⁺	Cat(i) ²⁺	Cat ³⁺	Cat ⁴⁺
ctDNA	0.7	8.7	5.5	3.4	-
DNApore	0/0 ^[c]	3.2/1.2 ^[c]	1.2/3.3 ^[c]	1.4/6.6 ^[c]	8.0

[a] Error of $\Delta T_m = \pm 0.5^\circ\text{C}$; [b] $r = [\text{compound}]/[\text{polynucleotide}]$; [c] Biphasic transitions.

6.2.3.2 Fluorimetric Titrations

The influence of increasing concentrations of ctDNA and DNApore on the emission spectra of **Cat**¹⁺, **Cat**²⁺, **Cat(i)**²⁺, **Cat**³⁺, and **Cat**⁴⁺ was investigated, the spectra obtained were normalized with respect to the emission of the single compound in potassium chloride solutions and the resulting changes are summarized in Figure 6.7 and Table 6.5. The interaction of **Cat**¹⁺ with ctDNA at pH 8 was not investigated as no interactions were observed at pH 7.

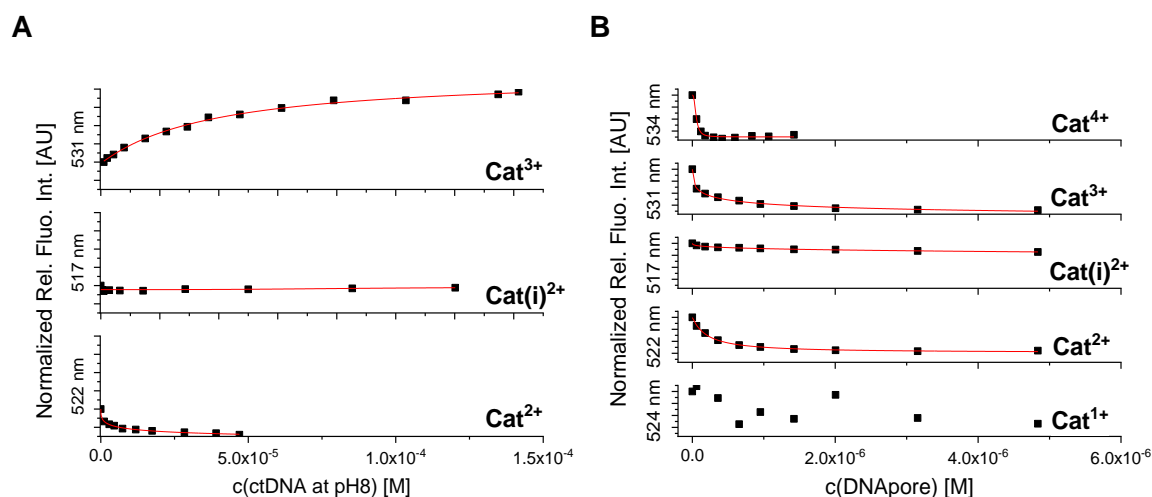


Figure 6.7: Normalized fluorimetric titration of **A)** Cat^{2+} ($\lambda_{\text{exc}} = 422 \text{ nm}$), Cat(i)^{2+} ($\lambda_{\text{exc}} = 417 \text{ nm}$), and Cat^{3+} ($\lambda_{\text{exc}} = 421 \text{ nm}$) with ctDNA and of **B)** Cat^{1+} ($\lambda_{\text{exc}} = 414 \text{ nm}$), Cat^{2+} ($\lambda_{\text{exc}} = 422 \text{ nm}$), Cat(i)^{2+} ($\lambda_{\text{exc}} = 417 \text{ nm}$), Cat^{3+} ($\lambda_{\text{exc}} = 421 \text{ nm}$), and Cat^{4+} ($\lambda_{\text{exc}} = 425 \text{ nm}$) with DNApore at pH 8 using $c(\text{Cat}^{2+}, \text{Cat(i)}^{2+}, \text{Cat}^{3+}) = 5 \times 10^{-7} \text{ mol L}^{-1}$, $c(\text{Cat}^{4+}) = 4 \times 10^{-7} \text{ mol L}^{-1}$.

Table 6.5: Binding constants^[a] (log K_s) of Cat^{1+} , Cat^{2+} , Cat(i)^{2+} , Cat^{3+} , and Cat^{4+} with polynucleotides at pH 8 calculated from fluorimetric titrations according to literature known procedures.^[221-222]

	Cat^{1+}	Cat^{2+}	Cat(i)^{2+}	Cat^{3+}	Cat^{4+}
ctDNA	-	6.8	^[b]	5.1	-
DNApore	^[b]	7.5	6.7	7.5	7.8

[a] Analyses of titration data by means of the Scatchard equation^[221] with von Hippel formalism^[222] gave values of the ratio $r = [\text{bound compound}]/[\text{polynucleotide}] = 0.2 - 0.3$; for easier comparison, all log K_s values were re-calculated for fixed $r = 0.25$ (ds-polynucleotides). Correlation coefficients were > 0.99 for all calculated K_s values. [b] Negligible emission change.

The emission of Cat(i)^{2+} does not change significantly with increasing concentration of ctDNA at pH 8 while at pH 7 a binding constant of 6.9 was obtained. For Cat^{2+} , a decrease of the emission intensity and a binding constant of 6.8 was observed pH 8, while at pH 7 an increase with a similar binding constant of 6.4 was obtained. The intensity of Cat^{3+} increases with binding constants of 6.5 and 5.1 at pH 7 and pH 8, respectively. The decreased binding constants obtained at pH 8 indicates weaker interaction of the bis-triarylborane with ctDNA at increased pH.

In the presence of DNApore, the emission of **Cat**¹⁺ does not change significantly, which indicates no interaction. For the other *bis*-triarylboranes, a decrease of the respective emission intensity was observed with binding constants that increase in the order **Cat(i)**²⁺ < **Cat**²⁺ ≈ **Cat**³⁺ < **Cat**⁴⁺ from 6.7 over 7.5 to 7.8 with increasing number of trimethylammonium groups.

6.2.3.3 Circular Dichroism Experiments

The change of the unique CD spectra of ctDNA and DNApore with increasing concentration of *bis*-triarylboranes was monitored in potassium chloride solutions at pH 8. The spectra obtained are summarized in Figure 6.8.

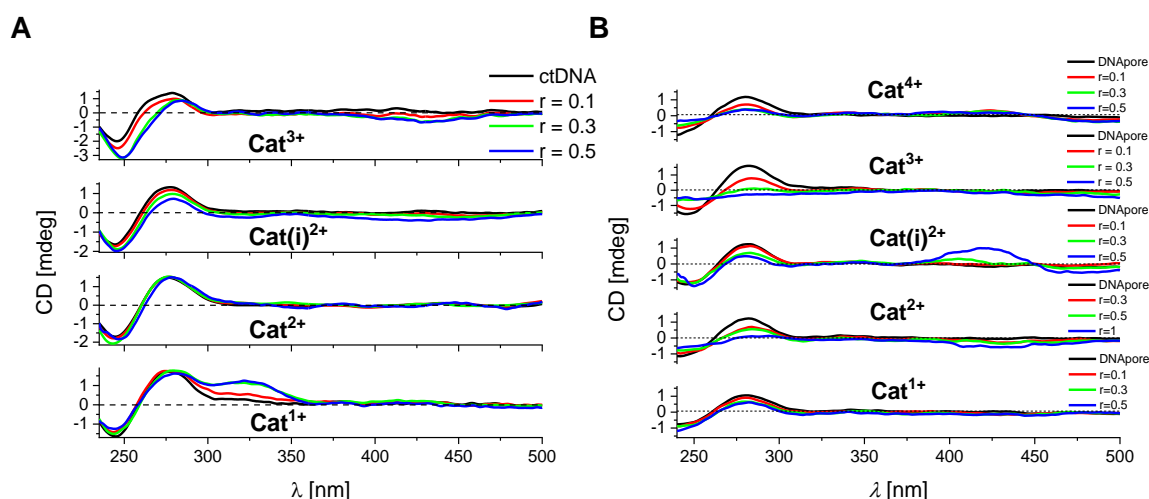


Figure 6.8: CD titration of **A)** ctDNA ($c = 2 \times 10^{-5} \text{ mol L}^{-1}$) and **B)** DNApore ($c = 5 \times 10^{-5} \text{ mol L}^{-1}$) with **Cat**¹⁺-**Cat**⁴⁺ at molar ratios $r_{[\text{dye}]/[\text{polynucleotide}]} = 0.1-1$ at pH 8.

The CD spectrum of ctDNA decreases and shifts bathochromically with increasing concentration of **Cat**³⁺ and **Cat(i)**²⁺, while in the presence of **Cat**²⁺ no significant changes are observed. In contrast, a new band arises at ca 325 nm with increasing concentration of **Cat**¹⁺ which was the only indication for any interaction of this compound with oligonucleotides.

In contrast to other polynucleotides, the chiral axis of the DNApore cannot be directly correlated to the usually well-defined chiral axes of typical ds-DNAs due to the six intertwined 50-mer oligonucleotides and, consequently, the tilted angles of the double helices with respect to the central axis of the DNApore. Thus, the following ICD signal assignments do not necessarily match those described in the literature.^[220, 223-224] However, due to the similar structure of the *bis*-triarylboranes studied and the same experimental

procedures applied, the results of these measurements were used for comparative conclusions within this series of compounds.

For **Cat**²⁺, weak, negative ICD bands at ca. 400-450 nm were observed which is characteristic for a perpendicular orientation of the transition moment of the chromophore with respect to the chiral axis of the DNApore. In contrast, addition of **Cat(i)**²⁺ to DNApore induced considerably strong ICD bands at 400-450 nm which fits the absorption spectra of the corresponding *bis*-triarylboranes perfectly. Thus, these positive ICD signals derive from the chromophores studied and suggest a tilted orientation by ca. 60° to the chiral axis of the DNApore. For **Cat**³⁺ and **Cat**⁴⁺, complete disintegration of the CD bands of DNApore suggests strong changes of the secondary structure of the latter upon binding of the compounds.

6.2.4 Interaction with Cells

The *bis*-triarylborane **Cat**⁴⁺ was reported to enter cells^[43] and to bind to DNA, RNA and proteins with different ratiometric read out.^[51] Hence, the influence of different numbers and distribution of charges on cell penetration and intracellular localization of **Cat**¹⁺, **Cat**²⁺, **Cat(i)**²⁺, and **Cat**³⁺ was investigated. However, as DNA and RNA binding studies showed that **Cat**¹⁺ does not bind to biomacromolecules (*vide supra*), this compound was not studied in cells.

6.2.4.1 MTT Assay

Due to the low stability of **Cat**²⁺ in DMEM with 10% FBS, only the cytotoxicity of **Cat(i)**²⁺ and **Cat**³⁺ to A549 and WI38 cells were investigated using the MTT assay.

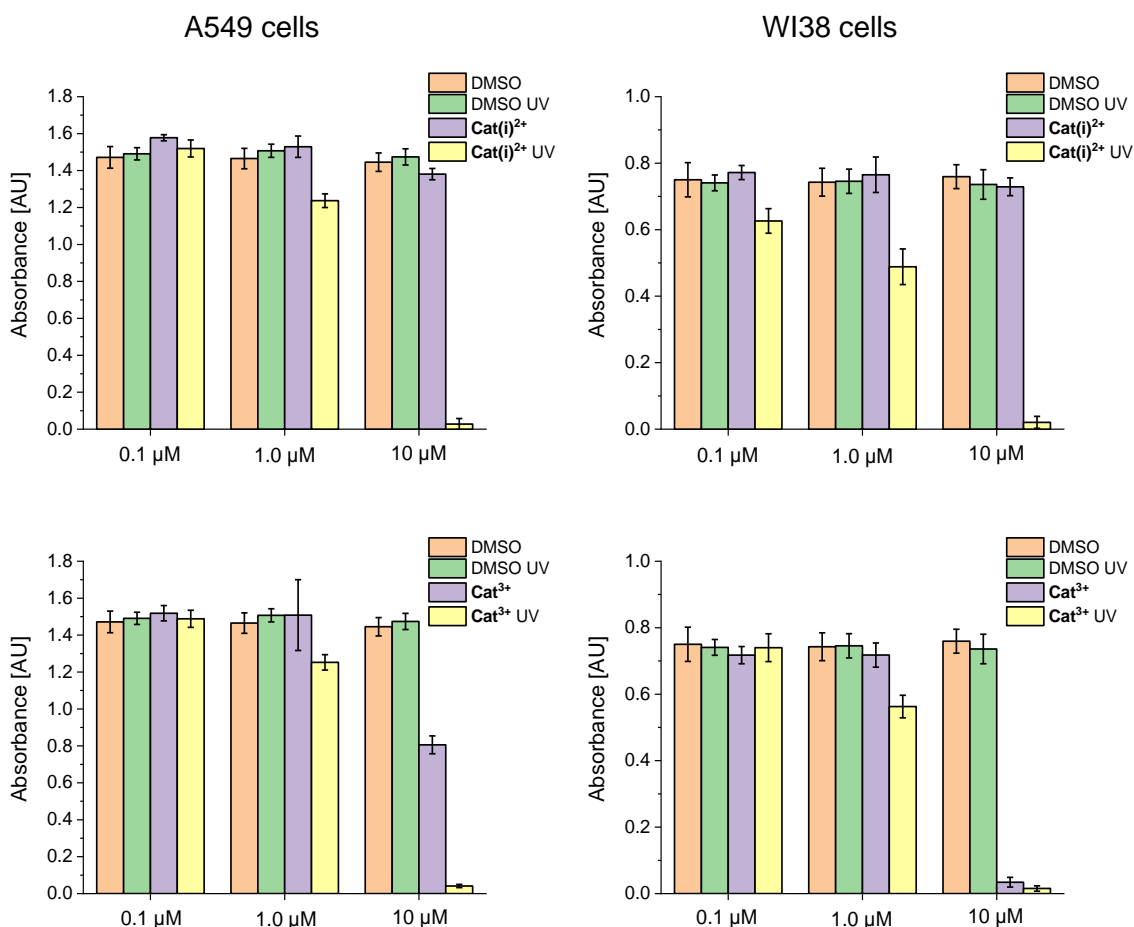


Figure 6.9: Cell survival of A549 and WI38 cells exposed to **Cat(i)**²⁺ and **Cat**³⁺, with or without UV exposure. Data are presented as mean \pm SD made in four replicates, relative to the control samples. Control samples are cells treated with DMSO in same concentration as compound tested. Representative data of three independent experiments which yielded similar results are shown.

The results are summarized in Figure 6.9 and show that the viability of both cell lines is drastically lowered in the presence of high concentrations of **Cat(i)**²⁺ and **Cat**³⁺ (10 $\mu\text{mol L}^{-1}$) and even stronger under irradiation with visible light (400-700 nm). In contrast, at lower concentrations and without irradiation, the viability of A549 and WI38 cells is barely influenced by the presence of either *bis*-triarylborane investigate.

6.2.4.2 Emission Bleaching and Photoinduced Cell Damage

To gain an initial impression of the behavior of **Cat**²⁺, **Cat(i)**²⁺, and **Cat**³⁺ in cells, A549 cells were incubated with each compound. The resulting fluorescence was monitored for up to 4 min by confocal microscopy, all images of which are shown in the appendix (Figure 11.59-Figure 11.64). As summarized in Figure 6.10, the intensity of the emission increases with increasing numbers of trimethylammonium groups in the order **Cat**²⁺ \approx **Cat(i)**²⁺ < **Cat**³⁺ as observed for the molar extinction coefficient in solution (*vide supra* and Chapter 4). However, the intensity of the emission decreases rapidly within ca. 30 s of irradiation for the three triarylboranes.

Figure 6.10A indicates that **Cat**²⁺ localizes at the outer limit of the cell and as bright spots in the middle of the cell. In contrast, for **Cat(i)**²⁺ and **Cat**³⁺, localization in the cytoplasm with a non-specific distribution is observed (Figure 6.10B,C). These indications were further investigated by co-localization experiments for **Cat(i)**²⁺ and **Cat**³⁺ (*vide infra*), but not for **Cat**²⁺ as the stability of the latter in Dulbecco Modified Eagle's Medium (DMEM) containing 10% fetal bovine serum (FBS) is not sufficient for these experiments.

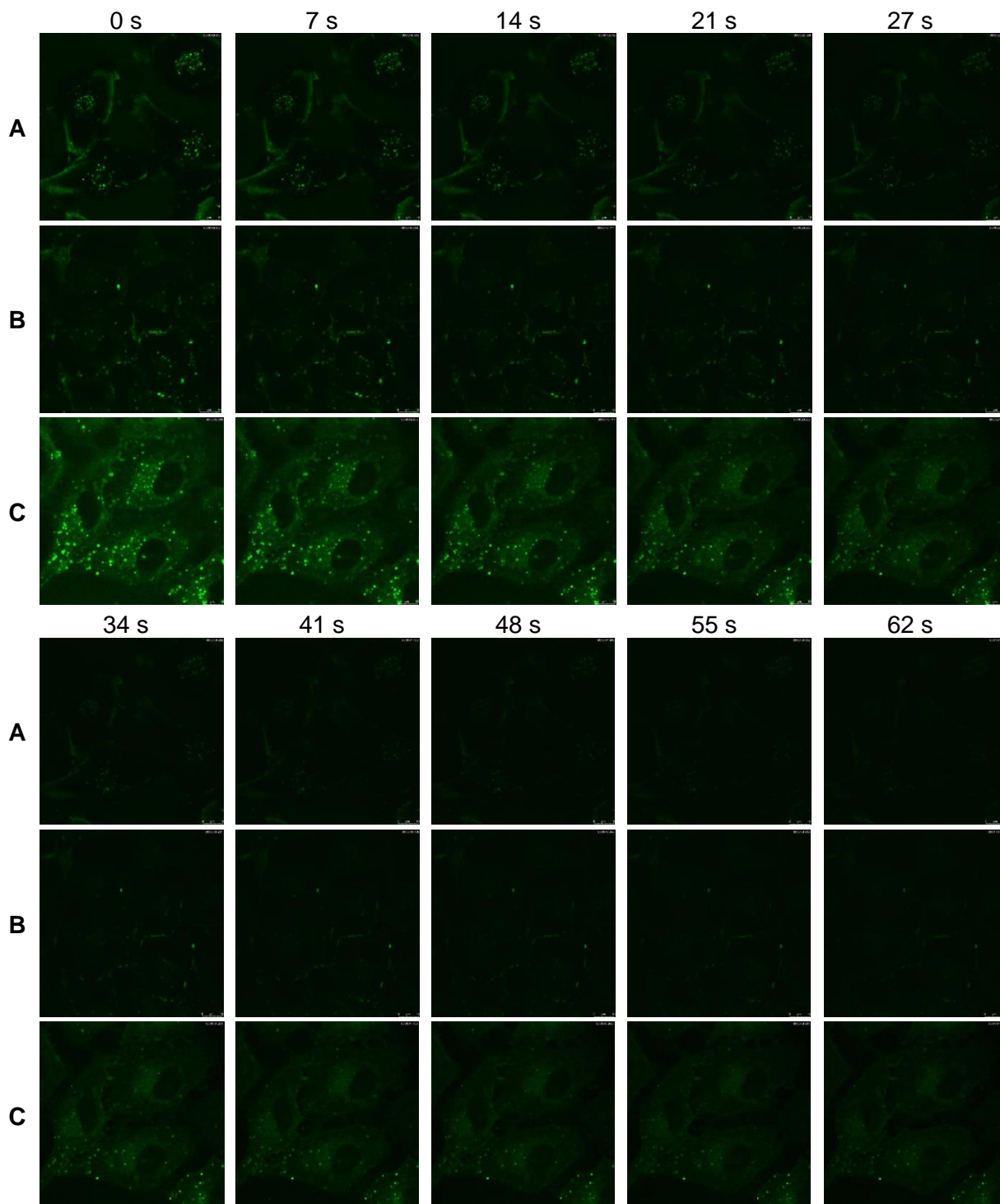


Figure 6.10: Images of the emission of A549 cells stained with **A) Cat^{2+}** , **B) $\text{Cat}(\text{i})^{2+}$** , and **C) Cat^{3+}** taken at times indicated showing fast bleaching of the emission of the *bis*-triarylboranes.

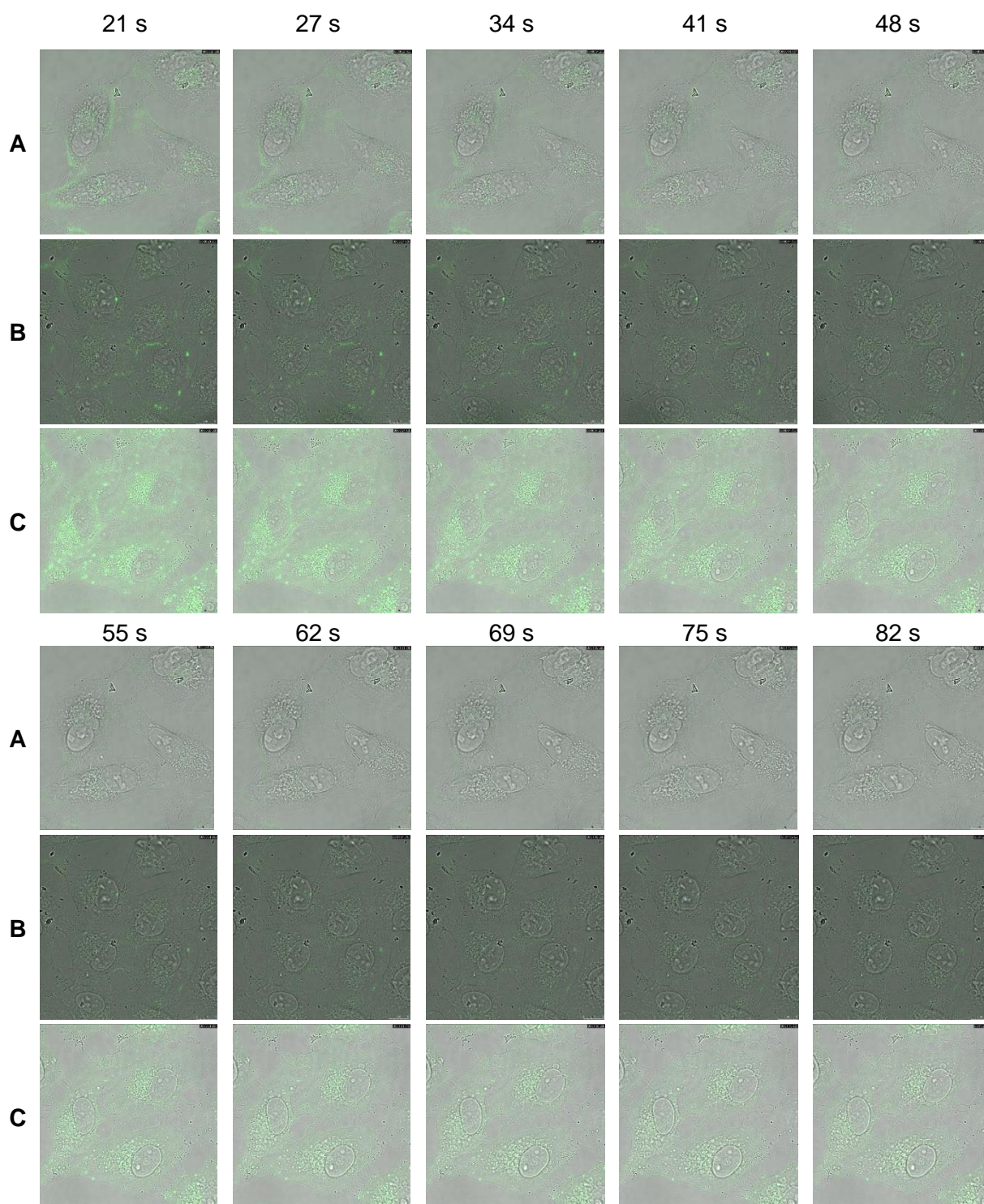


Figure 6.11: Images of the emission of A549 cells stained with **A) Cat²⁺**, **B) Cat(i)²⁺**, and **C) Cat³⁺** overlaid with bright field taken at times indicated showing fast bleaching of the emission of **Cat²⁺**, **Cat(i)²⁺**, and **Cat³⁺** and simultaneous cell blebbing.

Bright field images of these experiments (Figure 6.11) indicate cell blebbing while the compounds are fluorescent. As soon as the fluorescence is bleached, no further changes

of the cell structures is observed. As **Cat**²⁺, **Cat(i)**²⁺, and **Cat**³⁺ were found to sensitize singlet oxygen with an efficiency of ca. 0.6 (Chapter 4) in oxygen saturated solutions upon irradiation and ¹O₂ is known to lead to cell damage and cell death,^[179] it is suggested that cell blebbing is observed due to intracellular singlet oxygen sensitization of **Cat**²⁺, **Cat(i)**²⁺, and **Cat**³⁺.

6.2.4.3 Co-localization Studies

For these studies, fixed A549 cells were first incubated with primary antibodies against early endosome antigen 1 (EEA1), golgi apparatus (GM130) or lysosome membrane protein 1 (LAMP-1) and, after washing with PBS, with the fluorescently labeled anti-rabbit secondary antibody AF647. Upon binding of the fluorescent secondary antibody AF647 to either of the primary antibodies, the selectively stained organelle of the cell became visible. Thus, by comparison of the images obtained for the staining of **Cat(i)**²⁺ and **Cat**³⁺ with those of the fluorescent antibody (Figure 6.12, Figure 6.13), it was possible to calculate the Pearson correlation coefficient for the co-localization of the known staining dyes and *bis*-triarylboranes (Table 6.6). These values indicate that **Cat(i)**²⁺ and **Cat**³⁺ localize at lysosomes, golgi apparatus and early endosomes. For **Cat**³⁺, less localization is observed at the early endosomes compared to **Cat(i)**²⁺.

Table 6.6: Summary of Pearson correlation coefficients determined for **Cat(i)**²⁺ and **Cat**³⁺.

Compound	Commercial Staining Dye	Pearson Correlation Coefficient (R _r)
Cat(i) ²⁺	EEA1	0.24
	LAMP1	0.46
	GM130	0.37
Cat ³⁺	EEA1	0.08
	LAMP1	0.54
	GM130	0.39

Comparing these results with the previously reported selectivity of very similar, *tetra*-cationic compounds for lysosomes (Chapter1, Chapter 5) indicates that the number of charges largely influences the intracellular localization of *bis*-triarylboranes.

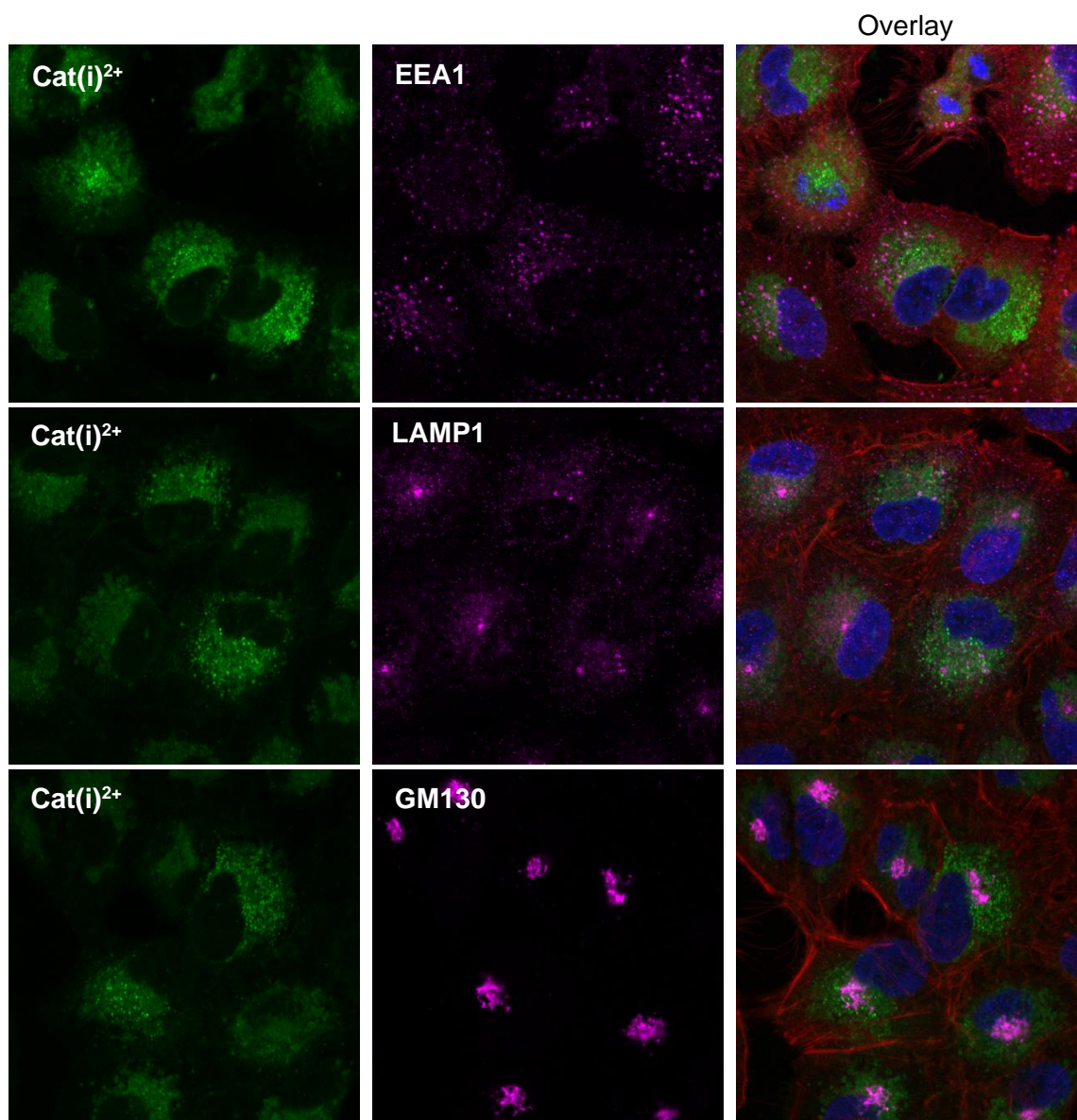


Figure 6.12: Intracellular localization of Cat(i)^{2+} in A549 cells. Co-localization of Cat(i)^{2+} with early endosomes (EEA1), golgi apparati (GM130) or lysosomes (LAMP1) observed by confocal microscopy. Cells were treated with $10 \mu\text{mol L}^{-1}$ of Cat(i)^{2+} for 90 min at 37°C . Nuclei were stained with DAPI. Co-localization was assessed by determining the Pearson correlation coefficient. The result is +1 for perfect correlation, 0 for no correlation, and -1 for perfect anti-correlation.

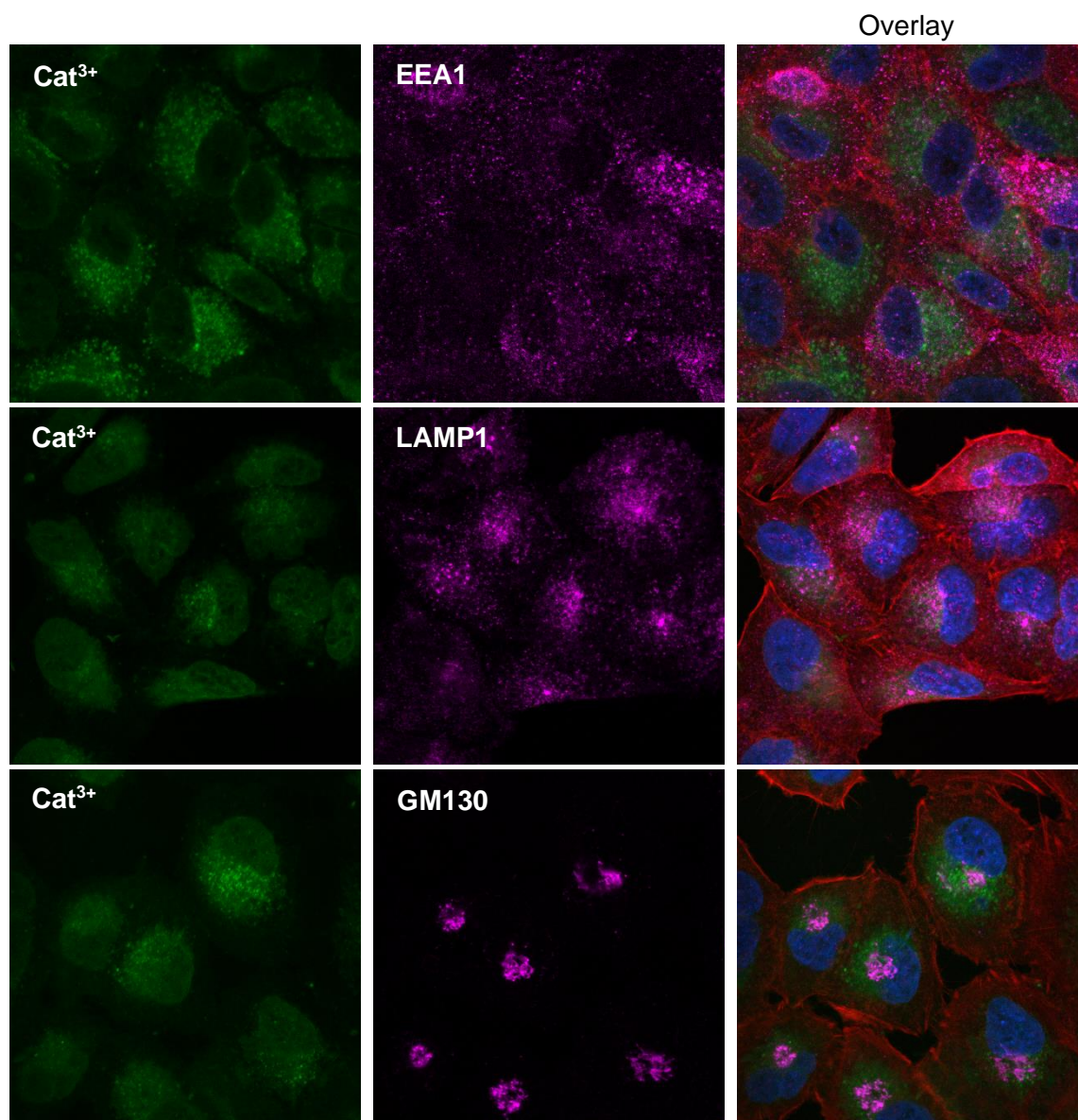


Figure 6.13: Intracellular localization of Cat^{3+} in A549 cells. Co-localization of Cat^{3+} with early endosomes (EEA1), lysosomes (LAMP1) or golgi apparati (GM130) observed by confocal microscopy. Cells were treated with $10 \mu\text{mol L}^{-1}$ of Cat^{3+} for 90 min at $37 \text{ }^\circ\text{C}$. Nuclei were stained with DAPI. Co-localization was assessed by determining the Pearson correlation coefficient. The result is +1 for perfect correlation, 0 for no correlation, and -1 for perfect anti-correlation.

6.3 Conclusions

The *mono*-cationic *bis*-triarylborane **Cat**¹⁺ does not interact with DNA, such as ctDNA or DNApore, nor RNA (pApU) as indicated by thermal melting experiments, fluorimetric titration, and CD spectroscopy. This behavior is very similar to some neutral analogues investigated earlier.^[52] Thus, one positive charge is not enough for the *bis*-triarylboranes to provide efficient interaction with polynucleotides. As a result, no further biological studies were conducted using this compound.

In contrast, **Cat**²⁺, **Cat(i)**²⁺, and **Cat**³⁺ are shown to bind to ctDNA and pApU at pH 7 presumably due to groove binding. At pH 8, the same compounds are shown to bind to ctDNA and DNApore, which consists of six intertwined oligonucleotides forming a cavity in the middle. This cavity provides enough space for the *bis*-triarylboranes. However, results obtained for the interaction between **Cat**²⁺, **Cat(i)**²⁺, and **Cat**³⁺ and DNApore suggest different binding modes. In the case of **Cat**²⁺, a perpendicular orientation of its transition moment to the chiral axis of the DNApore can be assumed, while for **Cat(i)**²⁺ a tilted orientation by ca. 60° is suggested. In contrast, for **Cat**³⁺ and **Cat**⁴⁺, strong changes of the secondary structure of DNApore upon binding of the boranes can be assumed.

Preliminary live cell imaging of A549 cells shows different staining patterns for **Cat**²⁺, **Cat(i)**²⁺, and **Cat**³⁺. Thus, not only are the DNA/RNA binding affinities affected by the number and distribution of charges of *bis*-triarylboranes, but also the cell penetration ability and their intracellular localization. However, fast bleaching of the compounds emission and simultaneous cell blebbing was observed for all three compounds, irrespective of the charge. Most likely, the cell blebbing results from intracellular formation of singlet oxygen as the *bis*-triarylboranes were found to be efficient singlet oxygen sensitizers.

Compounds **Cat(i)**²⁺ and **Cat**³⁺ are shown to be non-cytotoxic to A549 and WI38 cells up to concentration of 1.0 μmol L⁻¹. However, upon irradiation (400-700 nm), the viability of the cells is drastically lowered, most likely due to formation of singlet oxygen.

Co-localization experiments of A549 cells indicate that **Cat(i)**²⁺ stains lysosomes, golgi apparatus, and early endosomes with decreasing selectivity, while **Cat**³⁺ shows almost no co-localization with early endosomes but slightly increased localization at lysosomes.

Thus, these cationic *bis*-triarylboranes are promising candidates for photodynamic therapy due to their relatively high singlet-oxygen sensitizing efficiency and cell permeability, while the latter, among other properties, is influenced by the number of trimethylammonium groups and their distribution over the chromophore.

CHAPTER 7

PROOF-OF-CONCEPT INVESTIGATIONS OF H₂O₂-
CLEAVABLE ARYL BORONATE ESTERS AND
SUBSEQUENT FORMATION OF COUMARIN

internal or external trigger (therapeutic part) in one molecule, so-called theranostic agents are obtained. Furthermore, when such a compound releases another drug during the process, it is called a prodrug.^[226] Yan *et al.*^[8] demonstrated different kinds of such systems together with their basic functional principle. One of these systems^[227] and its cleavage in the presence of H_2O_2 is presented in Figure 7.2.

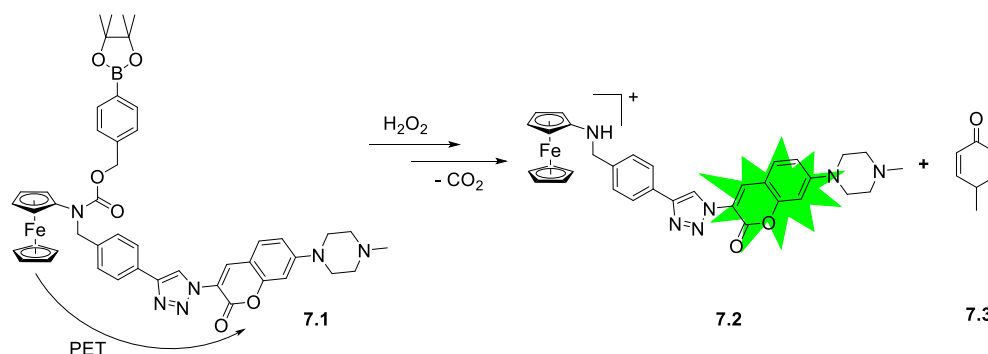


Figure 7.2: The structure of a prodrug system for the treatment of cancer and its reaction with H_2O_2 .^[227]

Prior to the cleavage of **7.1** with H_2O_2 , photoinduced energy transfer (PET) prevents fluorescence of the coumarin moiety incorporated into the system. Upon cleavage of the boronic ester and the amide, PET is lost and the fluorescence of the coumarin moiety is visible. Thus, increasing fluorescence of a stained cancer tissue indicates proceeding cleavage of the boronate moiety and increasing drug release.

Using the same basic principle of increasing fluorescence upon cleavage of a boronate ester and influenced by preliminary studies of Martina Raschig, Daul reported boronic esters of cinnamate acids and esters **7.4-7.8**, which form coumarin **7.10** upon reaction with H_2O_2 (Figure 7.3).^[10] However, **7.4-7.7** form coumarin only after light induced isomerization of the *trans*-double bond (Figure 7.3B).

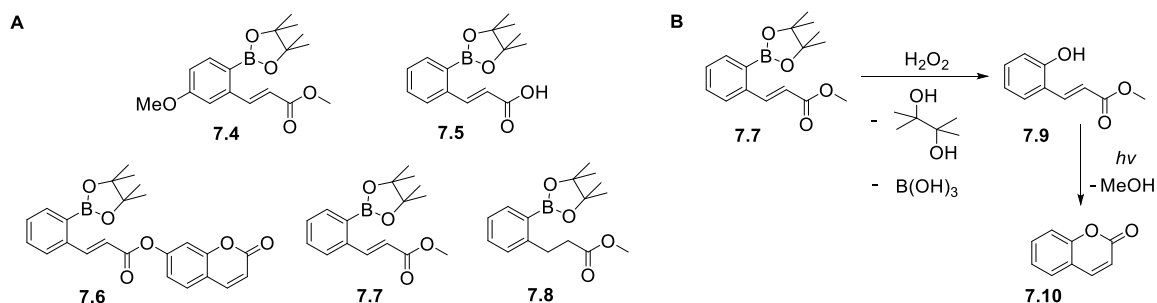


Figure 7.3: **A)** Molecules synthesized and preliminarily investigated by Daul and **B)** their reaction principle.^[10]

During the formation of coumarin, a second ester is cleaved, and methanol is released, which can be replaced by, *e. g.*, drugs in future investigations. Thus, the drug release in these systems is not only dependent on the cleavage of the boronate ester, but also requires light of a specific wavelength as a second trigger. Hence, such systems might increase the accuracy of drug release only at diseased tissues.

Daul reported the synthesized compounds to be slightly soluble in water and phosphate-buffered saline (PBS buffer) solutions and to have molar extinction coefficients in the range of ca. 1 000 to 28 000 L mol⁻¹ cm⁻¹, which increases with increasing size of the conjugated π system (Table 7.1). The water-solubilities of **7.4-7.7** are reported to be of the same magnitude, while the solubility of **7.8** was reported to be significantly enhanced. Compounds **7.5**, **7.7**, and **7.8** do not display any emission while **7.4** and **7.6** show weak emission with very low fluorescence quantum yields (Table 7.1).

Table 7.1: Properties of **7.4-7.8** reported previously.^[10] Photophysical data were determined in acetonitrile.

Compound	λ_{max}^{abs} [nm]	λ_{max}^{fl} [nm]	Apparent Stokes shift [cm ⁻¹]	Φ_f	ϵ [10 ³ L mol ⁻¹ cm ⁻¹]	max. water solubility [μ M]
7.5	276	-	-	-	19 000	20.8
7.4	280	386	9 800	-	13 000	37.7
7.7	276	-	-	-	21 500	32.1
7.6	289	454	12 600	0.02	28 000	17.8
7.8	273	-	-	-	1 000	555.2

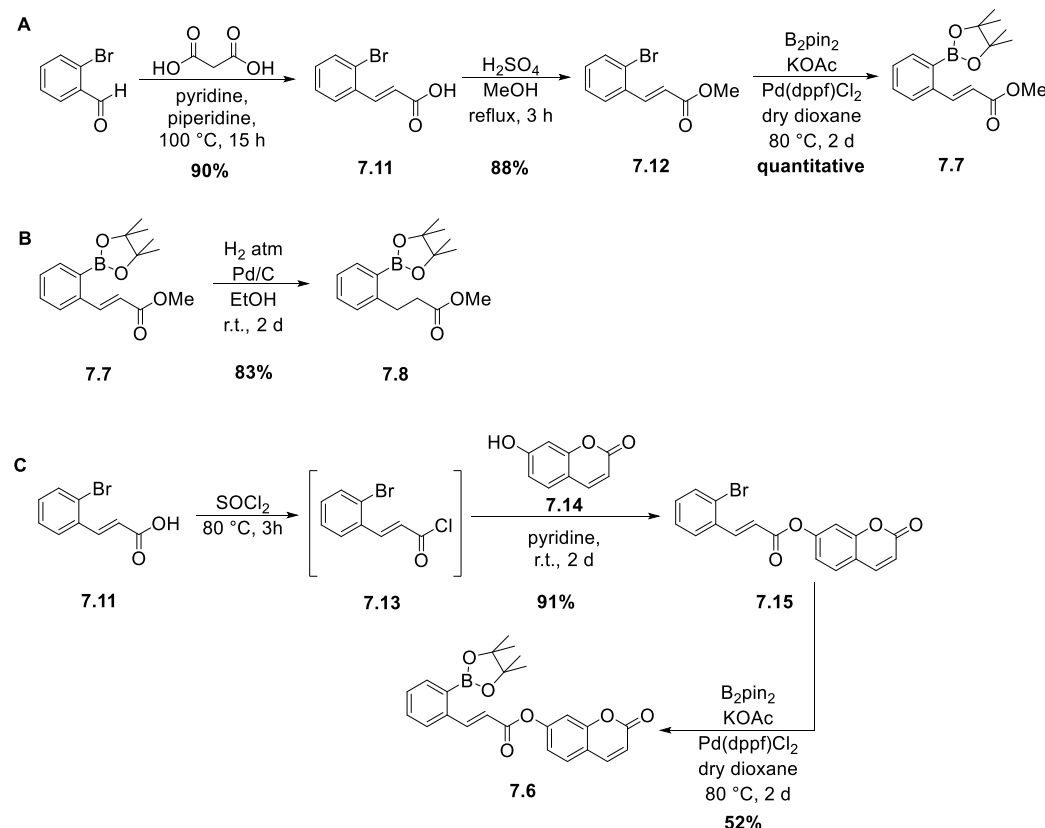
The double bond of **7.7** and **7.4** was reported to isomerize efficiently when irradiated with UV light (340 nm) for 1 h while the boronate esters are incompletely cleaved in aqueous solutions containing 20% acetonitrile upon addition of less than ca. 15 mol% H₂O₂ and stirring for 2 d. For **7.8**, complete cleavage of the boronate ester was reported after 18 h of reaction, but no cyclization was observed, as concluded from one ¹H NMR experiment. However, as no purification was carried out for this small-scale experiment and no exact amounts of added H₂O₂ was given, no direct comparison of the efficiency of the reaction sequence can be estimated. In summary, the Master's Thesis demonstrates that, using small amounts of H₂O₂, cleavage of the boronate ester is incomplete after reaction times of up to 2 d. Thus, only a small amount of the phenol derivative **7.9** is formed. As a result, the cleavage of the ester and the resulting formation of coumarin is not efficient at such low concentrations of H₂O₂.^[10]

To examine the behavior of these systems with larger amounts of H₂O₂, **7.7**, **7.6**, and **7.8** were re-synthesized giving the compounds in higher yields and purity. The corresponding photophysical properties and solubilities in water and PBS buffer were re-investigated and the cleavage of the boronate ester followed by light-induced cyclization was investigated in the presence of stoichiometric amounts of H₂O₂.

7.2 Results and Discussion

7.2.1 Synthesis

Following the synthetic strategy reported by Daul,^[10] it was possible to isolate the boronate ester **7.7** in 79% yield over 3 steps (Scheme 7.1A). In the first step, 2-bromo-cinnamic acid **7.11** was obtained in 90% yield from a Knoevenagel-Daubner reaction of 2-bromobenzaldehyde with malonic acid under basic conditions. Next, the acid functionality was converted into the methylester under acidic conditions giving **7.12** in 88% yield. In the last step, bromine was replaced by the Bpin functionality, giving **7.7** in quantitative yields.



Scheme 7.1: Reaction sequences to yield **A) 7.7**, **B) 7.8**, and **C) 7.6**.

The double bond of **7.7** was hydrogenated using palladium on charcoal under 10 bar of hydrogen giving **7.8** in 83% yield after 2 d (Scheme 7.1B).

To obtain **7.6** (Scheme 7.1C), the more reactive acid chloride **7.13** was synthesized with thionyl chloride and then added to a solution of umbelliferon **7.14** in dry pyridine. The precipitate obtained after addition of water was collected by filtration and washed with acetone to give **7.15** in 91% yield. Previously, a yield of 72% was reported.^[10] The yield of **7.6** was increased from 25%^[10] to 52%, presumably due to the use of dry dioxane and stirring of the catalytic system prior to addition of **7.15**.

7.2.2 Solubility in Water and PBS Buffer

To reproduce the solubility values of **7.6**, **7.7**, and **7.8** in water and to examine their solubility in PBS buffer, determination of their molar extinction coefficient in both solutions was attempted. However, it was not possible to obtain stock solutions with concentrations between 4 and 6×10^{-4} mol L⁻¹ in pure water, which confirms the low solubility of the compounds. Hence, the solubility of the compounds was examined by monitoring the change of the respective absorption spectra during addition of water to stock solutions in acetonitrile (Figure 7.4A) and vice versa (Figure 7.4B,C).

These measurements show that the absorption of **7.6** is not affected until the solution consists of ca. 4% acetonitrile in water with a concentration of 4.2×10^{-6} mol L⁻¹ (Figure 7.4A). However, when adding increasing amounts of acetonitrile stock solutions of **7.6** to pure water (Figure 7.4B), the absorption changes at concentrations of ca. 1.25×10^{-5} mol L⁻¹ indicating precipitation and, thus, the maximum solubility. This value is slightly lower than that reported earlier (1.8×10^{-5} mol L⁻¹).^[10] Using the same approach, **7.7** and **7.8** are shown to be soluble in water with small amounts of acetonitrile up to concentrations of ca. 7.5×10^{-5} mol L⁻¹ (Figure 7.4C) and 6.2×10^{-5} mol L⁻¹ (Figure 7.4D), which is significantly higher (3.2×10^{-5} mol L⁻¹) and lower (5.5×10^{-4} mol L⁻¹), respectively, than reported earlier using a different method of determination.^[10]

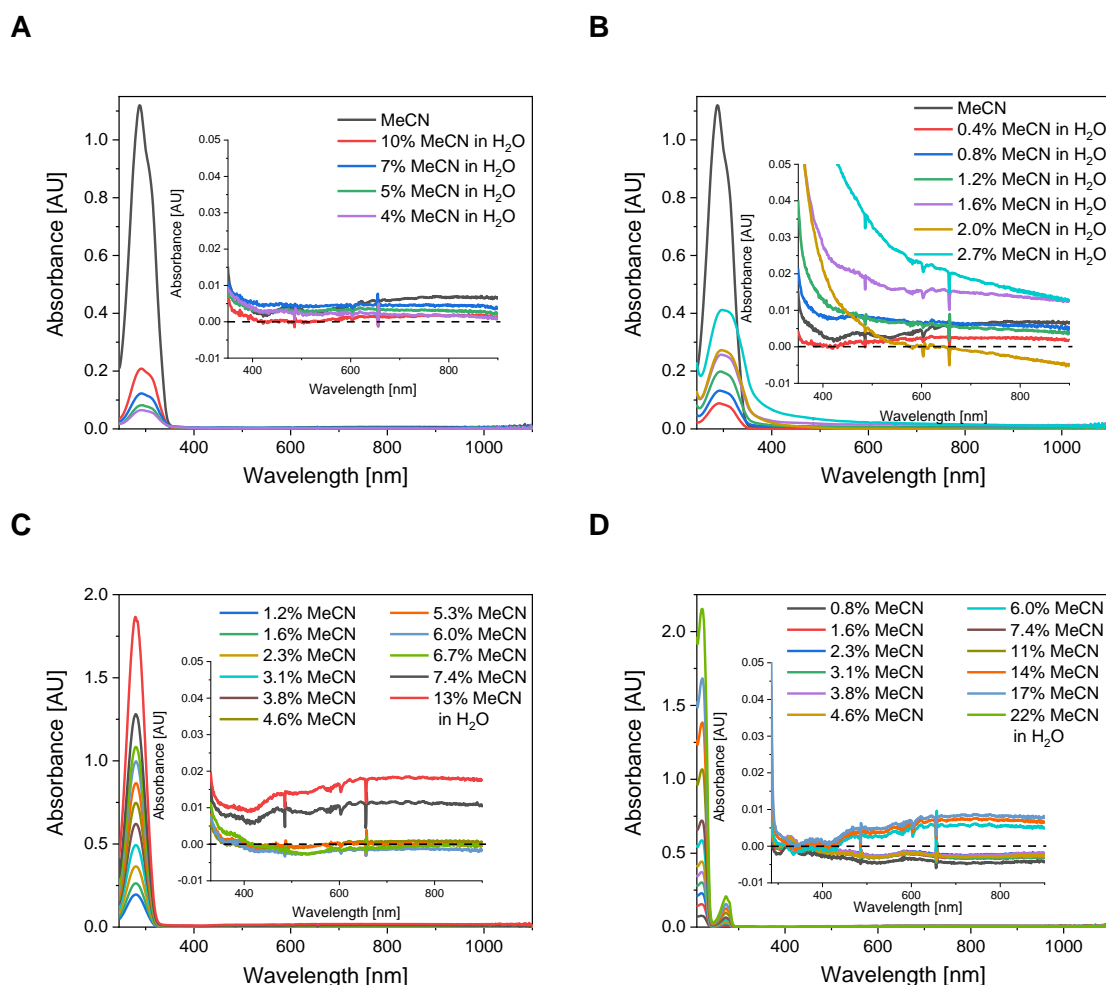


Figure 7.4: **A)** Absorption decrease of **7.6** with increasing amount of water ($c_1 = 1.05 \times 10^{-5} \text{ mol L}^{-1}$; $c_5 = 4.2 \times 10^{-6} \text{ mol L}^{-1}$). Absorption increase of **B)** **7.6** ($c_1 = 4.2 \times 10^{-6} \text{ mol L}^{-1}$, $c_7 = 2.9 \times 10^{-5} \text{ mol L}^{-1}$), **C)** **7.7** ($c_1 = 1.2 \times 10^{-5} \text{ mol L}^{-1}$, $c_{11} = 1.1 \times 10^{-4} \text{ mol L}^{-1}$); **D)** **7.8** ($c_0 = 8.2 \times 10^{-6} \text{ mol L}^{-1}$, $c_{12} = 2.2 \times 10^{-4} \text{ mol L}^{-1}$) upon addition of an acetonitrile stock solution to water.

Accordingly, the solubility of **7.6-7.8** was determined in PBS buffer (Figure 7.5). A maximum solubility of ca. $1.25 \times 10^{-5} \text{ mol L}^{-1}$ was obtained for **7.6**, which is very similar to its solubility in pure water (*vide supra*), while for **7.7**, no change of the absorption spectrum was observed for concentrations up to $1.1 \times 10^{-4} \text{ mol L}^{-1}$ (Figure 7.5B). This value is significantly higher than that observed in pure water. In the case of **7.8**, a change of the absorption maximum is observed at ca. $7.6 \times 10^{-5} \text{ mol L}^{-1}$, suggesting a slightly increased solubility of the compound in PBS buffer compared to pure water.

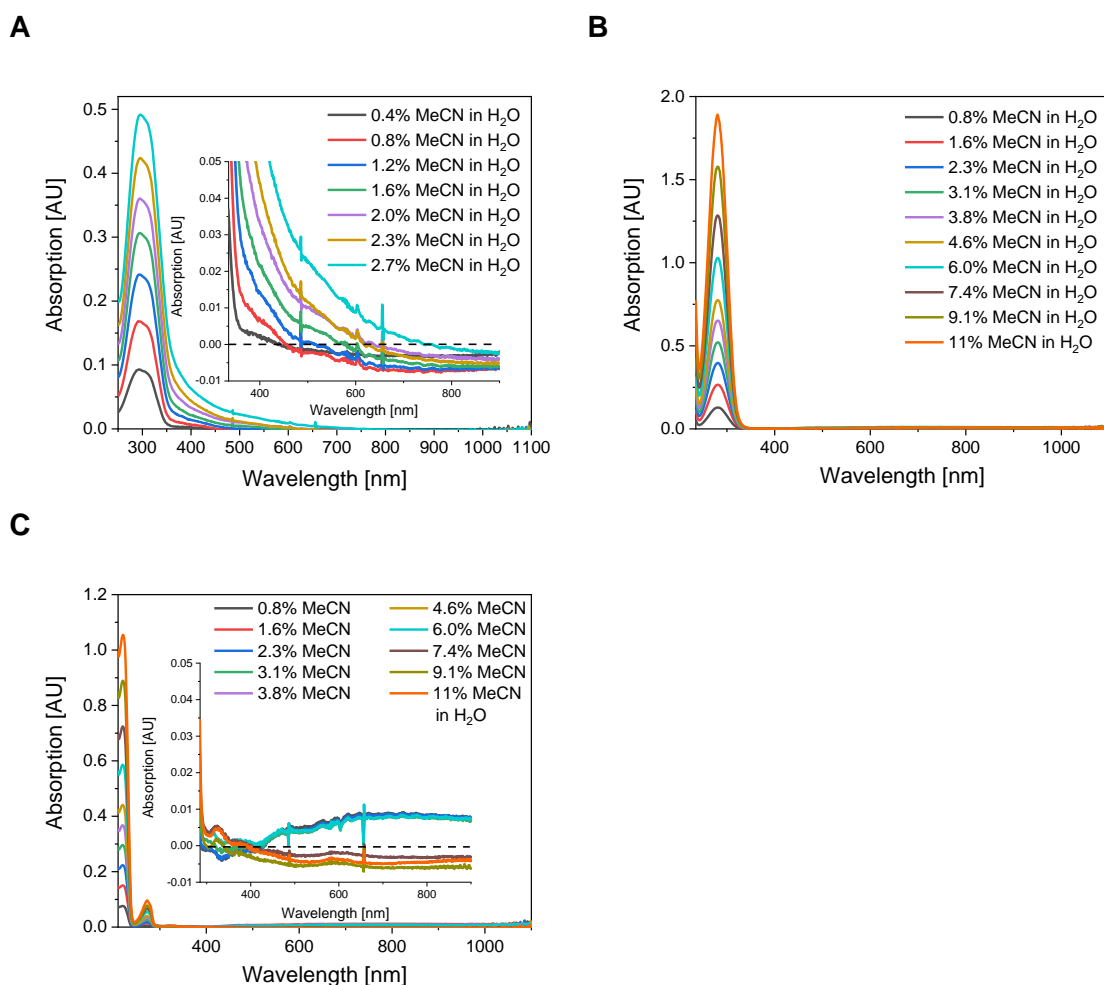


Figure 7.5: Absorption change of **A)** **7.6** ($c_0 = 4.2 \times 10^{-6} \text{ mol L}^{-1}$, $c_7 = 2.9 \times 10^{-5} \text{ mol L}^{-1}$), **B)** **7.7** ($c_0 = 8.0 \times 10^{-6} \text{ mol L}^{-1}$, $c_{10} = 1.1 \times 10^{-4} \text{ mol L}^{-1}$); **C)** **7.8** ($c_0 = 8.2 \times 10^{-6} \text{ mol L}^{-1}$, $c_{10} = 1.1 \times 10^{-4} \text{ mol L}^{-1}$) upon addition of an acetonitrile stock solution to water.

7.2.3 Photophysical Properties

The photophysical properties of **7.6-7.8** were determined in ethanol (dielectric constant: $\epsilon_r = 25 \text{ F m}^{-1}$), acetonitrile ($\epsilon_r = 38 \text{ F m}^{-1}$), and dilutions of different amounts of acetonitrile stock solutions in water and aqueous PBS buffer, with pure water having a ϵ_r of 80 F m^{-1} .^[166] The resulting spectra and data are summarized in Figure 7.6 and Table 7.2, respectively.

The absorption spectra of **7.6-7.8** are not solvatochromic. The compounds have molar extinction coefficients of ca. $15\,000 \text{ L mol}^{-1} \text{ cm}^{-1}$ in all solvents examined; only the value of **7.6** in acetonitrile is significantly higher ($32\,000 \text{ cm}^{-1}$). The absorption maxima shift bathochromically from 224 nm to 278 nm to 288 nm in acetonitrile with a more extended conjugated π -system in the order **7.8** < **7.7** < **7.6**. Compound **7.7** displays no emission

upon excitation at the absorption maximum, while **7.6** and **7.8** are slightly emissive when excited at 288 nm and 224 nm, respectively, with apparent Stokes shifts of ca. 10 000 cm⁻¹. The emission of **7.6** is slightly solvatochromic while the emission of **7.8** is not. However, in the case of **7.6**, irradiation with light leads to isomerization of the double bond, which results in a change of both absorption and emission spectra over time. Thus, it was not possible to determine fluorescence quantum yields or lifetimes for **7.6**. Due to the very weak emission of **7.8**, no such data are reported for the latter compound as well.

In summary, high molar extinction coefficients in all solvents examined and weak emission intensities are found for the basic structure of the studied prodrug system. However, the emission can be induced by attachment of a chromophore, such as umbelliferon in **7.6**.

In general, the data obtained are in accordance with the data reported previously.^[10] However, it must be noted that the previously reported data for **7.6** and **7.8** were obtained from compounds containing residual amounts of umbelliferon and **7.7**, respectively.

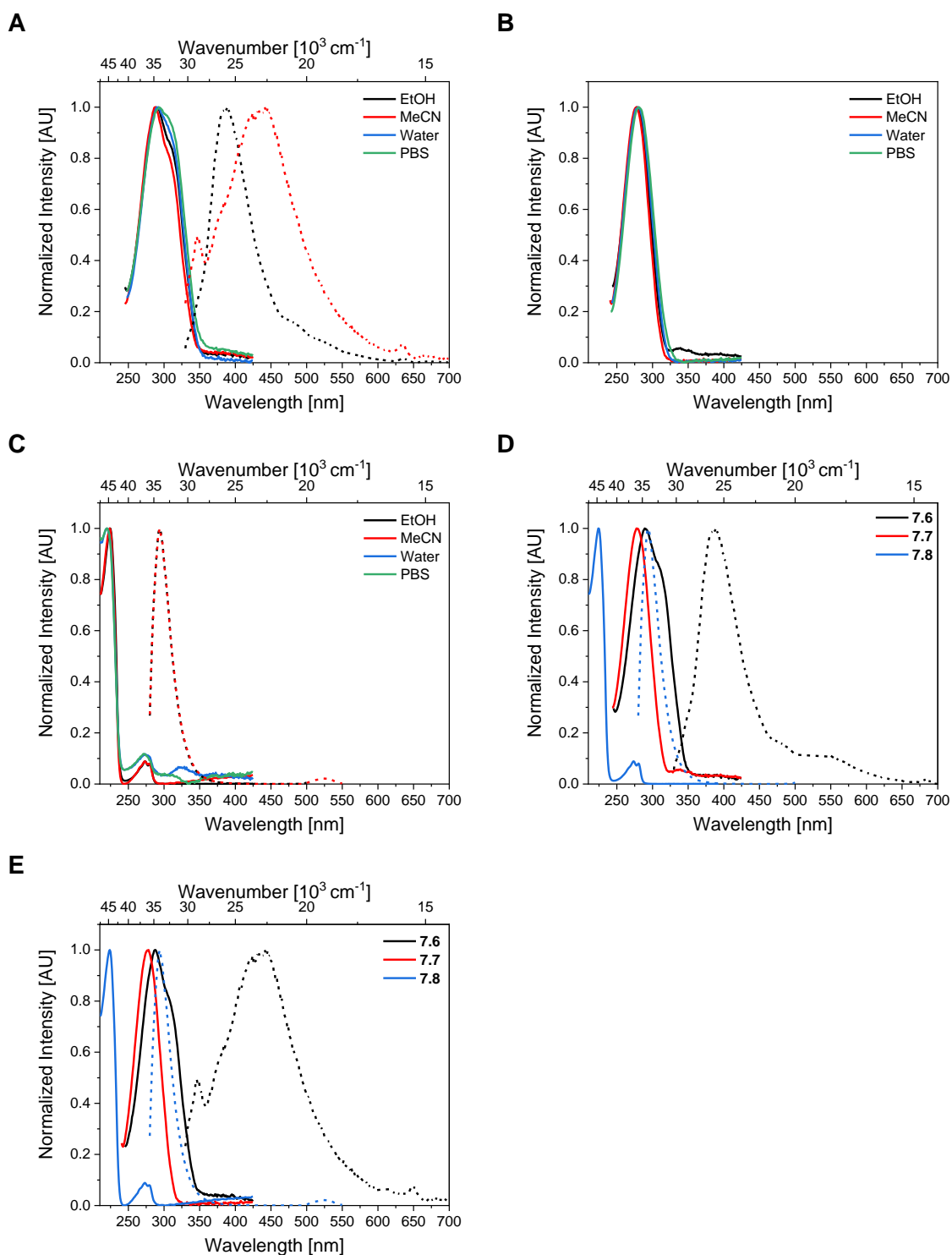


Figure 7.6: Absorption (solid lines) and emission (dotted lines; excitation at λ_{max}^{abs}) spectra of **A) 7.6**, **B) 7.7**, and **C) 7.8** in solvents of different polarity. Absorption (solid lines) and emission (dotted lines; excitation at λ_{max}^{abs}) spectra of **7.6-7.8** in **D) ethanol** and **E) acetonitrile**.

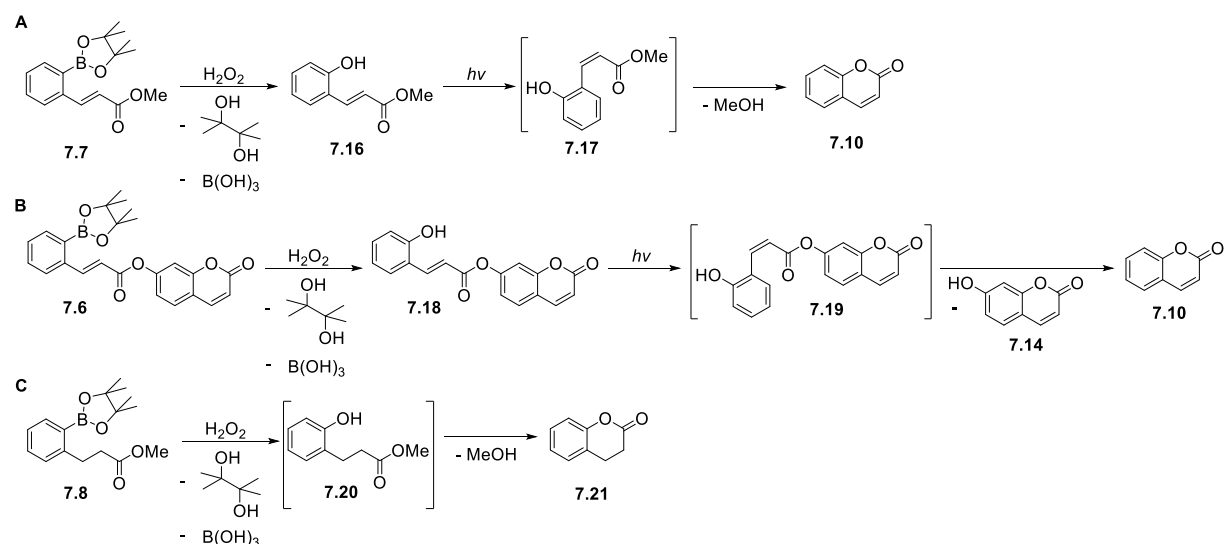
Table 7.2: Photophysical data of **7.6-7.8** determined in solvents of different polarity.

		λ_{max}^{abs} [nm]	λ_{max}^{fl} [nm]	Apparent Stokes shift [cm ⁻¹]	ϵ [L mol ⁻¹ cm ⁻¹]
7.6	EtOH	289	389	8 900	-
	MeCN	288	442	12 100	32 000
	Water [a]	292	-	-	13 000
	PBS [a]	293	-	-	16 000
7.7	EtOH	277	-	-	-
	MeCN	278	-	-	19 000
	Water [a]	280	-	-	10 000
	PBS [a]	281	-	-	17 000
7.8	EtOH	224	294	10 600	-
	MeCN	224	294	10 600	7 000
	Water [a]	220	-	-	17 000
	PBS [a]	220	-	-	10 000

[a] Solutions were prepared by addition of acetonitrile stock solutions to water/PBS buffer; final solutions contain less than 15% MeCN.

7.2.4 Cleavage experiments

The main goal of this work was to investigate whether the boronate ester moiety in the prodrug systems **7.6-7.8** is cleaved in the presence of H₂O₂ and if so, whether the resulting phenol derivative is able to react with the ester moiety to produce coumarin. In the case of **7.6** and **7.7**, light-induced isomerization of a double bond is required before the ester moiety can be cleaved (Scheme 8.1A,B) while for **7.8**, no light should be required to form dihydrocoumarin **7.21** (Scheme 8.1C).



Scheme 7.2: Expected reaction sequences of **A) 7.7**, **B) 7.6**, and **C) 7.8** upon cleavage of the boronate ester with H_2O_2 and subsequent irradiation.

Previous studies have shown that the boronate ester does not cleave completely in the presence of less than equimolar amounts of H_2O_2 after ca. 2 d.^[10] To study the behavior in the presence of equimolar amounts of H_2O_2 , solutions of **7.6**, **7.7**, and **7.8** in THF were treated with H_2O_2 and stirred in the dark at room temperature (WARNING: the use of H_2O_2 in THF generates instable peroxides which must be destroyed prior to any workup; see below). Quenching samples of each mixture after 40 min with an aqueous, saturated solution of iron(II) sulfate and subsequent HRMS measurements indicate the formation of **7.16** (m/z ca. 179) and **7.10** (m/z ca. 147) in the case of **7.7** (Figure 7.7A) and **7.18** (m/z ca. 309) and **7.10** (m/z ca. 147) in the case of **7.6** (Figure 7.8A). The molecular signals ($[\text{M}+\text{H}]^+$) of **7.7** and **7.6** are detected at m/z ca. 289 and 419, respectively. In both cases, an additional signal at m/z 257 is found, indicating cleavage of the ester moiety. Presumably, this cleavage proceeds during ionization as the same signal was found in the HRMS spectrum of pure **7.6** recorded for characterization of the compound (Figure 11.145). Thus, the boronate esters of **7.7** and **7.6** are cleaved after 40 min of reaction with H_2O_2 forming the phenol derivatives **7.16** and **7.18**, respectively. In addition, coumarin (m/z 147) was detected in both cases, although the reactions were stirred in the dark indicating that the energy of the light, which the measured samples were exposed to during the preparation of the HRMS measurement, was sufficient to isomerize the double bonds. Another explanation is that the ester of the phenol derivative is cleaved during ionization resulting in the same signal as expected for coumarin. In both cases, even after 24 h of stirring, starting material was detected (Figure 7.7B; Figure 7.8B). Very similar results were found for **7.8** (m/z ca. 291), as the phenol derivative **7.20** (m/z ca. 181) and dihydrocoumarin **7.21** (m/z ca. 149) are detected after 40 min and 24 h (Figure 7.9). Thus,

as expected, no irradiation is required for this last step in compound **7.8**, which does not contain a C=C double bond.

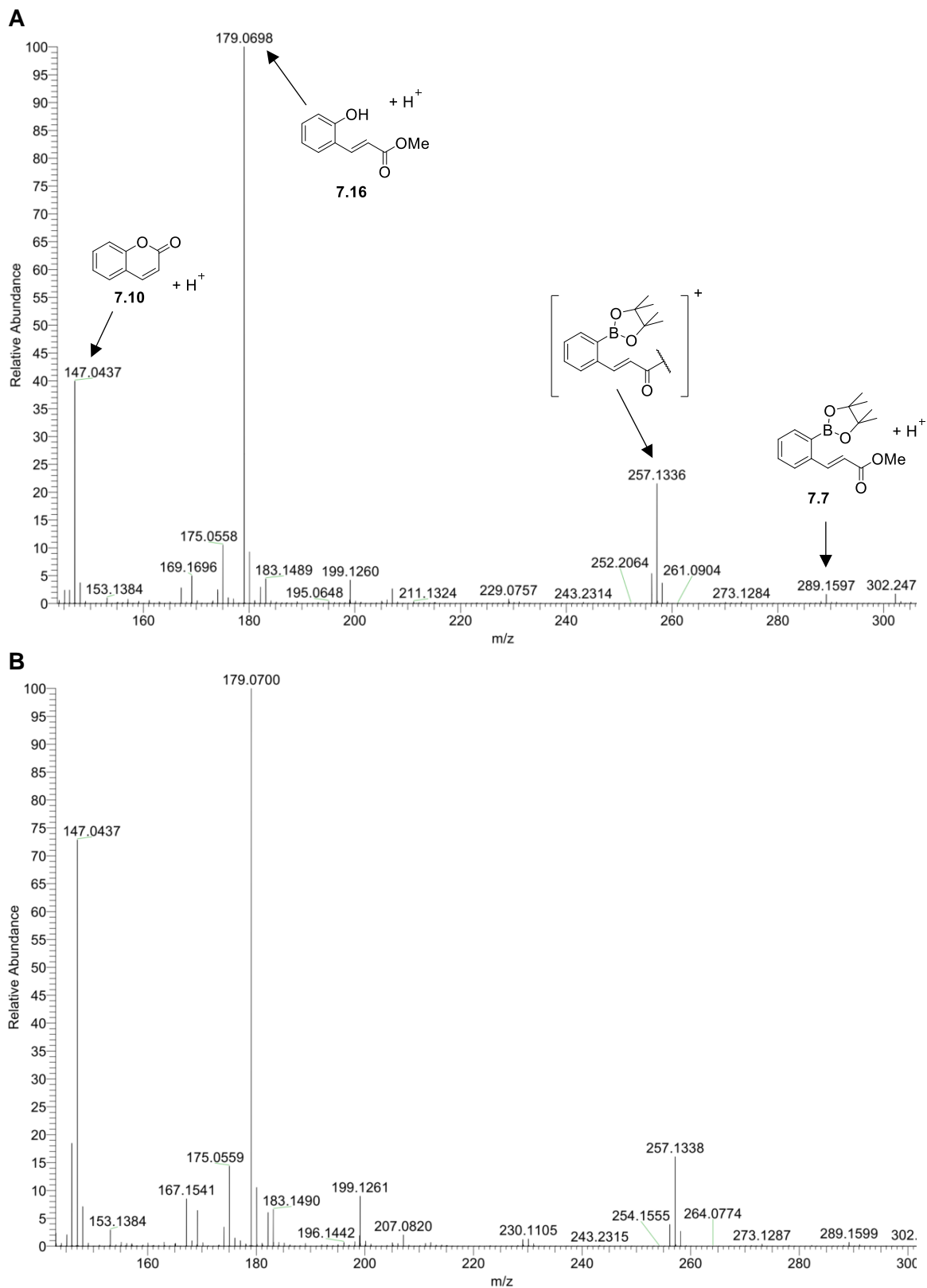


Figure 7.7: HRMS spectra (ASAP pos) of **7.7** recorded after **A)** 40 min and **B)** 24 h.

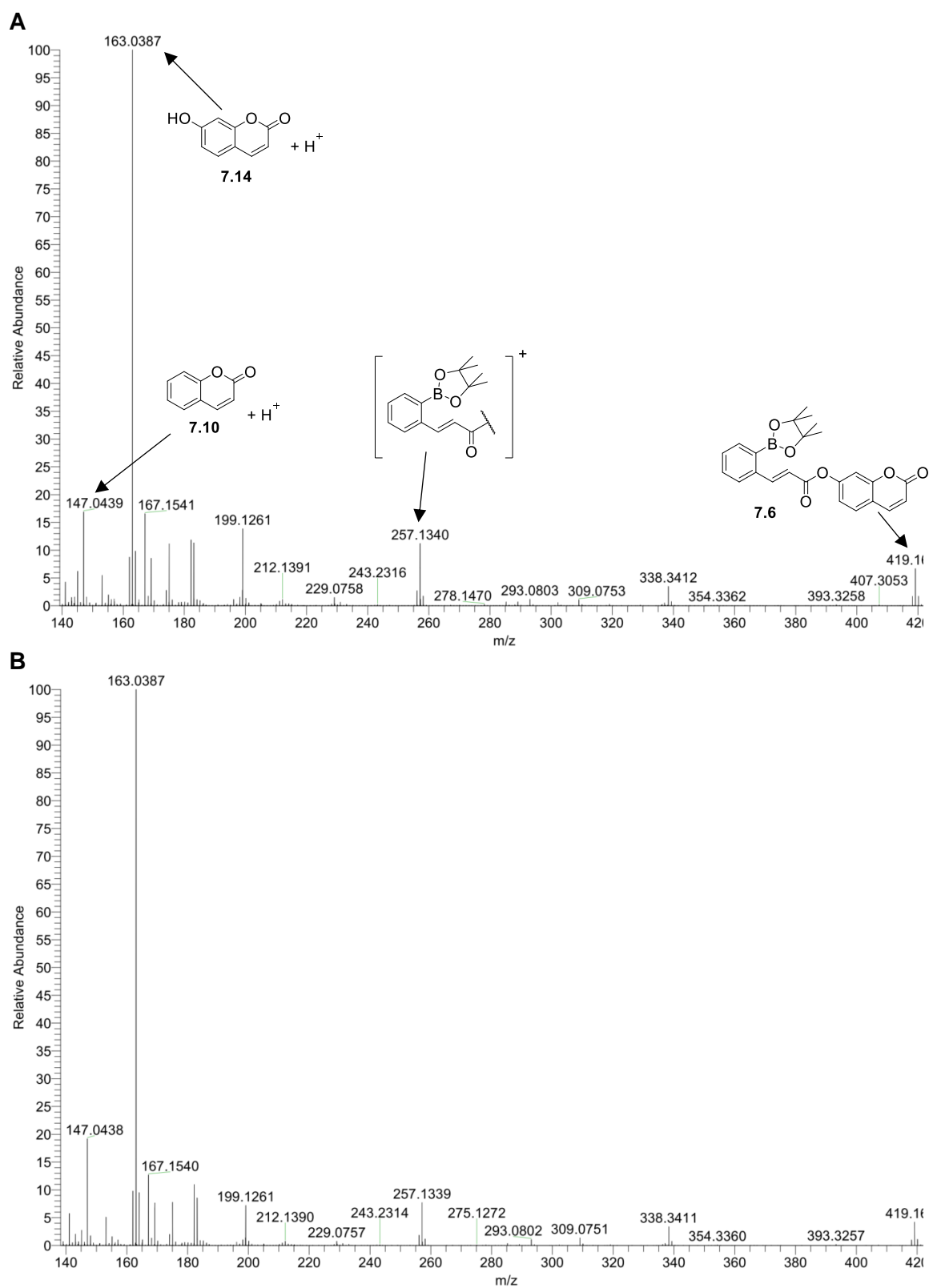
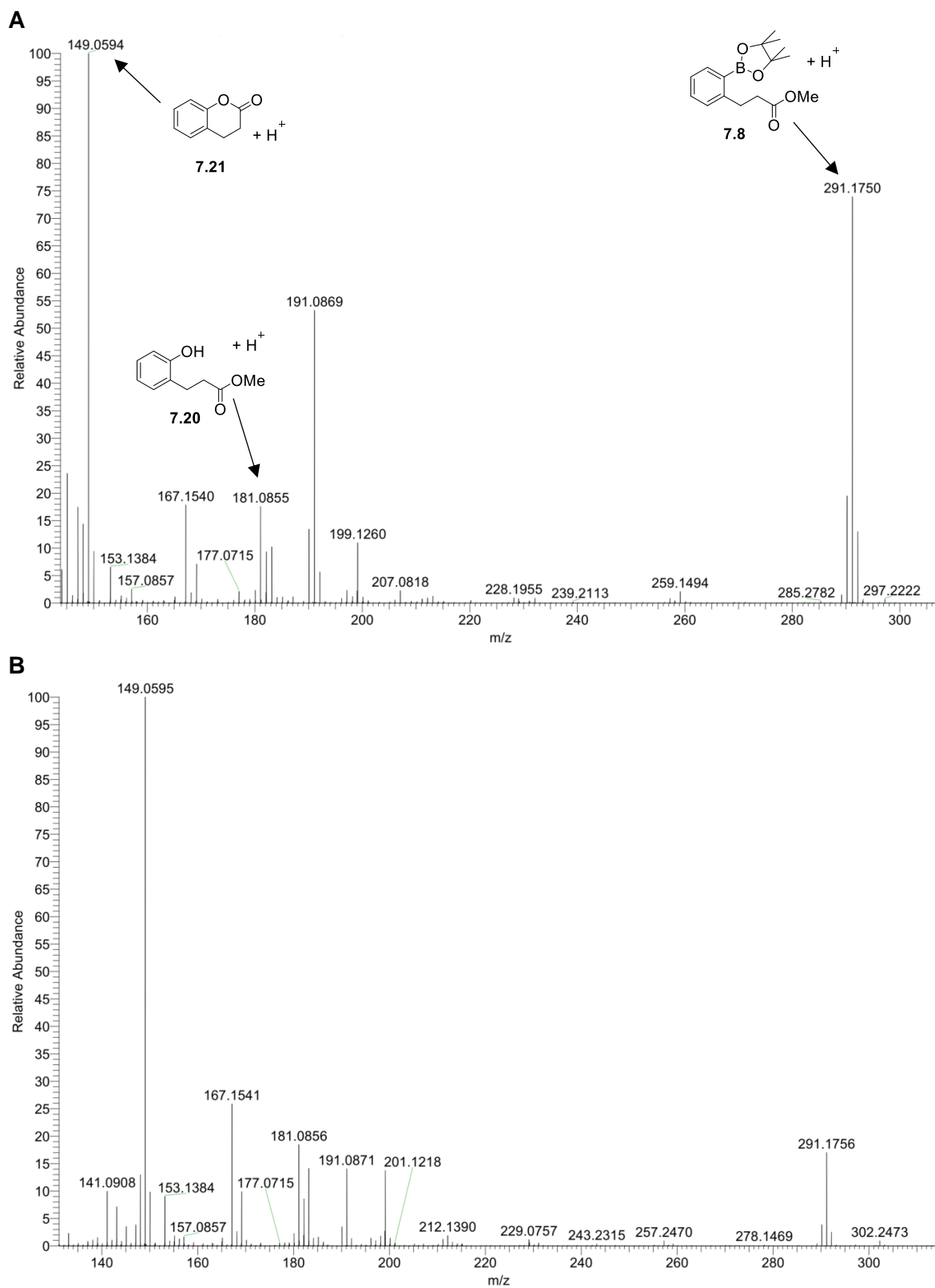


Figure 7.8: HRMS spectra (ASAP pos) of **7.6** recorded after **A**) 40 min and **B**) 24 h.

Figure 7.9: HRMS spectra (ASAP pos) of **7.8** recorded after **A)** 40 min and **B)** 24 h.

The photophysical data indicate that light in the range of ca. 250 to 310 nm is required to isomerize the double bond of **7.6** and **7.7**. Thus, solutions of **7.6** and **7.7** in CD₃CN were stirred under irradiation of two lamps (each ca. 4 W, 254 nm) for up to 1 h and the isomerization was monitored by ¹H NMR spectroscopy (Figure 7.10A,C). In a second experiment, reaction times of up to 4 h were examined (Figure 7.10B,D).

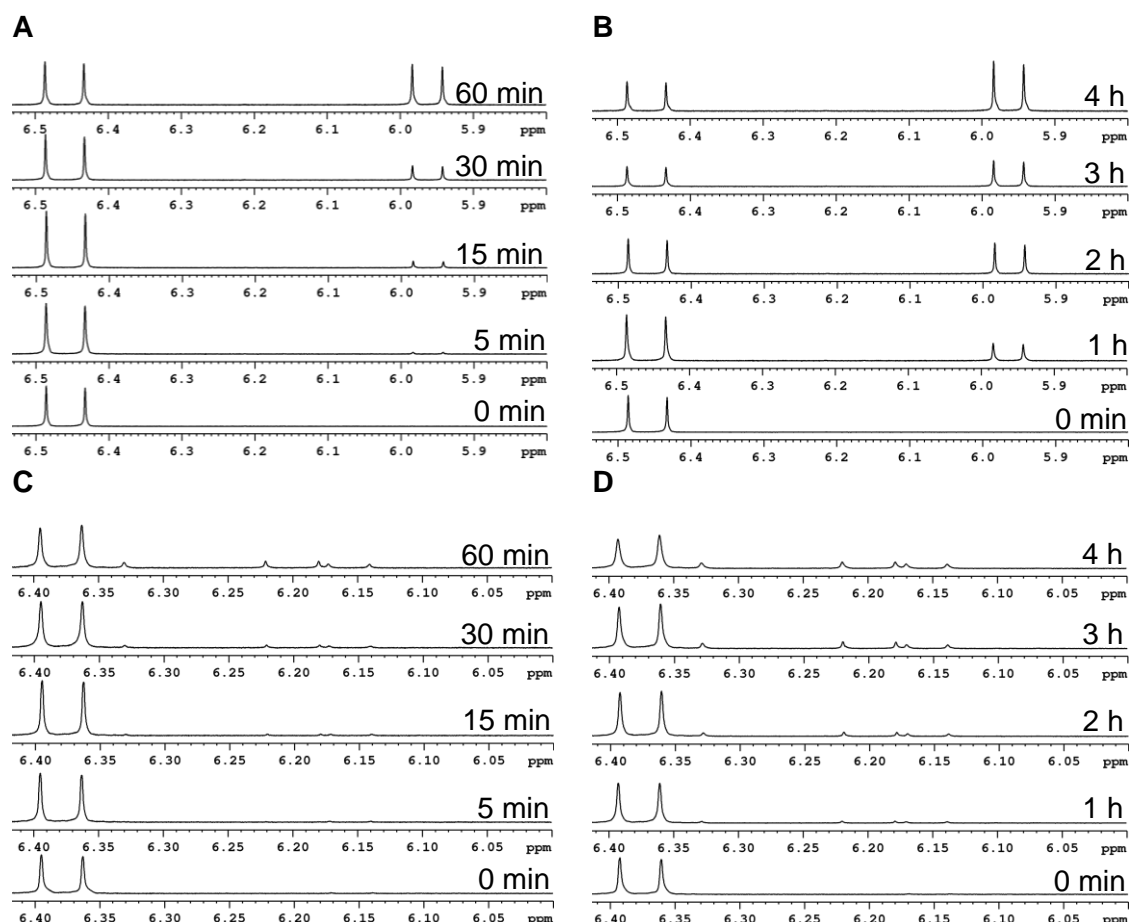
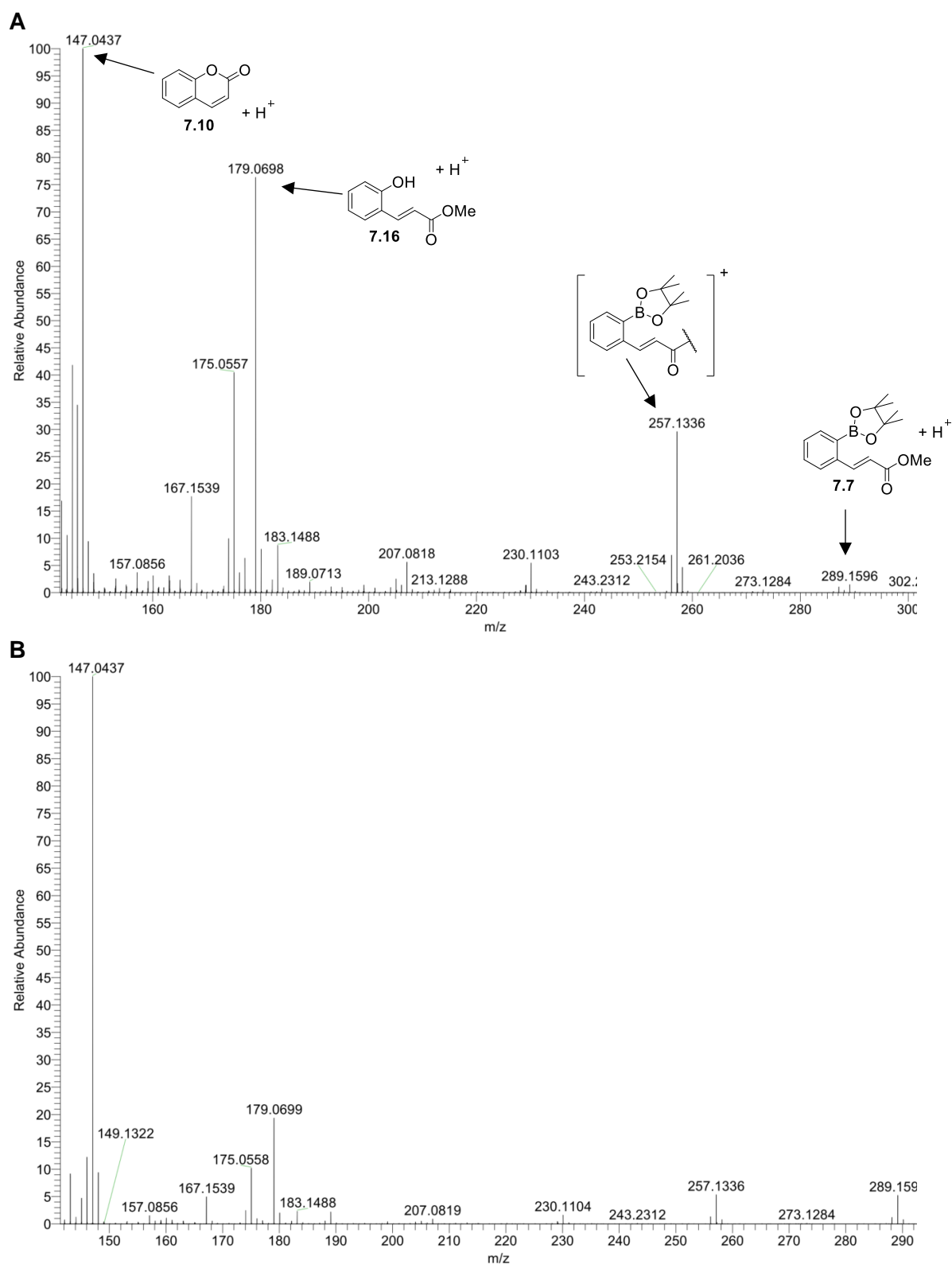


Figure 7.10: Isomerization of the C–C double bond of **7.7** (A, B) and **7.6** (C, D) under irradiation with light of the wavelength 245 nm monitored by ¹H NMR spectroscopy in CD₃CN at 300 MHz.

For **7.7**, signals indicating isomerization are visible after 5 min of irradiation (Figure 7.10A). After ca. 3 h, equivalent amounts of *trans*- and *cis*-isomer are observed (Figure 7.10B). However, even after 4 h of irradiation, **7.7** was not fully converted to the *cis*-isomer. The ³J coupling constant of the double bond decreases from 16 Hz (6.45 ppm) in the *trans*-isomer to 12 Hz (5.95 Hz) in the *cis*-isomer.

In contrast, for **7.6**, no clear change of the coupling constant and signals are observed, most likely caused by the attached umbelliferon moiety. However, some new signals between 6.45 ppm and 6.10 ppm can be observed after ca. 15 min of irradiation (Figure 7.10C).

Combining the results obtained for the cleavage of the boronate ester and the isomerization of the double bond in a second cleavage experiment shows that, after only 5 min of irradiation, the boronate ester of **7.7** is cleaved and coumarin is formed (Figure 7.11A). After ca. 6 h, coumarin **7.10** (m/z 147), phenol derivative **7.16** (m/z 179) and **7.7** (m/z 289) were detected (Figure 7.11B). For **7.6** (m/z 419), cleavage of the esters and the resulting formation of coumarin **7.10** (m/z 147) and umbelliferon **7.14** (m/z 163) are also detected after 5 min (Figure 7.12A). The same compounds are observed after 6 h of reaction (Figure 7.12B). For **7.8**, the second cleavage experiment conducted under ambient light shows that the starting material was cleaved after 1 h and **7.21** was formed (Figure 7.13A). The same compounds were detected after 46 h of stirring (Figure 7.13B). In summary, these experiments demonstrate that the formation of coumarin (**7.10**) begins after only 5 min of reaction for **7.6** and **7.7**, while dihydrocoumarin **7.21** was detected after 1 h in the case of **7.8**. Comparing these results with those reported previously^[10] indicates that increased amounts of H₂O₂ increases the rate of the reaction.

Figure 7.11: HRMS spectra (ASAP pos) of **7.7** recorded after **A**) 5 min and **B**) 6 h.

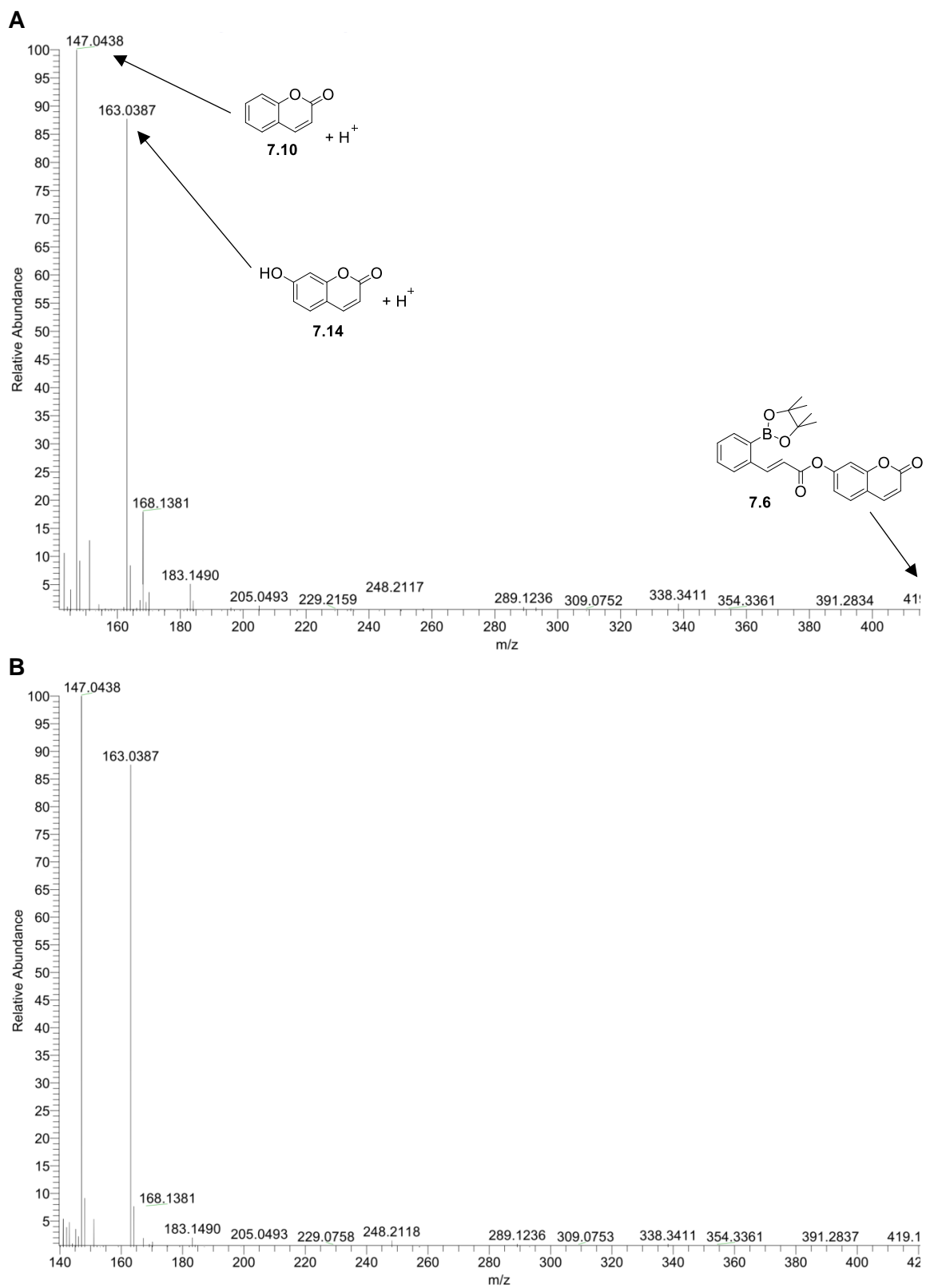


Figure 7.12: HRMS spectra (ASAP pos) of **7.6** recorded after **A**) 5 min and **B**) 6 h.

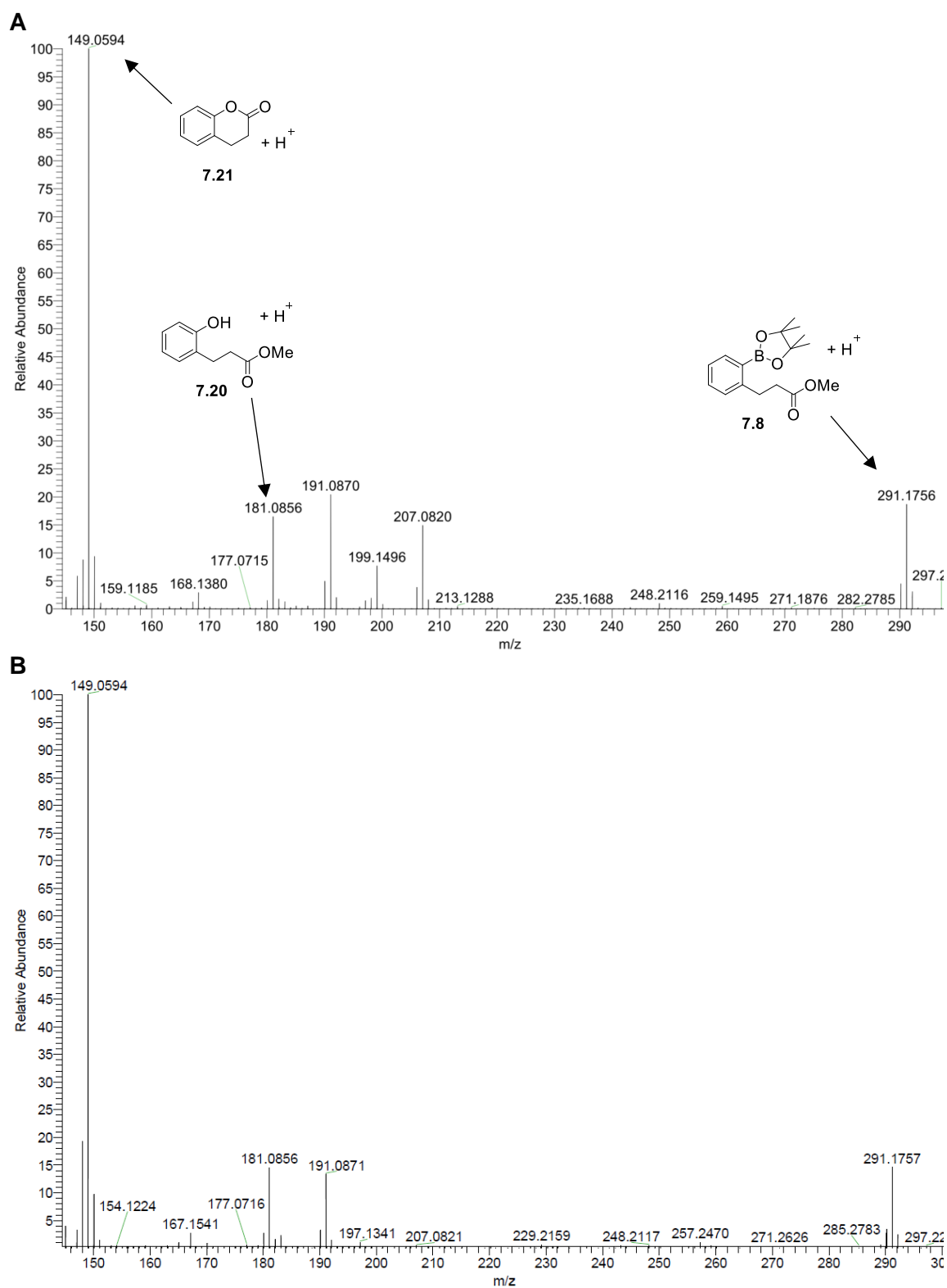


Figure 7.13: HRMS spectra (ASAP pos) of **7.8** recorded after **A**) 1 h and **B**) 46 h.

7.3 Conclusions

The syntheses of three prodrug systems **7.6-7.8** is described, with the compounds obtained in high yields of 47-79% over three to four steps. All three compounds are slightly soluble in water and aqueous PBS buffer when prepared from concentrated acetonitrile stock solutions. Examination of the photophysical properties demonstrated that the absorption spectra of **7.6-7.8** shift bathochromically with increasing size of the π system, which increases in the order **7.8** < **7.7** < **7.6**. The three compounds have high molar extinction coefficients of ca. 15 000 L mol⁻¹ cm⁻¹. Compound **7.7** is not emissive, while weak emission signals were detected for **7.6** and **7.8** resulting from umbelliferon and the benzene moiety, respectively.

Addition of stoichiometric amounts of H₂O₂ to THF solutions of **7.6-7.8** and stirring in the dark demonstrated the cleavage of the boronate ester functionality of the compounds after 40 min. Upon irradiation at 254 nm, isomerization of the double bonds of **7.6** and **7.7** indicate the formation of the *cis*-isomers after ca. 5 min and 15 min, respectively. Thus, a slower conversion for the compound with the coumarin ester substituent (**7.6**) can be assumed. Combination of irradiation and addition of stoichiometric amounts of H₂O₂ in one experiment indicate that coumarin is formed after a reaction time of 5 min in the cases of **7.7** and **7.6**. In the case of **7.8**, the sample was stirred under ambient light and cleavage of the esters was observed after 40 min of reaction by detection of dihydrocoumarin **7.21**.

In summary, these experiments indicate that prodrug systems such as **7.6-7.8** are good candidates for future investigations as their boronate ester and ester moieties are readily cleaved in a two-step process upon addition of stoichiometric amounts of H₂O₂. However, the compounds are only weakly fluorescent and, thus, it would not be easy to detect their intracellular localization. In addition, the light required for the isomerization of the double bond of **7.7** and **7.6** to yield coumarin is of high energy and, thus, has the potential to harm cells. Hence, the basic structure of such prodrug systems should be modified in future investigations such that the π system is extended to enhance the fluorescence efficiency and to require light of lower energy for the isomerization of the double bond. Potentially, the introduction of electron-donating and electron-accepting moieties at the benzene ring could solve both problems.

CHAPTER 8

SUMMARY / ZUSAMMENFASSUNG

8 Summary / Zusammenfassung

Parts of the following text and graphics are reproduced in a slightly modified form with the permission of Wiley VCH and The Royal Society of Chemistry.

8.1 Summary

8.1.1 Chapter 1

A short and general introduction to the structural motif of three-coordinate organoboron compounds is given, focusing on triarylboranes and boronic esters. A summary of the results reported for *tetra*-cationic *bis*-triarylboranes is given, demonstrating that the influence of different bridging units on, *e. g.*, photophysical and biological properties was investigated, while the influence of different numbers or distributions of the charge remained uninvestigated.

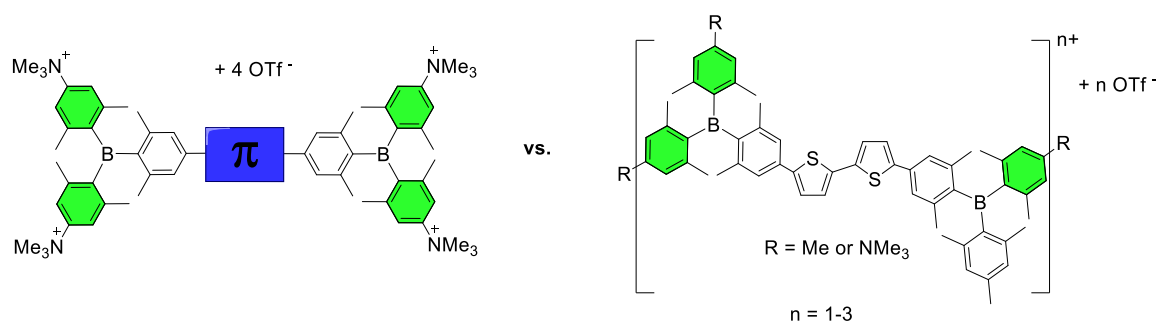


Figure 8.1: Previously studied compounds vs. target compounds.

8.1.2 Chapter 2

Chapter 2 summarizes the development of the synthesis of triarylboranes since their first isolation, which was reported in 1885. It is demonstrated that the synthetic approaches underwent various changes over the following century, some of which are still used in the present day, such as the generally applicable routes developed by Krause *et al.* in 1922, or by Grisdale *et al.* in 1972 at Eastman Kodak. Some other developments were not pursued further after their initial reports, such as the synthesis of two triarylboranes bearing three different aromatic groups by Mikhailov *et al.* in 1958. Various strategies have been pursued to synthesize specifically designed triarylboranes using the plethora of synthetic tools chemists of the 21st century have.

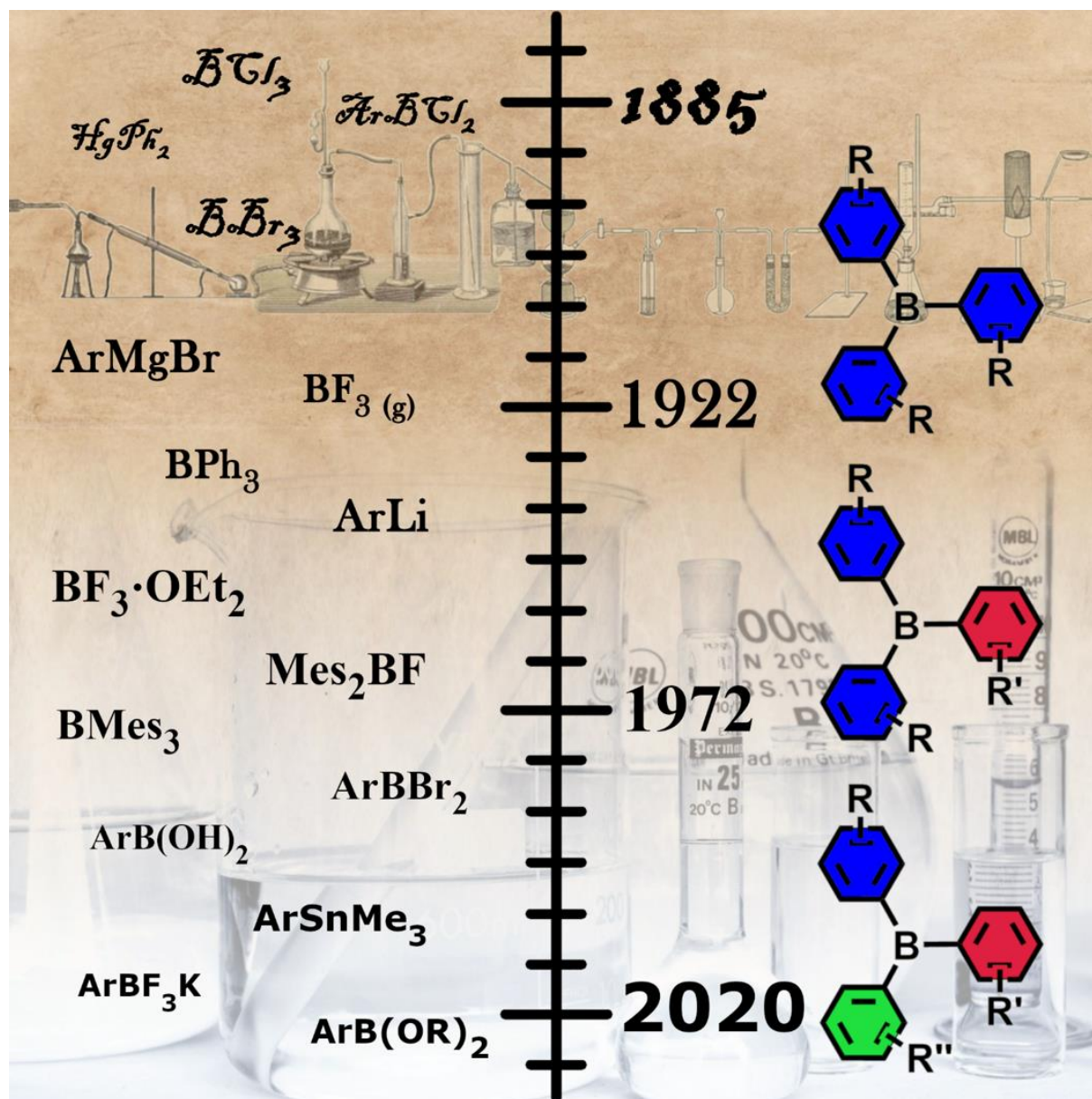
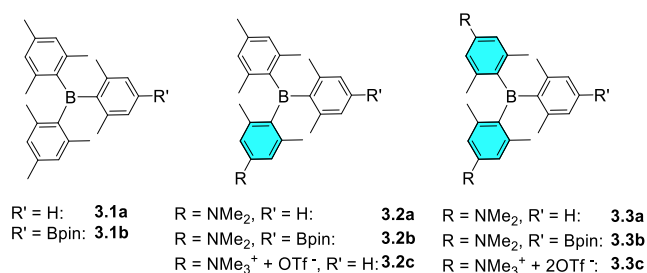
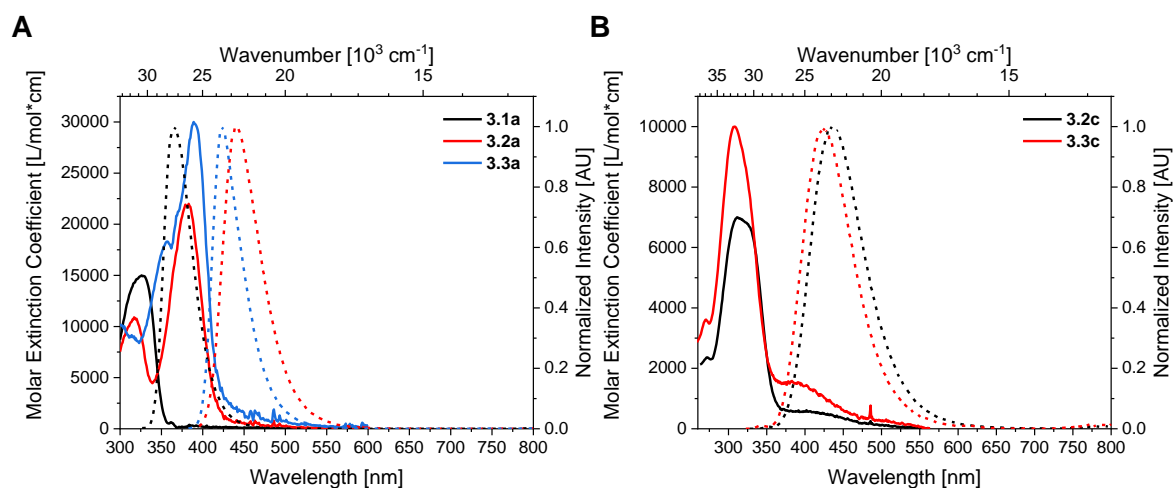


Figure 8.2: Frontispiece of the review summarizing the synthetic approaches to triarylboranes.^[57]

8.1.3 Chapter 3

Figure 8.3: Compounds **3.1-3.3**.

In this chapter, the synthesis of the amine-containing, unsymmetrically-substituted triarylborane **3.2a** and its C–H borylated derivative **3.2b** is presented. The methylation of the amine functionality of **3.2a** yielded the *mono*-cationic compound **3.2c**. Photophysical and electrochemical properties of **3.2a** and **3.2c** are discussed in comparison with those of **3.1a**, **3.3a**, and **3.3c**. The absorption and emission maxima shift bathochromically with increasing strength and number of donor substituents in the order **3.3c** < **3.2c** < **3.1** < **3.2a** < **3.3a**. The presented reduction potentials decrease with increasing electron density at the boron center. For the triarylboranes **3.1a**, **3.2c**, and **3.3c**, singlet oxygen sensitization efficiency is demonstrated to increase with increasing number of trimethylammonium groups. Thus, different numbers of dimethylamino- and trimethylammonium groups are shown to influence the properties of triarylboranes greatly.

Figure 8.4: Absorption (solid lines) and emission (dotted lines; excitation at λ_{max}^{abs}) spectra of **A)** **3.1a**, **3.2a**, and **3.3a** in hexane and of **B)** **3.2c** and **3.3c** in 1% acetonitrile in water.

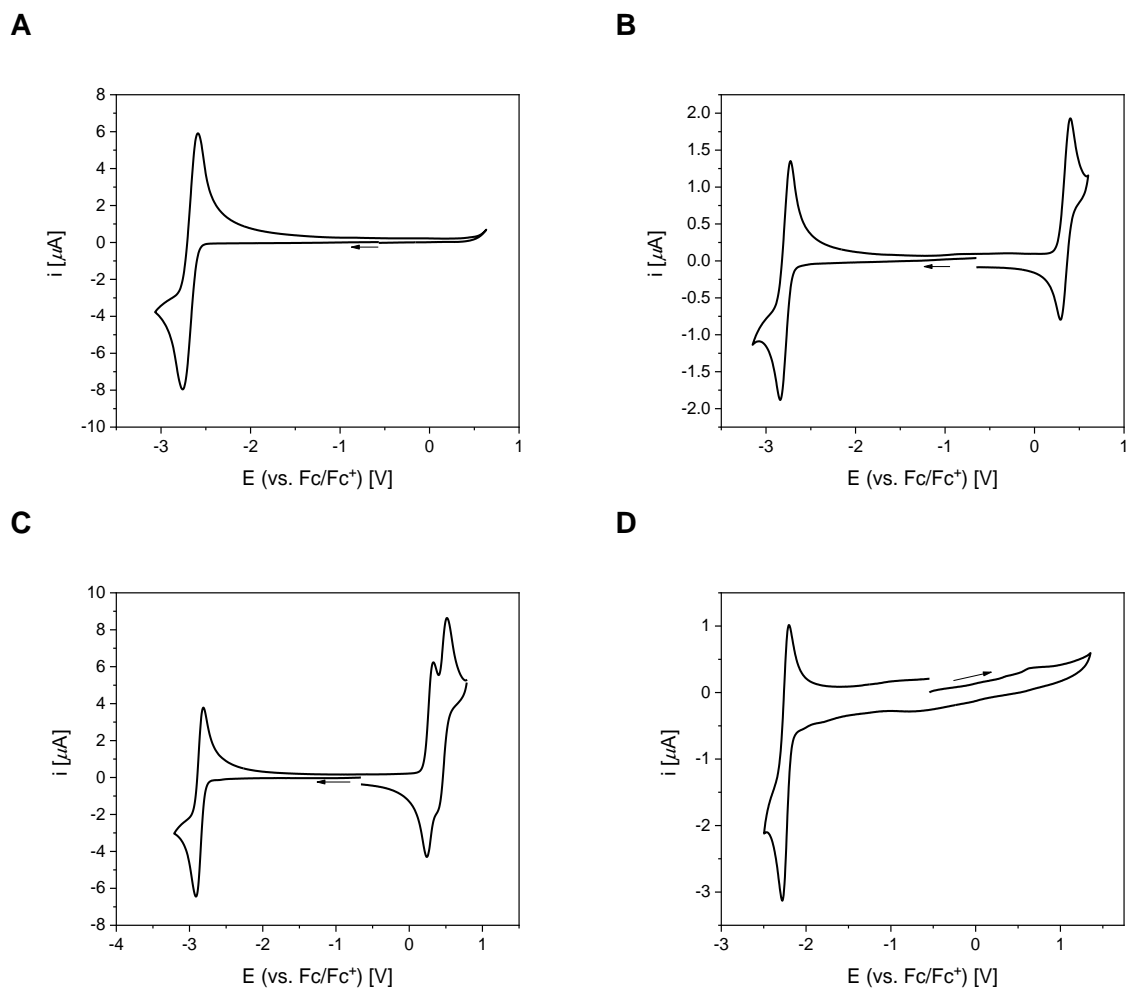


Figure 8.5: Cyclic voltammogram of **A) 3.1a**, **B) 3.2a**, and **C) 3.3a** in THF (scan rate: 250 mV s^{-1}). **D)** Cyclic voltammogram of **3.2c** in MeCN (scan rate: 250 mV s^{-1}).

8.1.4 Chapter 4

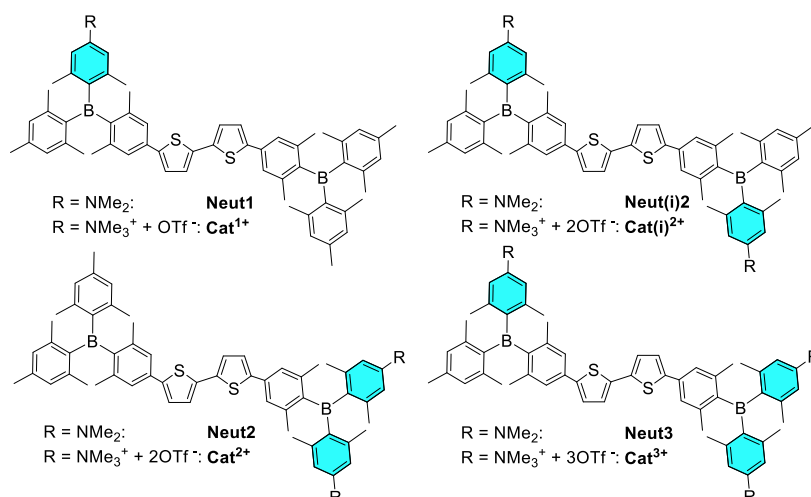


Figure 8.6: Selectively dimethylamino- and trimethylammonium-substituted compounds **Neut1-Neut3** and **Cat¹⁺-Cat³⁺**.

Using **3.2b**, the synthesis of the selectively dimethylamino- and trimethylammonium substituted *bis*-triarylboranes **Neut1**, **Neut2**, **Neut(i)2**, **Neut3** and **Cat¹⁺**, **Cat²⁺**, **Cat(i)²⁺**, **Cat³⁺**, respectively, is described. The photophysical properties of the neutral compounds are influenced by the number of dimethylamino groups. In contrast, the photophysical properties of the cationic compounds are influenced more by their dipole moment than by the number or distribution of trimethylammonium groups. The singlet oxygen sensitization efficiency of **Cat¹⁺**, **Cat²⁺**, **Cat(i)²⁺**, and **Cat³⁺** is shown to be ca. 0.6, irrespective of the number or distribution of charges.

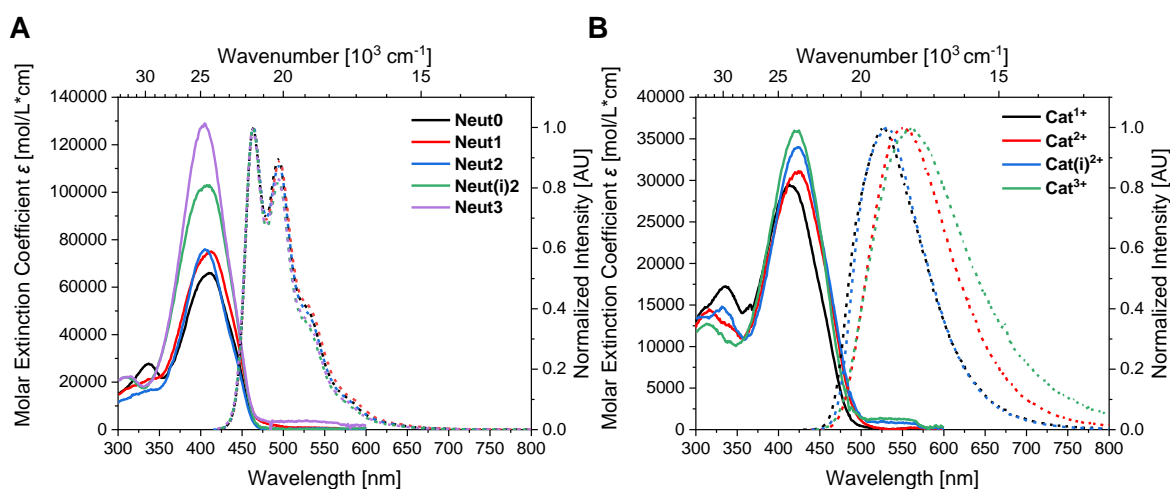


Figure 8.7: Absorption (solid lines) and emission (dotted lines; excitation at λ_{max}^{abs}) spectra of **A) Neut1**, **Neut2**, **Neut(i)2**, and **Neut3** in hexane and of **B) Cat¹⁺**, **Cat²⁺**, **Cat(i)²⁺**, and **Cat³⁺** in 1% acetonitrile in water.

The reduction and oxidation potentials of **Neut1**, **Neut2**, **Neut(i)2**, and **Neut3**, are very similar. Comparison with the potentials of the corresponding triarylboranes **3.1a**, **3.2a**, and **3.3a** reveals an increase by ca. 0.3-0.5 V upon connection of two triarylboranes with a bithiophene bridge. The influence of different electronic situations around the boron center of the cationic *bis*-triarylboranes **Cat¹⁺**, **Cat²⁺**, **Cat(i)²⁺**, and **Cat³⁺** is shown to be larger than the influence of the number or distribution of the charge.

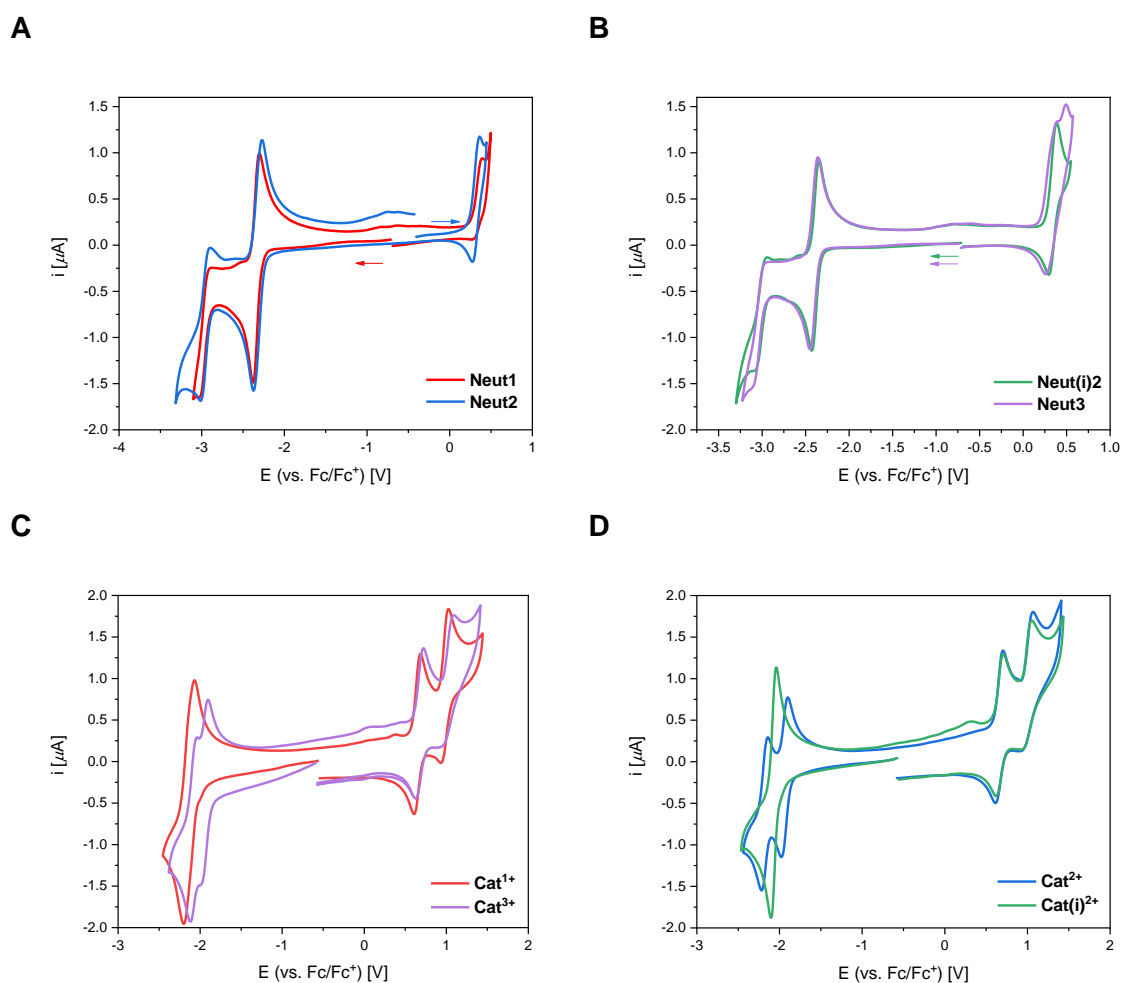


Figure 8.8: Comparison of cyclic voltammograms of **A) Neut0**, **Neut1**, **Neut2**, and **B) Neut(i)2**, **Neut3**, **Neut4** measured in THF vs. Fc/Fc⁺ (scan rate: 250 mV s⁻¹). Comparison of cyclic voltammograms of **C) Cat¹⁺** and **Cat³⁺** and **D) Cat²⁺** and **Cat(i)²⁺** measured in MeCN vs. Fc/Fc⁺ (scan rate: 250 mV s⁻¹).

The compounds **Cat¹⁺**, **Cat²⁺**, **Cat(i)²⁺**, and **Cat³⁺** are insoluble in pure water, but acetonitrile stock solutions can be diluted with water without precipitation until the solution contains less than 1% acetonitrile.

8.1.5 Chapter 5

Chapter 5 summarizes triarylboranes which have been used for intracellular imaging. Different approaches to water-solubility have been pursued by different groups, *e. g.*, incorporation into a polymeric structure or attachment of neutral and charged groups. Some of these compounds were designed to respond to specific changes in the cellular environment (pH, temperature, small molecules) or to biopolymers (DNA, RNA, and proteins). Adoption of standardized protocols for these biological investigations will help to move this field forward.

8.1.6 Chapter 6

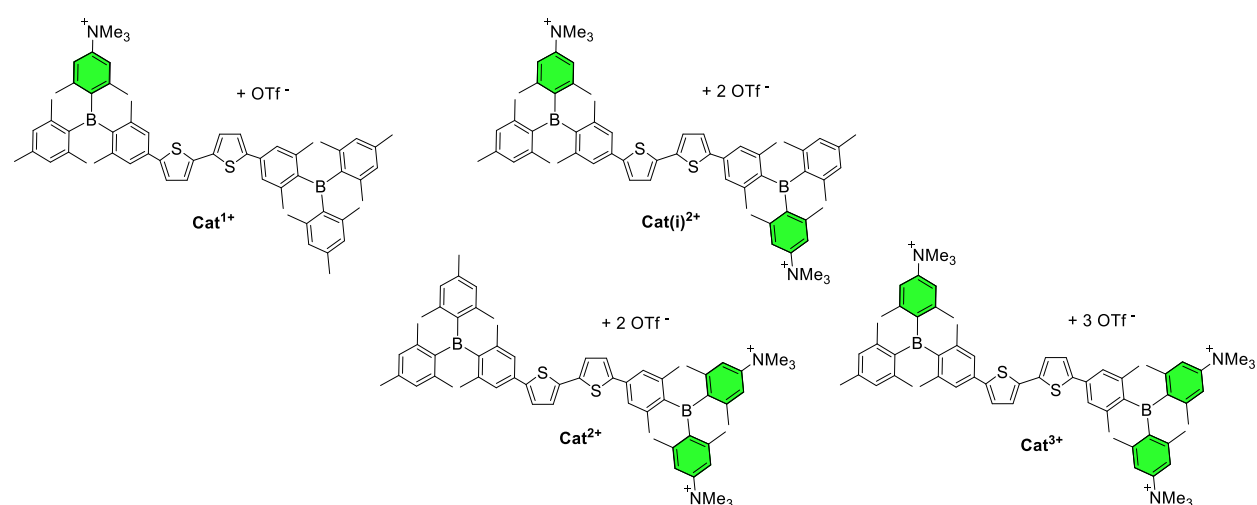


Figure 8.9: Compounds **Cat¹⁺**, **Cat²⁺**, **Cat(i)²⁺**, and **Cat³⁺**.

This chapter presents the interactions of **Cat¹⁺**, **Cat²⁺**, **Cat(i)²⁺**, and **Cat³⁺** with DNAs, RNA, and cells to examine the influence of different number and distribution of the charge. One trimethylammonium group is not sufficient for *bis*-triarylboranes to interact with DNA or RNA. In contrast, **Cat²⁺**, **Cat(i)²⁺**, and **Cat³⁺** interact with such biopolymers at pH 7 and 8. These interactions are demonstrated to be influenced by the number and distribution of charges such that, *e. g.*, the binding constants between **Cat²⁺**, **Cat(i)²⁺**, and **Cat³⁺** and DNApore increases with increasing number of charges.

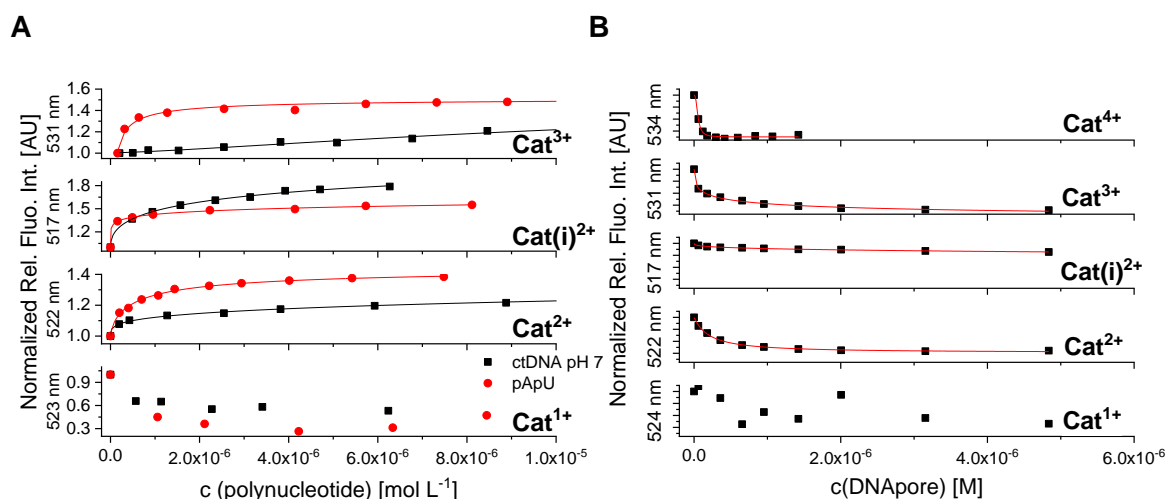


Figure 8.10: Normalized fluorimetric titration of **A)** Cat^{1+} ($c = 1 \times 10^{-7} \text{ mol L}^{-1}$; $\lambda_{\text{exc}} = 414 \text{ nm}$), Cat^{2+} ($c = 1 \times 10^{-7} \text{ mol L}^{-1}$; $\lambda_{\text{exc}} = 422 \text{ nm}$), Cat(i)^{2+} ($c = 1 \times 10^{-7} \text{ mol L}^{-1}$; $\lambda_{\text{exc}} = 417 \text{ nm}$), Cat^{3+} ($c = 1 \times 10^{-7} \text{ mol L}^{-1}$; $\lambda_{\text{exc}} = 421 \text{ nm}$) with ctDNA and pApU at pH 7 and of **B)** Cat^{1+} ($c = 5 \times 10^{-7} \text{ M}$; $\lambda_{\text{exc}} = 414 \text{ nm}$), Cat^{2+} ($c = 5 \times 10^{-7} \text{ M}$; $\lambda_{\text{exc}} = 422 \text{ nm}$), Cat(i)^{2+} ($c = 5 \times 10^{-7} \text{ M}$; $\lambda_{\text{exc}} = 417 \text{ nm}$), Cat^{3+} ($c = 5 \times 10^{-7} \text{ M}$; $\lambda_{\text{exc}} = 421 \text{ nm}$), and Cat^{4+} ($c = 4 \times 10^{-7} \text{ M}$; $\lambda_{\text{exc}} = 425 \text{ nm}$) with DNApore (pH 8 in 15 mM Tris-HCl, 300 mM KCl).

Using live cell imaging, Cat^{2+} , Cat(i)^{2+} , and Cat^{3+} are shown to be cell permeable. Inside A549 cells, the emission of Cat^{2+} , Cat(i)^{2+} , and Cat^{3+} is found to bleach within ca. 30 s with simultaneous cell blebbing, most likely due to formation of singlet oxygen. In addition, Cat(i)^{2+} and Cat^{3+} are non-cytotoxic to A549 and WI38 cells at concentrations of up to $1.0 \mu\text{M}$ in the dark. However, upon irradiation with visible light (400-700 nm) the viability of the cells is drastically lowered. Co-localization studies with primary antibodies showed that Cat(i)^{2+} and Cat^{3+} localize at lysosomes, golgi apparatus, and early endosomes of A549 cells.

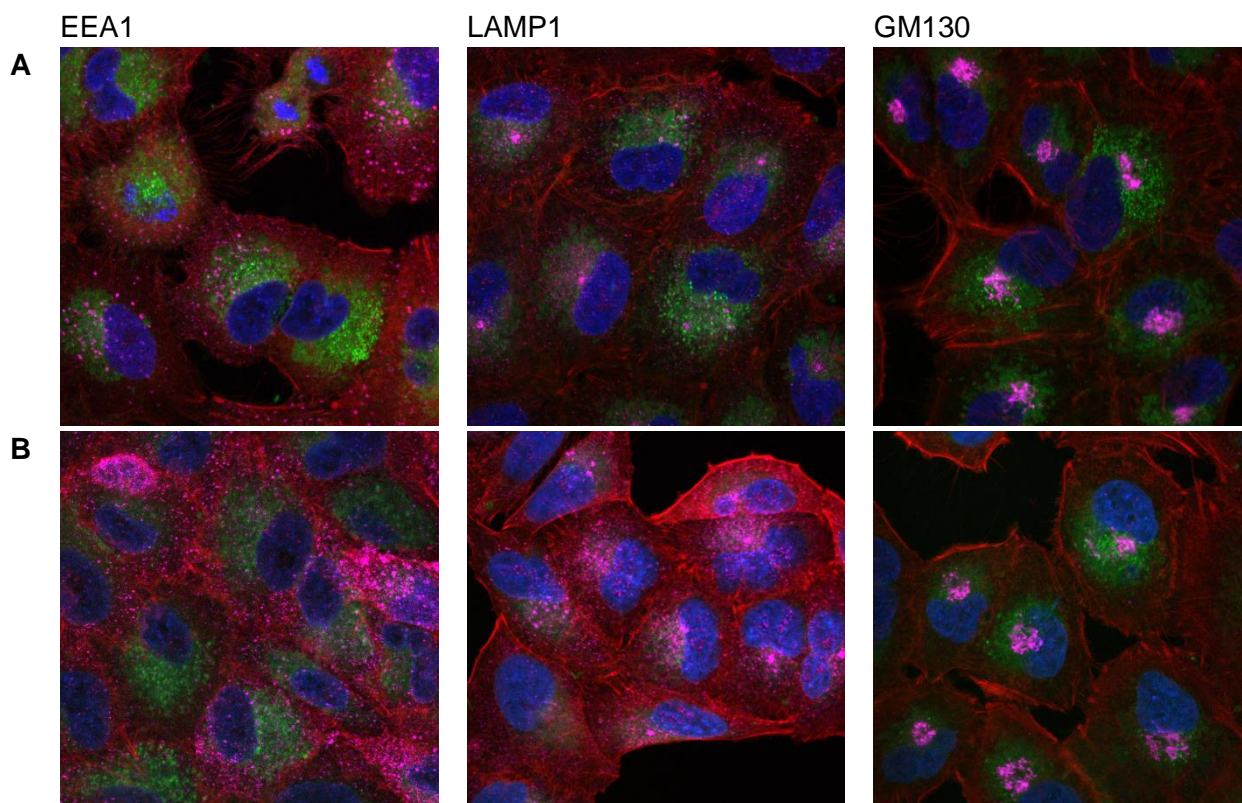
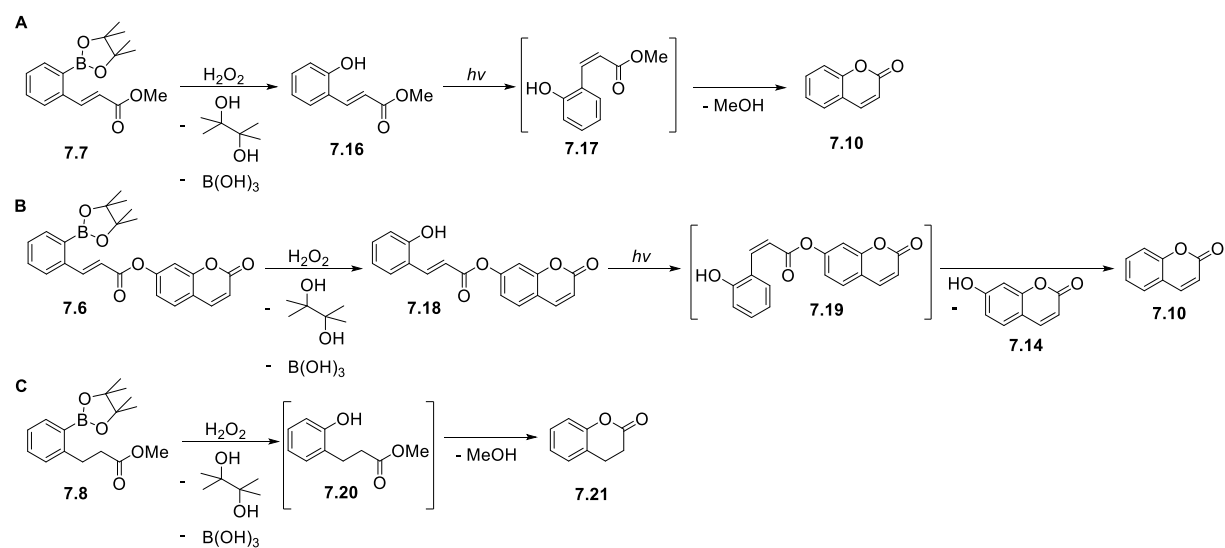


Figure 8.11: Intracellular localization of **A) Cat(i)²⁺** and **B) Cat³⁺** in A549 cells (10 $\mu\text{mol L}^{-1}$; 90 min; 37 $^{\circ}\text{C}$). Early endosomes (EEA1), lysosomes (LAMP1) or golgi apparatus (GM130) are stained with antibodies and monitored by confocal microscopy. Nuclei are stained with DAPI.

8.1.7 Chapter 7



Scheme 8.1: Reaction sequences of **A) 7.7**, **B) 7.6**, and **C) 7.8** upon cleavage of the boronate ester with H_2O_2 and subsequent irradiation.

The synthesis of three boronate esters **7.6-7.8** is described together with an investigation of their potential application as prodrug systems. Examination of the photophysical properties demonstrates high molar extinction coefficients of ca. $15\,000\text{ L mol}^{-1}\text{ cm}^{-1}$ for all compounds and a weak emission for **7.6** and **7.8**. The boronate esters of **7.6**, **7.7**, and **7.8** are shown to be cleaved efficiently in the presence of stoichiometric amounts of H_2O_2 . The intermediate phenol derivatives of **7.6** and **7.7** are shown to form coumarin upon irradiation with 254 nm *via* isomerization of the double bond. In contrast, the formation of dihydrocoumarin from the phenol derivative of **7.8** proceeds under ambient light.

8.2 Zusammenfassung

8.2.1 Kapitel 1

In diesem Kapitel wird die Struktur von dreifach-kordinierten, organischen Borverbindungen kurz und allgemein erklärt, wobei der Focus auf Triarylboranen und Borsäureestern gelegt wird. Eine anschließende Zusammenfassung der bisherigen Ergebnisse über vierfach kationische, *bis*-Triarylborane zeigt, dass der Einfluss der verbrückenden Einheit auf photophysikalische und biologische Eigenschaften bereits untersucht wurden, wohingegen der Einfluss von unterschiedlichen Anzahlen oder Verteilungen der Ladung nicht untersucht worden war.

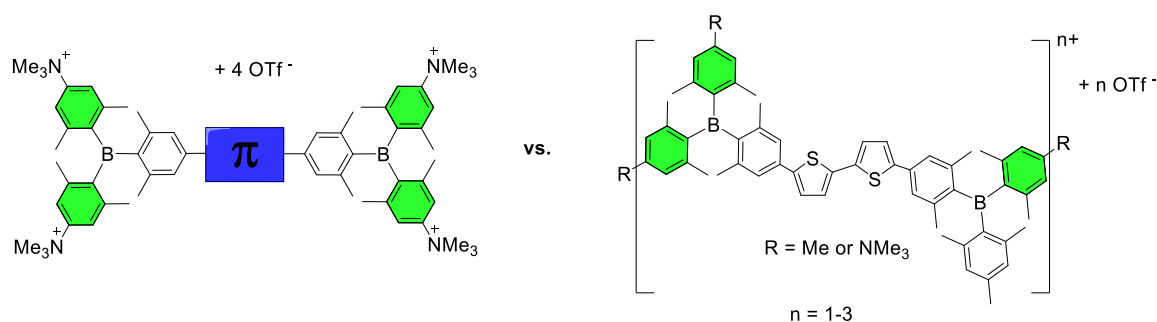


Abbildung 8.1: Gegenüberstellung der bisher untersuchten Strukturen und den Zielverbindungen dieser Arbeit.

8.2.2 Kapitel 2

In Kapitel 2 werden die Entwicklungen der Synthese von Triarylboranen seit ihrer ersten Isolierung im Jahr 1885 zusammengefasst. Es wird gezeigt, dass im Laufe des folgenden Jahrhunderts die synthetische Herangehensweise vielfältige Änderungen durchlaufen hat. Manche dieser Herangehensweisen werden heutzutage noch genutzt, wie die allgemein anwendbaren Syntheserouten, die 1922 von Krause *et al.* oder 1972 von Grisdale *et al.* bei Eastman Kodak entwickelt wurden. Andere Routen wurden nach ihrer ersten Publikation nicht weiter verfolgt, wie die 1958 von Mikhailov *et al.* publizierte Route, durch die zwei Triarylborane hergestellt werden konnten, bei denen drei unterschiedliche aromatische Systeme an das Borzentrum gebunden sind. Weiterhin wird gezeigt, dass unter Zuhilfenahme der großen Vielfalt an synthetischen Möglichkeiten, die Chemikern des 21. Jahrhunderts zur Verfügung stehen, unterschiedlichste Strategien verfolgt wurden, um speziell konzipierte Triarylborane herzustellen.

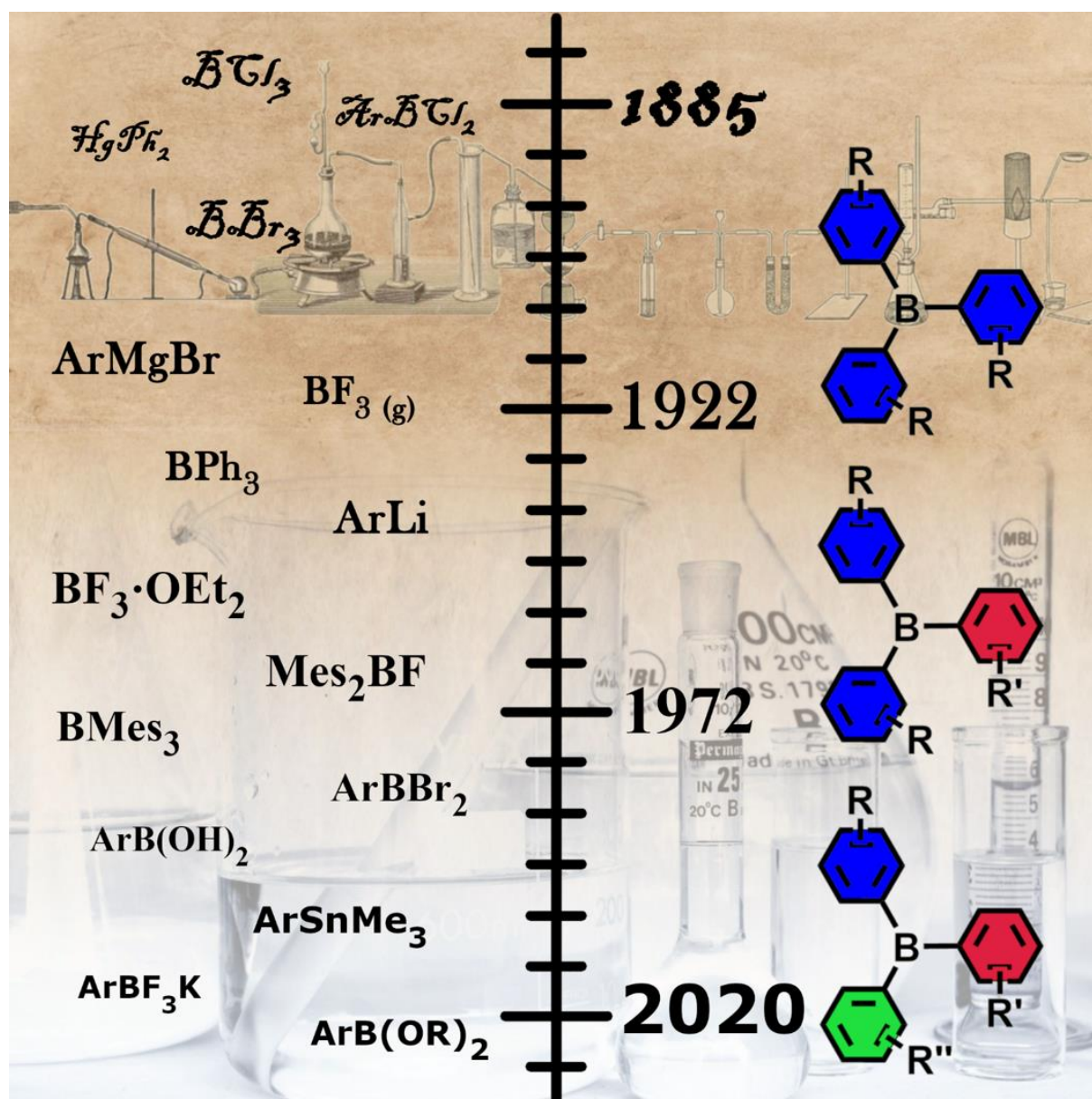
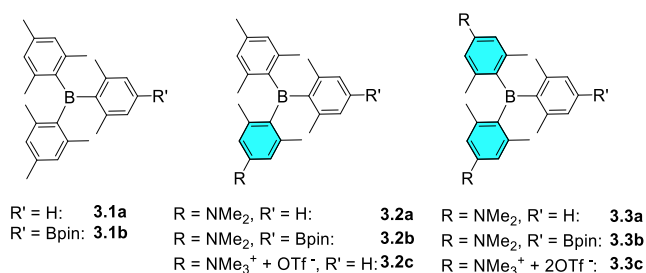


Abbildung 8.2: Titelbild des Übersichtsartikels, der die synthetischen Herangehensweisen zur Herstellung von Triarylboranen zusammenfasst.^[57]

8.2.3 Kapitel 3

Abbildung 8.3: Strukturen der Verbindungen **3.1-3.3**.

In diesem Kapitel wird die Synthese des aminierten, unsymmetrisch substituierten Triarylborans **3.2a** sowie des C–H borylierten Analogons **3.2b** gezeigt. Methylierung des Amins von **3.2a** führte zur Isolierung des einfachen Kations **3.2c**. Die photophysikalischen und elektrochemischen Eigenschaften von **3.2a** und **3.2c** werden mit den Eigenschaften von **3.1a**, **3.3a** und **3.3c** verglichen. Mit zunehmender Stärke des Elektronendonors erfahren die Absorptions- und Emissionsmaxima der Triarylborane eine Rotverschiebung, die in der Reihe **3.3c** < **3.2c** < **3.1** < **3.2a** < **3.3a** zunimmt. Im Gegenteil dazu nehmen die Werte der Reduktionspotentiale mit zunehmender Elektronendichte am Borzentrum ab. Für die Triarylborane **3.1a**, **3.2c** und **3.3c** wurde gezeigt, dass ihre Fähigkeit mit Singulett Sauerstoff zu reagieren mit zunehmender Anzahl an Trimethylammoniumgruppen zunimmt. In Summe wird gezeigt, dass unterschiedliche Anzahlen an Dimethylamino- und Trimethylammoniumgruppen großen Einfluss auf die Eigenschaften der Triarylborane haben.

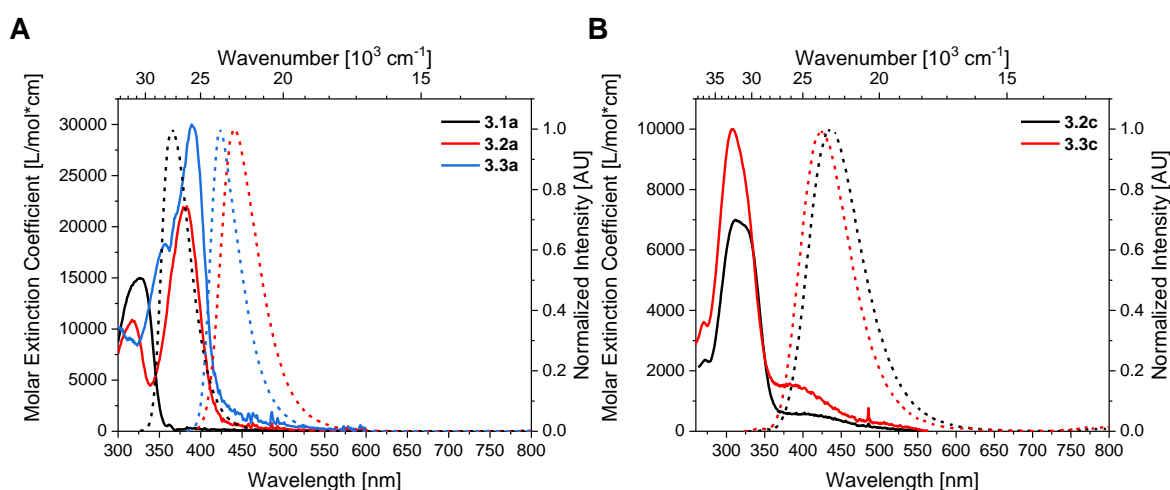


Abbildung 8.4: Absorptions- (durchgezogenen Linien) und Emissionsspektren (gestrichelte Linien; Anregung am λ_{max}^{abs}) von **A**) **3.1a**, **3.2a** und **3.3a** gemessen in Hexan und von **B**) **3.2c** und **3.3c** gemessen in einem Gemisch aus 1% Acetonitril in Wasser.

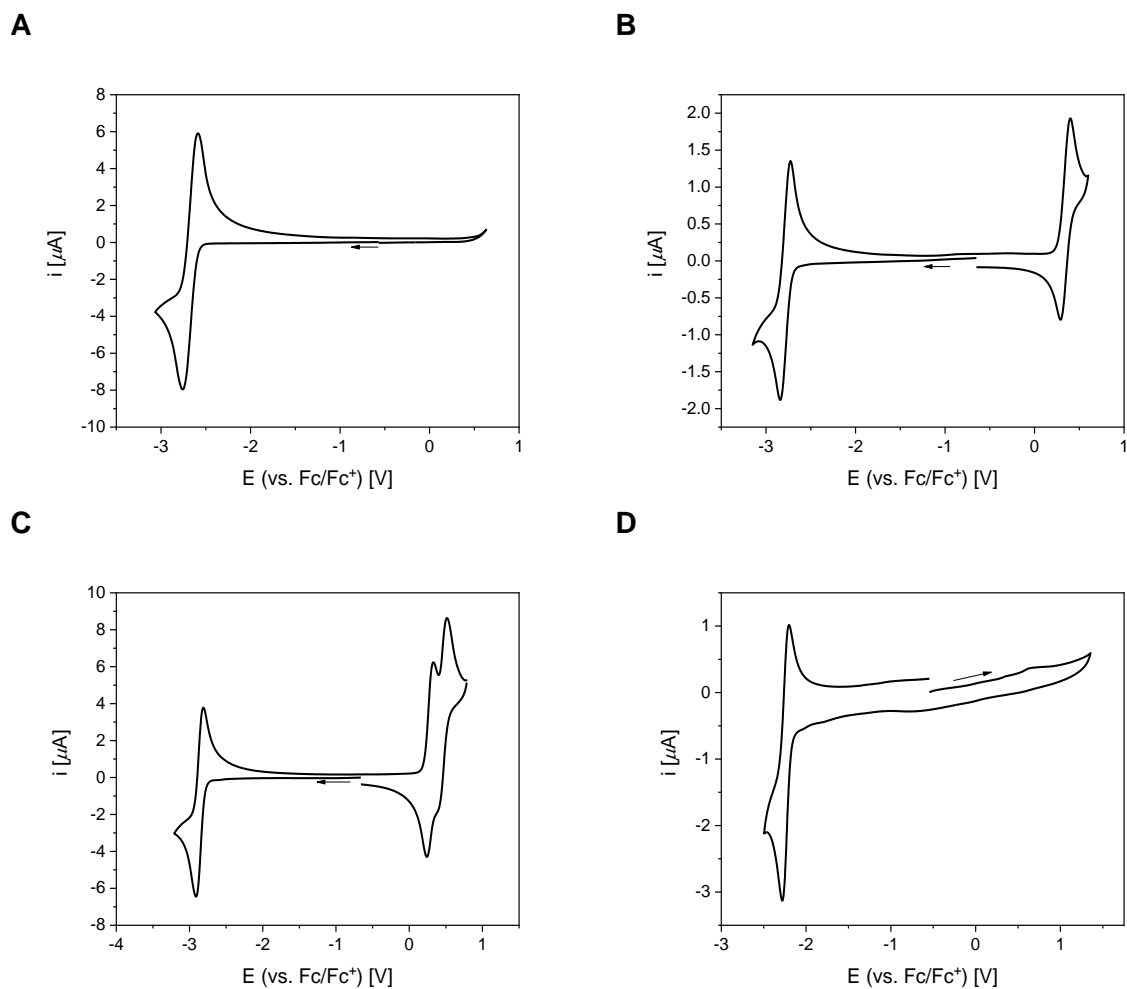


Abbildung 8.5: Cyclovoltammogramme von **A) 3.1a**, **B) 3.2a** und **C) 3.3a** gemessen in THF (Scanrate: 250 mV s^{-1}). **D)** Cyclovoltammogramm von **3.2c** gemessen in Acetonitril (Scanrate: 250 mV s^{-1}).

8.2.4 Kapitel 4

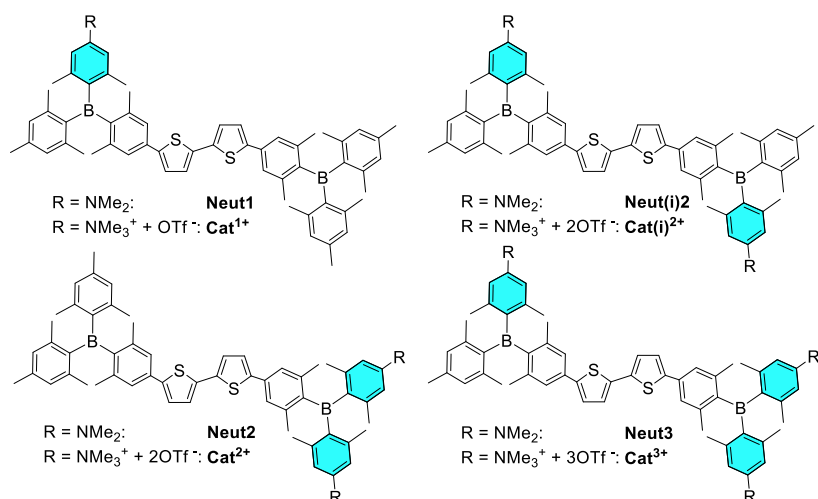


Abbildung 8.6: Verbindungen **Neut1-Neut3** und **Cat¹⁺-Cat³⁺**, die eine definierte Anzahl an Dimethylamino- und Trimethylammoniumgruppen tragen.

Unter Verwendung von **3.2b** wurden *bis*-Triarylborane **Neut1**, **Neut2**, **Neut(i)2**, **Neut3** und daraus **Cat¹⁺**, **Cat²⁺**, **Cat(i)²⁺**, **Cat³⁺** hergestellt, die eine definierte Anzahl an Dimethylamino- und Trimethylammoniumgruppen tragen. Es wird gezeigt, dass die photophysikalischen Eigenschaften der neutralen Verbindungen (**Neut1**, **Neut2**, **Neut(i)2**, **Neut3**) von der Anzahl an Dimethylaminogruppen beeinflusst werden. Im Gegensatz dazu werden die photophysikalischen Eigenschaften der kationischen Verbindungen (**Cat¹⁺**, **Cat²⁺**, **Cat(i)²⁺**, **Cat³⁺**) mehr durch ihr Dipolmoment als durch die Anzahl an Trimethylammoniumgruppen beeinflusst. Die Effizienz von **Cat¹⁺**, **Cat²⁺**, **Cat(i)²⁺** und **Cat³⁺** mit Singulett Sauerstoff zu reagieren ist ca. 0.6 und damit unabhängig von der Anzahl oder Verteilung von Trimethylammoniumgruppen.

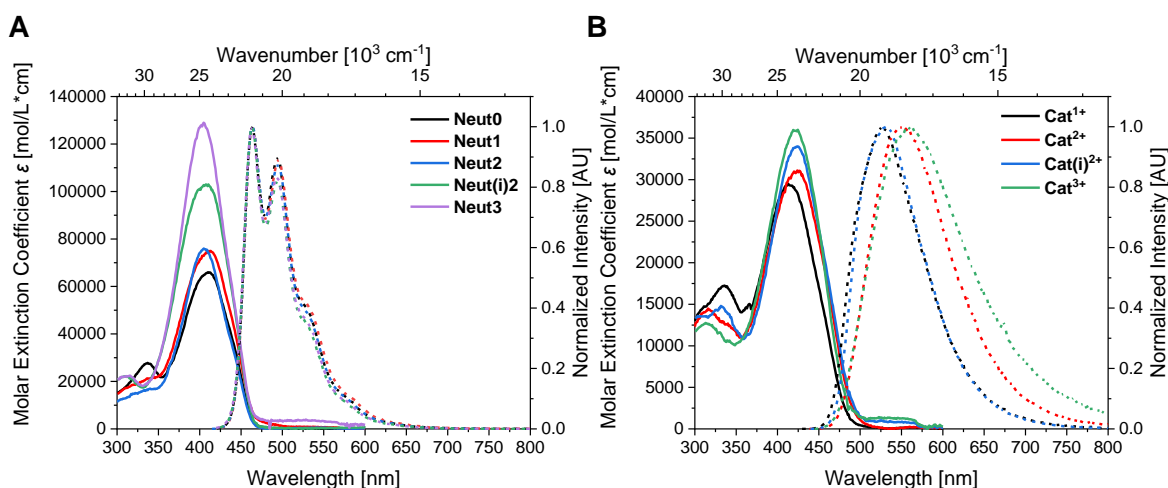


Abbildung 8.7: Absorptions- (durchgezogene Linien) und Emissionsspektren (gestrichelte Linien; Anregung am λ_{max}^{abs}) von **A) Neut1, Neut2, Neut(i)2** und **Neut3** gemessen in Hexan und von **B) Cat¹⁺, Cat²⁺, Cat(i)²⁺** und **Cat³⁺** gemessen in einem Gemisch von 1% Acetonitril in Wasser.

Die Oxidations- und Reduktionspotentiale von **Neut1, Neut2, Neut(i)2** und **Neut3** sind sich sehr ähnlich; im Vergleich zu den Potentialen der zugehörigen Triarylborane **3.1a, 3.2a** und **3.3a** sind sie um ca. 0.3-0.5 V höher. Deshalb kann festgehalten werden, dass der Einfluss von unterschiedlichen elektronischen Situationen am Borzentrum von kationischen *bis*-Triarylboranen wie **Cat¹⁺, Cat²⁺, Cat(i)²⁺** und **Cat³⁺** größer ist als der Einfluss der Anzahl oder der Verteilung der Ladung.

Es wird gezeigt, dass sich die Verbindungen **Cat¹⁺, Cat²⁺, Cat(i)²⁺** und **Cat³⁺** nicht in reinem Wasser lösen. Dennoch können deren Stammlösungen in Acetonitril ohne Bildung eines Niederschlags mit Wasser verdünnt werden bis der Anteil an Acetonitril in der resultierenden Lösung kleiner als 1% ist.

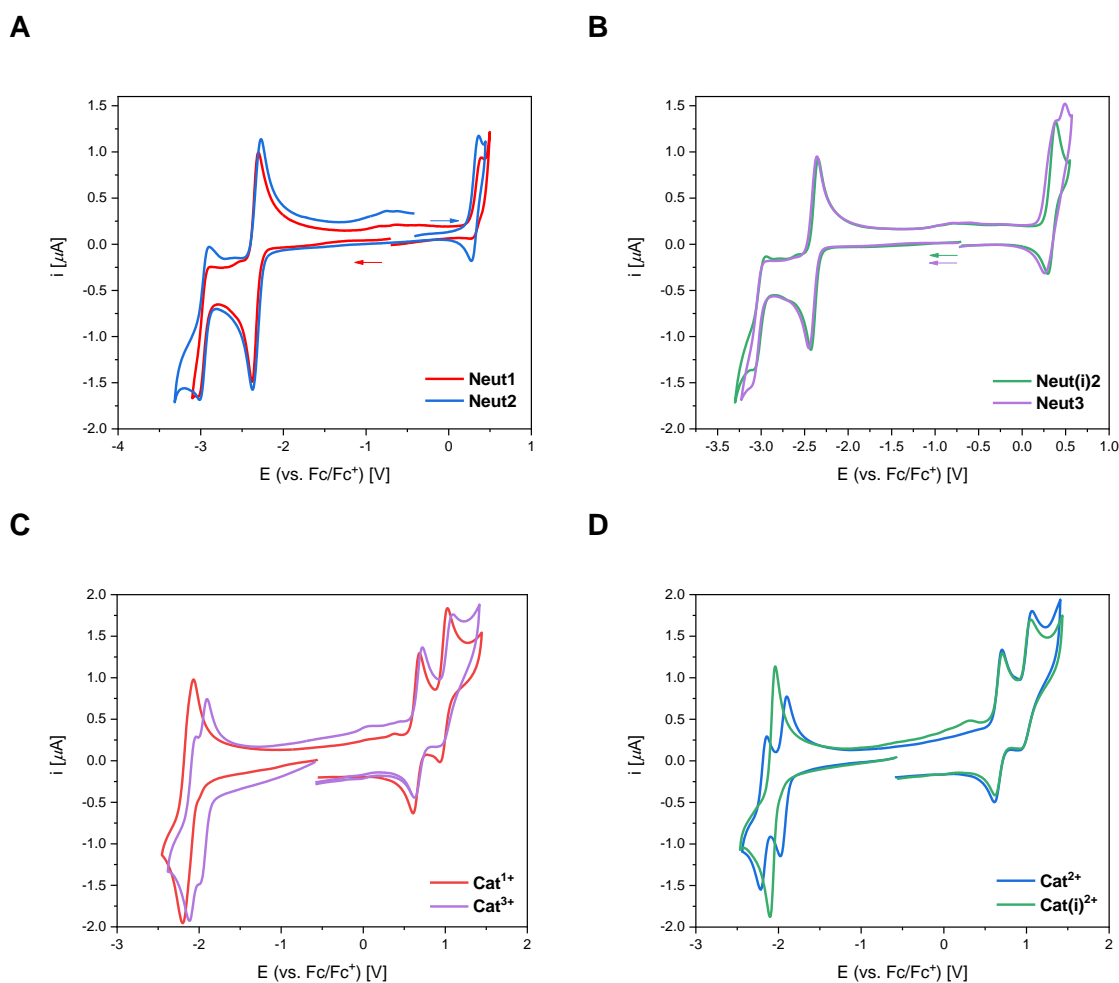
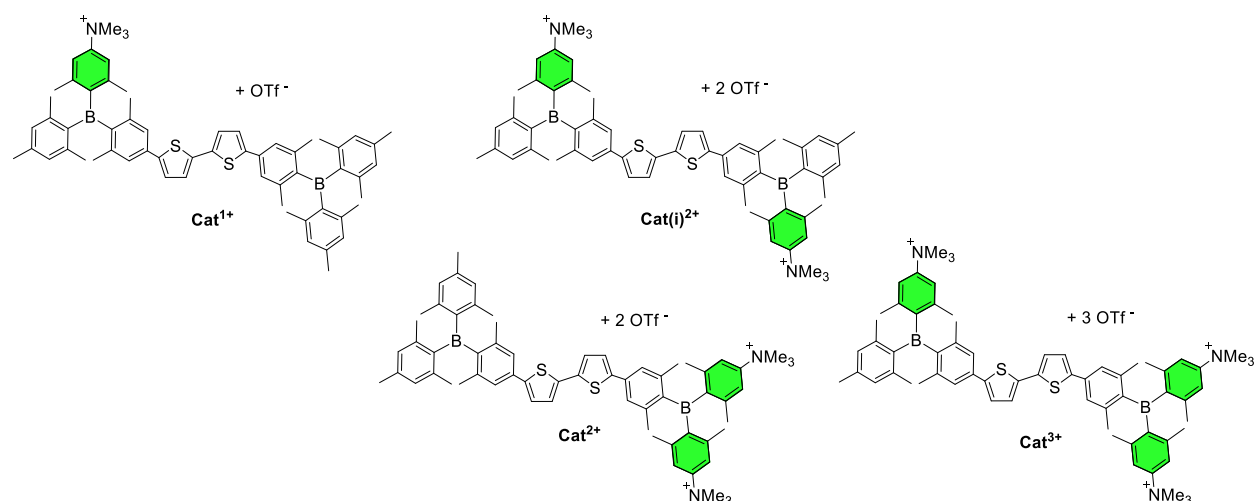


Abbildung 8.8: Vergleich der Cyclovoltammogramme von **A) Neut0, Neut1, Neut2** und **B) Neut(i)2, Neut3, Neut4** gemessen in THF gegen Fc/Fc^+ (Scanrate: 250 mV s^{-1}). Vergleich der Cyclovoltammogramme von **C) Cat^{1+} und Cat^{3+}** und **D) Cat^{2+} und $\text{Cat}(\text{i})^{2+}$** gemessen in Acetonitril gegen Fc/Fc^+ (Scanrate: 250 mV s^{-1}).

8.2.5 Kapitel 5

Kapitel 5 fasst Triarylborane zusammen, die für Bildgebung in Zellen verwendet wurden. Es wird gezeigt, dass unterschiedliche Gruppen unterschiedliche Strategien entwickelt haben, um die Verbindungen wasserlöslich zu machen, wie beispielsweise die Einbindung in polymere Strukturen oder durch Anbringung von neutralen oder geladenen Gruppen. Manche dieser Verbindungen wurden entwickelt um auf bestimmte Veränderungen der Umgebungen in Zellen (pH-Wert, Temperatur, kleine Moleküle) oder um auf Biopolymere (DNS, RNS und Proteine) zu reagieren.

8.2.6 Kapitel 6

Abbildung 8.9: Verbindungen Cat^{1+} , Cat^{2+} , $\text{Cat}(\text{i})^{2+}$ und Cat^{3+} .

In diesem Kapitel werden die Wechselwirkungen von Cat^{1+} , Cat^{2+} , $\text{Cat}(\text{i})^{2+}$ und Cat^{3+} mit DNS, RNS und Zellen gezeigt und der Einfluss von unterschiedlichen Anzahlen und Verteilungen der Ladung darauf untersucht. Es kann gezeigt werden, dass eine Trimethylammoniumgruppe nicht ausreicht, dass solche *bis*-Triarylborane mit DNS oder RNS wechselwirken. Im Gegensatz dazu wechselwirken Cat^{2+} , $\text{Cat}(\text{i})^{2+}$ und Cat^{3+} bei einem pH von 7 und 8 mit den untersuchten Biopolymeren. Zusätzlich wird gezeigt, dass diese Wechselwirkungen durch die Anzahl und Verteilung der Ladung beeinflusst wird, da beispielsweise die Bindungskonstanten zwischen Cat^{2+} , $\text{Cat}(\text{i})^{2+}$ und Cat^{3+} und DNApore mit zunehmender Anzahl an Ladungen größer werden.

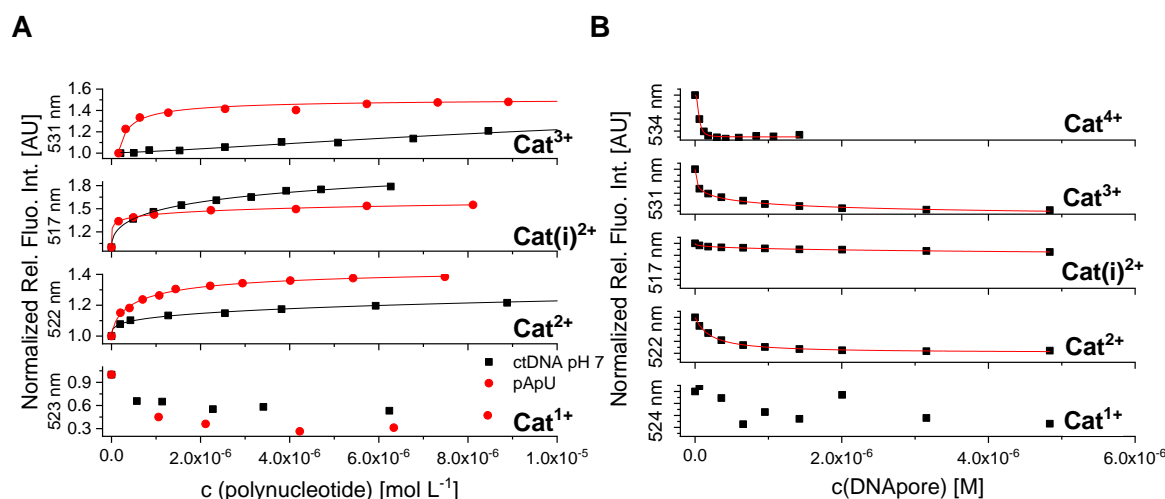


Abbildung 8.10: Änderungen der normalisierten Emissionsspektren **A)** **Cat**¹⁺ ($c = 1 \times 10^{-7} \text{ mol L}^{-1}$; $\lambda_{\text{exc}} = 414 \text{ nm}$), **Cat**²⁺ ($c = 1 \times 10^{-7} \text{ mol L}^{-1}$; $\lambda_{\text{exc}} = 422 \text{ nm}$), **Cat(i)**²⁺ ($c = 1 \times 10^{-7} \text{ mol L}^{-1}$; $\lambda_{\text{exc}} = 417 \text{ nm}$), **Cat**³⁺ ($c = 1 \times 10^{-7} \text{ mol L}^{-1}$; $\lambda_{\text{exc}} = 421 \text{ nm}$) mit zunehmender Konzentration an ctDNA und pApU bei pH 7 und von **B)** **Cat**¹⁺ ($c = 5 \times 10^{-7} \text{ M}$; $\lambda_{\text{exc}} = 414 \text{ nm}$), **Cat**²⁺ ($c = 5 \times 10^{-7} \text{ M}$; $\lambda_{\text{exc}} = 422 \text{ nm}$), **Cat(i)**²⁺ ($c = 5 \times 10^{-7} \text{ M}$; $\lambda_{\text{exc}} = 417 \text{ nm}$), **Cat**³⁺ ($c = 5 \times 10^{-7} \text{ M}$; $\lambda_{\text{exc}} = 421 \text{ nm}$), und **Cat**⁴⁺ ($c = 4 \times 10^{-7} \text{ M}$; $\lambda_{\text{exc}} = 425 \text{ nm}$) mit zunehmender Konzentration an DNApore bei pH 8 (15 mM Tris-HCl, 300 mM KCl).

Durch Bildgebung in lebenden Zellen konnte gezeigt werden, dass **Cat**²⁺, **Cat(i)**²⁺ und **Cat**³⁺ in der Lage sind durch die Zellwand in die Zellen zu gelangen. Es wird gezeigt, dass die Emission von **Cat**²⁺, **Cat(i)**²⁺ und **Cat**³⁺ in A549 Zellen innerhalb von ca. 30 s ausbleicht und dass die Zellen gleichzeitig aufplatzen, wahrscheinlich bedingt durch die Bildung von Singulett Sauerstoff. Zusätzlich kann gezeigt werden, dass **Cat(i)**²⁺ und **Cat**³⁺ im Dunkeln bis zu einer Konzentration von 1.0 μM nicht zytotoxisch für A549 und WI38 Zellen sind. Unter Bestrahlung mit sichtbarem Licht (400-700 nm) sinkt die Überlebensrate der Zellen drastisch. Untersuchungen der Co-Lokalisierung zwischen primären Antikörpern und **Cat(i)**²⁺ und **Cat**³⁺ zeigen, dass sich die *bis*-Triarylborane in Lysosomen, Golgi-Apparaten und frühen Endosomen von A549 Zellen anlagern.

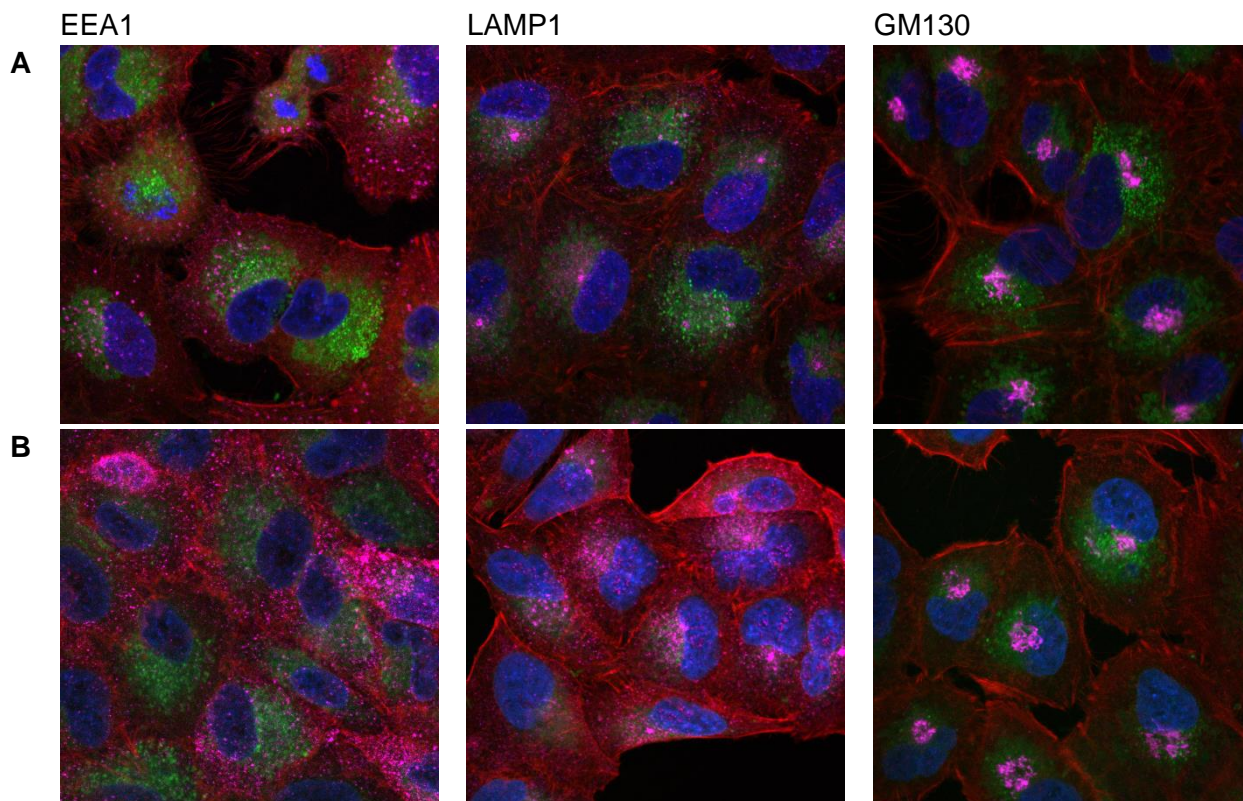


Abbildung 8.11: Intrazelluläre Lokalisierung von **A) Cat(i)²⁺** und **B) Cat³⁺** in A549 Zellen (10 $\mu\text{mol L}^{-1}$; 90 min; 37 °C). Frühe Endosomen (EEA1), Lysosomen (LAMP1) oder Golgi-Apparate (GM130) wurden mit Antikörpern angefärbt und mit konfokaler Mikroskopie beobachtet wurden. Die Zellkerne wurden mit DAPI angefärbt.

8.2.7 Kapitel 7

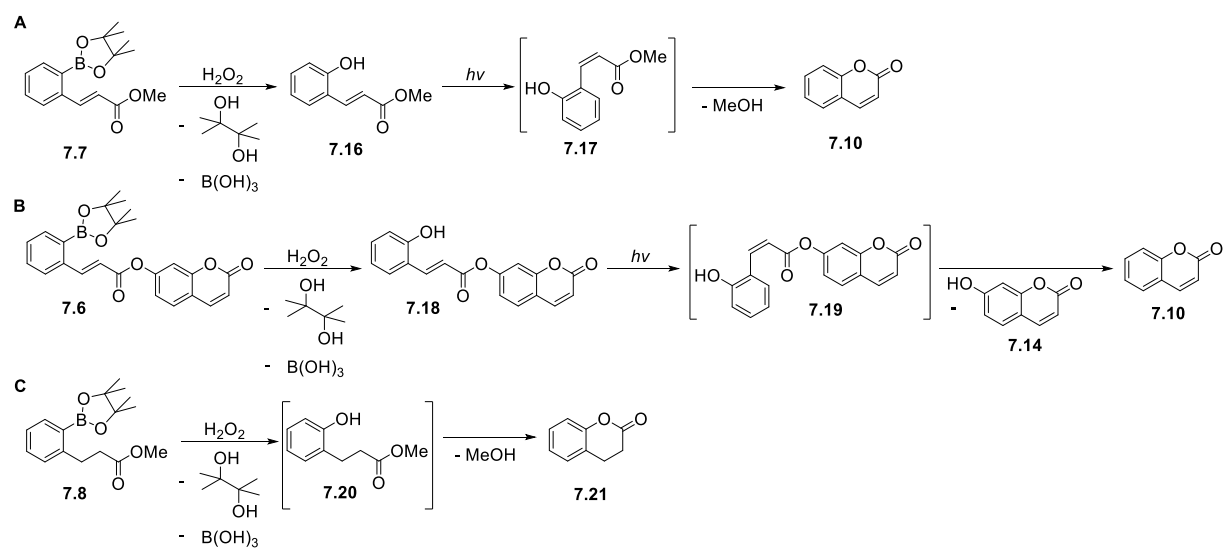


Abbildung 8.12: Reaktionsabfolge von **A) 7.7**, **B) 7.6** und **C) 7.8** eingeleitet durch die Spaltung des Borsäureesters mit H_2O_2 unter gleichzeitiger Bestrahlung mit Licht.

Es wird die Synthese der drei Borsäureester **7.6-7.8** zusammen mit unterschiedlichen Untersuchungen beschrieben um deren Einsatzmöglichkeiten als Vorläufermedikamente zu bestimmen. Untersuchungen der photophysikalischen Eigenschaften ergeben hohe molare Extinktionskoeffizienten von ca. $15\,000\text{ L mol}^{-1}\text{ cm}^{-1}$ für alle Verbindungen und eine schwache Emission für **7.6** und **7.8**. Es wird gezeigt, dass die Borsäureester von **7.6**, **7.7** und **7.8** in der Anwesenheit von stöchiometrischen Mengen H_2O_2 effizient gespalten werden. Des Weiteren konnte gezeigt werden, dass die Doppelbindungen der als Zwischenprodukte gebildeten Phenolderivate von **7.6** und **7.7** durch Bestrahlung mit Licht der Wellenlänge 254 nm isomerisieren und Coumarin gebildet wird. Im Gegensatz dazu verläuft die Bildung von Dihydrocoumarin aus dem Phenolderivat von **7.8** bei Raumbeleuchtung.

CHAPTER 9

EXPERIMENTAL

9 Experimental

9.1 General Experimental Details

Unless otherwise noted, all reactions were performed under an inert atmosphere of argon using standard Schlenk techniques or glovebox (Innovative Technology Inc.) techniques. For these reactions, oven-dried and additionally flame-dried glassware was used. Unless otherwise stated, every work up procedure described was performed open to the air. Each methylation of **5a**, **6a**, **Neut1**, **Neut2**, **Neut(i)2**, and **Neut3** was done in a new vial with a maximum volume of 5 mL (diameter: 19 mm, height: 40 mm) made from soda-lime glass provided by VWR. Solvents used for reactions under argon (THF, CH₂Cl₂, hexane, and Et₂O) were dried, deoxygenated and argon saturated using an Innovative Technology Inc. Pure Solvent Purification System. Deuterated solvents (CD₂Cl₂, C₆D₆, CD₃OD, CD₃CN, acetone-d₆) used for nuclear magnetic resonance spectroscopy were purchased from Sigma Aldrich. *n*-Butyllithium (2.5 M solution in hexane), *t*-butyllithium (1.7 M solution in pentane), 4,4'-di-*tert*-butyl-2,2'-dipyridyl (dtbpy), methyl triflate, and KHF₂ were purchased from Sigma Aldrich and used as received. 2-Iodo-5-bromo-1,3-dimethylbenzene was purchased from Apollo Scientific Limited and passed through a silica plug with hexane prior to use. *N,N*,3,5-Tetramethylaniline was purchased from TCI or Sigma Aldrich and used as received. 2-Dicyclohexylphosphino-2',6'-dimethoxybiphenyl (SPhos) was purchased from Oxchem and used as received. B₂pin₂ was kindly provided by AllylChem Co. Ltd. (Dalian, China). Leftovers of *bis*-[4-(trimethylammonium)-2,6-dimethylphenyl]-2,6-dimethylphenylborane *bis*-triflate **6c**^[56] from the initial synthesis were used for photophysical studies etc. after checking its purity by ¹H NMR spectroscopy. The leftovers of 5,5'-*bis*-[4-(2,6-dimethylphenyl)-dimesitylboryl]-2,2'-bithiophene **Neut0**^[54] were fully characterized after further purification as indicated below. Potassium (2,6-dimethylphenyl)-trifluoroborate **3.4**,^[55] 4-bromo-*N,N*,3,5-tetramethylaniline,^[228] 4-(*N,N*-dimethylamino)-2,6-dimethylphenyllithium,^[50] [Ir(COD)(μ-OMe)]₂,^[229] Pd₂dba₃-CHCl₃,^[230] 5,5'-dibromo-2,2'-bithiophene **4.4**,^[231] *bis*-[4-(*N,N*-dimethylamino)-2,6-dimethylphenyl]-2,6-dimethylphenylborane **3.3a**,^[43] *bis*-[4-(*N,N*-dimethylamino)-2,6-dimethylphenyl]-2,6-dimethyl-4-(4,4,5,5-tetramethyl-1,3,2-dioxaborolan-2-yl)phenylborane **3.3b**,^[43] 5,5'-*bis*-[4-[*bis*-[4-(*N,N*-dimethylamino)-2,6-dimethylphenyl]boryl]-3,5-dimethylphenyl]-2,2'-bithiophene **Neut4**,^[43] and 5,5'-*bis*-[4-[*bis*-[4-(*N,N,N*-trimethylammonium)-2,6-dimethylphenyl]boryl]-3,5-dimethylphenyl]-2,2'-bithiophene tetratriflate **Cat**⁴⁺ ^[43] were synthesized according to literature procedures. All other chemicals were obtained from commercial sources and used as received.

Reaction progress was monitored by thin layer chromatography (TLC) using plates pre-coated with a layer of either silica (Polygram® Sil G/UV254) with fluorescent indicator

UV254 or aluminum oxide, purchased from Marchery-Nagel. Automated flash column chromatography was performed using a Biotage® Isolera Four system on silica gel (Biotage SNAP KP-Sil or NH cartridges indicated with the cartridge size depending on substance mass according to the Biotage handbook), obtained from Biotage. Solvent gradients were applied as indicated. Solvents were generally removed using a rotary evaporator *in vacuo* at a maximum temperature of 50 °C. Preparative column chromatography was performed using silica gel 60 (0.040 – 0.063 mm) or aluminum oxide 90 (basic, activity I) purchased from Macherey-Nagel as the stationary phase and the solvent mixtures indicated.

^1H , $^{13}\text{C}\{^1\text{H}\}$, $^{11}\text{B}\{^1\text{H}\}$ **NMR spectra** were obtained, unless otherwise stated, at ambient temperature using a Bruker Avance 300 III (operating at 300 MHz for ^1H , 75 MHz for $^{13}\text{C}\{^1\text{H}\}$ and 96 MHz for $^{11}\text{B}\{^1\text{H}\}$), or a Bruker Avance 500 NMR spectrometer (operating at 500 MHz for ^1H , 125 MHz for $^{13}\text{C}\{^1\text{H}\}$, 160 MHz for $^{11}\text{B}\{^1\text{H}\}$, and 470.6 MHz for ^{19}F). Chemical shifts (δ) were referenced to solvent peaks as follows. ^1H NMR spectra were referenced *via* residual proton resonances of CD_2Cl_2 (5.32 ppm), C_6D_6 (7.16 ppm), CD_3OD (3.31 ppm), acetone- d_6 (2.05 ppm), and CD_3CN (1.94 ppm). ^{13}C NMR spectra were referenced to CD_2Cl_2 (53.84 ppm), C_6D_6 (128.06 ppm) CD_3OD (49.00 ppm), acetone- d_6 (29.84 ppm), and CD_3CN (1.32 ppm). ^{11}B NMR signals are quoted relative to external $\text{BF}_3\cdot\text{OEt}_2$. ^{19}F NMR signals are referenced relative to external and CFCl_3 .

Elemental analyses were performed on an Elementar vario MICRO cube elemental analyzer. It has to be noted that values of carbon obtained for most boron containing samples differ by approximately 1.5% possibly due to formation of boron carbide.^[232] For the analysis of boron-containing compounds, V_2O_5 was added, except for **3.2b**, **4.2**, **4.3**, **4.7**, **Neut1**, **Neut3**, **Cat¹⁺**, and **Cat³⁺**.

High-resolution mass spectrometry was performed with a Thermo Fisher Scientific Exactive Plus Orbitrap MS system. ESI measurements were performed with a HESI source at 50 °C. APCI and ASAP measurements were performed with an APCI source and Corona needle at 400 °C, unless otherwise noted. LIFDI measurements were performed with a Linden CMS LIFDI 700 unit.

Single-crystal X-ray diffraction. Crystals suitable for single-crystal X-ray diffraction were selected, coated in perfluoropolyether oil, and mounted on MiTeGen sample holders. Diffraction data for **3.2a** and **3.2b** were collected on a BRUKER X8-APEX II diffractometer with a CCD area detector and multi-layer mirror monochromated Mo-K_α radiation. Data were collected at 100 K or 296 K as indicated. The structures were solved using the intrinsic phasing method (SHELXT),^[233] refined with the SHELXL program^[234] and

expanded using Fourier techniques. All non-hydrogen atoms were refined anisotropically. Hydrogen atoms were included in structure factors calculations. All hydrogen atoms were assigned to idealized geometric positions. Diamond^[235] software was used for graphical representation. Crystal data and experimental details are listed in Table 11.3; full structural information has been deposited with the Cambridge Crystallographic Data Centre: CCDC-2045567 (**3.2a**) and 2045566 (**3.2b**).

All **photophysical measurements** were carried out at ambient conditions using HPLC grade solvents and standard quartz cuvettes (1 cm x 1 cm cross section). UV/Vis absorption spectra were recorded using an Agilent 1100 diode array UV/Vis spectrophotometer or a Perkin Elmer LAMBDA 465 UV/Vis spectrophotometer. Excitation, emission, lifetime, and quantum yield measurements were recorded using an Edinburgh Instruments FLSP920 spectrometer equipped with a 450 W Xenon arc lamp, double monochromators for the excitation and emission pathways, and a red-sensitive photomultiplier (PMT-R928P) or a near-IR PMT as detectors. The measurements were made in right-angle geometry mode and all spectra were fully corrected for the spectral response of the instrument. To avoid self-absorption, the concentration of all solutions used for photophysical measurements was lower than 10^{-5} M (OD ca. 0.1 at absorption maximum of lowest energy).

Fluorescence quantum yields of the samples were measured using a calibrated integrating sphere (150 mm inner diameter) from Edinburgh Instruments combined with the FLSP920 spectrometer described above. For solution-state measurements, the absorption maximum of lowest energy of the compound in the respective solvent was chosen for excitation. The emission spectra were measured with dilute samples (OD ca. 0.1 at the excitation wavelength).

Fluorescence lifetime measurements were conducted using the time-correlated single-photon counting method (TCSPC) on the FLSP920 spectrometer equipped with a high-speed photomultiplier tube positioned after a single emission monochromator. Lifetimes shorter than 0.5 ns were recorded at an Edinburgh Instruments FLS 980 fluorescence lifetime spectrometer equipped with a high speed PMT (H10720) detector using the laser diodes defined below. Measurements were made in right-angle geometry mode, and the emission was collected through a polarizer set to the magic angle (54.8°). Solutions were excited with either a 315 nm (pulse width 932.5 ps), 376 nm (pulse width 72.6 ps) or a 418 nm (pulse width 1.5 ns) pulsed diode laser at repetition rates of 1–5 MHz and counts were recorded at the emission maxima. The choice of laser was based on the largest absorption maximum of the respective compound. Decays were recorded to 10 000 counts

in the peak channel with a record length of at least 4 000 channels. The band-pass of the monochromator was adjusted to give a signal count rate of <20 KHz. Iterative reconvolution of the IRF with one decay function and nonlinear least-squares analysis were used to analyze the data. The quality of all decay fits was judged to be satisfactory based on the calculated values of the reduced χ^2 and Durbin–Watson parameters and visual inspection of the weighted and autocorrelated residuals.

Singlet oxygen sensitizing efficiency (Φ_{Δ}) of **3.1a**, **3.2c**, **3.3c**, and **Cat¹⁺ - Cat⁴⁺** was determined in acetonitrile solutions relative to a solution of perinaphthenone in acetonitrile by measuring the weak emission of ¹O₂ at ca. 1275 nm. Absorption spectra were recorded using the Perkin Elmer LAMBDA 465 UV/Vis spectrophotometer described above. Emission spectra were recorded using the Edinburgh Instruments FLSP920 spectrometer described above. Excitation was performed using the 450 W Xenon arc lamp while detection was performed using the near-IR PMT detector. Emission wavelengths shorter than 850 nm were removed using an optical filter to remove optical refractions of higher orders of the excitation light. Solutions were O₂ saturated by purging the solutions with pure oxygen for 20 min. Concentrations of solutions were adjusted to obtain an intersection of the absorption spectrum of perinaphthenone and the respective compound at an absorbance of ca. 0.15. The intersection of the spectra was at ca. 341 nm for the triarylboranes and at ca. 400 nm for the *bis*-triarylboranes. The values for the respective compounds were calculated relative to perinaphthenone which is known to have a Φ_{Δ} of 1 in acetonitrile^[180] by integration of the respective emission spectra between ca. 1240 and 1300 nm.

Molar extinction coefficients (ϵ) were determined from at least three dilutions of two independently prepared stock solutions ($c = 6.3 \times 10^{-4} - 5.0 \times 10^{-6}$ M) in the solvent(s) indicated and are average values from these measurements.

Solubility in water was determined for **Cat¹⁺**, **Cat²⁺**, **Cat(i)²⁺**, and **Cat³⁺** by measuring the absorbance of solutions in Millipore water ($c = 3.4$ M to 2.6 M) which were shaken in the dark for 3 d using a Janke & Kunkel IKA® VIBRAX® VXR. Absorption of the resulting “solutions” was measured using the Perkin Elmer LAMBDA 465 UV/Vis spectrophotometer described above. Solutions were filtered using CLEAR PA-45/13 syringe filters with polyamide (Nylon) membrane and a pore size of 0.45 μ m. To determine the solubility of **7.6-7.8** in water and PBS buffer, acetonitrile stock solutions with concentrations of 1.05×10^{-3} , 1.01×10^{-3} , and 1.03×10^{-3} M, respectively, were added to water or buffer filled standard quartz cuvettes (1 cm x 1 cm cross section). Absorption changes were monitored

by UV/Vis measurements. Precipitation and/or aggregation was indicated by change of the shape of the spectrum and/or by a raise of the baseline.

Cyclic voltammetry experiments were performed using a Gamry Instruments Reference 600 potentiostat. A standard three-electrode cell configuration was employed using a platinum disk working electrode, a platinum wire as counter electrode, and a silver wire, separated by a *Vycor* tip, serving as the reference electrode. Formal redox potentials are referenced to the ferrocene/ferrocenium ($[\text{Cp}_2\text{Fe}]^{+/0}$) redox couple as an internal standard. Tetra-*n*-butylammonium hexafluorophosphate ($[\text{nBu}_4\text{N}][\text{PF}_6]$) was used as supporting electrolyte. Compensation for resistive losses (iR drop) was employed for all measurements.

DFT and TD-DFT calculations were carried out with the Gaussian 09 (Rev. E.01) program package^[236] and were performed on a parallel cluster system. GaussView 5.0.9 was used to visualize the results, and to measure calculated structural parameters. Multitwfn^[237] was used to plot orbital surfaces (isovalue: $\pm 0.030 [\text{e}_0^{-3}]^{1/2}$). The ground-state geometries were optimized using the B3LYP functional^[238-240] in combination with the 6-31G(d) basis set.^[241-242] The optimized geometries were confirmed to be local minima by performing frequency calculations. Based on these optimized structures, the lowest-energy gas-phase vertical transitions were calculated (singlets, 10 states) by TD-DFT, using the Coulomb-attenuated functional CAM-B3LYP^[243] in combination with the 6-31G(d,p) basis set.

Optical Properties in Sodium Cacodylate. UV/Vis absorption spectra were recorded on a Varian Cary 100 Bio spectrometer; excitation and emission spectra were recorded on a Varian Cary Eclipse fluorimeter

Study of Interactions with DNA and RNA. Polynucleotides were purchased as noted: poly A – poly U (Sigma), calf thymus (ct)-DNA (Aldrich) and dissolved in sodium cacodylate buffer, ($I = 0.05 \text{ M}$, pH 7). The ctDNA was additionally sonicated and filtered through a 0.45 mm filter to obtain mostly short (ca. 100 base pairs) rod-like β -helical DNA fragments.^[244] The polynucleotide concentration was determined spectroscopically^[245] as the concentration of the phosphates, which corresponds to the concentration of the nucleobase.

Thermal melting experiments were performed on a Varian Cary 100 Bio spectrometer in quartz cuvettes (diameter: 1 cm). The measurements were carried out in aqueous buffer solution at pH 7 (sodium cacodylate buffer $I = 0.05 \text{ M}$) or pH 8 (15 mM Tris-HCl, 300 mM KCl), as indicated. Thermal melting curves for ds-DNA, ds-RNA, and their complexes with **Cat¹⁺**, **Cat²⁺**, **Cat(i)²⁺**, **Cat³⁺**, and **Cat⁴⁺** were determined by following the absorption change

at 260 nm as a function of temperature.^[218] T_m values are the midpoints of the transition curves determined from the maximum of the first derivative and checked graphically by the tangent method. The ΔT_m values were calculated subtracting T_m of the free nucleic acid from T_m of the complex. Every ΔT_m value reported here was the average of at least two measurements. The error in ΔT_m is ± 0.5 °C.

Fluorimetric titrations were performed in quartz cuvettes (diameter: 1 cm) on a Varian Cary Eclipse fluorimeter by adding portions of polynucleotide solution into the solution of the compound studied and excitation wavelengths of $\lambda_{exc} > 300$ nm were used to avoid absorption of excitation light by added polynucleotides. After mixing the polynucleotides with the compound investigated, equilibrium was reached in less than 120 s. Fluorescence spectra were analyzed at an excess of DNA/RNA ($r[dye]/[DNA] < 0.2$) to assure one dominant binding mode. To obtain binding constants (K_s), titration data were processed by means of non-linear fitting to the Scatchard equation^[221] using the McGhee, von Hippel formalism^[222] which gave values of the ratio of [bound compound]/[polynucleotide] in the range 0.1–0.3. For easier comparison, all k_s values were recalculated for the fixed $r = 0.25$ (for ds-DNA/RNA). Calculated values for k_s have satisfactory correlation coefficients (> 0.99).

Circular dichroism (CD) spectra were recorded on a JASCO J-815 spectropolarimeter at room temperature using quartz cuvettes (diameter: 1 cm) with a scan speed of 200 nm/min. A background spectrum of the buffer was subtracted from each spectrum and each spectrum was the result of three accumulations. CD experiments were performed by adding portions of a stock solution of the compound into the solution of polynucleotide ($c = 2 \times 10^{-5}$ M).

Cells. Experiments were performed using two human cell lines, epithelial human lung adenocarcinoma A549 (ATCC® CCL-185™) and human normal lung fibroblast WI-38 (ATCC® CCL-75™). Both cell lines adhere to plastic and glass surfaces and are maintained in the culture under same conditions. Cells were grown in Dulbecco Modified Eagle's Medium (DMEM, Sigma Aldrich, USA) supplemented with 10% of fetal bovine serum (FBS, Sigma Aldrich, USA) at 37 °C and 5% CO₂ in a humidified atmosphere. Cells were passaged twice per week to retain maximum confluence of 70-80%. Cells exhibiting normal morphology without any contamination signs were kept in culture and used in all further experiments. Two biological replicates were performed for all experiments.

Cytotoxicity Assay. Cytotoxic effect of the compounds was analyzed by the MTT assay.^[246] The compounds were dissolved in an appropriate volume of dimethyl sulfoxide solution (DMSO) under sterile conditions, to obtain a stock solution of 10 mM

concentration. Solutions were kept in the dark and stored at +4 °C to prevent degradation. Prior to each assay, fresh working solutions were prepared from stock solutions by diluting it with DMEM. Cells were seeded on 96 well plate at a concentration of 7×10^3 cells/well in 100 μ L of DMEM (10% FBS) and left in the incubator overnight (37 °C, 5% CO₂). The next day, 100 μ L of the working solution was added to the wells. The final concentration of compounds was obtained in the total volume of 200 μ L/well. All conditions were tested in quadruplicates. Cells treated with the same dilutions of DMSO represented the control, while cells treated only with DMEM (10% FBS) represented the negative control. The plate was then incubated for the next 72 h (37 °C, 5% CO₂). After the incubation, the medium was removed, and 40 μ L of MTT solution was added to each well. The plate was incubated for 3 h, allowing the formazan crystals to form. After 3 h, 170 μ L of DMSO was added in each well and the system was shaken for 20 min, allowing the crystals to dissolve. The absorbance of MTT-formazan product was measured with a microplate reader at 600 nm. The absorbance value directly correlates with the cell survival. For irradiation experiments, cells in MTT-prepared plates (see above), treated with the compounds studied, were irradiated for 5 min in a Luzchem reactor with visible light (400-700 nm, 8 lamps, total ≈ 8 W, dose: 50.6 mW m⁻²) at ca. 18 cm distance between the lamps and the cell-plate, 24, 48 and 72 h after starting the MTT test.

Co-localization Assay. A549 cells were seeded on glass slides in 24 well plates at a concentration of 3×10^4 cells/well and incubated in DMEM (37 °C, 5% CO₂) for 48 h, allowing cells to attach to the glass surface and to multiply. Then, cells were treated with a 10 μ M solution of the compound and incubated for 90 min at 37 °C. After incubation, cells were fixed with 2% paraformaldehyde (PFA, 12 min, r.t.), washed with PBS (3 x), permeabilized with 0.1% Triton/PBS (2 min, r.t.), washed with PBS (3 x), blocked in 3% BSA (30 min, r.t.), and incubated with primary antibody against early endosome antigen 1 (EEA1, Cell Signaling Technology, #2411, rabbit, 1:100 in 5% BSA), Golgi Apparatus (GM130, Cell Signaling Technology, #12480, rabbit, 1:2500 in 5% BSA) or Lysosome Associated Membrane Protein 1 (LAMP-1, abcam, ab2417, rabbit, 1:250 in 5% BSA). After incubation in primary antibody, cells were washed with PBS, and then incubated in fluorescently labeled anti-rabbit secondary antibody (AF647) (Cell Signaling Technology, #4414, 1:1000 in 5% BSA). Slides were incorporated in DAPI containing mounting medium. Actin filaments were labeled with Alexa Fluor® 555 Phalloidin (Cell Signaling Technology, #8953). Prepared slides were kept in the dark and visualized using a Leica SP8 X confocal microscope (Leica Microsystems). Co-localization was assessed by determining the Pearson correlation coefficient.

Live Cell Imaging. Live imaging of the cells treated with the compounds was performed on the A549 cell line. Cells were seeded in Ibidi imaging cell chambers (Ibidi®) in 500 μL of medium, at a concentration of 5×10^4 cells/well, and left in the cell incubator for 48 h (37°C , 5% CO_2). After two days, cells were treated with 10 μM solution of the compound to be studied and left in the cell incubator for 90 min to allow the compound to enter the cells.

Double bond isomerization. Solutions of **7.6** and **7.7** ($c = 35 \times 10^{-3}$ M) in CD_3CN were stirred in cylindrical quartz flasks for up to 4 h. The flasks were placed on a magnetic stirring plate between two lamps (254 nm, 4 W each). The distance between the lamps was ca. 15 cm. Samples to record ^1H NMR spectra were taken after 0, 5, 15, and 30 min, 1, 2, 3, and 4 h and measured at 300 MHz at r.t. The NMR samples were stored in amberized NMR tubes from Norell® until the measurement was over.

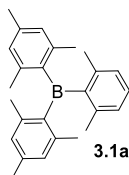
Cleavage of boronate esters with H_2O_2 . THF solutions of **7.6-7.8** ($c = 30 \times 10^{-3}$, 87×10^{-3} , and 43×10^{-3} M, respectively) with stoichiometric amounts of H_2O_2 were stirred in cylindrical quartz flasks for up to 46 h. First samples were taken after 5 min and added to an aqueous, saturated iron(II) sulfate solution. After extraction of the aqueous phase with Et_2O , HRMS spectra (ASAP) were recorded of the organic phase. With increasing reaction time, the time interval increased gradually. When combining cleavage and irradiation experiments, the concentration of the solutions was 50×10^{-3} M.

9.2 Synthesis

General procedure for the synthesis of Grignard reagents

Magnesium (2.5 eq.) was activated first by stirring overnight and then by addition and sublimation of catalytic amounts of iodine. After addition of dry THF (0.08 mL/mmol), undiluted bromo-arene (0.1 – 0.2 eq.) was added without stirring to start the reaction. If no heat evolution was visible, the solution was gently heated until the start of the reaction was clearly visible. Thereafter, bromo-arene (0.9 – 0.8 eq.) diluted with THF (0.24 mL/mmol) was added slowly to keep the reaction heating itself under slow stirring. After complete addition, the reaction was heated under stirring at reflux for another 1 – 2 h until GC-MS spectrometry confirmed the complete formation of the Grignard reagent. After cooling to room temperature, the Grignard reagent was transferred *via* a filtering canula into a second flask and used without further purification.

9.2.1 Chapter 3

Dimesityl-(2,6-dimethylphenyl)-borane 3.1a

The Grignard reagent was freshly prepared from magnesium (1.94 g, 79.7 mmol) and 2-bromomesitylene (12.0 mL, 79.7 mmol) in dry THF (40 mL) and, after cooling to 0 °C for 30 min, boron trifluoride etherate (4.3 mL, 35.0 mmol) was added dropwise. The solution was stirred at room temperature for 17 h. Afterwards, the solvent was removed *in vacuo* and the resulting solid was extracted with dry, hot hexane (4 x 40 mL). Removal of the solvent *in vacuo* yielded dimesitylfluoroborane **Mes₂BF** as a colorless solid which was used without further purification in the following step. The NMR spectra recorded match those reported in literature.^[247]

In a second flask, 1-bromo-2,6-dimethylbenzene (4.6 mL, 34.6 mmol) was dissolved in dry THF (30 mL), purged with argon for 5 min and cooled to -78 °C, and *tert*-butyl lithium (41 mL, c = 1.7 mol/L, 70 mmol) was added slowly. The solution was stirred for 15 min at -78 °C, warmed to room temperature and stirred for 2 h. The previously prepared dimesitylfluoroborane was dissolved in dry THF (15 mL) and added slowly to the solution of 2,6-dimethylphenyl lithium. The reaction was stirred at room temperature for 3 d and then water (40 mL) was added. The aqueous phase was extracted with hexane (3 x 40 mL). The combined organic phases were dried over magnesium sulfate and the solvent was removed *in vacuo*. The crude product was recrystallized from hexane two times yielding the product as clear colorless crystals (26.3 mmol, 9.33 g, 76%). For photophysical measurements, a small quantity was additionally purified *via* filtration through a silica gel plug using hexane.

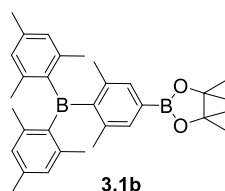
¹H NMR (500 MHz, CD₂Cl₂) δ = 7.14 (dd, *J* = 7.5 Hz, 1 H, CH), 6.92 (d, *J* = 7.5 Hz, 2 H, CH), 6.78 (s, 4 H, CH), 2.28 (s, 6 H, CH₃), 2.02 (s, 6 H, CH₃), 2.00 (s, 6 H, CH₃), 1.98 (s, 6 H, CH₃) ppm.

¹¹B{¹H} NMR (160 MHz, CD₂Cl₂) δ = 77 (br) ppm.

¹³C{¹H} NMR (125 MHz, CD₂Cl₂) δ = 147.8, 144.4, 141.0, 140.9, 140.6, 139.8, 129.6, 129.0, 129.0, 128.0, 23.0, 23.0, 22.9, 21.4 ppm.

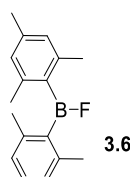
HRMS (EI⁻) *m/z*: [M+H]⁺ found: 355.2587; calc. for [C₂₆H₃₁B]: 355.2592 (|Δ| = 1.4 ppm).

Elem. Anal. Calc. (%) for C₂₆H₃₁B: C 88.13, H 8.82; found: C 88.12, H 8.91.

Dimesityl-4-(4,4,5,5-tetramethyl-1,3,2-dioxaborolan-2-yl)-2,6-dimethylphenylborane**3.1b**

Dimesityl-2,6-dimethylphenylborane **3.1a** (500 mg, 1.41 mmol), B_2pin_2 (431 mg, 1.70 mmol), dtbpy (8 mg, 29.4 μ mol) and $[Ir(COD)(\mu-OMe)]_2$ (10 mg, 14.8 μ mol) were dissolved in dry, degassed THF (17 mL) and stirred at 80 °C for 23 h. After cooling to room temperature and removing the solvent, the resulting brown oil was purified by automated flash column chromatography (silica gel, hexane/ CH_2Cl_2 1:1) yielding the product (612 mg, 1.27 mmol, 90%) as a colorless solid. The recorded 1H NMR spectrum matches that reported in literature.^[54, 248]

1H NMR (200 MHz, CD_2Cl_2) δ = 7.29 (s, 2 H, CH), 6.75 (s, 4 H, CH), 2.26 (s, 6 H, CH_3), 2.01 (s, 6 H, CH_3), 1.97 (s, 6 H, CH_3), 1.93 (s, 6 H, CH_3), 1.32 (s, 12 H, CH_3) ppm.

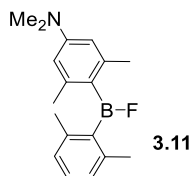
Mesityl-(2,6-dimethylphenyl)-fluoroborane 3.6

Potassium (2,6-dimethylphenyl)-trifluoroborate (5.0 g, 23.6 mmol) was dissolved in dry, degassed THF (50 mL). After dropwise addition of mesitylmagnesiumbromide (45 mL, 30.7 mmol, $c = 0.68$ M), the reaction mixture was stirred at room temperature for 18 h. Under an argon atmosphere, the solvent was removed *in vacuo*. The crude product was extracted with dry, hot hexane (4 x 40 mL). Removing the solvent yielded an off-white, crystalline solid (5.6 g, 22.0 mmol, 93%). The recorded NMR spectra match those reported in literature.^[55]

1H NMR (500 MHz, C_6D_6): δ = 7.09 (t, $J = 8$ Hz, 1 H, CH), 6.87 (d, $J = 8$ Hz, 2 H, CH), 6.68 (s, 2 H, CH), 2.27 (s, 3 H, CH_3), 2.27 (s, 3 H, CH_3), 2.26 (s, 3 H, CH_3), 2.26 (s, 3 H, CH_3), 2.08 (s, 3 H, CH_3) ppm.

$^{11}B\{^1H\}$ NMR (160 MHz, C_6D_6): δ = 53.70 (s) ppm.

$^{19}F\{^1H\}$ NMR (470 MHz, C_6D_6): δ = -13.31 (s) ppm.

[4-(*N,N*-dimethylamino)-2,6-dimethylphenyl]-(2,6-dimethylphenyl)-fluoroborane**3.11**

A Grignard reagent was prepared from magnesium (1.50 g, 61.7 mmol), 4-bromo-*N,N*,3,4-tetramethylaniline (7.03 g, 30.8 mmol) and dry, degassed THF (40 mL) while stirring under reflux for 2 h according to the general procedure described above. After cooling to room temperature, the solution was transferred *via* a filter cannula onto a solution of potassium 2,6-dimethylphenyl trifluoroborate (5.01 g, 23.6 mmol) in dry, degassed THF (50 mL). The mixture was stirred at room temperature for 18 h. After removing the solvent *in vacuo*, the remaining solid was extracted with dry, hot hexane (2 x 100 mL, 1 x 35 mL). Removing the solvent *in vacuo* yielded the product as a yellow oil (5.57 g, 19.7 mmol, 83%) which was used without further purification. It contained a small amount of residual *N,N*,3,5-tetramethylaniline.

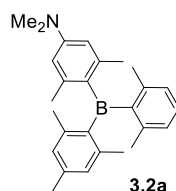
¹H NMR (500 MHz, C₆D₆) δ = 7.13 (m, 1 H, CH), 6.93 (m, 2 H, CH), 6.28 (s, 2 H, CH), 2.46 (s, 6 H, CH₃), 2.45 (s, 3 H, CH₃), 2.45 (s, 3 H, CH₃), 2.34 (s, 3 H, CH₃), 2.34 (s, 3 H, CH₃) ppm. (*N,N*,3,5-Tetramethylaniline: δ = 6.48 (s, 1 H, CH), 6.42 (s, 2 H, CH), 2.59 (s, 6 H, CH₃), 2.26 (s, 6 H, CH₃) ppm.)

¹¹B{¹H} NMR (160 MHz, C₆D₆) δ = 52.3 (s) ppm.

¹³C{¹H} NMR (125 MHz, C₆D₆) δ = 152.8, 147.9, 147.8, 141.6, 140.0, 140.0, 129.5, 129.5, 127.4, 122.5, 112.3, 39.3, 24.4, 24.3, 22.3 ppm. (*N,N*,3,5-Tetramethylaniline: δ = 151.4, 138.4, 119.4, 111.4, 40.5, 22.0 ppm.)

¹⁹F{¹H} NMR (470 MHz, C₆D₆) δ = -23.7 (s) ppm.

HRMS (LIFDI) m/z: [M]⁺ found: 283.1898; calc. for [C₁₈H₂₃BFN]: 283.1902 (| Δ | = 1.41 ppm).

[4-(*N,N*-dimethylamino)-2,6-dimethylphenyl]-(mesityl)-(2,6-dimethylphenyl)-borane
3.2a

Mesitylbromide (4.40 mL, 29.2 mmol) was dissolved in dry, degassed THF (45 mL). After cooling to $-78\text{ }^{\circ}\text{C}$, *t*BuLi (30.0 mL, 51 mmol, $c = 1.7\text{ M}$ in heptane) was added dropwise and the reaction was stirred at $-78\text{ }^{\circ}\text{C}$ for 30 min. After stirring at room temperature for 2 h, the reaction mixture was transferred *via* a transfer cannula to a solution of [(*N,N*-dimethylamino)-2,6-dimethylphenyl]-(2,6-dimethylphenyl)-fluoroborane (5.56 g, 19.6 mmol) in dry, degassed THF (60 mL). This mixture was stirred at room temperature for 3 d. After addition of water (50 mL), the aqueous phase was extracted with hexane (3 x 50 mL). The combined organic phases were washed with water (50 mL) and brine (3 x 120 mL), dried over magnesium sulfate and the solvent was removed *in vacuo*. The resulting crude product was purified *via* distillation (5×10^{-2} mbar, $80\text{ }^{\circ}\text{C}$) and column chromatography (aluminum oxide, neutral, pure hexane, then pure CH_2Cl_2) yielding the pure product as a yellow greenish, amorphous solid (4.30 g, 11.2 mmol, 48%).

$^1\text{H NMR}$ (500 MHz, CD_2Cl_2) $\delta = 7.20$ (t, $J = 7.5\text{ Hz}$, 1 H, CH), 6.90 (d, $J = 7.5\text{ Hz}$, 2 H, CH), 6.75 (s, 2 H, CH), 6.32 (s, 2 H, CH), 3.00 (s, 6 H, CH_3), 2.27 (s, 3 H, CH_3), 2.02 (br s, 3 H, CH_3), 1.97 (s, 6 H, CH_3), 1.95 (s, 6 H, CH_3) ppm.

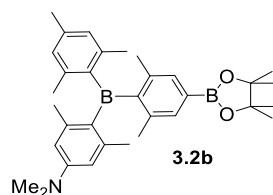
$^{11}\text{B}\{^1\text{H}\}$ NMR (160 MHz, CD_2Cl_2) $\delta = 75$ (br) ppm.

$^{13}\text{C}\{^1\text{H}\}$ NMR (125 MHz, CD_2Cl_2) $\delta = 152.0, 148.8, 145.4, 143.7, 143.6, 140.8, 140.5, 140.3, 139.0, 135.2, 129.0, 128.8, 127.7, 111.9, 111.9, 40.1, 24.0, 23.9, 23.1, 22.8, 22.7, 21.3$ ppm.

HRMS (EI $^-$) m/z : $[\text{M}+\text{H}]^+$ 384.2853; calc. for $[\text{C}_{27}\text{H}_{35}\text{BN}]$ 384.2857 ($|\Delta| = 1.04$ ppm).

Elem. Anal. Calc. (%) for $\text{C}_{27}\text{H}_{34}\text{BN}$: C 84.59, H 8.94, N 3.65; found: C 84.36, H 9.35, N 3.75.

[4-(*N,N*-Dimethylamino)-2,6-dimethylphenyl]-(mesityl)-[4-(4,4,5,5-tetramethyl-1,3,2-dioxaborolan-2-yl)2,6-dimethylphenyl]borane 3.2b



[4-(*N,N*-Dimethylamino)-2,6-dimethylphenyl]-(mesityl)-(2,6-dimethylphenyl)-borane **3.2a** (1.08 g, 2.82 mmol), *bis*-pinacolato diboron (822 mg, 3.24 mmol), 4,4'-di-*tert*-butyl-2,2'-dipyridyl (24 mg, dtbpy, 88.9 μ mol) and [Ir(COD)(μ -OMe)]₂ (24 mg, 35.6 μ mol) were dissolved in dry, degassed hexane (32 mL). The resulting solution was stirred at 80 °C for 1 d 18 h. After cooling to room temperature, the solvent was removed *in vacuo*. The resulting crude product was purified *via* flash column chromatography (NH column, 0-100% ethyl acetate in hexane) yielding the pure product as a yellow solid (1.18 g, 2.32 mmol, 89%).

¹H NMR (500 MHz, CD₂Cl₂) δ = 7.30 (s, 2 H, CH), 6.75 (s, 2 H, CH), 6.32 (m, 2 H, CH), 2.97 (s, 6 H, CH₃), 2.27 (s, 3 H, CH₃), 2.12–1.89 (m, 18 H, CH₃), 1.34 (s, 12 H, CH₃) ppm.

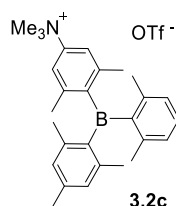
¹¹B{¹H} NMR (160 MHz, CD₂Cl₂) δ = 75.7 (br s), 31.0 (s) ppm.

¹³C{¹H} NMR (125 MHz, CD₂Cl₂) δ = 152.3, 152.1, 145.2, 143.8, 143.7, 139.5, 139.1, 135.0, 133.9, 111.9, 84.0, 40.1, 25.2, 24.1, 24.0, 21.4 ppm.

HRMS (EI⁻) *m/z*: [M+H]⁺ found: 510.3702; calc. for [C₃₃H₄₅B₂NO₂]: 510.3709 ($|\Delta|$ = 1.37 ppm).

Elem. Anal. Calc. (%) for C₃₃H₄₅B₂NO₂: C 77.82, H 8.91, N 2.75; found: C 77.50, H 9.20, N 2.85.

[4-(*N,N,N*-Trimethylammonium)-2,6-dimethylphenyl]-(mesityl)-(2,6-dimethylphenyl)-borane triflate 3.2c



[4-(*N,N*-Dimethylamino)-2,6-dimethylphenyl]-(mesityl)-(2,6-dimethylphenyl)borane **3.2a** (15 mg, 39.1 μmol) was dissolved in CH_2Cl_2 (2 mL). After addition of methyl triflate (17.5 μL , 156 μmol), the reaction mixture was stirred in the dark at room temperature for 17 h. Subsequently, hexane (7 mL) was added. The resulting solid was collected by filtration and washed with hexane (5 mL) yielding the product as a colorless solid (19 mg, 34.7 μmol , 89%). ^1H NMR spectroscopy in combination with absorption and emission spectroscopy revealed an impurity of 0.5% starting material. To obtain pure product for spectroscopy, parts of the product were further purified by washing with hexane (20 mL) and drying *in vacuo*.

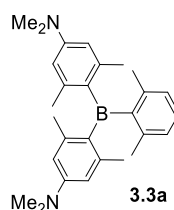
^1H NMR (500 MHz, CD_3OD) δ = 7.49 (s, 2 H, CH), 7.20 - 7.17 (m, 1 H, CH), 6.99 - 6.93 (m, 2 H, CH), 6.84 - 6.79 (m, 2 H, CH), 3.64 (s, 9 H, CH_3), 2.28 (s, 3 H, CH_3), 2.15 (s, 3 H, CH_3), 2.13 (s, 3 H, CH_3), 2.04 (s, 3 H, CH_3), 2.00 (s, 3 H, CH_3), 1.97 (s, 3 H, CH_3), 1.95 (s, 3 H, CH_3) ppm.

$^{11}\text{B}\{^1\text{H}\}$ NMR (160 MHz, CD_3OD) δ = 78 (br) ppm.

$^{13}\text{C}\{^1\text{H}\}$ NMR (125 MHz, CD_3OD) δ = 150.9, 149.1, 147.2, 144.6, 144.5, 144.0, 142.3, 142.1, 141.9, 141.7, 141.1, 131.4, 130.2, 130.0, 129.2, 129.1, 121.8 (q, $^1J_{\text{CF}}$ = 319 Hz), 119.6, 119.6, 57.4, 23.4, 23.2, 23.2, 23.2, 23.1, 21.3 ppm.

HRMS (ESI⁺) m/z : $[\text{M}-\text{OTf}]^+$ found: 398.3011; calc. for $[\text{C}_{28}\text{H}_{37}\text{BN}]$: 398.3014 ($|\Delta|$ = 0.75 ppm).

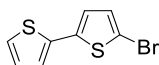
Elem. Anal. Calc. (%) for $\text{C}_{29}\text{H}_{37}\text{BF}_3\text{NO}_3\text{S}$: C 63.62, H 6.81, N 2.56, S 5.86; found: C 62.21, H 6.86, N 2.72, S 5.79.

Bis-[4-(*N,N*-dimethylamino)-2,6-dimethylphenyl]-2,6-dimethylphenylborane 3.3a

Potassium 2,6-dimethylphenyl trifluoroborate **3.4** (2.56 g, 12.1 mmol) was dissolved in THF (60 mL) and added dropwise to a solution of 4-(*N,N*-dimethylamino)-2,6-dimethylphenyllithium **3.7** (4.14 g, 26.7 mmol) in THF (55 mL). The reaction mixture was stirred at room temperature for 2 d. After the addition of water, the aqueous phase was extracted with hexane. The combined organic phases were washed with water and brine, dried over MgSO_4 and the solvent was removed *in vacuo*. The resulting crude product was purified by distillation (2×10^{-2} mbar, 90 °C) and column chromatography (aluminum oxide, basic, 10% EtOAc in hexane) yielding **3.3a** as a yellow solid (2.13 g, 5.17 mmol, 43%). The NMR spectrum matches that reported in literature.^[43]

^1H NMR (300 MHz, CD_2Cl_2) δ = 7.12 (dd, 1 H, J = 7.6 Hz, CH), 6.92 (d, 2 H, J = 7.6 Hz, CH), 6.36 (s, 4 H, CH), 2.98 (s, 12 H, CH_3), 2.08 (s, 6 H, CH_3), 2.06 (s, 6 H, CH_3), 1.97 (s, 6 H, CH_3) ppm.

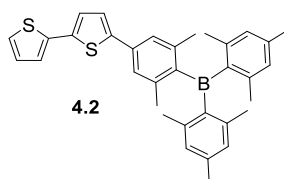
9.2.2 Chapter 4

5-Bromo-2,2'-bithiophene 4.1

4.1

Similarly to literature procedures,^[27-28] 2,2'-bithiophene (4.14 g, 24.9 mmol) was dissolved in DMF (140 mL) and cooled to 0 °C, and then NBS (4.33 g, 24.3 mmol) was added portion wise. After stirring for 15 min at 0 °C, the reaction mixture was allowed to warm to room temperature while stirring for 1 h. After addition of water (100 mL), the aqueous phase was extracted with CHCl₃ (2 x 80 mL). The combined organic phases were washed with water (1 x 80 mL), dried over magnesium sulfate and the solvent was removed *in vacuo*. The resulting green solid was further purified *via* a short way distillation yielding the product (3.62 g, 14.7 mmol, 59%) as a green solid. The ¹H NMR spectrum matches that reported in literature.^[29]

¹H NMR (300 MHz, CD₂Cl₂) δ = 7.26 (dd, J = 1 Hz, J = 5 Hz, 1 H, CH), 7.14 (ddd, J = 0.2 Hz, J = 1 Hz, J = 3.5 Hz, 1 H, CH), 7.02 (dd, J = 3.5 Hz, J = 5 Hz, 1 H, CH), 7.00 (d, J = 4 Hz, 1 H, CH), 6.94 (d, J = 4 Hz, 1 H, CH) ppm.

5-[4-(3,5-dimethylphenyl)-dimesitylboryl]-2,2'-bithiophene 4.2

5-Bromo-2,2'-bithiophene **4.1** (200 mg, 814 μmol), dimesityl-4-(4,4,5,5-tetramethyl-1,3,2-dioxaborolan-2-yl)-2,6-dimethylphenylborane **3.1b** (430 mg, 895 μmol) and KOH (275 mg, 4.89 mmol) were dissolved in toluene (6 mL) and water (3 mL). After purging the solution with argon for 4 min, $\text{Pd}_2(\text{dba})_3 \cdot \text{CHCl}_3$ (37.5 mg, 40.8 μmol) and SPhos (70.0 mg, 171 μmol) were added and the mixture was stirred at 85 $^\circ\text{C}$ for 22 h. After cooling to room temperature, the phases were separated, and the aqueous phase was extracted with hexane (4 x 20 mL). The combined organic phases were dried over magnesium sulfate. After removing the solvent *in vacuo*, the crude product was purified *via* flash column chromatography (silica gel, 0–100% ethyl acetate in hexane) yielding the product (298 mg, 575 μmol , 71%) as a yellow solid. The recorded spectra match those reported in literature.^[55]

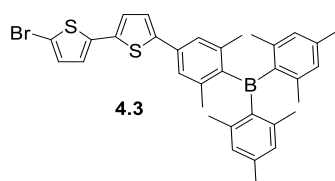
^1H NMR (500 MHz, CD_2Cl_2) δ = 7.30 (d, J = 4 Hz, 1 H, CH), 7.25 (dd, J = 1.0 Hz, J = 5 Hz, 1 H, CH), 7.23 (dd, J = 1 Hz, J = 4 Hz, 1 H, CH), 7.22 (s, 2 H, CH), 7.17 (d, J = 4 Hz, 1 H, CH), 7.05 (dd, J = 4 Hz, J = 5 Hz, 1 H, CH), 6.79 (2 br s, 2 H, CH), 2.29 (s, 6 H, CH_3), 2.06 (s, 6 H, CH_3), 2.03 (s, 6 H, CH_3), 2.01 (s, 6 H, CH_3) ppm.

$^{11}\text{B}\{^1\text{H}\}$ NMR (160 MHz, CD_2Cl_2) δ = 78 (br) ppm.

$^{13}\text{C}\{^1\text{H}\}$ NMR (125 MHz, CD_2Cl_2) δ = 147.6, 144.3, 143.6, 141.7, 141.0, 140.9, 139.9, 137.8, 136.8, 129.0, 128.3, 125.0, 124.9, 124.8, 124.1, 124.0, 23.1, 23.1, 23.0, 21.4 ppm.

HRMS (EI^-) m/z : $[\text{M}]^-$ 518.2281; calc. for $[\text{C}_{34}\text{H}_{35}\text{BS}_2]$ 518.2279 ($|\Delta|$ = 0.4 ppm).

Elem. Anal. Calc. (%) for $\text{C}_{34}\text{H}_{35}\text{BS}_2$: C 78.75, H 6.80, S 12.36; found: C 78.68, H 6.87, S 12.40.

5'-Bromo-5-[4-(3,5-dimethylphenyl)-dimesitylboryl]-2,2'-bithiophene 4.3

Under ambient conditions, 5-[4-(3,5-dimethylphenyl)-dimesitylboryl]-2,2'-bithiophene **4.2** (200 mg, 386 μmol) was dissolved in DMF (5.0 mL) and cooled to 0 °C. After portion wise addition of NBS (69 mg, 386 μmol), the reaction mixture was stirred at 0 °C for 15 min. After warming to room temperature, the solution was stirred for an additional 3 h. As GC-MS showed consumption of NBS, water (10 mL) was added. The resulting yellow precipitate was collected by filtration and washed with water (25 mL). Subsequently, the solid was dissolved in CH_2Cl_2 , washed with water, the organic phase was separated and dried over magnesium sulfate. Removal of the solvent *in vacuo* yielded the product (214 mg, 358 μmol , 93%) as a yellow solid. The recorded spectra match those reported in literature.^[55]

^1H NMR (500 MHz, CD_2Cl_2) δ = 7.28 (d, J = 4 Hz, 1 H, CH), 7.20 (s, 2 H, CH), 7.11 (d, J = 4 Hz, 1 H, CH), 7.01 (d, J = 4 Hz, 1 H, CH), 6.97 (d, J = 4 Hz, 1 H, CH), 6.78 (s, 4 H, CH), 2.28 (s, 6 H, CH_3), 2.05 (s, 6 H, CH_3), 2.02 (s, 6 H, CH_3), 2.00 (s, 6 H, CH_3) ppm.

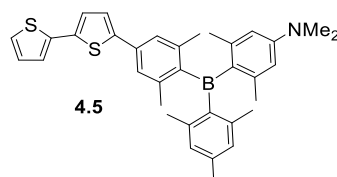
$^{11}\text{B}\{^1\text{H}\}$ NMR (160 MHz, CD_2Cl_2) δ = 77 (br) ppm.

$^{13}\text{C}\{^1\text{H}\}$ NMR (125 MHz, CD_2Cl_2) δ = 147.8, 144.2, 144.2, 141.7, 141.1, 140.9, 139.9, 139.5, 135.6, 134.5, 131.3, 129.0, 125.3, 124.9, 124.1, 111.1, 23.1, 23.0, 23.0, 21.4 ppm.

HRMS (EI^-) m/z : [$\text{M}^- - \text{H}^+$] 595.1316; calc. for $[\text{C}_{34}\text{H}_{33}\text{BBrS}_2]$ 595.1306 ($|\Delta|$ = 1.7 ppm).

Elem. Anal. Calc. (%) for $\text{C}_{34}\text{H}_{34}\text{BBrS}_2$: C 68.35, H 5.74, S 10.73; found: C 68.00, H 5.92, S 10.47.

5-[4-(2,6-Dimethylphenyl)-(4-(*N,N*-dimethylamino)-2,6-dimethylphenyl)-mesitylboryl]-2,2'-bithiophene 4.5



The compound 5-bromo-2,2'-bithiophene **4.1** (700 mg, 2.86 mmol), [(*N,N*-dimethylamino)-2,6-dimethylphenyl]-(mesityl)-[4-(4,4,5,5-tetramethyl-1,3,2-dioxaborolan-2-yl)-2,6-dimethylphenyl]borane **3.2b** (1.60 g, 3.14 mmol) and KOH (978 mg, 17.4 mmol) were dissolved in toluene (24 mL) and water (12 mL). After purging the solution with argon for 5 min, Pd₂dba₃·CHCl₃ (138 mg, 151 μmol) and SPhos (240 mg, 585 μmol) were added in one portion. The reaction mixture was stirred at 85 °C for 2 d. After cooling to room temperature, the phases were separated, and the aqueous phase was extracted with hexane (3 x 25 mL). The combined organic phases were dried over magnesium sulfate and the solvent was removed *in vacuo*. The resulting crude product was purified *via* preparative column chromatography (silica gel, 10% ethyl acetate in hexane). The product was isolated as a yellow foam (1.46 g, 2.67 mmol, 93%). A portion of this foam was further purified by preparative thin-layer chromatography (PSC plates (silica gel, 2 mm), 5% ethyl acetate in hexane) to yield pure product as a yellow solid.

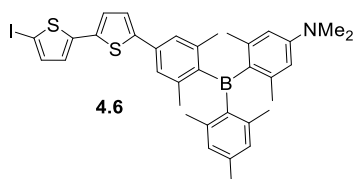
¹H NMR (500 MHz, CD₂Cl₂) δ = 7.29 (m, 1 H, CH), 7.25 (m, 1 H, CH), 7.22 (m, 1 H, CH), 7.20 (s, 2 H, CH), 7.16 (m, 1 H, CH), 7.04 (m, 1 H, CH), 6.76 (s, 2 H, CH), 6.32 (s, 2 H, CH), 2.97 (s, 6 H, CH₃) 2.27 (s, 3 H, CH₃), 2.15 – 1.95 (m, 18 H, CH₃) ppm.

¹¹B{¹H} NMR (160 MHz, CD₂Cl₂) δ = 75 (br) ppm.

¹³C{¹H} NMR (125 MHz, CD₂Cl₂) δ = 152.1, 148.8, 145.3, 143.9, 143.7, 143.6, 139.1, 137.9, 136.5, 135.1, 134.1, 128.8, 128.3, 125.0, 124.7, 124.7, 123.9, 123.8, 111.9, 111.8, 40.1, 24.1, 24.0, 21.3 ppm.

HRMS (EI⁻) *m/z*: [M+H]⁺ found: 548.2604; calc. for [C₃₅H₃₉BNS₂]: 548.2611 (|Δ| = 1.3 ppm).

Elem. Anal. Calc. (%) for C₃₅H₃₈BNS₂: C 76.76, H 6.99, N 2.56, S 11.71; found: C 77.10, H 7.03, N 2.74, S 11.32.

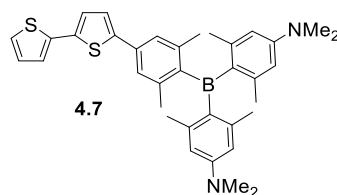
5-Iodo-5'-[4-(2,6-dimethylphenyl)-(4-(*N,N*-dimethylamino)-2,6-dimethylphenyl)-mesitylboryl]-2,2'-bithiophene 4.6

At $-78\text{ }^{\circ}\text{C}$, *n*-butyl lithium (0.35 mL, $c = 2.5\text{ M}$, 880 μmol) was added dropwise to a solution of 5-[4-(2,6-dimethylphenyl)-(4-(*N,N*-dimethylamino)-2,6-dimethylphenyl)-mesitylboryl]-2,2'-bithiophene **4.5** (399 mg, 730 μmol) in dry, degassed THF (3 mL). After stirring at $-78\text{ }^{\circ}\text{C}$ for 1.5 h, iodine (388 mg, 1.53 mmol) was added in one portion and the solution was allowed to warm to room temperature and then stirred for 18 h. The reaction was quenched by addition of water (5 mL) and diethyl ether (5 mL). The aqueous phase was extracted with diethyl ether (3 x 3 mL). The combined organic phase was washed with an aqueous, saturated sodium thiosulfate solution (1 x 10 mL), separated, and dried over magnesium sulfate and the solvent was removed *in vacuo* yielding a mixture of starting material and product (438 mg, purity $\approx 80\%$) which was used without further purification for further reaction.

$^1\text{H NMR}$ (500 MHz, CD_2Cl_2) $\delta = 7.27$ (d, $J = 4\text{ Hz}$, 1 H, CH), 7.20 – 7.17 (m, 3 H, CH), 7.11 (d, $J = 4\text{ Hz}$, 1 H, CH), 6.89 (d, $J = 4\text{ Hz}$, 1 H, CH), 6.75 (s, 2 H, CH), 6.32 (s, 2 H, CH), 2.96 (s, 6 H, CH_3), 2.27 (s, 3 H, CH_3), 2.13 – 1.94 (m, 18 H, CH_3) ppm.

HRMS (EI^-) m/z : $[\text{M}+\text{H}]^+$ found: 674.1565; calc. for $[\text{C}_{35}\text{H}_{38}\text{BINS}_2]$: 674.1578 ($|\Delta| = 1.9\text{ ppm}$).

5-[4-Bis-[4-(*N,N*-dimethylamino)-2,6-dimethylphenyl]-3,5-dimethylphenylboryl]-2,2'-bithiophene 4.7



The compounds 5-bromo-2,2'-bithiophene **4.1** (526 mg, 2.04 mmol), bis-[4-(*N,N*-dimethylamino)-2,6-dimethylphenyl]-2,6-dimethyl-4-(4,4,5,5-tetramethyl-1,3,2-dioxaborolan-2-yl)phenylborane **3.3b** (1.21 g, 2.24 mmol) and KOH (638 mg, 11.4 mmol) were dissolved in a mixture of toluene (20 mL) and water (10 mL). After purging the solution with argon for 5 min, SPhos (185 mg, 451 μ mol) and Pd₂(dba)₃·CHCl₃ (95 mg, 104 μ mol) were added in one portion. The reaction mixture was stirred at 85 °C for 41 h. After cooling to room temperature, the phases were separated, and the aqueous phase was extracted with hexane (5 x 15 mL). The combined organic phase was dried over magnesium sulfate and the solvent was removed *in vacuo*. The resulting crude product was purified *via* flash column chromatography (silica gel, 0–10% ethyl acetate in hexane) yielding the product (937 mg, 1.62 mmol, 80%) as a yellow solid.

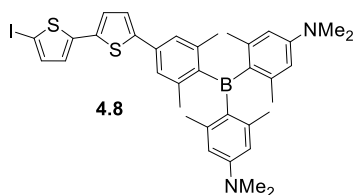
¹H NMR (500 MHz, CD₂Cl₂) δ = 7.29 (d, *J* = 4 Hz, 1 H, CH), 7.24 (dd, *J* = 1 Hz, *J* = 5 Hz, 1 H, CH), 7.22 (dd, *J* = 1 Hz, *J* = 4 Hz, 1 H, CH), 7.20 (s, 2 H, CH), 7.17 (d, *J* = 4 Hz, 1 H, CH), 7.05 (dd, *J* = 4 Hz, *J* = 5 Hz, 1 H, CH), 6.34 (s, 4 H, CH), 6.33 (s, 4 H, CH), 2.96 (s, 12 H, CH₃), 2.09 (s, 6 H, CH₃), 2.04 (s, 6 H, CH₃), 1.99 (s, 6 H, CH₃) ppm.

¹¹B{¹H} NMR (160 MHz, CD₂Cl₂) δ = 74 (br) ppm.

¹³C{¹H} NMR (125 MHz, CD₂Cl₂) δ = 151.7, 149.8, 144.1, 143.3, 142.9, 141.4, 138.0, 136.4, 136.1, 133.8, 128.3, 125.0, 124.7, 124.6, 123.9, 123.6, 111.9, 111.8, 40.2, 21.0, 23.9, 23.0 ppm.

HRMS (EI⁺) *m/z*: [M+H]⁺ 577.2874; calc. for [C₃₆H₄₂BN₂S₂] 577.2877 ($|\Delta|$ = 0.5 ppm).

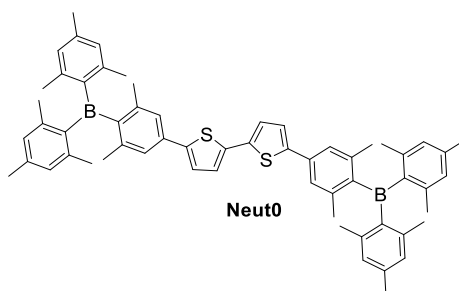
Elem. Anal. Calc. (%) for C₃₆H₄₁BN₂S₂: C 74.98, H 7.17, N 4.86, S 11.12; found: C 74.98, H 7.53, N 5.03, S 10.77.

5'-Iodo-5-[4-bis-[4-(*N,N*-dimethylamino)-2,6-dimethylphenyl]-3,5-dimethylphenylboryl]-2,2'-bithiophene 4.8

At $-78\text{ }^{\circ}\text{C}$, *n*-butyl lithium (0.35 mL, $c = 2.5\text{ M}$, 880 μmol) was added dropwise to a solution of 5-[4-(4-bis-[4-(*N,N*-dimethylamino)-2,6-dimethylphenyl]-3,5-dimethylphenylboryl)-2,2'-bithiophene **4.7** (400 mg, 690 μmol) in dry, degassed THF (3 mL). After stirring at $-78\text{ }^{\circ}\text{C}$ for 1.5 h, iodine (359 mg, 1.41 mmol) was added in one portion and the solution was stirred at room temperature for 18 h. The reaction was quenched by addition of water (5 mL) and diethyl ether (5 mL). The aqueous phase was extracted with diethyl ether (3 x 3 mL). The combined organic phase was washed with an aqueous, saturated sodium thiosulfate solution (10 mL), dried over magnesium sulfate and the solvent was removed *in vacuo* yielding a mixture of starting material and product (460 mg, purity $\approx 80\%$) which was used without further purification for further reaction.

$^1\text{H NMR}$ (500 MHz, CD_2Cl_2) $\delta = 7.26$ (d, $J = 4\text{ Hz}$, 1 H, CH), 7.20 – 7.17 (m, 3 H, CH), 7.11 (d, $J = 4\text{ Hz}$, 1 H, CH), 6.89 (d, $J = 4\text{ Hz}$, 1 H, CH), 6.32 (s, 4 H, CH), 2.95 (s, 12 H, CH_3), 2.09 – 1.94 (m, 18 H, CH_3) ppm.

HRMS (EI^-) m/z : $[\text{M}+\text{H}]^+$ found: 703.1836; calc. for $[\text{C}_{36}\text{H}_{41}\text{BIN}_2\text{S}_2]$: 703.1843 ($|\Delta| = 1.0\text{ ppm}$).

5,5'-Bis-[4-(2,6-dimethylphenyl)-dimesitylboryl]-2,2'-bithiophene Neut0

Compound 5,5'-bis-[4-(2,6-dimethylphenyl)-dimesitylboryl]-2,2'-bithiophene **Neut0** has been synthesized by Schleier in 2016.^[54] Prior to photophysical measurements, a small quantity was further purified by column chromatography (silica gel, 0-8% ethyl acetate in hexane) and by precipitation from a saturated diethyl ether solution with methanol. Subsequently, the compound was fully characterized as indicated below.

¹H NMR (500 MHz, CD₂Cl₂): δ = 7.31 (d, J = 4 Hz, 2 H, CH), 7.21 – 7.20 (m, 4 H, CH), 7.19 (d, J = 4 Hz, 2 H, CH), 6.77 (s, 4 H, CH), 6.77 (s, 4 H, CH), 2.27 (s, 12 H, CH₃), 2.05 (s, 12 H, CH₃), 2.01 (s, 12 H, CH₃), 1.99 (s, 12 H, CH₃) ppm.

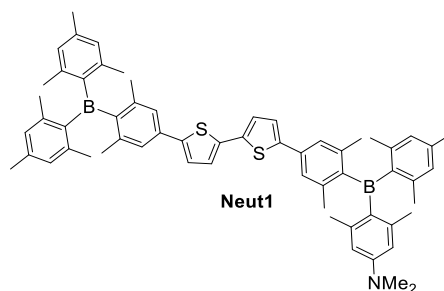
¹³C{¹H} NMR (125 MHz, CD₂Cl₂): δ = 143.9, 143.2, 141.3, 140.6, 140.5, 136.5, 134.3, 128.6, 124.5, 124.4, 123.7, 22.6, 22.6, 22.5, 20.9 ppm.

It was not possible to obtain a **¹¹B{¹H} NMR** spectrum (160 MHz) due to the low solubility of **Neut0** in CD₂Cl₂ and acetone-d₆.

HRMS (EI⁻) m/z : [M+H]⁺ found: 871.4701; calc. for [C₆₀H₆₅B₂NS₂]: 871.4708 ($|\Delta|$ = 0.8 ppm).

Elem. Anal. Calc. (%) for C₆₀H₆₄B₂NS₂: C 82.75, H 7.41, N 1.56, S 7.36; found: C 81.75, H 7.49, N 1.39, S 7.07.

5'-[4-(2,6-Dimethylphenyl)-(4-(*N,N*-dimethylamino)-2,6-dimethylphenyl)-mesitylboryl]-5-[4-(2,6-dimethylphenyl)-dimesitylboryl]-2,2'-bithiophene Neut1



The compounds 5'-bromo-5-[4-(3,5-dimethylphenyl)-dimesitylboryl]-2,2'-bithiophene **4.3** (276 mg, 462 μmol), [4-(*N,N*-dimethylamino)-2,6-dimethylphenyl]-(mesityl)-[4-(4,4,5,5-tetramethyl-1,3,2-dioxaborolan-2-yl)2,6-dimethylphenyl]borane **3.2b** (258 mg, 506 μmol) and KOH (167 mg, 2.98 mmol) were dissolved in toluene (4 mL) and water (2 mL). After purging the solution with argon for 10 min, Pd₂dba₃·CHCl₃ (22 mg, 24.0 μmol) and SPhos (40 mg, 97.4 μmol) were added in one portion. The reaction mixture was stirred at 85 °C for 2 d. After cooling to room temperature, the phases were separated, and the aqueous phase was extracted with hexane (5 x 20 mL). The combined organic phase was washed with brine (3 x 30 mL), dried over magnesium sulfate and the solvent was removed *in vacuo*. The resulting crude product was purified *via* preparative thin layer chromatography (PSC plates (silica gel, 2 mm), 3% ethyl acetate in hexane). The resulting solid was further purified by precipitation from a saturated diethyl ether solution with methanol, yielding the product as an orange yellow solid (180 mg, 200 μmol , 43%).

¹H NMR (500 MHz, CD₂Cl₂) δ = 7.31 (d, *J* = 4 Hz, 1 H, CH), 7.30 (d, *J* = 4 Hz, 1 H, CH), 7.23 (s, 2 H, CH), 7.21 (br s, 2 H, CH), 7.19 (d, *J* = 4 Hz, 2 H, CH), 6.79 (s, 4 H, CH), 6.77 (br s, 2 H, CH), 6.33 (s, 2 H, CH), 2.97 (s, 6 H, CH₃), 2.28 (s, 6 H, CH₃), 2.28 (s, 3 H, CH₃), 2.07 – 1.97 (m, 36 H, CH₃) ppm.

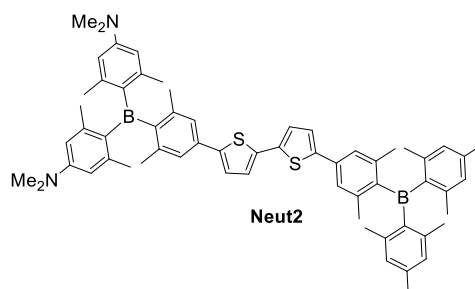
¹¹B{¹H} NMR (160 MHz, CD₂Cl₂) δ = 78 (br) ppm.

¹³C{¹H} NMR (125 MHz, CD₂Cl₂) δ = 152.1, 148.9, 147.6, 145.3, 144.3, 143.9, 143.8, 143.6, 143.5, 141.7, 141.0, 140.9, 139.9, 139.1, 137.0, 136.7, 135.1, 134.7, 134.2, 129.0, 128.8, 124.9, 124.8, 124.7, 124.2, 123.9, 111.9, 111.9, 40.1, 24.1, 24.0, 23.1, 23.1, 23.0, 21.4, 21.3 ppm.

HRMS (EI⁻) *m/z*: [M+H]⁺ found: 900.4960; calc. for [C₆₁H₆₇B₂NS₂]: 900.4974 ($|\Delta|$ = 1.6 ppm).

Elem. Anal. Calc. (%) for C₆₁H₆₇B₂NS₂: C 81.41, H 7.50, N 1.56, S 7.12; found: C 80.87, H 7.51, N 1.39, S 7.26.

5'-[4-(2,6-Dimethylphenyl)-bis-(4-(*N,N*-dimethylamino)-2,6-dimethylphenyl)-boryl]-5-[4-(2,6-dimethylphenyl)-dimesitylboryl]-2,2'-bithiophene Neut2



The compounds 5'-bromo-5-[4-(3,5-dimethylphenyl)-dimesitylboryl]-2,2'-bithiophene **4.3** (350 mg, 586 μmol), bis-[4-(*N,N*-dimethylamino)-2,6-dimethylphenyl]-2,6-dimethyl-4-(4,4,5,5-tetramethyl-1,3,2dioxaborolan-2-yl)-phenylborane **3.3b** (353 mg, 644 μmol) and KOH (205 mg, 3.65 mmol) were dissolved in toluene (14 mL) and water (7 mL). After purging the solution with argon for 10 min, $\text{Pd}_2(\text{dba})_3 \cdot \text{CHCl}_3$ (27 mg, 29.5 μmol) and SPhos (53 mg, 129 μmol) were added. The resulting solution was stirred at 85 °C for 42 h. After cooling to room temperature, the phases were separated, and the aqueous phase was extracted with hexane (4 x 20 mL). The combined organic phase was dried over magnesium sulfate. After removing the solvent *in vacuo*, the crude product was further purified *via* flash column chromatography (silica gel, 0–100% ethyl acetate in hexane). The resulting orange oil was further purified by precipitation from a saturated diethyl ether solution with methanol, yielding the product (320 mg, 344 μmol , 59%) as a yellow fine powder. The recorded spectra match those reported in literature.^[55]

^1H NMR (500 MHz, CD_2Cl_2) δ = 7.31 (d, J = 4 Hz, 1 H, CH), 7.30 (d, J = 4 Hz, 1 H, CH), 7.23 (br s, 2 H, CH), 7.20 (br s, 2 H, CH), 7.19 (d, J = 4 Hz, 2 H, CH), 6.79 (2 br s, 2 H, CH), 6.34 (br s, 2 H, CH), 6.33 (br s, 2 H, CH), 2.96 (s, 12 H, CH_3), 2.29 (s, 6 H, CH_3), 2.09 (s, 6 H, CH_3), 2.07 (s, 6 H, CH_3), 2.03 (br s, 12 H, CH_3), 2.01 (s, 6 H, CH_3), 2.00 (br s, 6 H, CH_3) ppm.

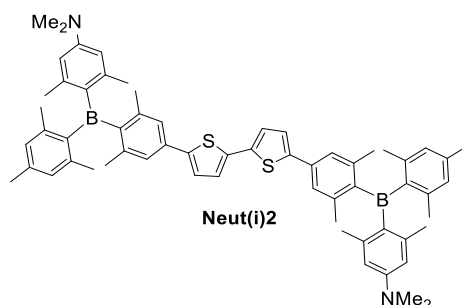
$^{11}\text{B}\{^1\text{H}\}$ NMR (160 MHz, CD_2Cl_2) δ = 77 (br) ppm.

$^{13}\text{C}\{^1\text{H}\}$ NMR (125 MHz, CD_2Cl_2) δ = 151.7, 149.9, 147.6, 144.3, 144.2, 143.4, 143.3, 142.9, 141.7, 141.4, 141.0, 140.9, 139.9, 137.1, 136.5, 136.1, 134.8, 133.7, 129.0, 124.9, 124.8, 124.6, 124.2, 123.8, 111.9, 111.8, 40.2, 24.1, 23.9, 23.1, 23.1, 23.1, 23.0, 21.4 ppm.

HRMS (EI^-) m/z : $[\text{M}+\text{H}]^+$ 929.5224; calc. for $[\text{C}_{62}\text{H}_{71}\text{B}_2\text{N}_2\text{S}_2]$ 929.5239 ($|\Delta|$ = 1.6 ppm).

Elem. Anal. Calc. (%) for $\text{C}_{62}\text{H}_{70}\text{B}_2\text{N}_2\text{S}_2$: C 80.16, H 7.60, N 3.02, S 6.90; found: C 80.36, H 7.64, N 3.31, S 6.55.

5,5'-Bis-[4-(2,6-Dimethylphenyl)-(4-(*N,N*-dimethylamino)-2,6-dimethylphenyl)-mesitylboryl]-2,2'-bithiophene Neut(i)2



The compounds 5,5'-dibromo-2,2'-bithiophene **4.1** (164 mg, 505 μmol), [(*N,N*-dimethylamino)-2,6-dimethylphenyl]-(mesityl)-[4-(4,4,5,5-tetramethyl-1,3,2-dioxaborolan-2-yl)-2,6-dimethylphenyl]borane **3.2b** (566 mg, 1.11 mmol) and KOH (195 mg, 3.48 mmol) were dissolved in toluene (4 mL) and water (2 mL). After purging the solution with argon for 5 min, $\text{Pd}_2\text{dba}_3 \cdot \text{CHCl}_3$ (23 mg, 25.1 μmol) and SPhos (43 mg, 105 μmol) were added in one portion. The reaction mixture was stirred at 85 $^\circ\text{C}$ for 44 h. After cooling to room temperature, the phases were separated, and the aqueous phase was extracted with hexane (6 x 15 mL). The combined organic phase was dried over magnesium sulfate and the solvent was removed *in vacuo*. The resulting crude product was purified *via* preparative column chromatography (Alox 90, basic, 5% ethyl acetate in hexane). The resulting solid was further purified by precipitation from a saturated diethyl ether solution with methanol, yielding the product as a yellow-orange solid (250 mg, 269 μmol , 53%).

^1H NMR (500 MHz, CD_2Cl_2) δ = 7.30 (d, J = 4 Hz, 2 H, CH), 7.20 (br s, 4 H, CH), 7.18 (d, J = 4 Hz, 2 H, CH), 6.76 (br s, 4 H, CH), 6.32 (br s, 4 H, CH), 2.97 (s, 12 H, CH_3), 2.27 (s, 6 H, CH_3), 2.12 – 1.95 (m, 36 H, CH_3) ppm.

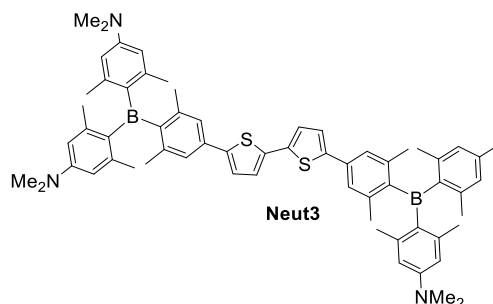
$^{11}\text{B}\{^1\text{H}\}$ NMR (160 MHz, CD_2Cl_2) δ = 75 (br) ppm.

$^{13}\text{C}\{^1\text{H}\}$ NMR (125 MHz, CD_2Cl_2) δ = 152.1, 148.8, 145.3, 143.8, 143.7, 143.6, 139.1, 136.7, 135.1, 134.1, 128.8, 124.8, 124.7, 123.9, 111.9, 111.8, 40.1, 24.1, 24.0, 23.2, 23.1, 22.9, 21.3 ppm.

HRMS (EI^-) m/z : $[\text{M}+\text{H}]^+$ found: 929.5219; calc. for $[\text{C}_{62}\text{H}_{70}\text{B}_2\text{N}_2\text{S}_2]$: 929.5239 ($|\Delta|$ = 2.2 ppm).

Elem. Anal. Calc. (%) for $\text{C}_{62}\text{H}_{70}\text{B}_2\text{N}_2\text{S}_2$: C 80.16, H 7.60, N 3.02, S 6.90; found: C 79.62, H 7.85, N 2.90, S 7.48.

5'-[4-(2,6-Dimethylphenyl)-(4-(*N,N*-dimethylamino)-2,6-dimethylphenyl)-mesitylboryl]-5-[4-(2,6-dimethylphenyl)-bis-(4-(*N,N*-dimethylamino)-2,6-dimethylphenyl)boryl]-2,2'-bithiophene Neut3



Entry A: 5-Iodo-5-[4-(3,5-dimethylphenyl)-bis-(4-(*N,N*-dimethylamino)-2,6-dimethylphenyl)-boryl]-2,2'-bithiophene **4.8** (460 mg, 655 μmol , purity $\approx 80\%$), [4-(*N,N*-dimethylamino)-2,6-dimethylphenyl]-(mesityl)-[4-(4,4,5,5-tetramethyl-1,3,2-dioxaborolan-2-yl)-2,6-dimethylphenyl]borane **3.2b** (367 mg, 720 μmol) and KOH (285 mg, 5.08 mmol) were dissolved in toluene (6 mL) and water (3 mL). After purging the solution with argon for 4 min, $\text{Pd}_2\text{dba}_3\cdot\text{CHCl}_3$ (30 mg, 33 μmol) and SPhos (60 mg, 146 μmol) were added in one portion. The reaction mixture was stirred at 85 $^\circ\text{C}$ for 44 h. After cooling to room temperature, the aqueous phase was extracted with hexane (3 x 20 mL). The combined organic phase was dried over magnesium sulfate and the solvent was removed *in vacuo*. The resulting crude product was purified *via* column chromatography (silica gel, 10% ethyl acetate in hexane). The resulting solid was further purified by precipitation from a saturated diethyl ether solution with methanol, yielding the product as a yellow-orange solid (31 μmol , 30 mg, 6%).

Entry B: 5-Iodo-5'-[4-(2,6-dimethylphenyl)-(4-(*N,N*-dimethylamino)-2,6-dimethylphenyl)-mesitylboryl]-2,2'-bithiophene **4.6** (438 mg, 650 μmol , purity $\approx 80\%$), [bis-(4-(*N,N*-dimethylamino)-2,6-dimethylphenyl)]-[4-(4,4,5,5-tetramethyl-1,3,2-dioxaborolan-2-yl)-2,6-dimethylphenyl]borane **3.3b** (385 mg, 715 μmol) and KOH (295 mg, 5.26 mmol) were dissolved in toluene (6 mL) and water (3 mL). After purging the solution with argon for 4 min, $\text{Pd}_2\text{dba}_3\cdot\text{CHCl}_3$ (30 mg, 32.8 μmol) and SPhos (60 mg, 146 μmol) were added in one portion. The reaction mixture was stirred at 85 $^\circ\text{C}$ for 44 h. After cooling to room temperature, the phases were separated, and the aqueous phase was extracted with hexane (3 x 20 mL). The combined organic phase was dried over magnesium sulfate and the solvent was removed *in vacuo*. The resulting crude product was purified *via* column chromatography (silica gel, 10% ethyl acetate in hexane). The resulting solid was further purified by precipitation from a saturated diethyl ether solution with methanol, yielding the product as a yellow-orange solid (300 mg, 120 μmol , 60%).

^1H NMR (500 MHz, CD_2Cl_2) δ = 7.31 – 7.28 (m, 2 H, CH), 7.21 – 7.17 (m, 6 H, CH), 6.76 (s, 2 H, CH), 6.32 (s, 6 H, CH), 2.97 (s, 6 H, CH_3), 2.95 (s, 12 H, CH_3), 2.27 (s, 3 H, CH_3), 2.08 – 1.95 (m, 36 H, CH_3) ppm.

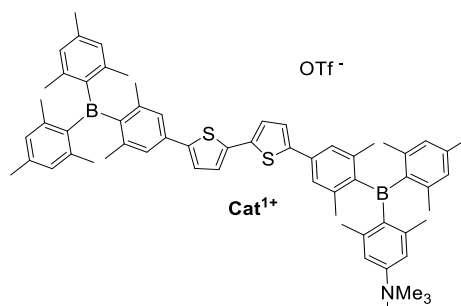
$^{11}\text{B}\{^1\text{H}\}$ NMR (160 MHz, CD_2Cl_2) δ = 75 (br) ppm.

$^{13}\text{C}\{^1\text{H}\}$ NMR (125 MHz, CD_2Cl_2) δ = 152.1, 151.7, 149.9, 148.8, 145.3, 144.0, 143.7, 143.7, 143.6, 143.3, 142.9, 141.4, 139.1, 136.8, 136.5, 136.1, 135.1, 134.1, 133.7, 128.8, 124.8, 124.7, 124.5, 123.9, 123.7, 111.9, 111.8, 40.2, 40.1, 24.1, 24.0, 24.0, 23.8, 23.0, 21.3 ppm.

HRMS (EI^-) m/z : $[\text{M}+\text{H}]^+$ found: 958.5473; calc. for $[\text{C}_{63}\text{H}_{74}\text{B}_2\text{N}_3\text{S}_2]$: 958.5505 ($|\Delta|$ = 3.3 ppm).

Elem. Anal. Calc. (%) for $\text{C}_{63}\text{H}_{73}\text{B}_2\text{N}_3\text{S}_2$: C 78.98, H 7.68, N 4.39, S 6.69; found: C 78.69, H 7.70, N 4.33, S 6.68.

**5'-[4-(2,6-Dimethylphenyl)-(4-(*N,N,N*-trimethylammonium)-2,6-dimethylphenyl)-mesitylboryl]-5-[4-(2,6-dimethylphenyl)-dimesitylboryl]-2,2'-bithiophene triflate
Cat¹⁺**



The compound 5'-[4-(2,6-dimethylphenyl)-(4-(*N,N*-dimethylamino)-2,6-dimethylphenyl)-mesitylboryl]-5-[4-(2,6-dimethylphenyl)-dimesitylboryl]-2,2'-bithiophene **Neut1** (15 mg, 16.7 μmol) was dissolved in dry, degassed CH_2Cl_2 (2 mL). After addition of methyl triflate (15.0 μL , 133 μmol), the reaction mixture was stirred in the dark at room temperature for 3 d. Subsequently, hexane (7 mL) was added. The resulting solid was collected by filtration and washed with hexane (8 mL) yielding the product as an orange yellow solid (15 mg, 14.8 μmol , 88%).

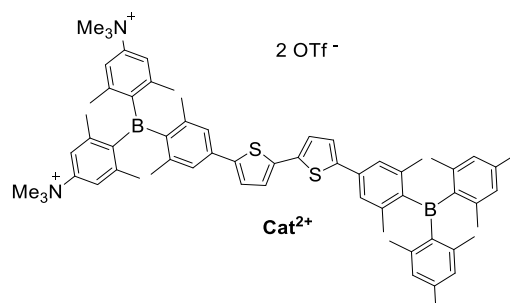
¹H NMR (500 MHz, CD_2Cl_2) δ = 7.51 (s, 2 H, CH), 7.41 (d, J = 4 Hz, 1 H, CH), 7.37 (d, J = 4 Hz, 1 H, CH), 7.30 (s, 1 H, CH), 7.27 (s, 1 H, CH), 7.25 – 7.23 (m, 2 H, CH), 7.23 (s, 2 H, CH), 6.85 (s, 1 H, CH), 6.82 (s, 2 H, CH), 6.78 (s, 4 H, CH), 3.65 (s, 9 H, CH_3), 2.29 (s, 3 H, CH_3), 2.27 (s, 6 H, CH_3), 2.20 (s, 3 H, CH_3), 2.17 (s, 3 H, CH_3), 2.10 (s, 3 H, CH_3), 2.07 (s, 3 H, CH_3), 2.05 (s, 6 H, CH_3), 2.03 (s, 3 H, CH_3), 2.01 (s, 6 H, CH_3), 1.98 (s, 6 H, CH_3), 1.96 (s, 3 H, CH_3) ppm.

¹³C{¹H} NMR (125 MHz, CD_2Cl_2) δ = 150.9, 149.1, 148.5, 146.9, 145.1, 144.6, 144.6, 44.5, 144.0, 143.8, 143.2, 142.6, 142.4, 142.3, 142.1, 141.9, 141.7, 141.6, 140.9, 138.3, 137.6, 137.0, 136.0, 130.2, 130.1, 129.8, 129.8, 125.9, 125.8, 125.8, 125.7, 126.6, 125.2, 121.8 (q, $^1J_{\text{CF}}$ = 316 Hz), 119.6, 57.5, 23.5, 23.4, 23.4, 23.3, 23.2, 23.2, 23.1, 21.3, 23.3 ppm.

HRMS (ESI⁺) m/z : $[\text{M}-\text{OTf}]^+$ found: 914.5115; calc. for $[\text{C}_{62}\text{H}_{70}\text{B}_2\text{NS}_2]$: 914.5130 ($|\Delta|$ = 1.6 ppm).

Elem. Anal. Calc. (%) for $\text{C}_{63}\text{H}_{70}\text{B}_2\text{F}_3\text{NO}_3\text{S}_3$: C 71.11, H 6.63, N 1.32, S 9.04; found: C 67.93, H 6.63, N 1.28, S 8.78.

5'-[4-(2,6-Dimethylphenyl)-bis-(4-(*N,N,N*-trimethylammonium)-2,6-dimethylphenyl)-boryl]-5-[4-(2,6-dimethylphenyl)-dimesitylboryl]-2,2'-bithiophene bis-triflate Cat²⁺



The compound 5'-[4-(2,6-dimethylphenyl)-bis-(4-(*N,N*-dimethylamino)-2,6-dimethylphenyl)-boryl]-5-[4-(2,6-dimethylphenyl)-dimesitylboryl]-2,2'-bithiophene **Neut2** (15 mg, 16.1 μmol) was dissolved in dry, degassed CH_2Cl_2 (2.0 mL). After addition of methyl triflate (15.0 μL , 132 μmol), the reaction mixture was stirred in the dark at room temperature for 3 d. Subsequently, hexane (7 mL) was added. The resulting solid was collected by filtration and washed with diethyl ether (10 mL) yielding the product (14 mg, 11.1 μmol , 69%) as a yellow orange solid.

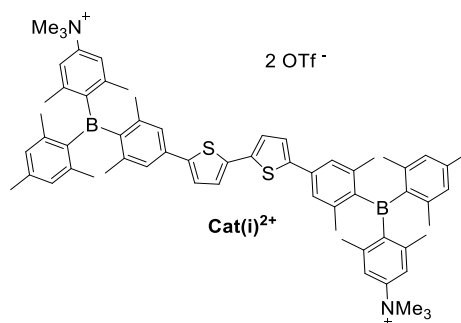
¹H NMR (500 MHz, CD_3OD) δ = 7.58 (br s, 2 H, CH), 7.57 (br s, 2 H, CH), 7.46 (d, J = 4 Hz, 1 H, CH), 7.39 (d, J = 4 Hz, 1 H, CH), 7.34 (br s, 2 H, CH), 7.27 (d, J = 4 Hz, 1 H, CH), 7.26 (d, J = 4 Hz, 1 H, CH), 7.24 (br s, 2 H, CH), 3.66 (s, 18 H, CH_3), 2.27 (s, 6 H, CH_3), 2.25 (br s, 6 H, CH_3), 2.16 (br s, 6 H, CH_3), 2.08 (s, 6 H, CH_3), 2.05 (s, 6 H, CH_3), 2.02 (s, 6 H, CH_3), 1.98 (s, 6 H, CH_3) ppm.

¹³C{¹H} NMR (125 MHz, CD_3OD) δ = 149.6, 149.4, 148.6, 145.6, 145.1, 144.8, 144.6, 144.5, 143.3, 143.1, 142.5, 141.8, 141.6, 140.6, 138.7, 137.8, 137.5, 135.9, 129.8, 129.8, 126.1, 126.0, 126.0, 125.8, 125.6, 125.2, 121.8 (q, $^1J_{\text{CF}}$ = 318 Hz) 120.1, 120.0, 57.5, 23.7, 23.5, 23.4, 23.3, 23.3, 23.2, 21.4 ppm.

HRMS (EI⁺) m/z : $[\text{M}-2\text{OTf}]^+$ 479.2803; calc. for $[\text{C}_{64}\text{H}_{76}\text{B}_2\text{N}_2\text{S}_2]$ 479.2813 ($|\Delta|$ = 2.1 ppm).

Elem. Anal. Calc. (%) for $\text{C}_{66}\text{H}_{76}\text{B}_2\text{F}_6\text{N}_2\text{O}_6\text{S}_2$: C 63.06, H 6.09, N 2.23, S 10.20; found: C 60.69, H 6.68, N 1.95, S 10.86.

5,5'-Bis-[4-(2,6-Dimethylphenyl)-(4-(*N,N*-dimethylammonium)-2,6-dimethylphenyl)-mesitylboryl]-2,2'-bithiophene *bis*-triflate **Cat(i)²⁺**



The compound 5,5'-*bis*-[4-(2,6-dimethylphenyl)-(4-(*N,N*-dimethylamino)-2,6-dimethylphenyl)-mesitylboryl]-2,2'-bithiophene **Neut(i)2** (15 mg, 16.1 μmol) was dissolved in dry CH_2Cl_2 (2 mL). After addition of methyl triflate (15.0 μL , 129 μmol), the reaction mixture was stirred in the dark at room temperature for 17 h. The resulting solid was collected by filtration and washed with diethyl ether (3 x 2 mL) yielding the product as a yellow solid (10 mg, 7.95 μmol , 49%).

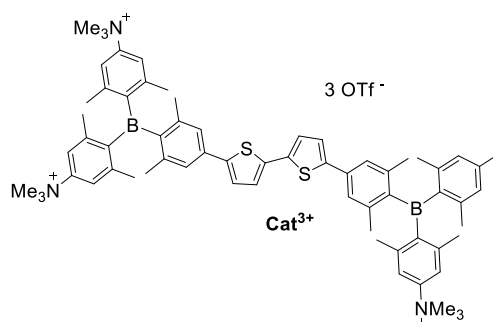
¹H NMR (500 MHz, CD_3OD) δ = 7.51 (s, 4 H, CH), 7.42 (d, J = 4 Hz, 2 H, CH), 7.30 (m, 4 H, CH), 7.26 (d, J = 4 Hz, 2 H, CH), 6.84 (m, 4 H, CH), 3.65 (s, 18 H, CH_3), 2.29 (s, 6 H, CH_3), 2.20 (s, 6 H, CH_3), 2.17 (s, 6 H, CH_3), 2.10 (s, 6 H, CH_3), 2.07 (s, 6 H, CH_3), 2.04 (s, 6 H, CH_3), 1.97 (s, 6 H, CH_3) ppm.

¹³C{¹H} NMR (125 MHz, CD_3OD) δ = 150.8, 149.1, 147.0, 144.6, 144.5, 144.0, 143.2, 142.5, 142.3, 142.2, 141.7, 138.1, 136.9, 130.2, 130.1, 125.9, 125.9, 125.8, 125.7, 121.8 (q, $^1J_{\text{CF}}$ = 318 Hz), 119.6, 57.5, 23.4, 23.4, 23.3, 23.3, 23.2, 21.3 ppm.

HRMS (ESI⁺) m/z : $[\text{M}-2\text{OTf}]^+$ found: 479.2818; calc. for $[\text{C}_{64}\text{H}_{76}\text{B}_2\text{N}_2\text{S}_2]$: 479.2813 ($|\Delta|$ = 1.0 ppm).

Elem. Anal. Calc. (%) for $\text{C}_{66}\text{H}_{76}\text{B}_2\text{F}_6\text{N}_2\text{O}_6\text{S}_4$: C 63.06, H 6.09, N 2.23, S 10.20; found: C 61.50, H 6.13, N 2.12, S 9.74.

5'-[4-(2,6-Dimethylphenyl)-(4-(*N,N,N*-trimethylammonium)-2,6-dimethylphenyl)-mesitylboryl]-5-[4-(2,6-dimethylphenyl)-*bis*-(4-(*N,N,N*-trimethylammonium)-2,6-dimethylphenyl)boryl]-2,2'-bithiophene *tris*-triflate **Cat³⁺**



The compound 5'-[4-(2,6-dimethylphenyl)-(4-(*N,N*-dimethylamino)-2,6-dimethylphenyl)-mesitylboryl]-5-[4-(2,6-dimethylphenyl)-*bis*-(4-(*N,N*-dimethylamino)-2,6-dimethylphenyl)boryl]-2,2'-bithiophene **Neut3** (15 mg, 15.6 μmol) was dissolved in dry CH_2Cl_2 (2 mL). After addition of methyl triflate (21.3 μL , 188 μmol), the reaction mixture was stirred in the dark at room temperature for 21 h. The resulting solid was collected by filtration and washed with diethyl ether (4 x 2 mL) yielding the product as a yellow solid (13 mg, 8.96 μmol , 57%).

¹H NMR (500 MHz, CD_3OD) δ = 7.57 (s, 4 H, CH), 7.51 (s, 2 H, CH), 7.46 (d, J = 4 Hz, 1 H, CH), 7.42 (d, J = 4 Hz, 1 H, CH), 7.34 (s, 2 H, CH), 7.31 – 7.28 (m, 2 H, CH), 7.28 – 7.26 (m, 2 H, CH), 6.83 (m, 2 H, CH), 3.66 (s, 18 H, CH_3), 3.65 (s, 9 H, CH_3), 2.28 (s, 3 H, CH_3), 2.25 (s, 6 H, CH_3), 2.20 (s, 3 H, CH_3), 2.16 (s, 3 H, CH_3), 2.15 (s, 6 H, CH_3), 2.10 (s, 3 H, CH_3), 2.08 (s, 6 H, CH_3), 2.07 (s, 3 H, CH_3), 2.03 (s, 3 H, CH_3), 1.96 (s, 3 H, CH_3) ppm.

¹³C{¹H} NMR (125 MHz, CD_3OD) δ = 150.8, 149.7, 149.4, 149.1, 147.1, 145.7, 144.9, 144.6, 144.5, 144.4, 144.2, 144.0, 143.5, 143.2, 143.1, 142.5, 142.2, 142.1, 141.8, 138.5, 138.0, 137.8, 136.8, 130.1, 130.1, 126.2, 126.7, 126.0, 125.9, 125.8, 125.7, 121.8 (q, $^1J_{\text{CF}}$ = 318 Hz), 120.1, 120.1, 119.6, 57.5, 23.6, 23.4, 23.4, 23.4, 23.4, 23.3, 23.2, 21.3 ppm.

HRMS (ESI⁺) m/z : $[\text{M}-3\text{OTf}]^{3+}$ found: 334.2039; calc. for $[\text{C}_{66}\text{H}_{82}\text{B}_2\text{N}_3\text{S}_2]$: 334.2040 ($|\Delta|$ = 0.30 ppm).

Elem. Anal. Calc. (%) for $\text{C}_{69}\text{H}_{82}\text{B}_2\text{F}_9\text{N}_3\text{O}_9\text{S}_5$: C 57.14, H 5.70, N 2.90, S 9.93; found: C 52.95, H 5.69, N 2.81, S 10.95.

9.2.3 Chapter 6

Preparation of DNA nanopores

Oligonucleotides (P1, P2, P3, P4, P5, P6; 50% G-C pairs; exact composition of DNApore: Table 9.1) were dissolved in Tris-HCl buffer, pH 8 (15 mM Tris-HCl, 300 mM KCl), $c(P_i) = 2 \times 10^{-2}$ M. All concentrations are expressed as the concentration of phosphates (same as nucleobases). Equimolar concentrations of each oligonucleotide (5×10^{-4} M) were mixed and heated in a UV/Vis thermo-block at 95 °C for 15 min, then slowly cooled (0.5 °C per minute) to 10 °C. The overall DNA nanopore concentration $c(P1-6) = 3 \times 10^{-3}$ M. Nanopore formation was confirmed by thermal melting experiments (UV/Vis-monitored and DSC-monitored), showing clear and reproducible denaturation profiles.

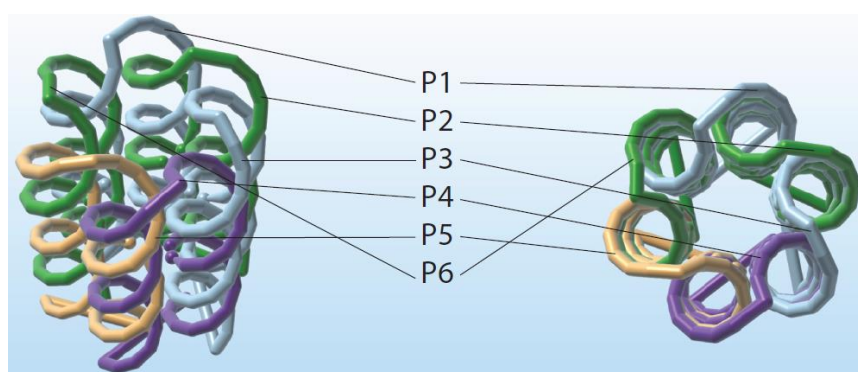
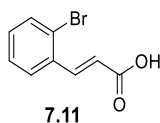


Figure 9.1: Schematic representation of DNApore.

Table 9.1: Composition of oligonucleotides P1-P6 used for synthesis of DNApore.

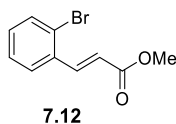
P1	AGCGAACGTGGATTTTGTCCGACATCGGCAAGCTCCCTTTTTCGACTATT
P2	CCGATGTCGGACTTTTACACGATCTTCGCCTGCTGGGTTTTGGGAGCTTG
P3	CGAAGATCGTGTTTTTCCACAGTTGATTGCCCTTCACTTTTCCCAGCAGG
P4	AATCAACTGTGGTTTTTCTCACTGGTGATTAGAATGCTTTTGTGAAGGGC
P5	TCACCAGTGAGATTTTTGTTCGTACCAGGTGCATGGATTTTTGCATTCTAA
P6	CCTGGTACGACATTTTTCCACGTTTCGCTAATAGTCGATTTTATCCATGCA

9.2.4 Chapter 7

(E)-3-(2-Bromophenyl)acrylic acid 7.11

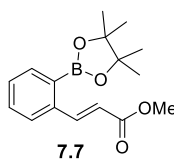
To a mixture of 2-bromobenzaldehyde (5 mL, 43.0 mmol) in pyridine (6.4 mL), malonic acid (5.81 g, 55.9 mmol) and piperidine (0.44 mL, 4.44 mmol) was added. The reaction mixture was stirred at 100 °C for 15 h. After cooling to room temperature, an aqueous HCl solution (15% HCl, 150 mL) was added to the reaction mixture. The resulting precipitate was collected by filtration, washed with water (5 x 10 mL), and dried *in vacuo* to yield the pure product as a white crystalline solid (8.81 g, 38.8 mmol, 90%). The recorded ¹H NMR spectrum matches that reported in literature.^[10, 249]

¹H NMR (500 MHz, acetone-d₆) δ = 8.03 (d, *J* = 16 Hz, 1 H, *CH*), 7.88 (dd, *J* = 2 Hz, *J* = 8 Hz, 1 H, *CH*), 7.71 (dd, *J* = 2 Hz, *J* = 8 Hz, 1 H, *CH*), 7.79 – 7.42 (m, 1 H, *CH*), 7.40 – 7.33 (m, 1 H, *CH*), 6.54 (d, *J* = 16 Hz, 1 H, *CH*) ppm.

Methyl-(E)-3-(2-bromophenyl)acrylate 7.12

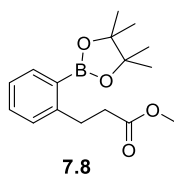
Sulfuric acid (18 M, 7.0 mL) was added to a solution of (*E*)-3-(2-bromophenyl)acrylic acid **7.11** (5.0 g, 22.0 mmol) in methanol (167 mL). The mixture was stirred under reflux for 3 h. After cooling to room temperature, water (100 mL) and brine (100 mL) were added. The aqueous phase was extracted with diethyl ether (4 x 50 mL). The combined organic phases were dried over sodium sulfate and the solvent was removed *in vacuo* yielding the product as a pale yellow oil (4.68 g, 19.4 mmol, 88%) which solidifies over time. The recorded ¹H NMR spectrum matches that reported in literature.^[250]

¹H NMR (300 MHz, acetone-d₆) δ = 8.01 (d, *J* = 16 Hz, 1 H, *CH*), 7.87 (dd, *J* = 2 Hz, *J* = 8 Hz, 1 H, *CH*), 7.70 (dd, *J* = 2 Hz, *J* = 8 Hz, 1 H, *CH*), 7.49 (m, 1 H, *CH*), 7.40 – 7.33 (m, 1 H, *CH*), 6.56 (d, *J* = 16 Hz, 1 H, *CH*), 3.78 (s, 3 H, *CH*₃) ppm.

Methyl-(E)-3-(2-(4,4,5,5-tetramethyl-1,3,2-dioxaborolan-2-yl)phenyl)acrylate 7.7

A solution of *bis*-(pinacolato)diboron (2.73 g, 10.8 mmol), potassium acetate (1.23 g, 12.5 mmol) and Pd(dppf)Cl₂ (303 mg, 0.41 mmol) in dry, degassed 1,4-dioxane (20 mL) was stirred at room temperature for 20 min. Thereafter, a solution of methyl-(*E*)-3-(2-bromophenyl)acrylate **7.12** (2.0 g, 8.30 mmol) in dry, degassed dioxane (30 mL) was added. The resulting reaction mixture was stirred at 80 °C for 2 d. After cooling to room temperature, the reaction was filtered over a silica plug, washed with diethyl ether (4 x 50 mL) and the solvent was removed *in vacuo*. The crude product was purified by column chromatography (silica gel, 10% ethyl acetate in hexane) to yield the pure product as a pale yellow solid (2.36 g, 8.19 mmol, 99%). The recorded ¹H NMR spectrum matches that reported in literature.^[10]

¹H NMR (300 MHz, CD₂Cl₂) δ = 8.52 (d, *J* = 16 Hz, 1H, *CH*), 7.81 (dd, *J* = 2 Hz, *J* = 7 Hz, 1H, *CH*), 7.72–7.68 (m, 1H, *CH*), 7.49 – 7.42 (m, 1 H, *CH*), 7.40 – 7.34 (m, 1 H, *CH*), 6.38 (d, *J* = 16 Hz, 1H, *CH*), 3.78 (s, 3H, *CH*₃), 1.37 (s, 12H, *CH*₃) ppm.

Methyl-3-(2-(4,4,5,5-tetramethyl-1,3,2-dioxaborolan-2-yl)phenyl)propanoate 7.8

The synthesis was adapted from ref. 250.^[251] An autoclave was equipped with a mixture of methyl-(*E*)-3-(2-(4,4,5,5-tetramethyl-1,3,2-dioxaborolan-2-yl)phenyl)acrylate **7.7** (397 mg, 1.38 mmol) and palladium on charcoal (Pd/C, 55 mg, 523 μ mol) in ethanol (20 mL). This mixture was stirred under hydrogen atmosphere (10 bar) for 2 d. Filtration over celite, two times over silica and subsequent removal of the solvent yielded the pure product as a colorless oil (330 mg, 1.14 mmol, 83%). The recorded ^1H NMR spectrum matches that reported in literature.^[10]

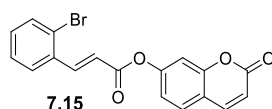
^1H NMR (500 MHz, acetone- d_6) δ = 7.74 (dd, J = 2 Hz, J = 7 Hz, 1 H, CH), 7.38 – 7.34 (m, 1 H, CH), 7.24 – 7.22 (m, 1 H, CH), 7.22 – 7.18 (m, 1 H, CH), 3.61 (s, 3 H, CH₃), 3.19 – 3.15 (m, 2 H, CH₂), 2.58 – 2.54 (m, 2 H, CH₂), 1.35 (s, 12 H, CH₃) ppm.

^{11}B NMR (160 MHz, acetone- d_6) δ = 31 (s) ppm.

^{13}C NMR (125 MHz, acetone- d_6) δ = 173.5, 148.6, 137.0, 131.9, 130.1, 126.3, 84.3, 51.5, 37.6, 31.8, 25.1 ppm.

HRMS (EI⁺) m/z : [M+H]⁺ 291.1751; calc. for [C₁₆H₂₄BO₄] 291.1762 ($|\Delta|$ = 3.78 ppm).

Elem. Anal. Calc. (%) for C₁₆H₂₃BO₄: C 66.23, H 7.99; found: C: 63.92, H: 7.70.

2-Oxo-2H-chromen-7-yl-(E)-3-(2-bromophenyl)acrylate 7.15

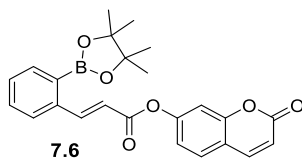
The synthesis was adapted from ref. 251.^[252] Under an argon atmosphere, methyl-(E)-3-(2-bromophenyl)acrylate **7.11** (3.03 g, 13.3 mmol) was dissolved in thionyl chloride (4.1 mL, 56.2 mmol) and stirred at 80 °C for 3.5 h. After cooling to room temperature, thionyl chloride was removed *in vacuo* yielding a dark brown solid. Under an argon atmosphere, this solid was added in one portion to a solution of umbelliferone (1.78 g, 11.0 mmol) in dry pyridine (6 mL). The solution was stirred at room temperature for 2 d. Addition of water (25 mL) led to precipitation. The precipitate was collected by filtration and washed with water (3 x 15 mL). The resulting brown solid was washed with acetone (2 x 10 mL) yielding the pure product as a greyish solid (3.71 g, 9.99 mmol, 91%). The recorded ¹H NMR spectrum matches that reported in literature.^[10]

¹H NMR (500 MHz, CD₂Cl₂) δ = 8.25 (d, *J* = 16 Hz, 1 H, CH), 7.76 – 7.72 (m, 2 H, CH), 7.69 – 7.66 (m, 1 H, CH), 7.56 (dd, *J* = 0.5 Hz, *J* = 8.5 Hz, 1 H, CH), 7.43 – 7.39 (m, 1 H, CH), 7.33 – 7.29 (m, 1 H, CH), 7.23 – 7.21 (m, 1 H, CH), 7.16 (dd, *J* = 2 Hz, *J* = 8.5 Hz, 1 H, CH), 6.62 (d, *J* = 16 Hz, 1 H, CH), 6.38 (d, *J* = 10 Hz, 1 H, CH) ppm.

¹³C NMR (125 MHz, CD₂Cl₂) δ = 164.5, 160.5, 155.2, 153.7, 145.8, 143.2, 134.4, 133.9, 132.3, 129.1, 128.5, 128.4, 125.9, 119.9, 118.7, 117.2, 116.4, 110.7 ppm.

HRMS (EI⁺) *m/z*: [M+H]⁺ 372.9879; calc. for [C₁₈H₁₂BrO₄] 372.9893 (|Δ| = 3.75 ppm).

Elem. Anal. Calc. (%) for C₁₈H₁₁BrO₄: C 58.25, H 2.99; found: C: 58.10, H: 3.12.

2-Oxo-2H-chromen-7-yl-(E)-3-(2-(4,4,5,5-tetramethyl-1,3,2-dioxaborolan-2-yl)phenyl)acrylate 7.6

Under an argon atmosphere, 2-oxo-2H-chromen-7-yl-(E)-3-(2-bromophenyl)acrylate **7.15** (900 mg, 2.84 mmol), *bis*-pinacolato diboron (1.14 g, 4.49 mmol), Pd(dppf)Cl₂ (210 mg, 280 μmol) and potassium acetate (420 mg, 4.29 mmol) were dissolved in dry and degassed 1,4-dioxane (18 mL). The reaction mixture was stirred at 80 °C for 4 d. After cooling to room temperature, diethyl ether (10 mL) was added, and the solution was filtered over a silica plug. Removing the solvent yielded the crude product as a dark brown oil which was further purified by column chromatography (silica gel, 50% ethyl acetate in hexane). The product containing fraction was dissolved in dichloromethane. Upon addition of hexane, an off-white solid precipitated which was collected by filtration. Drying the solid *in vacuo* yielded the pure product as an off-white solid (613 mg, 1.47 mmol, 52%) which contained small amounts (ca. 2.5%) of residual B₂pin₂. The recorded ¹H NMR spectrum matches that reported in literature.^[10]

¹H NMR (500 MHz, CD₂Cl₂) δ = 8.81 (d, *J* = 16 Hz, 1 H, CH), 7.88 – 7.85 (m, 1 H, CH), 7.81 – 7.78 (m, 1 H, CH), 7.75 – 7.73 (m, 1 H, CH), 7.55 (dd, *J* = 0.5 Hz, *J* = 8 Hz, 1 H, CH), 7.54 – 7.50 (m, 1 H, CH), 7.45 – 7.42 (m, 1 H, CH), 7.23 – 7.22 (m, 1 H, CH), 7.17 (dd, *J* = 2 Hz, *J* = 8 Hz, 1 H, CH), 6.58 (d, *J* = 16 Hz, 1 H, CH), 6.37 (d, *J* = 9 Hz, 1 H, CH), 1.37 (s, 12 H, CH₃) ppm.

¹¹B NMR (160 MHz, CD₂Cl₂) δ = 31 (s) ppm.

¹³C NMR (125 MHz, CD₂Cl₂) δ = 165.1, 160.6, 155.2, 154.0, 148.8, 143.3, 140.0, 136.7, 131.6, 130.1, 129.0, 128.8, 126.2, 118.8, 117.6, 117.0, 116.3, 110.6, 84.7, 25.1 ppm.

HRMS (EI⁺) *m/z*: [M+H]⁺ 419.1654; calc. for [C₂₄H₂₄BO₆] 419.1660 (|Δ| = 1.43 ppm).

Elem. Anal. Calc. (%) for C₂₄H₂₃BO₆: C 68.92, H 5.54; found: C: 68.85, H: 5.61.

CHAPTER 10

REFERENCES

10 References

- [1] A. Paramore, S. Frantz, *Nat. Rev Drug. Discov.* **2003**, *2*, 611-612.
- [2] M. M. Hansen, R. A. Jolly, R. J. Linder, *Org. Process Res. Dev.* **2015**, *19*, 1507-1516.
- [3] B. Ames, N., F. D. Lee, W. E. Durston, *Proc. Natl. Acad. Sci. U. S. A.* **1973**, *70*, 782-786.
- [4] K. Mortelmans, E. Zeigerb, *Mutat. Res., Fundam. Mol. Mech. Mutagen.* **2000**, *455*, 29-60.
- [5] S. Gronowitz, Y. Zhang, A.-B. Hörnfeldt, *Acta Chem. Scand.* **1992**, *46*, 654-660.
- [6] K. E. Broaders, S. Grandhe, J. M. Frechet, *J. Am. Chem. Soc.* **2011**, *133*, 756-758.
- [7] C. Achilli, A. Ciana, M. Fagnoni, C. Balduini, G. Minetti, *Cent. Eur. J. Chem.* **2013**, *11*, 137-139.
- [8] K. C. Yan, A. C. Sedgwick, Y. Zang, G. R. Chen, X. P. He, J. Li, J. Yoon, T. D. James, *Small Methods* **2019**, *3*, 1900013.
- [9] E. A. Veal, A. M. Day, B. A. Morgan, *Mol. Cell* **2007**, *26*, 1-14.
- [10] W. Daul, Julius-Maximilians-Universität Würzburg (Würzburg), **2019**.
- [11] S. Darses, J.-P. Genet, *Chem. Rev.* **2008**, *108*, 288-325.
- [12] G. A. Molander, D. L. Sandrock, *Curr. Opin. Drug Discovery Dev.* **2009**, *12*, 811-823.
- [13] M. Ferger, Julius-Maximilians-Universität Würzburg (Würzburg), **2021**.
- [14] H. C. Brown, V. H. Dodson, *J. Am. Chem. Soc.* **1957**, *79*, 2302-2306.
- [15] X. Yin, J. Chen, R. A. Lalancette, T. B. Marder, F. Jäkle, *Angew. Chem. Int. Ed.* **2014**, *53*, 9761-9765; *Angew. Chem.* **2014**, *126*, 9919-9923.
- [16] Z. Zhou, A. Wakamiya, T. Kushida, S. Yamaguchi, *J. Am. Chem. Soc.* **2012**, *134*, 4529-4532.
- [17] T. J. Weismann, J. C. Schug, *J. Chem. Phys.* **1964**, *40*, 956-966.
- [18] C. D. Entwistle, T. B. Marder, *Angew. Chem. Int. Ed.* **2002**, *41*, 2927-2931; *Angew. Chem.* **2002**, *114*, 3051-3056.
- [19] C. D. Entwistle, T. B. Marder, *Chem. Mater.* **2004**, *16*, 4574-4585.
- [20] Z. M. Hudson, S. Wang, *Acc. Chem. Res.* **2009**, *42*, 1584-1596.
- [21] L. Ji, S. Griesbeck, T. B. Marder, *Chem. Sci.* **2017**, *8*, 846-863.
- [22] C. Jiménez, A. Enríquez-Cabrera, O. González-Antonio, J. Ordóñez-Hernández, P. Lacroix, P. Labra-Vázquez, N. Farfán, R. Santillan, *Inorganics* **2018**, *6*, 131.
- [23] J.-B. Li, H.-W. Liu, T. Fu, R. Wang, X.-B. Zhang, W. Tan, *Trends in Chemistry* **2019**, *1*, 224-234.
- [24] S. K. Mellerup, S. Wang, *Chem. Soc. Rev.* **2019**, *48*, 3537-3549.

- [25] S. K. Mellerup, S. Wang, *Trends in Chemistry* **2019**, *1*, 77-89.
- [26] Z. M. Hudson, S. Wang, *Dalton Trans.* **2011**, *40*, 7805-7816.
- [27] G. Turkoglu, M. E. Cinar, T. Ozturk, *Molecules* **2017**, *22*, 1522-1544.
- [28] Y. Yu, C. Dong, A. F. Alahmadi, B. Meng, J. Liu, F. Jäkke, L. Wang, *Journal of Materials Chemistry C* **2019**, *7*, 7427-7432.
- [29] K. C. Song, K. M. Lee, N. V. Nghia, W. Y. Sung, Y. Do, M. H. Lee, *Organometallics* **2013**, *32*, 817-823.
- [30] H. Zhao, L. A. Leamer, F. P. Gabbaï, *Dalton Trans.* **2013**, *42*, 8164-8178.
- [31] G. Turkoglu, M. E. Cinar, T. Ozturk, *Eur. J. Org. Chem.* **2017**, *2017*, 4552-4561.
- [32] J. Liu, C. Zhang, J. Dong, J. Zhu, C. Shen, G. Yang, X. Zhang, *New J. Chem.* **2017**, *41*, 4733-4737.
- [33] H. J. Li, S. K. Mellerup, X. Wang, S. Wang, *Org. Lett.* **2019**, *21*, 2838-2842.
- [34] H. R. Bhat, P. S. S. Gupta, S. Biswal, M. K. Rana, *ACS Omega* **2019**, *4*, 4505-4518.
- [35] X. Li, X. Guo, L. Cao, Z. Xun, S. Wang, S. Li, Y. Li, G. Yang, *Angew. Chem. Int. Ed.* **2014**, *53*, 7809-7813; *Angew. Chem.* **2014**, *126*, 7943-7947.
- [36] X. Guo, X. Zhang, S. Wang, S. Li, R. Hu, Y. Li, G. Yang, *Anal. Chim. Acta* **2015**, *869*, 81-88.
- [37] J. Liu, X. Guo, R. Hu, J. Xu, S. Wang, S. Li, Y. Li, G. Yang, *Anal. Chem.* **2015**, *87*, 3694-3698.
- [38] J. Liu, X. Guo, R. Hu, X. Liu, S. Wang, S. Li, Y. Li, G. Yang, *Anal. Chem.* **2016**, *88*, 1052-1057.
- [39] J. Liu, C. Zhang, J. Dong, J. Zhu, C. Shen, G. Yang, X. Zhang, *RSC Advances* **2017**, *7*, 14511-14515.
- [40] J. Liu, S. Zhang, C. Zhang, J. Dong, C. Shen, J. Zhu, H. Xu, M. Fu, G. Yang, X. Zhang, *Chem. Commun.* **2017**, *53*, 11476-11479.
- [41] S. Pagidi, N. K. Kalluvettukuzhy, P. Thilagar, *Langmuir* **2018**, *34*, 8170-8177.
- [42] J. Liu, S. Li, S. Zhang, C. Shen, J. Zhu, G. Yang, X. Zhang, *Sens. Actuators, B* **2018**, *261*, 531-536.
- [43] S. Griesbeck, Z. Zhang, M. Gutmann, T. Lühmann, R. M. Edkins, G. Clermont, A. N. Lazar, M. Haehnel, K. Edkins, A. Eichhorn, M. Blanchard-Desce, L. Meinel, T. B. Marder, *Chem. Eur. J.* **2016**, *22*, 14701-14706.
- [44] S. Griesbeck, M. Ferger, C. Czernetzi, C. Wang, R. Bertermann, A. Friedrich, M. Haehnel, D. Sieh, M. Taki, S. Yamaguchi, T. B. Marder, *Chem. Eur. J.* **2019**, *25*, 7679-7688.

- [45] S. Griesbeck, E. Michail, F. Rauch, H. Ogasawara, C. Wang, Y. Sato, R. Edkins, Z. Zhang, M. Taki, C. Lambert, S. Yamaguchi, T. B. Marder, *Chem. Eur. J.* **2019**, *25*, 13164-13175.
- [46] S. Griesbeck, E. Michail, C. Wang, H. Ogasawara, S. Lorenzen, L. Gerstner, T. Zang, J. Nitsch, Y. Sato, R. Bertermann, M. Taki, C. Lambert, S. Yamaguchi, T. B. Marder, *Chem. Sci.* **2019**, *10*, 5405-5422.
- [47] J. Liu, K. Cheng, C. Yang, J. Zhu, C. Shen, X. Zhang, X. Liu, G. Yang, *Anal. Chem.* **2019**, *91*, 6340-6344.
- [48] J. Liu, S. Zhang, J. Zhu, X. Liu, G. Yang, X. Zhang, *Anal. Bioanal. Chem.* **2019**, *411*, 5223-5231.
- [49] J. Liu, S. Zhang, B. Zhao, C. Shen, X. Zhang, G. Yang, *Biosens. Bioelectron.* **2019**, *142*, 111497.
- [50] C.-W. Chiu, Y. Kim, F. P. Gabbaï, *J. Am. Chem. Soc.* **2009**, *131*, 60-61.
- [51] Z. Ban, S. Griesbeck, S. Tomic, J. Nitsch, T. B. Marder, I. Piantanida, *Chem. Eur. J.* **2020**, *26*, 2195-2203.
- [52] H. Amini, Z. Ban, M. Ferger, S. Lorenzen, F. Rauch, A. Friedrich, I. Crnolatac, A. Kendel, S. Miljanic, I. Piantanida, T. B. Marder, *Chem. Eur. J.* **2020**, *26*, 6017-6028.
- [53] M. Ferger, Z. Ban, I. Krosi, S. Tomic, L. Dietrich, S. Lorenzen, F. Rauch, D. Sieh, A. Friedrich, S. Griesbeck, A. Kendel, S. Miljanic, I. Piantanida, T. B. Marder, *Chem. Eur. J.* **2021**.
- [54] D. Schleier, Julius-Maximilians-Universität Würzburg (Würzburg), **2016**.
- [55] S. Berger, Julius-Maximilians-Universität Würzburg (Würzburg), **2018**.
- [56] S. Griesbeck, Julius-Maximilians-Universität Würzburg (Würzburg), **2014**.
- [57] S. M. Berger, M. Ferger, T. B. Marder, *Chem. Eur. J.* **2021**, *27*, 7043-7058.
- [58] M. F. Lappert, *Chem. Rev.* **1956**, *56*, 959-1064.
- [59] J. L. Carden, A. Dasgupta, R. L. Melen, *Chem. Soc. Rev.* **2020**, *49*, 1706-1725.
- [60] A. Michaelis, *Liebigs Ann. Chem.* **1885**, *229*, 295-334.
- [61] W. E. Piers, D. J. Morrison, M. Parvez, *Synlett* **2004**, 2429-2433.
- [62] Á. Gyömöre, M. Bakos, T. Földes, I. Pápai, A. Domján, T. Soós, *ACS Catalysis* **2015**, *5*, 5366-5372.
- [63] K. Schickedanz, T. Trageser, M. Bolte, H. W. Lerner, M. Wagner, *Chem. Commun.* **2015**, *51*, 15808-15810.
- [64] J. Merz, J. Fink, A. Friedrich, I. Krummenacher, H. H. Al Mamari, S. Lorenzen, M. Haehnel, A. Eichhorn, M. Moos, M. Holzapfel, H. Braunschweig, C. Lambert, A. Steffen, L. Ji, T. B. Marder, *Chem. Eur. J.* **2017**, *23*, 13164-13180.

- [65] J. Merz, A. Steffen, J. Nitsch, J. Fink, C. B. Schurger, A. Friedrich, I. Krummenacher, H. Braunschweig, M. Moos, D. Mims, C. Lambert, T. B. Marder, *Chem. Sci.* **2019**, *10*, 7516-7534.
- [66] M. Ito, E. Ito, M. Hirai, S. Yamaguchi, *J. Org. Chem.* **2018**, *83*, 8449-8456.
- [67] J. He, F. Rauch, M. Finze, T. B. Marder, *Chem. Sci.* **2021**, *12*, 128-147.
- [68] E. von Grotthuss, A. John, T. Kaese, M. Wagner, *Asian Journal of Organic Chemistry* **2018**, *7*, 37-53.
- [69] H. Budy, J. Gilmer, T. Trageser, M. Wagner, *Eur. J. Inorg. Chem.* **2020**, *2020*, 4148-4162.
- [70] A. Escande, M. J. Ingleson, *Chem. Commun.* **2015**, *51*, 6257-6274.
- [71] A. Michaelis, P. Becker, *Ber. Dtsch. Chem. Ges.* **1880**, *13*, 58-61.
- [72] A. Michaelis, P. Becker, *Ber. Dtsch. Chem. Ges.* **1882**, *15*, 180-185.
- [73] A. Michaelis, A. Reese, *Ber. Dtsch. Chem. Ges.* **1882**, *15*, 1610-1610.
- [74] A. Michaelis, A. Reese, *Ber. Dtsch. Chem. Ges.* **1882**, *15*, 2876-2877.
- [75] A. Michaelis, *Ber. Dtsch. Chem. Ges.* **1889**, *22*, 241-243.
- [76] A. Dequasie, *The Green Flame: Surviving Government Secrecy, Vol. 1*, American Chemical Society, Washington, DC (USA), **1991**.
- [77] L. Gattermann, *Ber. Dtsch. Chem. Ges.* **1889**, *22*, 186-197.
- [78] A. Michaelis, *Ber. Dtsch. Chem. Ges.* **1894**, *27*, 244-262.
- [79] A. Michaelis, *Liebigs Ann. Chem.* **1901**, *315*, 19-43.
- [80] V. Grignard, *C.R. Hebd. Seances Acad. Sci.* **1900**, *130*, 1322-1324.
- [81] E. Khotinsky, M. Melamed, *Ber. Dtsch. Chem. Ges.* **1909**, *42*, 3090-3096.
- [82] W. Strecker, *Ber. Dtsch. Chem. Ges.* **1910**, *43*, 1131-1136.
- [83] W. König, W. Scharnbeck, *J. Prakt. Chem.* **1930**, *128*, 153-170.
- [84] K. Albrecht, V. Kaiser, R. Boese, J. Adams, D. E. Kaufmann, *J. Chem. Soc., Perkin Trans. 2* **2000**, 2153-2157.
- [85] Y. Gu, H. Pritzkow, W. Siebert, *Eur. J. Inorg. Chem.* **2001**, *2*, 373-379.
- [86] A. Pron, G. Zhou, H. Norouzi-Arasi, M. Baumgarten, K. Müllen, *Org. Lett.* **2009**, *11*, 3550-3553.
- [87] A. Tsurusaki, T. Sasamori, A. Wakamiya, S. Yamaguchi, K. Nagura, S. Irle, N. Tokitoh, *Angew. Chem. Int. Ed.* **2011**, *50*, 10940-10943; *Angew. Chem.* **2011**, *123*, 11132-11135.
- [88] A. Sengupta, A. Doshi, F. Jäkle, R. M. Peetz, *Journal of Polymer Science Part A: Polymer Chemistry* **2015**, *53*, 1707-1718.
- [89] H. Schiff, *Ann. Chem. Supl.* **1867**, *5*, 154-218.
- [90] E. Krause, R. Nitsche, *Ber. Dtsch. Chem. Ges.* **1921**, *54*, 2784-2791.
- [91] E. Krause, R. Nitsche, *Ber. Dtsch. Chem. Ges.* **1922**, *55*, 1261-1265.

- [92] E. Krause, *Ber. Dtsch. Chem. Ges.* **1924**, *57*, 216-217.
- [93] E. Krause, H. Polack, *Ber. Dtsch. Chem. Ges.* **1926**, *59*, 777-785.
- [94] E. Krause, H. Polack, *Ber. Dtsch. Chem. Ges.* **1928**, *61*, 271-276.
- [95] E. Krause, P. Nobbe, *Ber. Dtsch. Chem. Ges.* **1930**, *63*, 934-942.
- [96] E. Krause, P. Nobbe, *Ber. Dtsch. Chem. Ges.* **1931**, *64*, 2112-2116.
- [97] G. Wittig, P. Raff, *Liebigs Ann. Chem.* **1951**, *573*, 195-209.
- [98] J. D. Hoefelmeyer, F. P. Gabbaï, *Organometallics* **2002**, *21*, 982-985.
- [99] J. E. Borger, A. W. Ehlers, M. Lutz, J. C. Slootweg, K. Lammertsma, *Angew. Chem. Int. Ed.* **2014**, *53*, 12836-12839.
- [100] A. Chardon, A. Osi, D. Mahaut, T. H. Doan, N. Tumanov, J. Wouters, L. Fusaro, B. Champagne, G. Berionni, *Angew. Chem. Int. Ed.* **2020**, *59*, 12402-12406.
- [101] H. C. Brown, S. Sujish, *J. Am. Chem. Soc.* **1945**, *70*, 2793-2802.
- [102] G. Wittig, G. Keicher, *Naturwissenschaften* **1947**, *34*, 216.
- [103] G. Wittig, G. Keicher, A. Rückert, P. Raff, *Liebigs Ann. Chem.* **1949**, *563*, 110-126.
- [104] G. Wittig, W. Herwig, *Chem. Ber.* **1955**, *88*, 962-976.
- [105] Z. Wu, J. Nitsch, J. Schuster, A. Friedrich, K. Edkins, M. Loebnitz, F. Dinkelbach, V. Stepanenko, F. Würthner, C. M. Marian, L. Ji, T. B. Marder, *Angew. Chem. Int. Ed.* **2020**, *59*, 17137-17144; *Angew. Chem.* **2020**, *132*, 17285-17292.
- [106] R. T. Hawkins, W. J. Lennarz, H. R. Snyder, *J. Am. Chem. Soc.* **1960**, *82*, 3053-3059.
- [107] H. E. Ramsden, A. E. Balint, W. R. Whitford, J. J. Walburn, R. Cserr, *J. Org. Chem.* **1957**, *22*, 1202-1206.
- [108] J. L. R. Williams, J. C. Doty, P. J. Grisdale, R. Searle, T. H. Regan, G. P. Happ, D. P. Maier, *J. Am. Chem. Soc.* **1967**, *89*, 5153-5157.
- [109] J. C. Doty, B. Babb, P. J. Grisdale, M. Glogowski, J. L. R. Williams, *J. Organomet. Chem.* **1972**, *38*, 229-236.
- [110] H. Gilman, L. O. Moore, *J. Am. Chem. Soc.* **1958**, *80*, 3609-3611.
- [111] W. Gerrard, M. Howarth, E. F. Mooney, D. E. Pratt, *J. Chem. Soc.* **1963**, 1582-1584.
- [112] B. E. Carpenter, W. E. Piers, R. McDonald, *Can. J. Chem.* **2001**, *79*, 291-295.
- [113] V. C. Williams, W. E. Piers, W. Clegg, M. R. J. Elsegood, S. Collins, T. B. Marder, *J. Am. Chem. Soc.* **1999**, *121*, 3244-3245.
- [114] Y. Sun, W. E. Piers, M. Parvez, *Can. J. Chem.* **1998**, *76*, 513-517.
- [115] A. Sundararaman, F. Jäkle, *J. Organomet. Chem.* **2003**, *681*, 134-142.
- [116] A. E. Ashley, T. J. Herrington, G. G. Wildgoose, H. Zaher, A. L. Thompson, N. H. Rees, T. Krämer, D. O'Hare, *J. Am. Chem. Soc.* **2011**, *133*, 14727-14740.

- [117] P. Chen, A. S. Marshall, S.-H. Chi, X. Yin, J. W. Perry, F. Jäkle, *Chem. Eur. J.* **2015**, *21*, 18237-18247.
- [118] P. Chen, X. Yin, N. Baser-Kirazli, F. Jäkle, *Angew. Chem. Int. Ed.* **2015**, *54*, 10768-10772.
- [119] J. E. Burch, W. Gerrard, M. Howarth, E. F. Mooney, *J. Chem. Soc.* **1960**, 4916-4918.
- [120] T. Chivers, *Can. J. Chem.* **1970**, *48*, 3856-3859.
- [121] A. Sundararaman, M. Victor, R. Varughese, F. Jäkle, *J. Am. Chem. Soc.* **2005**, *127*, 13748-13749.
- [122] P. Chen, F. Jäkle, *J. Am. Chem. Soc.* **2011**, *133*, 20142-20145.
- [123] X. Yin, F. Guo, R. A. Lalancette, F. Jäkle, *Macromolecules* **2016**, *49*, 537-546.
- [124] W. Haubold, J. Herdtle, W. Gollinger, W. Einholz, *J. Organomet. Chem.* **1986**, *35*, 1-8.
- [125] D. Kaufmann, *Chem. Ber.* **1987**, *120*, 853-854.
- [126] D. Kaufmann, *Chem. Ber.* **1987**, *120*, 901-905.
- [127] M. J. Sharp, W. Cheng, V. Snieckus, *Tetrahedron Lett.* **1987**, *28*, 5093-5096.
- [128] Y. Qin, G. Cheng, A. Sundararaman, F. Jäkle, *J. Am. Chem. Soc.* **2002**, *124*, 12672-12673.
- [129] Y. Qin, G. Cheng, O. Achara, K. Parab, F. Jäkle, *Macromolecules* **2004**, *37*, 7123-7131.
- [130] A. Lik, L. Fritze, L. Müller, H. Helten, *J. Am. Chem. Soc.* **2017**, *139*, 5692-5695.
- [131] H. Helten, L. Fritze, N. Riensch, *Synthesis* **2018**, *51*, 399-406.
- [132] A. Lik, S. Jenthra, L. Fritze, L. Muller, K. N. Truong, H. Helten, *Chem. Eur. J.* **2018**, *24*, 11961-11972.
- [133] R. D. Chambers, H. C. Clark, C. J. Willis, *J. Am. Chem. Soc.* **1960**, *82*, 5298-5301.
- [134] S. L. Stafford, *Can. J. Chem.* **1963**, *41*, 807-808.
- [135] R. D. Chambers, T. Chivers, D. A. Pyk, *J. Chem. Soc.* **1965**, 5144-5145.
- [136] D. Thierig, F. Umland, *Naturwissenschaften* **1967**, *54*, 563.
- [137] G. Bir, W. Schacht, D. Kaufmann, *J. Organomet. Chem.* **1988**, *340*, 267-271.
- [138] E. Vedejs, R. W. Chapman, S. C. Fields, S. Lin, M. R. Schrimpf, *J. Org. Chem.* **1995**, *60*, 3020-3027.
- [139] G. A. Molander, N. Ellis, *Acc. Chem. Res.* **2007**, *40*, 275-286.
- [140] É. Dorkó, B. Kótai, T. Földes, Á. Gyömöre, I. Pápai, T. Soós, *J. Organomet. Chem.* **2017**, *847*, 258-262.
- [141] É. Dorkó, M. Szabó, B. Kótai, I. Pápai, A. Domján, T. Soós, *Angew. Chem. Int. Ed.* **2017**, *56*, 9512-9516; *Angew. Chem.* **2017**, *129*, 9640-9644.

- [142] Y. Hoshimoto, T. Kinoshita, S. Hazra, M. Ohashi, S. Ogoshi, *J. Am. Chem. Soc.* **2018**, *140*, 7292-7300.
- [143] K. Schickedanz, J. Radtke, M. Bolte, H. W. Lerner, M. Wagner, *J. Am. Chem. Soc.* **2017**, *139*, 2842-2851.
- [144] E. Yamamoto, K. Izumi, R. Shishido, T. Seki, N. Tokodai, H. Ito, *Chem. Eur. J.* **2016**, *22*, 17547-17551.
- [145] R. Shishido, I. Sasaki, T. Seki, T. Ishiyama, H. Ito, *Chem. Eur. J.* **2019**, *25*, 12924-12928.
- [146] P. J. Grisdale, J. L. R. Williams, M. E. Glogowski, B. E. Babb, *J. Org. Chem.* **1971**, *36*, 544-549.
- [147] R. L. Letsinger, N. Remes, *J. Am. Chem. Soc.* **1955**, *77*, 2489-2491.
- [148] B. M. Mikhailov, T. V. Kostroma, N. S. Fedotov, *Chemisches Zentralblatt* **1958**, *129*, 10916-10917.
- [149] A. Pelter, K. Smith, D. Buss, Z. Jin, *Heteroat. Chem.* **1992**, *3*, 275-277.
- [150] R. J. Blagg, G. G. Wildgoose, *RSC Advances* **2016**, *6*, 42421-42427.
- [151] K. Parab, K. Venkatasubbaiah, F. Jäkle, *J. Am. Chem. Soc.* **2006**, *128*, 12879-12885.
- [152] A. Sundararaman, K. Venkatasubbaiah, M. Victor, L. N. Zakharov, A. L. Rheingold, F. Jäkle, *J. Am. Chem. Soc.* **2006**, *128*, 16554-16565.
- [153] H. Li, A. Sundararaman, T. Pakkirisamy, K. Venkatasubbaiah, F. Schödel, F. Jäkle, *Macromolecules* **2011**, *44*, 95-103.
- [154] K. Parab, A. Doshi, F. Cheng, F. Jäkle, *Macromolecules* **2011**, *44*, 5961-5967.
- [155] X. Yin, K. Liu, Y. Ren, R. A. Lalancette, Y. L. Loo, F. Jäkle, *Chem. Sci.* **2017**, *8*, 5497-5505.
- [156] M. J. Kelly, R. Tirfoin, J. Gilbert, S. Aldridge, *J. Organomet. Chem.* **2014**, *769*, 11-16.
- [157] M. Ferger, S. M. Berger, F. Rauch, M. Schönitz, J. Rühle, J. Krebs, A. Friedrich, T. B. Marder, *Chem. Eur. J.* **2021**, *27*, 9094-9101.
- [158] T. Ishiyama, J. Takagi, K. Ishida, N. Miyaura, N. R. Anastasi, J. F. Hartwig, *J. Am. Chem. Soc.* **2002**, *24*, 390-391.
- [159] I. A. I. Mkhallid, J. H. Barnard, T. B. Marder, J. M. Murphy, J. F. Hartwig, *Chem. Rev.* **2010**, *110*, 890-931.
- [160] S. Yamaguchi, T. Shirasaka, K. Tamao, *Org. Lett.* **2000**, *2*, 4129-4132.
- [161] J. F. Blount, P. Finocchiaro, D. Gust, K. Mislow, *J. Am. Chem. Soc.* **1973**, *95*, 7018-7029.
- [162] M. M. Olmstead, P. P. Power, *J. Am. Chem. Soc.* **1986**, *108*, 4235-4236.
- [163] J. D. Andose, K. Mislow, *J. Am. Chem. Soc.* **1974**, *96*, 2168-2176.

- [164] K. Mislow, *Acc. Chem. Res.* **1976**, *9*, 26-33.
- [165] W. L. Jia, M. J. Moran, Y.-Y. Yuan, Z. H. Lu, S. Wang, *J. Mater. Chem.* **2005**, *15*.
- [166] J. Clayden, N. Greeves, S. Warren, *Organic Chemistry*, Oxford University Press, New York, **2012**.
- [167] M. J. Peach, P. Benfield, T. Helgaker, D. J. Tozer, *J. Chem. Phys.* **2008**, *128*, 044118.
- [168] R. Stahl, C. Lambert, C. Kaiser, R. Wortmann, R. Jakober, *Chem. Eur. J.* **2006**, *12*, 2358-2370.
- [169] Z. Zhang, R. M. Edkins, J. Nitsch, K. Fucke, A. Steffen, L. E. Longobardi, D. W. Stephan, C. Lambert, T. B. Marder, *Chem. Sci.* **2015**, *6*, 308-321.
- [170] M. Feger, Julius-Maximilians-Universität Würzburg (Würzburg), **2016**.
- [171] N. G. Connelly, W. E. Geiger, *Chem. Rev.* **1996**, *96*, 877-910.
- [172] D. Tsiplakides, D. Archonta, C. G. Vayenas, *Top. Catal.* **2007**, *44*, 469-479.
- [173] D. T. Sawyer, J. L. Roberts, *Experimental Electrochemistry for Chemists*, Wiley-Interscience, New York, **1974**.
- [174] D. Reitzenstein, T. Quast, F. Kanal, M. Kullmann, S. Ruetzel, M. S. Hammer, C. Deibel, V. Dyakonov, T. Brixner, C. Lambert, *Chem. Mater.* **2010**, *22*, 6641-6655.
- [175] J. Gierschner, J. Cornil, H. J. Egelhaaf, *Advanced Materials* **2007**, *19*, 173-191.
- [176] S. Porcel, G. Bouhadir, N. Saffon, L. Maron, D. Bourissou, *Angew. Chem. Int. Ed.* **2010**, *49*, 6186-6189; *Angew. Chem.* **2010**, *122*, 6322-6325.
- [177] K. Liu, R. A. Lalancette, F. Jäkle, *J. Am. Chem. Soc.* **2019**, *141*, 7453-7462.
- [178] B. Chandra, R. Soman, B. Sathish Kumar, K. V. J. Jose, P. K. Panda, *Org. Lett.* **2020**, *22*, 9735-9739.
- [179] P. R. Ogilby, *Chem. Soc. Rev.* **2010**, *39*, 3181-3209.
- [180] R. Schmidt, C. Tanielian, R. Dunsbach, C. Wolff, *J. Photochem. Photobiol. A Chem.* **1994**, *79*, 11-17.
- [181] M. Bregnhøj, M. Westberg, B. F. Minaev, P. R. Ogilby, *Acc. Chem. Res.* **2017**, *50*, 1920-1927.
- [182] W. Li, D. Liu, F. Shen, D. Ma, Z. Wang, T. Feng, Y. Xu, B. Yang, Y. Ma, *Adv. Funct. Mater.* **2012**, *22*, 2797-2803.
- [183] S. Zhang, W. Li, L. Yao, Y. Pan, F. Shen, R. Xiao, B. Yang, Y. Ma, *Chem. Commun.* **2013**, *49*, 11302-11304.
- [184] L. Yao, S. Zhang, R. Wang, W. Li, F. Shen, B. Yang, Y. Ma, *Angew. Chem. Int. Ed.* **2014**, *53*, 2119-2123; *Angew. Chem.* **2014**, *126*, 2151-2155.
- [185] A. D. Buckingham, *Q. Rev. Chem. Soc.* **1959**, *13*, 183-241.
- [186] S. Griesbeck, Dissertation thesis, Julius-Maximilians-Universität Würzburg (Würzburg), **2019**.

- [187] N. Elgrishi, K. J. Rountree, B. D. McCarthy, E. S. Rountree, T. T. Eisenhart, J. L. Dempsey, *J. Chem. Educ.* **2017**, *95*, 197-206.
- [188] E. M. Null, University of Iowa **2014**.
- [189] S. Tanaka, T. Enoki, H. Imoto, Y. Ooyama, J. Ohshita, T. Kato, K. Naka, *Macromolecules* **2020**, *53*, 2006-2013.
- [190] Y. Yang, Q. Guo, H. Chen, Z. Zhou, Z. Guo, Z. Shen, *Chem. Commun.* **2013**, *49*, 3940-3942.
- [191] S. Berger, T. B. Marder, *Mater. Horiz.* **2021**, DOI: 10.1039/d1031mh00696g.
- [192] V. Prakash Reddy, E. Sinn, N. Hosmane, *J. Organomet. Chem.* **2015**, *798*, 5-12.
- [193] P. A. Gale, C. Caltagirone, *Coord. Chem. Rev.* **2018**, *354*, 2-27.
- [194] B. M. Squeo, M. Pasini, *Supramol. Chem.* **2020**, *32*, 56-70.
- [195] T. M. Grant, D. S. Josey, K. L. Sampson, T. Mudigonda, T. P. Bender, B. H. Lessard, *Chem. Rec.* **2019**, *19*, 1093-1112.
- [196] J. Dong, C. H. Zhang, B. Zhao, X. M. Zhang, Z. W. Leng, J. Liu, *Dyes Pigm.* **2020**, *174*, 108077-108082.
- [197] B. R. Shaw, M. I. Dobrikov, X. Wang, J. Wang, K. He, J.-L. Lin, P. Li, V. Rait, Z. A. Sergueeva, D. S. Sergueev, *Ann. N.Y. Acad. Sci.* **2003**, *1002*, 12-29.
- [198] B. S. Burnham, *Curr. Med. Chem.* **2005**, *12*, 1995-2010.
- [199] A. Loudet, K. Burgess, *Chem. Rev.* **2007**, *107*, 4891-4932.
- [200] C. R. Wade, A. E. J. Broomsgrove, S. Aldridge, F. P. Gabbai, *Chem. Rev.* **2010**, *110*, 3958-3984.
- [201] Z. Liu, Z. Jiang, M. Yan, X. Wang, *Front. Chem.* **2019**, *7*, 712.
- [202] K. Chansaenpak, B. Vabre, F. P. Gabbai, *Chem. Soc. Rev.* **2016**, *45*, 954-971.
- [203] N. Boens, V. Leen, W. Dehaen, *Chem. Soc. Rev.* **2012**, *41*, 1130-1172.
- [204] Y. S. Marfin, A. V. Solomonov, A. S. Timin, E. V. Rumyantsev, *Curr. Med. Chem.* **2017**, *24*, 2745-2772.
- [205] C. S. Kue, S. Y. Ng, S. H. Voon, A. Kamkaew, L. Y. Chung, L. V. Kiew, H. B. Lee, *Photochem. Photobiol. Sci.* **2018**, *17*, 1691-1708.
- [206] K. Hu, Z. Yang, L. Zhang, L. Xie, L. Wang, H. Xu, L. Josephson, S. H. Liang, M.-R. Zhang, *Coord. Chem. Rev.* **2020**, *405*.
- [207] C. A. Perks, A. J. Mill, G. Constantine, K. G. Harrison, J. A. Gibson, *Brit. J. Radiol.* **1988**, *61*, 1115-1126.
- [208] R. F. Barth, J. C. Grecula, *Appl. Radiat. Isot.* **2020**, *160*, 109029.
- [209] D. S. Novopashina, M. A. Vorobyeva, A. Venyaminova, *Front. Chem.* **2021**, *9*, 619052.
- [210] Y. Kim, F. P. Gabbai, *J. Am. Chem. Soc.* **2009**, *131*, 3363-3369.

- [211] T. Agou, M. Sekine, J. Kobayashi, T. Kawashima, *Chem. Eur. J.* **2009**, *15*, 5056-5062.
- [212] S. Mukherjee, P. Thilagar, *Journal of Materials Chemistry C* **2016**, *4*, 2647-2662.
- [213] Y. Y. Ma, J. L. Yin, G. H. Li, W. J. Gao, W. Y. Lin, *Coord. Chem. Rev.* **2020**, *406*.
- [214] L. Feng, Y. Zhao, *View* **2020**, *1*.
- [215] Y. Sugihara, N. Inai, M. Taki, T. Baumgartner, R. Kawakami, T. Saitou, T. Imamura, T. Yanai, S. Yamaguchi, *Chem. Sci.* **2021**, *12*, 6333-6341.
- [216] X. Li, X. Guo, L. Cao, Z. Xun, S. Wang, S. Li, Y. Li, G. Yang, *Angew. Chem.* **2014**, *126*, 7943-7947.
- [217] M. Demeunynck, C. Bailly, W. D. Wilson, *DNA and RNA Binders*, Wiley-VCH, Weinheim, Germany, **2002**.
- [218] J.-L. Mergny, L. Lacroix, *Oligonucleotides* **2003**, *13*, 515-537.
- [219] N. C. Garbett, P. A. Ragazzon, J. B. Chaires, *Nat. Protoc.* **2007**, *2*, 3166-3172.
- [220] T. Smidlehner, I. Piantanida, G. Pescitelli, *Beilstein J. Org. Chem.* **2018**, *14*, 84-105.
- [221] G. Scatchard, *Ann. N.Y. Acad. Sci.* **1949**, *51*, 660-672.
- [222] J. D. McGhee, P. H. von Hippel, *J. Mol. Biol.* **1974**, *86*, 469-489.
- [223] A. Rodger, B. Nordén, *Circular Dichroism and Linear Dichroism*, Oxford University Press, New York, **1997**.
- [224] M. Eriksson, B. Nordén, *Methods in Enzymology*, Vol. 340, Academic Press, San Diego, **2001**.
- [225] M. Białek, M. Czauderna, K. Krajewska, W. Przybylski, *Journal of Animal and Feed Sciences* **2019**, *28*, 307-320.
- [226] X. Peng, V. Gandhi, *Therapeutic Delivery* **2012**, *3*, 823-833.
- [227] S. Daum, M. S. V. Reshetnikov, M. Sisa, T. Dumych, M. D. Lootsik, R. Bilyy, E. Bila, C. Janko, C. Alexiou, M. Herrmann, L. Sellner, A. Mokhir, *Angew. Chem. Int. Ed.* **2017**, *56*, 15545-15549; *Angew. Chem.* **2017**, *129*, 15751-15755.
- [228] E. Zysman-Colman, K. Arias, J. S. Siegel, *Can. J. Chem.* **2009**, *87*, 440-447.
- [229] R. Uson, L. A. Oro, J. A. Cabeza, H. E. B. Bryndza, M. P. Stepro, *Inorg. Synth.* **1985**, *23*, 126-130.
- [230] S. S. Zalesskiy, V. P. Ananikov, *Organometallics* **2012**, *31*, 2302-2309.
- [231] S. Colella, M. Mazzeo, R. Grisorio, E. Fabiano, G. Melcarne, S. Carallo, M. D. Angione, L. Torsi, G. P. Suranna, F. della Sala, P. Mastrorilli, G. Gigli, *Chem. Commun.* **2010**, *46*, 6273-6275.
- [232] J. H. Barnard, J. C. Collings, A. Whiting, S. A. Przyborski, T. B. Marder, *Chem. Eur. J.* **2009**, *15*, 11430-11442.
- [233] G. M. Sheldrick, *Acta Crystallogr.* **2015**, *71*, 3-8.

- [234] G. M. Sheldrick, *Acta Crystallogr.* **2008**, *64*, 112-122.
- [235] K. Brandenburg, *Diamond (Version 4.4.0), Crystal and Molecular Structure Visualization* **2017**.
- [236] M. J. Frisch, G. W. Trucks, H. B. Schlegel, G. E. Scuseria, M. A. Robb, J. R. Cheeseman, G. Scalmani, V. Barone, B. Mennucci, G. A. Petersson, H. Nakatsuji, M. Caricato, X. Li, H. P. Hratchian, A. F. Izmaylov, J. Bloino, G. Zheng, J. L. Sonnenberg, M. Hada, M. Ehara, K. Toyota, R. Fukuda, J. Hasegawa, M. Ishida, T. Nakajima, Y. Honda, O. Kitao, H. Nakai, T. Vreven, J. A. Montgomery Jr, J. E. Peralta, F. Ogliaro, M. Bearpark, J. J. Heyd, E. Brothers, K. N. Kudin, V. N. Staroverov, R. Kobayashi, J. Normand, K. Raghavachari, A. Rendell, J. C. Burant, S. S. Iyengar, J. Tomasi, M. Cossi, N. Rega, J. M. Millam, M. Klene, J. E. Knox, J. B. Cross, V. Bakken, C. Adamo, J. Jaramillo, R. Gomperts, R. E. Stratmann, O. Yazyev, A. J. Austin, R. Cammi, C. Pomelli, J. W. Ochterski, R. L. Martin, K. Morokuma, V. G. Zakrzewski, G. A. Voth, P. Salvador, J. J. Dannenberg, S. Dapprich, A. D. Daniels, O. Farkas, J. B. Foresman, J. V. Ortiz, J. Cioslowski, D. J. Fox, *Gaussian 09, Revision E.01*, Gaussian, Inc., Wallingford CT, **2009**.
- [237] T. Lu, F. Chen, *J. Comput. Chem.* **2012**, *33*, 580-592.
- [238] A. D. Becke, *J. Chem. Phys.* **1993**, *98*, 5648-5652.
- [239] C. Lee, W. Yang, R. G. Parr, *Phys. Rev. B Condens. Matter.* **1988**, *37*, 785-789.
- [240] P. J. Stephens, F. J. Devlin, C. F. Chabalowski, M. J. Frisch, *J. Phys. Chem. A* **1994**, *98*, 11623-11627.
- [241] G. A. Petersson, A. Bennett, T. G. Tensfeldt, M. A. Al-Laham, W. A. Shirley, *J. Chem. Phys.* **1988**, *89*, 2193-2218.
- [242] G. A. Petersson, M. A. Al-Laham, *J. Chem. Phys.* **1991**, *94*, 6081-6090.
- [243] T. Yanai, D. P. Tew, N. C. Handy, *Chem. Phys. Lett.* **2004**, *393*, 51-57.
- [244] J. B. Chaires, N. Dattagupta, D. M. Crothers, *Biochemistry* **1982**, *21*, 3933-3940.
- [245] L.-M. Tumir, I. Piantanida, I. J. Cindri, T. Hrenar, Z. Mei, M. ini, *J. Phys. Org. Chem.* **2003**, *16*, 891-899.
- [246] T. Mosmann, *J. Immunol. Methods* **1983**, *65*, 55-63.
- [247] C. Chazalotte, M. Riviere-Baudet, A. Scozzafava, F. Abbate, Z. Ben Maarouf, C. T. Supuran, *J. Enzym. Inhib. Med. Chem.* **2001**, *16*, 125-133.
- [248] N. Suzuki, K. Suda, D. Yokogawa, H. Kitoh-Nishioka, S. Irle, A. Ando, L. M. G. Abegao, K. Kamada, A. Fukazawa, S. Yamaguchi, *Chem. Sci.* **2018**, *9*, 2666-2673.
- [249] T. B. Nguyen, A. Al-Mourabit, *Photochem. Photobiol. Sci.* **2016**, *15*, 1115-1119.
- [250] J. M. Percy, H. Emerson, J. W. Fyfe, A. R. Kennedy, S. Maciuk, D. Orr, L. Rathouska, J. M. Redmond, P. G. Wilson, *Chem. Eur. J.* **2016**, *22*, 12166-12175.
- [251] K. E. Judd, L. Caggiano, *Org. Biomol. Chem.* **2011**, *9*, 5201-5210.

- [252] L. Li, P. Zhao, J. Hu, J. Liu, Y. Liu, Z. Wang, Y. Xia, Y. Dai, L. Chen, *Eur. J. Med. Chem.* **2015**, 93, 300-307.

CHAPTER 11

APPENDIX

11 Appendix

11.1 Cyclic Voltammograms

Table 11.1: Peak-to-peak splitting of triarylboranes and *bis*-triarylboranes investigated.

Compound	Peak-to-peak splitting compound [V]	Peak-to-peak splitting Fc/Fc ⁺ [V]
3.1a	0.215	0.105
3.2a	Red: 0.165 Ox: 0.160	0.090
3.3a	Red: 0.100 Ox1: 0.095 Ox2: 0.115	0.100
3.2c	0.080	0.080
3.3c	0.080	0.080
Neut0	Rev red: 0.080 Irrev red: 0.125	0.085
Neut1	Rev red: 0.075 Irrev red: 0.135 Ox: 0.070	0.075
Neut2	Rev red: 0.100 Irrev red: 0.125 Ox: 0.090	0.109
Neut(i)2	Rev red: 0.095 Irrev red: 0.140 Ox: 0.100	0.110
Neut3	Rev red: 0.090 Irrev red: 0.205 Ox1: 0.125 (Ox2: 0.230)	0.095
Neut4	Rev red: 0.100 Irrev red: 0.115 Ox: 0.100	0.109
Cat¹⁺	Red: 0.130 Ox1: 0.075 Ox2: 0.095	0.075
Cat²⁺	Red1: 0.075 Red2: 0.085 Ox1: 0.085 Ox2: 0.130	0.070
Cat(i)²⁺	Red: 0.065 Ox1: 0.090 Ox2: 0.150	0.080
Cat³⁺	Red1: 0.075 Red2: 0.070 Ox1: 0.090 Ox2: 0.165	0.080

11.1.1 Chapter 3

11.1.1.1 Neutral Triarylboranes

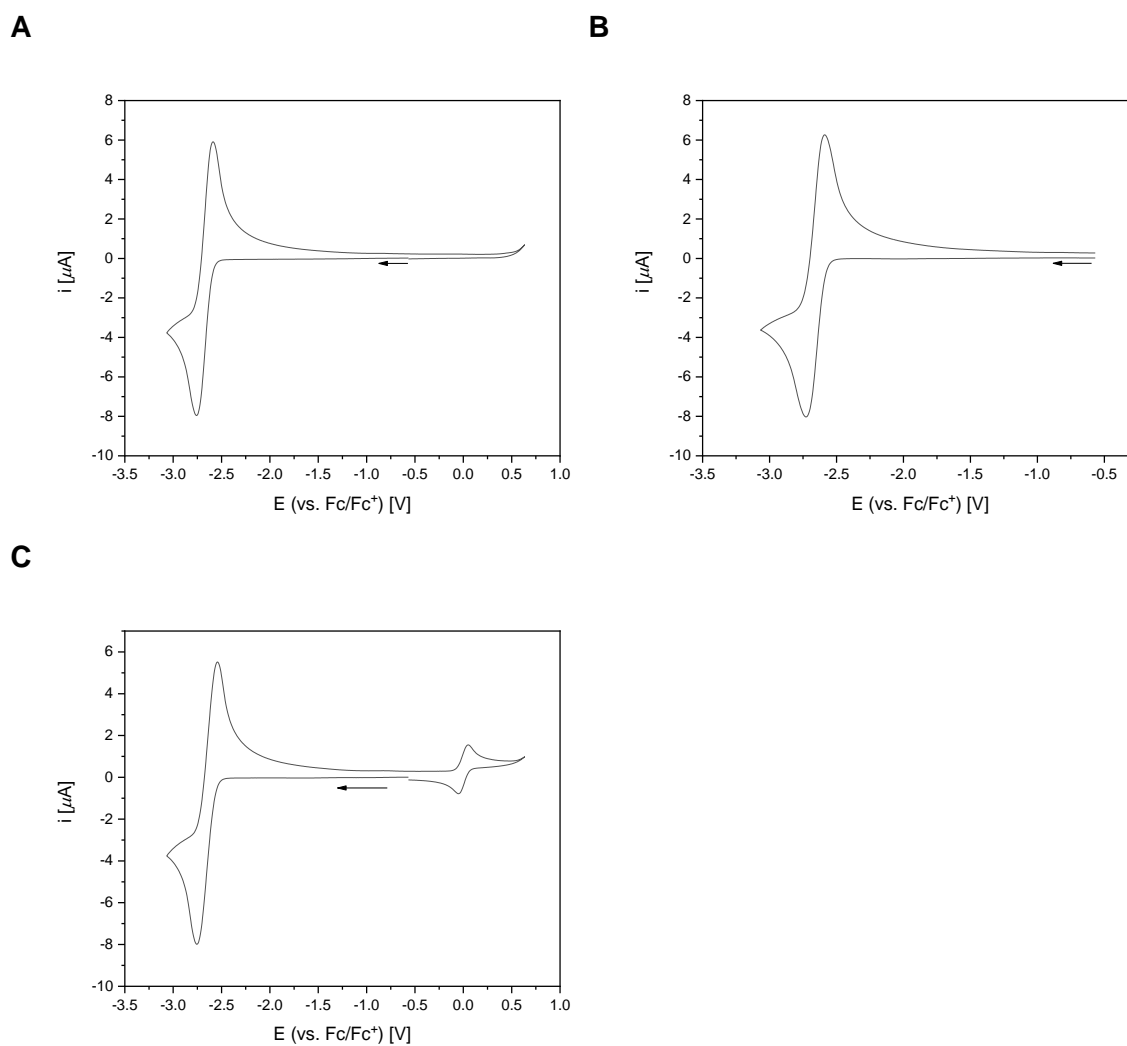


Figure 11.1: **A)** Cyclic voltammogram of **3.1a** in THF. **B)** Reversible Reduction of **3.1a** in THF. **C)** Cyclic voltammogram of **3.1a** in THF in the presence of Fc/Fc⁺.

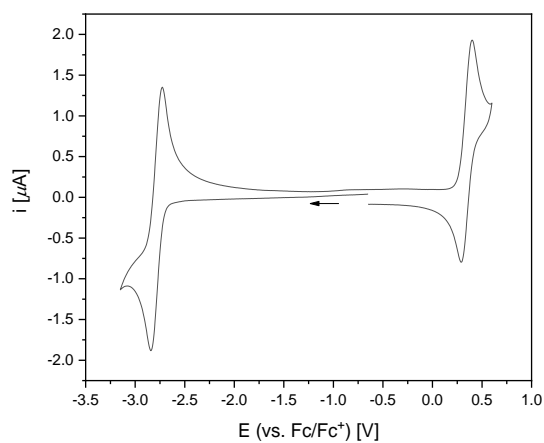
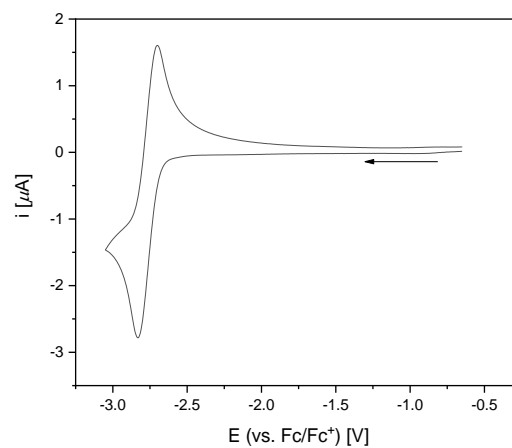
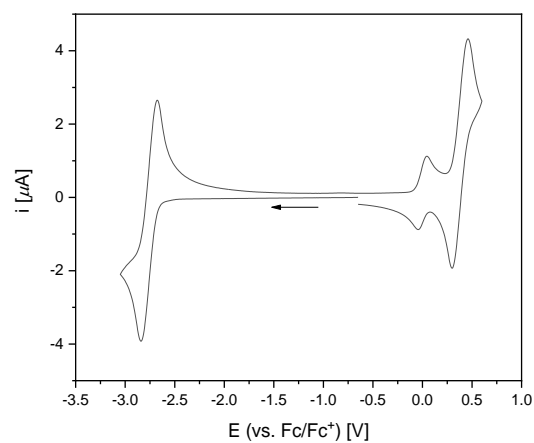
A**B****C**

Figure 11.2: **A)** Cyclic voltammogram of **3.2a** in THF. **B)** Partially reversible reduction of **3.2a** in THF. **C)** Cyclic voltammogram of **3.2a** in THF in the presence of Fc/Fc^+ .

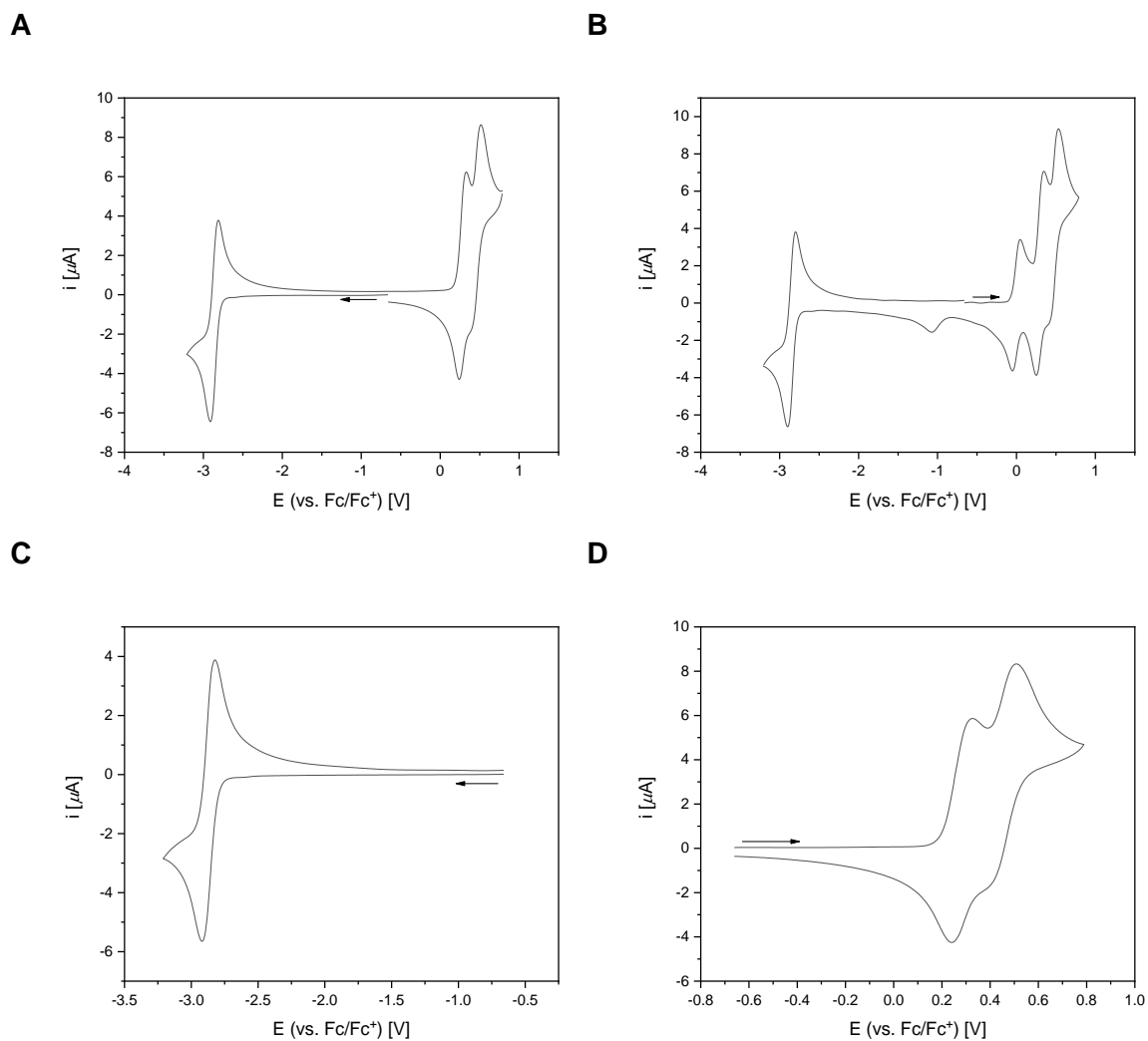


Figure 11.3: **A)** Cyclic voltammogram of **3.3a** in THF. **B)** Cyclic voltammogram of **3.3a** in THF in the presence of Fc/Fc^+ . **C)** Partially reversible reduction of **3.3a** in THF. **D)** Reversible oxidations of **3.3a** in THF.

11.1.1.2 Cationic Triarylboranes

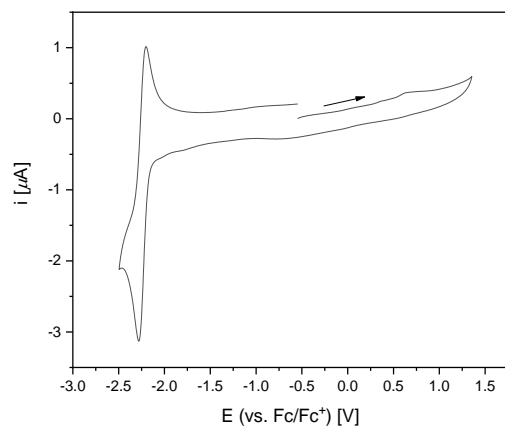
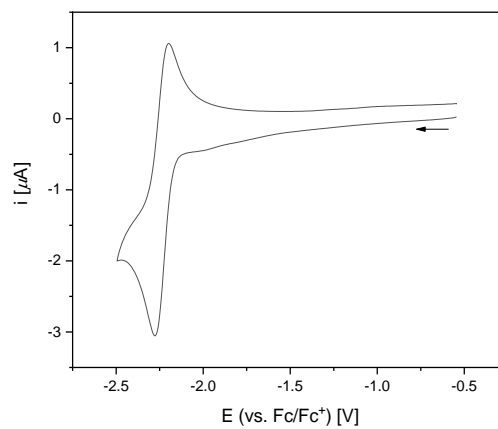
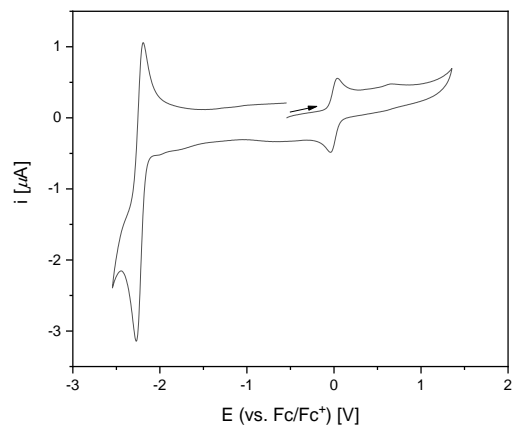
A**B****C**

Figure 11.4: **A**) Cyclic voltammogram of **3.2c** in MeCN. **B**) Reversible reduction of **3.2c** in MeCN. **C**) Cyclic voltammogram of **3.2c** in MeCN in the presence of Fc/Fc^+ .

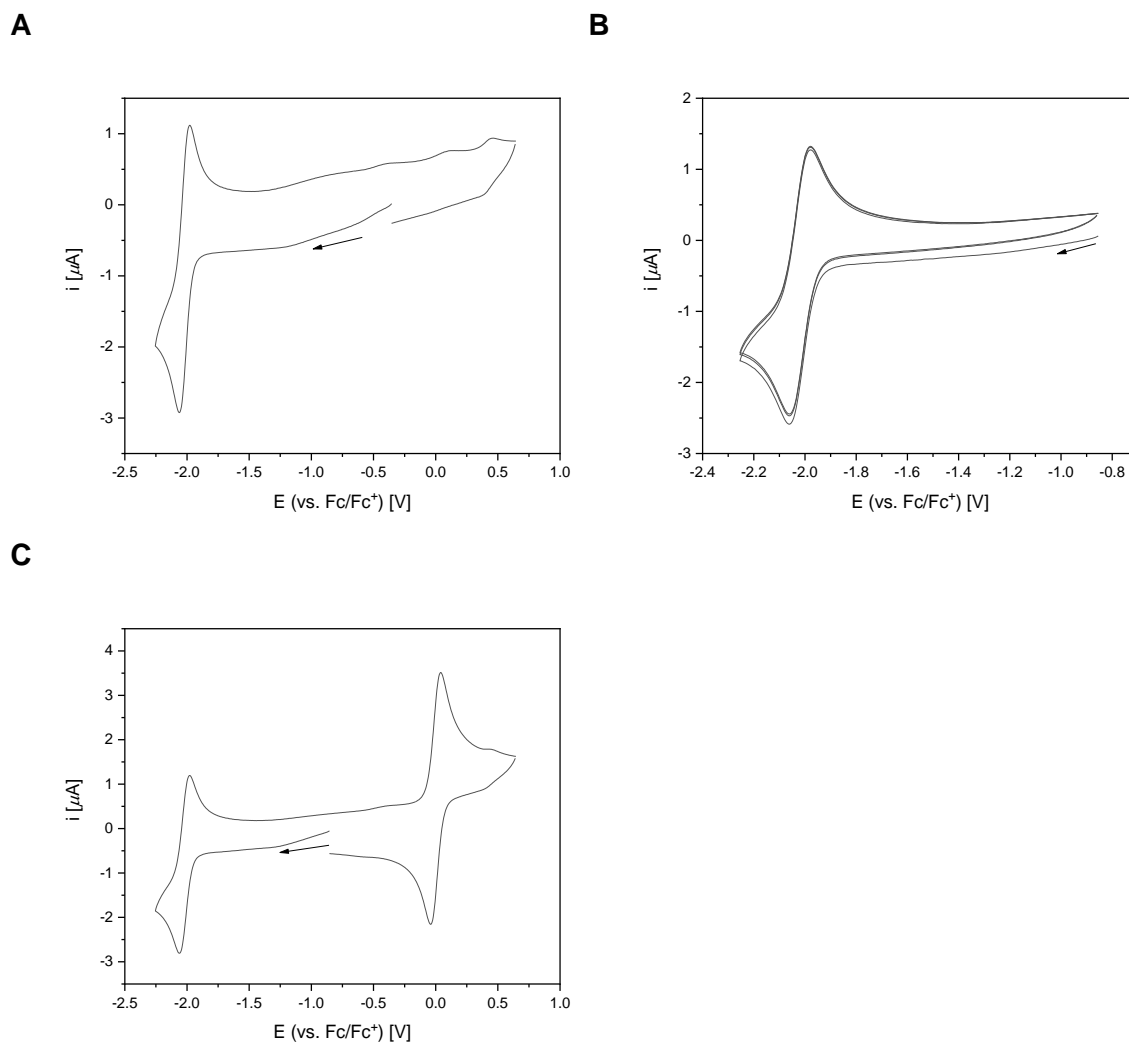


Figure 11.5: **A**) Cyclic voltammogram of **3.3c** in MeCN. **B**) Reversible reduction of **3.3c** in MeCN. **C**) Cyclic voltammogram of **3.3c** in MeCN in the presence of Fc/Fc⁺.

11.1.2 Chapter 4

11.1.2.1 Neutral bis-Triarylboranes

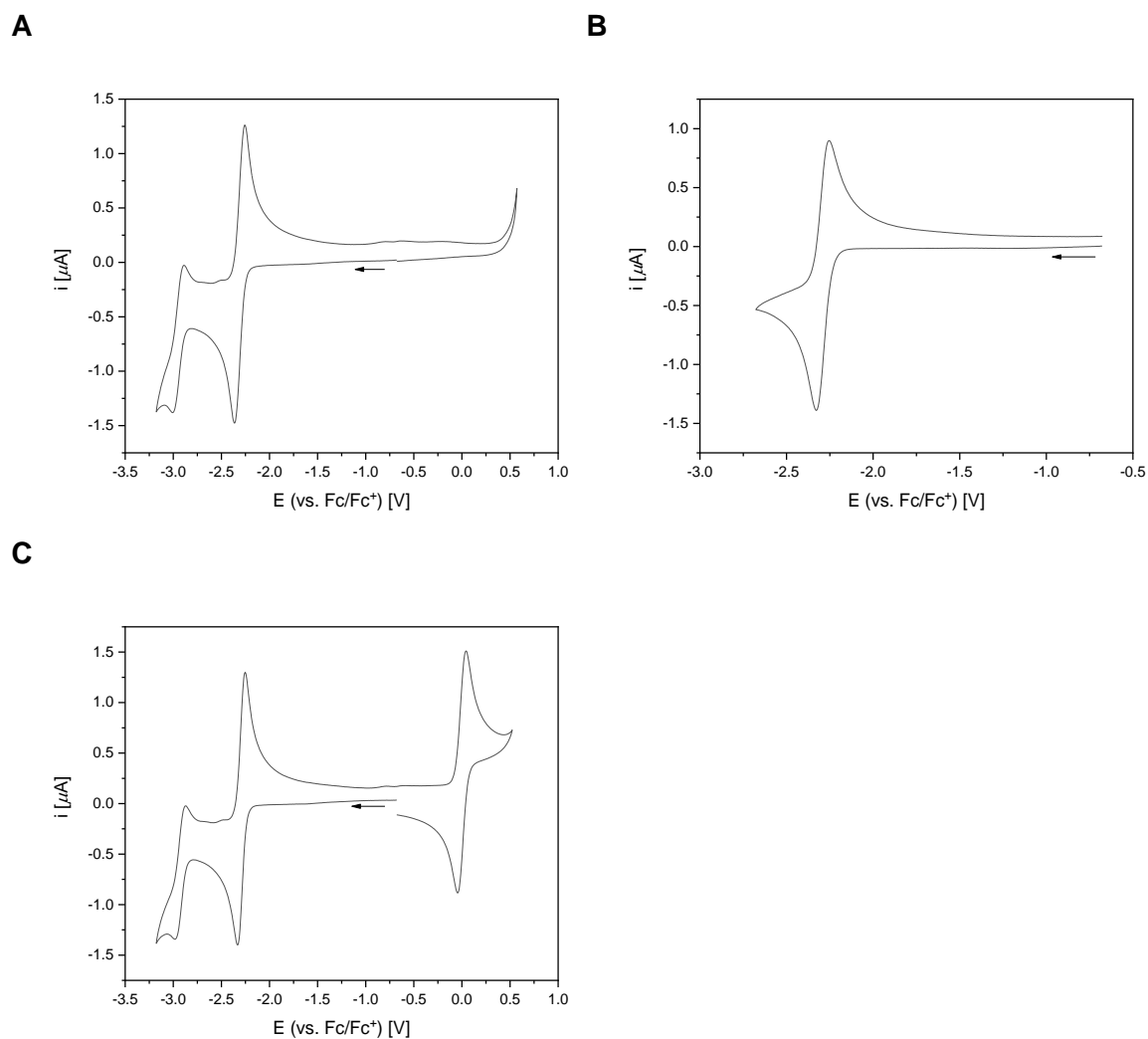


Figure 11.6: **A)** Cyclic voltammogram of **Neut0** in THF. **B)** Reversible Reduction of **Neut0** in THF. **C)** Cyclic voltammogram of **Neut0** in THF in the presence of Fc/Fc^+ .

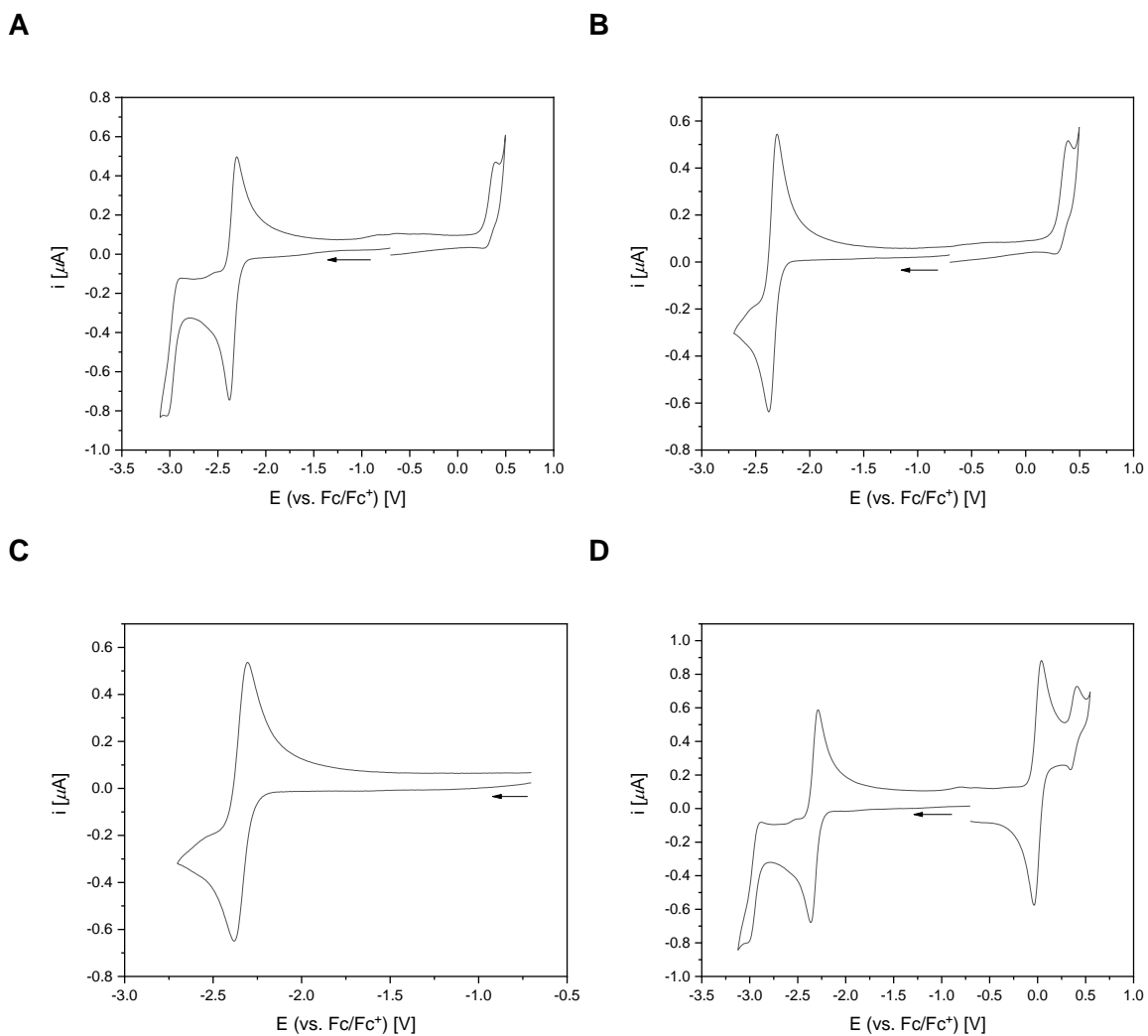


Figure 11.7: **A)** Cyclic voltammogram of **Neut1** in THF. **B)** First reduction and first oxidation of **Neut1** in THF. **C)** Reversible Reduction of **Neut1** in THF. **D)** Cyclic voltammogram of **Neut1** in THF in the presence of Fc/Fc^+ .

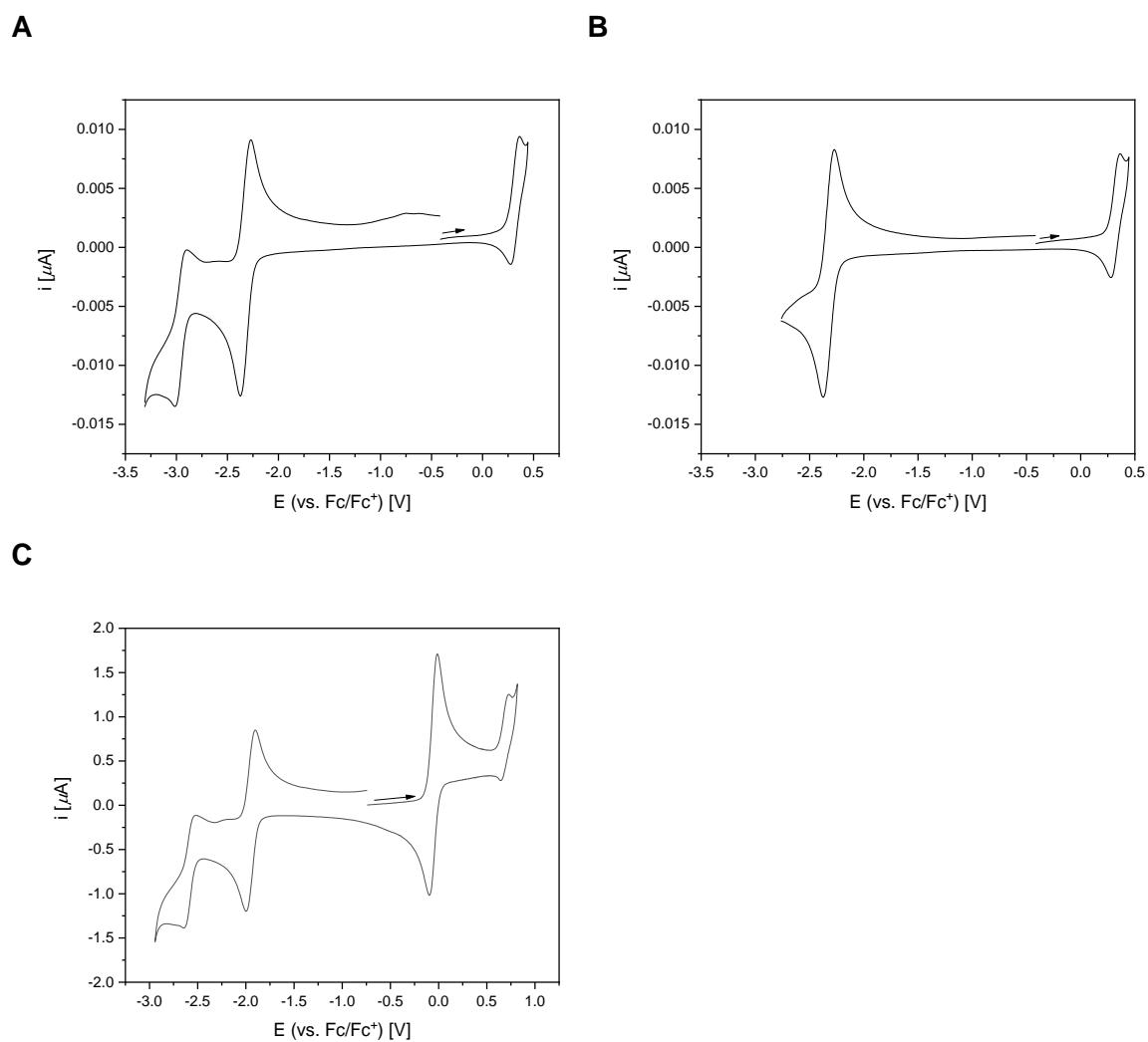


Figure 11.8: **A)** Cyclic voltammogram of **Neut2** in THF. **B)** First reduction and first oxidation of **Neut2** in THF. **C)** Cyclic voltammogram of **Neut2** in THF in the presence of Fc/Fc^+ .

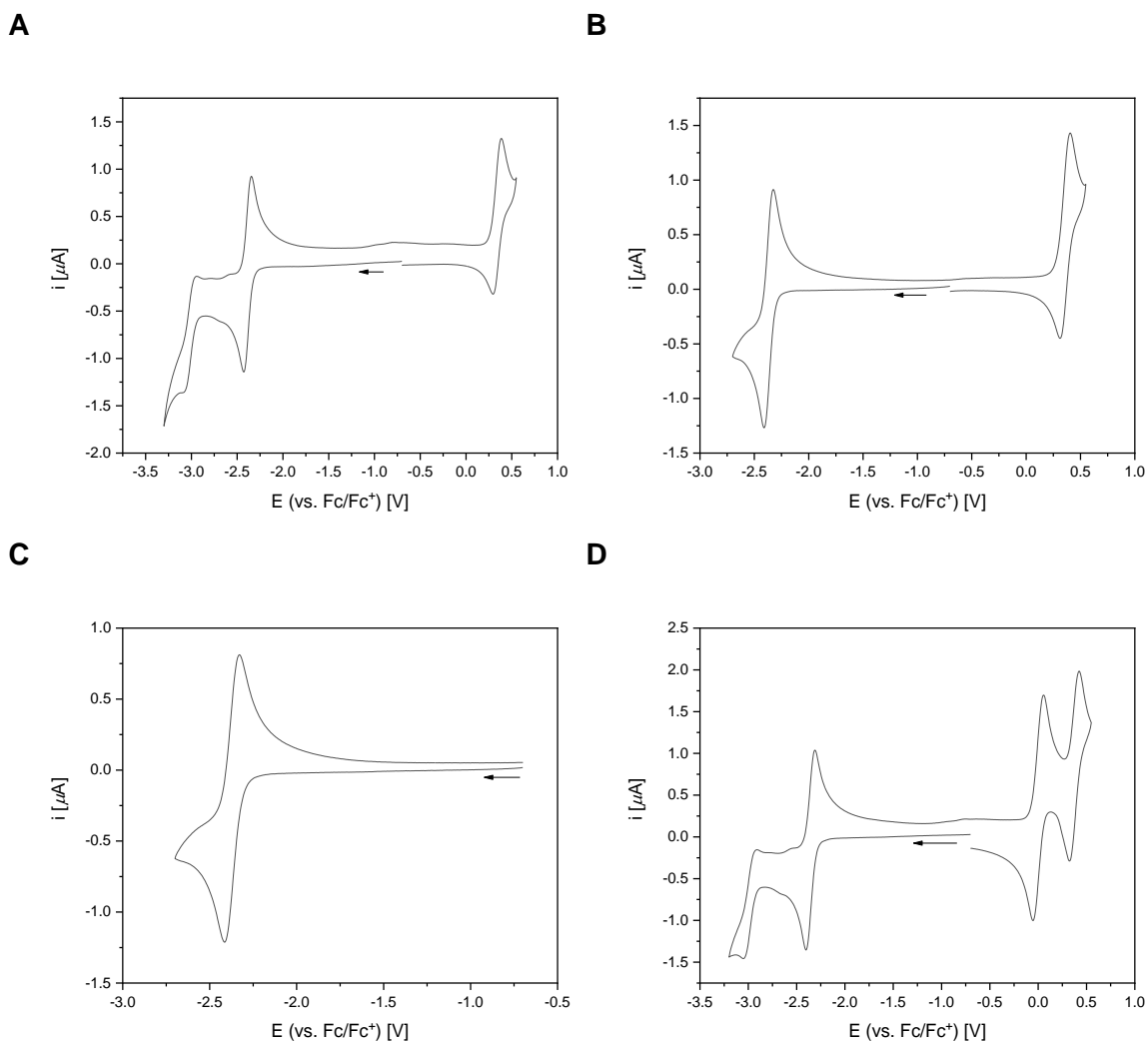


Figure 11.9: **A)** Cyclic voltammogram of **Neut(i)2** in THF. **B)** First reduction and first oxidation of **Neut(i)2** in THF. **C)** Reversible Reduction of **Neut(i)2** in THF. **D)** Cyclic voltammogram of **Neut(i)2** in THF in the presence of Fc/Fc^+ .

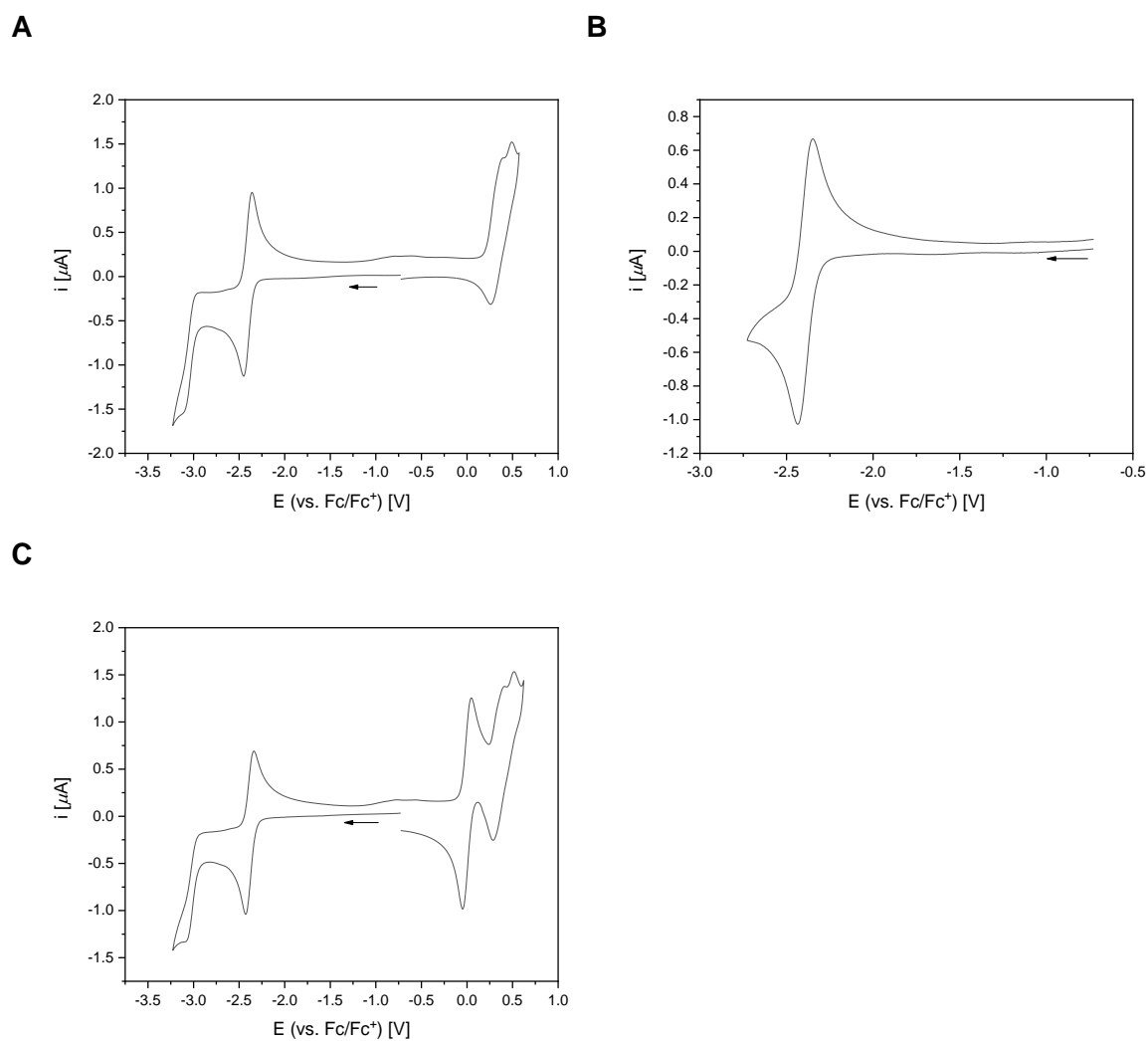


Figure 11.10: **A)** Cyclic voltammogram of **Neut3** in THF. **B)** Reversible reduction of **Neut3** in THF. **C)** Cyclic voltammogram of **Neut3** in THF in the presence of Fc/Fc^+ .

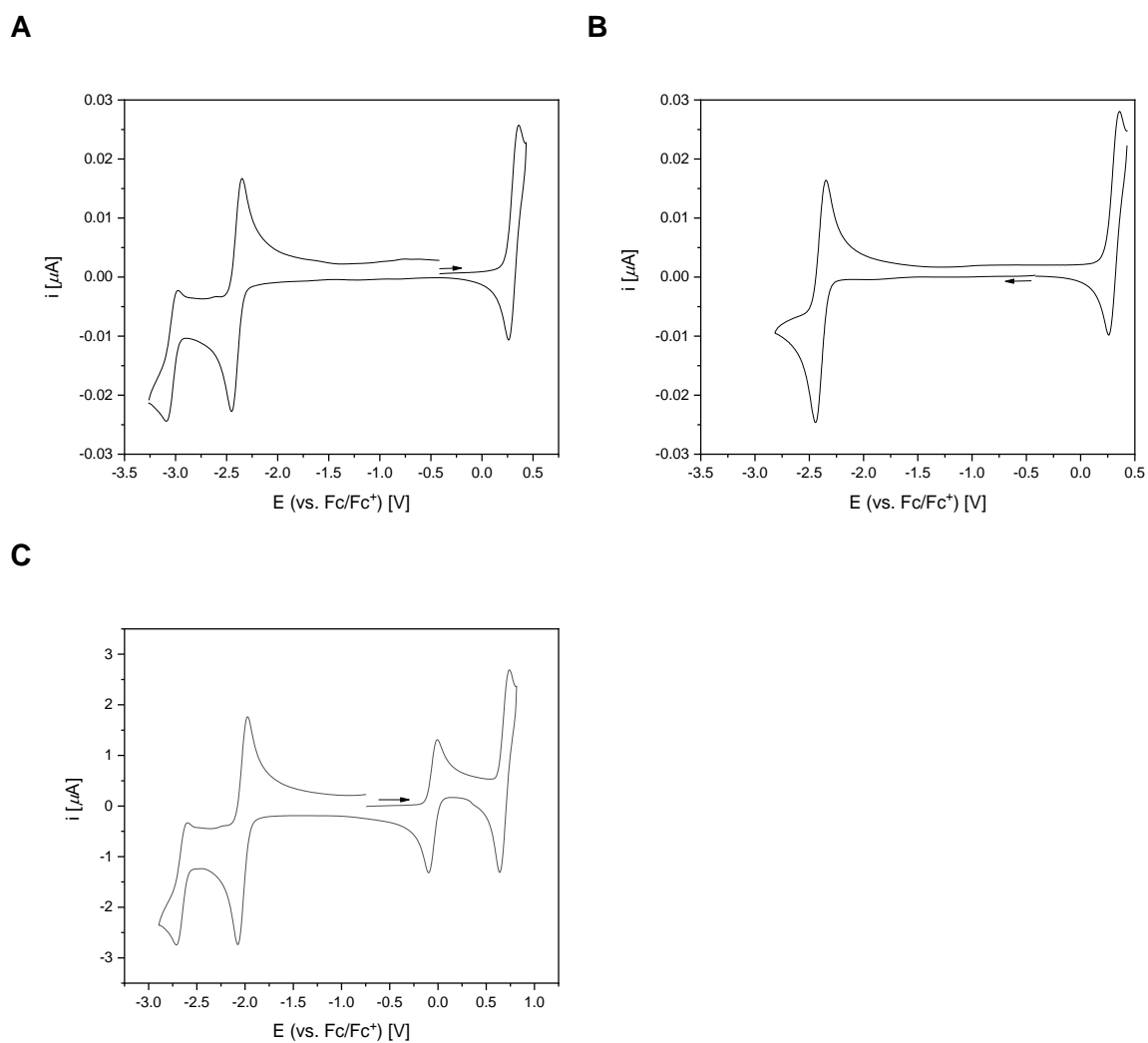


Figure 11.11: **A)** Cyclic voltammogram of **Neut4** in THF. **B)** First reduction and first oxidation of **Neut4** in THF. **C)** Cyclic voltammogram of **Neut4** in THF in the presence of Fc/Fc^+ .

11.1.2.2 Cationic bis-Triarylboranes

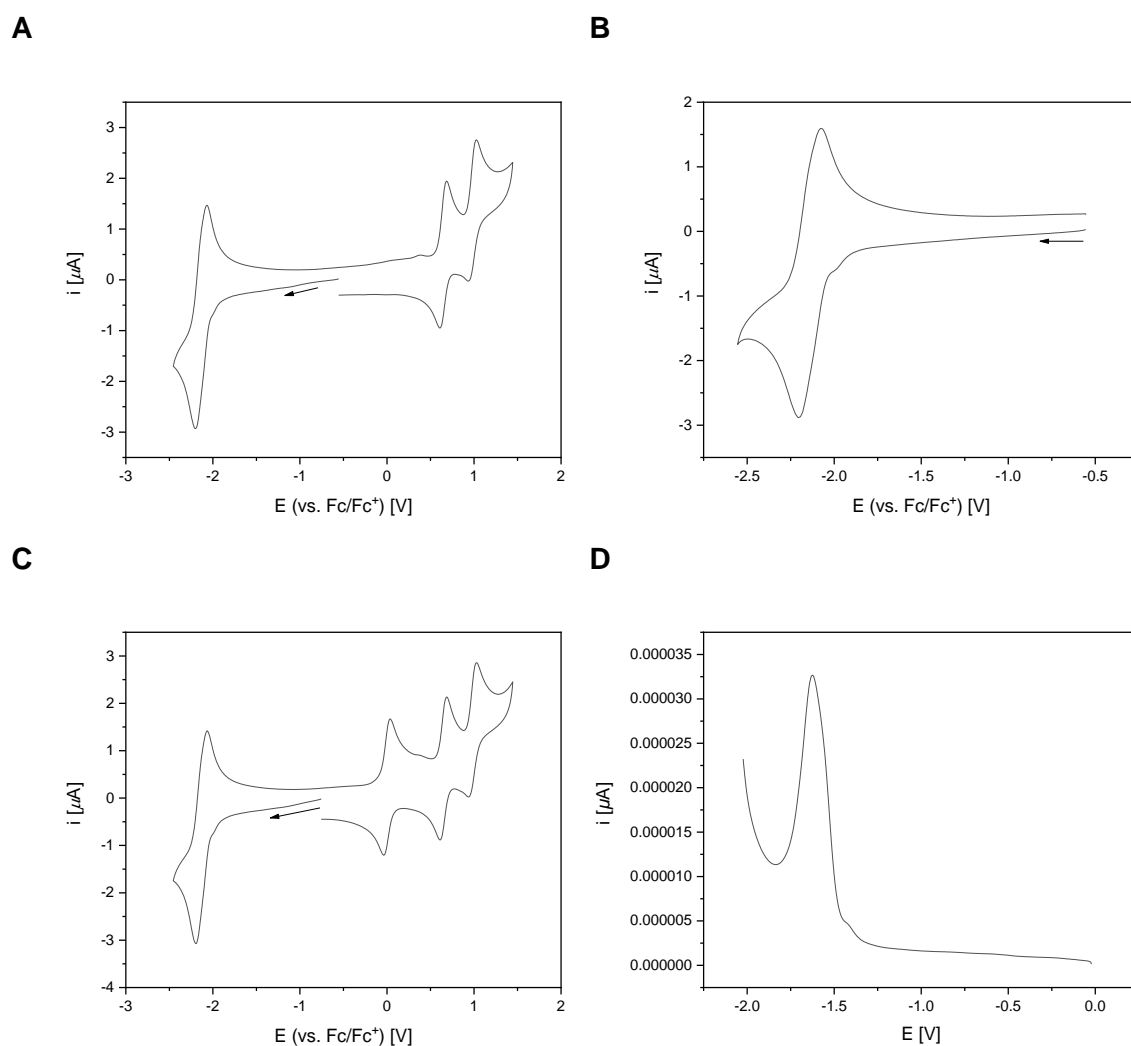


Figure 11.12: **A)** Cyclic voltammogram of Cat^{1+} in MeCN. **B)** Reversible reduction of Cat^{1+} in MeCN. **C)** Cyclic voltammogram of Cat^{1+} in MeCN in the presence of Fc/Fc^+ . **D)** Square wave experiment for Cat^{1+} in THF.

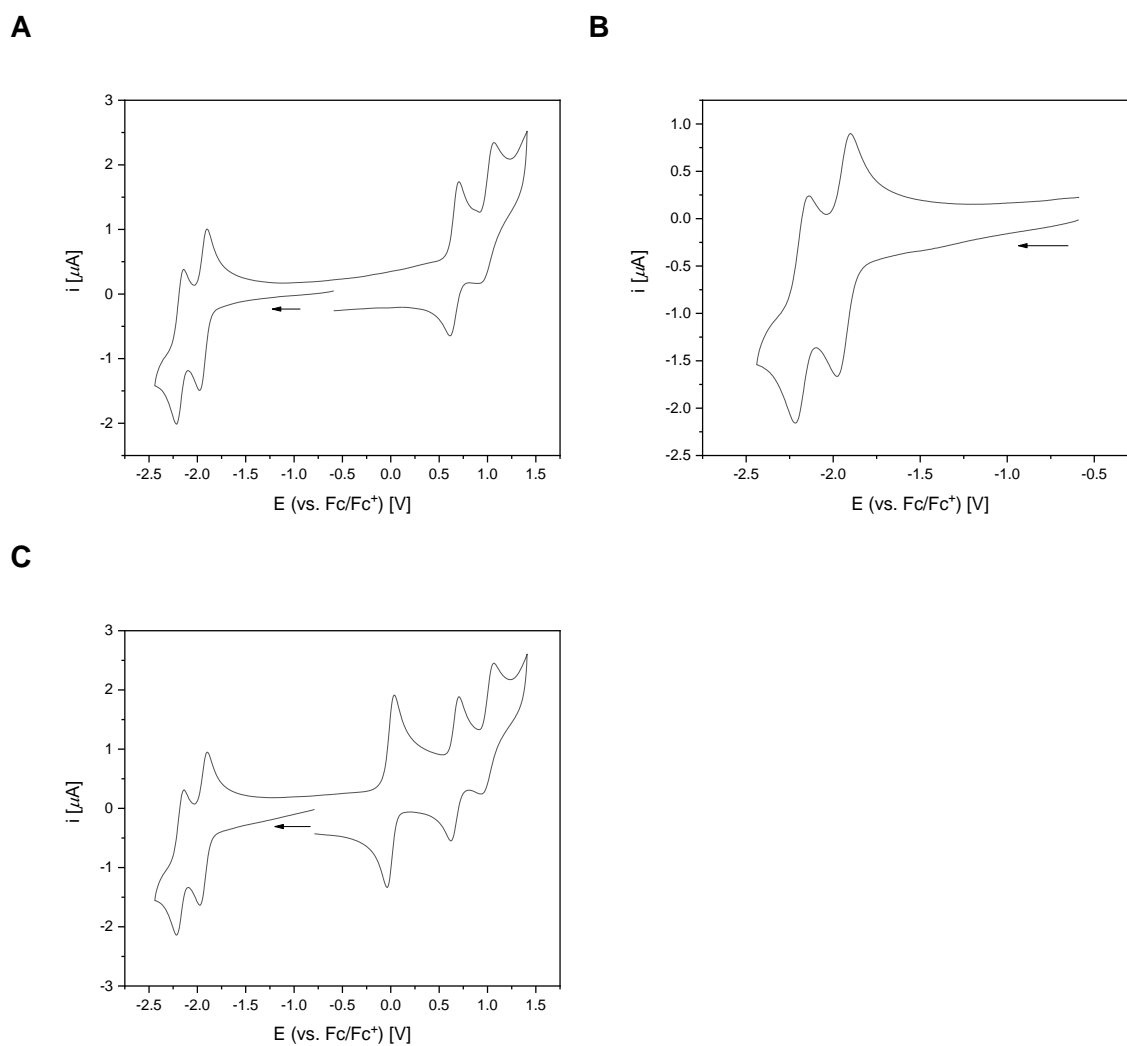


Figure 11.13: **A)** Cyclic voltammogram of Cat^{2+} in MeCN. **B)** Reversible reduction of Cat^{2+} in MeCN. **C)** Cyclic voltammogram of Cat^{2+} in MeCN in the presence of Fc/Fc^+ .

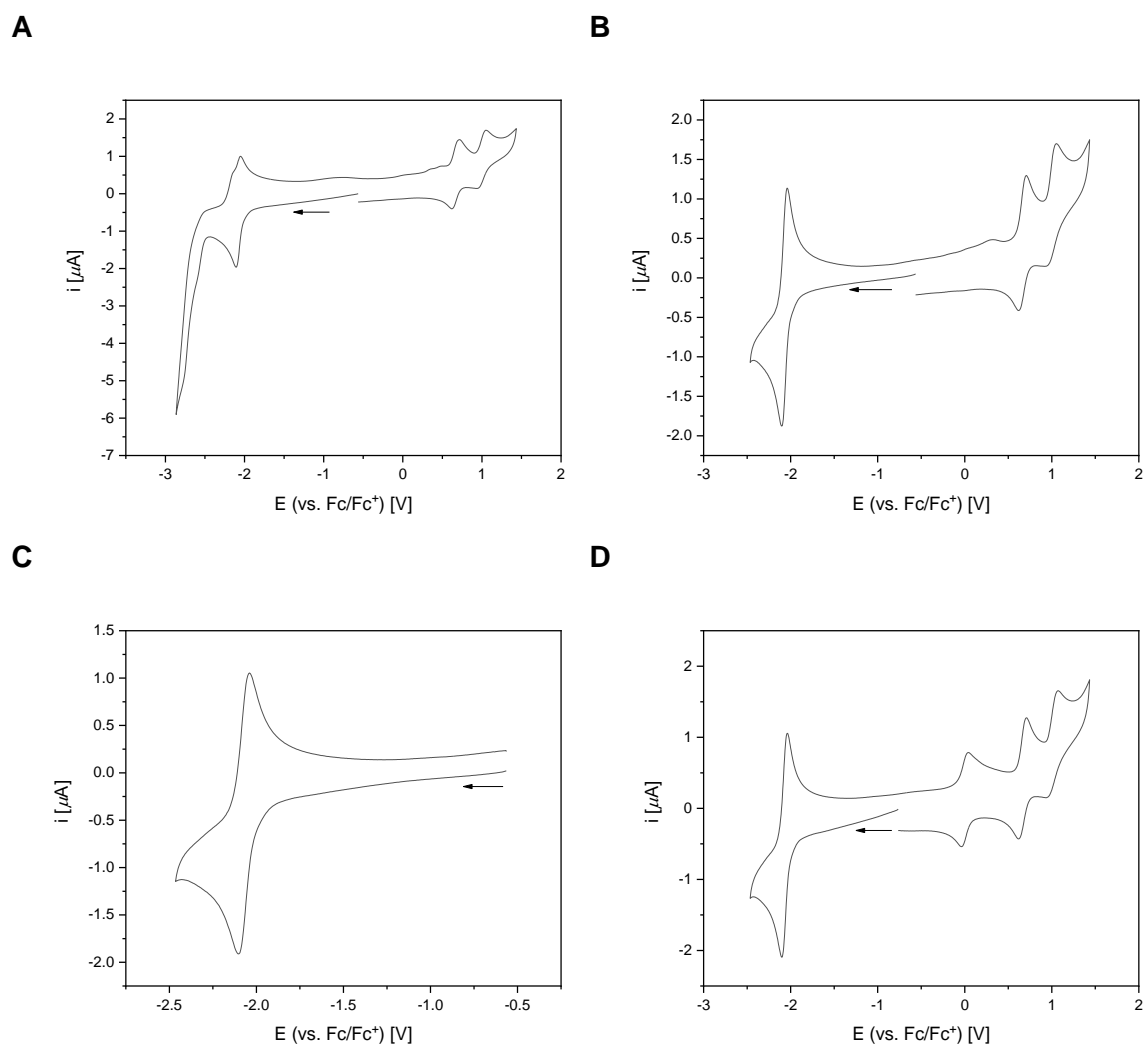


Figure 11.14: **A)** Cyclic voltammogram of $\text{Cat}(\text{i})^{2+}$ in MeCN. **B)** Cyclic voltammogram of $\text{Cat}(\text{i})^{2+}$ in MeCN without irreversible reduction. **C)** Reversible reduction of $\text{Cat}(\text{i})^{2+}$ in MeCN. **D)** Cyclic voltammogram of $\text{Cat}(\text{i})^{2+}$ in MeCN in the presence of Fc/Fc^+ .

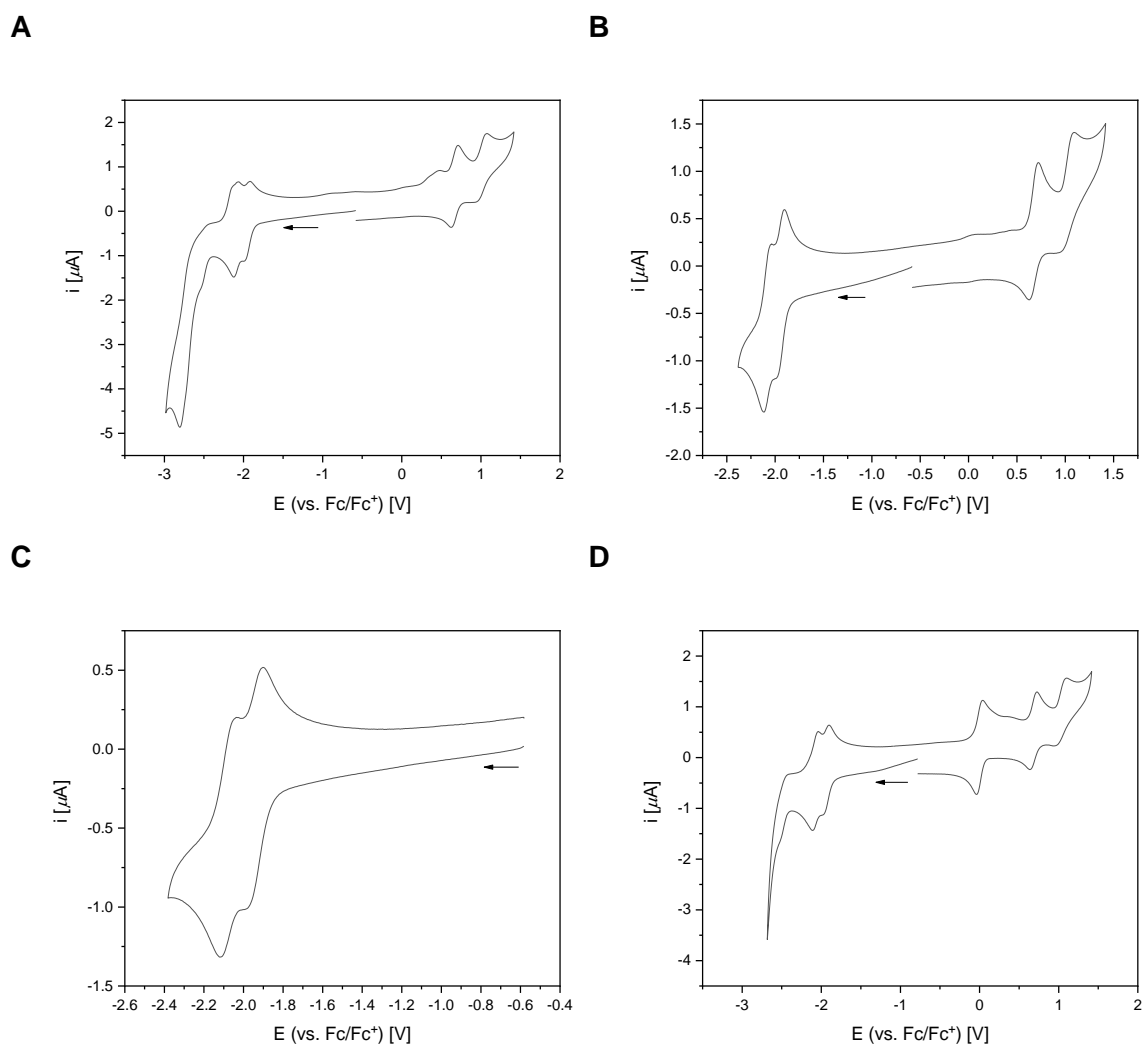


Figure 11.15: **A)** Cyclic voltammogram of Cat^{3+} in MeCN. **B)** Cyclic voltammogram of Cat^{3+} in MeCN without irreversible reduction. **C)** Reversible reduction of Cat^{3+} in MeCN. **D)** Cyclic voltammogram of Cat^{3+} in MeCN in the presence of Fc/Fc^+ .

11.2 Singlet Oxygen Sensitization

Note that absorption and emission spectra of all compounds recorded after the singlet oxygen measurement remained unchanged (**Fehler! Verweisquelle konnte nicht gefunden werden.**,).

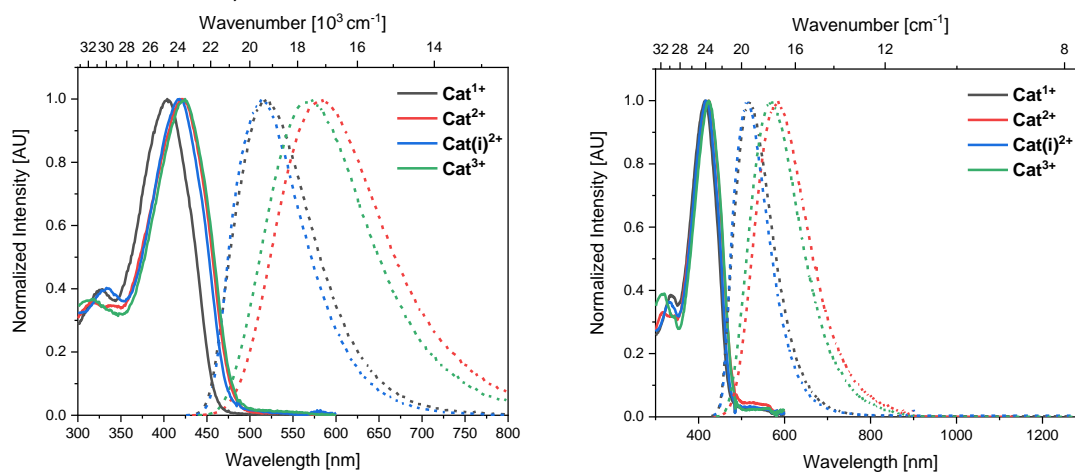


Figure 11.16: Comparison of absorption and emission spectra of **Cat¹⁺-Cat³⁺** recorded in acetonitrile before (left) and after (right) singlet oxygen measurement. [Note: emission measured from 430-900 nm with the red-sensitive photomultiplier (PMT-R928P) detector, and from 900.5 to 1300 nm with the near-IR PMT detector described in the general experimental details.]

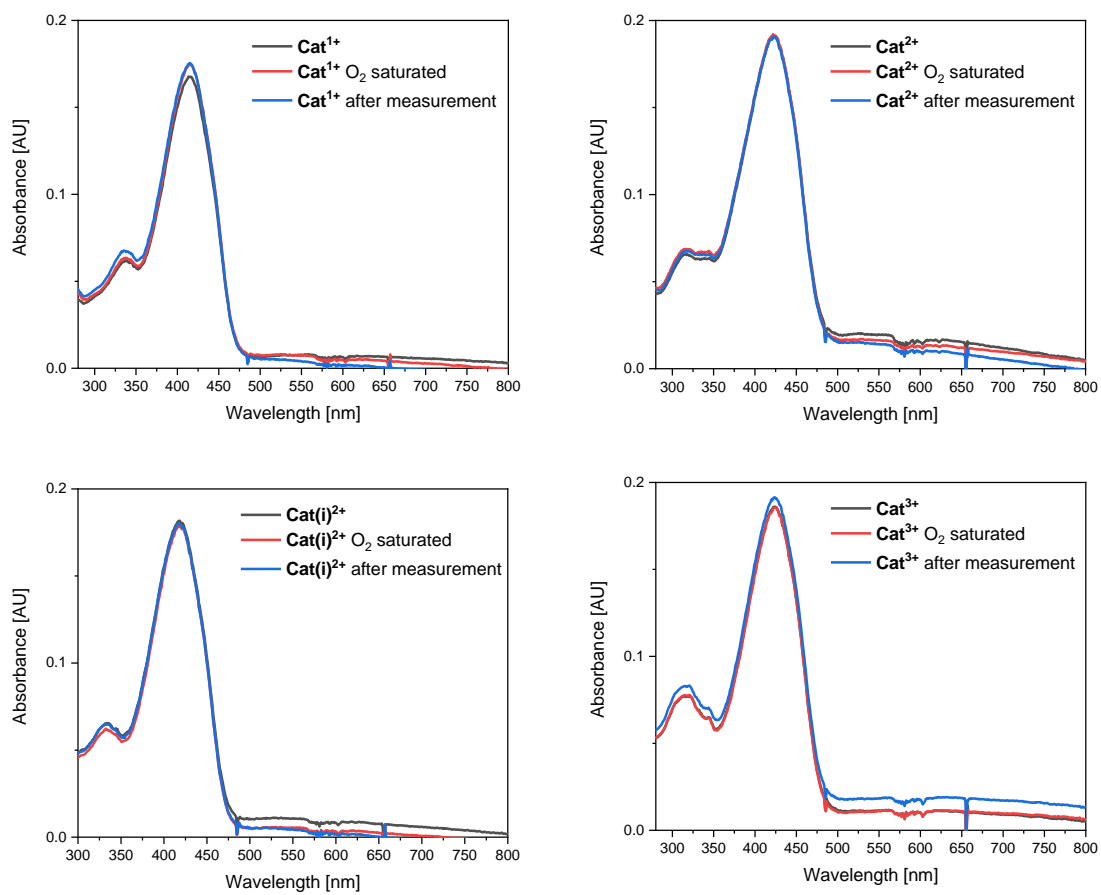


Figure 11.17: Absorption spectra of **Cat¹⁺**-**Cat³⁺** in solution, in O₂ saturated solution and after measurement of singlet oxygen sensing.

11.3 Studies in Buffered Solutions

11.3.1 Chapter 6

11.3.1.1 Physico-Chemical Properties of **Cat¹⁺-Cat³⁺** in Buffered Solution

11.3.1.1.1 Solubility in Sodium Cacodylate at pH 7

DMSO stock solutions of **Cat¹⁺**, **Cat²⁺**, **Cat(i)²⁺** and **Cat³⁺** were diluted with sodium cacodylate solutions (pH 7, I = 0.05 M) to concentrations of ca. $2 \times 10^{-5} - 8 \times 10^{-6}$ M. The corresponding absorption maxima and molar extinction coefficients are very similar for buffered solutions containing small amounts of DMSO and water solutions containing max. 1% acetonitrile (Table 11.2). The same is true for the respective emission spectra. However, upon heating, the emission of **Cat¹⁺**, **Cat²⁺**, and **Cat³⁺** is quenched by ca. 40-50%. In contrast, the emission of **Cat(i)²⁺** increases by ca. 15% upon heating. After cooling to room temperature, the emission of **Cat²⁺** and **Cat³⁺** was restored, while the spectra of **Cat¹⁺** and **Cat(i)²⁺** were not.

11.3.1.1.2 Stability of UV/Vis Spectra

The UV/Vis spectra of examined compounds were recorded in sodium cacodylate buffer (c = 0.05 M) at pH 7 (Figure 11.18-Figure 11.21). Absorbancies of aqueous solutions of the compounds were proportional to their concentrations up to concentrations $c = 2 \times 10^{-5}$ M. The absorption maxima and the corresponding molar extinction coefficients are given in Table 11.2.

Table 11.2: Absorption maxima and molar extinction coefficient of **Cat¹⁺-Cat³⁺** determined in 1% MeCN in water and DMSO in sodium cacodylate.

	DMSO in sodium cacodylate		1% MeCN in water	
	λ_{max}^{abs} [nm]	ϵ [L mol ⁻¹ cm ⁻¹]	λ_{max}^{abs} [nm]	ϵ [L mol ⁻¹ cm ⁻¹]
Cat¹⁺	414	33 300 ±600	415	29 500 ±1 200
Cat²⁺	422	37 700 ±900	424	31 100 ±300
Cat(i)²⁺	417	30 800 ±200	424	34 000 ±1 500
Cat³⁺	421	30 900 ±700	423	36 000 ±900

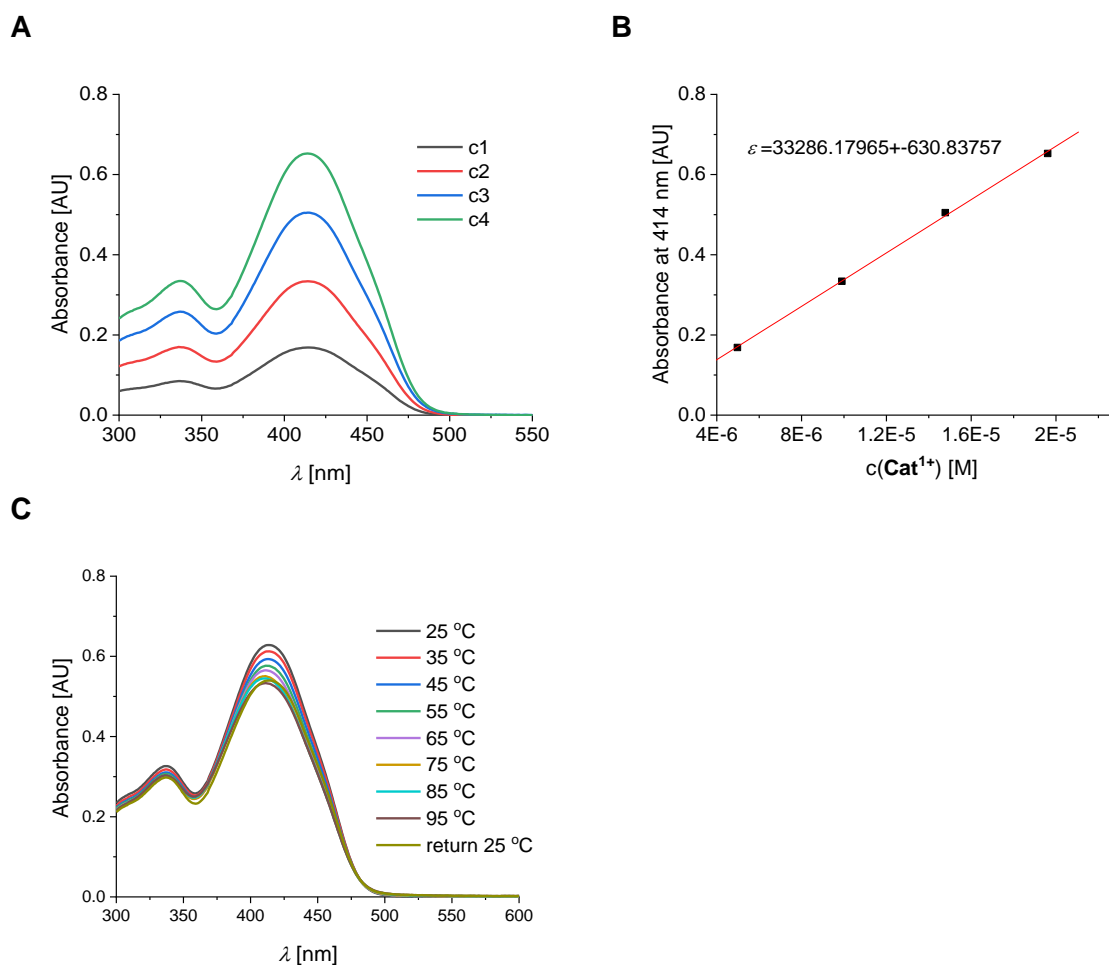


Figure 11.18: **A**) UV/Vis spectra of Cat^{1+} ($c = 4.9 \times 10^{-6} - 2 \times 10^{-5}$ M). **B**) Linear dependence (—) of the absorbance at 414 nm (■) on the concentration of Cat^{1+} . **C**) Temperature dependence ($T = 25$ °C – 95 °C) of UV/Vis spectra ($c = 2 \times 10^{-5}$ M; sodium cacodylate buffer, pH = 7, $I = 0.05$ M).

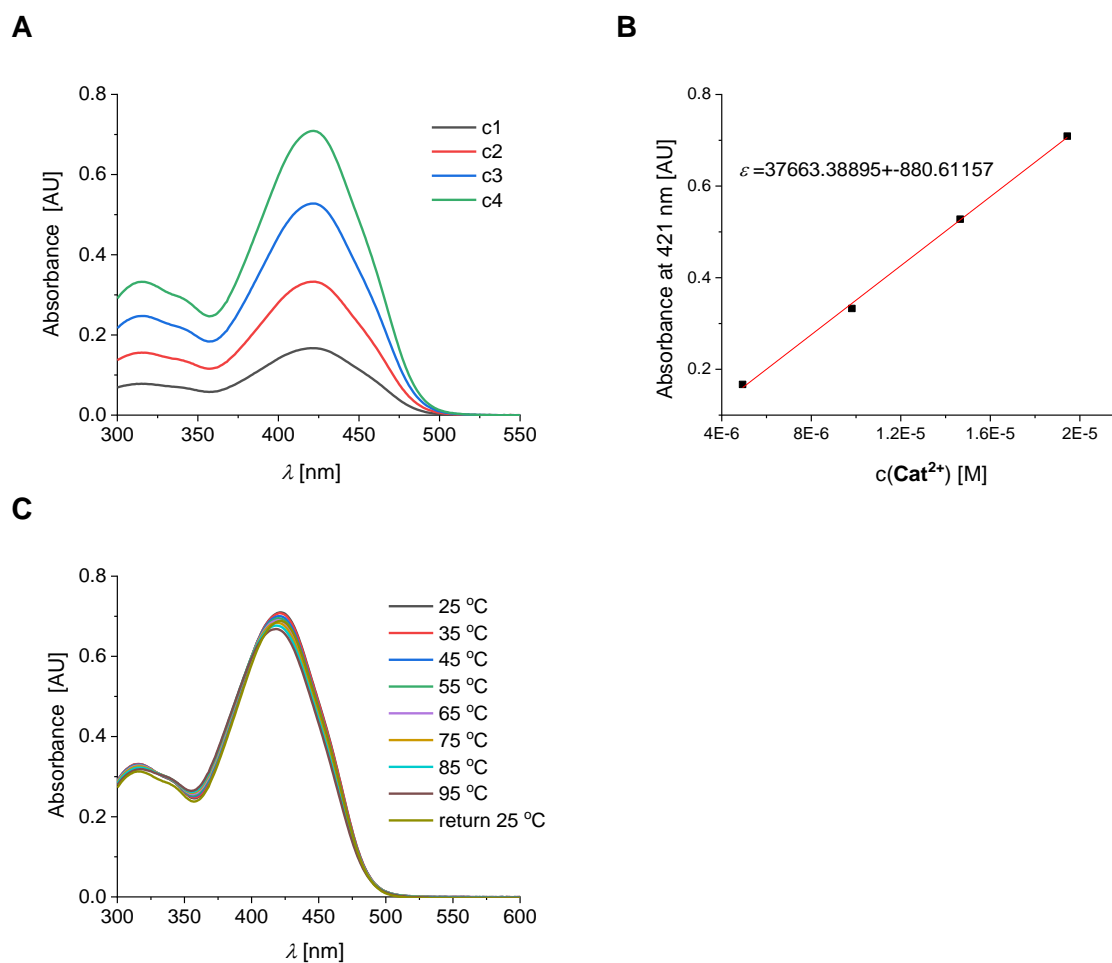


Figure 11.19: **A**) UV/Vis spectra of Cat^{2+} ($c = 4.9 \times 10^{-6} - 2 \times 10^{-5}$ M). **B**) Linear dependence (—) of the absorbance at 422 nm (■) on the concentration of Cat^{2+} . **C**) Temperature dependence ($T = 25\text{ °C} - 95\text{ °C}$) of the UV/Vis spectra ($c = 2 \times 10^{-5}$ M; sodium cacodylate buffer, $\text{pH} = 7$, $I = 0.05$ M).

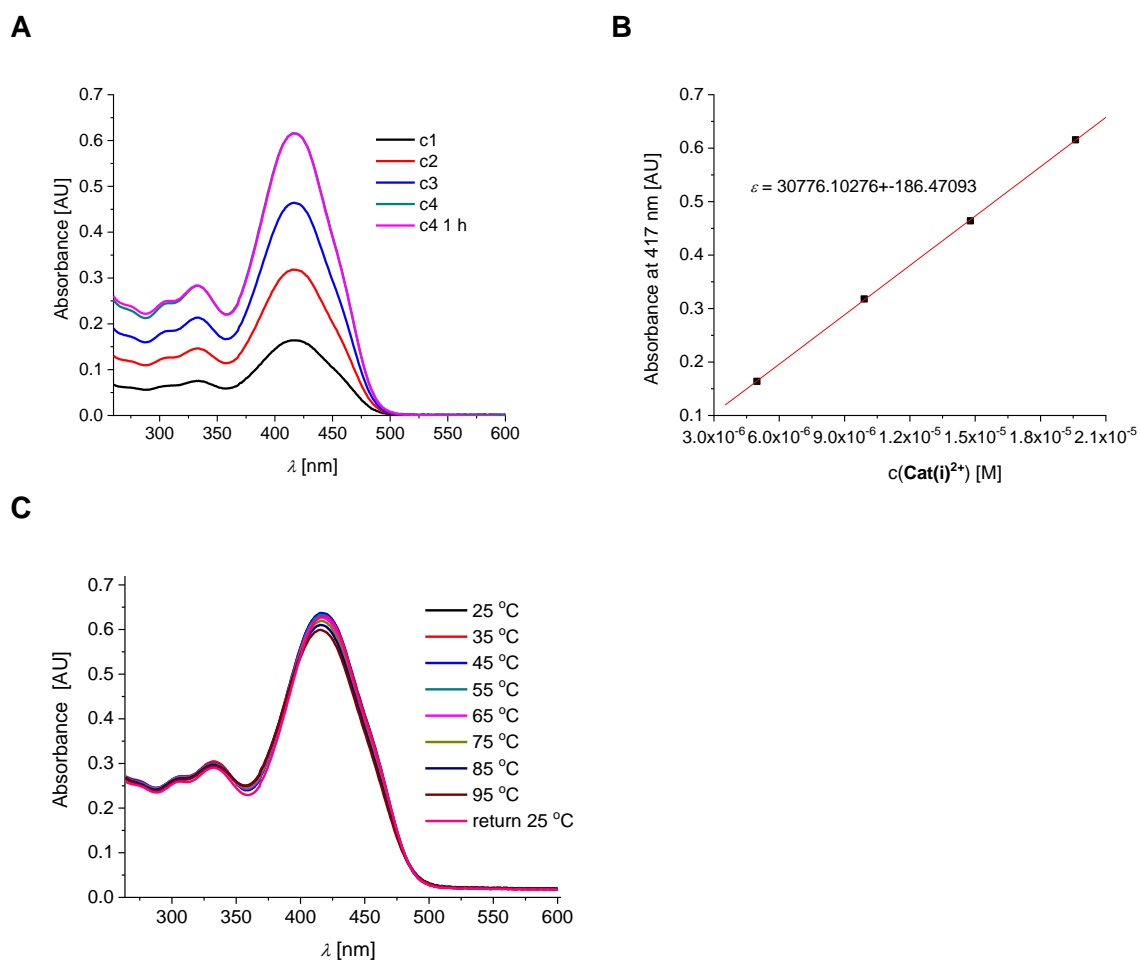


Figure 11.20: **A**) UV/Vis spectra of Cat(i)^{2+} ($c = 5 \times 10^{-6} - 2 \times 10^{-5}$ M). **B**) Linear dependence (—) of the absorbance at 417 nm (■) on the concentration of Cat(i)^{2+} . **C**) Temperature dependence ($T = 25 \text{ }^\circ\text{C} - 95 \text{ }^\circ\text{C}$) of UV/Vis spectra ($c = 2 \times 10^{-5}$ M; sodium cacodylate buffer, pH = 7, $I = 0.05$ M).

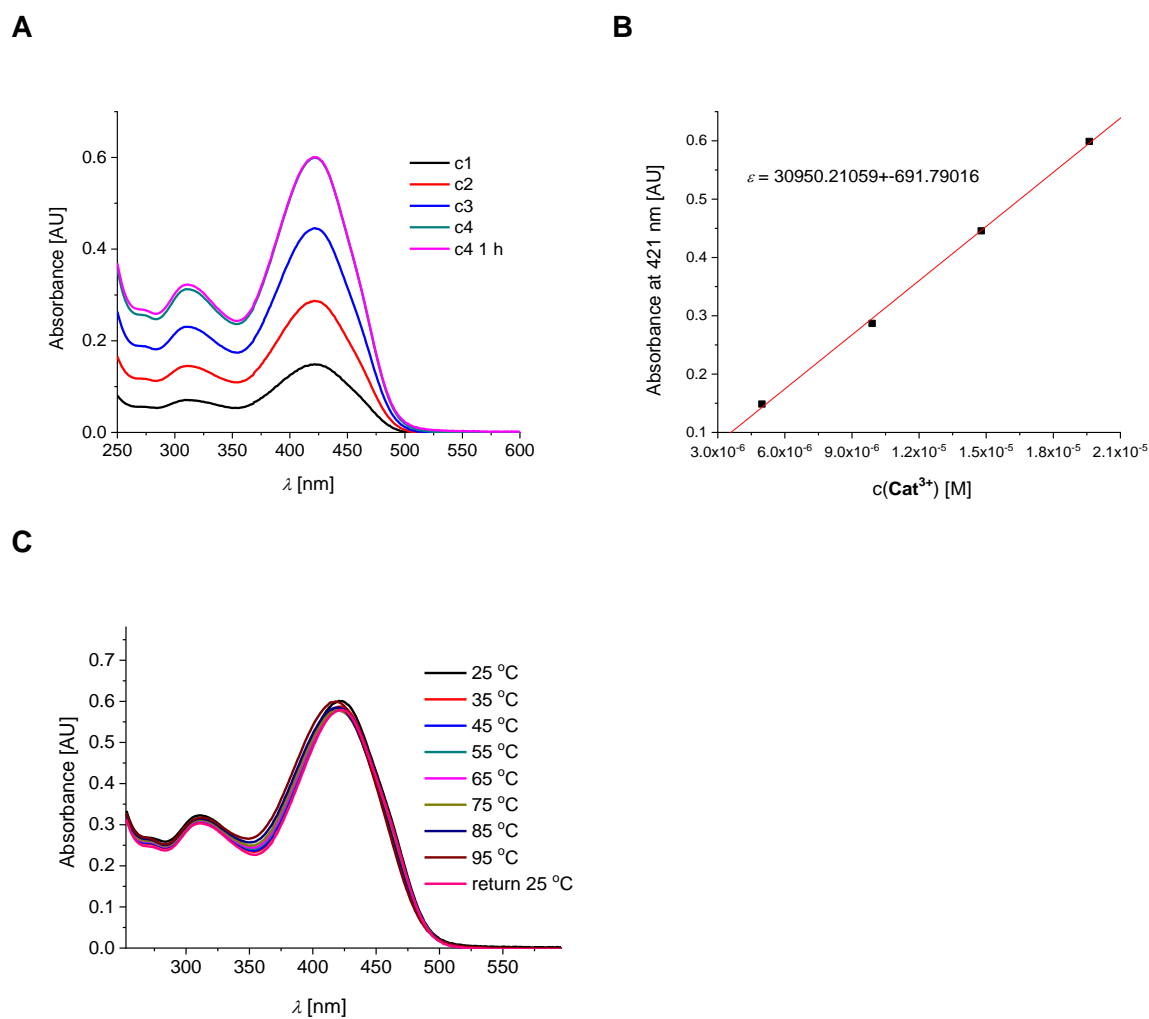


Figure 11.21: **A**) UV/Vis spectra of Cat^{3+} ($c = 5 \times 10^{-6} - 2 \times 10^{-5}$ M). **B**) Linear dependence (—) of the absorbance at 421 nm (■) on the concentration of Cat^{3+} . **C**) Temperature dependence ($T = 25\text{ °C} - 95\text{ °C}$) of UV/Vis spectra ($c = 2 \times 10^{-5}$ M; sodium cacodylate buffer, $\text{pH} = 7$, $I = 0.05$ M).

11.3.1.1.3 Fluorimetric Spectra

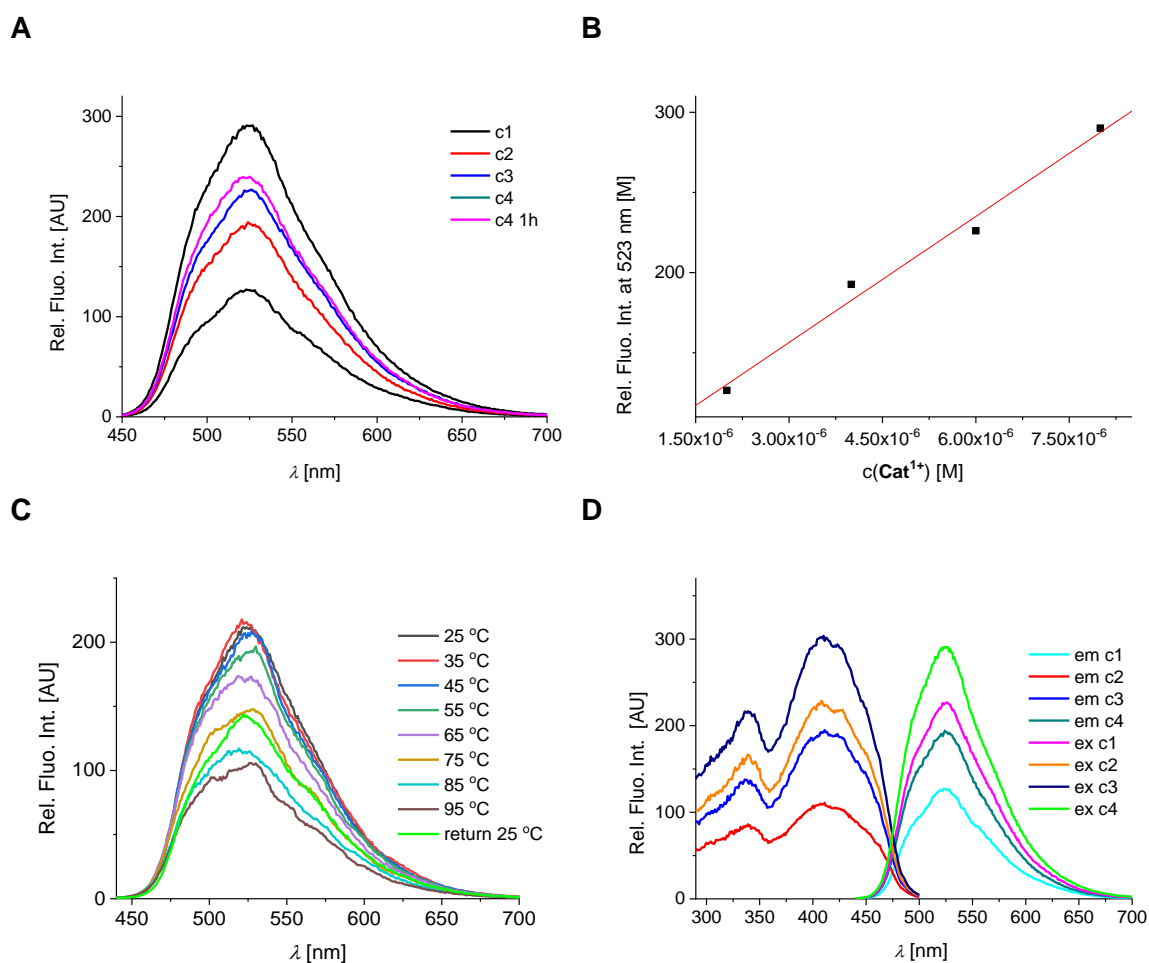


Figure 11.22: **A)** Emission spectra of Cat^{1+} ($\lambda_{\text{exc}} = 414 \text{ nm}$; $c = 2 \times 10^{-6} - 8 \times 10^{-6} \text{ M}$). **B)** Linear dependence (—) of the fluorescence intensity ($\lambda_{\text{exc}} = 414 \text{ nm}$, $\lambda_{\text{em}} = 523 \text{ nm}$) (■) on the concentration of Cat^{1+} . **C)** Influence of temperature increase ($T = 25 \text{ °C} - 95 \text{ °C}$) on fluorescence spectra of Cat^{1+} ($c = 8 \times 10^{-6} \text{ M}$; sodium cacodylate buffer, $\text{pH} = 7$, $I = 0.05 \text{ M}$). **D)** Comparison of emission and excitation spectra ($\lambda_{\text{em}} = 523 \text{ nm}$).

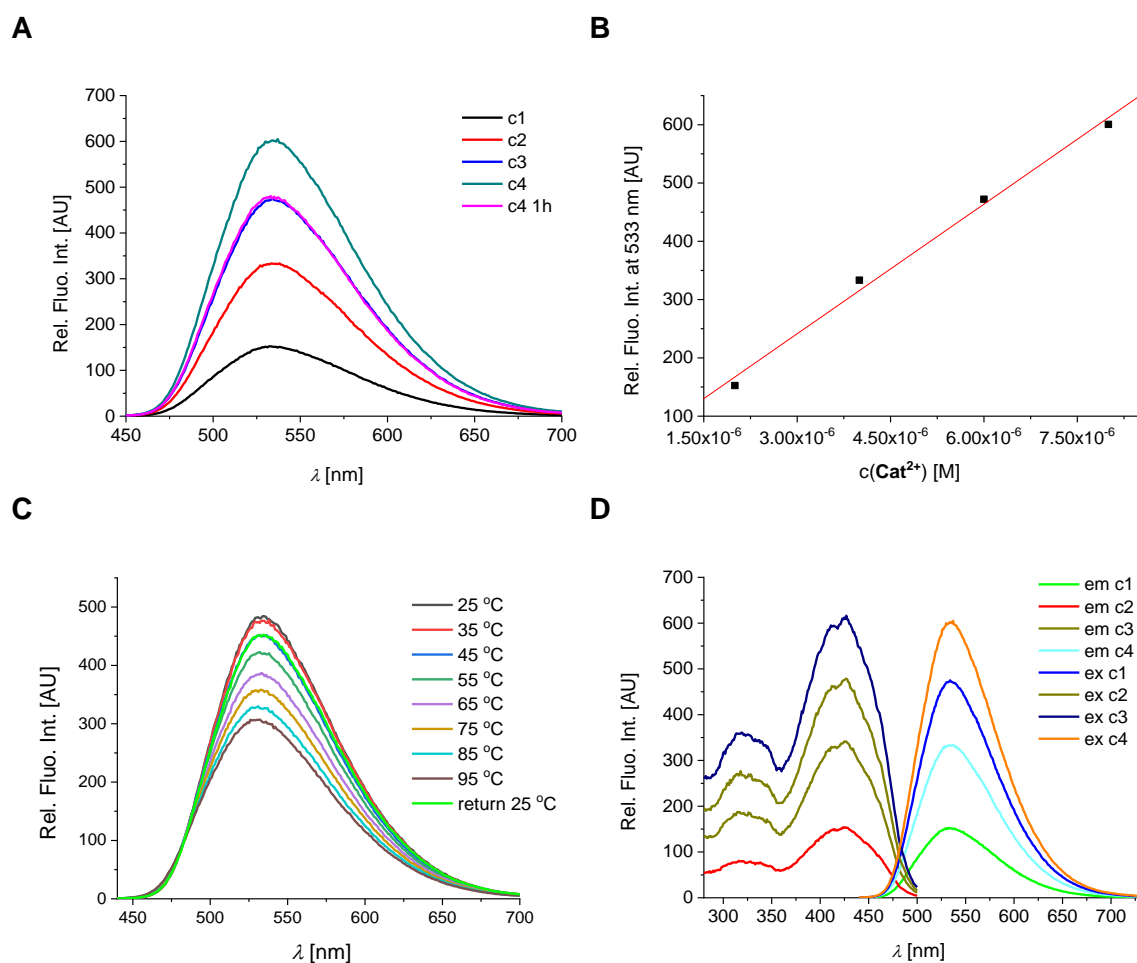


Figure 11.23: **A**) Emission spectra of Cat^{2+} ($\lambda_{\text{exc}} = 422$ nm; $c = 2 \times 10^{-6} - 8 \times 10^{-6}$ M). **B**) Linear dependence (—) of the fluorescence intensity ($\lambda_{\text{exc}} = 422$ nm, $\lambda_{\text{em}} = 533$ nm) (■) on the concentration of Cat^{2+} . **C**) Influence of temperature increase ($T = 25$ °C – 95 °C) on fluorescence spectra of Cat^{2+} ($c = 8 \times 10^{-6}$ M; sodium cacodylate buffer, pH = 7, $I = 0.05$ M). **D**) Comparison of emission and excitation spectra ($\lambda_{\text{em}} = 533$ nm).

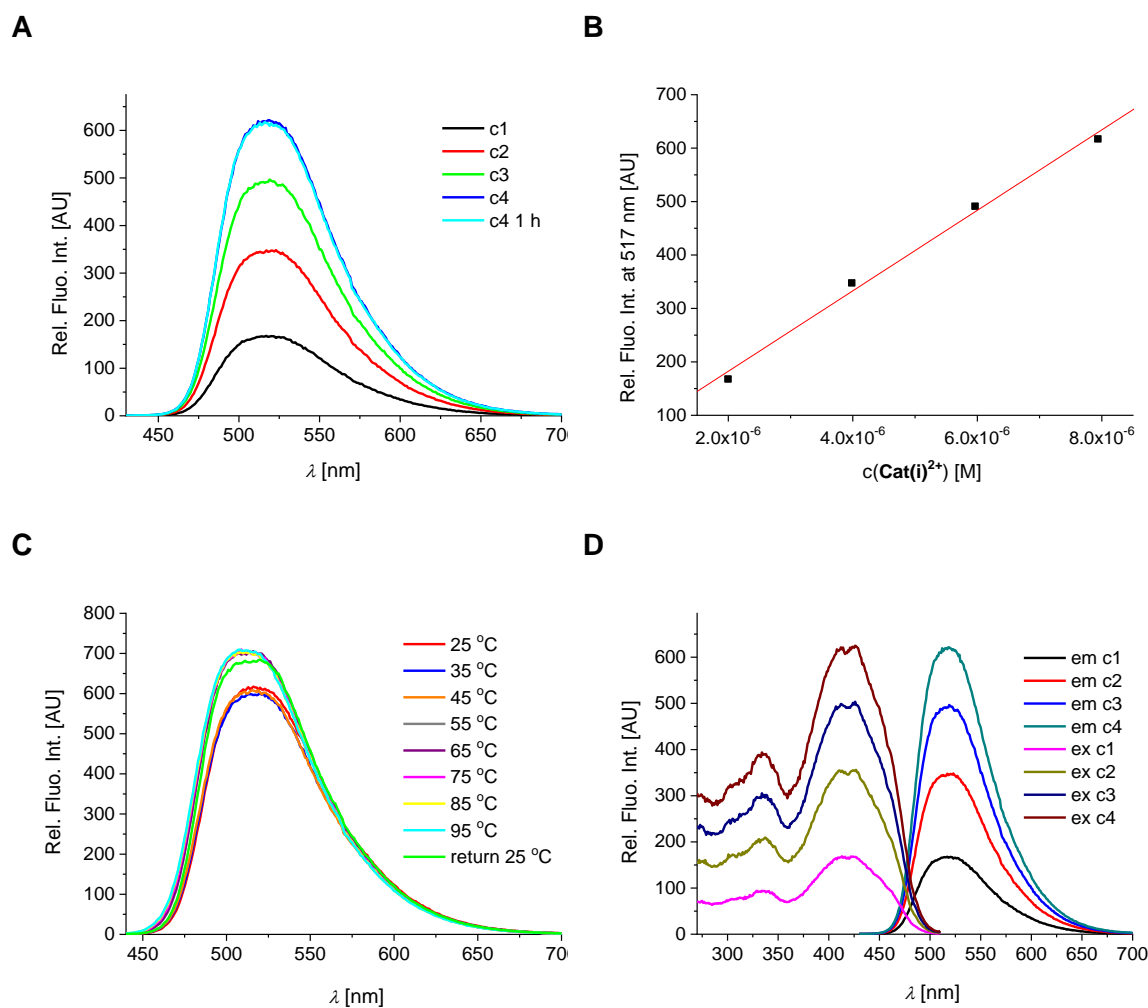


Figure 11.24: **A)** Emission spectra of Cat(i)^{2+} ($\lambda_{\text{exc}} = 417$ nm; $c = 2 \times 10^{-6} - 8 \times 10^{-6}$ M). **B)** Linear dependence (—) of the fluorescence intensity ($\lambda_{\text{exc}} = 417$ nm, $\lambda_{\text{em}} = 517$ nm) (■) on the concentration of Cat(i)^{2+} . **C)** Influence of temperature increase ($T = 25$ °C – 95 °C) on fluorescence spectra of Cat(i)^{2+} ($c = 8 \times 10^{-6}$ M; sodium cacodylate buffer, pH = 7, $I = 0.05$ M). **D)** Comparison of emission and excitation spectra ($\lambda_{\text{em}} = 517$ nm).

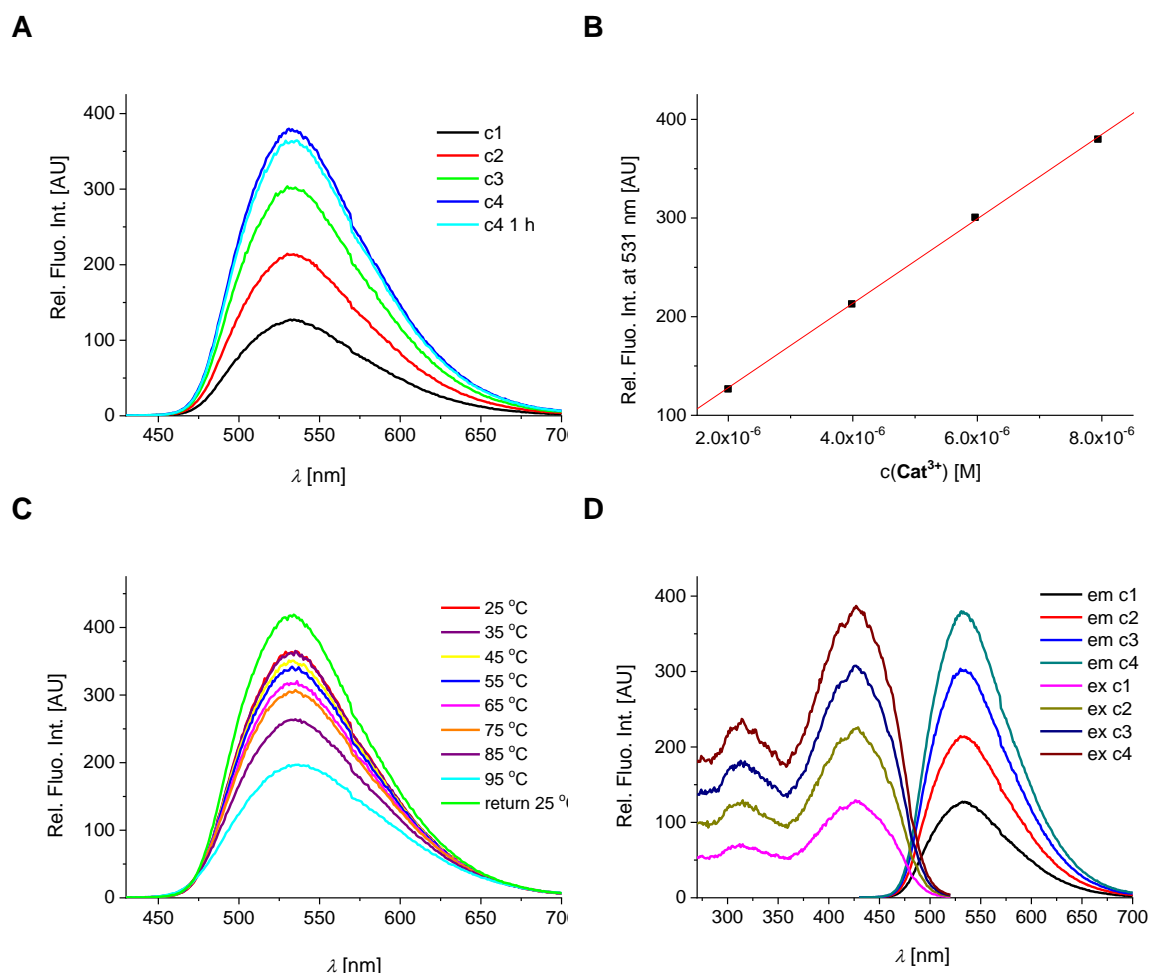


Figure 11.25: **A)** Emission spectra of Cat^{3+} ($\lambda_{\text{exc}} = 421$ nm; $c = 2 \times 10^{-6} - 8 \times 10^{-6}$ M). **B)** Linear dependence (—) of the fluorescence intensity ($\lambda_{\text{exc}} = 421$ nm, $\lambda_{\text{em}} = 531$ nm) (■) on the concentration of Cat^{3+} . **C)** Influence of temperature increase ($T = 25$ °C – 95 °C) on fluorescence spectra of Cat^{3+} ($c = 8 \times 10^{-6}$ M; sodium cacodylate buffer, pH = 7, $I = 0.05$ M). **D)** Comparison of emission and excitation spectra ($\lambda_{\text{em}} = 531$ nm).

11.3.1.2 Interaction of Cat^{1+} - Cat^{3+} with ctDNA, and pApU at pH 7

11.3.1.2.1 Thermal Melting Experiments

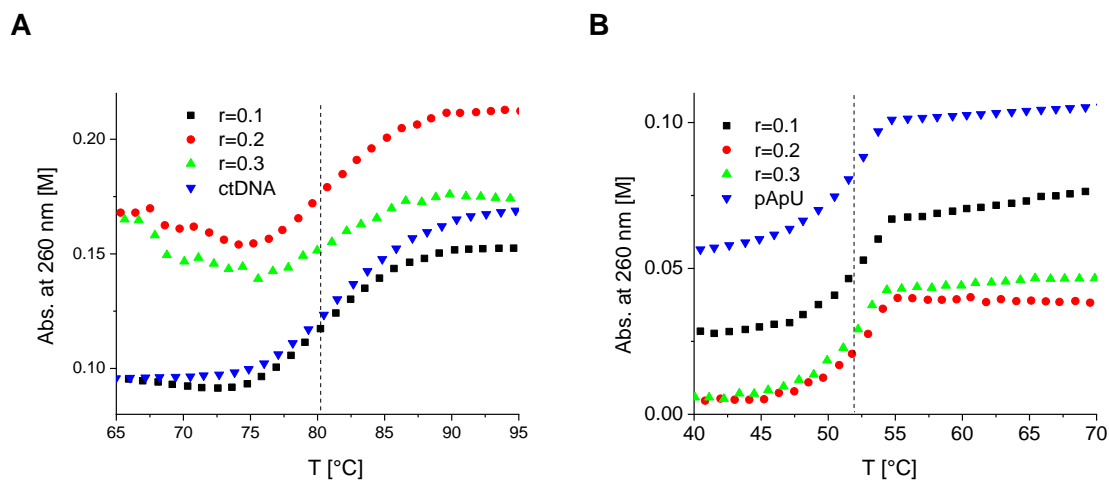


Figure 11.26: **A)** Thermal denaturation curves of ctDNA ($c(\text{ctDNA}) = 2.26 \times 10^{-5}$ M, $r_{[\text{Cat}^{1+}]/[\text{ctDNA}]} = 0.1$ to 0.3) at pH 7 (sodium cacodylate buffer, $I = 0.05$ M) upon addition of Cat^{1+} . Error in ΔT_m values: ± 0.5 °C. **B)** Thermal denaturation curves of pApU ($c(\text{pApU}) = 2.49 \times 10^{-5}$ M, $r_{[\text{Cat}^{1+}]/[\text{pApU}]} = 0.1$ to 0.3) at pH 7 (sodium cacodylate buffer, $I = 0.05$ M) upon addition of Cat^{1+} . Error in ΔT_m values: ± 0.5 °C. The vertical lines are added to chart the changes of the melting temperatures.

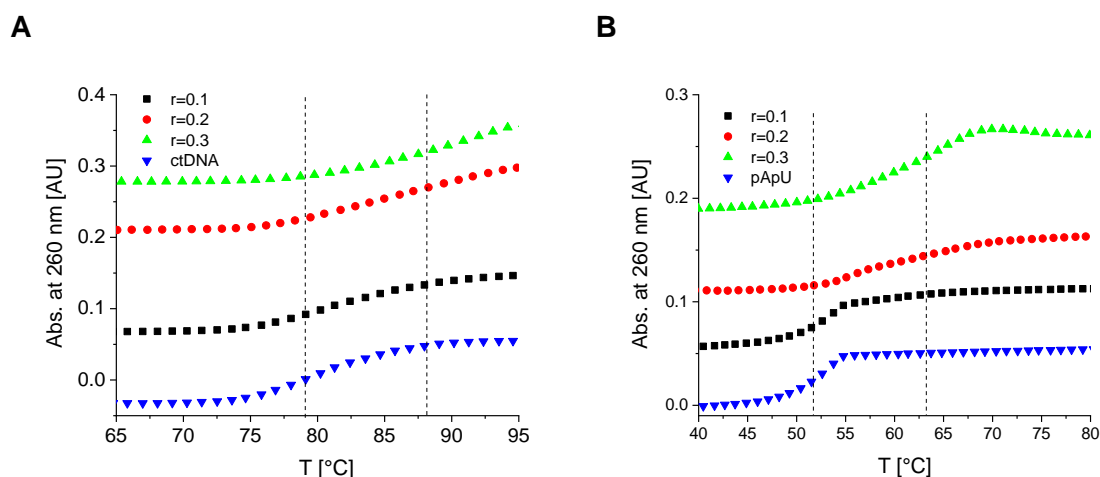


Figure 11.27: **A)** Thermal denaturation curves of ctDNA ($c(\text{ctDNA}) = 2.26 \times 10^{-5}$ M, $r_{[\text{Cat}^{2+}]/[\text{ctDNA}]} = 0.1$ to 0.3) at pH 7 (sodium cacodylate buffer, $I = 0.05$ M) upon addition of Cat^{2+} . Error in ΔT_m values: ± 0.5 °C. **B)** Thermal denaturation curves of pApU ($c(\text{pApU}) = 2.49 \times 10^{-5}$ M, $r_{[\text{Cat}^{2+}]/[\text{pApU}]} = 0.1$ to 0.3) at pH 7 (sodium cacodylate buffer, $I = 0.05$ M) upon addition of Cat^{2+} . Error in ΔT_m values: ± 0.5 °C. The vertical lines are added to chart the changes of the melting temperatures.

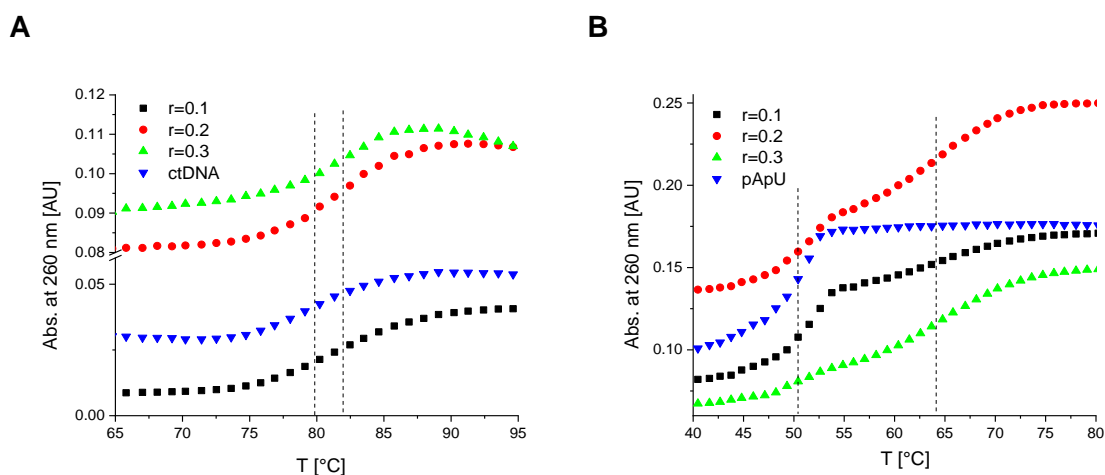


Figure 11.28: **A**) Thermal denaturation curves of ctDNA ($c(\text{ctDNA}) = 2.26 \times 10^{-5}$ M, $r_{[\text{Cat}(i)^{2+}]/[\text{ctDNA}]} = 0.1$ to 0.3) at pH 7 (sodium cacodylate buffer, $I = 0.05$ M) upon addition of **Cat(i)²⁺**. Error in ΔT_m values: ± 0.5 °C. **B**) Thermal denaturation curves of pApU ($c(\text{pApU}) = 2.49 \times 10^{-5}$ M, $r_{[\text{Cat}(i)^{2+}]/[\text{pApU}]} = 0.1$ to 0.3) at pH 7 (sodium cacodylate buffer, $I = 0.05$ M) upon addition of **Cat(i)²⁺**. Error in ΔT_m values: ± 0.5 °C. The vertical lines are added to chart the changes of the melting temperatures.

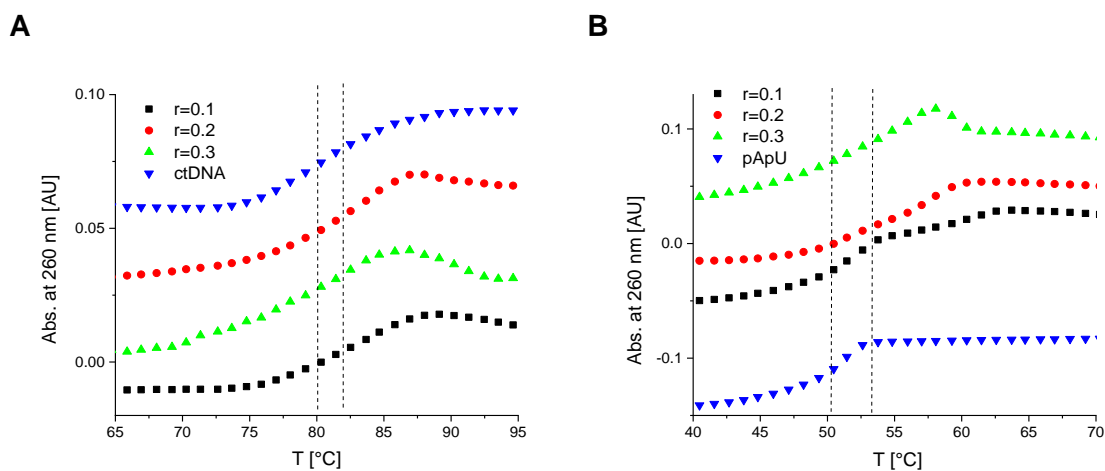


Figure 11.29: **A**) Thermal denaturation curves of ctDNA ($c(\text{ctDNA}) = 2.26 \times 10^{-5}$ M, $r_{[\text{Cat}^{3+}]/[\text{ctDNA}]} = 0.1$ to 0.3) at pH 7 (sodium cacodylate buffer, $I = 0.05$ M) upon addition of **Cat³⁺**. Error in ΔT_m values: ± 0.5 °C. **B**) Thermal denaturation curves of pApU ($c(\text{pApU}) = 2.49 \times 10^{-5}$ M, $r_{[\text{Cat}^{3+}]/[\text{pApU}]} = 0.1$ to 0.3) at pH 7 (sodium cacodylate buffer, $I = 0.05$ M) upon addition of **Cat³⁺**. Error in ΔT_m values: ± 0.5 °C. The vertical lines are added to chart the changes of the melting temperatures.

11.3.1.2.2 Fluorimetric Titrations

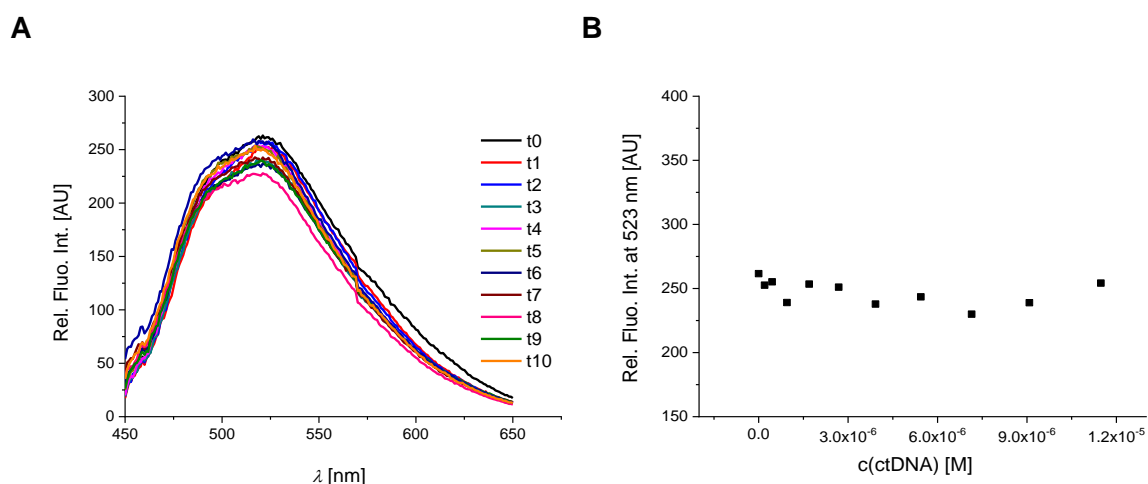


Figure 11.30: **A)** Fluorimetric titration of Cat^{1+} ($c = 1 \times 10^{-7}$ M; $\lambda_{\text{exc}} = 414$ nm; pH 7, sodium cacodylate buffer, $I = 0.05$ M) with ctDNA. **B)** Dependence of fluorescence of Cat^{1+} at $\lambda_{\text{max}} = 523$ nm on $c(\text{ctDNA})$.

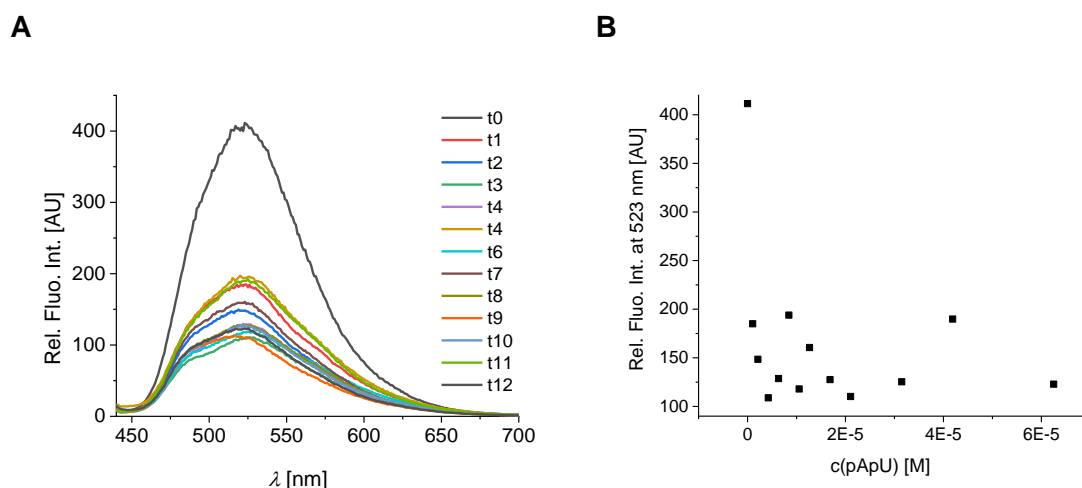


Figure 11.31: **A)** Fluorimetric titration of Cat^{1+} ($c = 5 \times 10^{-7}$ M; $\lambda_{\text{exc}} = 414$ nm; pH 7, sodium cacodylate buffer, $I = 0.05$ M) with pApU. **B)** Dependence of fluorescence of Cat^{1+} at $\lambda_{\text{max}} = 523$ nm on $c(\text{pApU})$. It has to be noted that during the measurement, formation of colloids was observed.

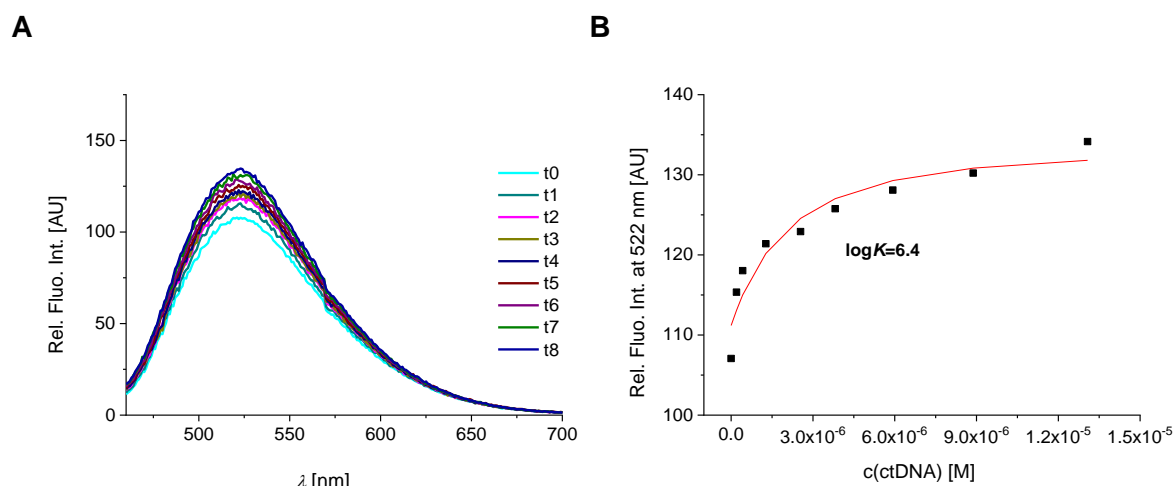


Figure 11.32: **A)** Fluorimetric titration of Cat^{2+} ($c = 1 \times 10^{-7}$ M; $\lambda_{\text{exc}} = 422$ nm; pH 7, sodium cacodylate buffer, $I = 0.05$ M) with ctDNA. **B)** Dependence of fluorescence of Cat^{2+} at $\lambda_{\text{max}} = 522$ nm on $c(\text{ctDNA})$.

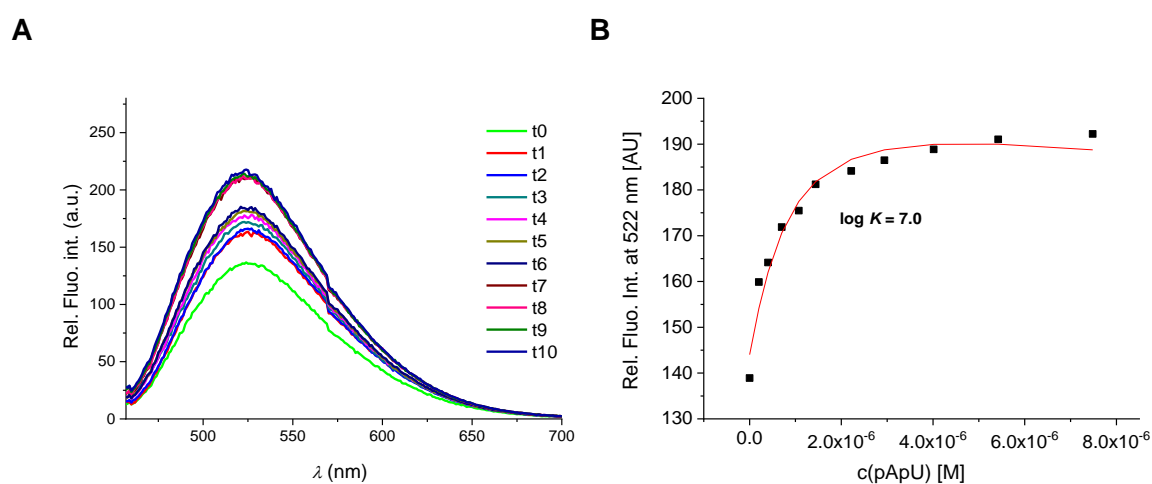


Figure 11.33: **A)** Fluorimetric titration of Cat^{2+} ($c = 1 \times 10^{-7}$ M; $\lambda_{\text{exc}} = 422$ nm; pH 7, sodium cacodylate buffer, $I = 0.05$ M) with pApU. **B)** Dependence of fluorescence of Cat^{2+} at $\lambda_{\text{max}} = 522$ nm on $c(\text{pApU})$.

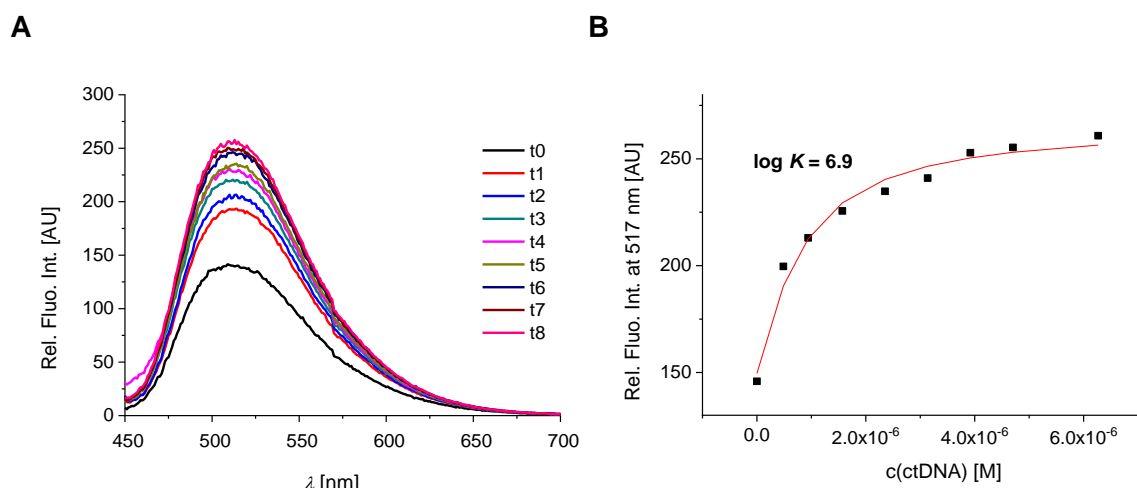


Figure 11.34: **A**) Fluorimetric titration of **Cat(i)²⁺** ($c = 1 \times 10^{-7}$ M; $\lambda_{\text{exc}} = 417$ nm; pH 7, sodium cacodylate buffer, $I = 0.05$ M) with ctDNA. **B**) Dependence of fluorescence of **Cat(i)²⁺** at $\lambda_{\text{max}} = 517$ nm on $c(\text{ctDNA})$.

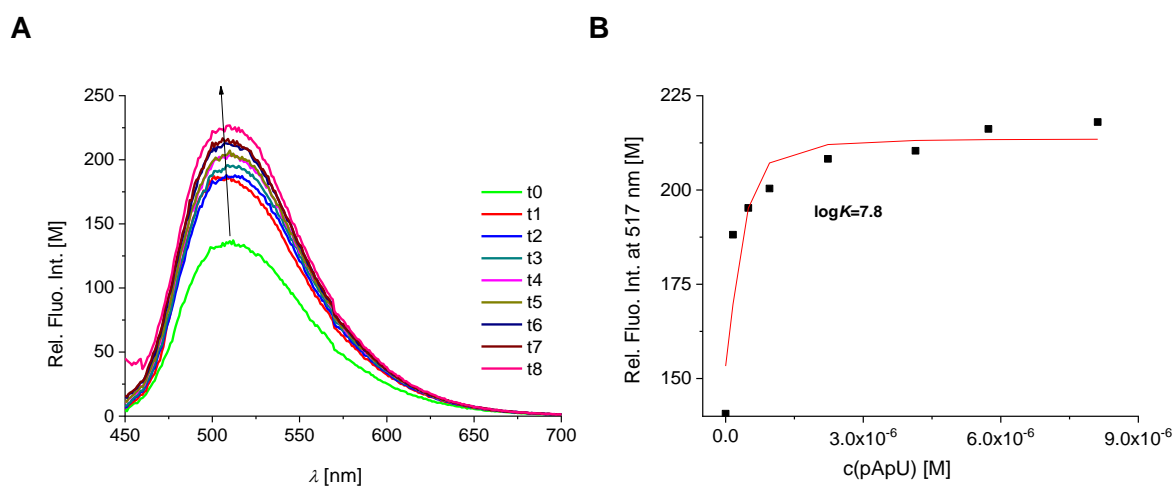


Figure 11.35: **A**) Fluorimetric titration of **Cat(i)²⁺** ($c = 1 \times 10^{-7}$ M; $\lambda_{\text{exc}} = 417$ nm; pH 7, sodium cacodylate buffer, $I = 0.05$ M) with pApU. **B**) Dependence of fluorescence of **Cat(i)²⁺** at $\lambda_{\text{max}} = 517$ nm on $c(\text{pApU})$.

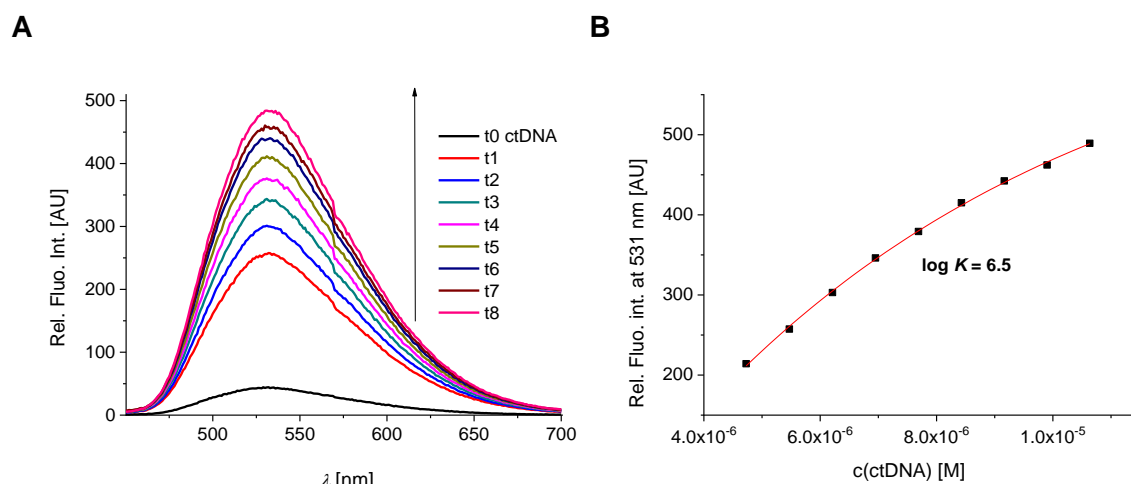


Figure 11.36: **A)** Fluorimetric titration of ctDNA ($c = 1 \times 10^{-7}$ M; $\lambda_{\text{exc}} = 421$ nm; pH 7, sodium cacodylate buffer, $I = 0.05$ M) with Cat^{3+} . **B)** Dependence of fluorescence of Cat^{3+} at $\lambda_{\text{max}} = 531$ nm on $c(\text{ctDNA})$.

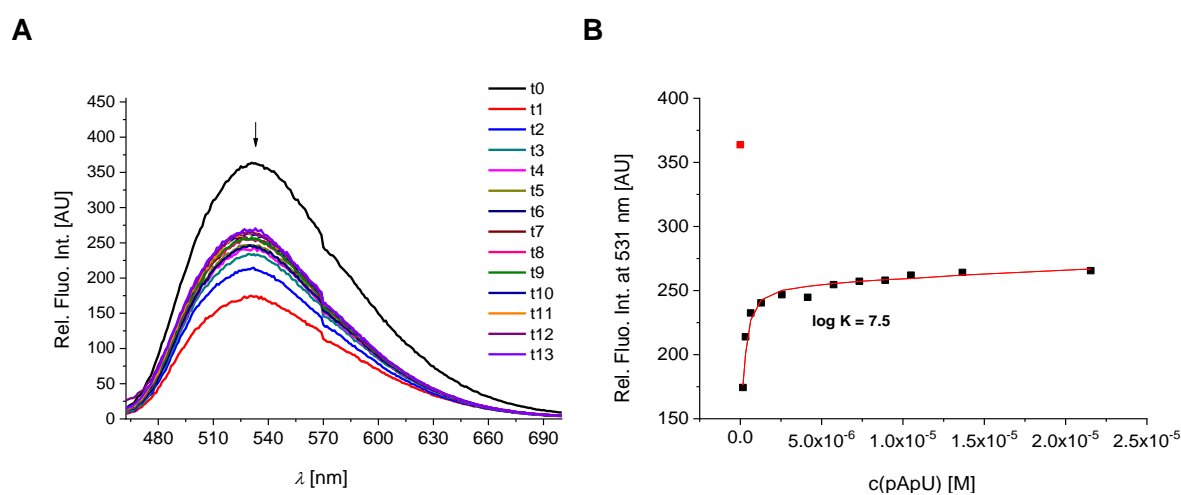


Figure 11.37: **A)** Fluorimetric titration of Cat^{3+} ($c = 1 \times 10^{-7}$ M; $\lambda_{\text{exc}} = 421$ nm; pH 7, sodium cacodylate buffer, $I = 0.05$ M) with pApU. **B)** Dependence of fluorescence of Cat^{3+} at $\lambda_{\text{max}} = 531$ nm on $c(\text{pApU})$.

11.3.1.2.3 Circular Dichroism Experiments

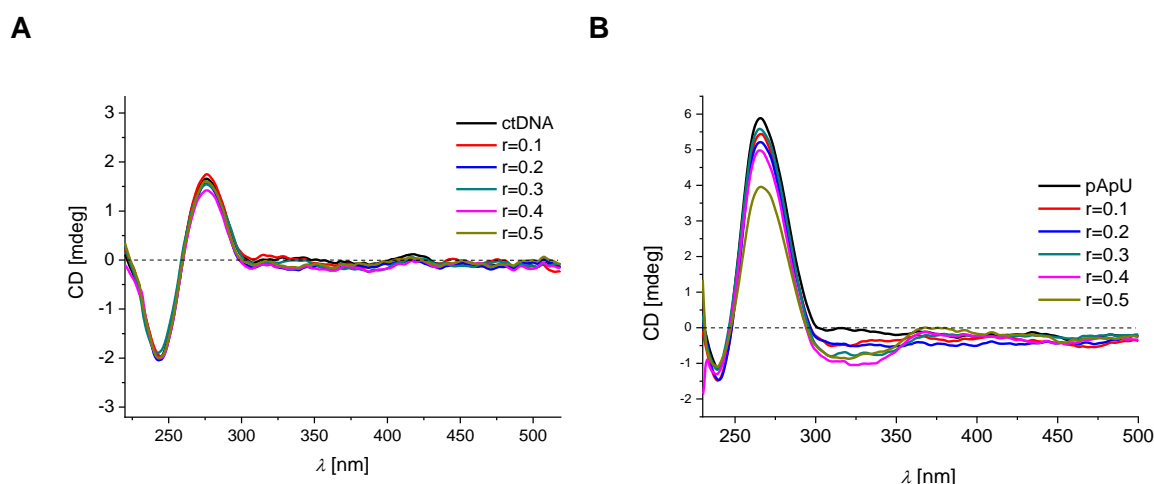


Figure 11.38: **A**) CD titration of ctDNA ($c(\text{ctDNA}) = 2 \times 10^{-5}$ M; pH 7, sodium cacodylate buffer, $I = 0.05$ M) with **Cat¹⁺** at molar ratios $r_{[\text{compound}]/[\text{polynucleotide}]} = 0.1 - 0.5$. **B**) CD titration of pApU ($c(\text{pApU}) = 2.5 \times 10^{-5}$ M; pH 7, sodium cacodylate buffer, $I = 0.05$ M) with **Cat¹⁺** at molar ratios $r_{[\text{compound}]/[\text{polynucleotide}]} = 0.1 - 0.5$.

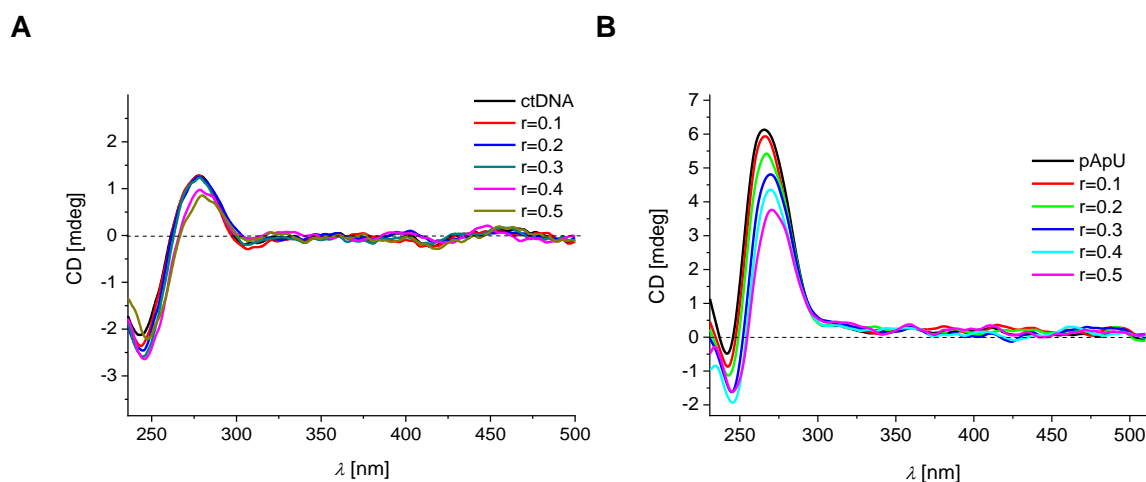


Figure 11.39: **A**) CD titration of ctDNA ($c(\text{ctDNA}) = 2 \times 10^{-5}$ M; pH 7, sodium cacodylate buffer, $I = 0.05$ M) with **Cat²⁺** at molar ratios $r_{[\text{compound}]/[\text{polynucleotide}]} = 0.1 - 0.5$. **B**) CD titration of pApU ($c(\text{pApU}) = 2.5 \times 10^{-5}$ M; pH 7, sodium cacodylate buffer, $I = 0.05$ M) with **Cat²⁺** at molar ratios $r_{[\text{compound}]/[\text{polynucleotide}]} = 0.1 - 0.5$.

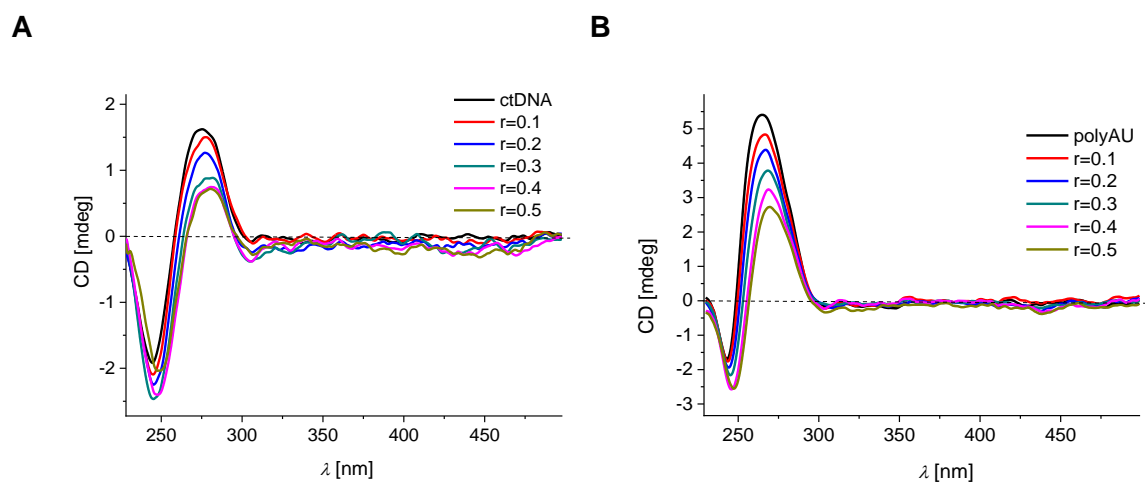


Figure 11.40: **A**) CD titration of ctDNA ($c(\text{ctDNA}) = 2 \times 10^{-5}$ M; pH 7, sodium cacodylate buffer, $I = 0.05$ M) with Cat(i)^{2+} at molar ratios $r_{[\text{compound}]/[\text{polynucleotide}]} = 0.1 - 0.5$. **B**) CD titration of pApU ($c(\text{pApU}) = 2.5 \times 10^{-5}$ M; pH 7, sodium cacodylate buffer, $I = 0.05$ M) with Cat(i)^{2+} at molar ratios $r_{[\text{compound}]/[\text{polynucleotide}]} = 0.1 - 0.5$.

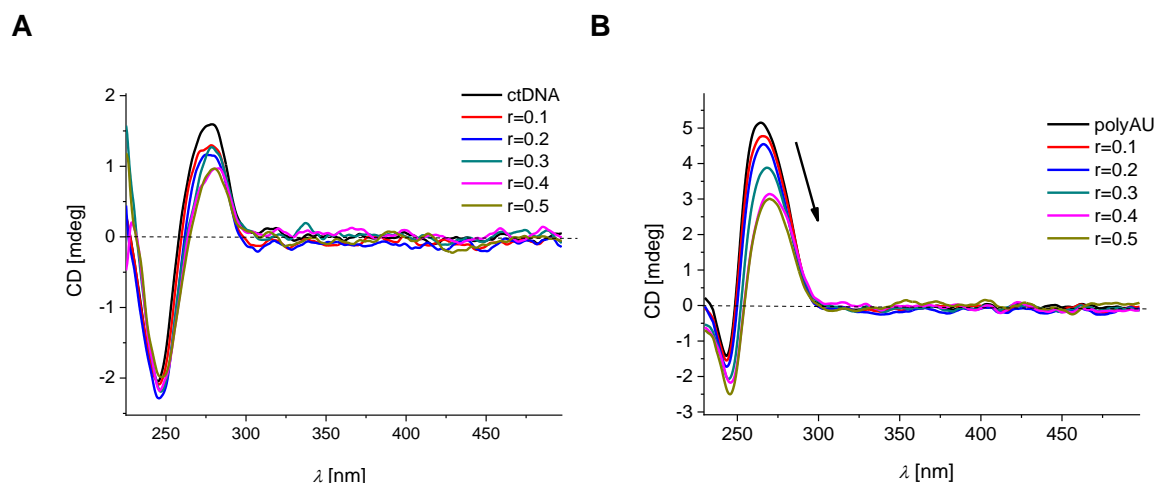


Figure 11.41: **A**) CD titration of ctDNA ($c(\text{ctDNA}) = 2 \times 10^{-5}$ M; pH 7, sodium cacodylate buffer, $I = 0.05$ M) with Cat^{3+} at molar ratios $r_{[\text{compound}]/[\text{polynucleotide}]} = 0.1 - 0.5$. **B**) CD titration of pApU ($c(\text{pApU}) = 2.5 \times 10^{-5}$ M; pH 7, sodium cacodylate buffer, $I = 0.05$ M) with Cat^{3+} at molar ratios $r_{[\text{compound}]/[\text{polynucleotide}]} = 0.1 - 0.5$.

11.3.1.3 Interaction of **Cat¹⁺-Cat⁴⁺** with ctDNA, and DNApore at pH 8

11.3.1.3.1 Thermal Melting Experiments

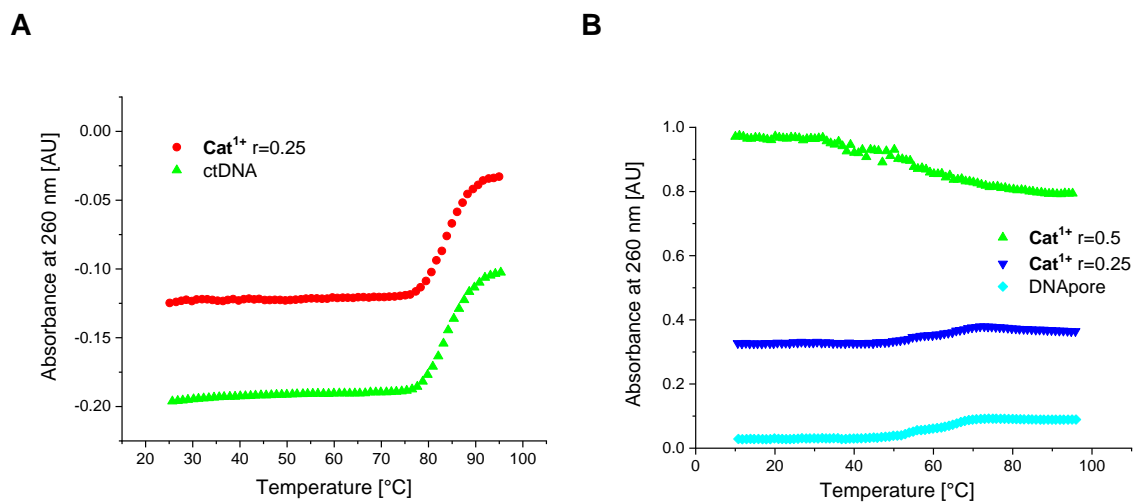


Figure 11.42: Thermal denaturation curves of **A)** ctDNA ($c(\text{ctDNA}) = 2.26 \times 10^{-5}$ M, $r_{[\text{Cat}^{1+}]/[\text{ctDNA}]} = 0.25$) and **B)** DNApore ($c(\text{DNApore}) = 2 \times 10^{-5}$ M, $r_{[\text{Cat}^{1+}]/[\text{DNApore}]} = 0.25$ to 0.5) at pH 8 (15 mM Tris-HCl, 300 mM KCl) upon addition of **Cat¹⁺**. Error in ΔT_m values: ± 0.5 °C.

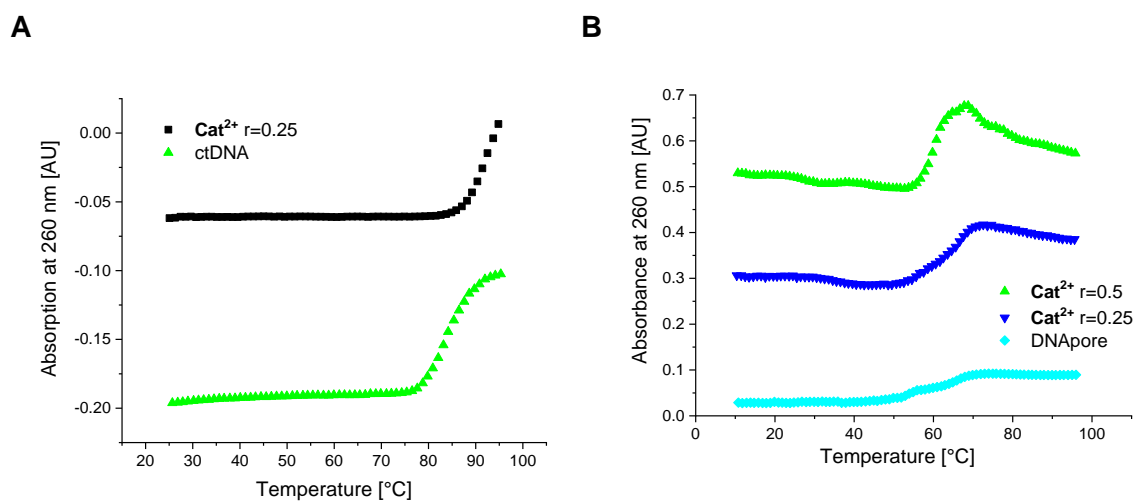


Figure 11.43: Thermal denaturation curves of **A)** ctDNA ($c(\text{ctDNA}) = 2.26 \times 10^{-5}$ M, $r_{[\text{Cat}^{2+}]/[\text{ctDNA}]} = 0.25$) and **B)** DNApore ($c(\text{DNApore}) = 2.49 \times 10^{-5}$ M, $r_{[\text{Cat}^{2+}]/[\text{DNApore}]} = 0.25$ to 0.5) at pH 8 (15 mM Tris-HCl, 300 mM KCl) upon addition of **Cat²⁺**. Error in ΔT_m values: ± 0.5 °C.

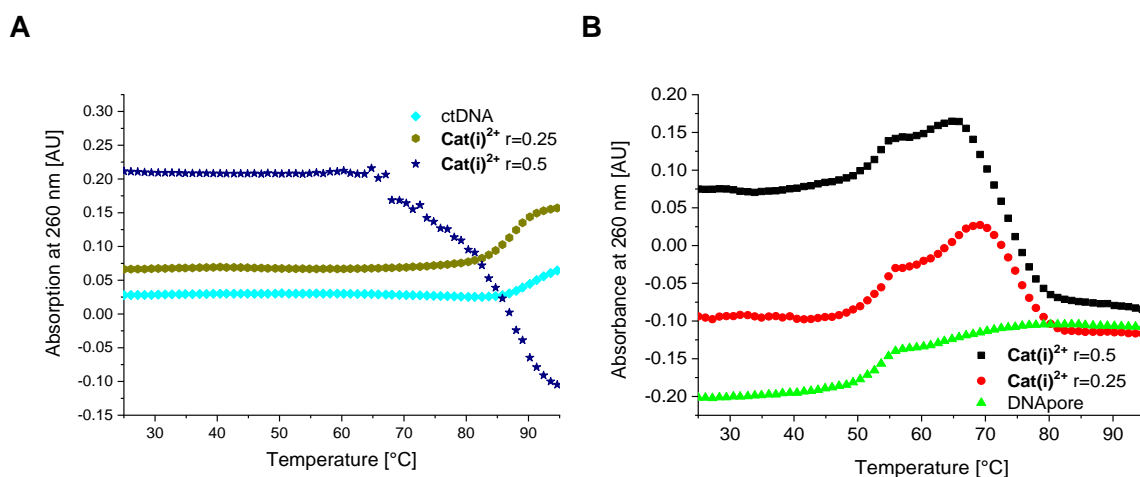


Figure 11.44: Thermal denaturation curves of **A**) ctDNA ($c(\text{ctDNA}) = 2.26 \times 10^{-5} \text{ M}$, $r_{[\text{Cat}(i)^{2+}]/[\text{ctDNA}]} = 0.25$ to 0.5) and **B**) DNApore ($c(\text{DNApore}) = 1.05 \times 10^{-6} \text{ M}$, $r_{[\text{Cat}(i)^{2+}]/[\text{DNApore}]} = 0.25$ to 0.5) at pH 8 (15 mM Tris-HCl, 300 mM KCl) upon addition of **Cat(i)²⁺**. Error in ΔT_m values: $\pm 0.5 \text{ }^\circ\text{C}$.

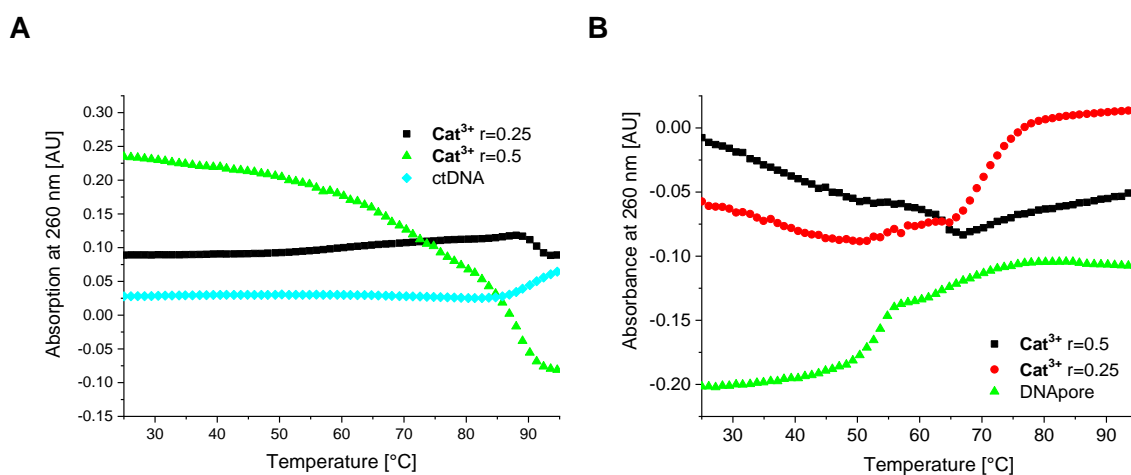


Figure 11.45: Thermal denaturation curves of **A**) ctDNA ($c(\text{ctDNA}) = 2.26 \times 10^{-5} \text{ M}$, $r_{[\text{Cat}^{3+}]/[\text{ctDNA}]} = 0.25$ to 0.5) and **B**) DNApore ($c(\text{DNApore}) = 1.05 \times 10^{-6} \text{ M}$, $r_{[\text{Cat}^{3+}]/[\text{DNApore}]} = 0.25$ to 0.5) at pH 8 (15 mM Tris-HCl, 300 mM KCl) upon addition of **Cat³⁺**. Error in ΔT_m values: $\pm 0.5 \text{ }^\circ\text{C}$.

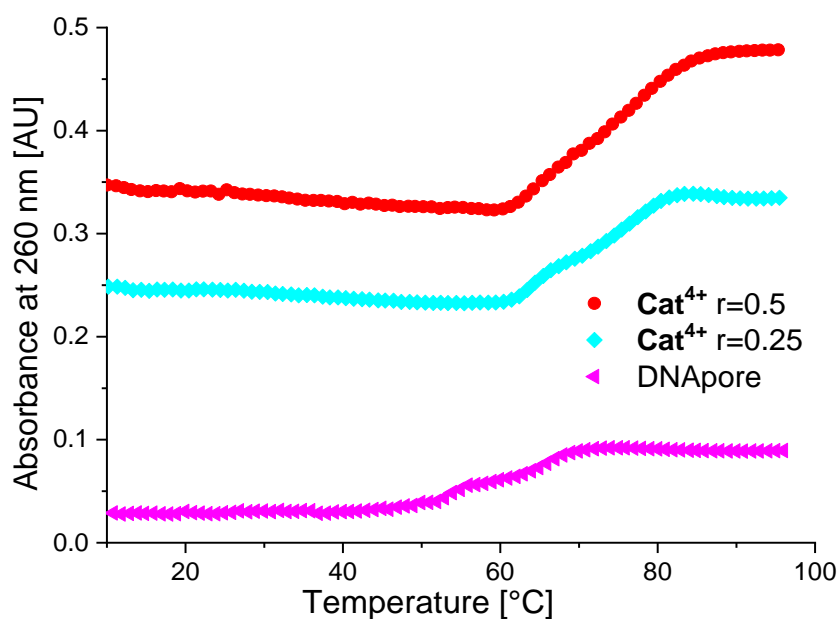


Figure S1: Thermal denaturation curves of DNApore ($c(\text{DNApore}) = 2 \times 10^{-5} \text{ M}$, $r_{[\text{Cat}^{4+}]/[\text{DNApore}]} = 0.25 \text{ to } 0.5$) at pH 8 (15 mM Tris-HCl, 300 mM KCl) upon addition of Cat^{4+} . Error in ΔT_m values: $\pm 0.5 \text{ } ^\circ\text{C}$.

11.3.1.3.2 Fluorimetric Titrations

Fluorimetric titration of Cat^{1+} with ctDNA at pH 8 (15 mM Tris-HCl, 300 mM KCl) was not performed as the titration at pH 7 showed no binding between Cat^{1+} and ctDNA.

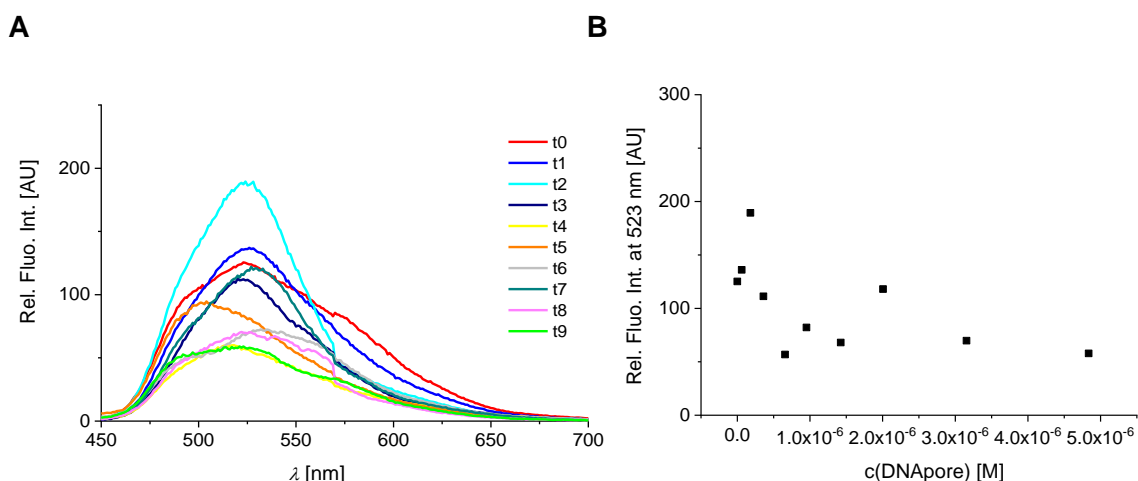


Figure 11.46: **A)** Fluorimetric titration of Cat^{1+} ($c = 5 \times 10^{-7} \text{ M}$; $\lambda_{\text{exc}} = 414 \text{ nm}$; pH 8, 15 mM Tris-HCl, 300 mM KCl) with DNApore. **B)** Dependence of fluorescence of Cat^{1+} at $\lambda_{\text{max}} = 524 \text{ nm}$ on $c(\text{DNApore})$. It has to be noted that during the measurement, formation of colloids was observed.

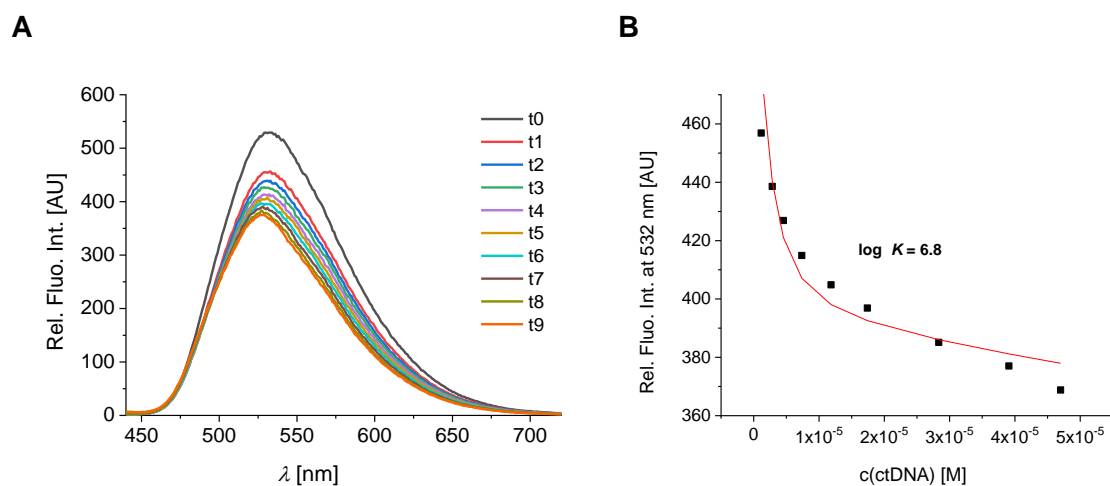


Figure 11.47: **A)** Fluorimetric titration of Cat^{2+} ($c = 4 \times 10^{-7}$ M; $\lambda_{\text{exc}} = 422$ nm; pH 8, 15 mM Tris-HCl, 300 mM KCl) with ctDNA. **B)** Dependence of fluorescence at $\lambda_{\text{max}} = 532$ nm on $c(\text{ctDNA})$.

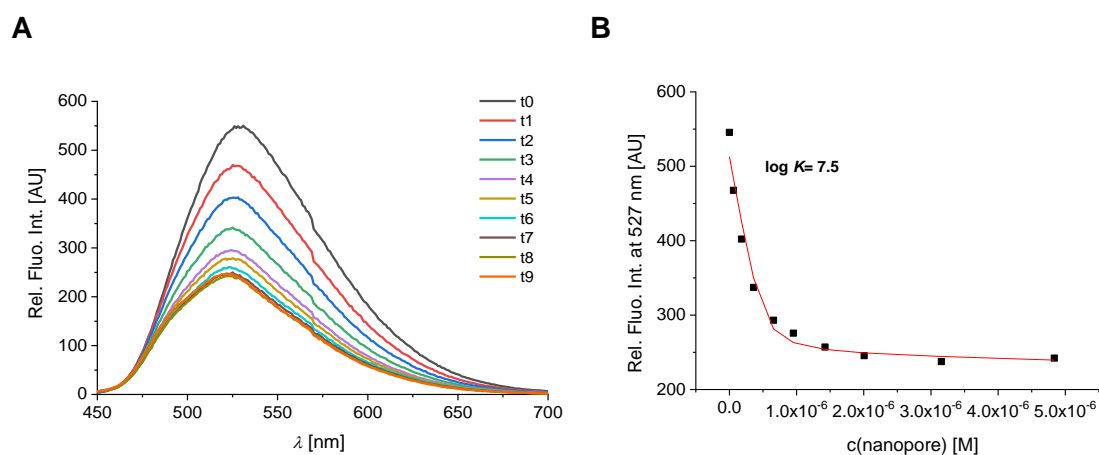


Figure 11.48: **A)** Fluorimetric titration of Cat^{2+} ($c = 5 \times 10^{-7}$ M; $\lambda_{\text{exc}} = 422$ nm; pH 8, 15 mM Tris-HCl, 300 mM KCl) with DNApore. **B)** Dependence of fluorescence of Cat^{2+} at $\lambda_{\text{max}} = 527$ nm on $c(\text{DNApore})$.

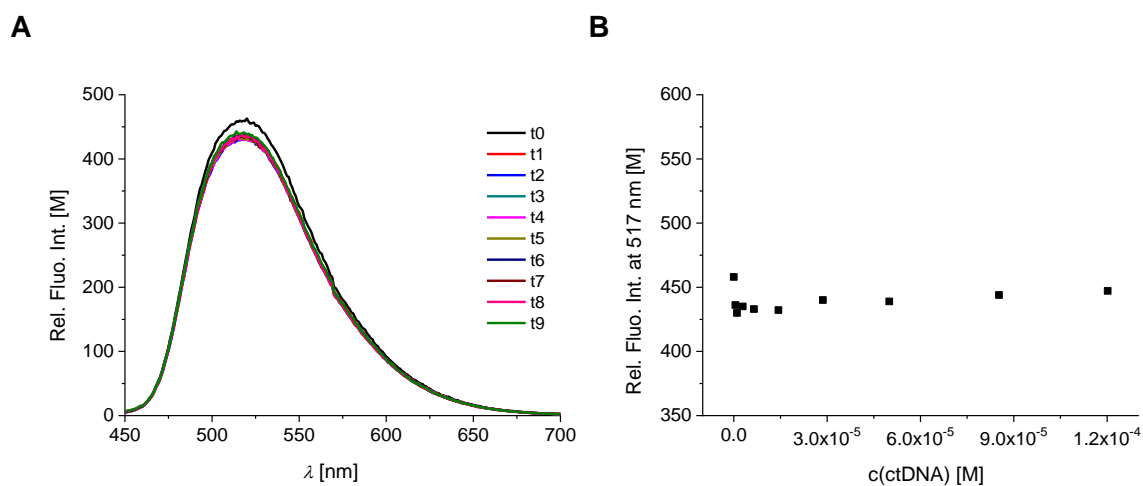


Figure 11.49: **A**) Fluorimetric titration of Cat(i)^{2+} ($c = 5 \times 10^{-7}$ M; $\lambda_{\text{exc}} = 417$ nm; pH 8, 15 mM Tris-HCl, 300 mM KCl) with ctDNA. **B**) Dependence of fluorescence of Cat(i)^{2+} at $\lambda_{\text{max}} = 517$ nm on $c(\text{ctDNA})$.

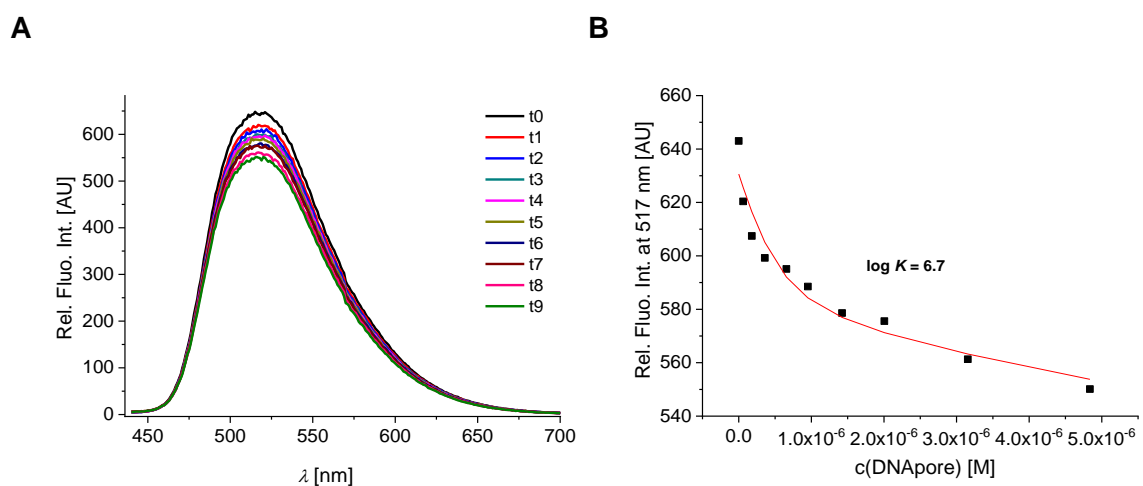


Figure 11.50: Fluorimetric titration of Cat(i)^{2+} ($c = 5 \times 10^{-7}$ M; $\lambda_{\text{exc}} = 417$ nm; pH 8, 15 mM Tris-HCl, 300 mM KCl) with DNApore. **B**) Dependence of fluorescence of Cat(i)^{2+} at $\lambda_{\text{max}} = 517$ nm on $c(\text{DNApore})$.

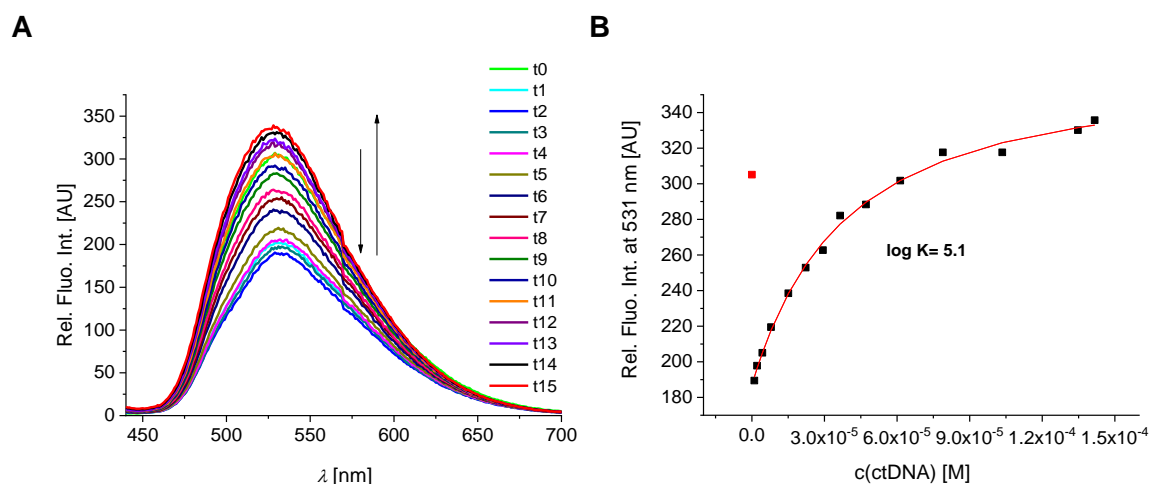


Figure 11.51: **A)** Fluorimetric titration of Cat^{3+} ($c = 5 \times 10^{-7}$ M; $\lambda_{\text{exc}} = 421$ nm; pH 8, 15 mM Tris-HCl, 300 mM KCl) with ctDNA. **B)** Dependence of fluorescence of Cat^{3+} at $\lambda_{\text{max}} = 531$ nm on $c(\text{ctDNA})$.

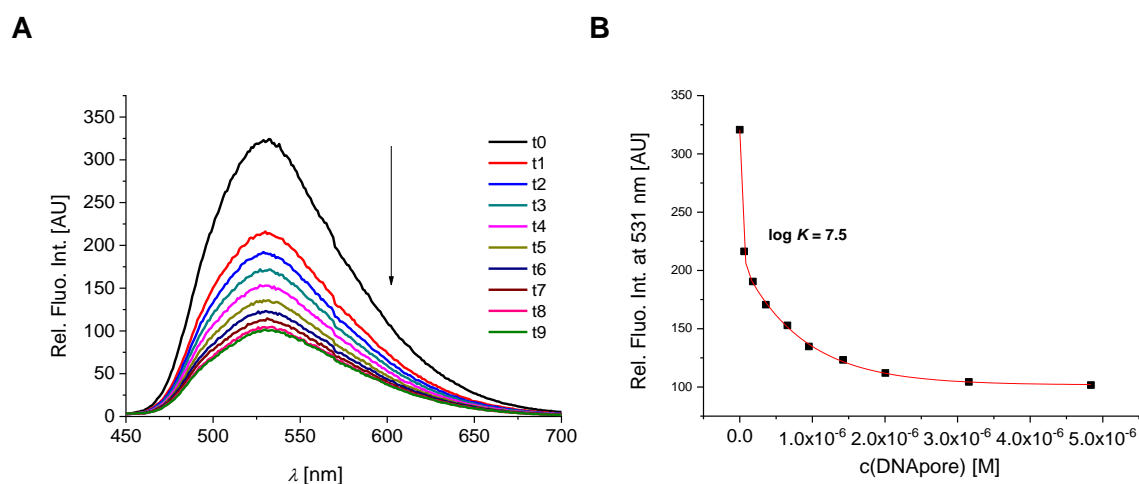


Figure 11.52: **A)** Fluorimetric titration of Cat^{3+} ($c = 5 \times 10^{-7}$ M; $\lambda_{\text{exc}} = 421$ nm; pH 8, 15 mM Tris-HCl, 300 mM KCl) with DNApore. **B)** Dependence of fluorescence of Cat^{3+} at $\lambda_{\text{max}} = 531$ nm on $c(\text{DNApore})$.

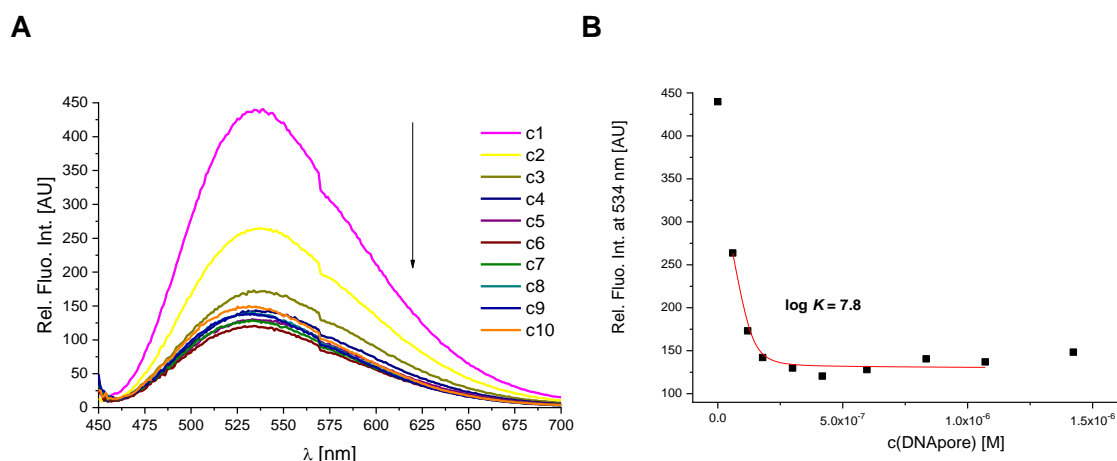


Figure 11.53: **A)** Fluorimetric titration of **Cat⁴⁺** ($c = 4 \times 10^{-7}$ M; $\lambda_{\text{exc}} = 425$ nm; pH 8, 15 mM Tris-HCl, 300 mM KCl) with DNApore. **B)** Dependence of fluorescence of **Cat⁴⁺** at $\lambda_{\text{max}} = 534$ nm on $c(\text{DNApore})$.

11.3.1.3.3 Circular Dichroism Experiments

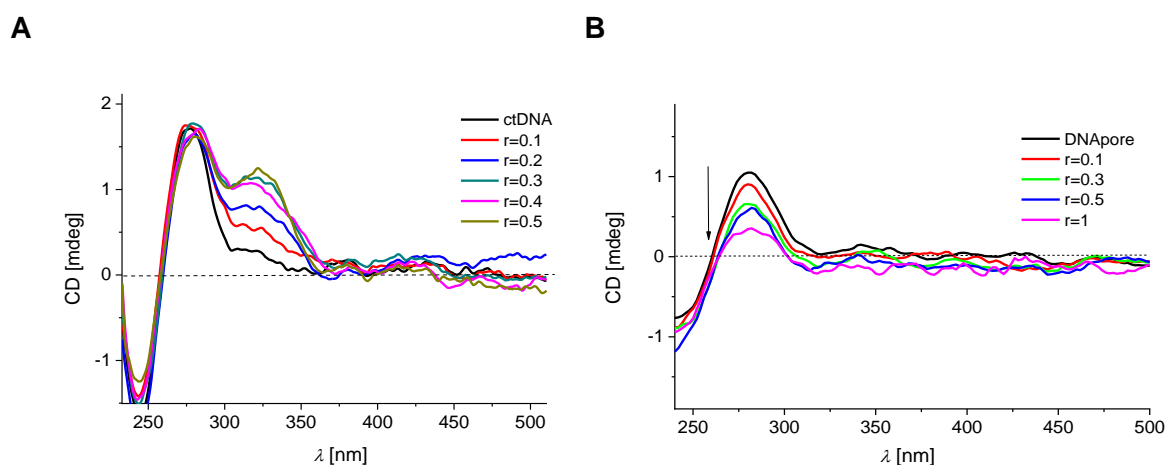


Figure 11.54: **A)** CD titration of ctDNA ($c(\text{ctDNA}) = 2 \times 10^{-5}$ M; pH 8, 15 mM Tris-HCl, 300 mM KCl) with **Cat¹⁺** at molar ratios $r_{[\text{compound}]/[\text{polynucleotide}]} = 0.1 - 0.5$. **B)** CD titration of DNApore ($c(\text{DNApore}) = 2.5 \times 10^{-5}$ M; pH 8, 15 mM Tris-HCl, 300 mM KCl) with **Cat¹⁺** at molar ratios $r_{[\text{compound}]/[\text{polynucleotide}]} = 0.1 - 1$.

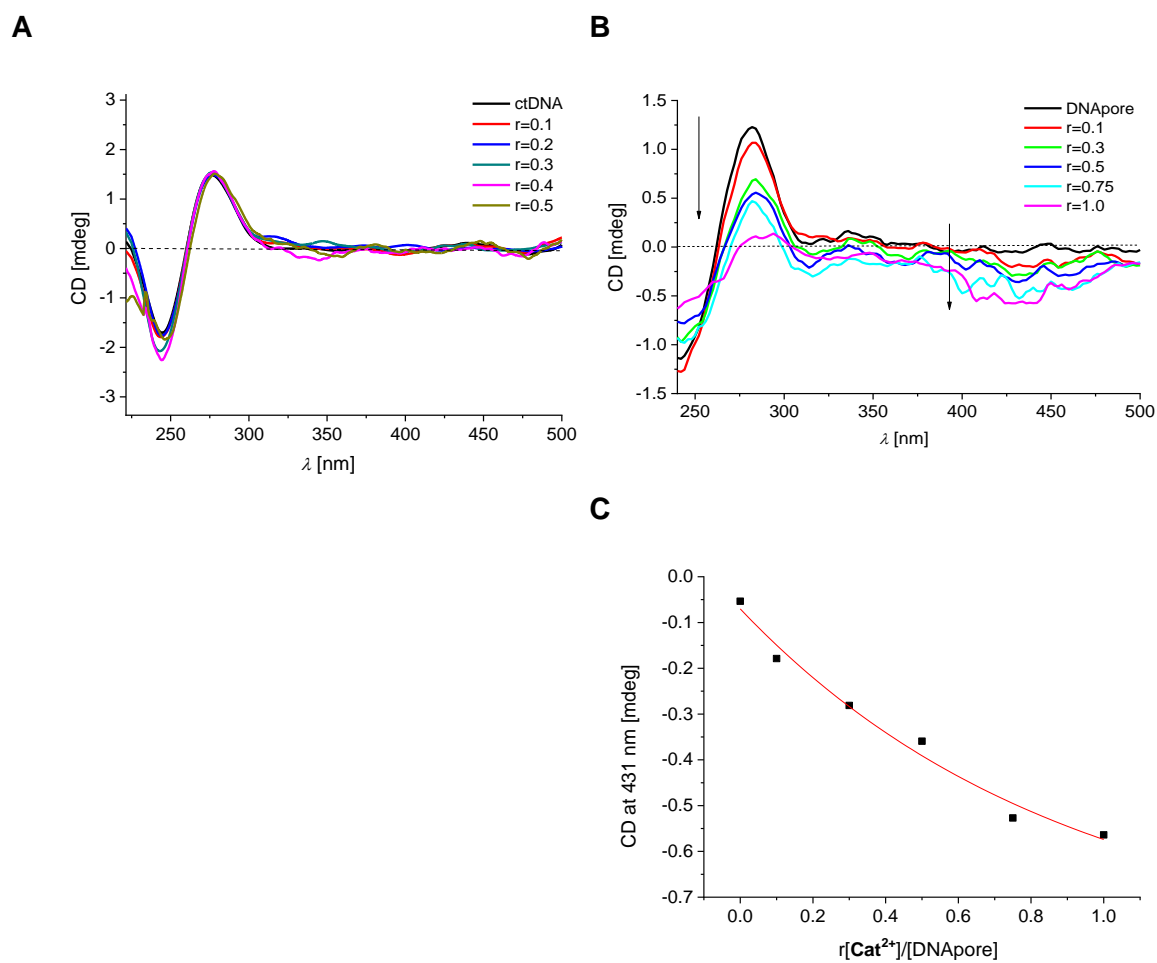


Figure 11.55: **A)** CD titration of ctDNA ($c(\text{ctDNA}) = 2 \times 10^{-5}$ M; pH 8, 15 mM Tris-HCl, 300 mM KCl) with Cat^{2+} at molar ratios $r_{[\text{compound}]/[\text{polynucleotide}]} = 0.1 - 0.5$. **B)** CD titration of DNApore ($c(\text{DNApore}) = 5 \times 10^{-5}$ M; pH 8, 15 mM Tris-HCl, 300 mM KCl) with Cat^{2+} at molar ratios $r_{[\text{compound}]/[\text{polynucleotide}]} = 0.1 - 1$. **C)** Dependence of CD signal of DNApore at $\lambda_{\text{max}} = 431$ nm on $c(\text{Cat}^{2+})$.

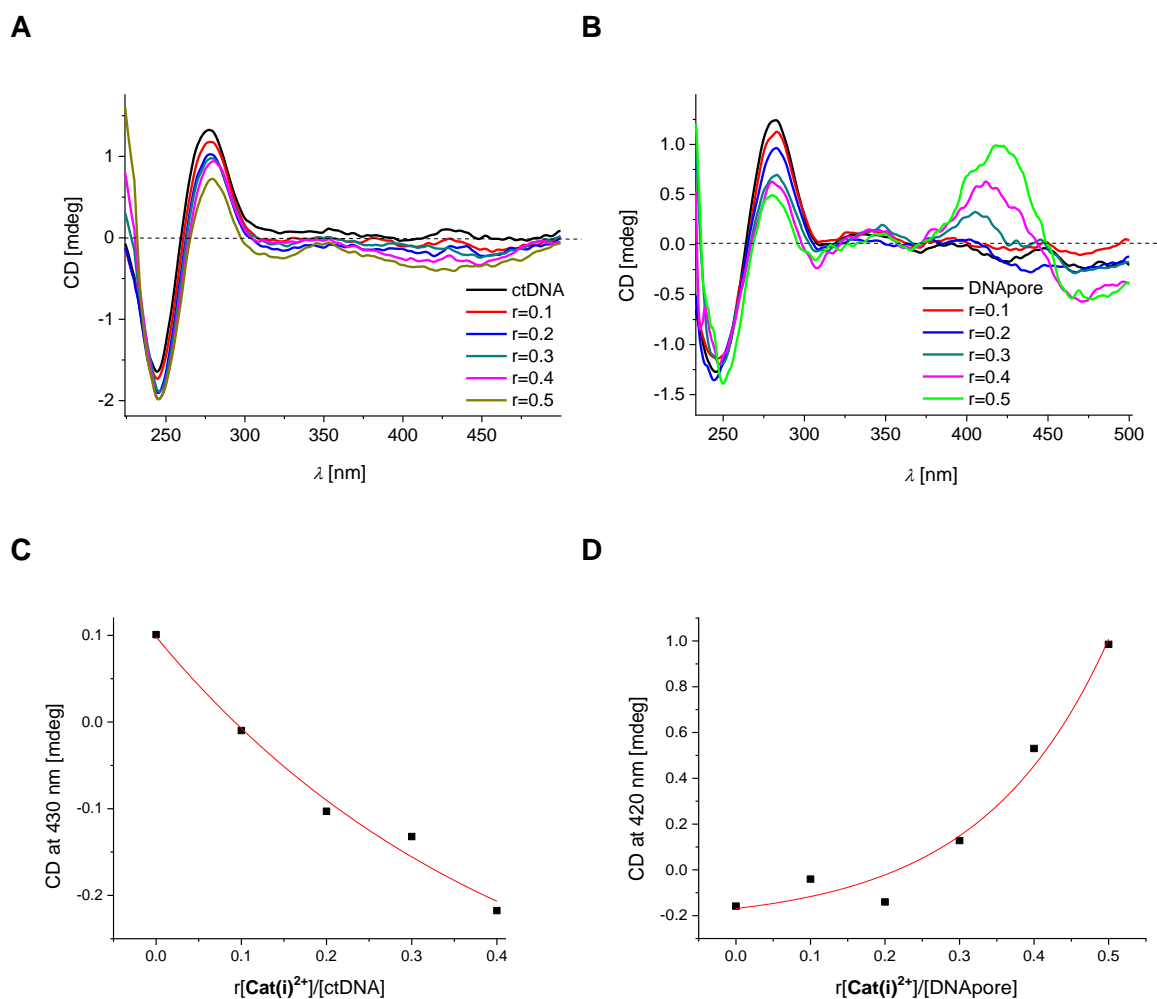


Figure 11.56: **A)** CD titration of ctDNA ($c(\text{ctDNA}) = 2 \times 10^{-5}$ M; pH 8, 15 mM Tris-HCl, 300 mM KCl) with Cat(i)^{2+} at molar ratios $r_{[\text{compound}]/[\text{polynucleotide}]} = 0.1 - 0.5$. **B)** CD titration of DNApore ($c(\text{DNApore}) = 5 \times 10^{-5}$ M; pH 8, 15 mM Tris-HCl, 300 mM KCl) with Cat(i)^{2+} at molar ratios $r_{[\text{compound}]/[\text{polynucleotide}]} = 0.1 - 0.5$. **C)** Dependence of CD signal of ctDNA at $\lambda_{\text{max}} = 430$ nm on $c(\text{Cat(i)}^{2+})$. **D)** Dependence of CD signal of DNApore at $\lambda_{\text{max}} = 420$ nm on $c(\text{Cat(i)}^{2+})$.

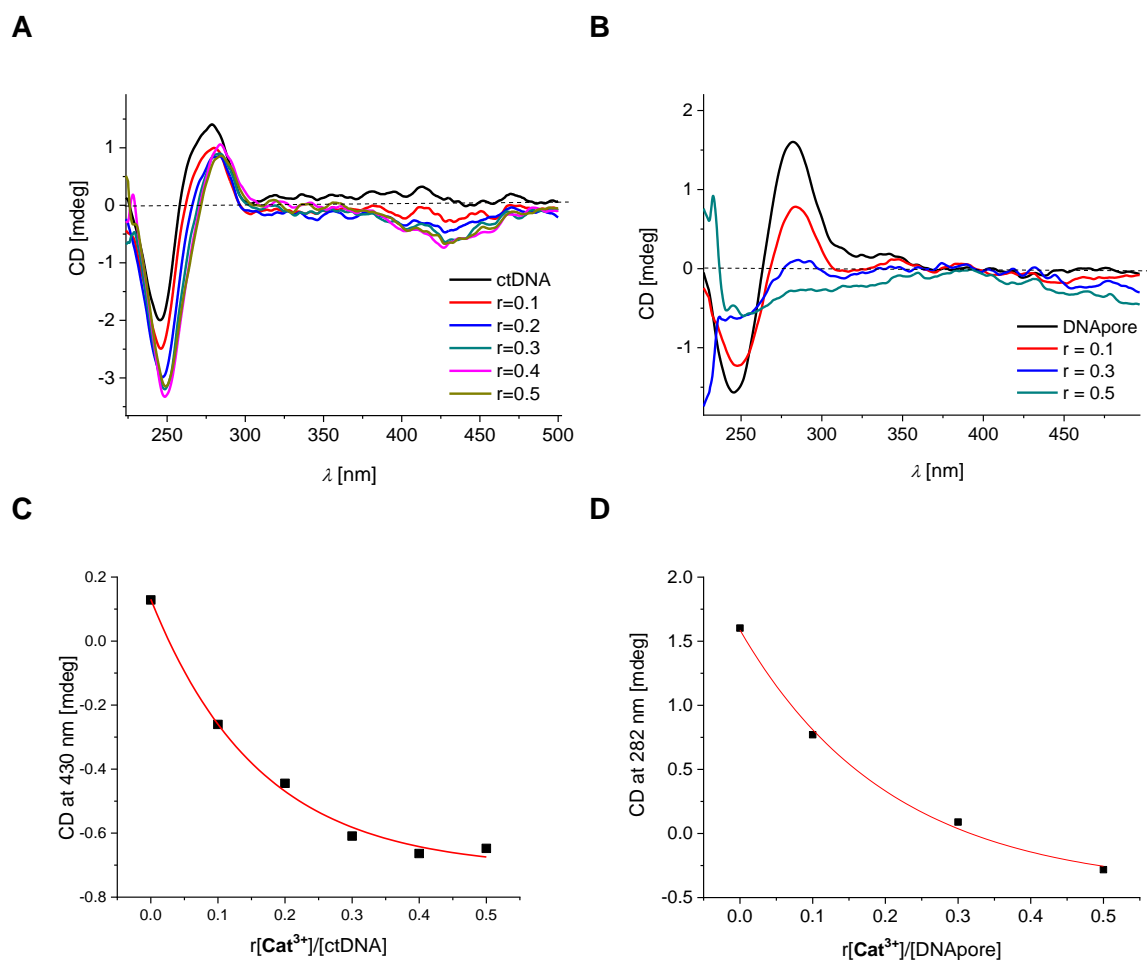


Figure 11.57: **A)** CD titration of ctDNA ($c(\text{ctDNA}) = 2 \times 10^{-5}$ M; pH 8, 15 mM Tris-HCl, 300 mM KCl) with Cat^{3+} at molar ratios $r_{[\text{compound}]/[\text{polynucleotide}]} = 0.1 - 0.5$. **B)** CD titration of DNApore ($c(\text{DNApore}) = 5 \times 10^{-5}$ M; pH 8, 15 mM Tris-HCl, 300 mM KCl) with Cat^{3+} at molar ratios $r_{[\text{compound}]/[\text{polynucleotide}]} = 0.1 - 0.5$. **C)** Dependence of CD signal of ctDNA at $\lambda_{\text{max}} = 430$ nm on $c(\text{Cat}^{3+})$. **D)** Dependence of CD signal of DNApore at $\lambda_{\text{max}} = 282$ nm on $c(\text{Cat}^{3+})$.

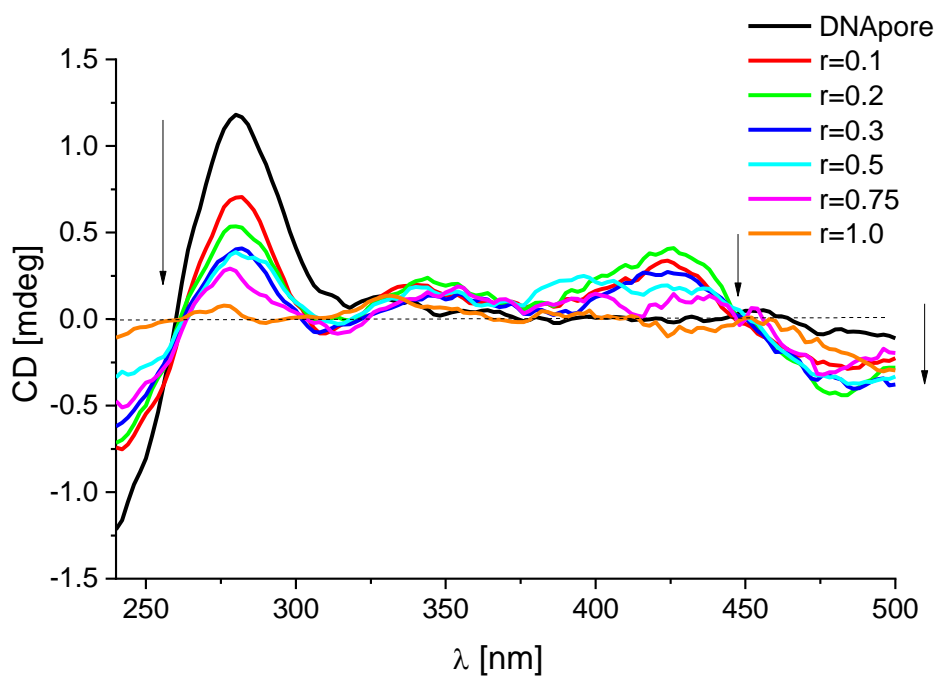


Figure 11.58: CD titration of DNApore ($c(\text{DNApore}) = 5 \times 10^{-5} \text{ M}$; pH 8, 15 mM Tris-HCl, 300 mM KCl) with **Cat⁴⁺** at molar ratios $r_{[\text{compound}]/[\text{polynucleotide}]} = 0.1 - 1$.

11.3.1.1 Cell Studies

11.3.1.1.1 Photoinduced Cell Damage

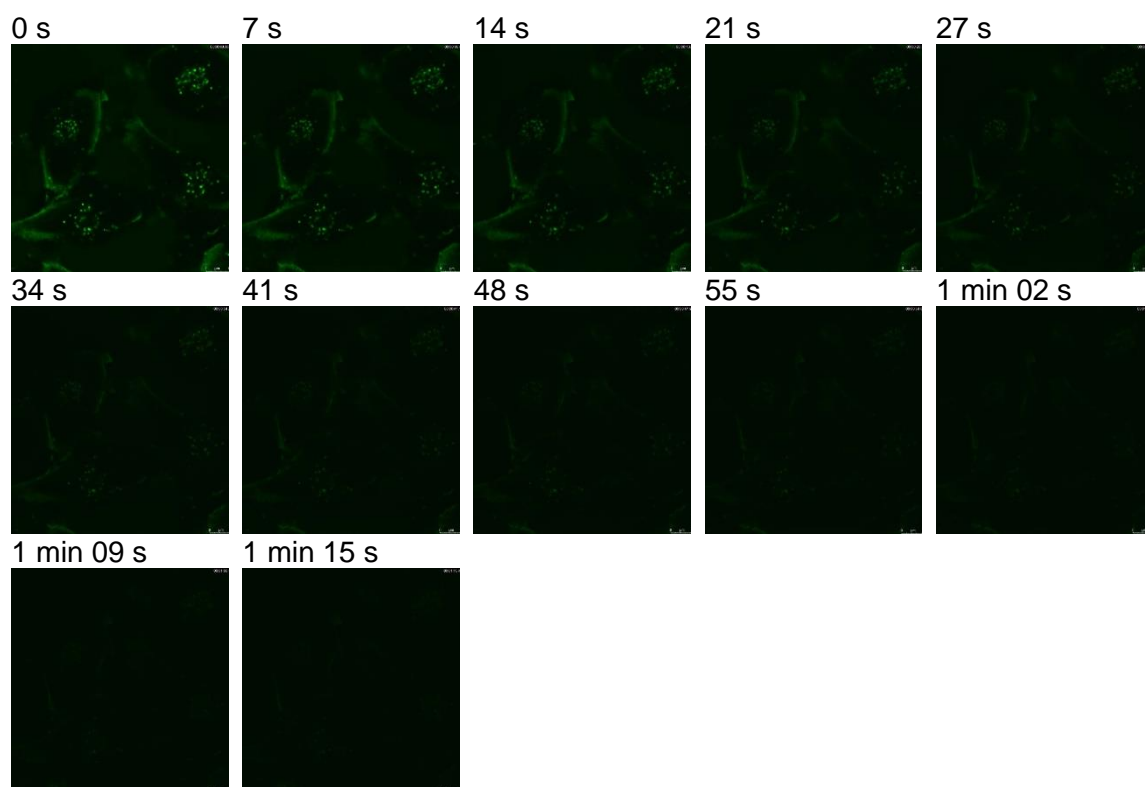
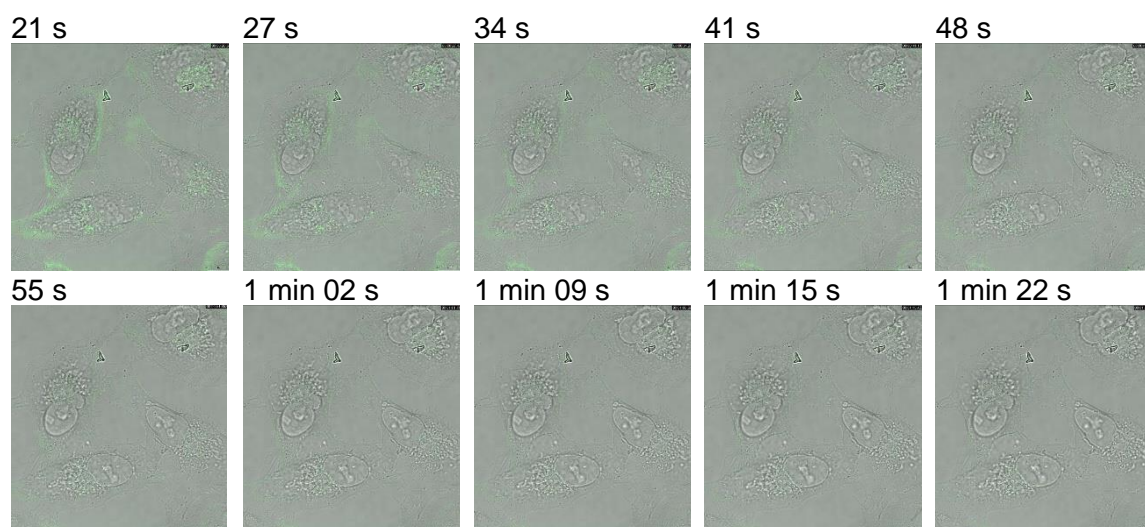


Figure 11.59: Emission of A549 cells stained with **Cat²⁺**. Images were taken at times indicated showing fast bleaching of the emission of **Cat²⁺**.



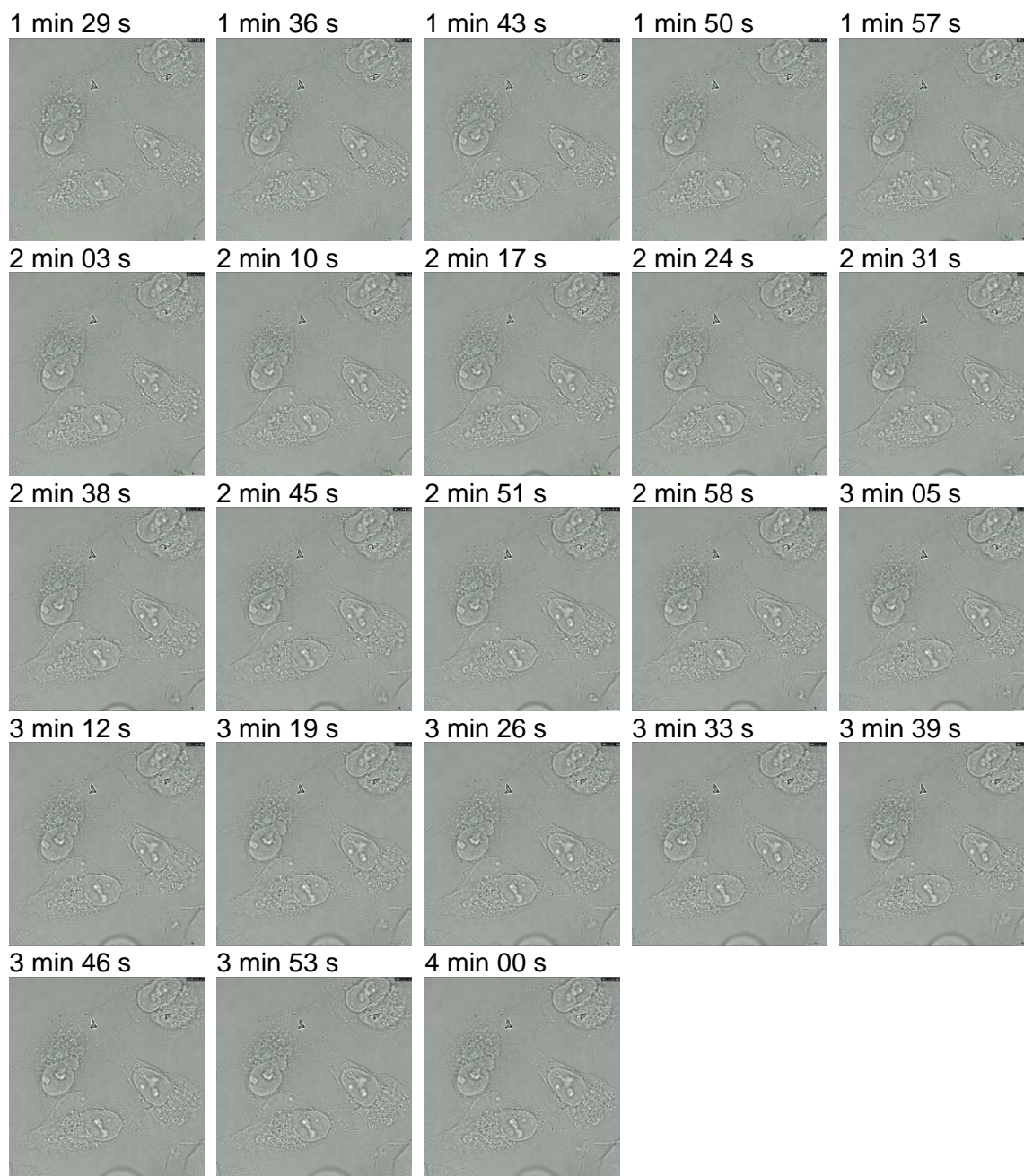


Figure 11.60: Emission of A549 cells stained with **Cat²⁺** overlaid with bright field images. Images were taken at times indicated showing fast bleaching of the emission of **Cat²⁺** and simultaneous cell blebbing.

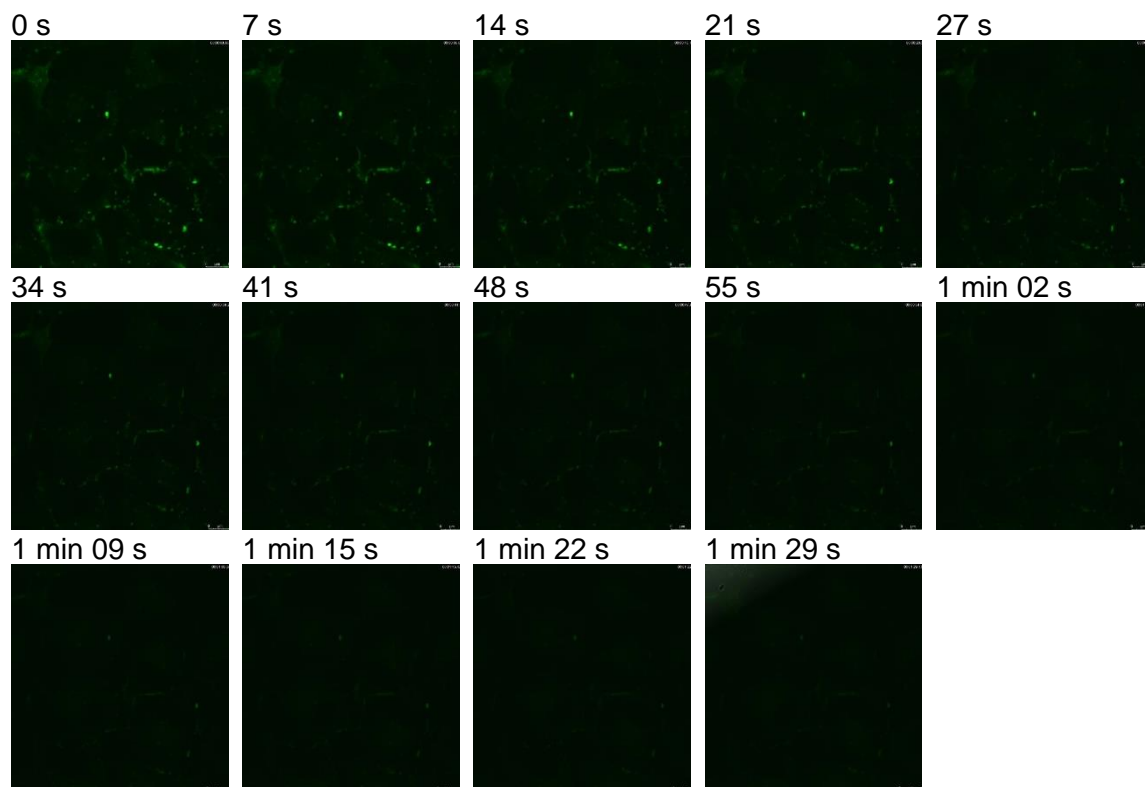


Figure 11.61: Emission of A549 cells stained with Cat(i)^{2+} . Images were taken at times indicated showing fast bleaching of the emission of Cat(i)^{2+} .

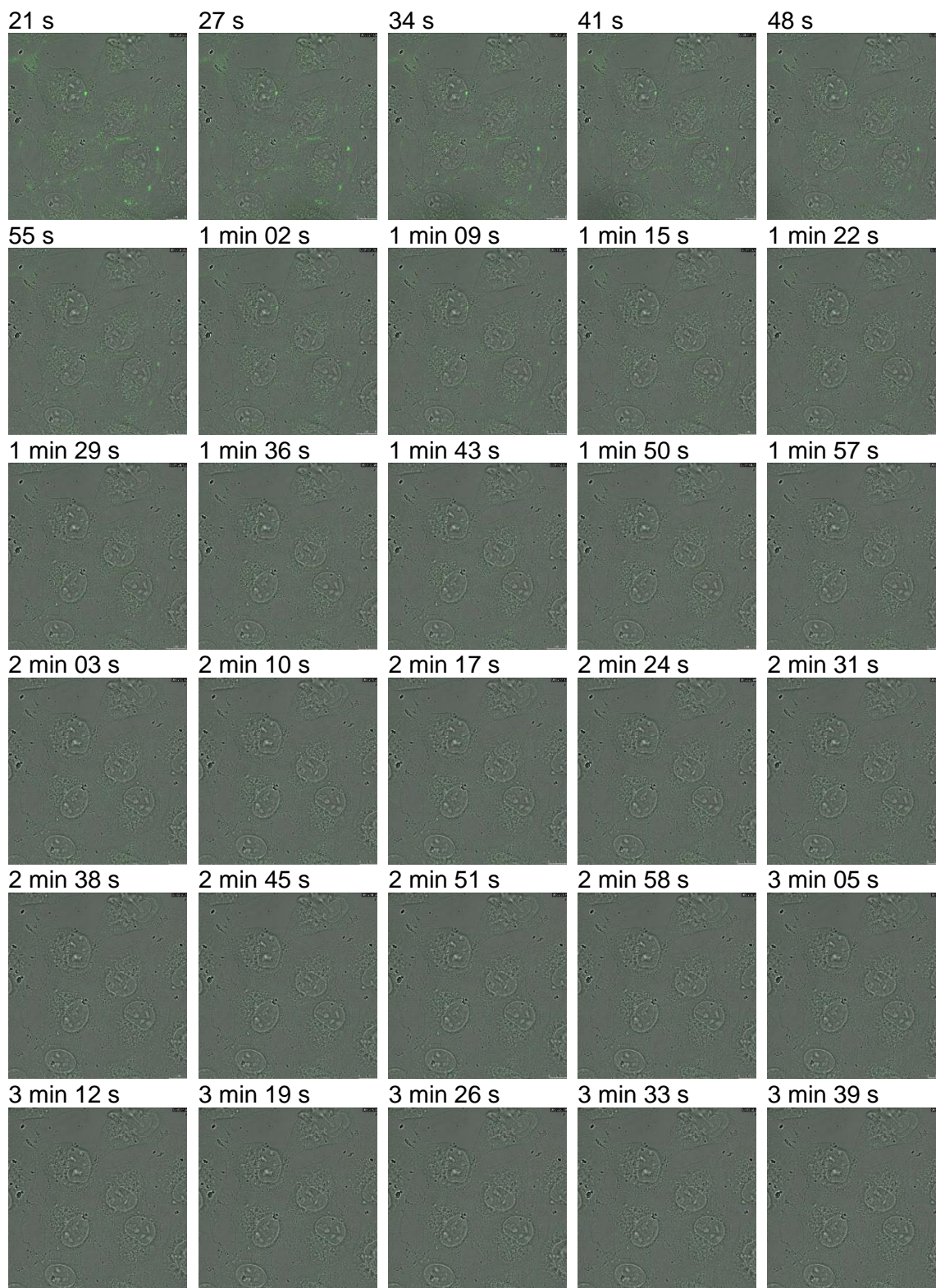


Figure 11.62: Emission of A549 cells stained with **Cat(i)²⁺** overlaid with bright field images. Images were taken at times indicated showing fast bleaching of the emission of **Cat(i)²⁺** and simultaneous cell blebbing.

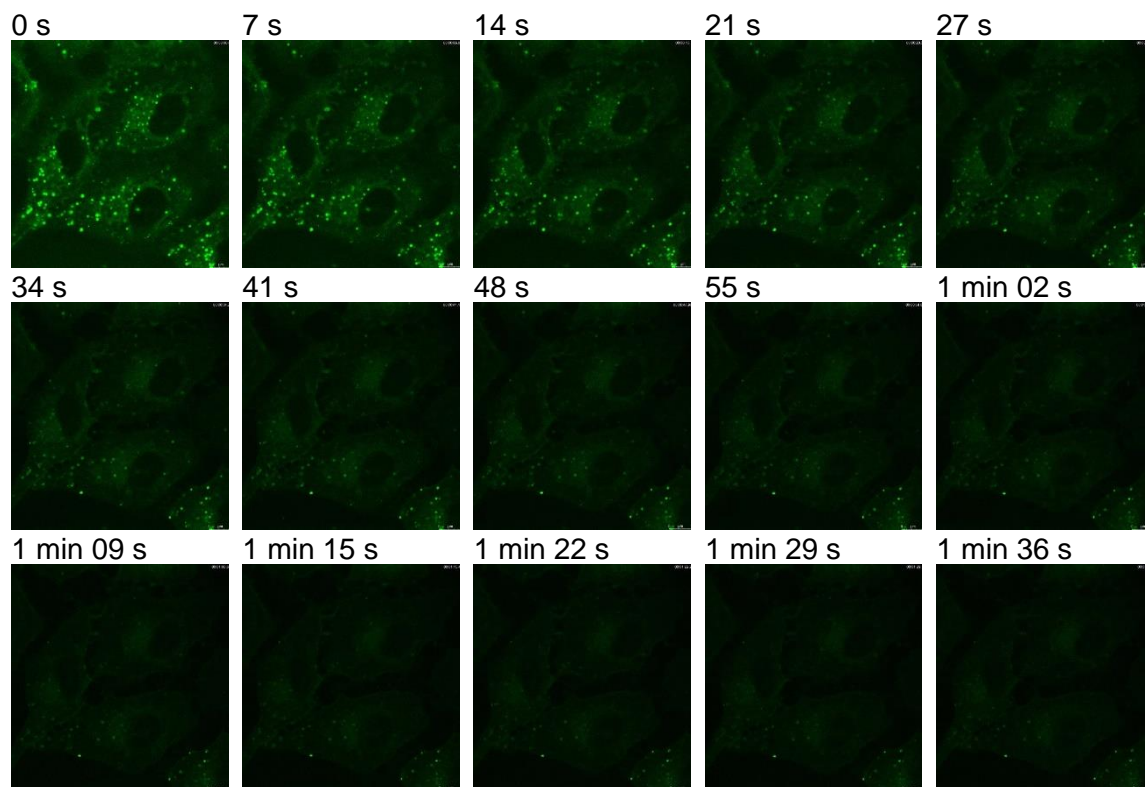


Figure 11.63: Emission of A549 cells stained with Cat^{3+} . Images were taken at times indicated showing fast bleaching of the emission of Cat^{3+} .

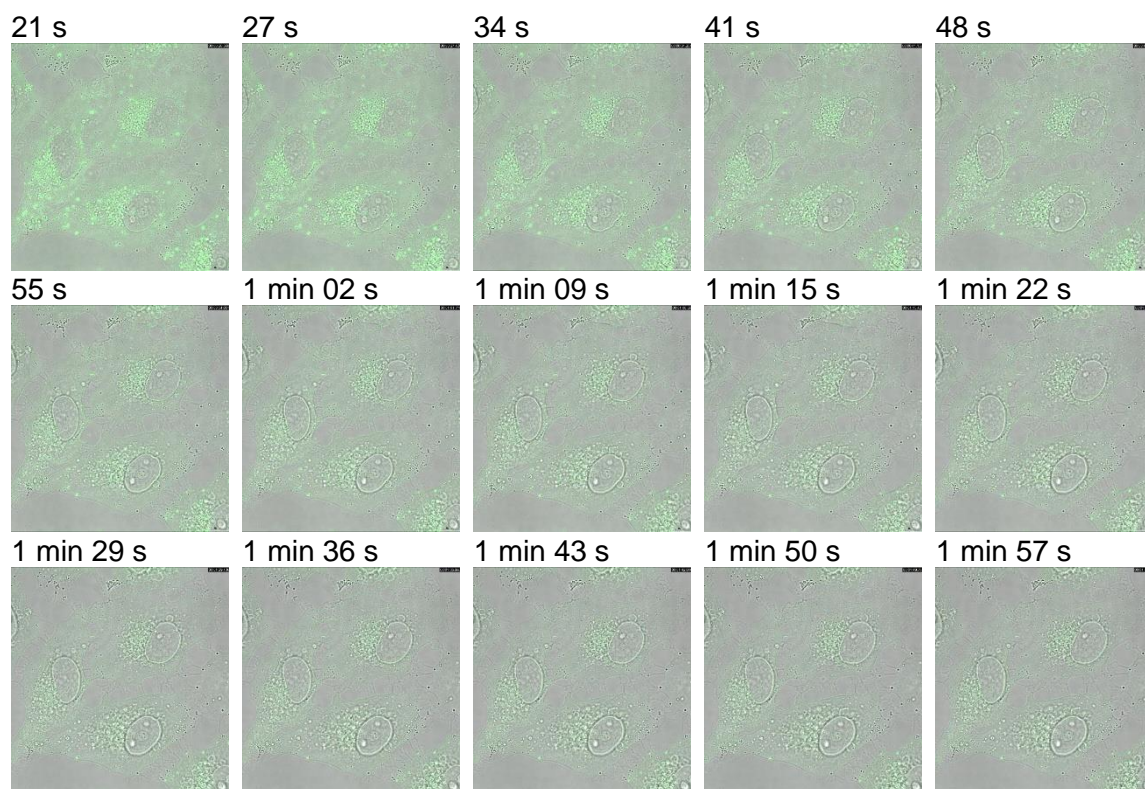
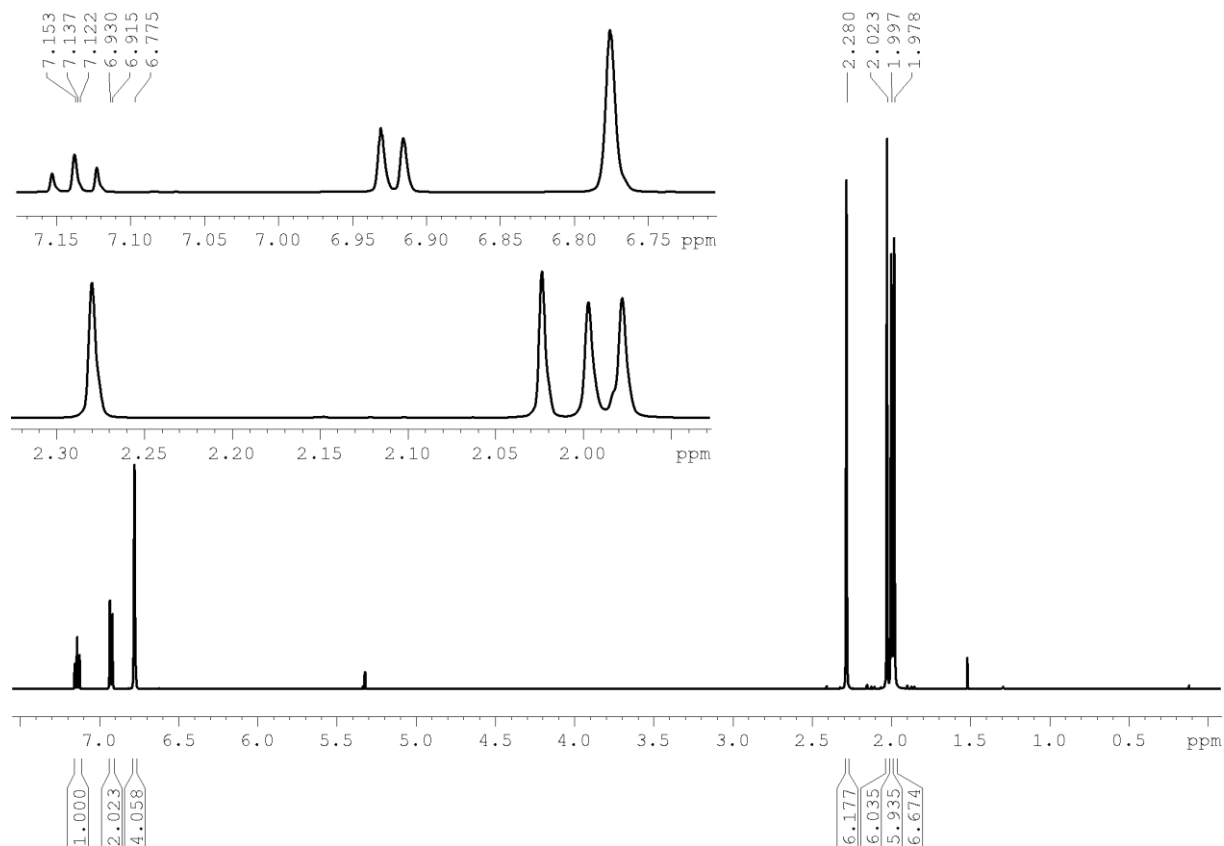
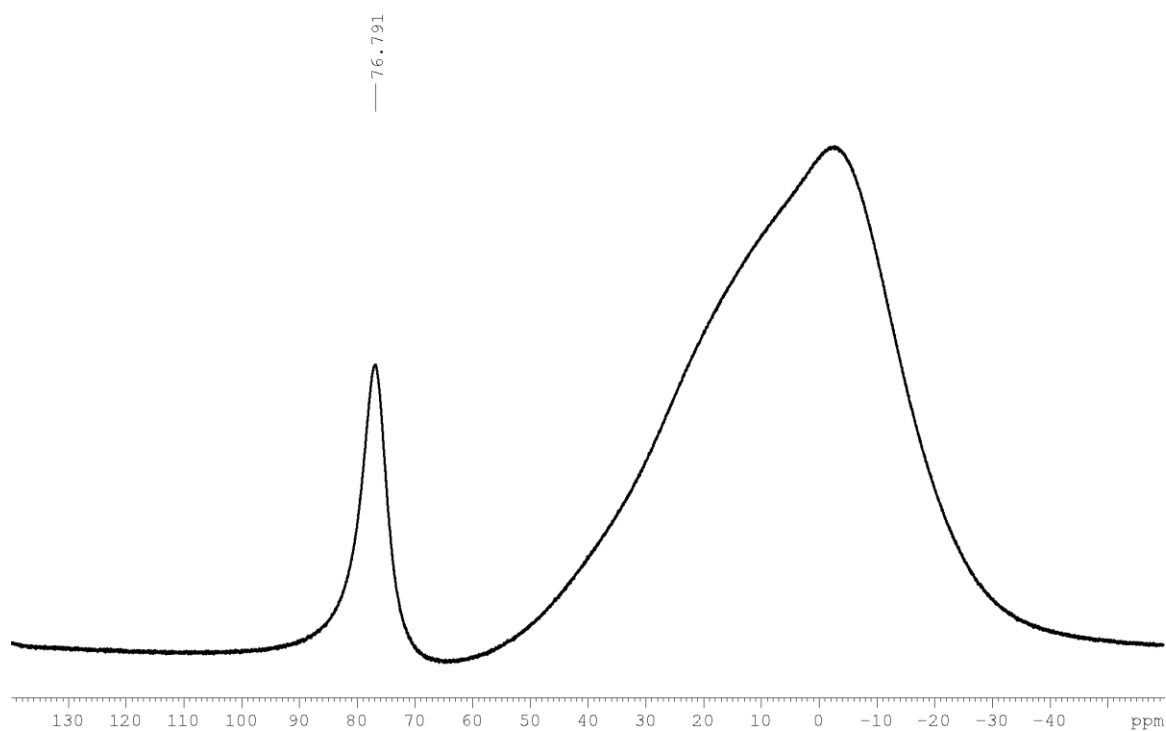




Figure 11.64: Emission of A549 cells stained with Cat^{3+} overlaid with bright field images. Images were taken at times indicated showing fast bleaching of the emission of Cat^{3+} and simultaneous cell blebbing.

11.4 NMR Spectra

11.4.1 Chapter 3

Figure 11.65: ^1H NMR spectrum of compound **3.1a** recorded in CD_2Cl_2 at 500 MHz.Figure 11.66: $^{11}\text{B}\{^1\text{H}\}$ NMR spectrum of compound **3.1a** recorded in CD_2Cl_2 at 160 MHz.

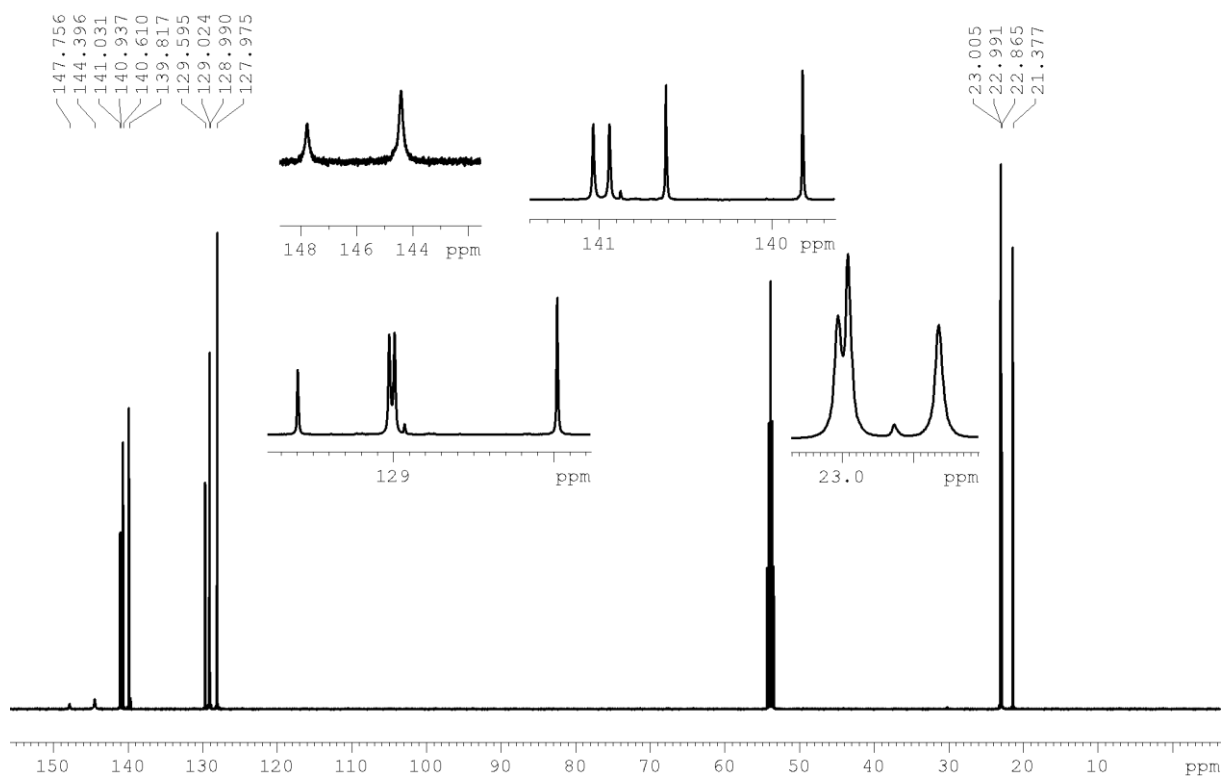


Figure 11.67: $^{13}\text{C}\{^1\text{H}\}$ NMR spectrum of compound **3.1a** recorded in CD_2Cl_2 at 125 MHz.

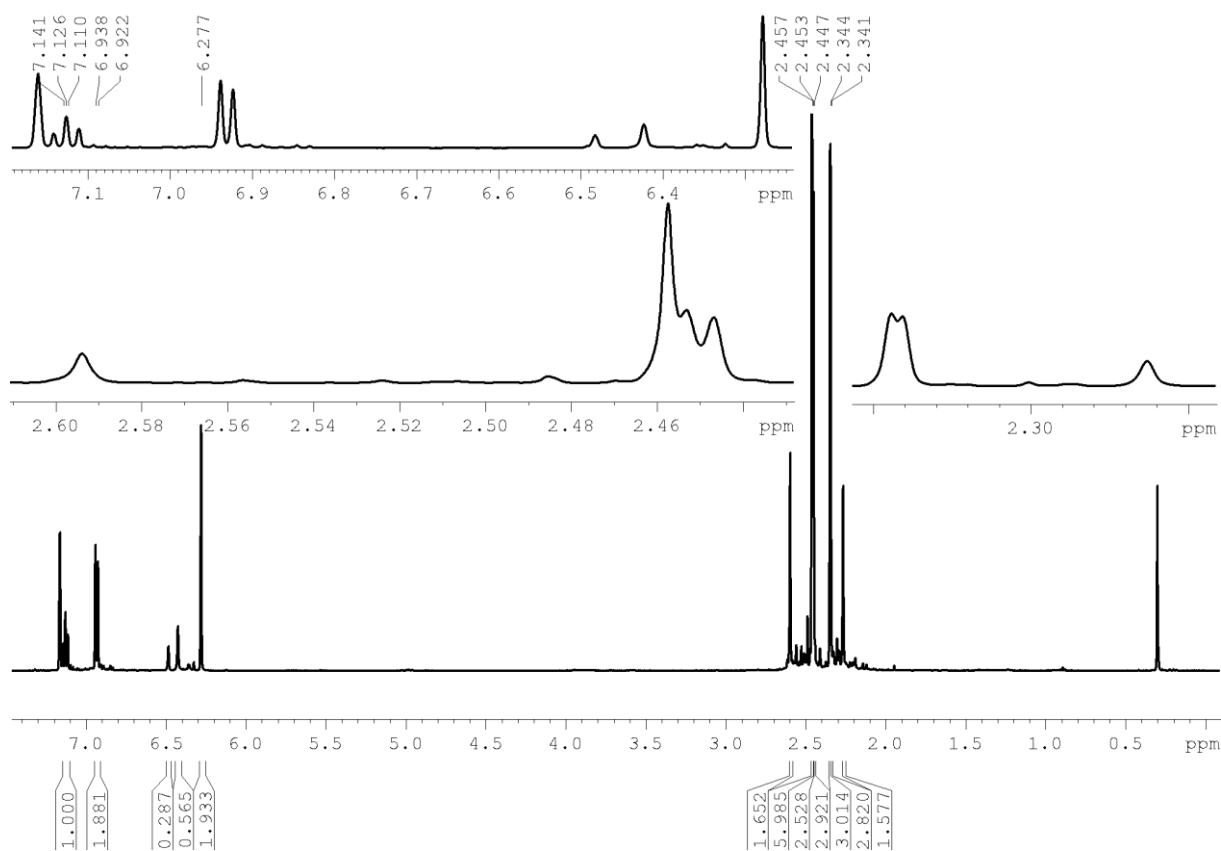


Figure 11.68: ^1H NMR spectrum of **3.11** in C_6D_6 at 500 MHz.

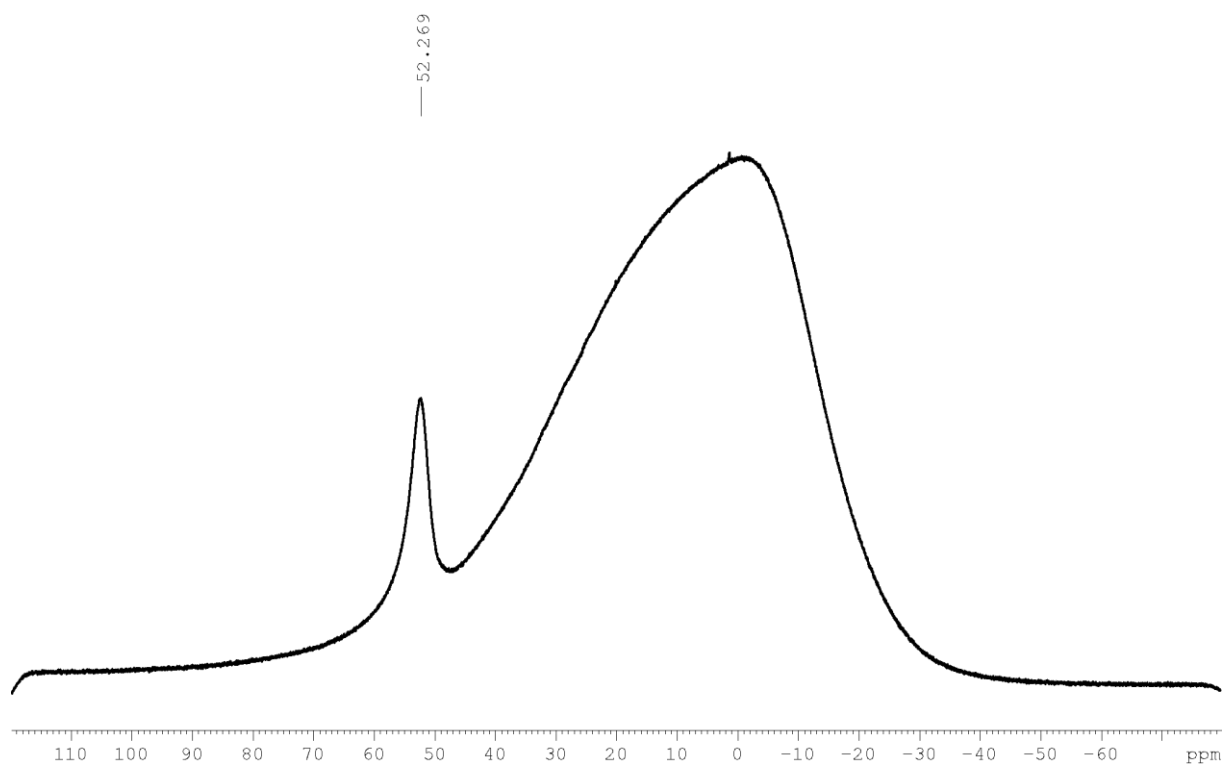


Figure 11.69: $^{11}\text{B}\{^1\text{H}\}$ NMR spectrum of **3.11** in C_6D_6 at 160 MHz.

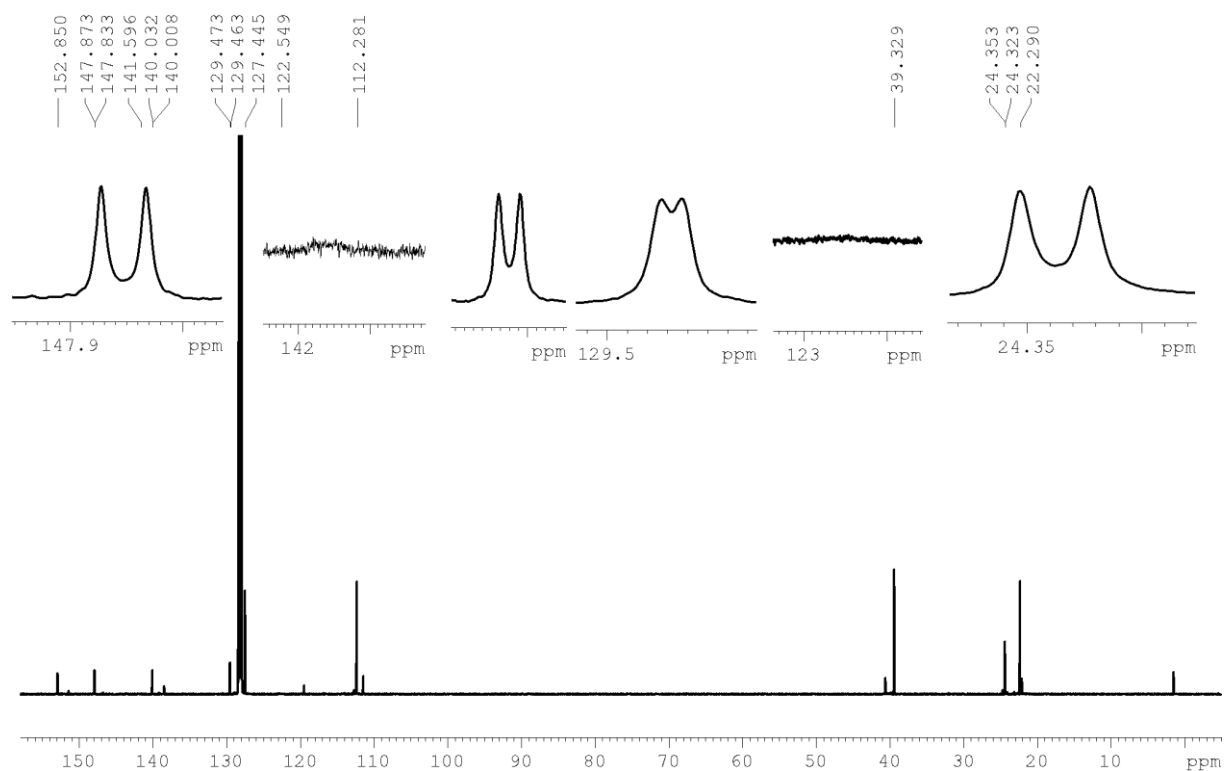


Figure 11.70: $^{13}\text{C}\{^1\text{H}\}$ NMR spectrum of **3.11** in C_6D_6 at 125 MHz.

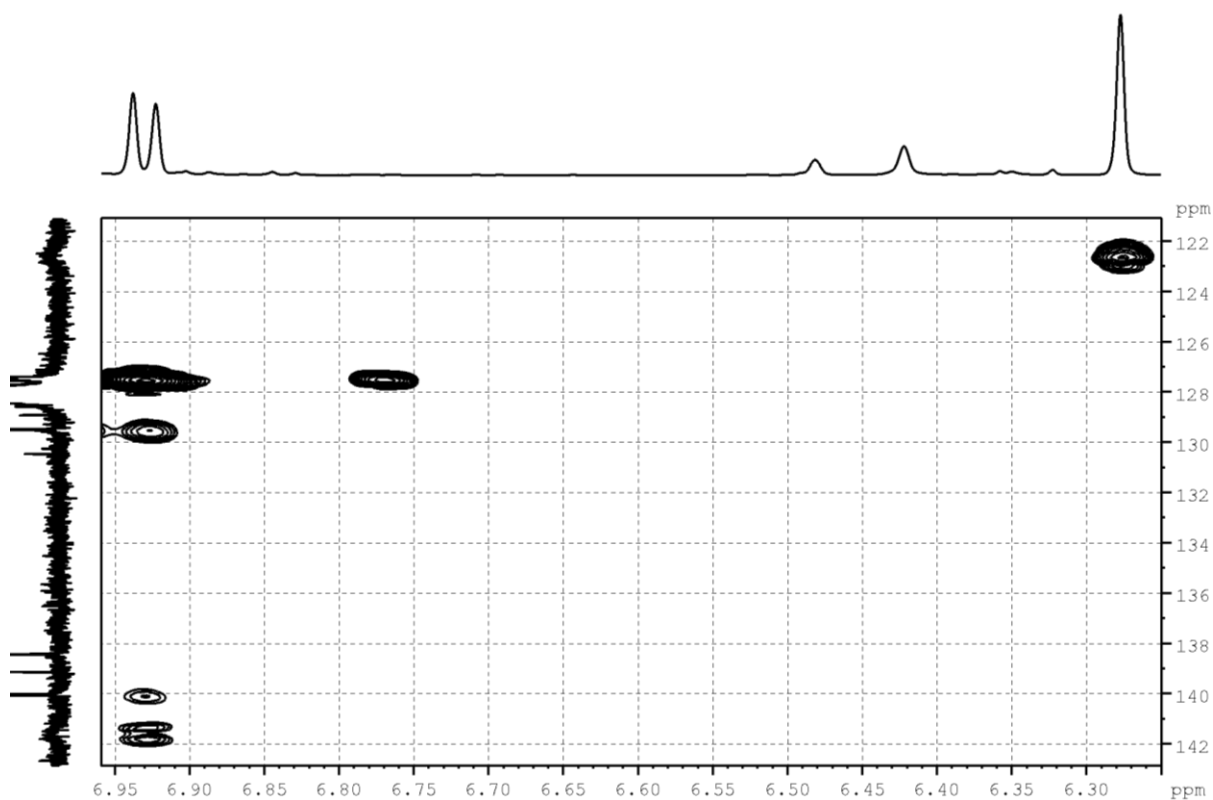


Figure 11.71: ^1H - ^{13}C HMBC NMR spectrum of **3.11** in C_6D_6 at 500 MHz.

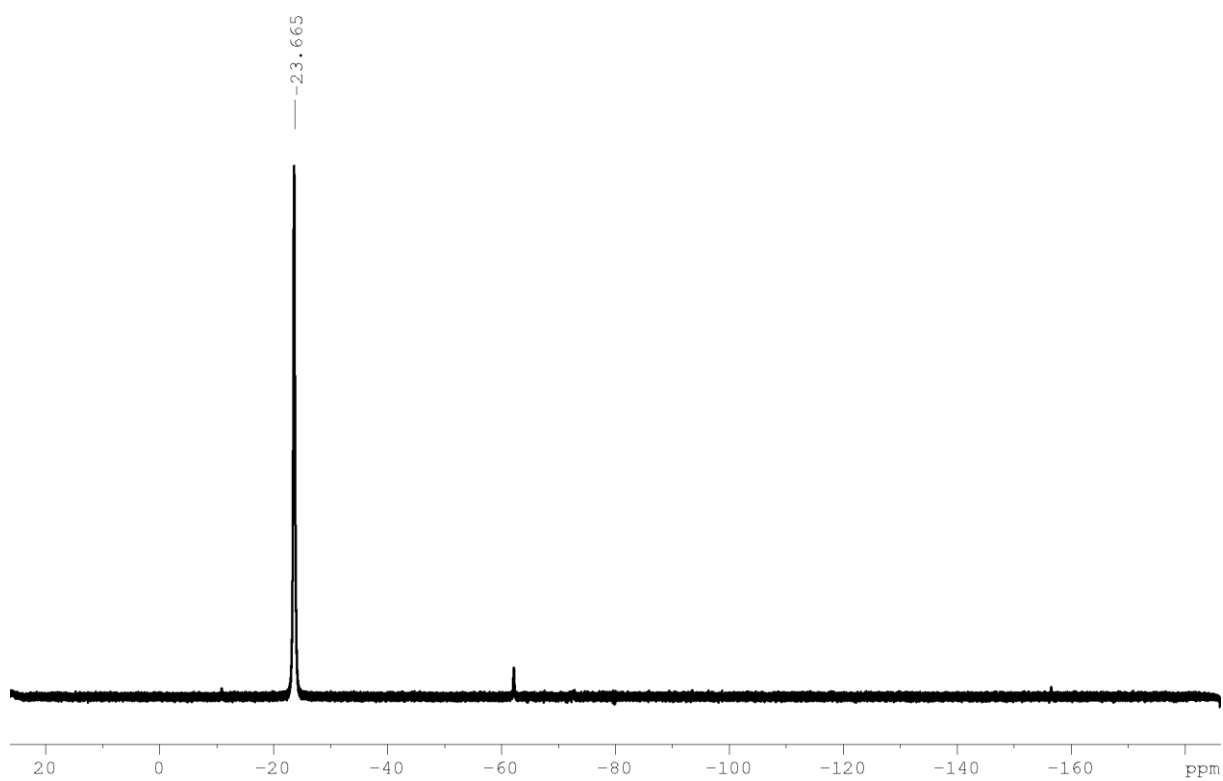


Figure 11.72: ^{19}F NMR spectrum of **3.11** in C_6D_6 at 470 MHz.

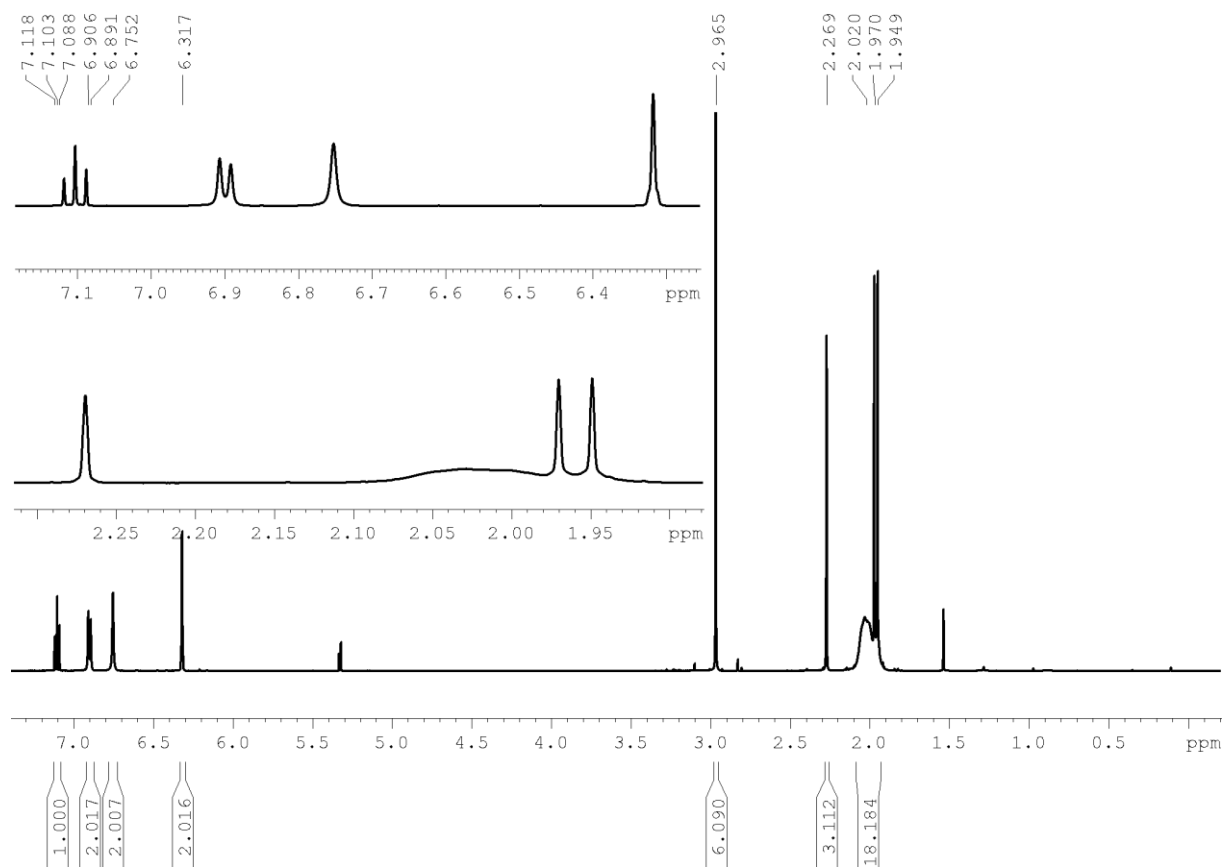


Figure 11.73: ^1H NMR spectrum of **3.2a** in CD_2Cl_2 at 500 MHz.

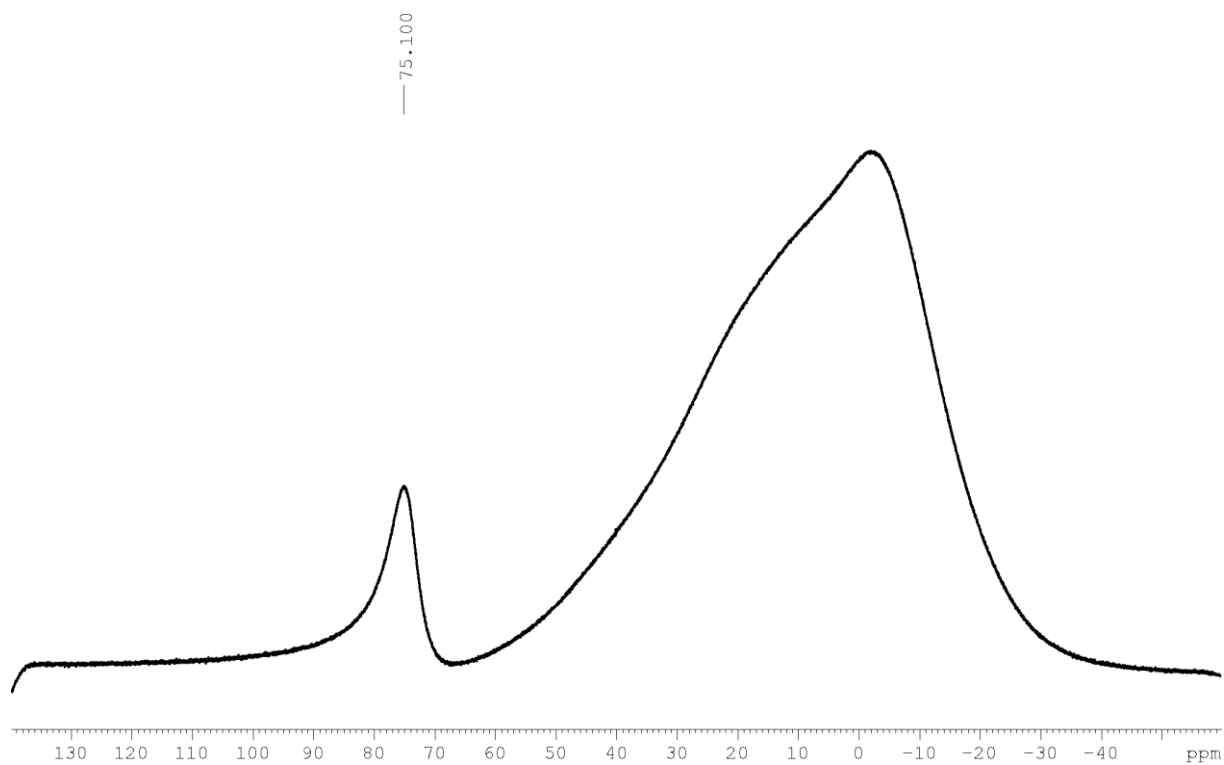


Figure 11.74: $^{11}\text{B}\{^1\text{H}\}$ NMR spectrum of **3.2a** in CD_2Cl_2 at 160 MHz.

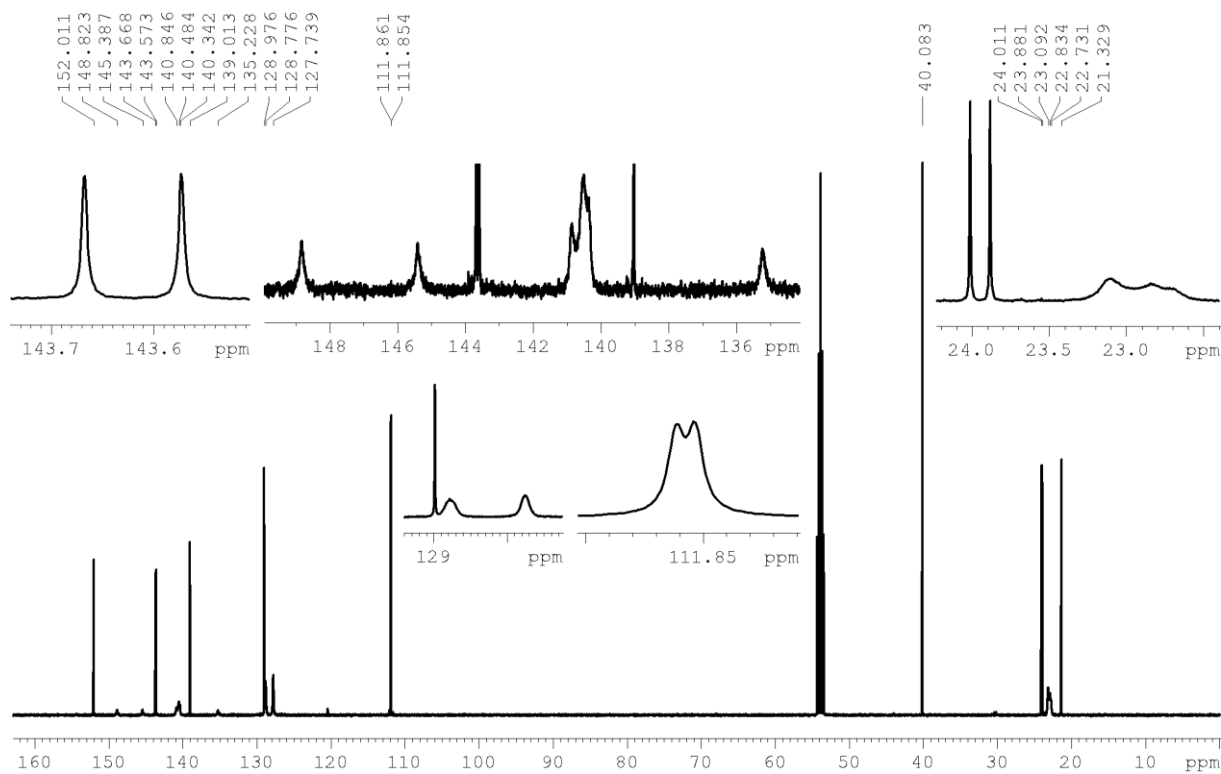


Figure 11.75: $^{13}\text{C}\{^1\text{H}\}$ NMR spectrum of **3.2a** in CD_2Cl_2 at 125 MHz.

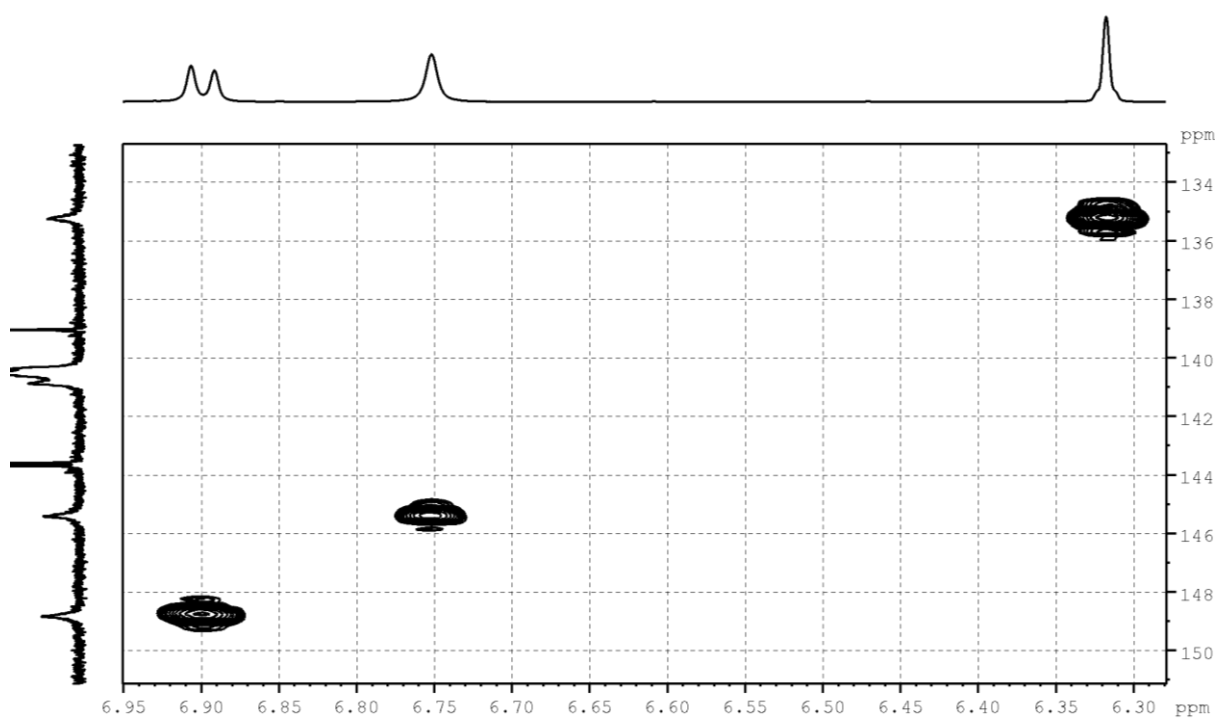
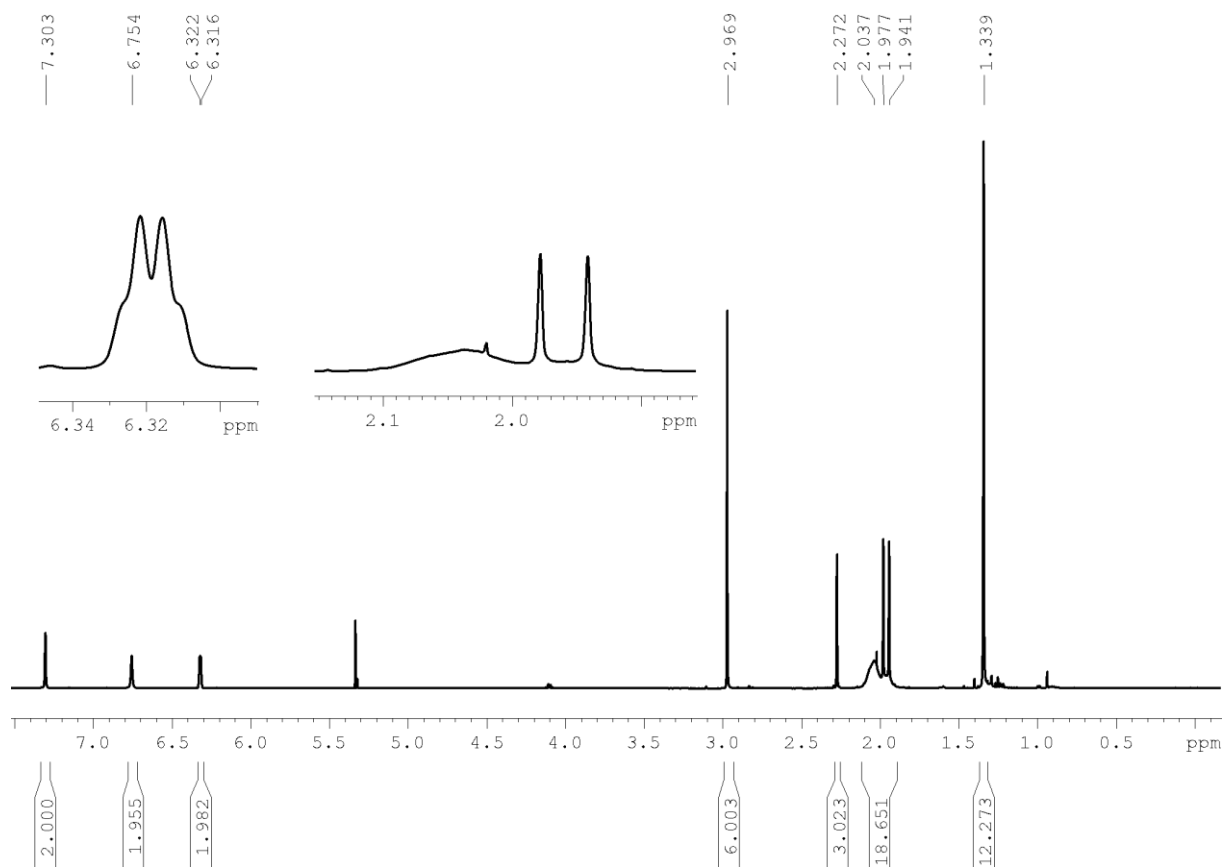
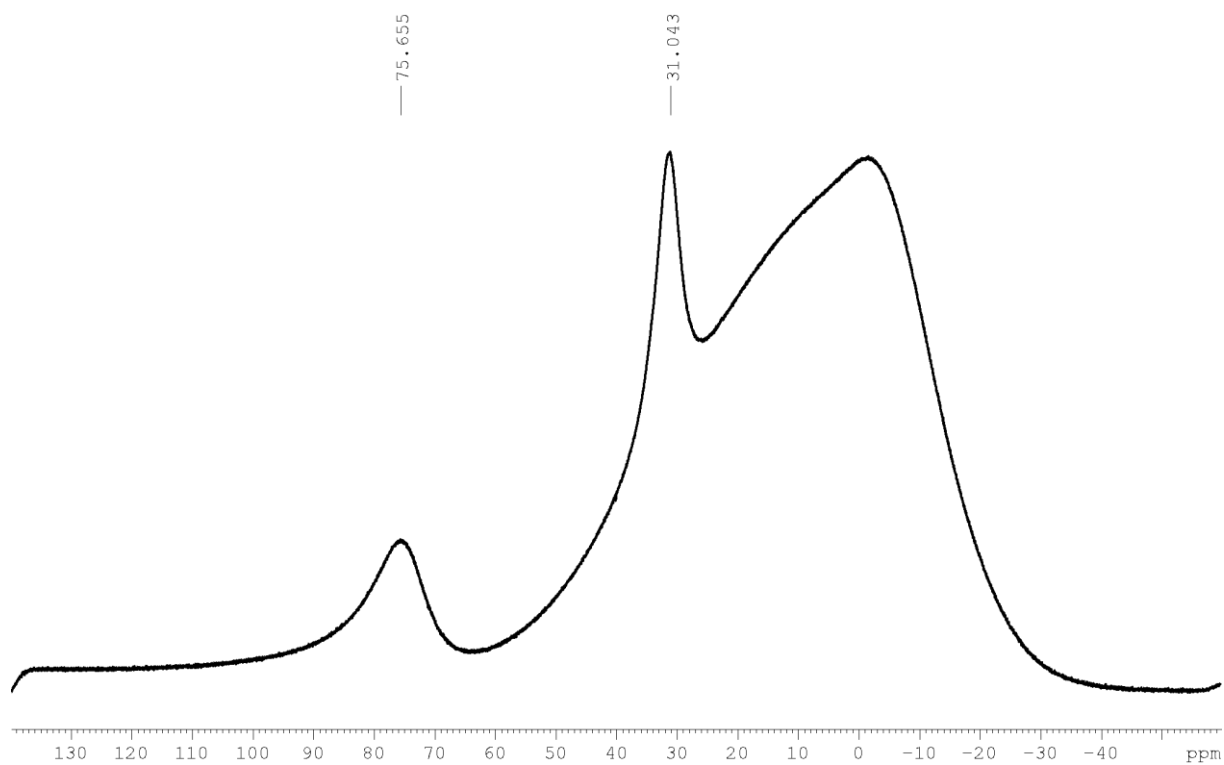


Figure 11.76: $^1\text{H} - ^{13}\text{C}$ HMBC NMR spectrum of **3.2a** in CD_2Cl_2 at 500 MHz.

Figure 11.77: ^1H NMR spectrum of **3.2b** in CD_2Cl_2 at 500 MHz.Figure 11.78: $^{11}\text{B}\{^1\text{H}\}$ NMR spectrum of **3.2b** in CD_2Cl_2 at 160 MHz.

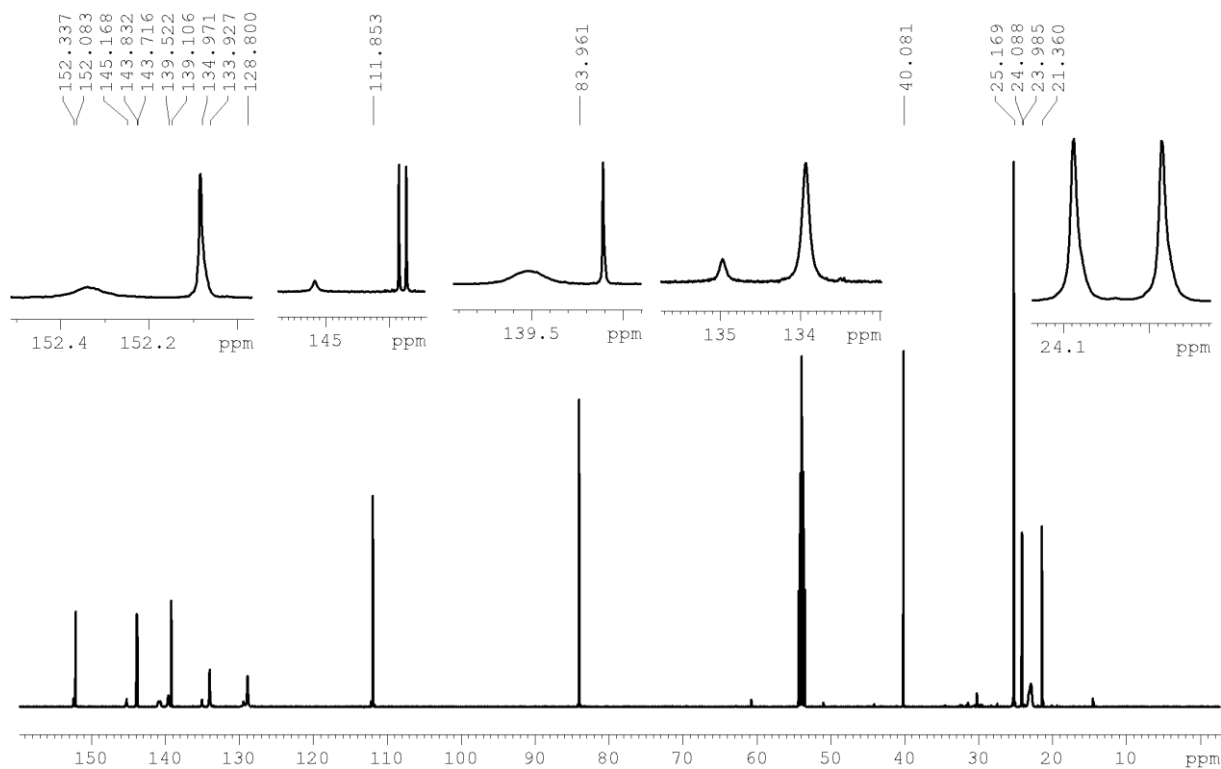


Figure 11.79: $^{13}\text{C}\{^1\text{H}\}$ NMR spectrum of **3.2b** in CD_2Cl_2 at 125 MHz.

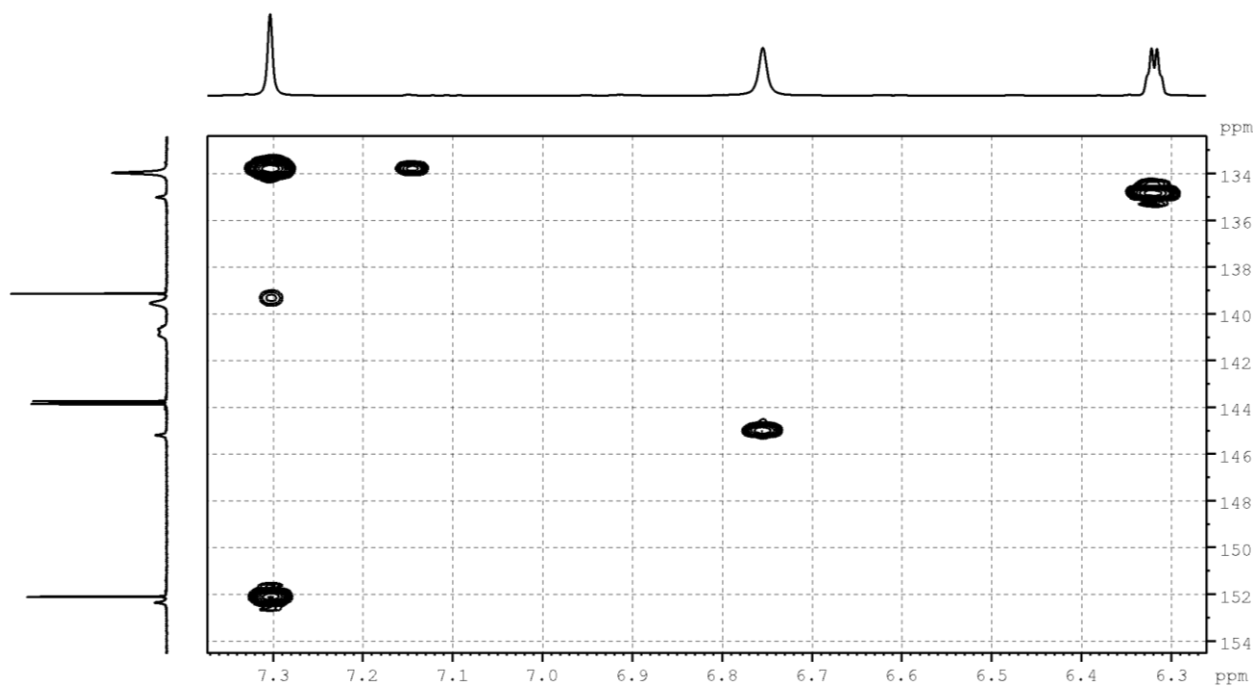


Figure 11.80: $^1\text{H} - ^{13}\text{C}$ HMBC NMR spectrum of **3.2b** in CD_2Cl_2 at 500 MHz.

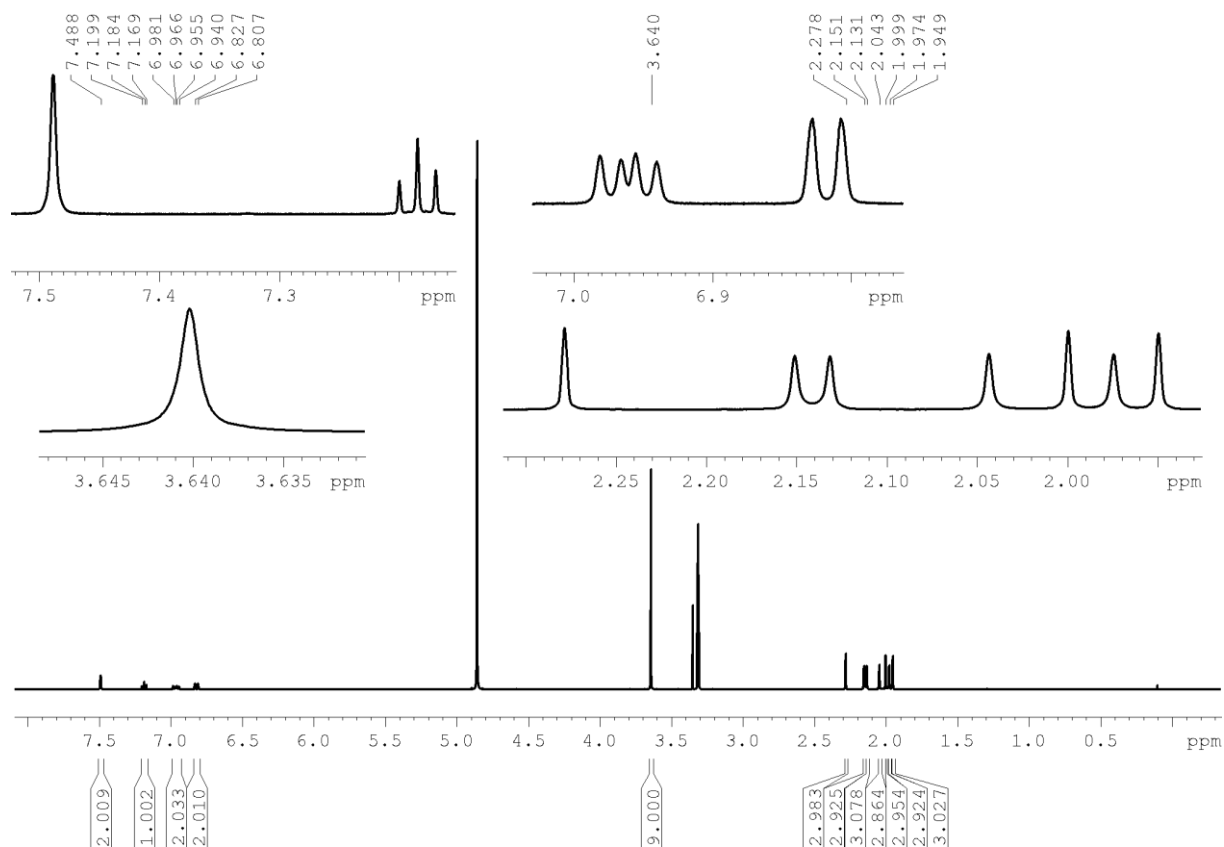


Figure 11.81: ^1H NMR spectrum of compound **3.2c** recorded in CD_3OD at 500 MHz.

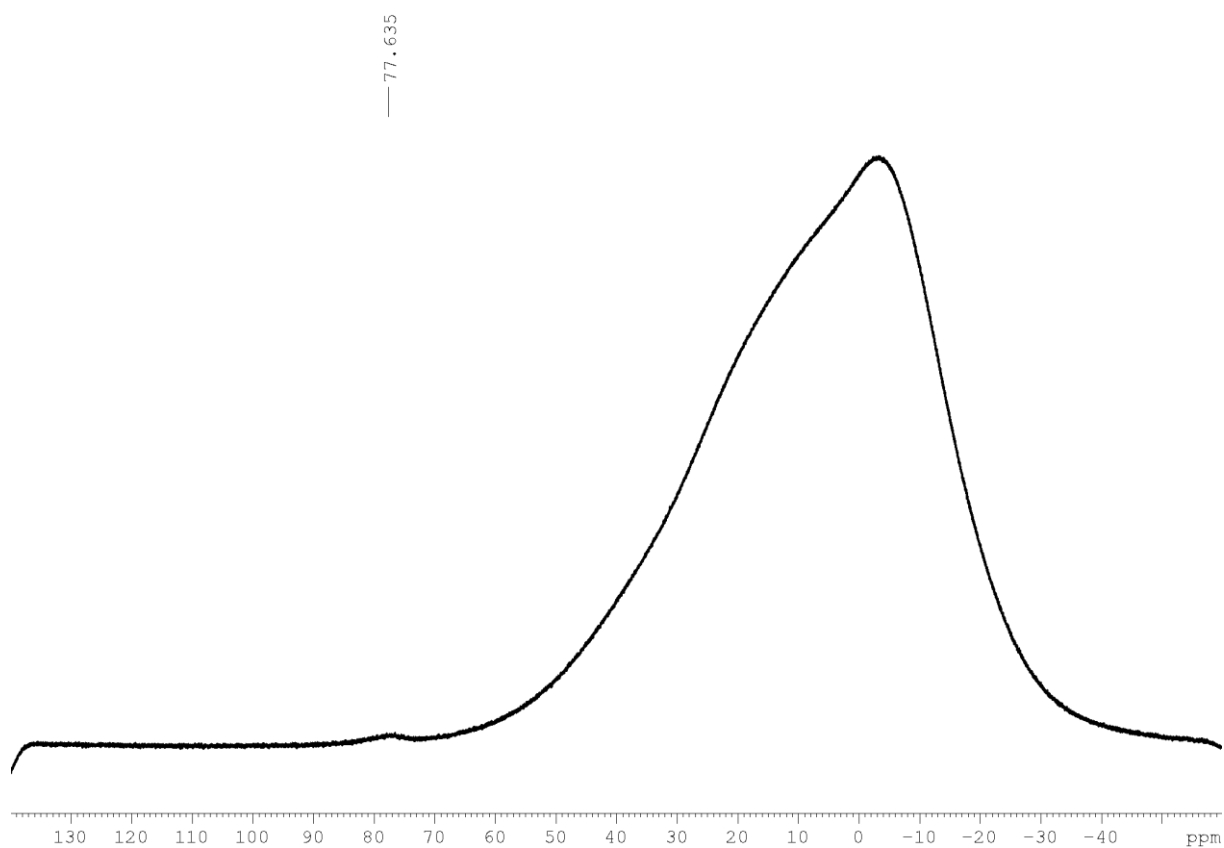


Figure 11.82: $^{11}\text{B}\{^1\text{H}\}$ NMR spectrum of compound **3.2c** recorded in CD_3OD at 160 MHz.

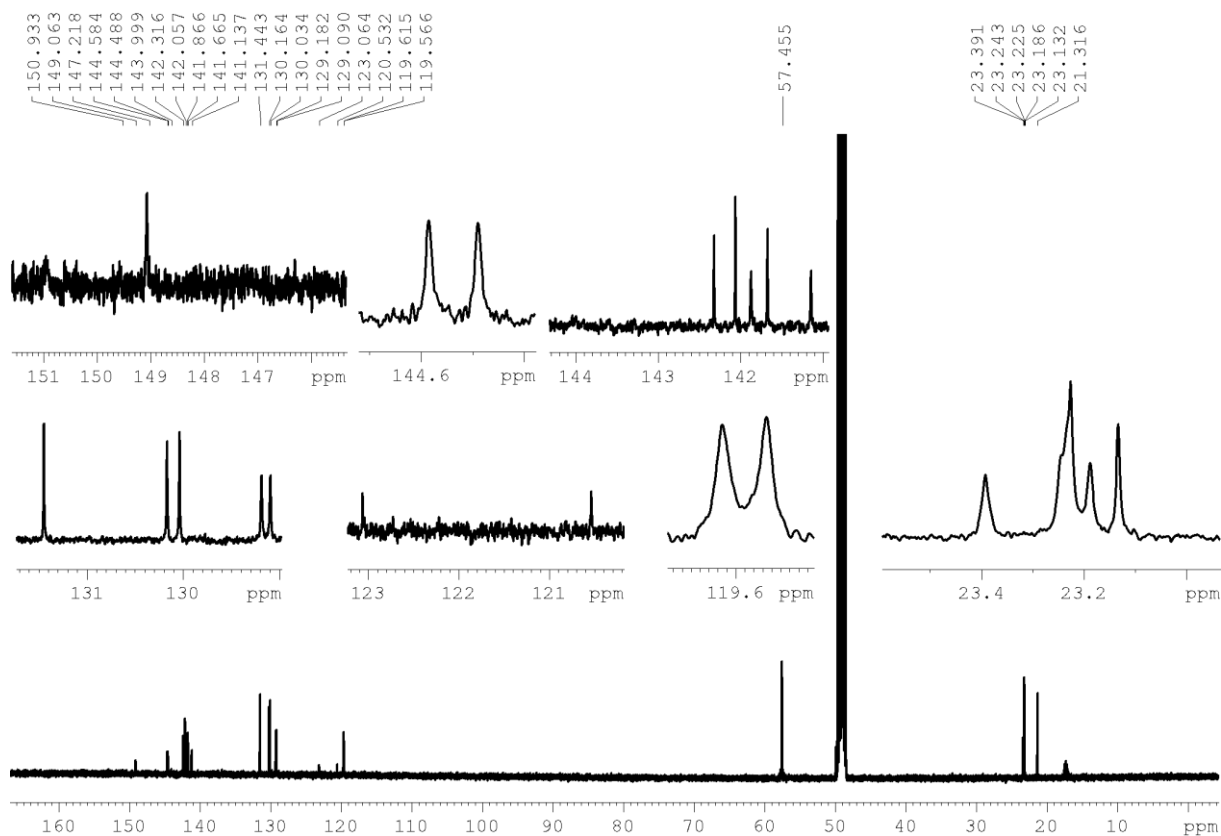


Figure 11.83: $^{13}\text{C}\{^1\text{H}\}$ NMR spectrum of compound **3.2c** recorded in CD_3OD at 125 MHz.

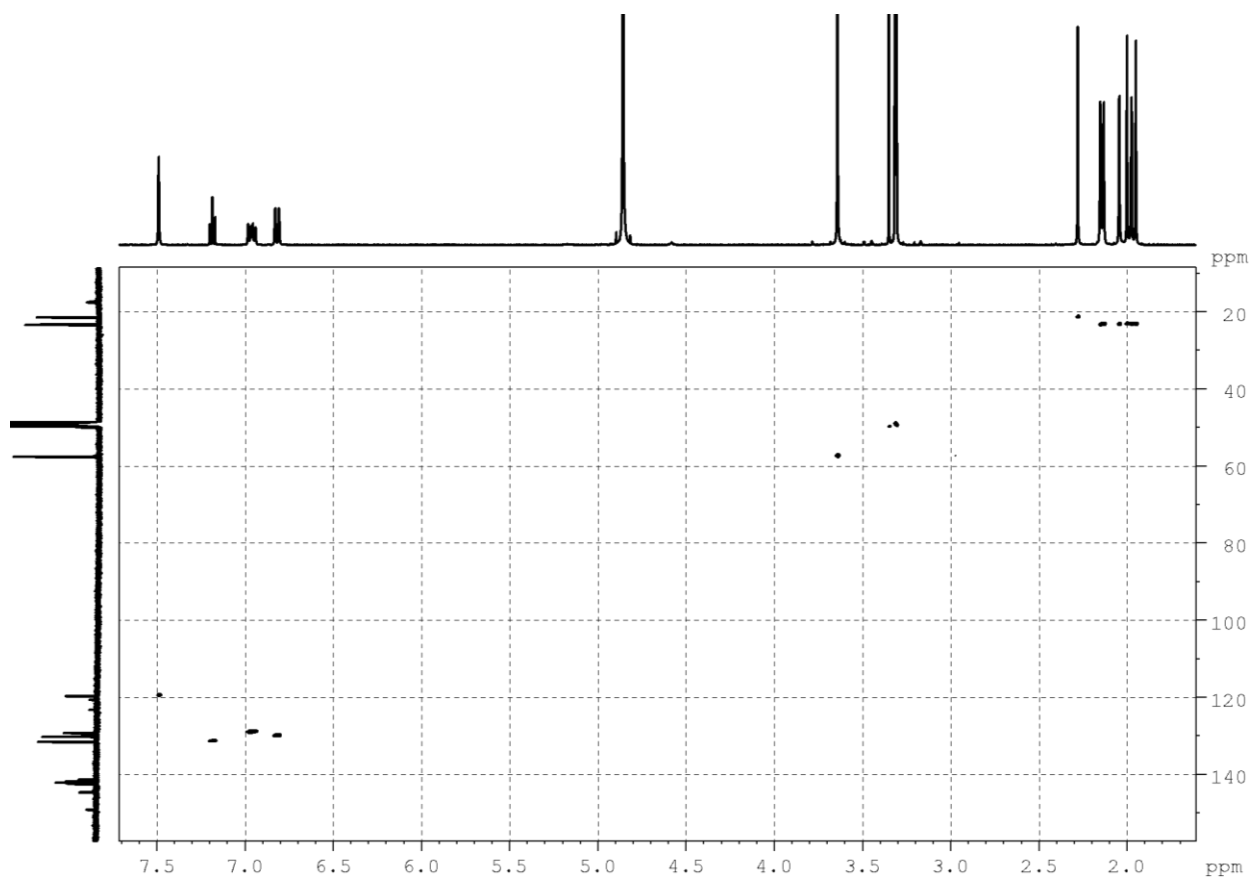


Figure 11.84: $^1\text{H} - ^{13}\text{C}$ HSQC spectrum of compound **3.2c** recorded in CD_3OD at 500 MHz.

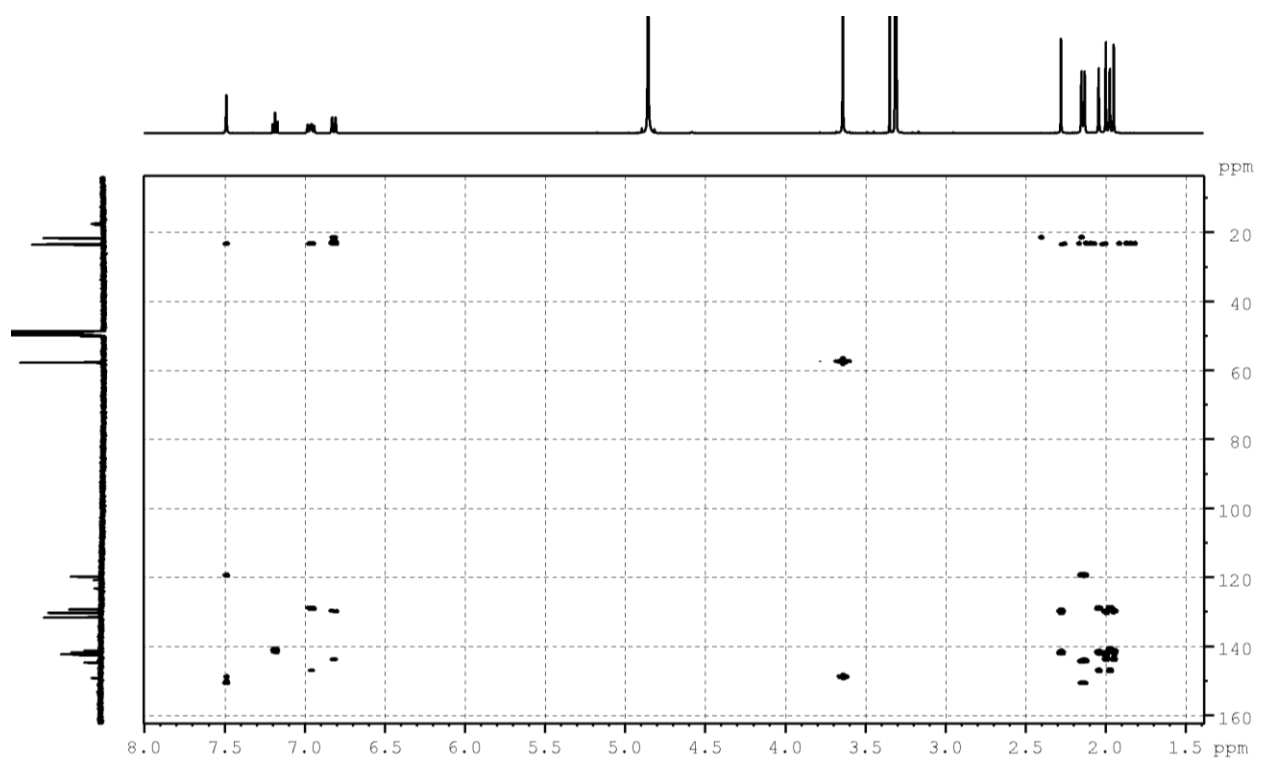
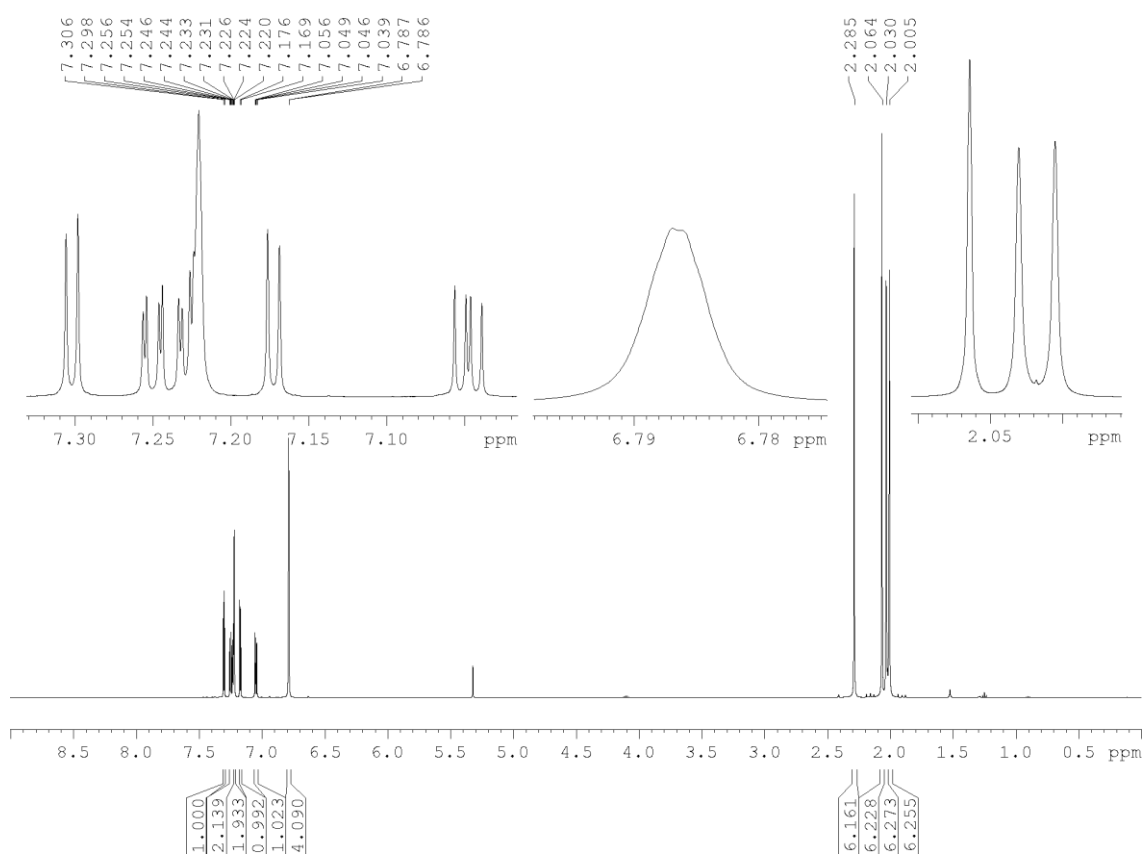
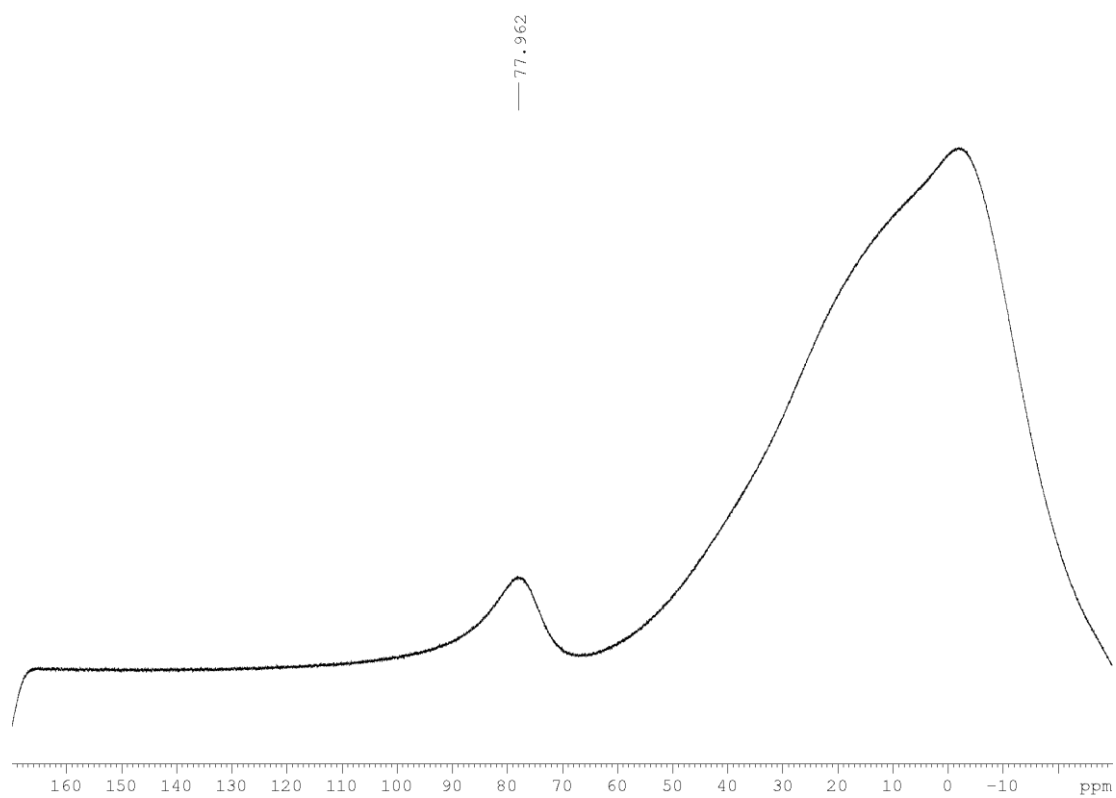


Figure 11.85: ^1H – ^{13}C HMBC spectrum of compound **3.2c** recorded in CD_3OD at 500 MHz.

11.4.2 Chapter 4

Figure 11.86: ^1H NMR spectrum of **4.2** recorded in CD_2Cl_2 at 500 MHz.Figure 11.87: $^{11}\text{B}\{^1\text{H}\}$ NMR spectrum of **4.2** recorded in CD_2Cl_2 at 160 MHz.

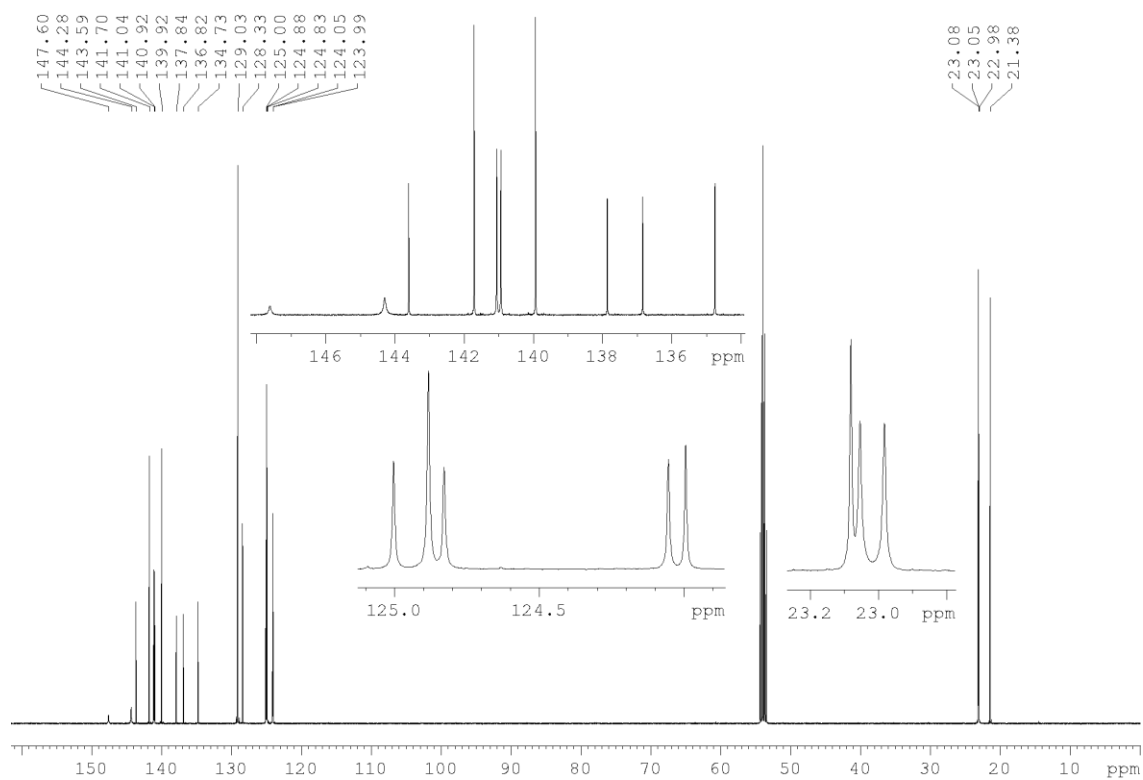


Figure 11.88: $^{13}\text{C}\{^1\text{H}\}$ NMR spectrum of **4.2** recorded in CD_2Cl_2 at 125 MHz.

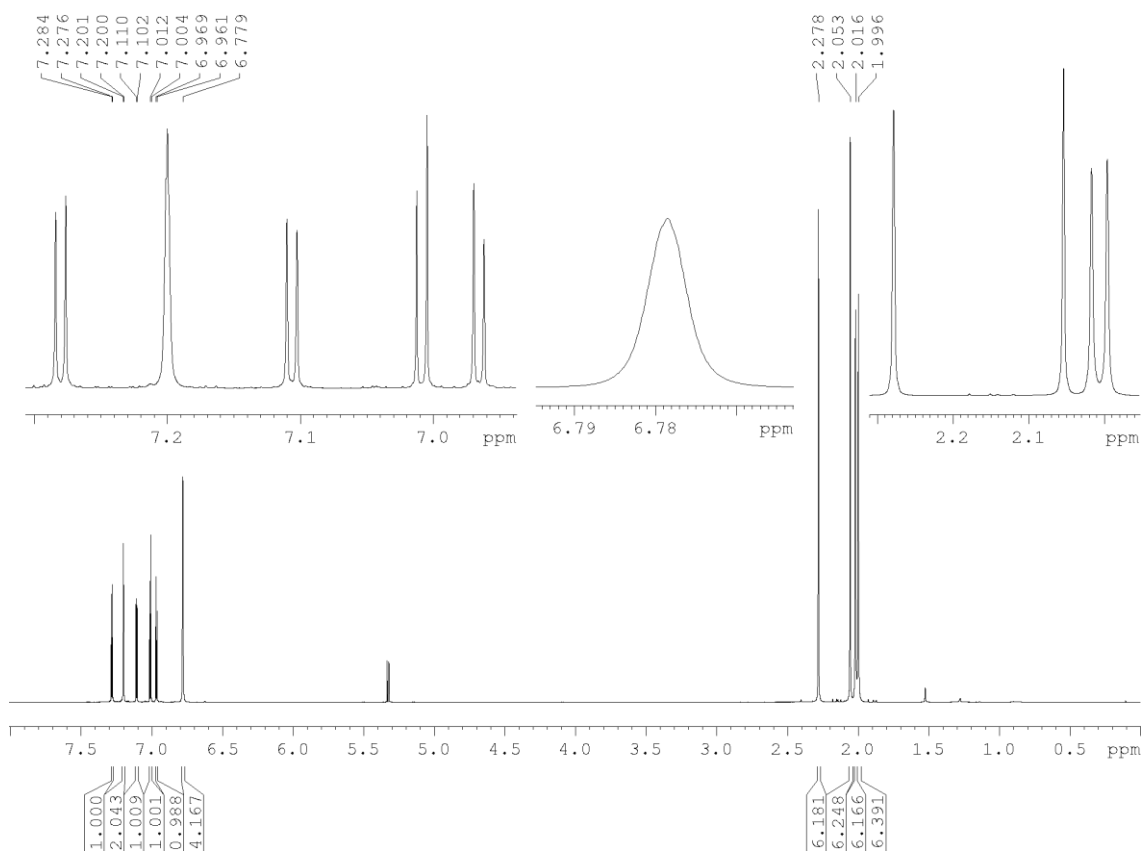


Figure 11.89: ^1H NMR spectrum of **4.3** recorded in CD_2Cl_2 at 500 MHz.

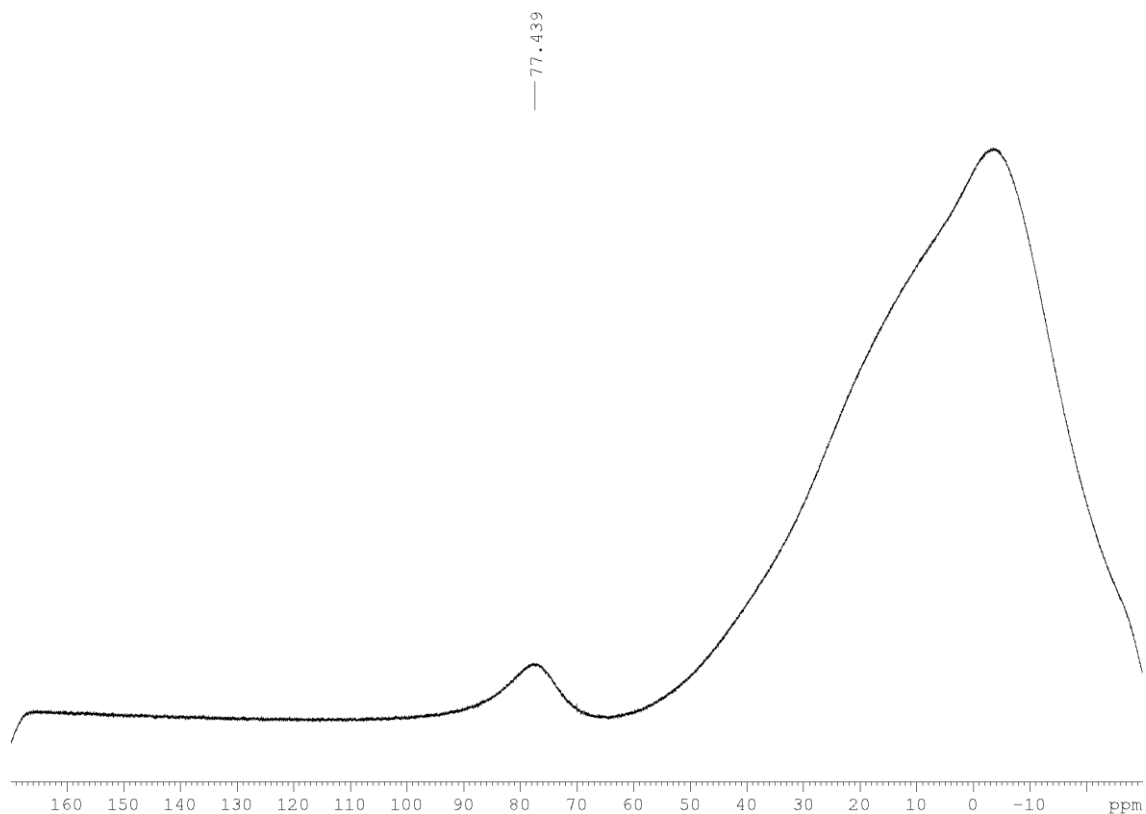


Figure 11.90: $^{11}\text{B}\{^1\text{H}\}$ NMR spectrum of **4.3** recorded in CD_2Cl_2 at 160 MHz.

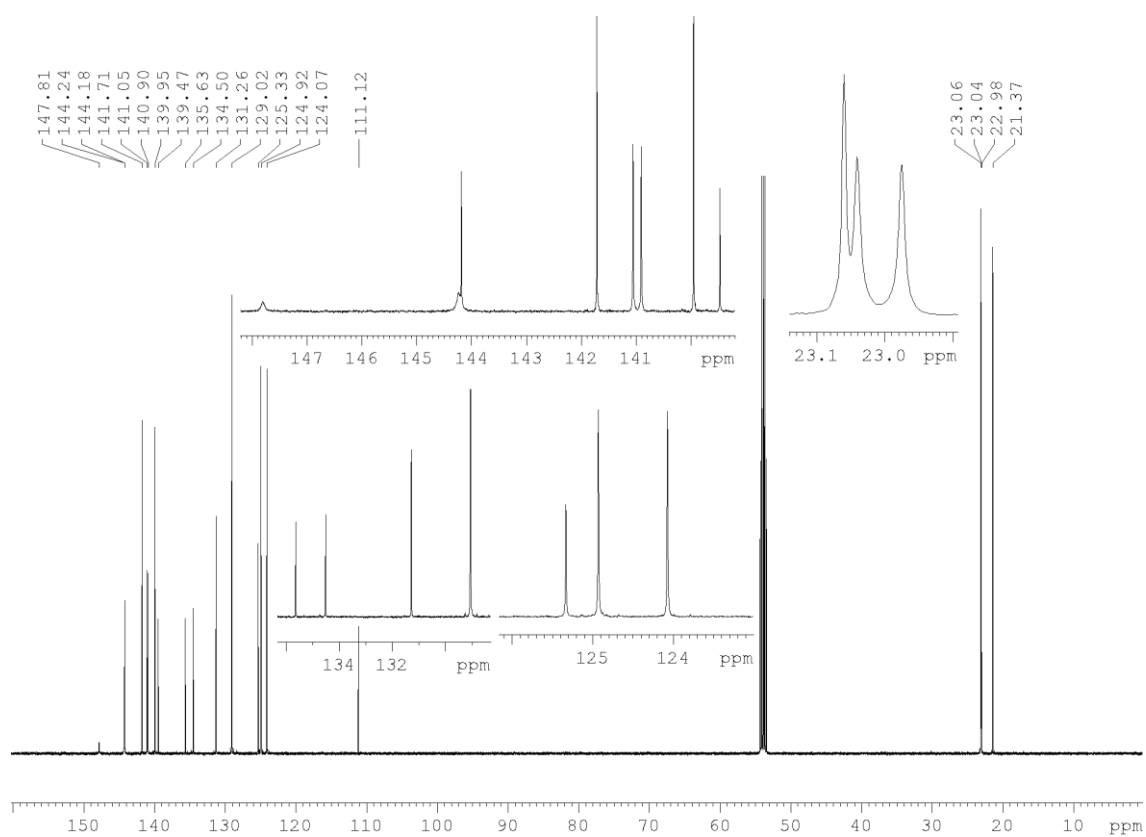


Figure 11.91: $^{13}\text{C}\{^1\text{H}\}$ NMR spectrum of **4.3** recorded in CD_2Cl_2 at 125 MHz.

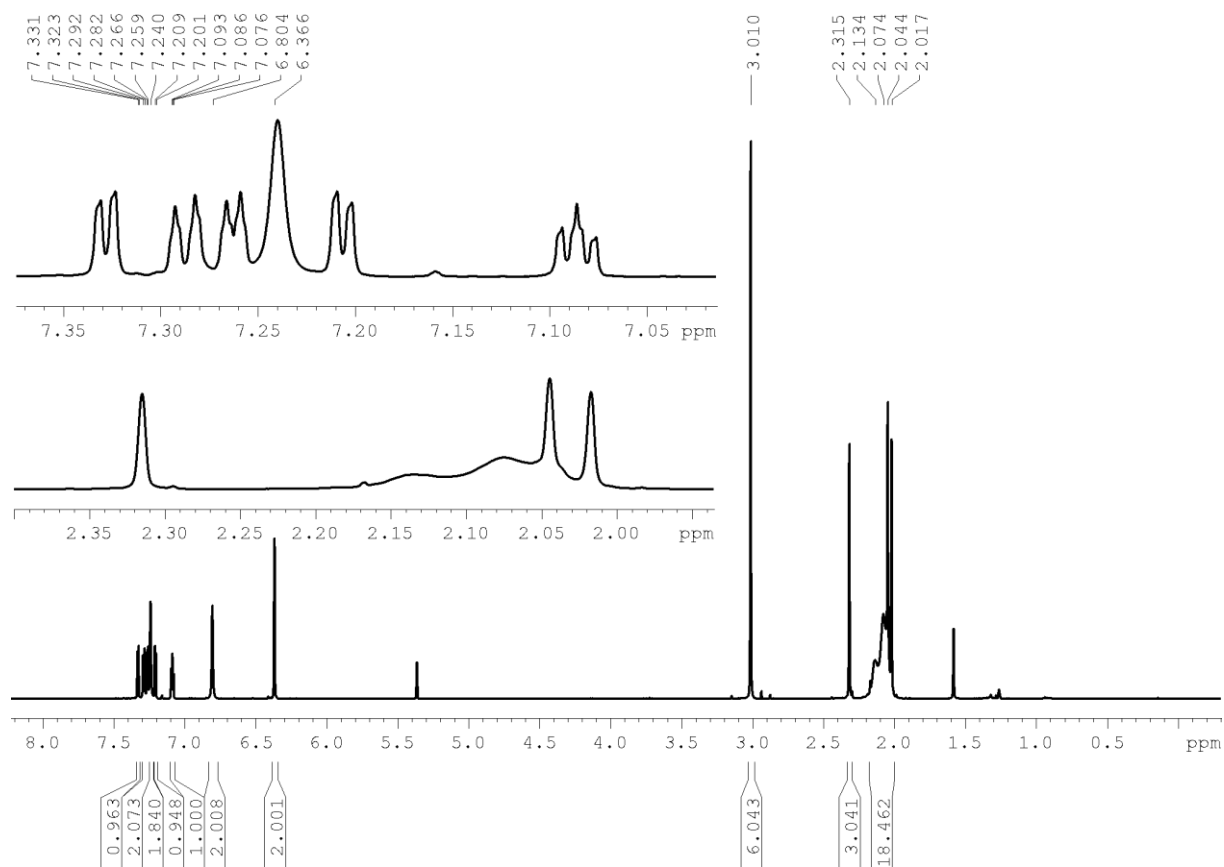


Figure 11.92: ^1H NMR spectrum of **4.5** recorded in CD_2Cl_2 at 500 MHz.

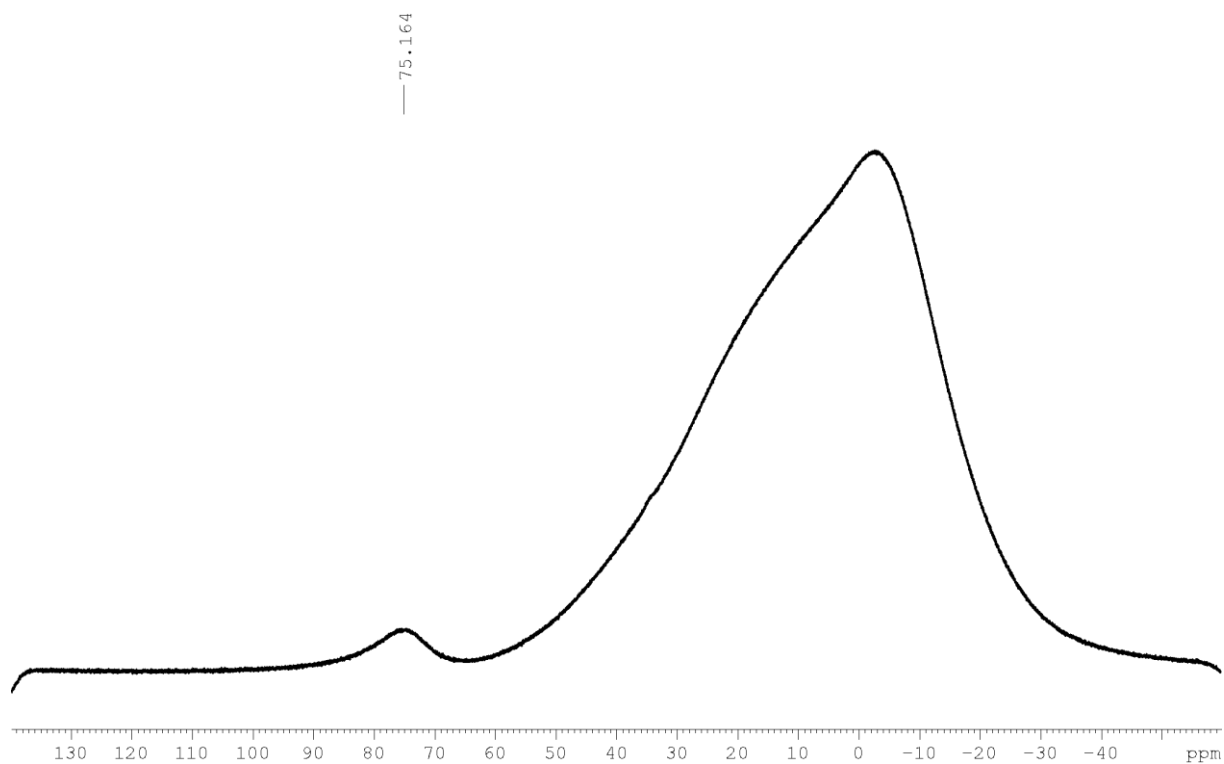


Figure 11.93: $^{11}\text{B}\{^1\text{H}\}$ NMR spectrum of **4.5** recorded in CD_2Cl_2 at 160 MHz.

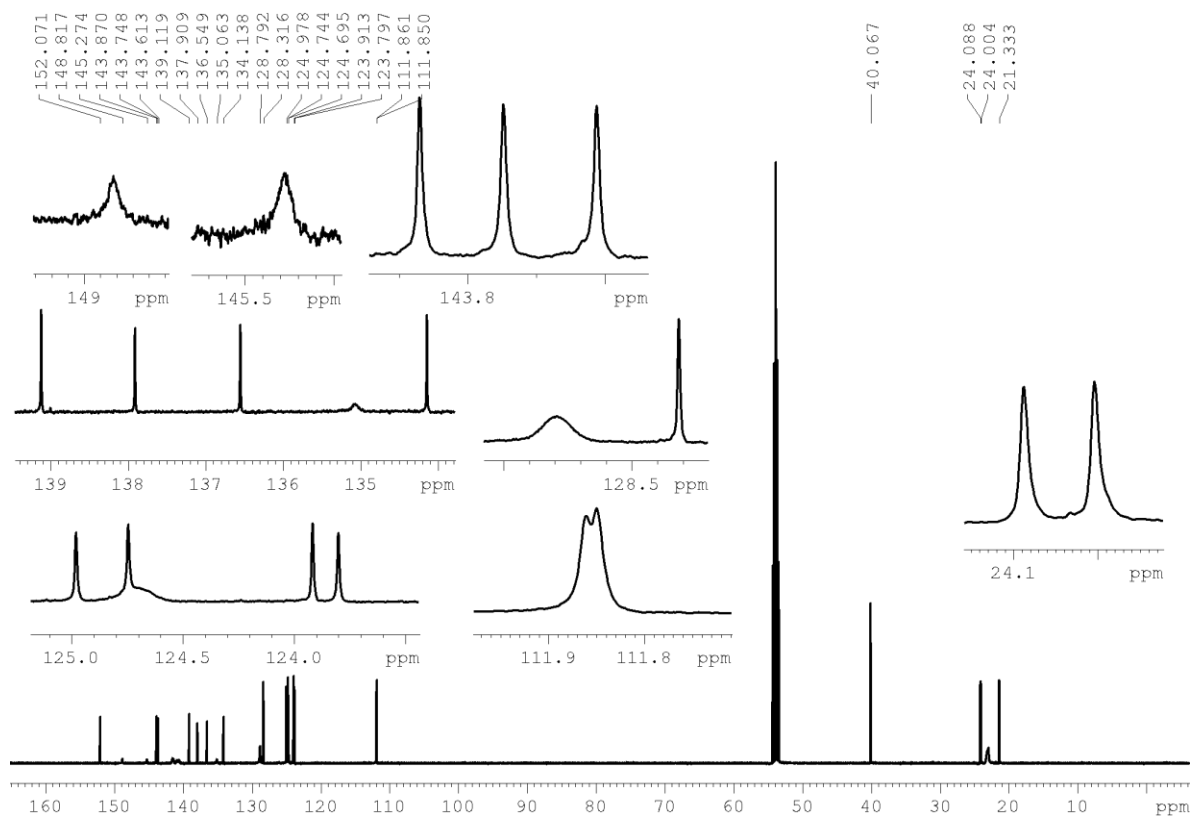


Figure 11.94: $^{13}\text{C}\{^1\text{H}\}$ NMR spectrum of **4.5** recorded in CD_2Cl_2 at 125 MHz.

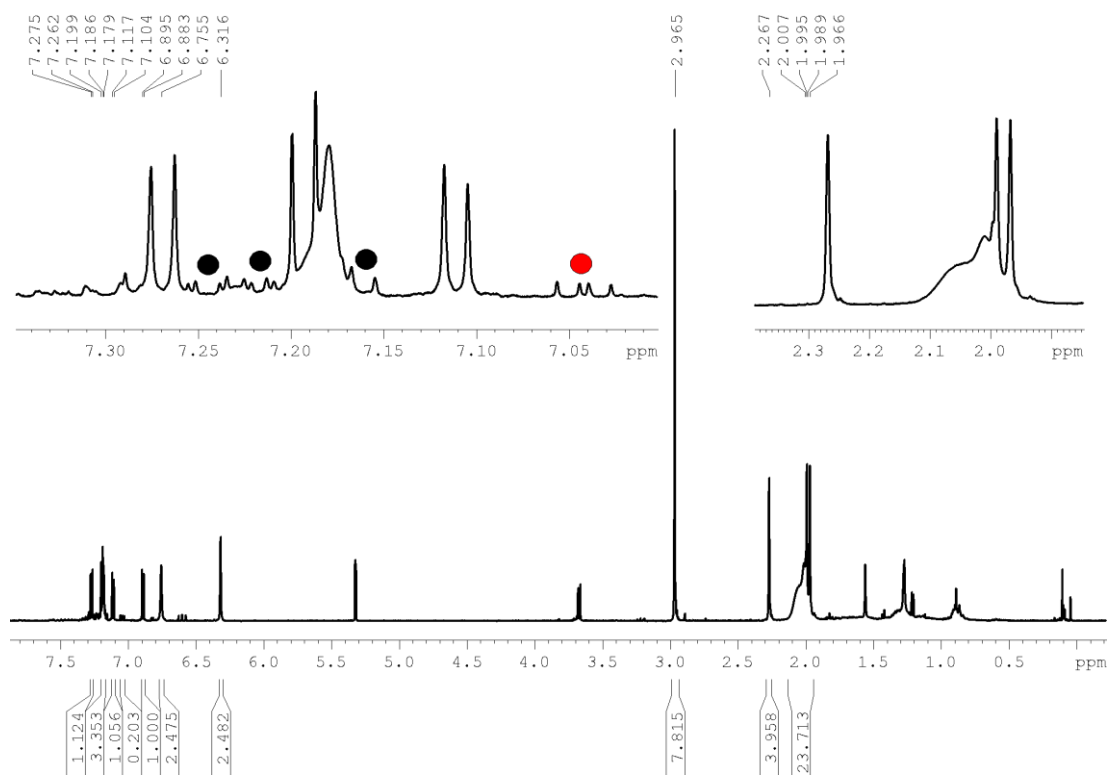


Figure 11.95: ^1H NMR spectrum of compound **4.6** recorded in CD_2Cl_2 at 300 MHz. Dots mark remaining starting material. Red dot marks signal which was used for estimation of ratio of starting material to product.

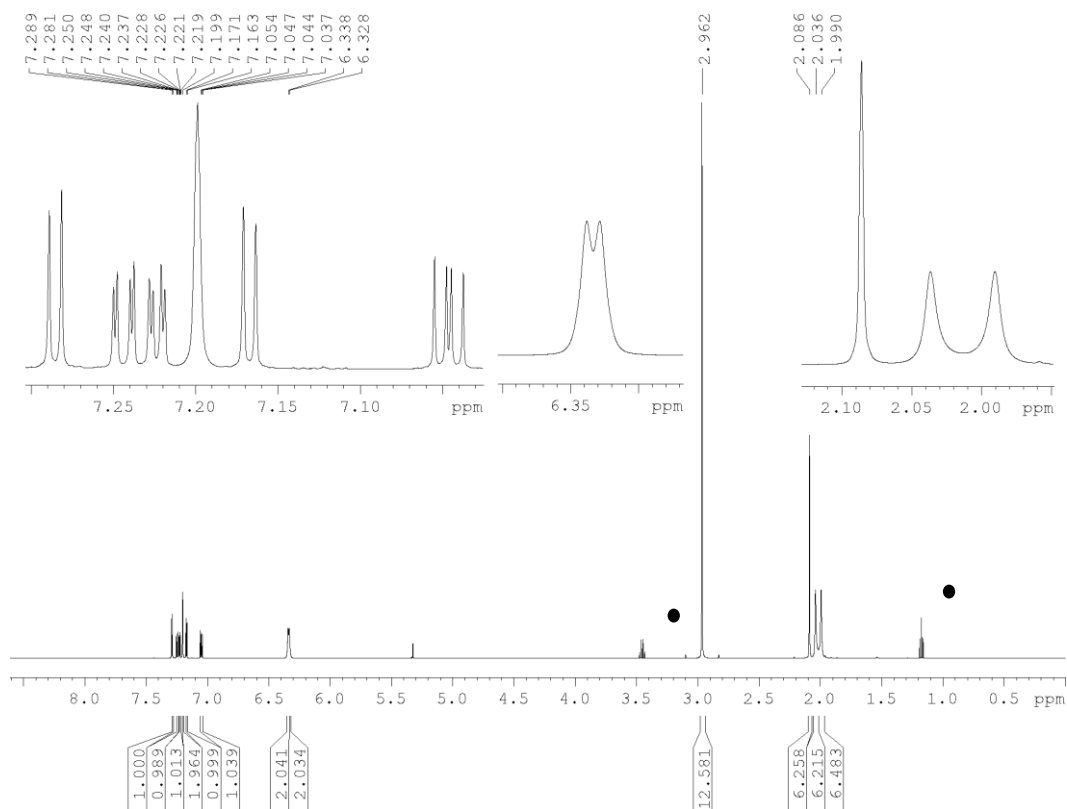


Figure 11.96: ^1H NMR spectrum of **4.7** recorded in CD_2Cl_2 at 500 MHz. Dots mark remaining diethyl ether.

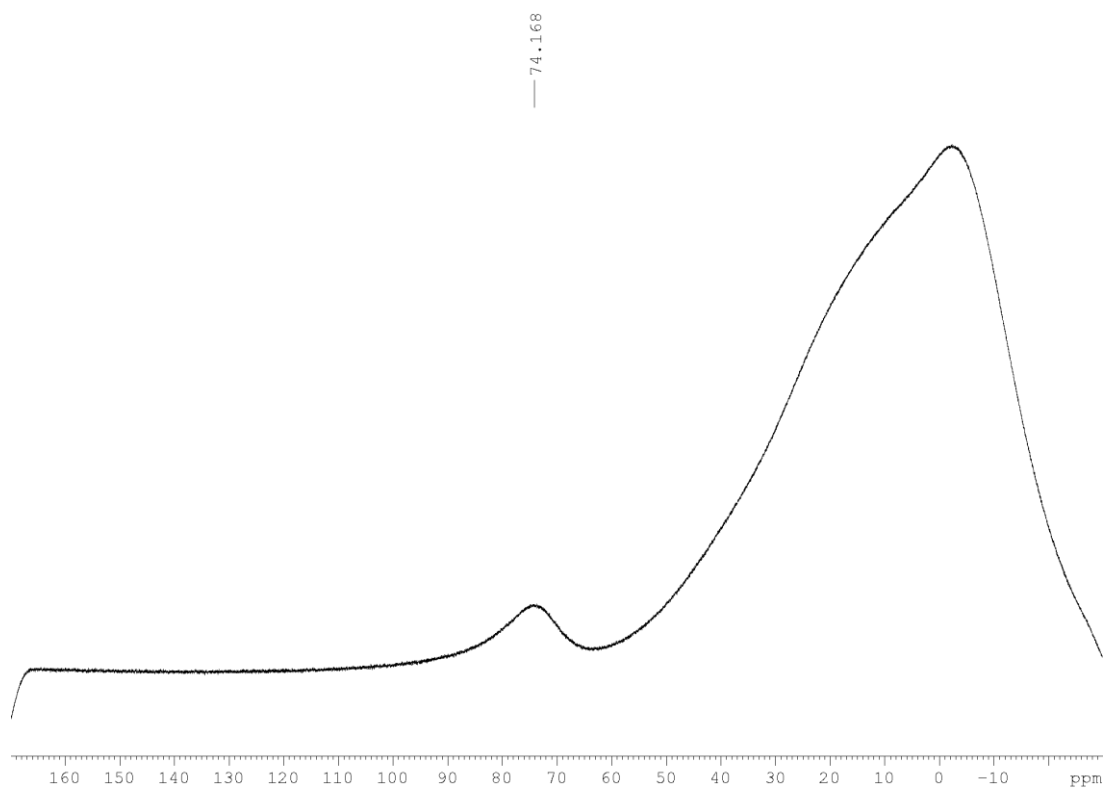


Figure 11.97: $^{11}\text{B}\{^1\text{H}\}$ NMR spectrum of **4.7** recorded in CD_2Cl_2 at 160 MHz.

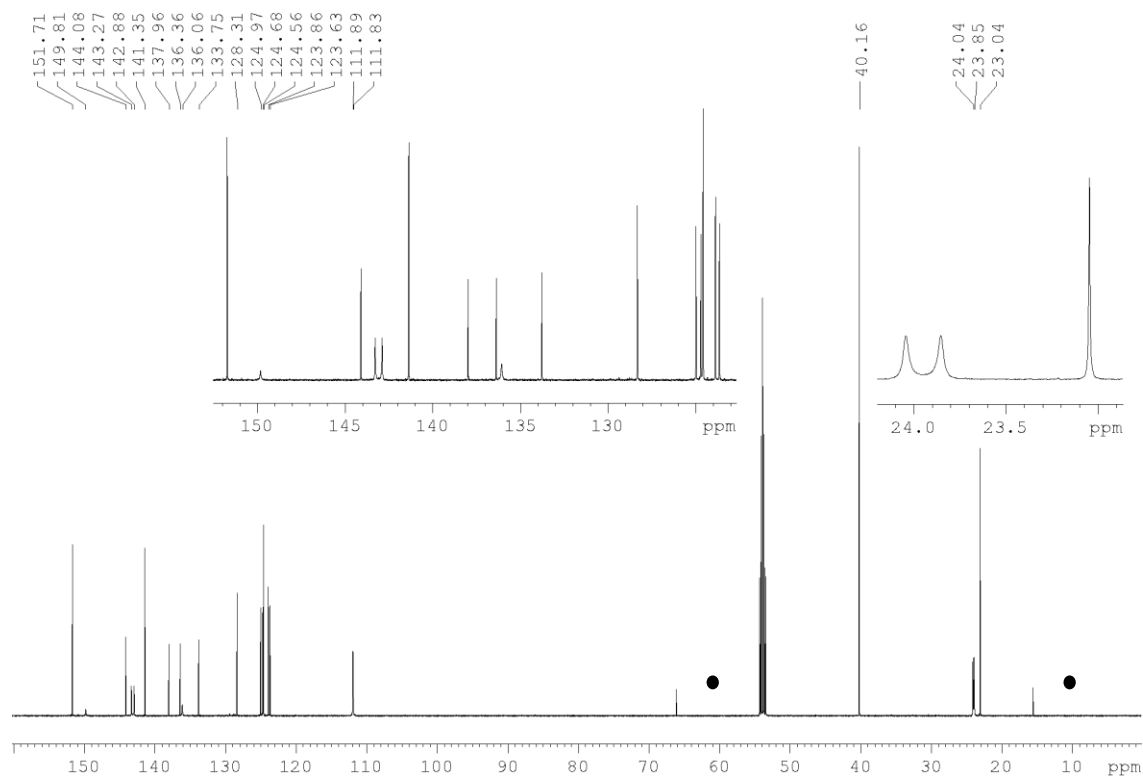


Figure 11.98: $^{13}\text{C}\{^1\text{H}\}$ NMR spectrum of **4.7** recorded in CD_2Cl_2 at 125 MHz. Dots mark remaining diethyl ether.

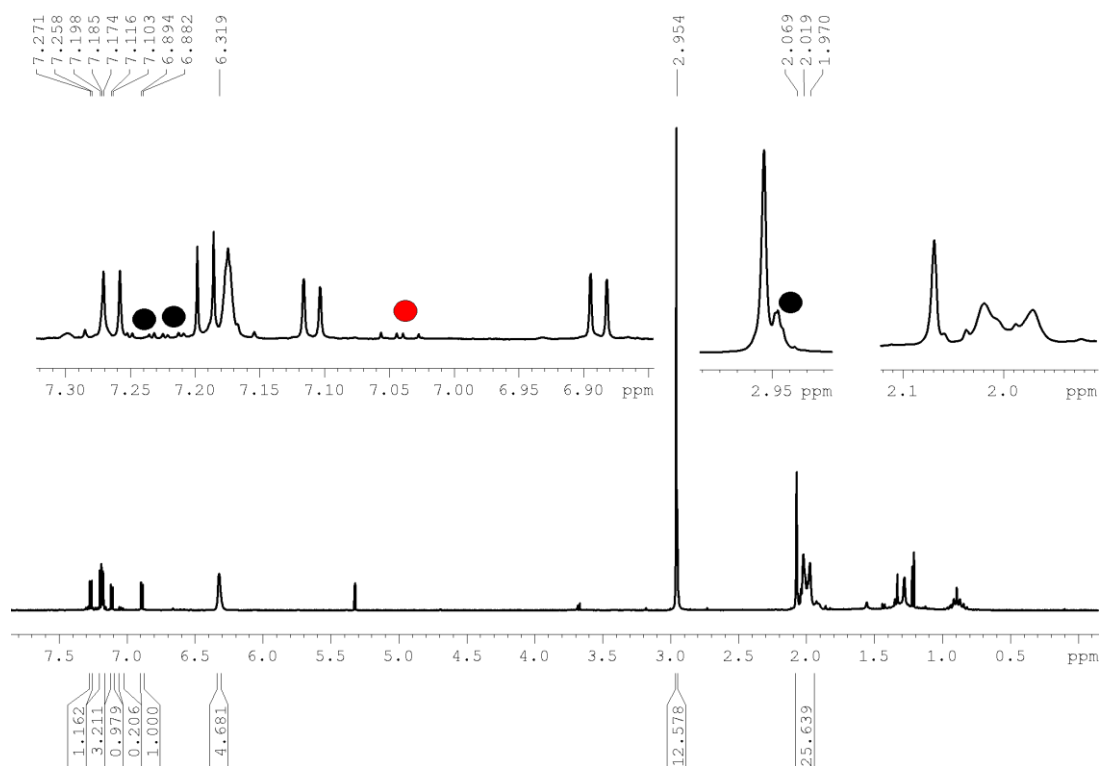


Figure 11.99: ^1H NMR spectrum of compound **4.8** recorded in CD_2Cl_2 at 300 MHz. Dots mark remaining starting material. Red dot marks signal which was used for estimation of ratio of starting material to product.

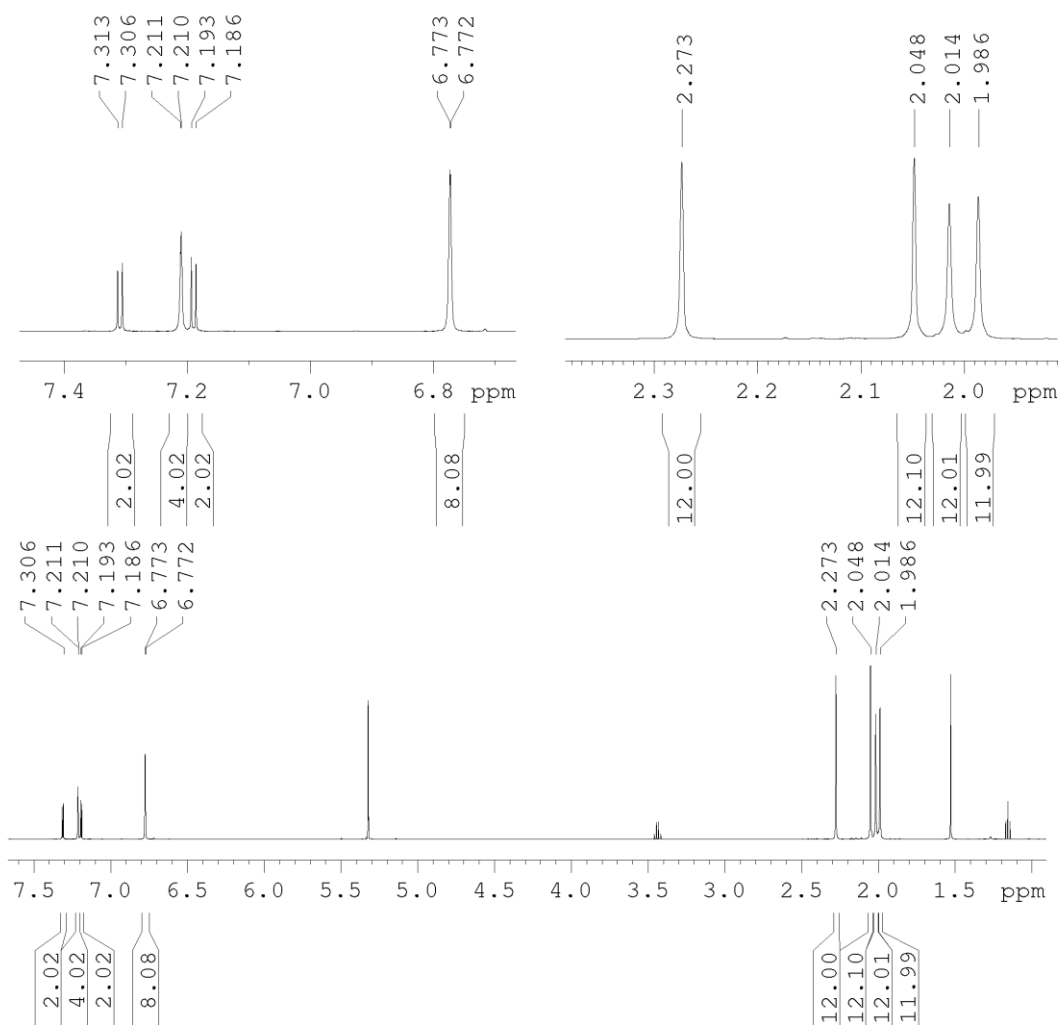


Figure 11.100: ^1H NMR spectrum of compound **Neut0** recorded in CD_2Cl_2 at 500 MHz.

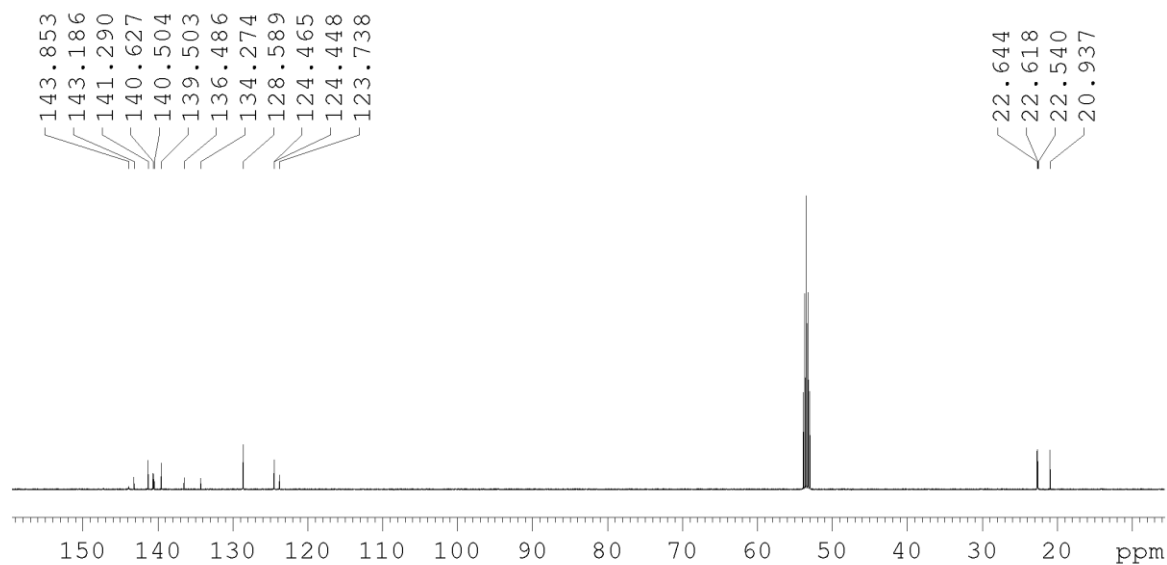


Figure 11.101: $^{13}\text{C}\{^1\text{H}\}$ NMR spectrum of compound **Neut0** recorded in CD_2Cl_2 at 125 MHz.

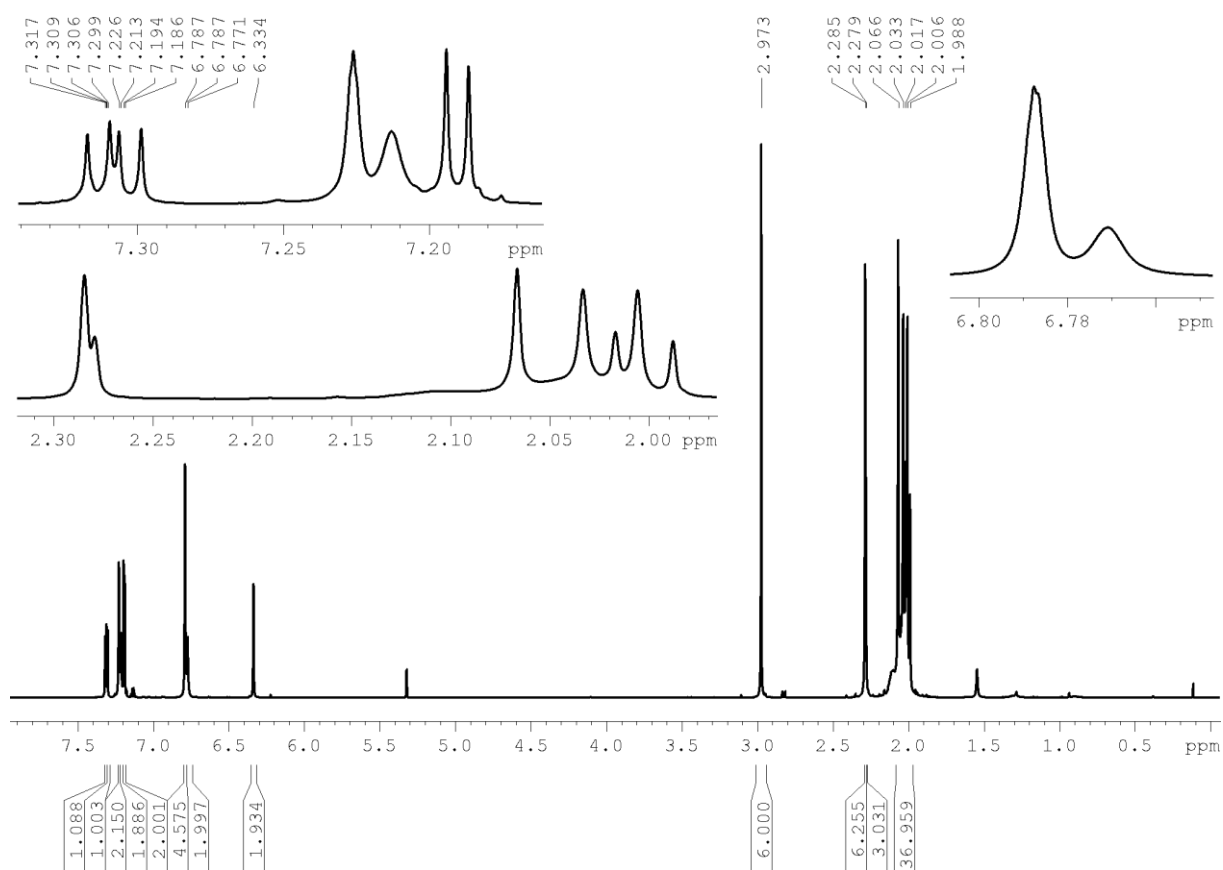


Figure 11.102: ^1H NMR spectrum of compound **Neut1** recorded in CD_2Cl_2 at 500 MHz.

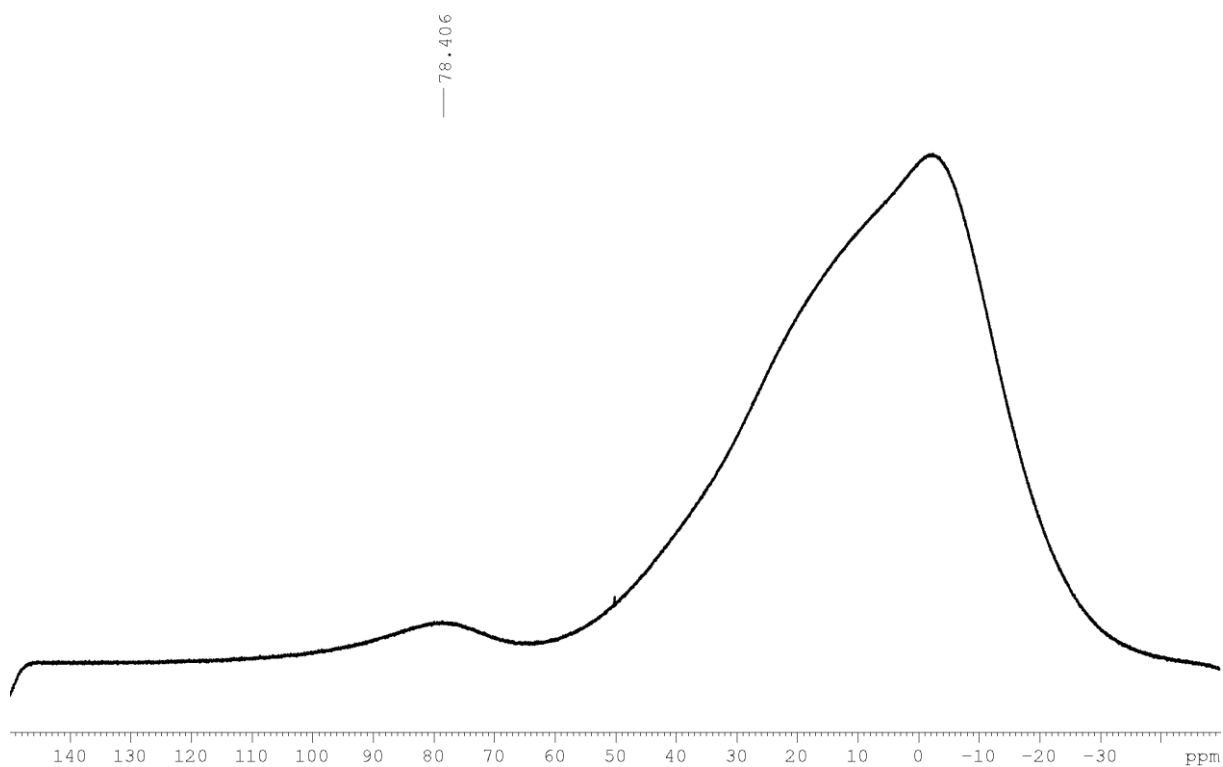


Figure 11.103: $^{11}\text{B}\{^1\text{H}\}$ NMR spectrum of compound **Neut1** recorded in CD_2Cl_2 at 160 MHz.

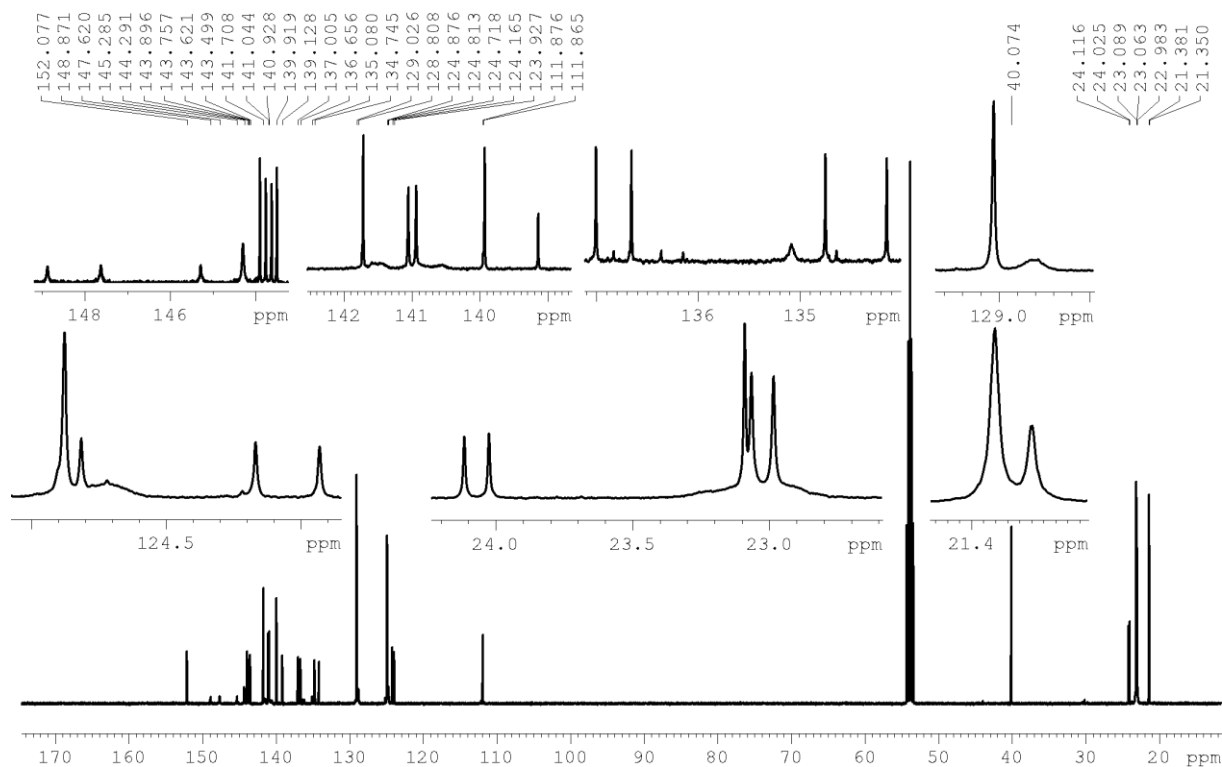


Figure 11.104: $^{13}\text{C}\{^1\text{H}\}$ NMR spectrum of compound **Neut1** recorded in CD_2Cl_2 at 125 MHz.

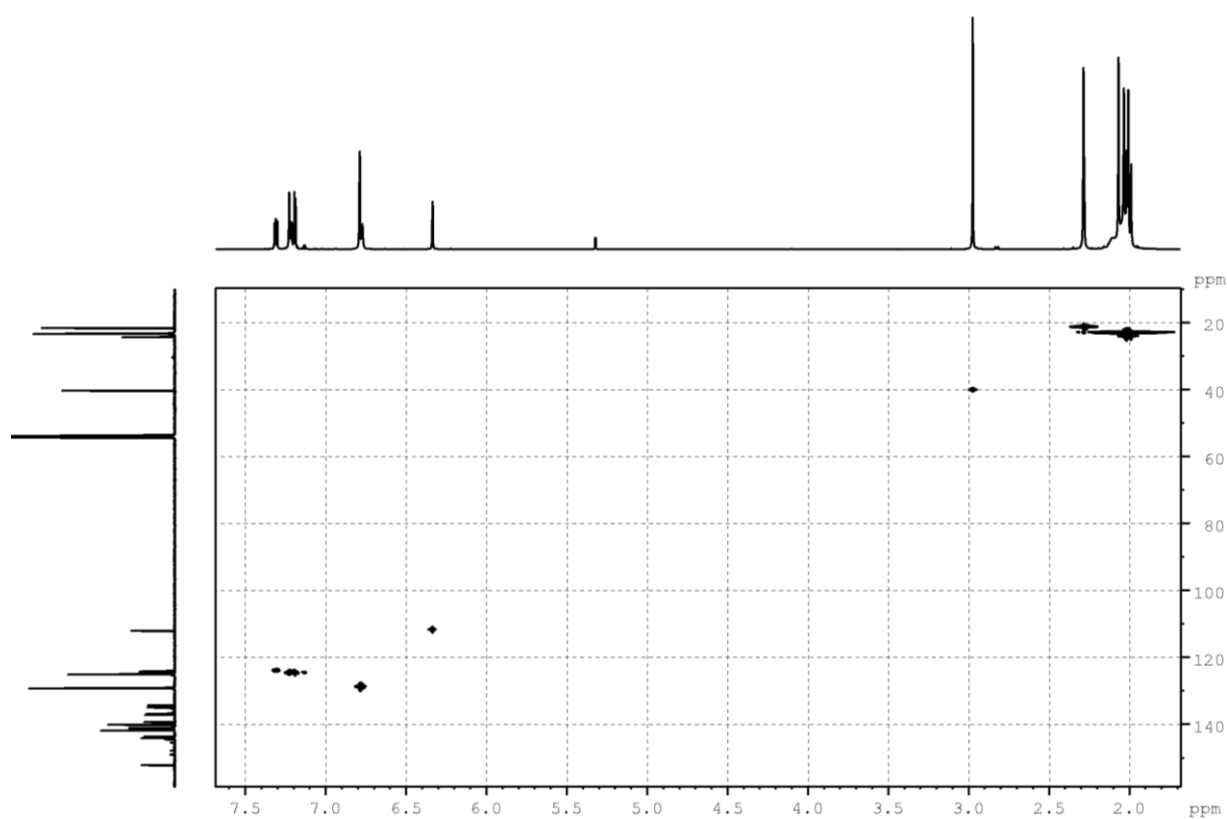


Figure 11.105: $^1\text{H} - ^{13}\text{C}$ HSQC spectrum of compound **Neut1** recorded in CD_2Cl_2 at 500 MHz.

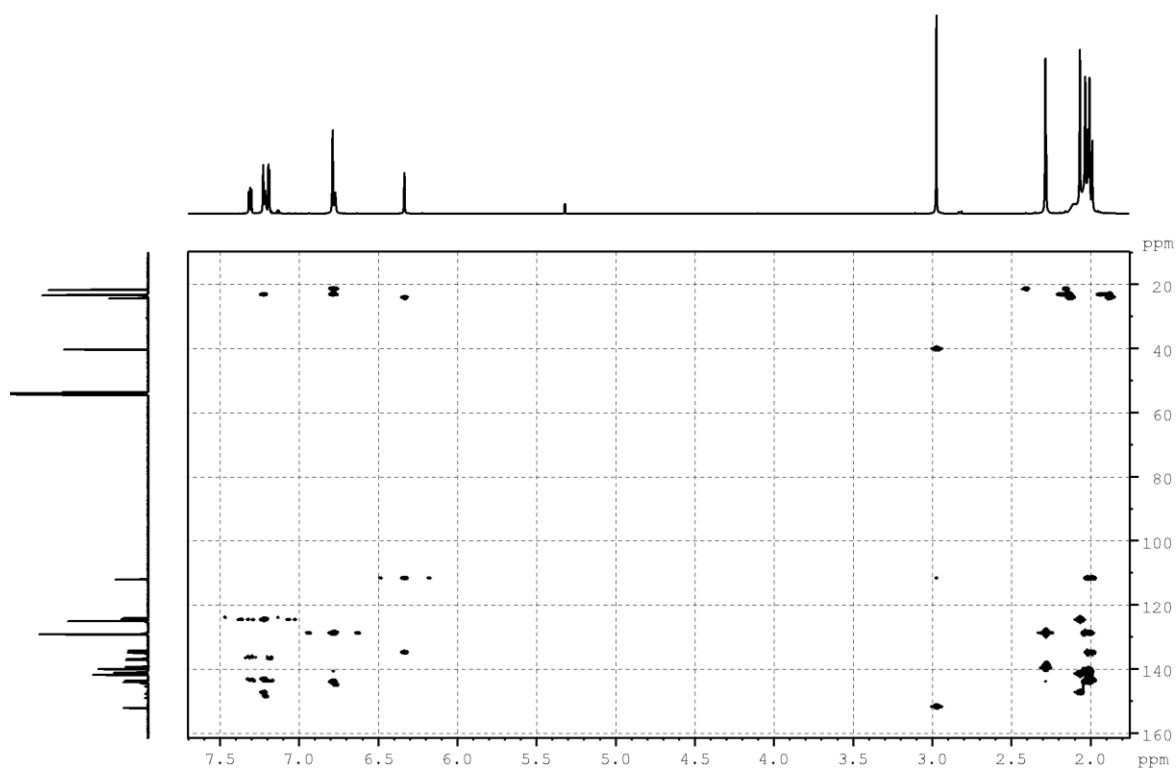


Figure 11.106: $^1\text{H} - ^{13}\text{C}$ HMBC spectrum of compound **Neut1** recorded in CD_2Cl_2 at 500 MHz.

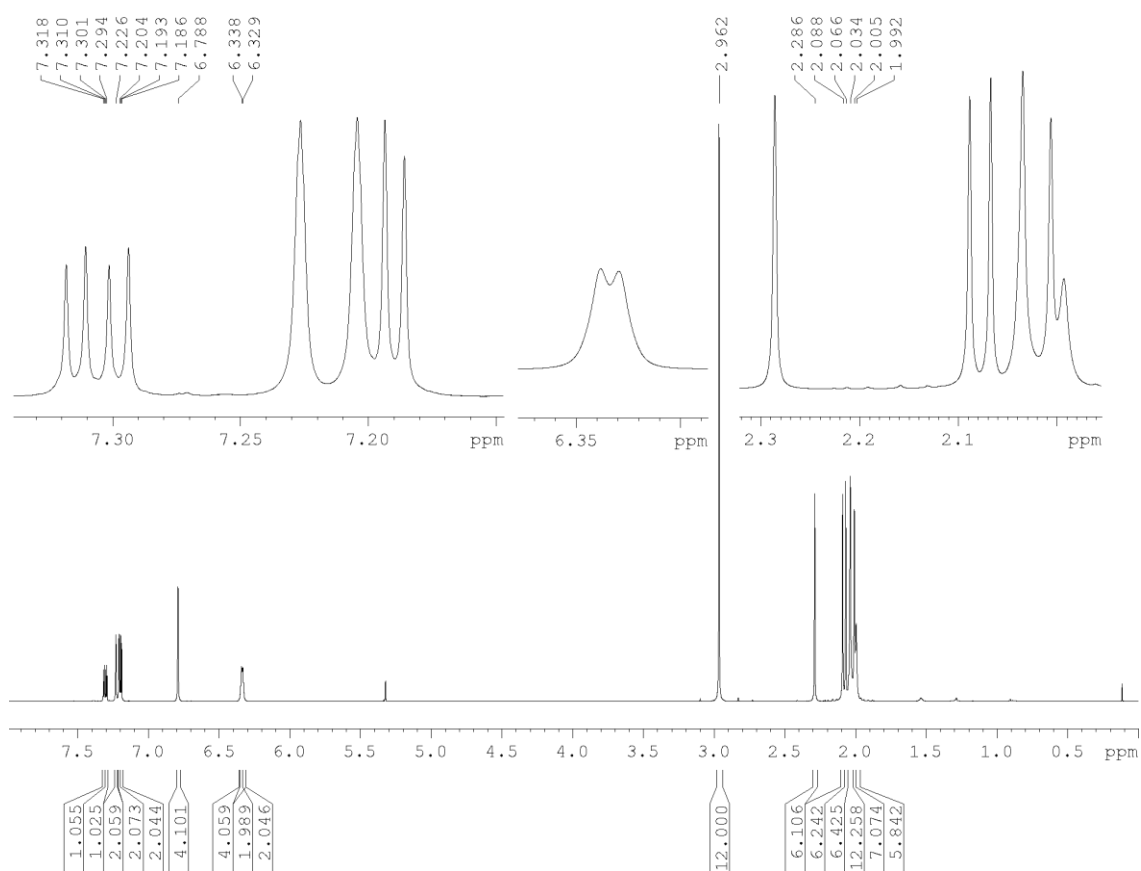


Figure 11.107: ^1H NMR spectrum of **Neut2** recorded in CD_2Cl_2 at 500 MHz.

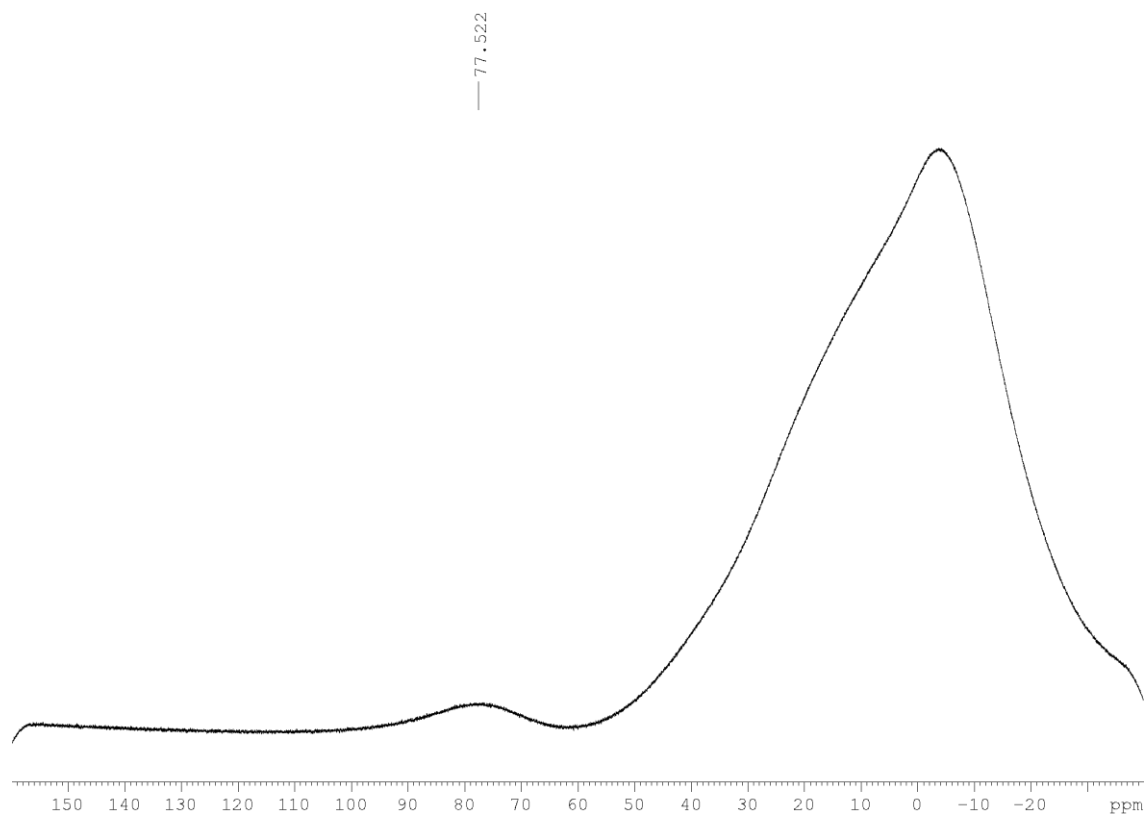


Figure 11.108: $^{11}\text{B}\{^1\text{H}\}$ NMR spectrum of **Neut2** recorded in CD_2Cl_2 at 160 MHz.

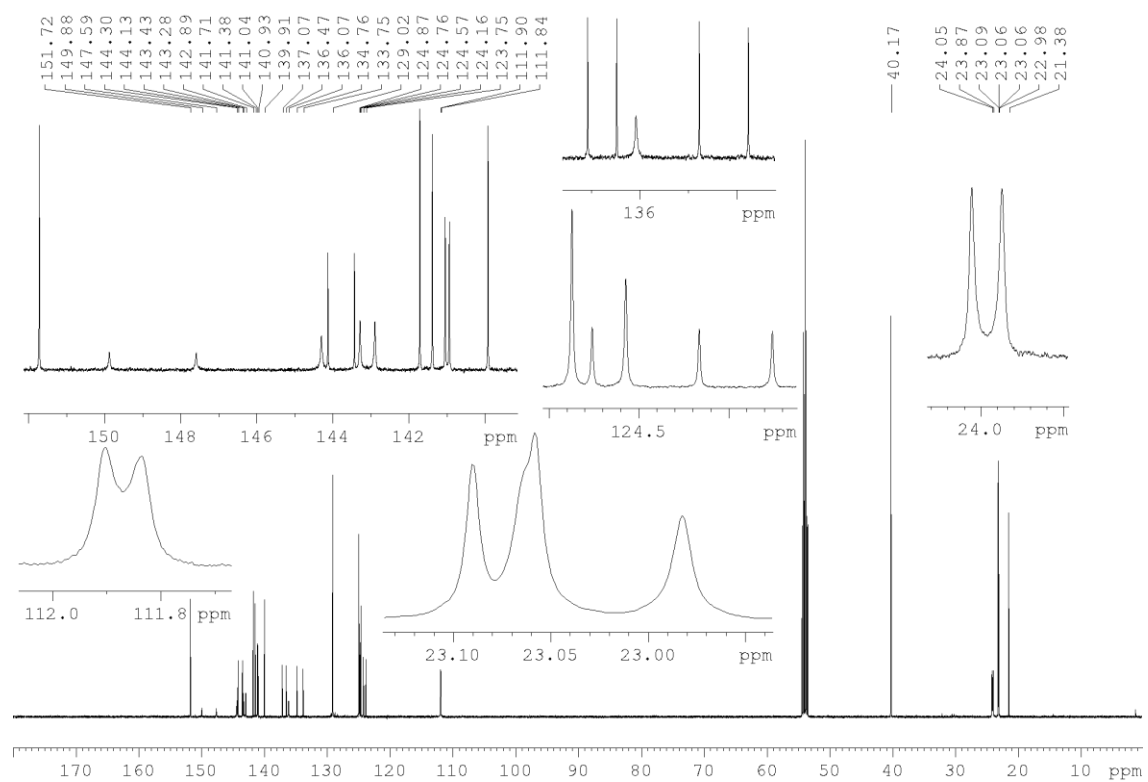


Figure 11.109: $^{13}\text{C}\{^1\text{H}\}$ NMR spectrum of **Neut2** recorded in CD_2Cl_2 at 125 MHz.

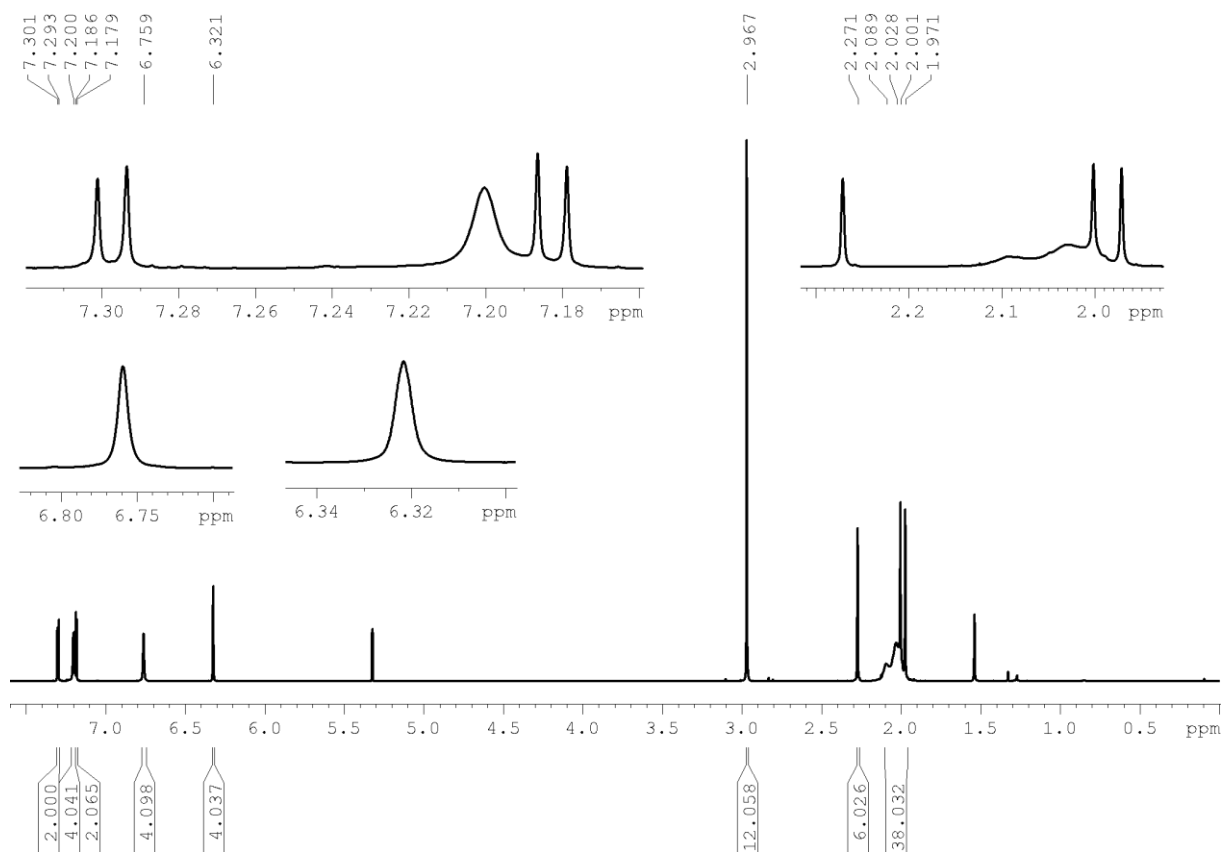


Figure 11.110: ^1H NMR spectrum of compound **Neut(i)2** recorded in CD_2Cl_2 at 500 MHz.

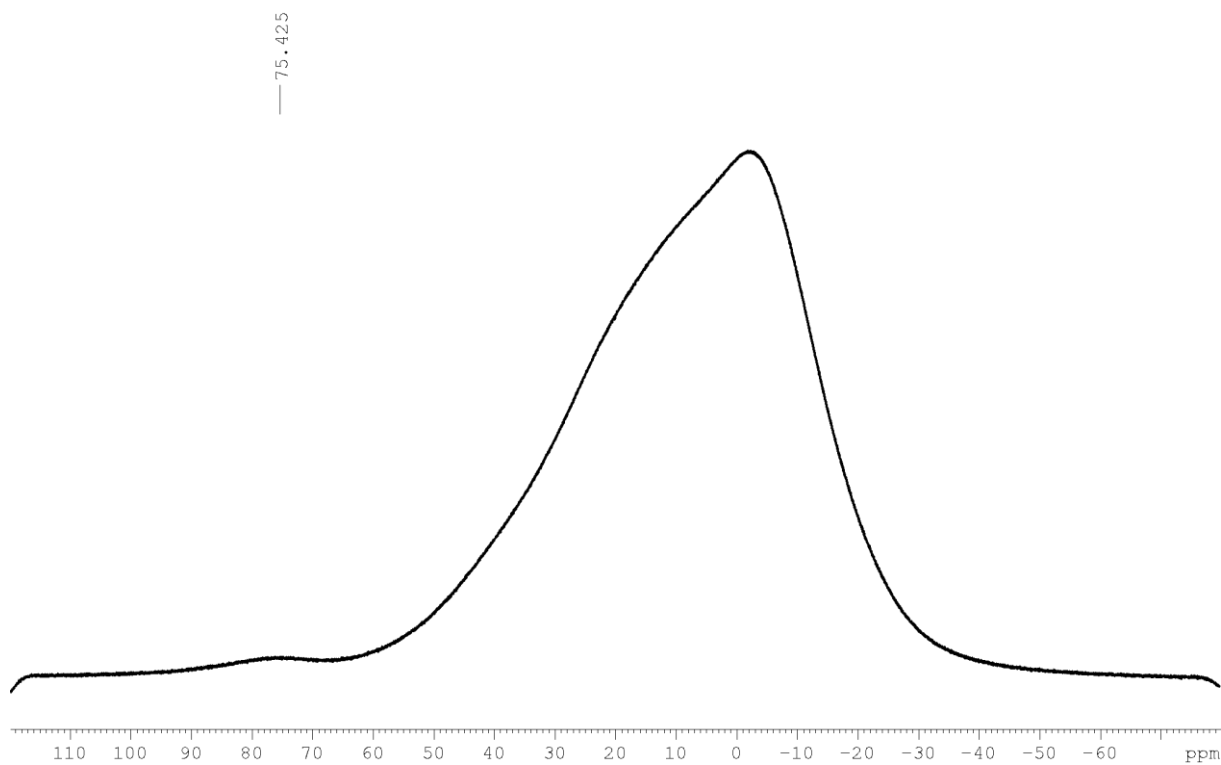


Figure 11.111: $^{11}\text{B}\{^1\text{H}\}$ NMR spectrum of compound **Neut(i)2** recorded in CD_2Cl_2 at 160 MHz.

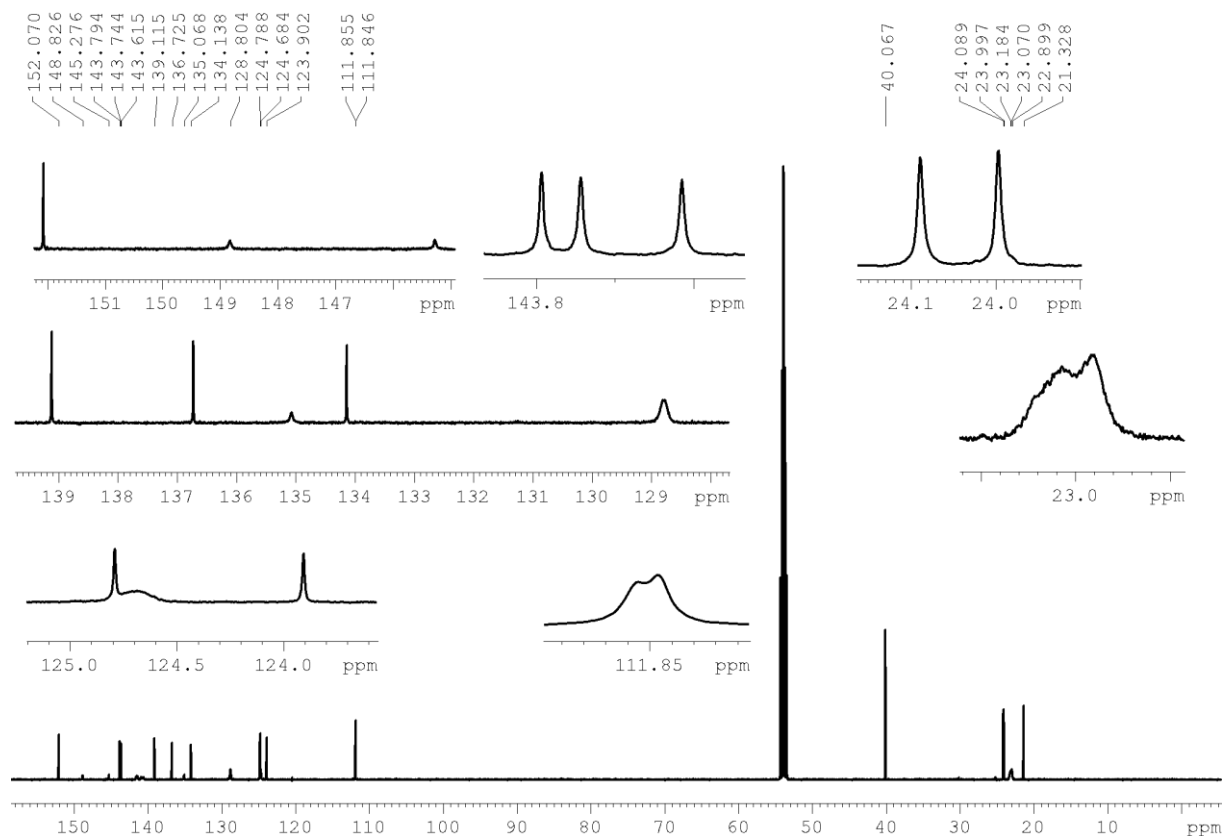


Figure 11.112: $^{13}\text{C}\{^1\text{H}\}$ NMR spectrum of compound **Neut(i)2** recorded in CD_2Cl_2 at 125 MHz.

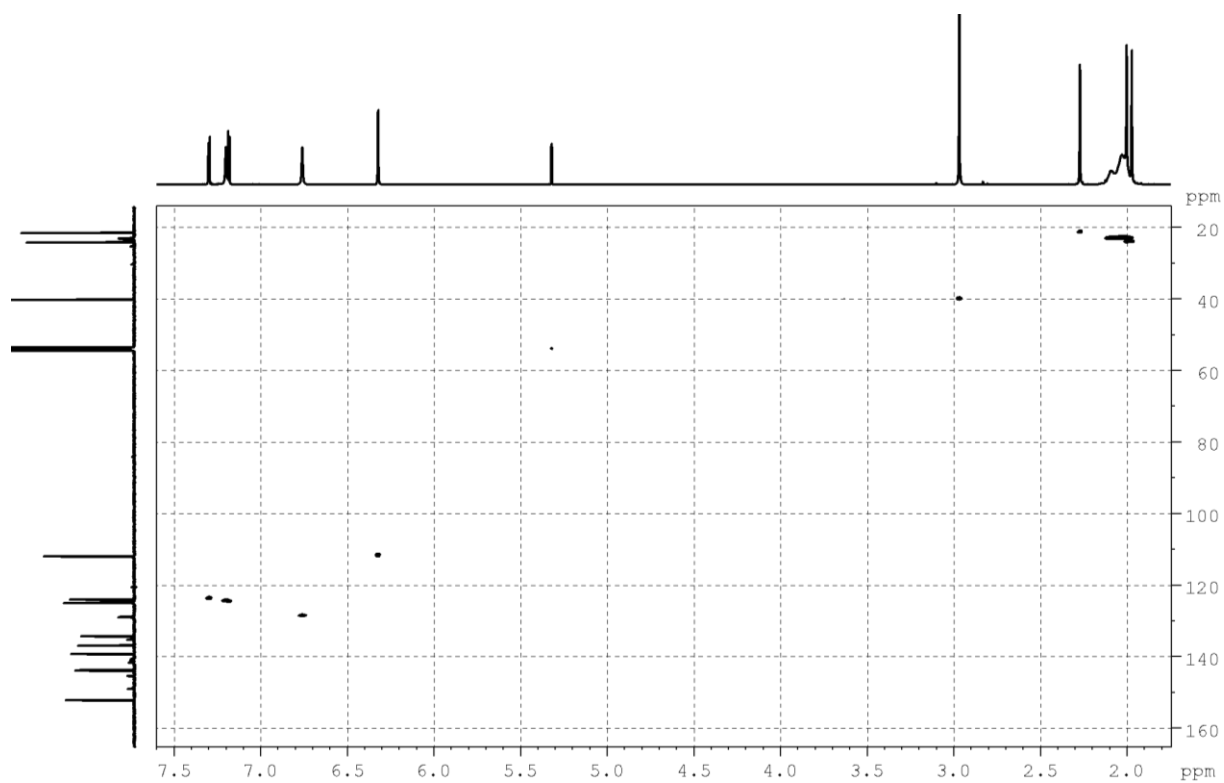


Figure 11.113: $^1\text{H} - ^{13}\text{C}$ HSQC spectrum of compound **Neut(i)2** recorded in CD_2Cl_2 at 500 MHz.

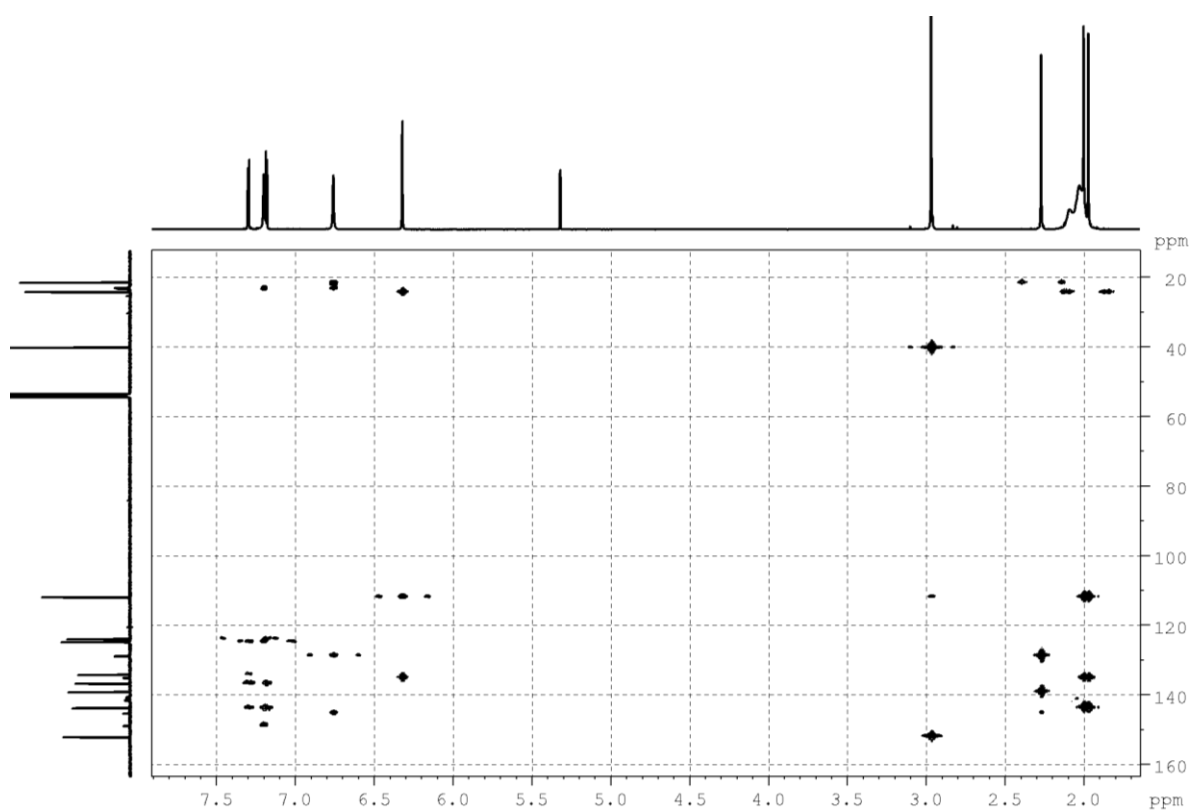


Figure 11.114: $^1\text{H} - ^{13}\text{C}$ HMBC spectrum of compound **Neut(i)2** recorded in CD_2Cl_2 at 500 MHz.

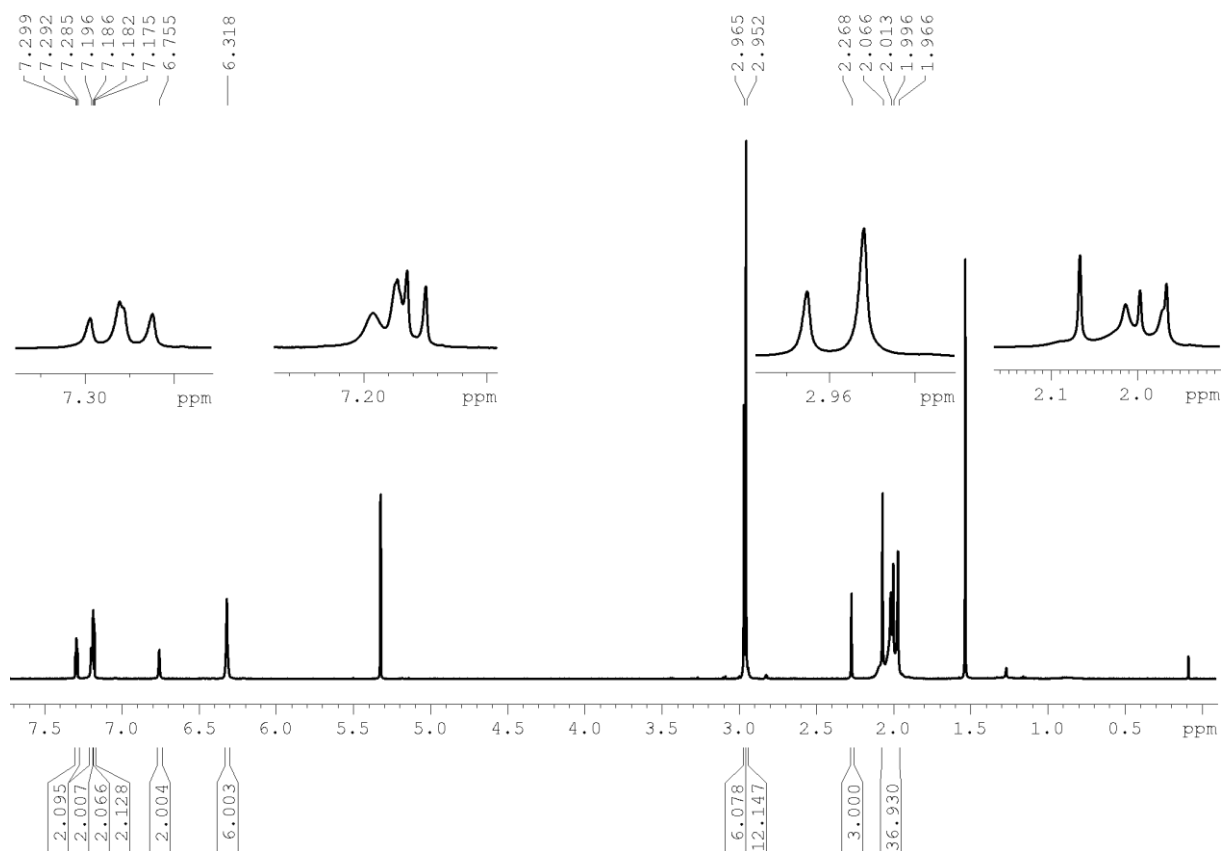


Figure 11.115: ^1H NMR spectrum of compound **Neut3** recorded in CD_2Cl_2 at 500 MHz.

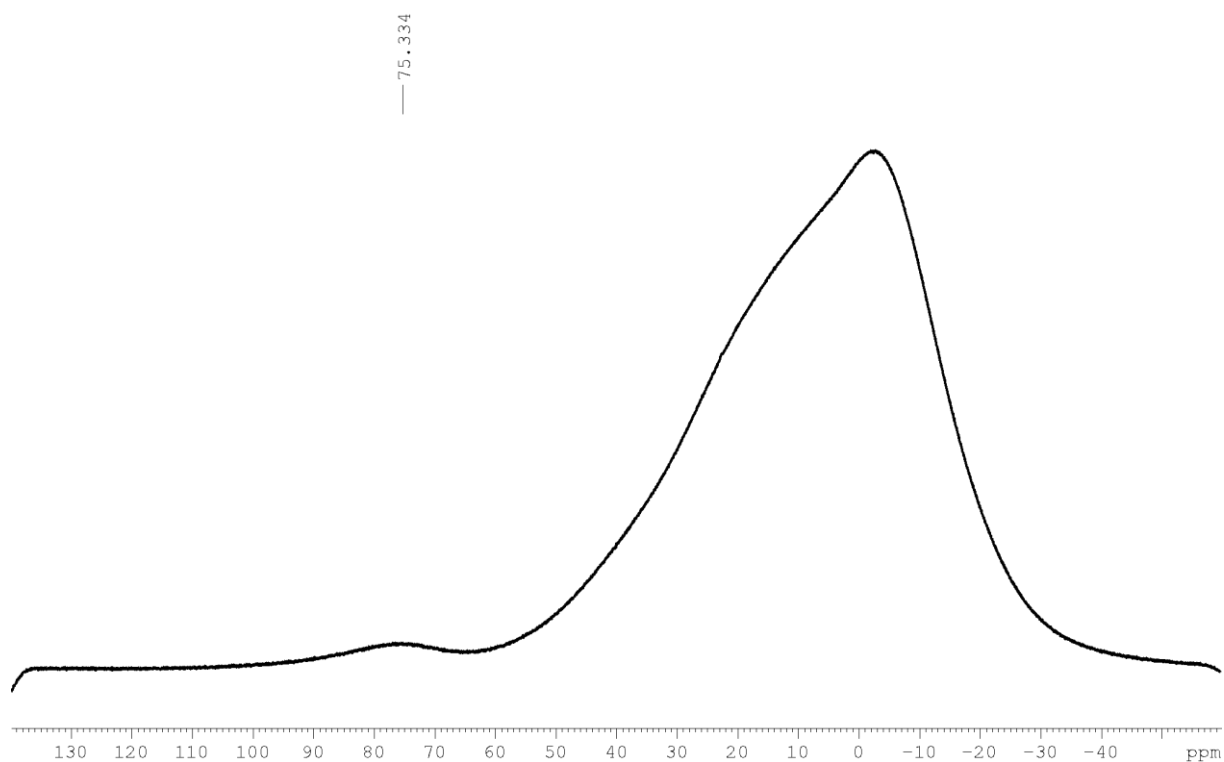


Figure 11.116: $^{11}\text{B}\{^1\text{H}\}$ NMR spectrum of compound **Neut3** recorded in CD_2Cl_2 at 160 MHz.

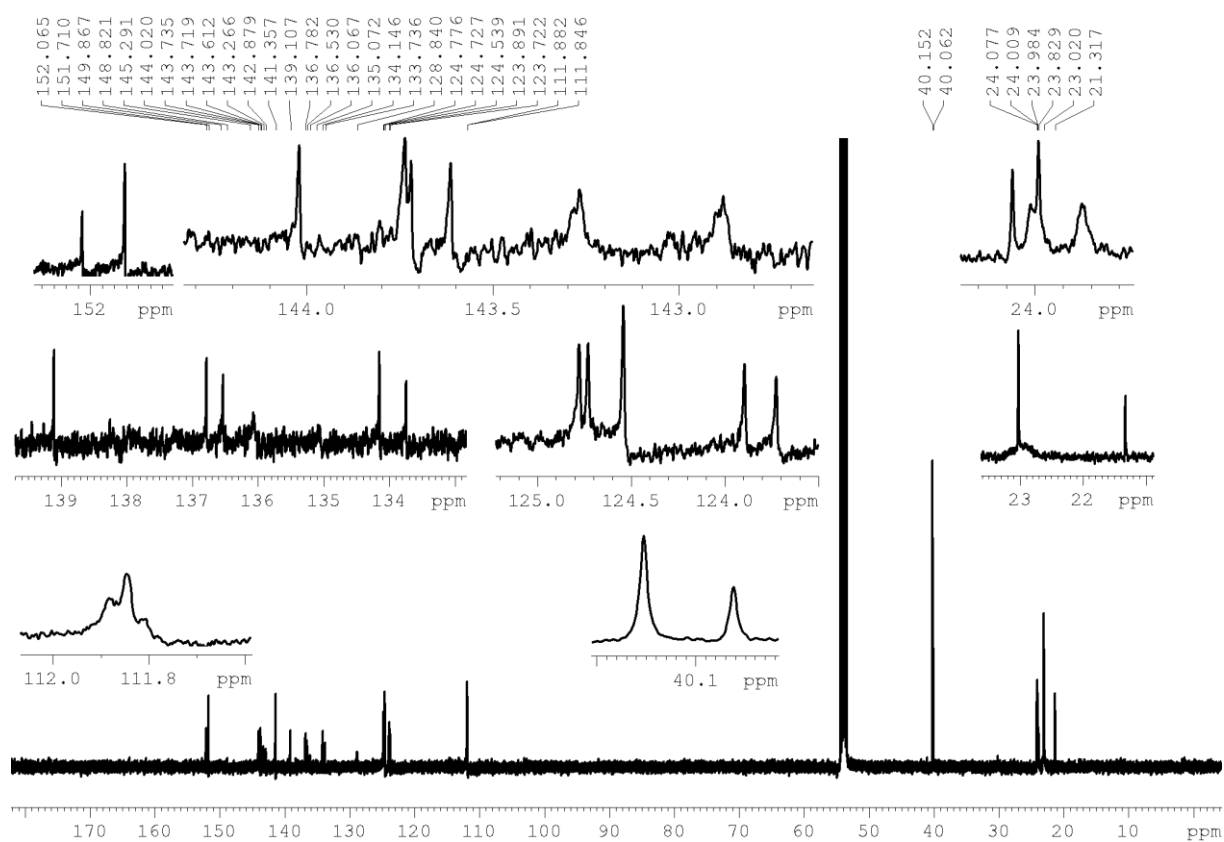


Figure 11.117: $^{13}\text{C}\{^1\text{H}\}$ NMR spectrum of compound **Neut3** recorded in CD_2Cl_2 at 125 MHz.

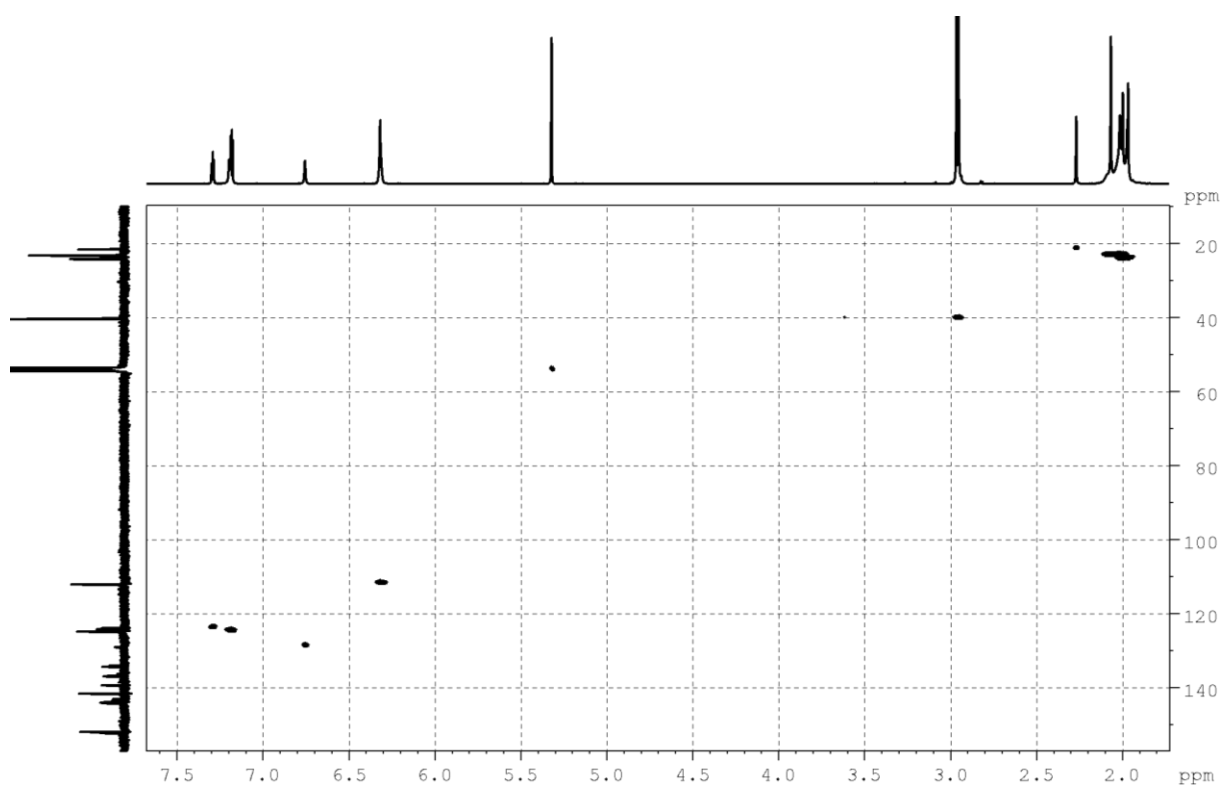


Figure 11.118: ^1H - ^{13}C HSQC spectrum of compound **Neut3** recorded in CD_2Cl_2 at 500 MHz.

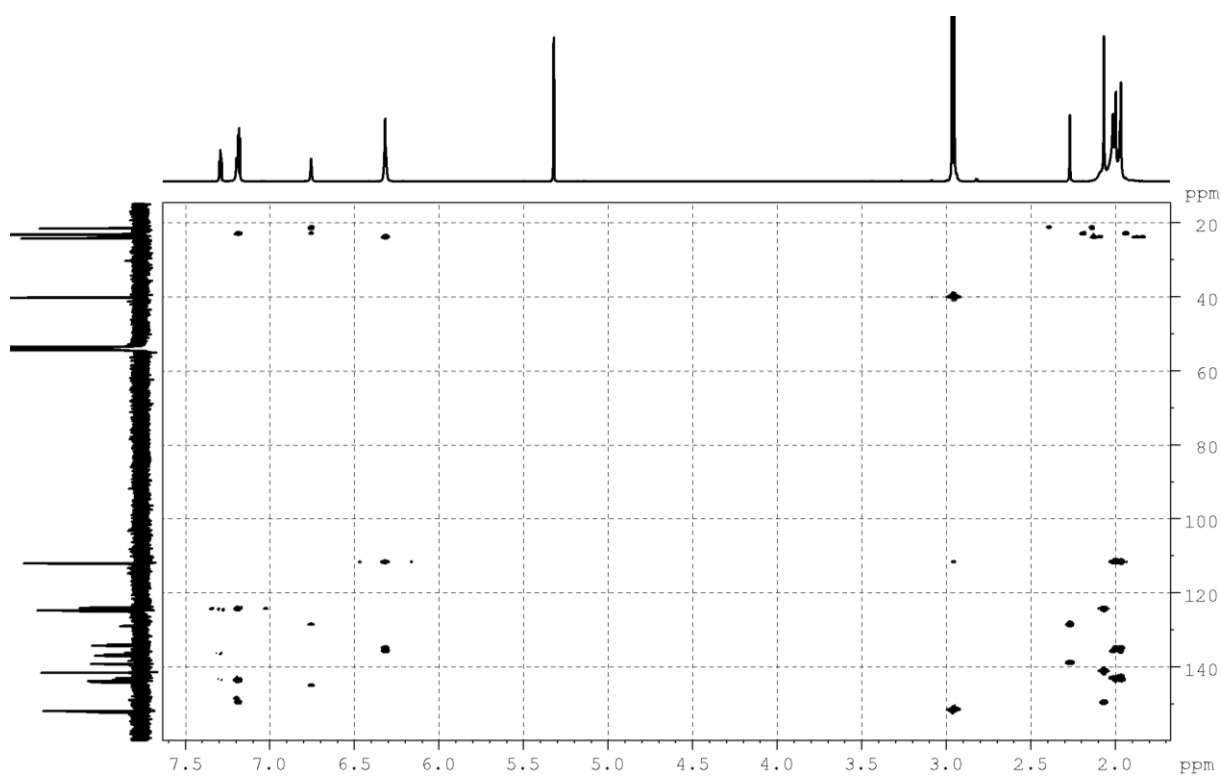


Figure 11.119: ^1H - ^{13}C HMBC spectrum of compound **Neut3** recorded in CD_2Cl_2 at 500 MHz.

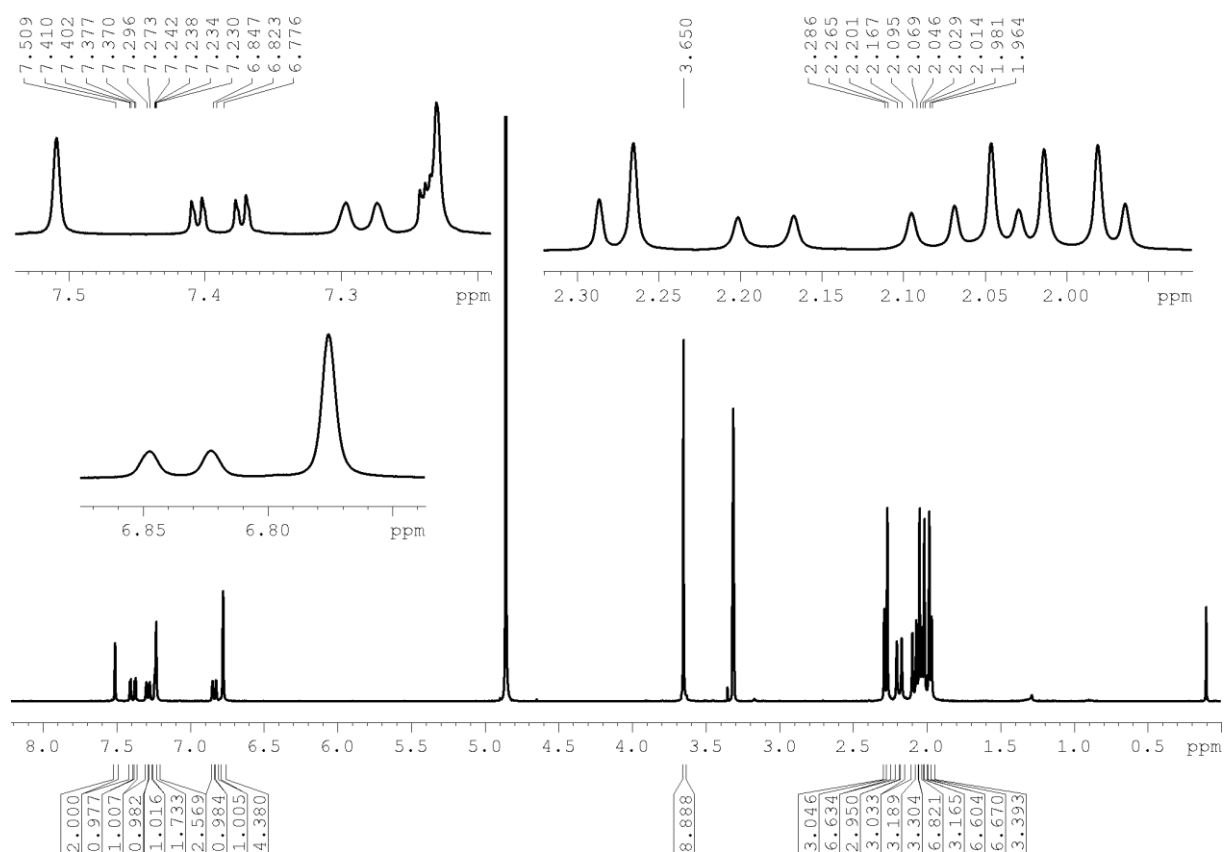


Figure 11.120: ^1H NMR spectrum of compound **Cat¹⁺** recorded in CD_3OD at 500 MHz.

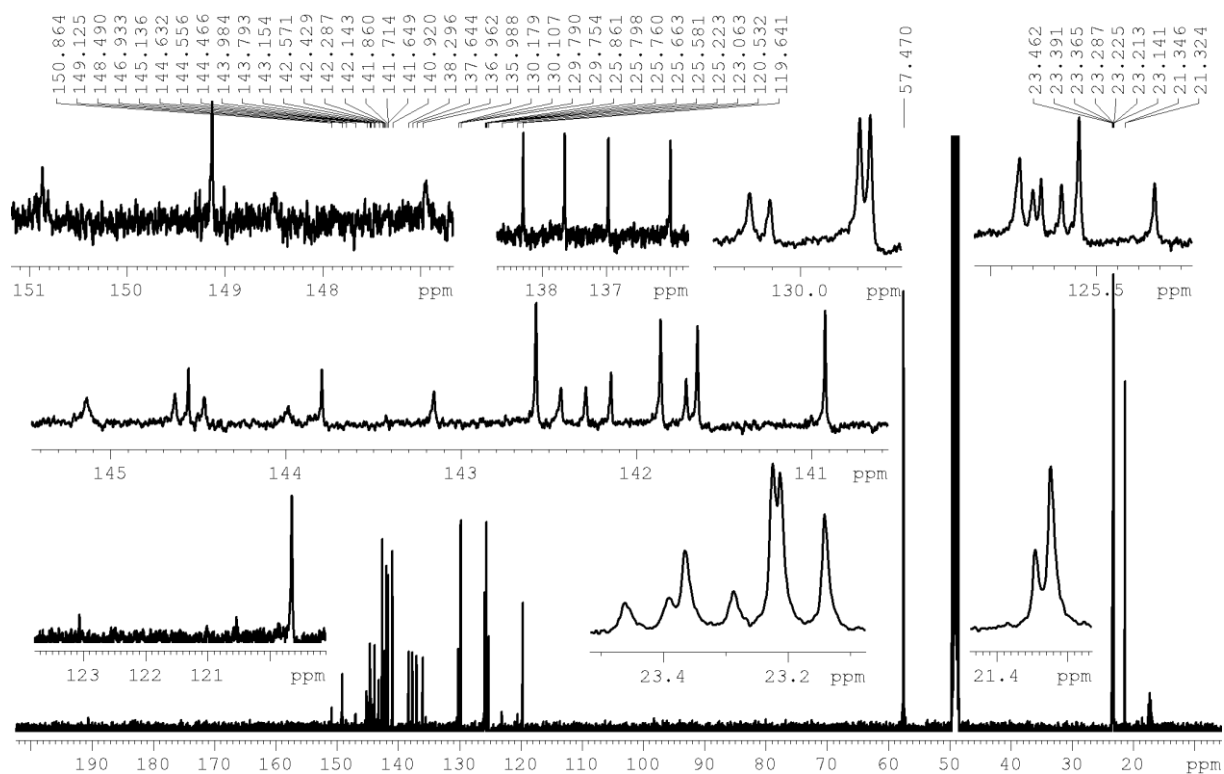


Figure 11.121: $^{13}\text{C}\{^1\text{H}\}$ NMR spectrum of compound **Cat¹⁺** recorded in CD_3OD at 125 MHz.

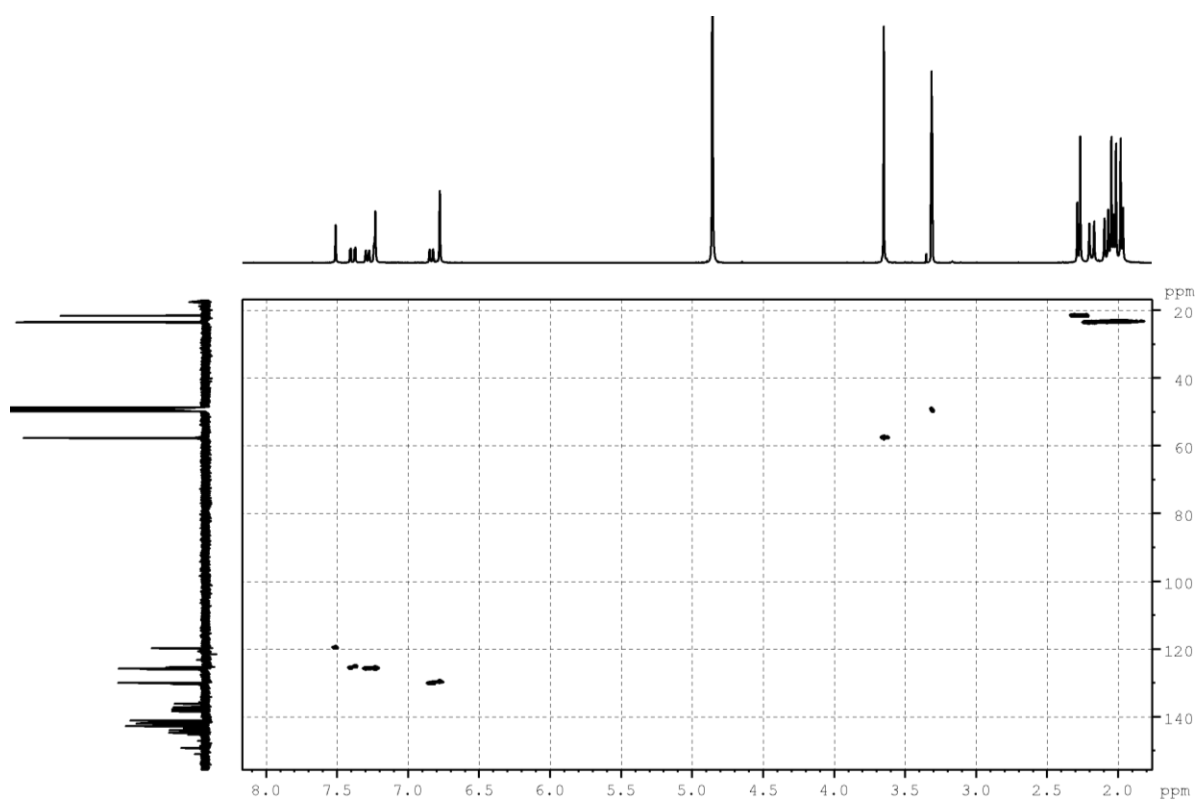


Figure 11.122: ^1H – ^{13}C HSQC spectrum of compound **Cat¹⁺** recorded in CD_3OD at 500 MHz.

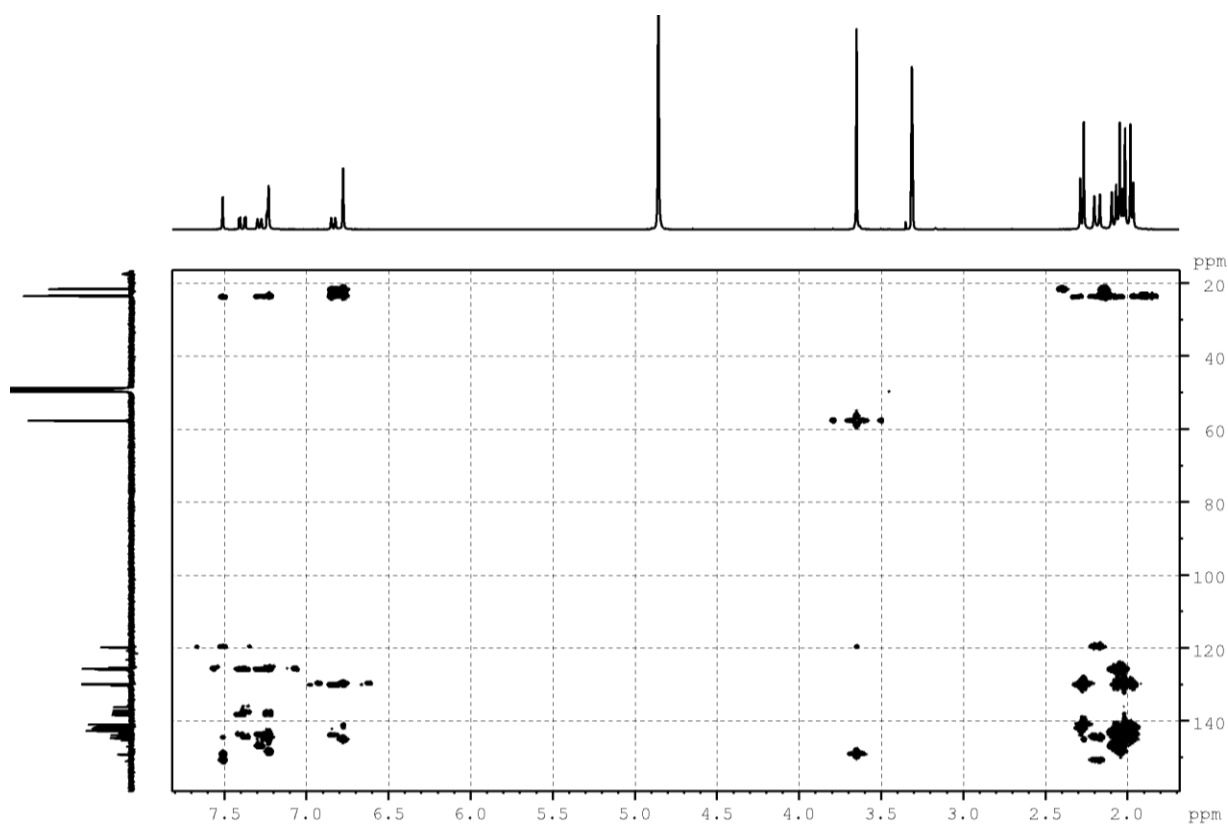


Figure 11.123: ^1H – ^{13}C HMBC spectrum of compound **Cat¹⁺** recorded in CD_3OD at 500 MHz.

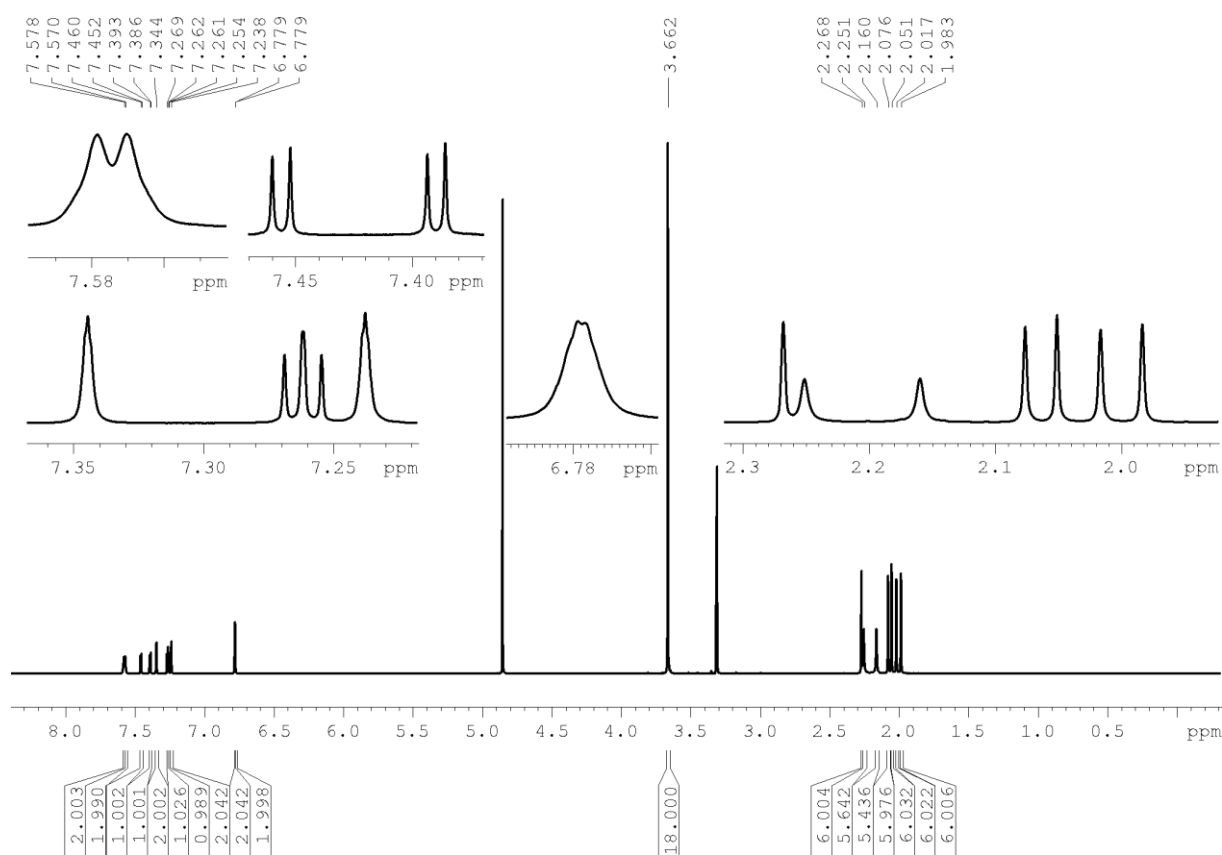


Figure 11.124: ^1H NMR spectrum of Cat^{2+} recorded in CD_3OD at 500 MHz.

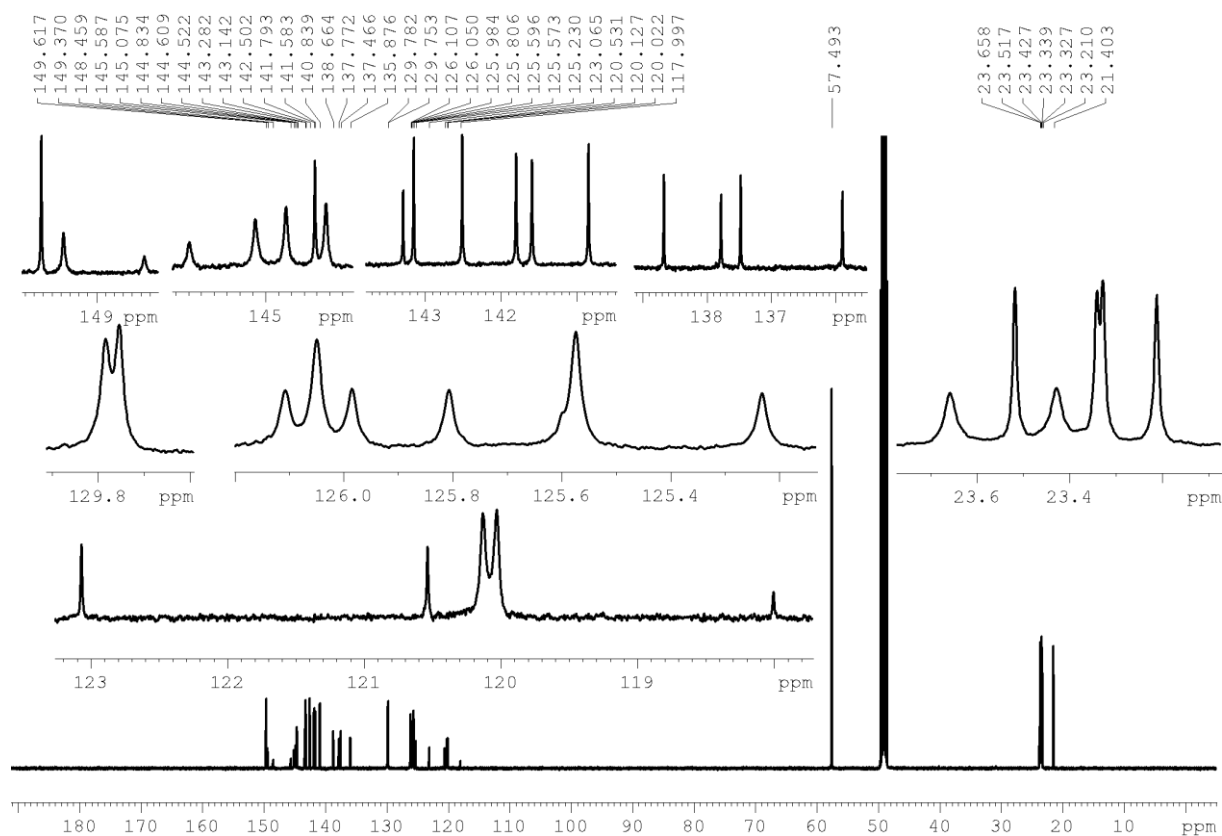


Figure 11.125: $^{13}\text{C}\{^1\text{H}\}$ NMR spectrum of Cat^{2+} recorded in CD_3OD at 125 MHz.

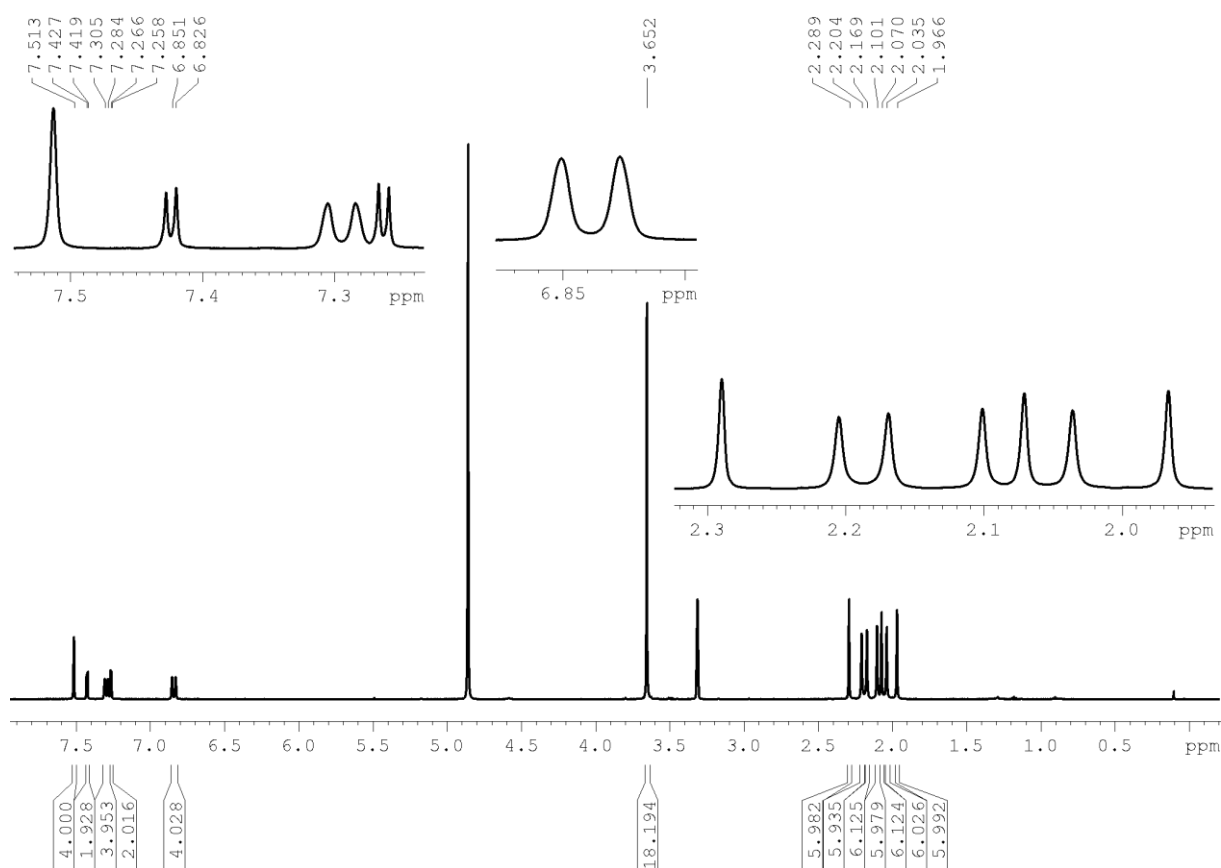


Figure 11.126: ^1H NMR spectrum of Cat(i)^{2+} recorded in CD_3OD at 500 MHz.

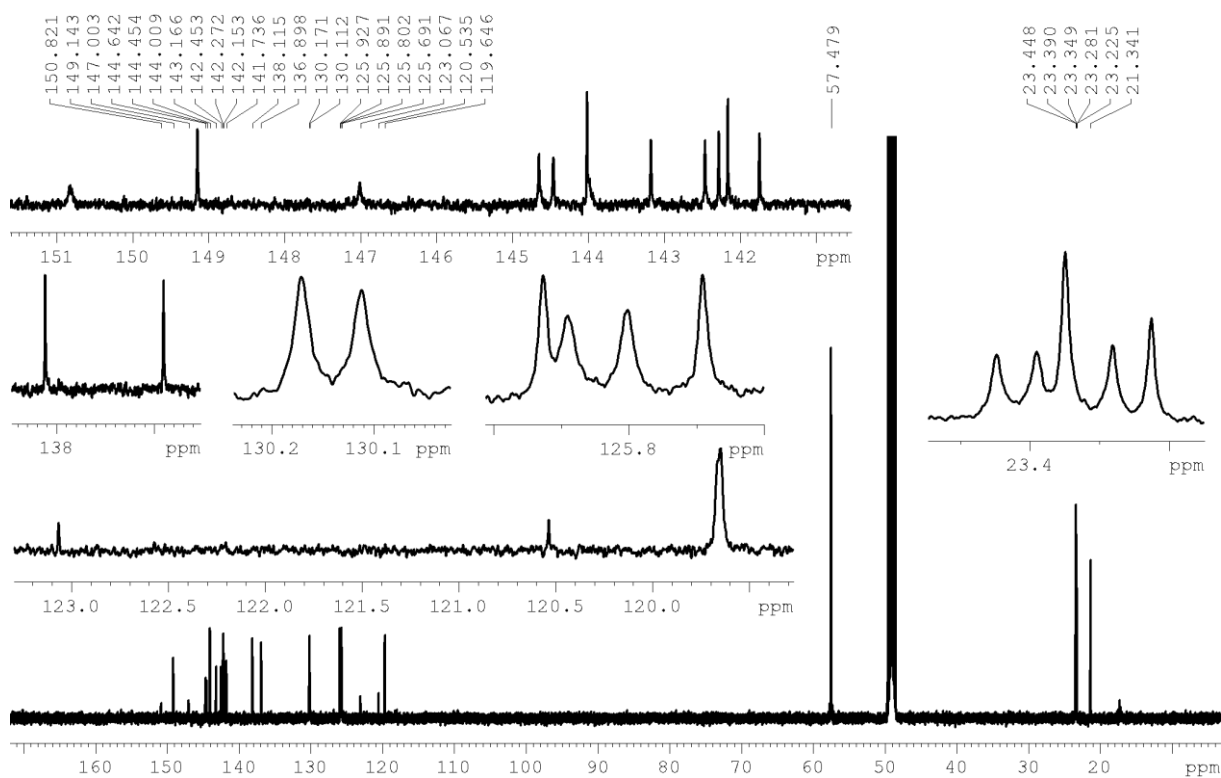


Figure 11.127: $^{13}\text{C}\{^1\text{H}\}$ NMR spectrum of Cat(i)^{2+} recorded in CD_3OD at 125 MHz.

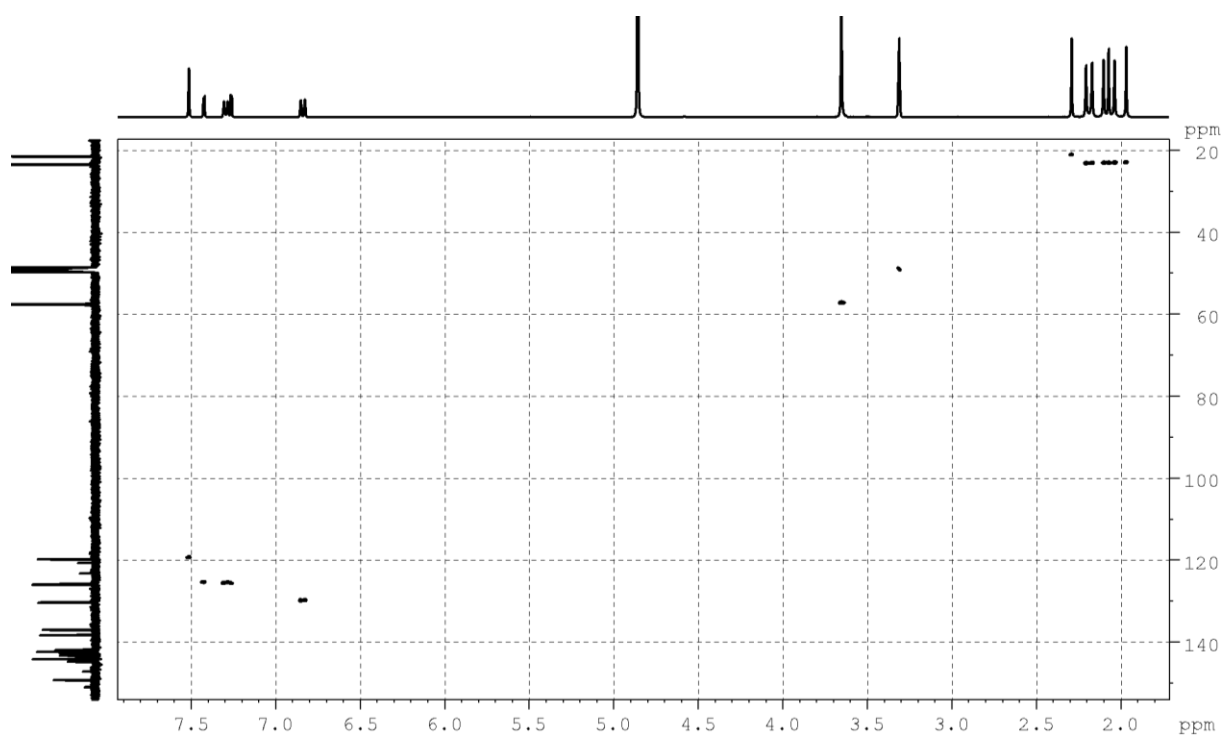


Figure 11.128: ^1H – ^{13}C HSQC spectrum of compound **Cat(i) $^{2+}$** recorded in CD_3OD at 500 MHz.

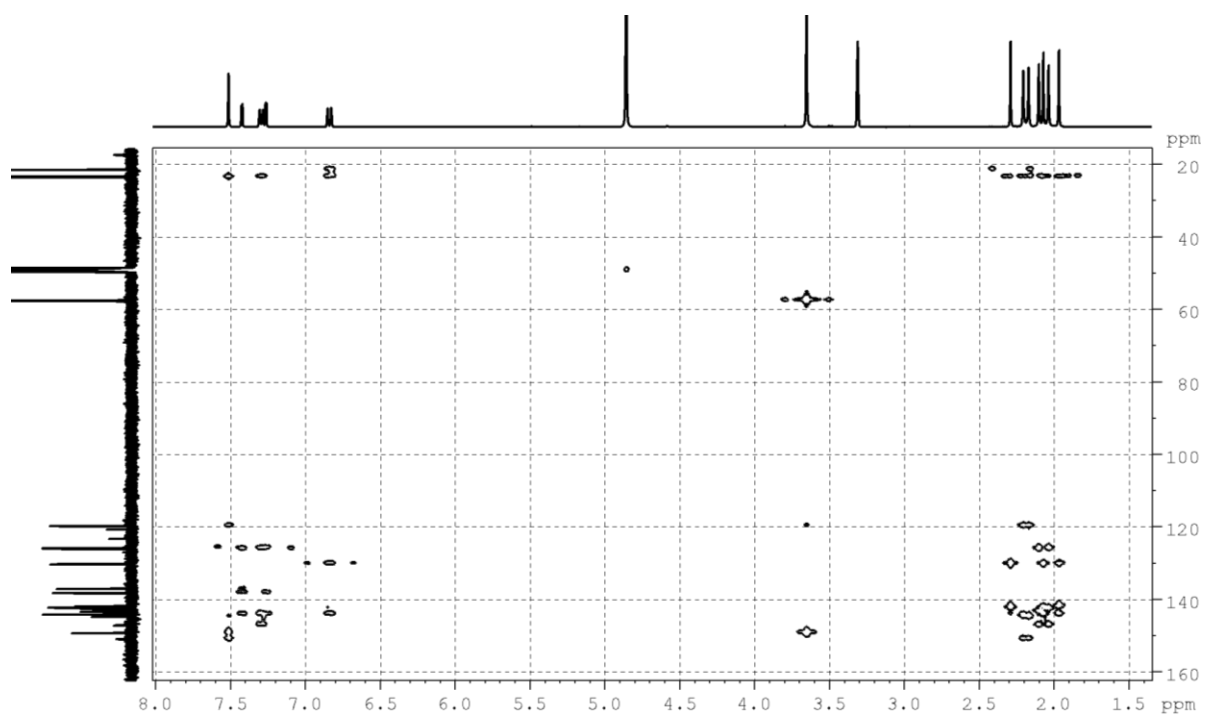
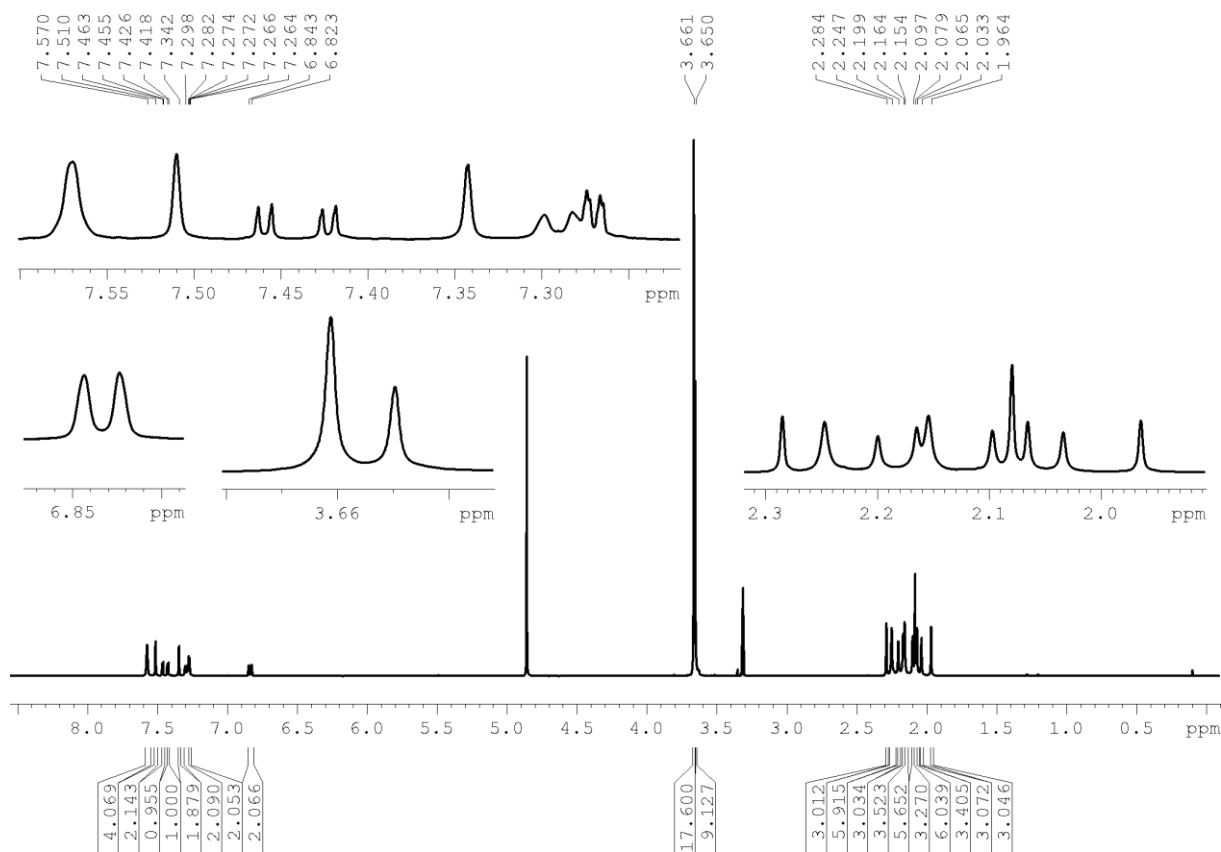
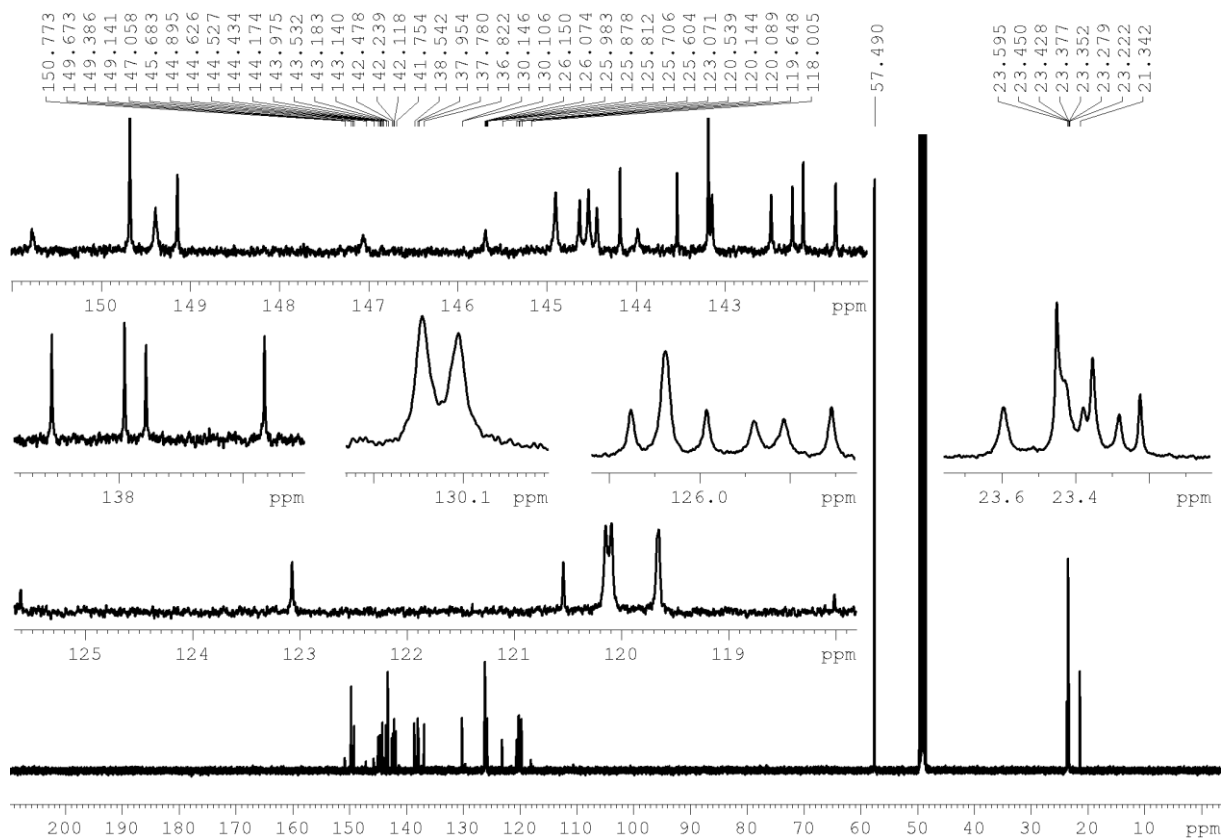


Figure 11.129: ^1H – ^{13}C HMBC spectrum of compound **Cat(i) $^{2+}$** recorded in CD_3OD at 500 MHz.

Figure 11.130: ^1H NMR spectrum of Cat^{3+} recorded in CD_3OD at 500 MHz.Figure 11.131: $^{13}\text{C}\{^1\text{H}\}$ NMR spectrum of Cat^{3+} recorded in CD_3OD at 125 MHz.

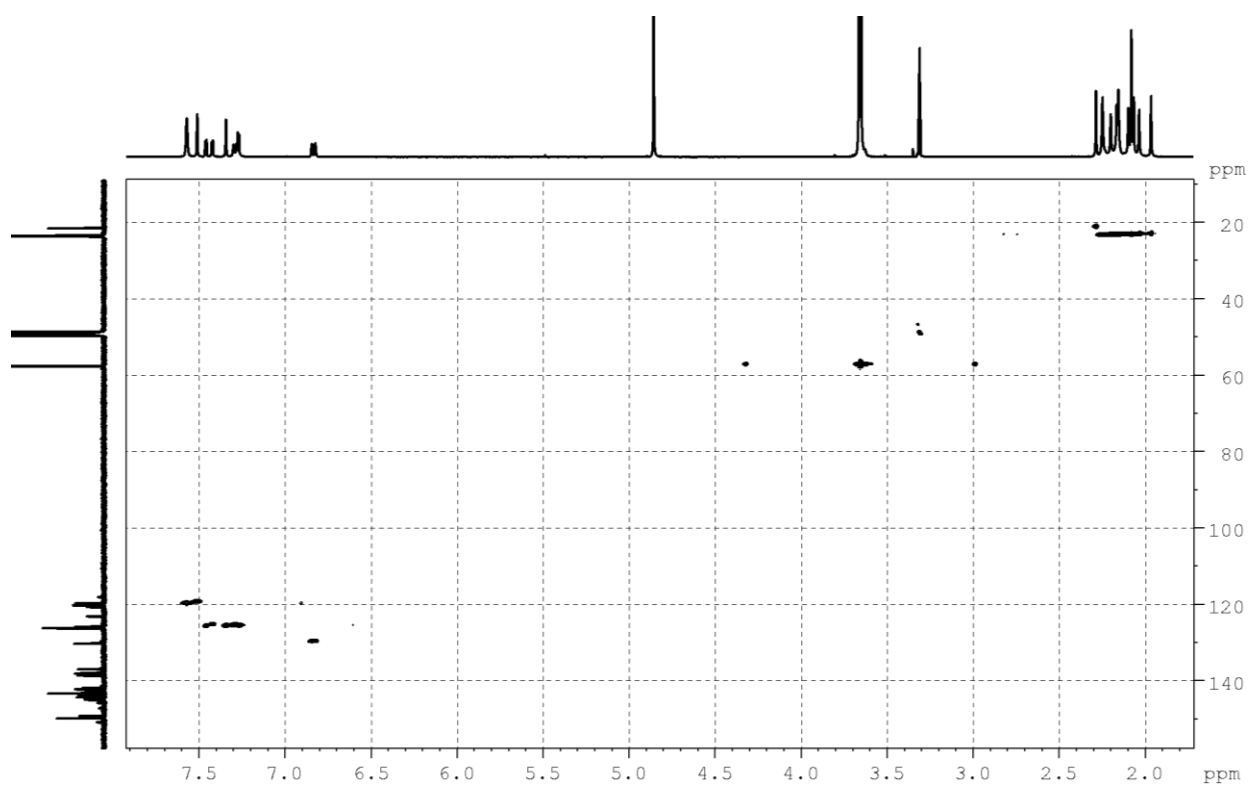


Figure 11.132: ^1H - ^{13}C HSQC spectrum of compound **Cat³⁺** recorded in CD_3OD at 500 MHz.

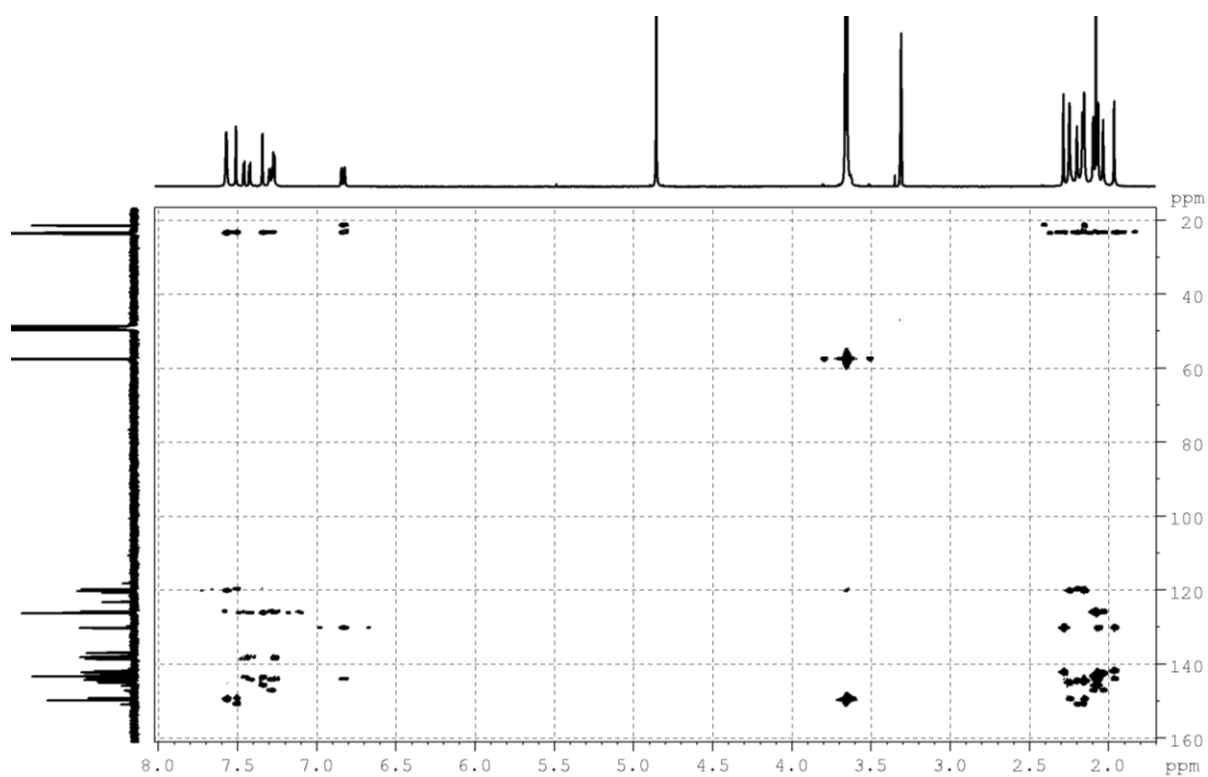
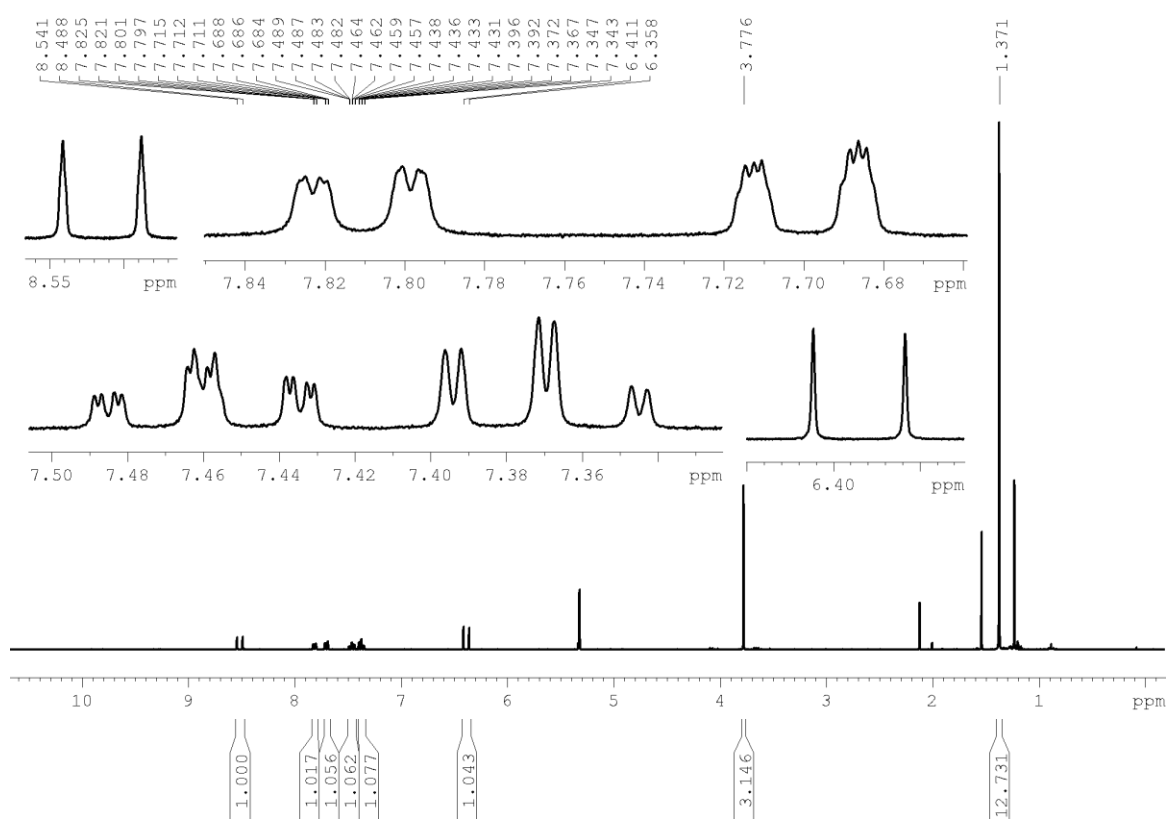
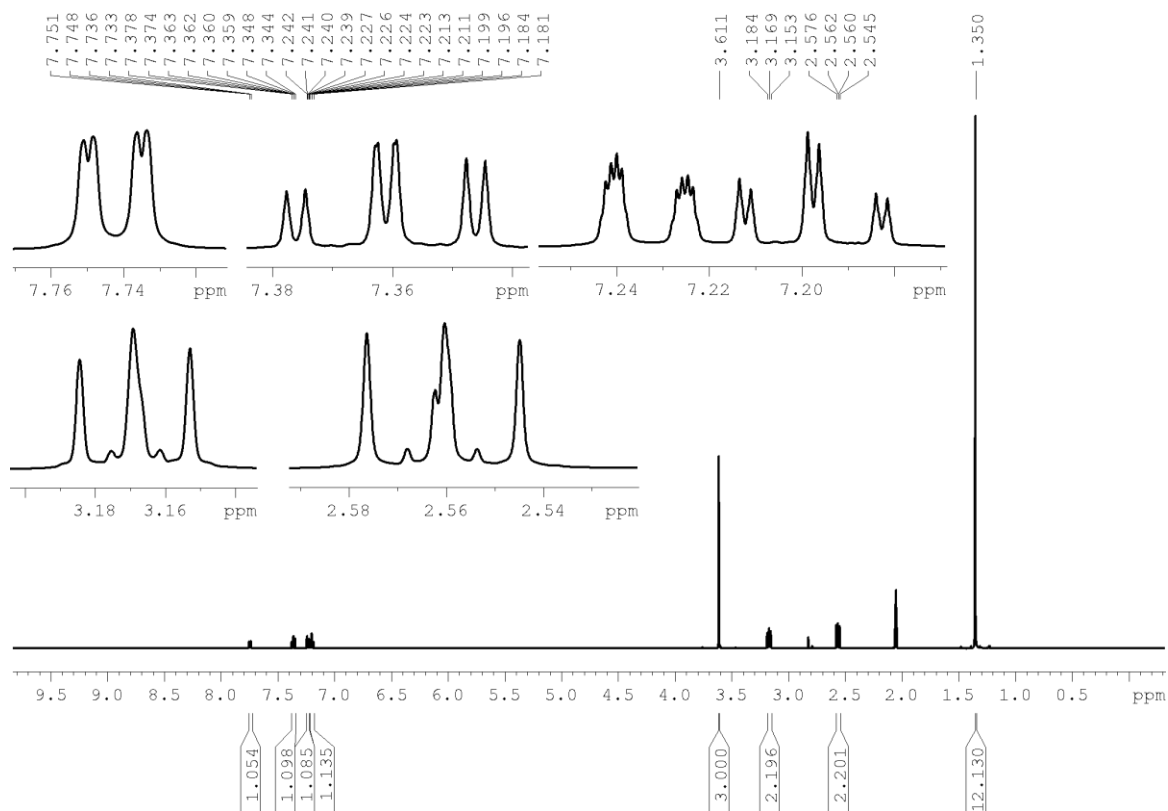


Figure 11.133: ^1H - ^{13}C HMBC spectrum of compound **Cat³⁺** recorded in CD_3OD at 500 MHz.

11.4.3 Chapter 7

Figure 11.134: ^1H NMR spectrum of **7.7** recorded in CD_2Cl_2 at 300 MHz.Figure 11.135: ^1H NMR spectrum of **7.8** recorded in CD_2Cl_2 at 500 MHz.

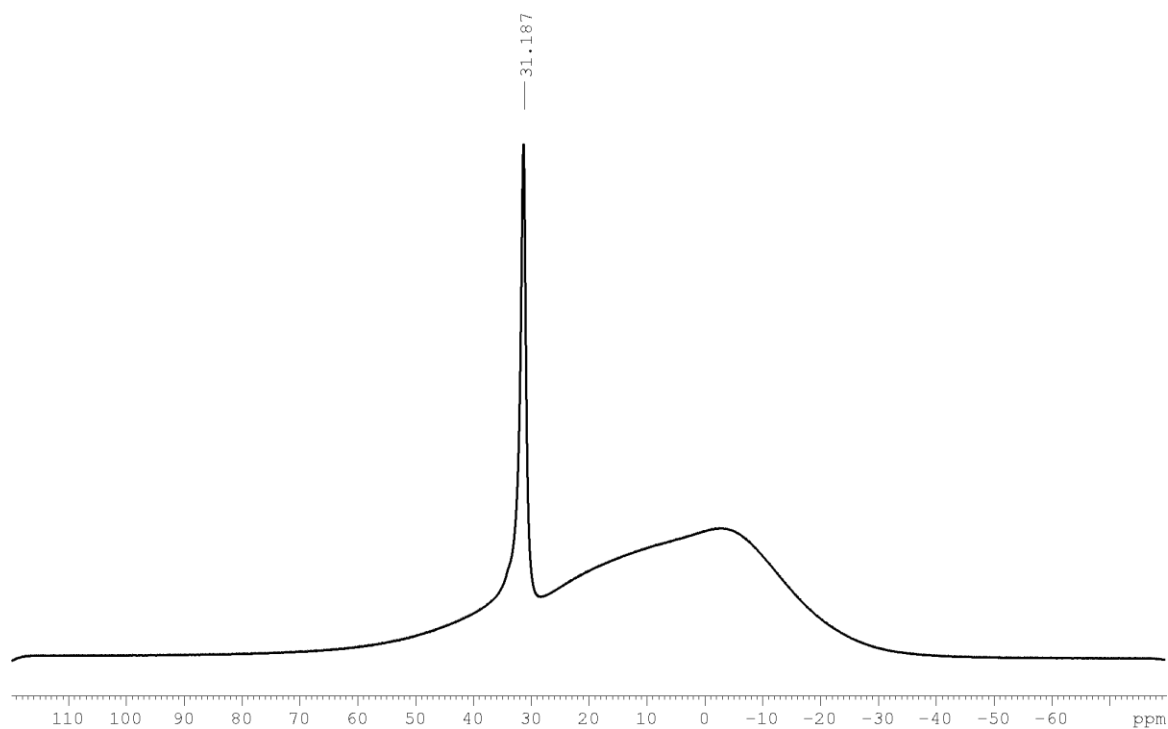


Figure 11.136: $^{11}\text{B}\{^1\text{H}\}$ NMR spectrum of **7.8** recorded in CD_2Cl_2 at 160 MHz.

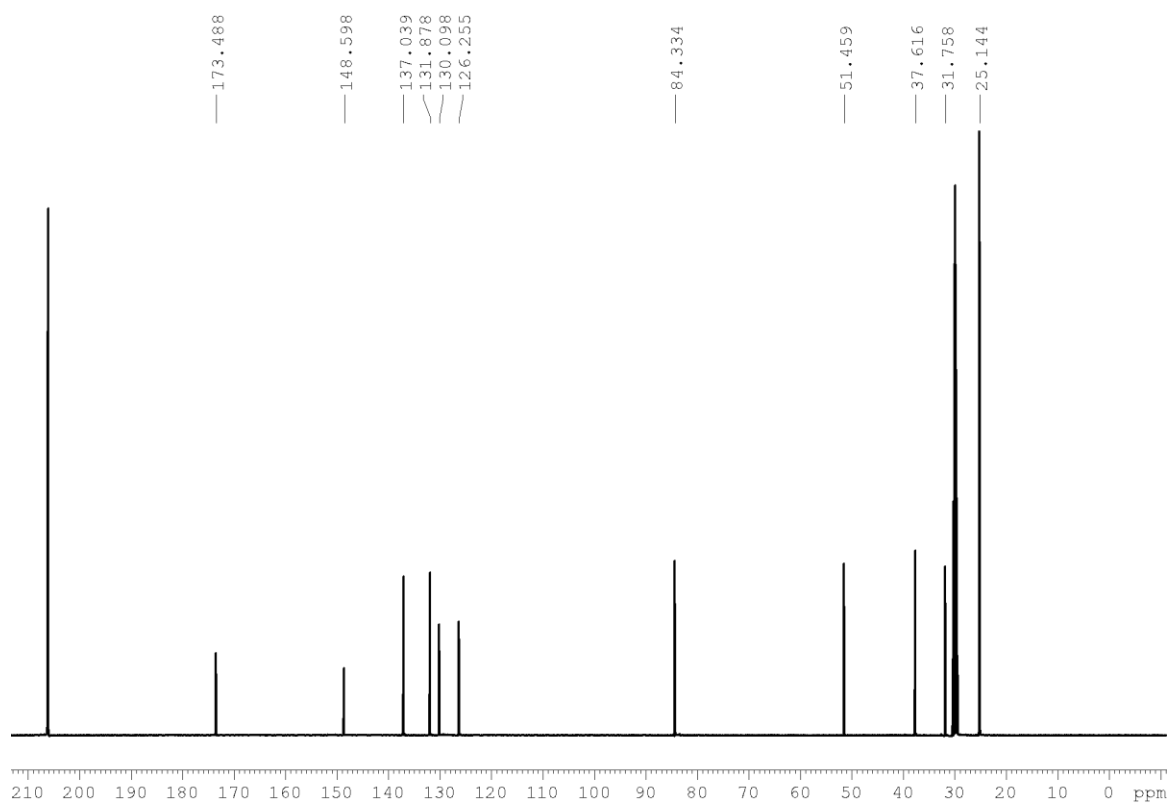


Figure 11.137: $^{13}\text{C}\{^1\text{H}\}$ NMR spectrum of **7.8** recorded in CD_2Cl_2 at 125 MHz.

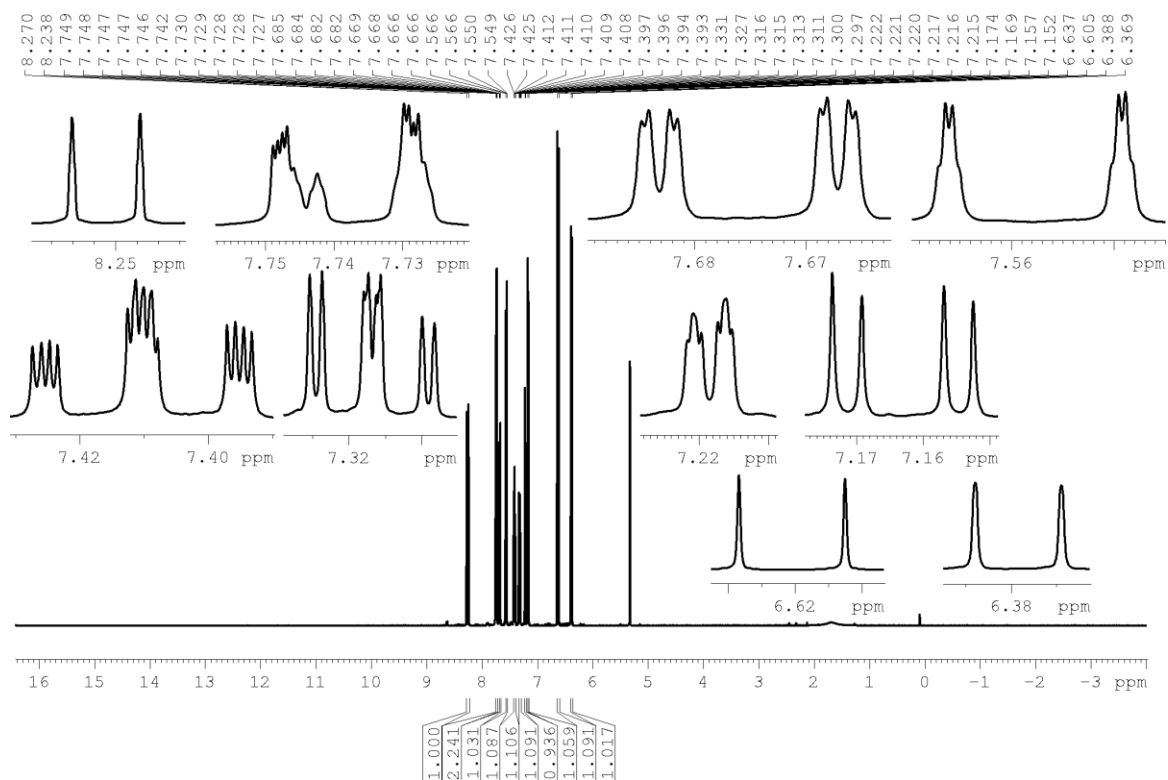


Figure 11.138: ^1H NMR spectrum of **7.15** recorded in CD_2Cl_2 at 500 MHz.

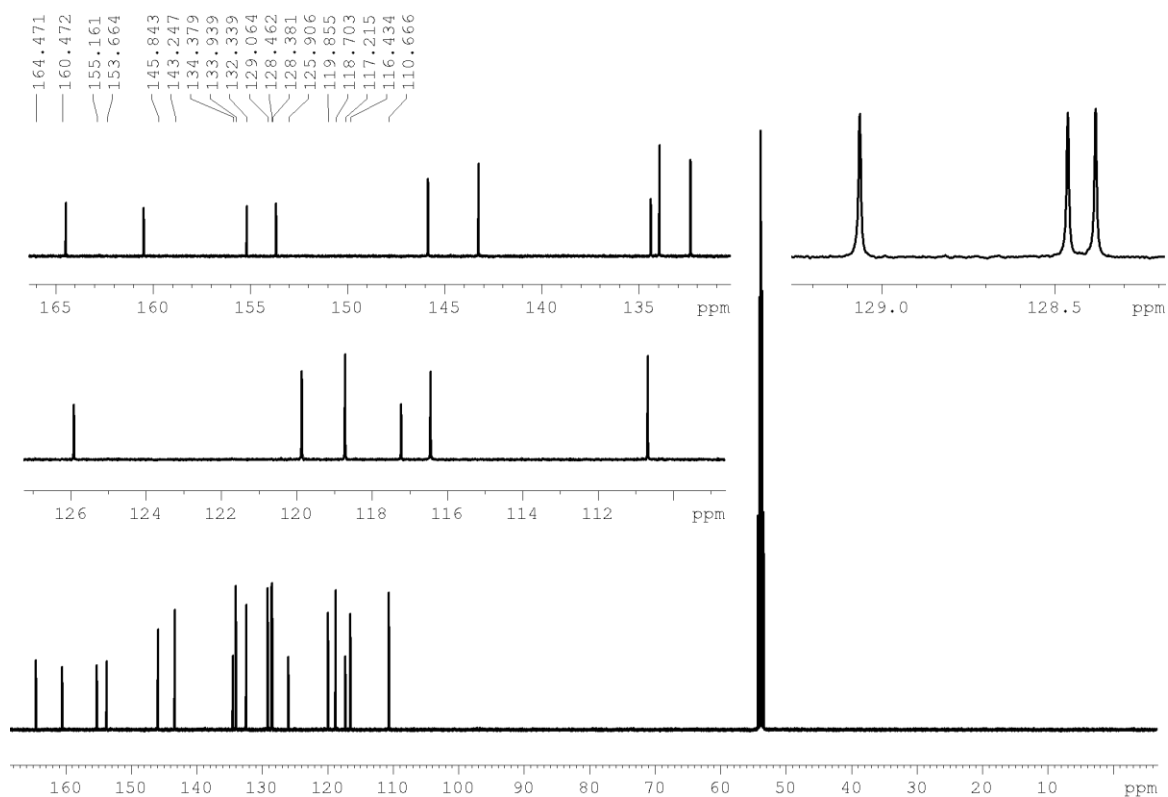


Figure 11.139: $^{13}\text{C}\{^1\text{H}\}$ NMR spectrum of **7.15** recorded in CD_2Cl_2 at 125 MHz.

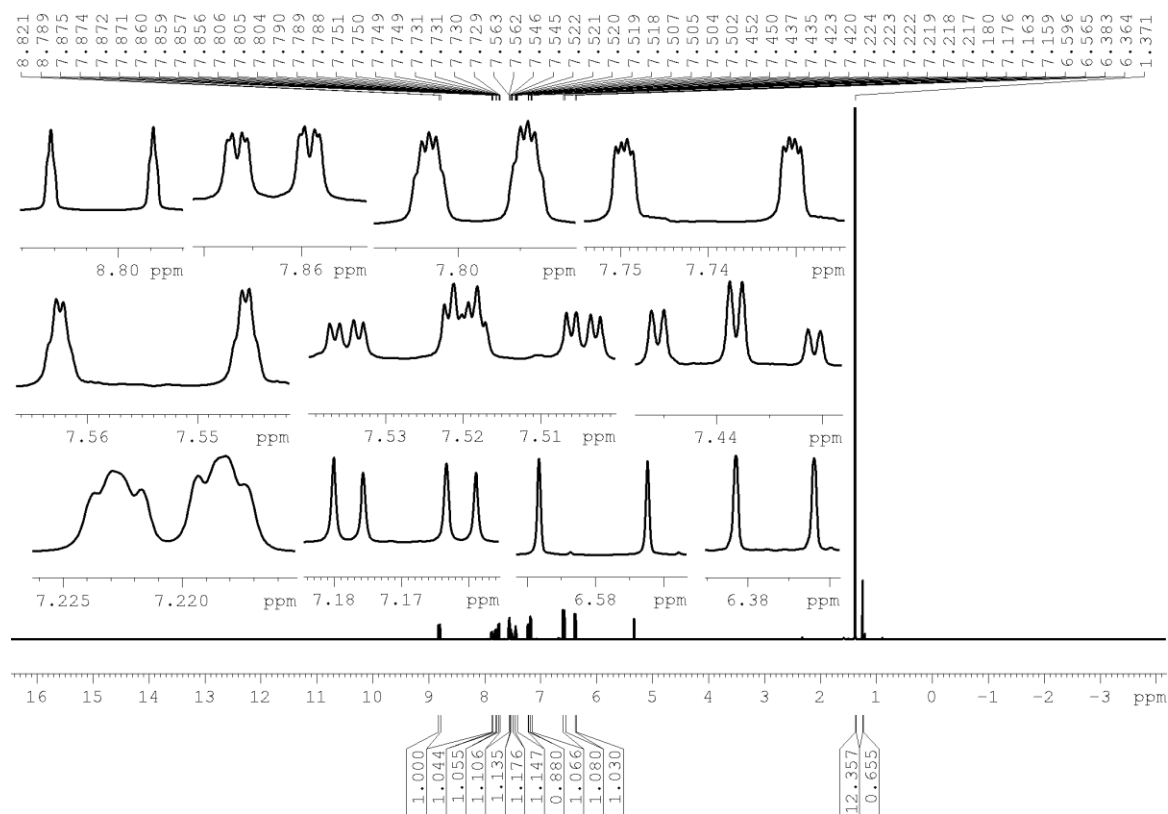


Figure 11.140: ^1H NMR spectrum of **7.6** recorded in CD_2Cl_2 at 500 MHz.

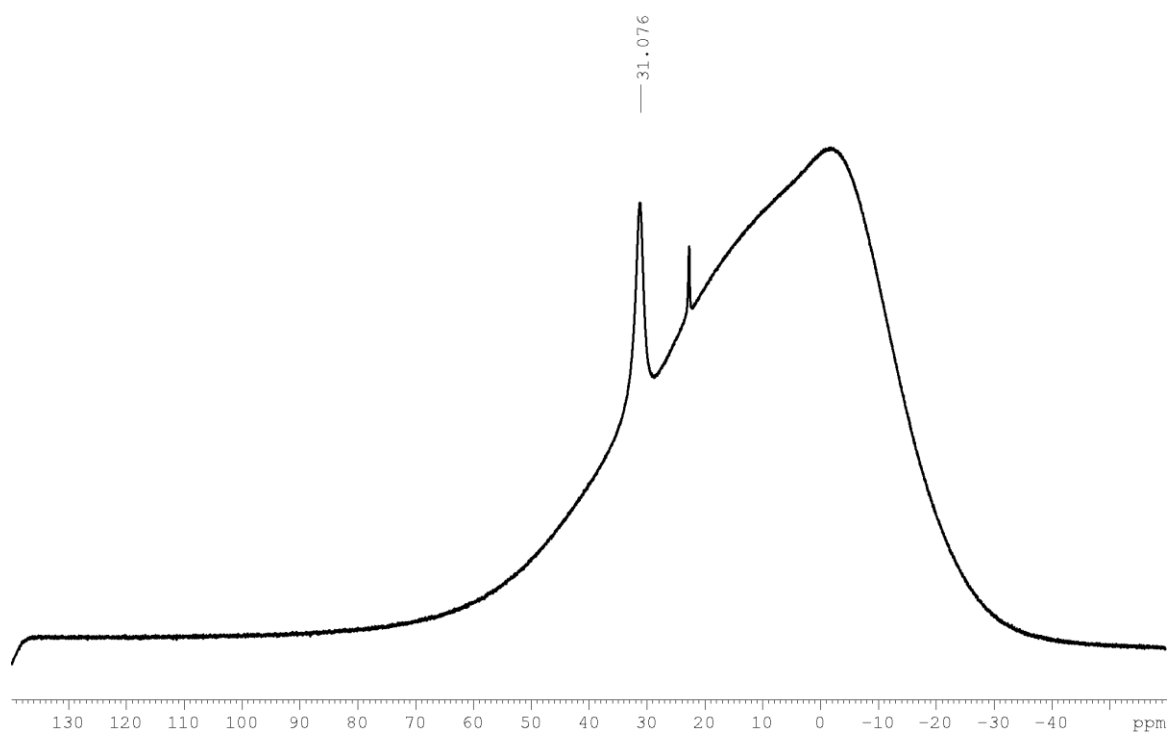


Figure 11.141: $^{11}\text{B}\{^1\text{H}\}$ NMR spectrum of **7.6** recorded in CD_2Cl_2 at 160 MHz.

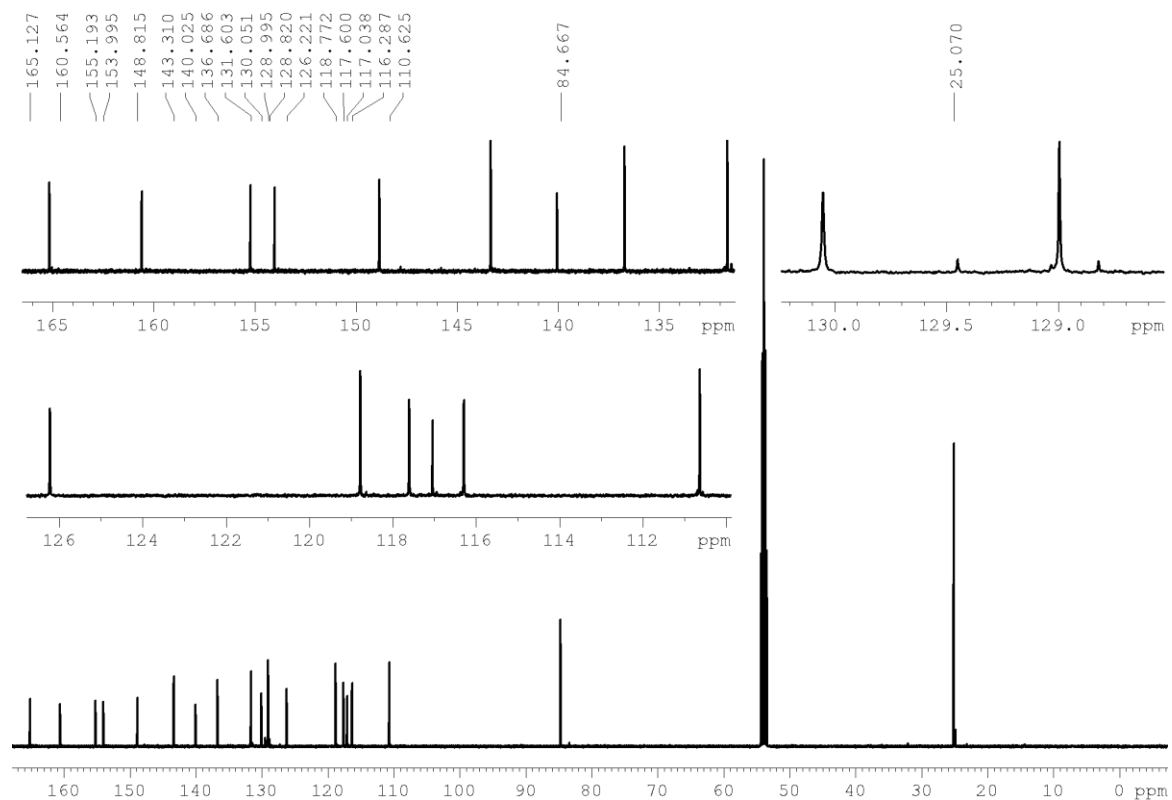
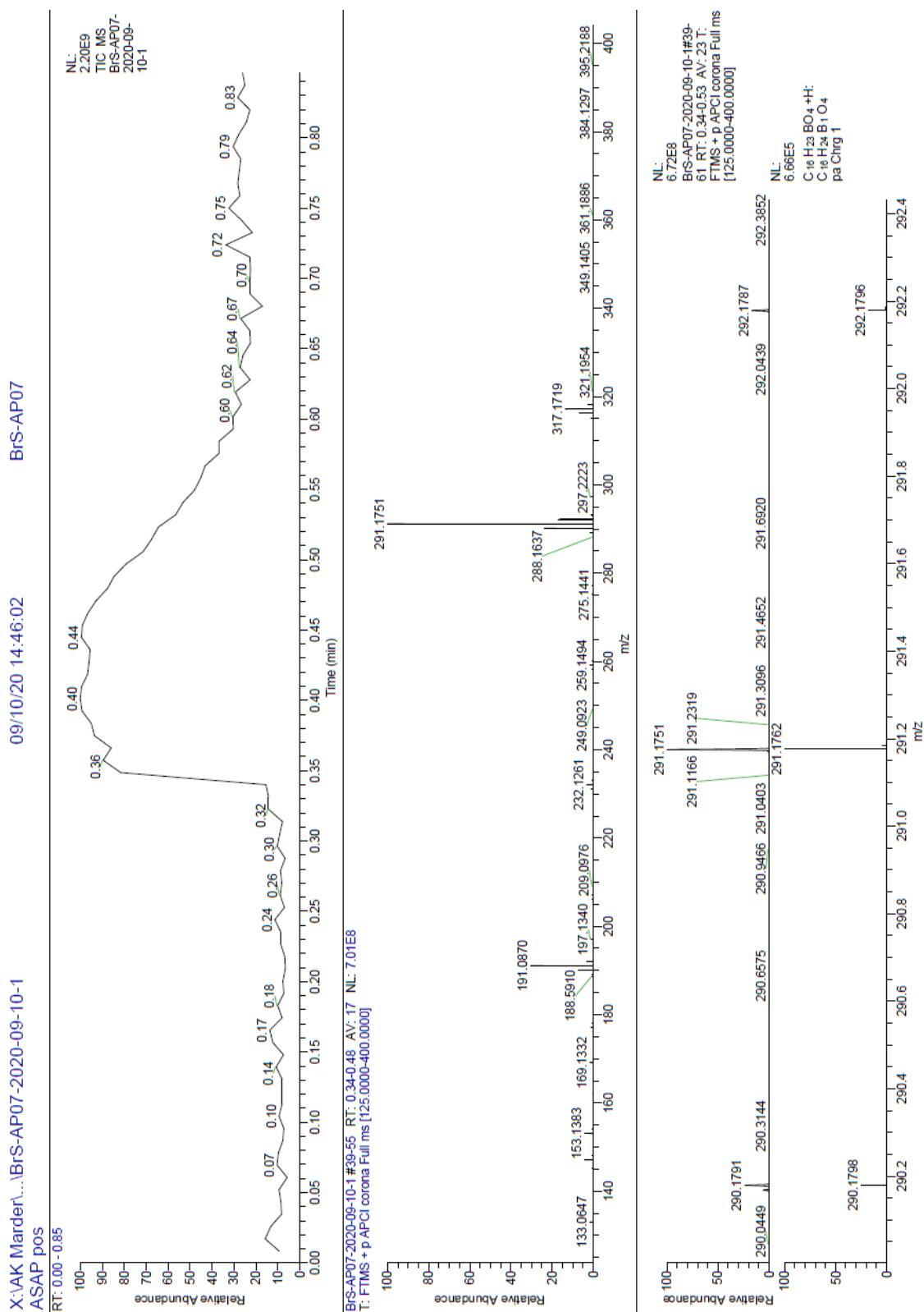


Figure 11.142: $^{13}\text{C}\{^1\text{H}\}$ NMR spectrum of **7.6** recorded in CD_2Cl_2 at 125 MHz.

11.5 HRMS Spectra

11.5.1 Chapter 7

Figure 11.143: HRMS spectrum (ASAP pos) of **7.8** recorded for characterization.

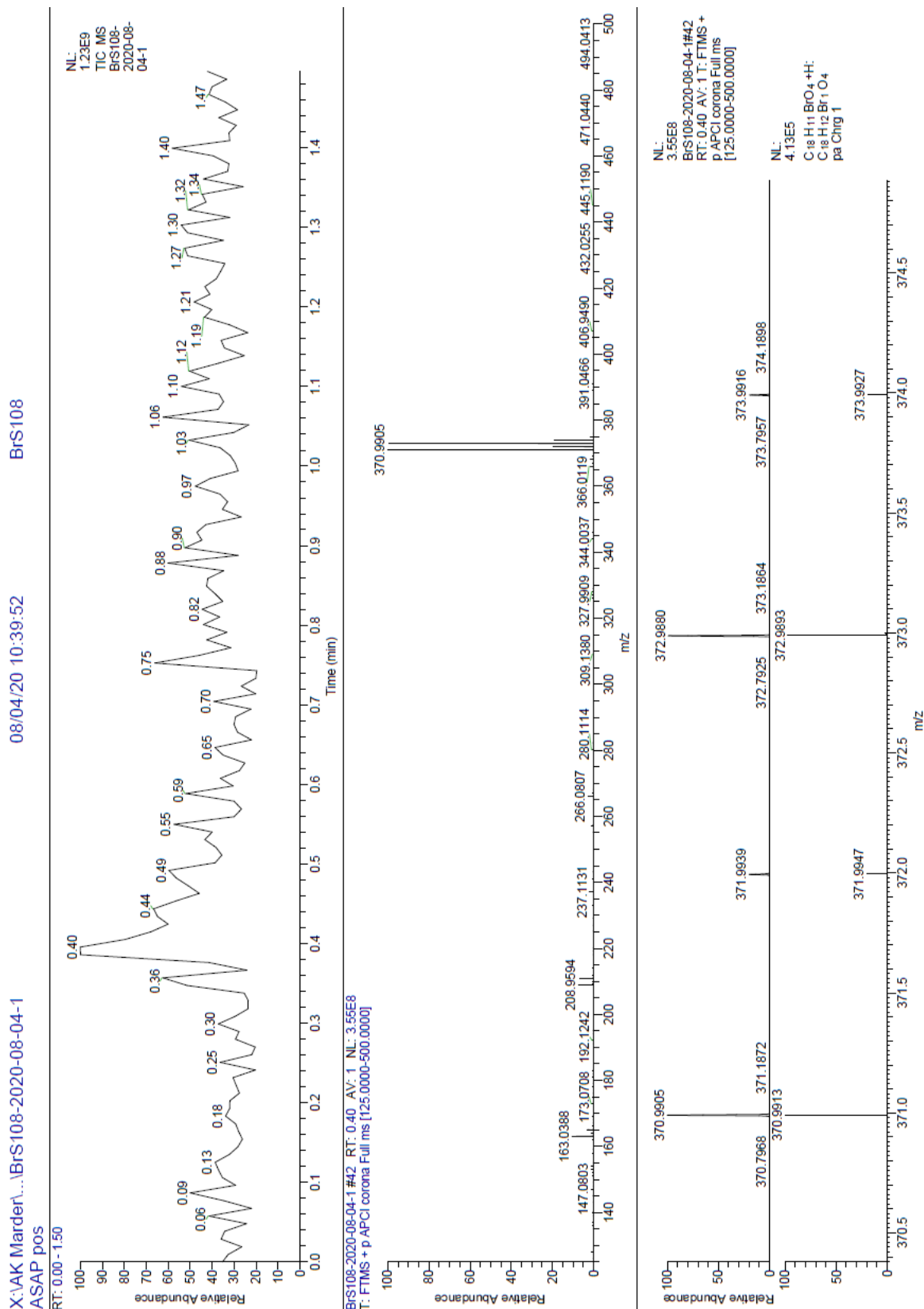


Figure 11.144: HRMS spectrum (ASAP pos) of **7.15** recorded for characterization.

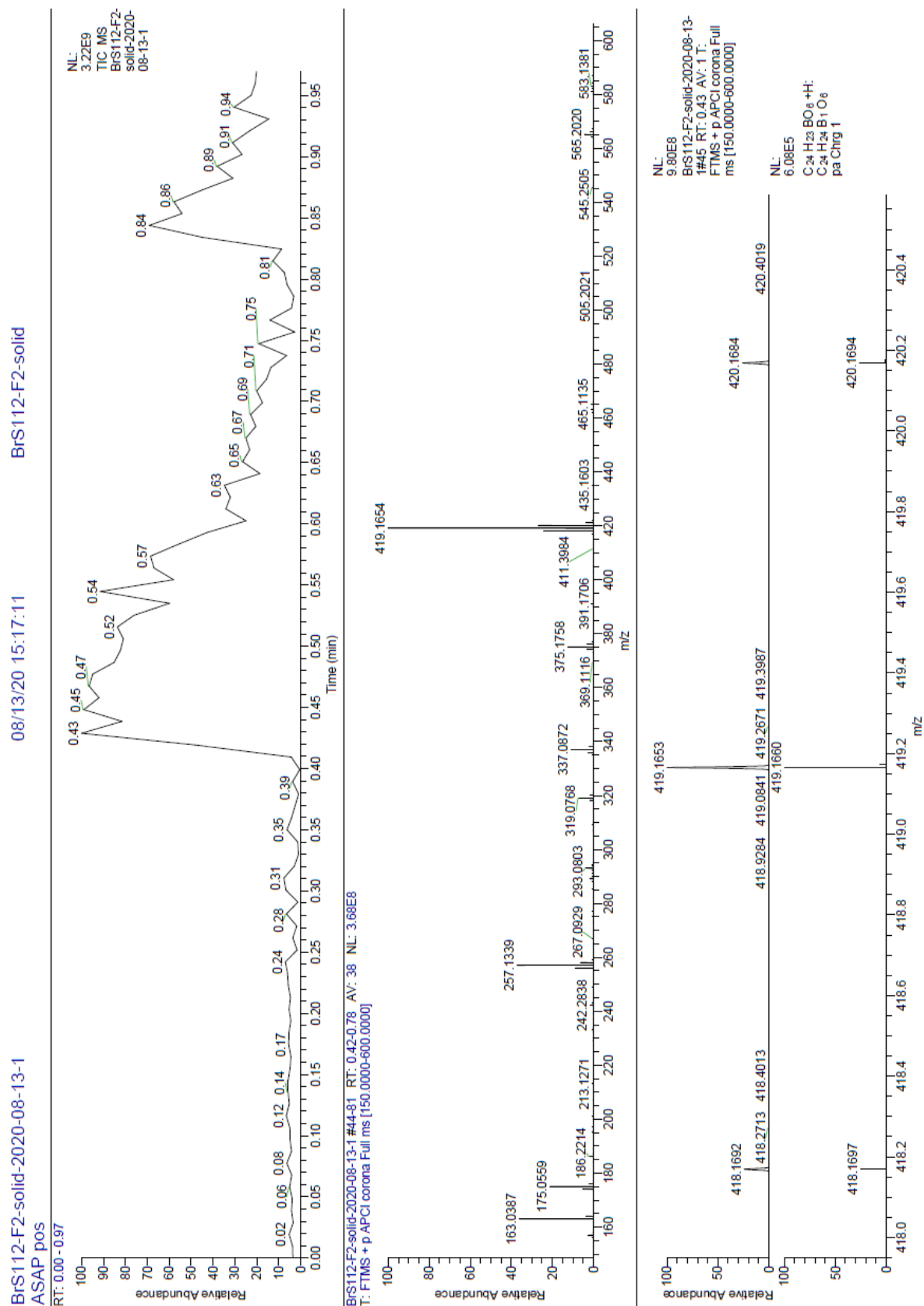


Figure 11.145: HRMS spectrum (ASAP pos) of 7.6 recorded for characterization.

11.6 Crystal Structures

11.6.1 Chapter 3

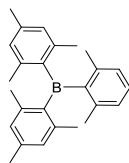
Table 11.3: Single-crystal X-ray diffraction data and structure refinements of **3.2a** and **3.2b**.

Data	3.2a	3.2b
CCDC number	2045567	2045566
Empirical formula	C ₅₅ H ₇₀ B ₂ Cl ₂ N ₂	C ₃₃ H ₄₅ B ₂ NO ₂
Formula weight (g·mol ⁻¹)	851.65	509.32
Temperature (K)	100(2)	296(2)
Radiation, λ (Å)	Mo-K α 0.71073	Mo-K α 0.71073
Crystal system	Triclinic	Monoclinic
Space group	$P\bar{1}$	$P2_1/c$
<i>Unit cell dimensions</i>		
a (Å)	8.193(4)	8.102(5)
b (Å)	16.849(8)	22.572(5)
c (Å)	18.995(9)	16.990(4)
α (°)	113.933(11)	90
β (°)	92.463(16)	91.67(2)
γ (°)	95.778(10)	90
Volume (Å ³)	2374.3(19)	3106(2)
Z	2	4
Calculated density (Mg·m ⁻³)	1.191	1.089
Abs. coefficient (mm ⁻¹)	0.176	0.065
$F(000)$	916	1104
Theta range for collection	1.367 to 26.395°	1.501 to 26.773°
Reflections collected	79205	54729
Independent reflections	9726	6616
Minimum/maximum transmission	0.7101/0.7454	0.7208/0.7449
Refinement method	Full-matrix on F^2	least-squares Full-matrix on F^2
Data / parameters / restraints	9726 / 596 / 120	6616 / 356 / 0
Goodness-of-fit on F^2	1.016	1.034
Final R indices [$I > 2\sigma(I)$]	$R_1 = 0.0502$, $wR^2 = 0.1184$	$R_1 = 0.0437$, $wR^2 = 0.1128$
R indices (all data)	$R_1 = 0.0846$, $wR^2 = 0.1361$	$R_1 = 0.0527$, $wR^2 = 0.1202$
Max./min. residual electron density (e·Å ⁻³)	0.390 / -0.314	0.332 / -0.252

11.7 TD-DFT Calculations

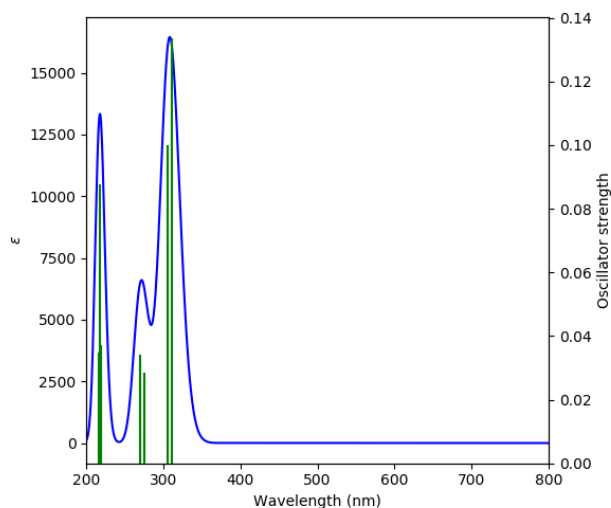
11.7.1 Chapter 3

3.1a

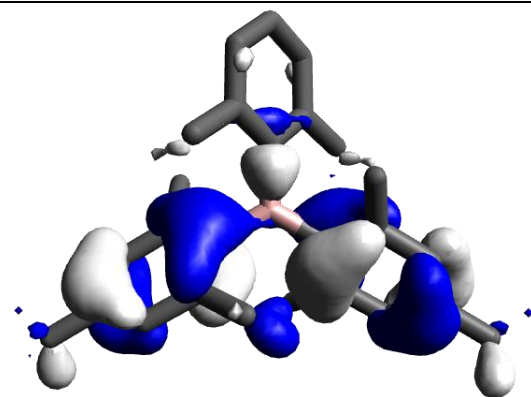


Functional used: TD-DFT CAM-B3LYP 6-31G(d,p), gas phase

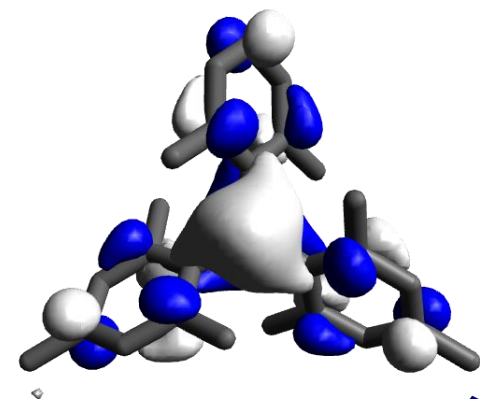
Calculated Absorption Spectrum



Orbital	Energy [eV]	Symmetry
L+4	0.39	B
L+3	0.33	A
L+2	0.00	A
L+1	-0.01	B
LUMO	-1.60	B
HOMO	-5.94	A
H-1	-6.02	B
H-2	-6.17	A
H-3	-6.26	A
H-4	-6.26	B

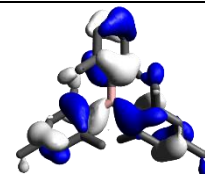
Orbitals Relevant for $S_1 \leftarrow S_0$ Transition

HOMO

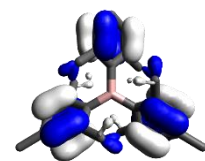


LUMO

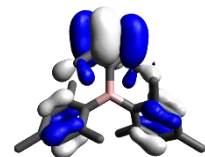
Other Relevant Orbitals



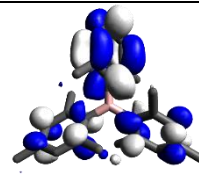
HOMO-1



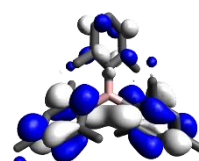
HOMO-2



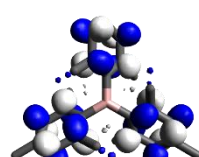
HOMO-3



LUMO+1



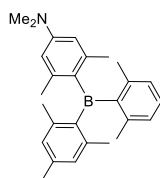
LUMO+2



LUMO+3

Table 11.4: Lowest energy singlet electronic transitions of **3.1a** (TD-DFT CAM-B3LYP 6-31G(d,p), gas phase).

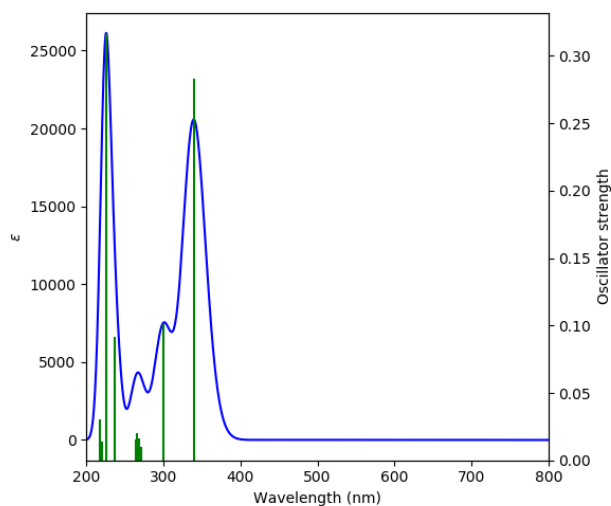
State	E [eV]	λ [nm]	f	Symmetry	Major Contributions	Δ
1	3.98	310	0.134	B	HOMO->LUMO (93%)	0.583
2	4.07	305	0.010	A	H-1->LUMO (91%)	0.634
3	4.51	275	0.028	B	H-2->LUMO (86%)	0.521
4	4.59	270	0.031	A	H-4->LUMO (82%)	0.494
5	4.60	269	0.034	B	H-3->LUMO (84%)	0.506
6	4.74	261	0.000	A	H-5->LUMO (90%)	0.682
7	5.66	219	0.037	B	H-4->L+2 (17%), H-1->L+3 (10%), HOMO->L+1 (12%), HOMO->L+4 (19%)	0.639
8	5.66	219	0.028	A	H-4->LUMO (14%), H-2->L+2 (12%), HOMO->L+3 (18%)	0.655
9	5.71	217	0.088	B	H-6->LUMO (40%)	0.625
10	5.74	216	0.035	B	H-6->LUMO (28%), H-3->L+1 (12%), H-1->L+2 (15%)	0.651



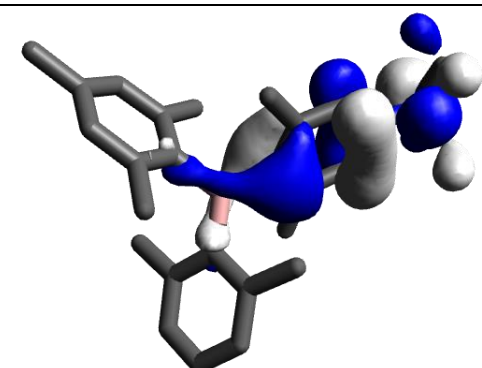
3.2a

Functional used: TD-DFT CAM-B3LYP
6-31G(d,p), gas phase

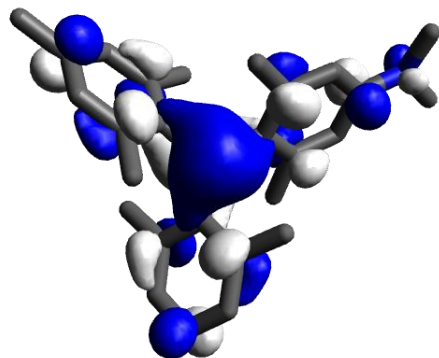
Calculated Absorption Spectrum



Orbital	Energy [eV]	Symmetry
L+4	0.52	A
L+3	0.48	A
L+2	0.30	A
L+1	0.12	A
LUMO	-1.36	A
HOMO	-5.02	A
H-1	-5.83	A
H-2	-6.03	A
H-3	-6.05	A
H-4	-6.12	A

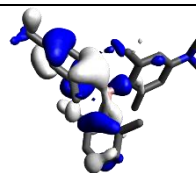
Orbitals Relevant for $S_1 \leftarrow S_0$ Transition

HOMO

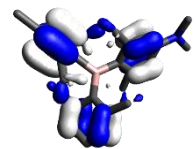


LUMO

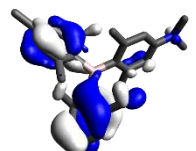
Other Relevant Orbitals



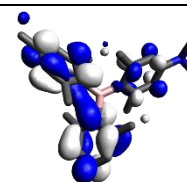
HOMO-1



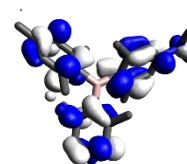
HOMO-2



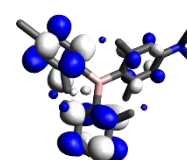
HOMO-3



LUMO+1



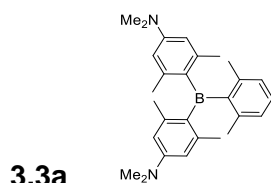
LUMO+2



LUMO+3

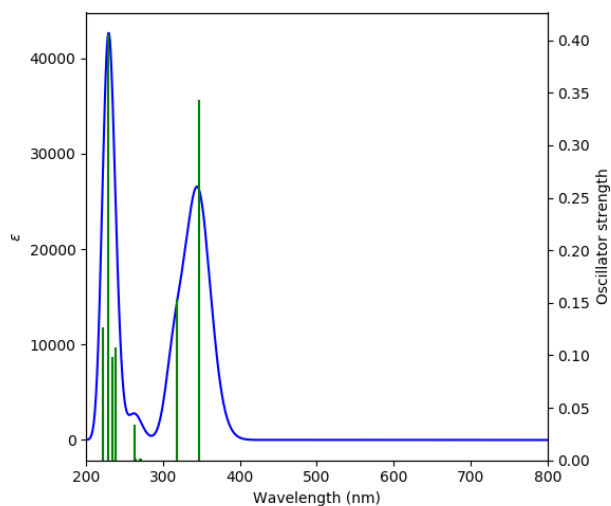
Table 11.5: Lowest energy singlet electronic transitions of **3.2a** (TD-DFT CAM-B3LYP 6-31G(d,p), gas phase).

State	E [eV]	λ [nm]	f	Symmetry	Major Contributions	Δ
1	3.65	339	0.283	A	HOMO->LUMO (87%)	0.495
2	4.13	300	0.101	A	H-1->LUMO (87%)	0.572
3	4.57	271	0.010	A	H-2->LUMO (66%), HOMO->L+4 (11%)	0.511
4	4.61	269	0.016	A	H-3->LUMO (79%)	0.576
5	4.68	265	0.020	A	H-5->LUMO (56%), H-2->LUMO (13%)	0.521
6	4.69	264	0.015	A	H-4->LUMO (83%)	0.580
7	5.24	237	0.091	A	H-5->LUMO (26%), HOMO->L+1 (24%), HOMO->L+4 (33%)	0.495
8	5.50	225	0.316	A	H-7->LUMO (11%), H-6->LUMO (24%), HOMO->L+2 (36%), HOMO->L+5 (11%)	0.565
9	5.64	220	0.014	A	H-1->L+3 (15%), HOMO->L+2 (13%)	0.631
10	5.71	217	0.030	A	H-4->L+1 (14%), HOMO->L+2 (10%)	0.621



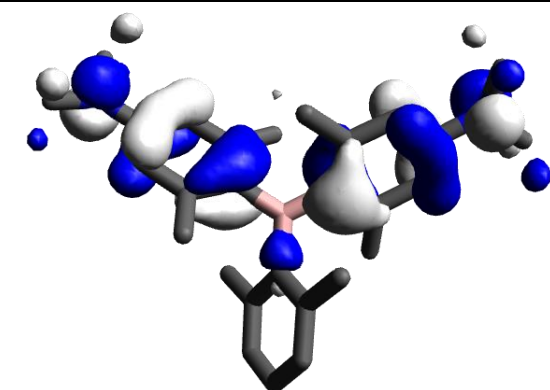
Functional used: TD-DFT CAM-B3LYP
6-31G(d,p), gas phase

Calculated Absorption Spectrum

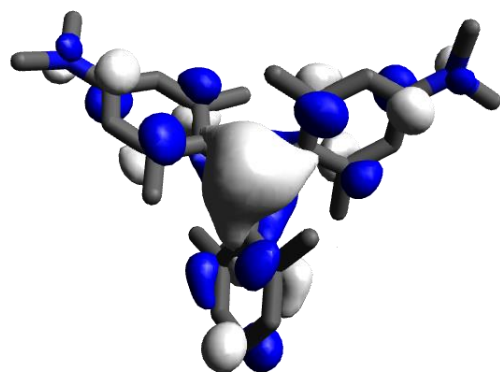


Orbital	Energy [eV]	Symmetry
L+4	0.67	A
L+3	0.61	A
L+2	0.46	A
L+1	0.31	A
LUMO	-1.16	A
HOMO	-4.79	A
H-1	-4.98	A
H-2	-5.89	A
H-3	-5.91	A
H-4	-5.99	A

Orbitals Relevant for $S_1 \leftarrow S_0$ Transition

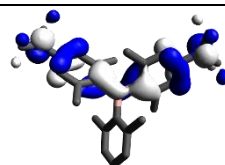


HOMO

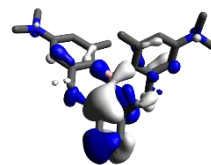


LUMO

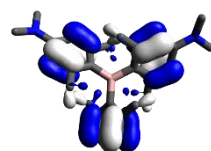
Other Relevant Orbitals



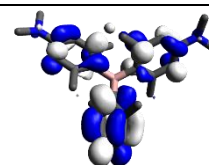
HOMO-1



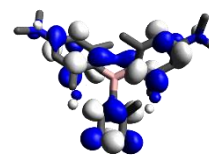
HOMO-2



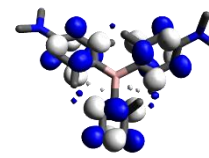
HOMO-3



LUMO+1



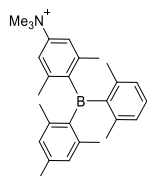
LUMO+2



LUMO+3

Table 11.6: Lowest energy singlet electronic transitions of **3.3a** (TD-DFT CAM-B3LYP 6-31G(d,p), gas phase).

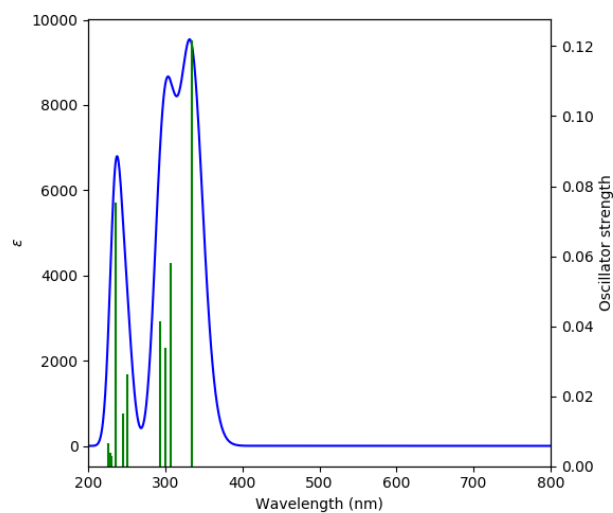
State	E [eV]	λ [nm]	f	Symmetry	Major Contributions	Δ
1	3.58	346	0.343	A	HOMO->LUMO (90%)	0.517
2	3.90	318	0.154	A	H-2->LUMO (12%), H-1->LUMO (81%)	0.575
3	4.57	271	0.001	A	H-2->LUMO (81%), H-1->LUMO (12%)	0.567
4	4.60	270	0.002	A	H-3->LUMO (56%)	0.527
5	4.69	265	0.001	A	H-5->LUMO (52%), H-1->L+4 (10%), HOMO->L+3 (12%)	0.545
6	4.72	263	0.034	A	H-4->LUMO (62%), H-3->LUMO (16%)	0.514
7	5.21	238	0.108	A	H-4->LUMO (14%), H-3->LUMO (19%), H-1->L+3 (12%), HOMO->L+1 (24%), HOMO->L+4 (16%)	0.553
8	5.30	234	0.100	A	H-5->LUMO (44%), H-1->L+1 (14%), H-1->L+4 (11%), HOMO->L+3 (16%)	0.552
9	5.43	229	0.406	A	H-8->LUMO (11%), H-6->LUMO (24%), H-1->L+2 (14%), HOMO->L+1 (25%)	0.606
10	5.61	221	0.126	A	H-1->L+1 (14%), HOMO->L+2 (43%), HOMO->L+5 (21%)	0.641



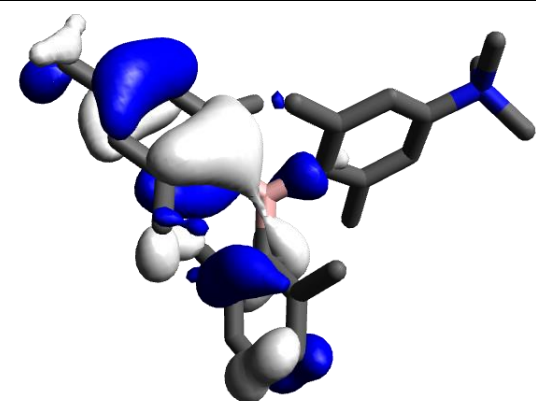
3.2c

Functional used: TD-DFT CAM-B3LYP
6-31G(d,p), gas phase

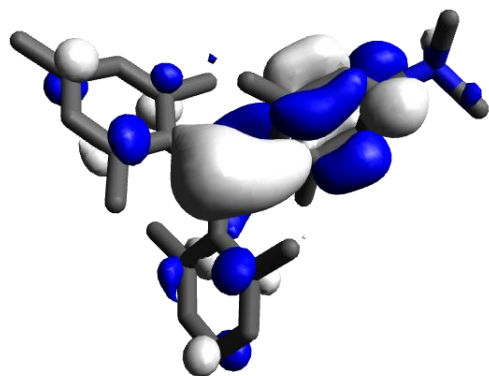
Calculated Absorption Spectrum



Orbital	Energy [eV]	Symmetry
L+4	-2.17	A
L+3	-2.37	A
L+2	-3.25	A
L+1	-3.36	A
LUMO	-4.36	A
HOMO	-8.23	A
H-1	-8.37	A
H-2	-8.46	A
H-3	-8.55	A
H-4	-9.58	A

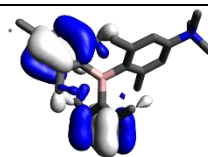
Orbitals Relevant for $S_1 \leftarrow S_0$ Transition

HOMO

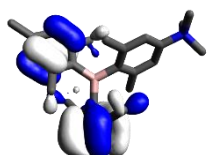


LUMO

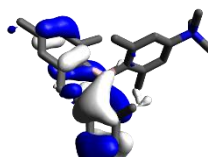
Other Relevant Orbitals



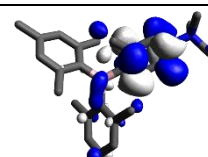
HOMO-1



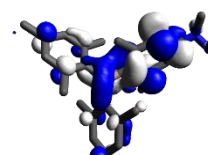
HOMO-2



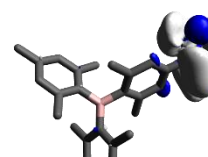
HOMO-3



LUMO+1



LUMO+2

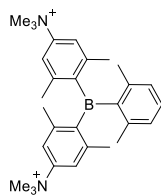


LUMO+3

Table 11.7: Lowest energy singlet electronic transitions of **3.2c** (TD-DFT CAM-B3LYP 6-31G(d,p), gas phase).

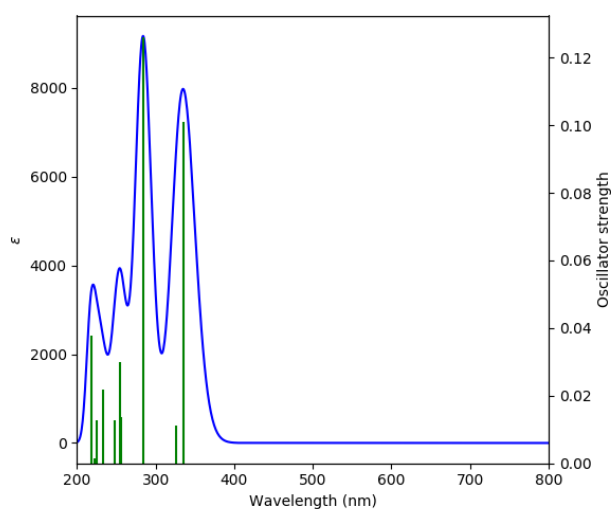
State	E [eV]	λ [nm]	f	Symmetry	Major Contributions	Δ
1	3.71	334	0.122	A	HOMO->LUMO (87%)	0.462
2	4.03	308	0.058	A	H-3->LUMO (54%), H-2->LUMO (17%), H-1->LUMO (14%)	0.473
3	4.14	300	0.034	A	H-3->LUMO (13%), H-1->LUMO (72%)	0.405
4	4.24	293	0.041	A	H-3->LUMO (17%), H-2->LUMO (68%)	0.397
5	4.96	250	0.026	A	H-4->LUMO (83%)	0.695
6	5.05	246	0.015	A	H-5->LUMO (62%), H-4->L+1 (14%)	0.565
7	5.25	236	0.075	A	HOMO->L+1 (31%), HOMO->L+2 (43%)	0.411
8	5.40	230	0.003	A	H-1->L+1 (10%), H-1->L+2 (21%)	0.481
9	5.41	229	0.004	A	H-2->LUMO (10%), H-2->L+2 (23%)	0.511
10	5.48	226	0.006	A	HOMO->L+1 (51%), HOMO->L+2 (32%)	0.364

3.3c

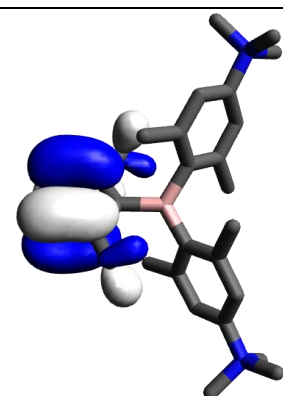


Functional used: TD-DFT CAM-B3LYP 6-31G(d,p), gas phase

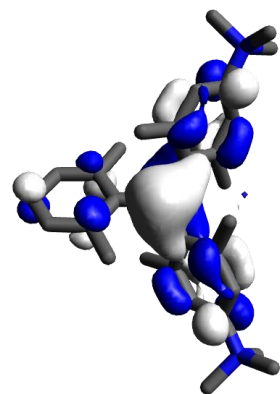
Calculated Absorption Spectrum



Orbital	Energy [eV]	Symmetry
L+4	-5.01	A
L+3	-5.44	A
L+2	-5.50	A
L+1	-5.83	A
LUMO	-6.90	A
HOMO	-10.62	A
H-1	-10.79	A
H-2	-11.69	A
H-3	-11.9	A
H-4	-11.92	A

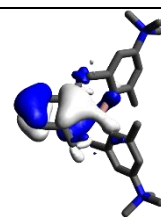
Orbitals Relevant for $S_1 \leftarrow S_0$ Transition

HOMO

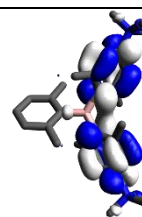


LUMO

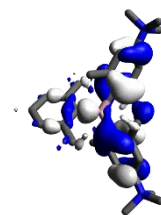
Other Relevant Orbitals



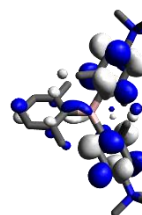
HOMO-1



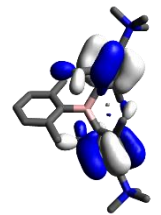
LUMO+1



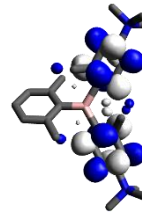
HOMO-2



LUMO+2



HOMO-3



LUMO+3

Table 11.8: Lowest energy singlet electronic transitions of **3.3c** (TD-DFT CAM-B3LYP 6-31G(d,p), gas phase).

State	E [eV]	λ [nm]	f	Symmetry	Major Contributions	Δ
1	3.69	336	0.101	A	H-1->LUMO (92%)	0.472
2	3.80	326	0.011	A	HOMO->LUMO (92%)	0.286
3	4.36	284	0.126	A	H-2->LUMO (90%)	0.654
4	4.85	256	0.014	A	H-4->L+1 (11%), H-3->LUMO (73%)	0.580
5	4.86	255	0.030	A	H-4->LUMO (70%), H-3->L+1 (12%)	0.568
6	4.99	249	0.013	A	H-5->LUMO (87%)	0.692
7	5.32	233	0.022	A	H-1->L+1 (52%), H-1->L+5 (10%), HOMO->L+2 (10%), HOMO->L+4 (15%)	0.342
8	5.50	225	0.013	A	H-1->L+1 (37%), H-1->L+5 (11%), HOMO->L+2 (19%), HOMO->L+4 (16%)	0.349
9	5.56	223	0.001	A	HOMO->L+1 (94%)	0.136
10	5.69	218	0.038	A	H-1->L+2 (61%), H-1->L+4 (12%)	0.468

11.7.2 Chapter 4

11.7.2.1 Sulfur Atoms of Bithiophene on Same Side

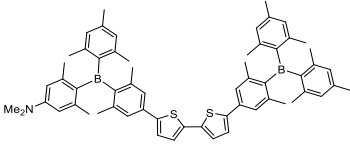
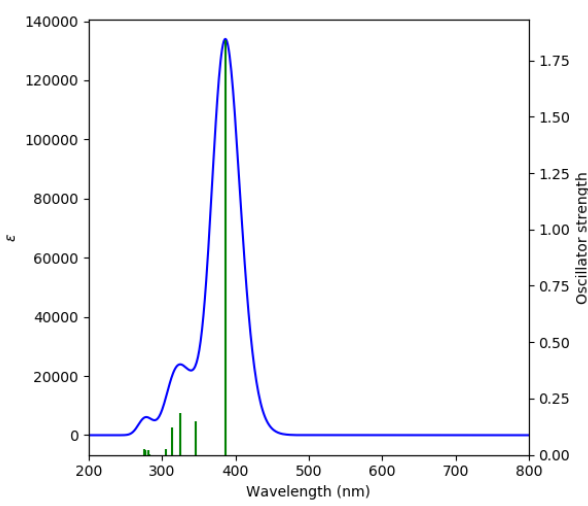
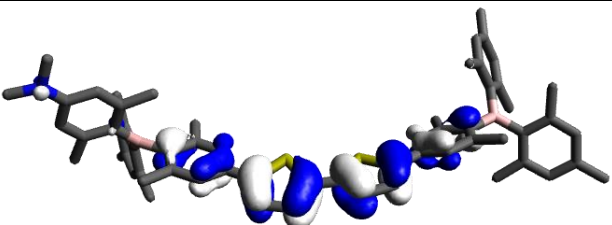
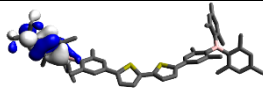
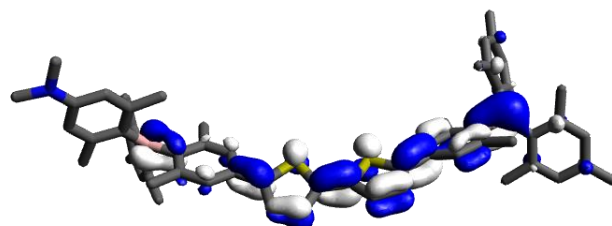
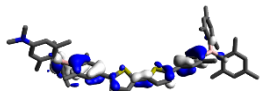
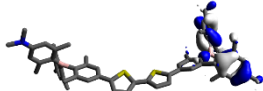
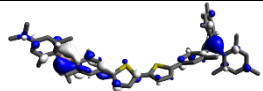
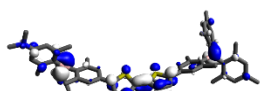
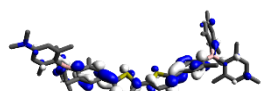
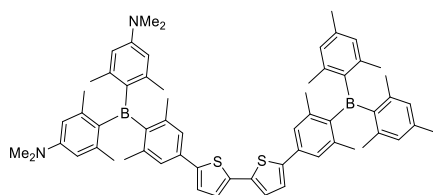
Neut1		Functional used: TD-DFT CAM-B3LYP 6-31G(d,p), gas phase		
				
Calculated Absorption Spectrum		Orbital	Energy [eV]	Symmetry
		L+4	-0.02	A
		L+3	-0.41	A
		L+2	-1.13	A
		L+1	-1.54	A
		LUMO	-1.85	A
		HOMO	-4.89	A
		H-1	-5.06	A
		H-2	-5.82	A
		H-3	-5.93	A
		H-4	-5.95	A
Orbitals Relevant for $S_1 \leftarrow S_0$ Transition		Other Relevant Orbitals		
				
HOMO		HOMO-1		
				
LUMO		HOMO-2		
				
		HOMO-3		
				
		LUMO+1		
				
		LUMO+2		
				
		LUMO+3		

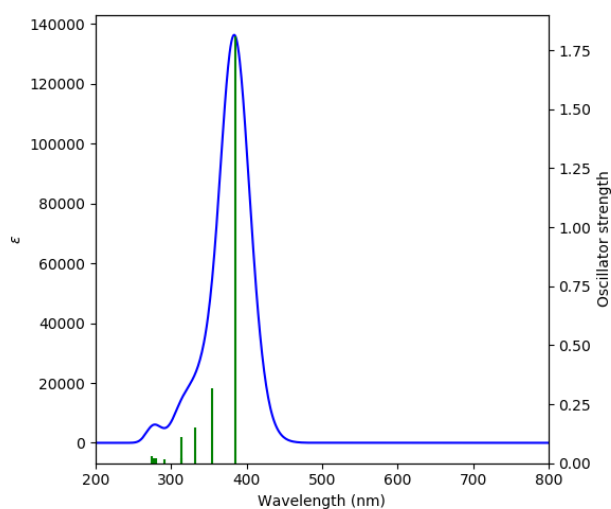
Table 11.9: Lowest energy singlet electronic transitions of **Neut1** (TD-DFT CAM-B3LYP 6-31G(d,p), gas phase).

State	E [eV]	λ [nm]	f	Symmetry	Major Contributions	Λ
1	3.21	387	1.841	A	HOMO->LUMO (76%)	0.667
2	3.59	346	0.148	A	H-1->LUMO (20%), H-1->L+1 (34%), H-1->L+2 (16%), HOMO->L+1 (10%)	0.388
3	3.82	325	0.184	A	H-2->LUMO (23%), HOMO->L+1 (36%)	0.544
4	3.94	314	0.120	A	H-3->LUMO (48%), H-3->L+1 (34%), H-3->L+2 (10%)	0.362
5	4.07	305	0.024	A	H-2->L+1 (28%), HOMO->L+2 (31%)	0.588
6	4.37	284	0.004	A	H-6->LUMO (12%), H-4->L+1 (28%), HOMO->L+1 (15%)	0.529
7	4.41	281	0.022	A	H-11->LUMO (37%), H-7->LUMO (22%), H-7->L+1 (11%)	0.376
8	4.47	278	0.023	A	H-8->LUMO (10%), H-6->L+1 (15%)	0.450
9	4.48	277	0.011	A	H-6->LUMO (12%), HOMO->L+2 (11%)	0.467
10	4.50	275	0.026	A	H-11->LUMO (22%), H-7->LUMO (23%), H-7->L+1 (20%)	0.364

**Neut2**

Functional used: TD-DFT CAM-B3LYP
6-31G(d,p), gas phase

Calculated Absorption Spectrum



Orbital

Energy [eV]

Symmetry

L+4	-0.01	A
L+3	-0.33	A
L+2	-1.04	A
L+1	-1.44	A
LUMO	-1.80	A
HOMO	-4.83	A
H-1	-4.84	A
H-2	-5.05	A
H-3	-5.79	A
H-4	-5.92	A

Orbitals Relevant for $S_1 \leftarrow S_0$ Transition

Other Relevant Orbitals

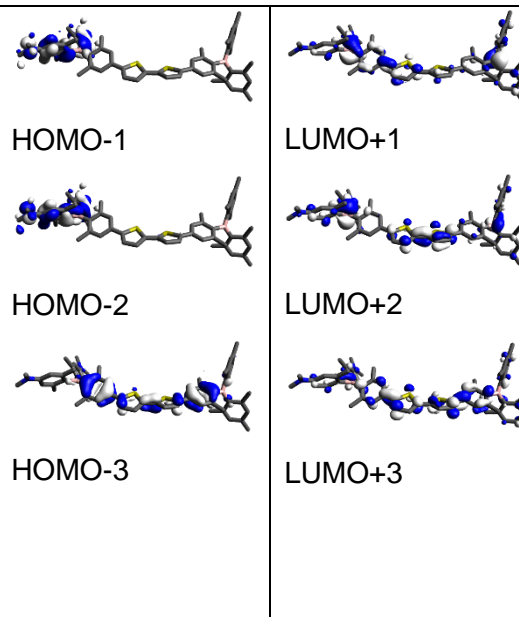
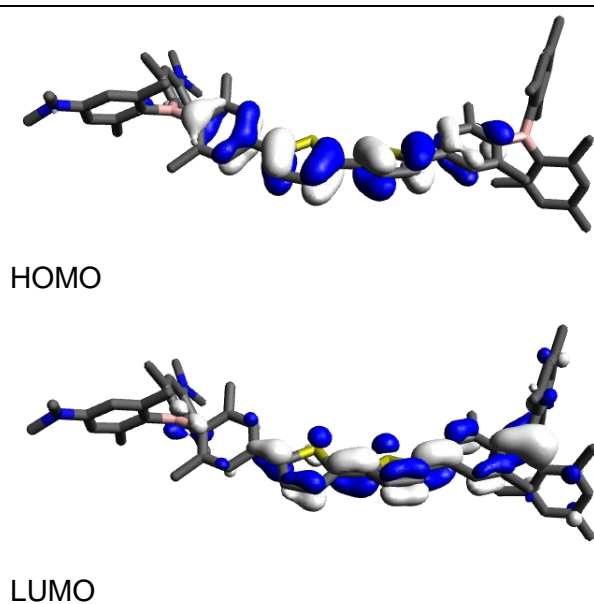
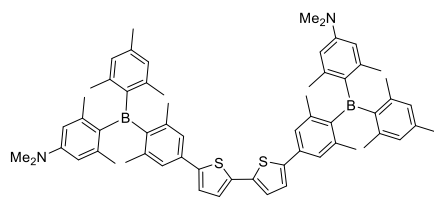


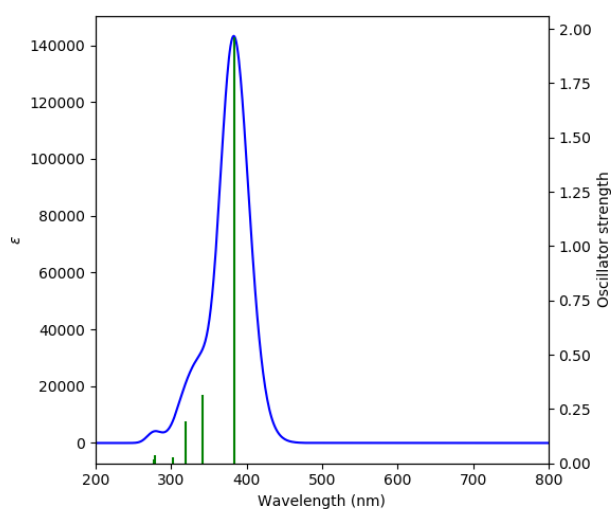
Table 11.10: Lowest energy singlet electronic transitions of **Neut2** (TD-DFT CAM-B3LYP 6-31G(d,p), gas phase).

State	E [eV]	λ [nm]	f	Symmetry	Major Contributions	Δ
1	3.22	385	1.810	A	HOMO->LUMO (73%)	0.646
2	3.50	354	0.317	A	H-1->LUMO (15%), H-1->L+1 (46%), H-1->L+2 (29%)	0.305
3	3.73	332	0.152	A	H-3->LUMO (16%), H-2->L+1 (11%), HOMO->L+1 (33%)	0.531
4	3.95	314	0.113	A	H-4->LUMO (46%), H-4->L+1 (25%)	0.379
5	3.96	313	0.021	A	H-4->LUMO (10%), H-2->L+1 (21%), HOMO->L+2 (13%)	0.492
6	4.26	291	0.015	A	H-3->L+1 (16%), H-2->L+1 (12%), HOMO->L+2 (23%)	0.522
7	4.42	280	0.020	A	H-11->LUMO (37%), H-8->LUMO (27%), H-8->L+1 (10%)	0.386
8	4.47	278	0.019	A	H-7->LUMO (16%), H-7->L+1 (10%), H-6->LUMO (10%), H-6->L+1 (11%), HOMO->L+2 (14%)	0.545
9	4.50	276	0.010	A	H-9->LUMO (19%), H-9->L+1 (29%), H-5->L+1 (13%)	0.344
10	4.51	275	0.029	A	H-11->LUMO (27%), H-8->LUMO (24%) H-8->L+1 (17%)	0.370

**Neut(i)2**

Functional used: TD-DFT CAM-B3LYP 6-31G(d,p), gas phase

Calculated Absorption Spectrum

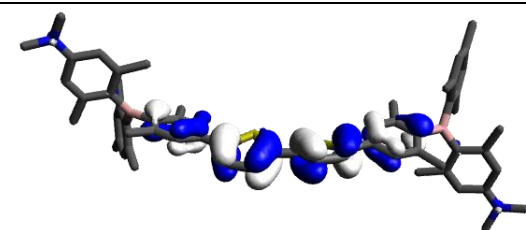


Orbital

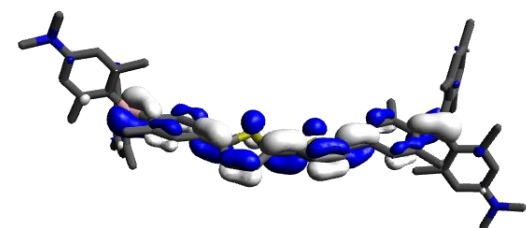
Energy [eV]

Symmetry

L+4	0.16	B
L+3	-0.36	A
L+2	-1.04	B
L+1	-1.43	A
LUMO	-1.72	B
HOMO	-4.83	A
H-1	-5.02	B
H-2	-5.05	A
H-3	-5.76	B
H-4	-5.89	A

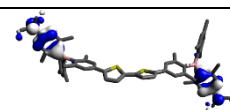
Orbitals Relevant for $S_1 \leftarrow S_0$ Transition

HOMO

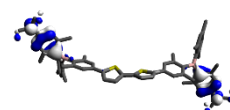


LUMO

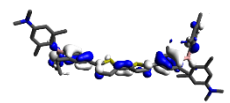
Other Relevant Orbitals



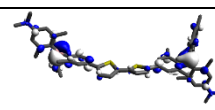
HOMO-1



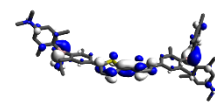
HOMO-2



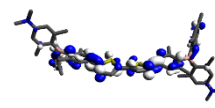
HOMO-3



LUMO+1



LUMO+2



LUMO+3

Table 11.11: Lowest energy singlet electronic transitions of **Neut(i)2** (TD-DFT CAM-B3LYP 6-31G(d,p), gas phase).

State	E [eV]	λ [nm]	f	Symmetry	Major Contributions	Δ
1	3.23	383	1.963	B	HOMO->LUMO (78%)	0.690
2	3.57	347	0	A	H-2->L+1 (29%), H-1->LUMO (30%), H-1->L+2 (13%), HOMO->L+1 (13%)	0.427
3	3.63	342	0.314	B	H-2->LUMO (33%), H-2->L+2 (11%), H-1->L+1 (36%)	0.460
4	3.88	320	0.191	A	H-4->L+1 (11%), H-3->LUMO (25%), HOMO->L+1 (34%)	0.557
5	4.10	303	0.027	B	H-4->LUMO (15%), H-3->L+1 (28%), HOMO->L+2 (29%)	0.5721
6	4.36	285	2E-4	A	H-5->LUMO (20%), H-4->L+1 (30%), HOMO->L+1 (15%)	0.434
7	4.44	279	0.036	B	H-5->L+1 (28%), H-4->LUMO (15%), HOMO->L+2 (20%)	0.544
8	4.47	277	0.017	A	H-11->LUMO (19%), H-10->L+1 (10%), H-9->LUMO (14%), H-8->L+1 (11%)	0.461
9	4.48	277	0.002	B	H-10->LUMO (17%), H-8->LUMO (12%), H-7->L+1 (11%), H-6->LUMO (10%)	0.468
10	4.56	272	1E-4	A	H-11->LUMO (10%), H-7->LUMO (15%), H-7->L+2 (13%), H-6->L+1 (25%)	0.434

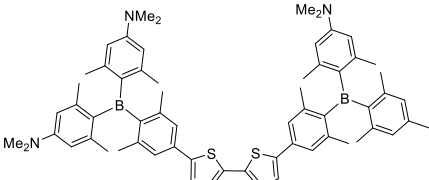
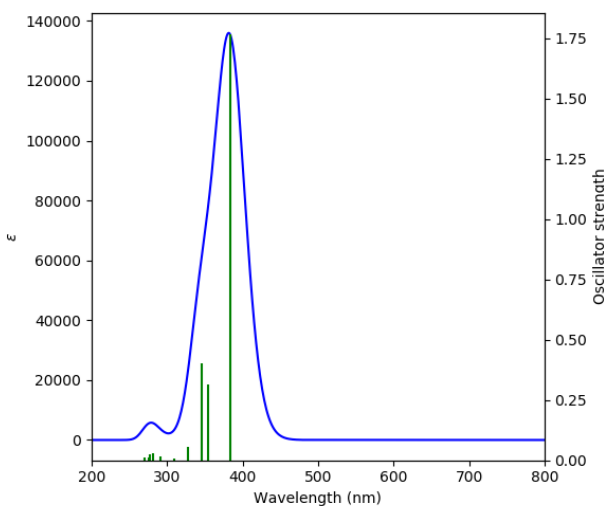
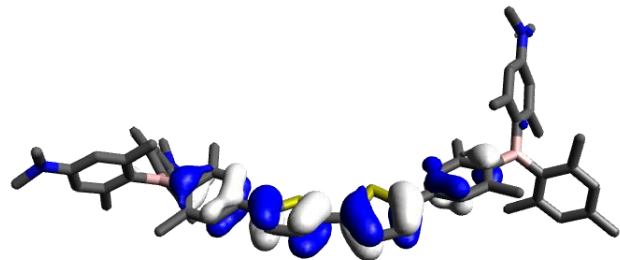
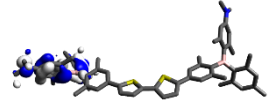
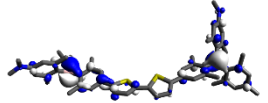
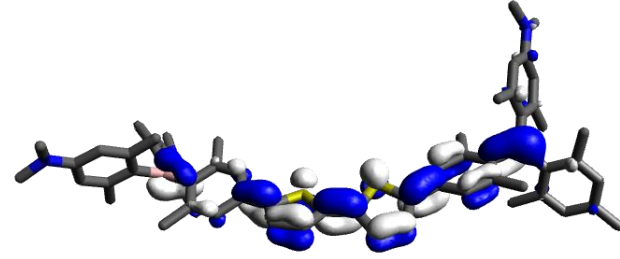
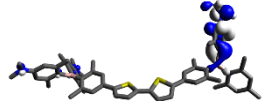
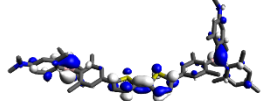
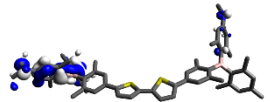
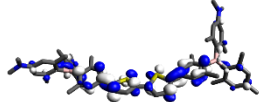
Neut3		Functional used: TD-DFT CAM-B3LYP 6-31G(d,p), gas phase	
			
Calculated Absorption Spectrum		Orbital	Energy [eV]
		L+4	0.16
		L+3	-0.29
		L+2	-0.95
		L+1	-1.34
		LUMO	-1.67
		HOMO	-4.77
		H-1	-4.81
		H-2	-5.01
		H-3	-5.04
		H-4	-5.73
Orbitals Relevant for $S_1 \leftarrow S_0$ Transition		Other Relevant Orbitals	
 <p>HOMO</p>		 <p>HOMO-1</p>	 <p>LUMO+1</p>
 <p>LUMO</p>		 <p>HOMO-2</p>	 <p>LUMO+2</p>
		 <p>HOMO-3</p>	 <p>LUMO+3</p>

Table 11.12: Lowest energy singlet electronic transitions of **Neut3** (TD-DFT CAM-B3LYP 6-31G(d,p), gas phase).

State	E [eV]	λ [nm]	f	Symmetry	Major Contributions	Δ
1	3.23	384	1.768	A	HOMO->LUMO (78%)	0.691
2	3.51	354	0.315	A	H-1->LUMO (24%), H-1->L+1 (44%), H-1->L+2 (22%)	0.297
3	3.59	345	0.404	A	H-2->LUMO (37%), H-2->L+1 (21%), H-2->L+2 (10%), HOMO->L+1 (11%)	0.410
4	3.78	328	0.054	A	H-4->LUMO (11%), H-3->LUMO (17%), H-2->L+1 (11%), HOMO->L+1 (21%)	0.506
5	4.00	310	0.007	A	H-4->LUMO (13%), H-3->L+1 (19%), HOMO->L+1 (14%), HOMO->L+2 (12%)	0.548
6	4.26	291	0.016	A	H-5->LUMO (13%), H-4->L+1 (15%), H-3->L+1 (11%), HOMO->L+1 (11%), HOMO->L+2 (17%)	0.5224
7	4.41	281	0.029	A	H-5->LUMO (16%), H-5->L+1 (22%), HOMO->L+2 (19%)	0.511
8	4.47	278	0.023	A	H-11->LUMO (21%), H-9->LUMO (16%), H-7->LUMO (11%)	0.371
9	4.50	276	0.011	A	H-10->LUMO (26%), H-10->L+1 (23%), H-6->L+1 (12%)	0.351
10	4.58	271	0.014	A	H-10->L+1 (10%), H-6->L+1 (19%), H-6->L+2 (15%)	0.332

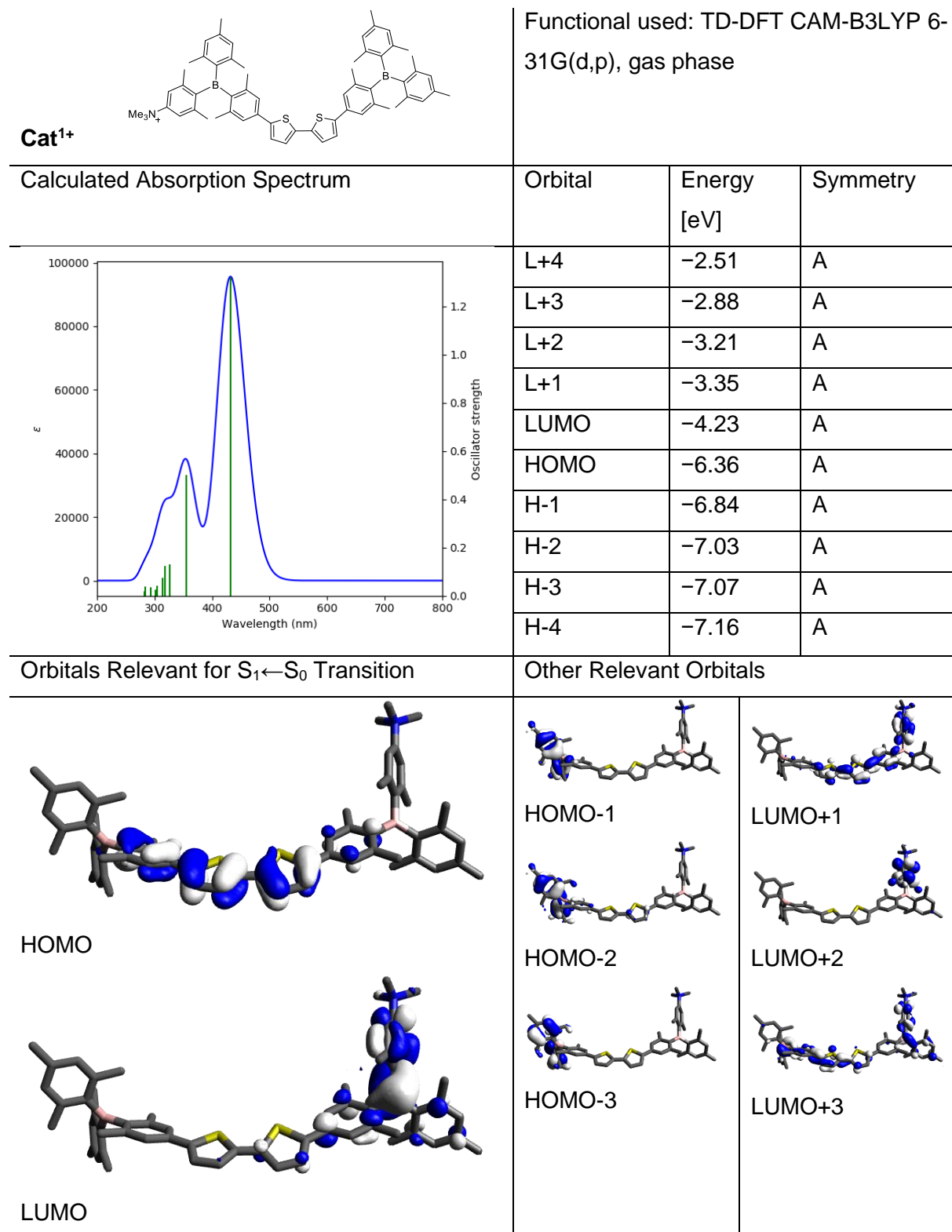


Table 11.13: Lowest energy singlet electronic transitions of **Cat**¹⁺ (TD-DFT CAM-B3LYP 6-31G(d,p), gas phase).

State	E [eV]	λ [nm]	f	Symmetry	Major Contributions	Δ
1	2.87	432	1.32	A	HOMO->LUMO (60%), HOMO->L+1 (18%)	0.353
2	3.48	356	0.500	A	HOMO->L+1 (41%), HOMO->L+3 (22%)	0.519
3	3.79	327	0.129	A	H-8->LUMO (12%), H-7->LUMO (57%), HOMO->LUMO (10%)	0.410
4	3.89	318	0.125	A	H-1->L+3 (31%), H-1->L+4 (46%)	0.344
5	3.95	314	0.074	A	H-2->L+3 (12%), H-2->L+4 (14%), HOMO->L+4 (26%)	0.502
6	4.07	304	0.040	A	H-10->LUMO (19%), H-9->LUMO (16%), H-5->LUMO (21%), HOMO->LUMO (14%)	0.370
7	4.11	302	0.024	A	H-9->LUMO (58%)	0.402
8	4.22	294	0.036	A	H-12->LUMO (15%), H-11->LUMO (50%)	0.399
9	4.38	283	0.038	A	H-2->L+3 (14%), H-2->L+4 (14%), HOMO->L+3 (29%)	0.542
10	4.39	282	0.019	A	H-6->L+3 (14%), H-3->L+3 (18%), H-3->L+4 (24%)	0.259

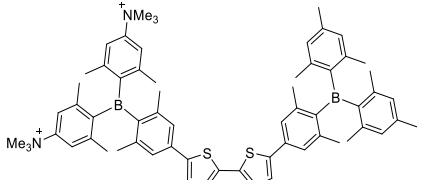
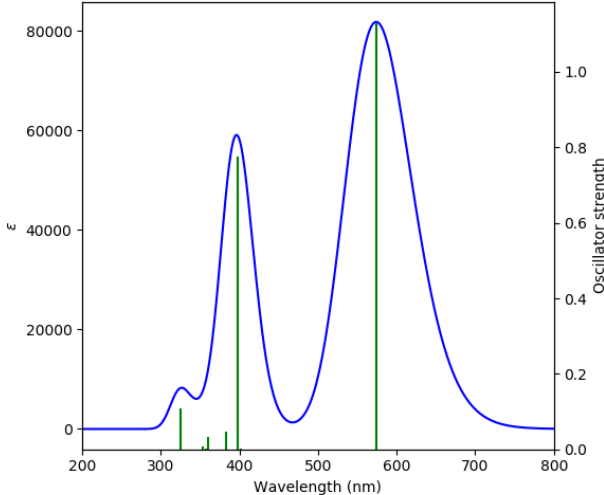
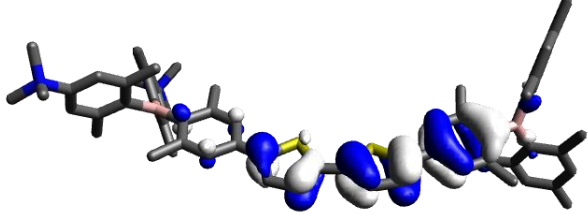
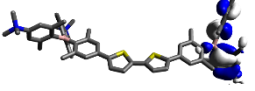
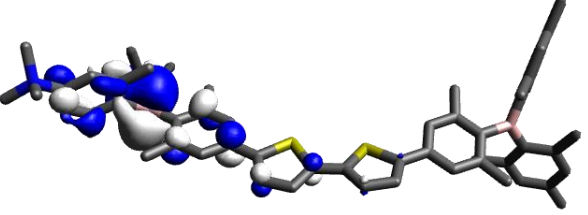
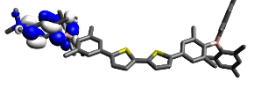
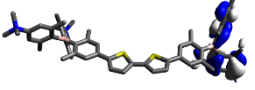
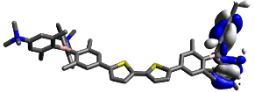
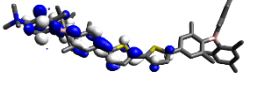
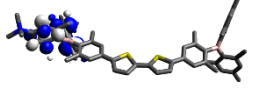
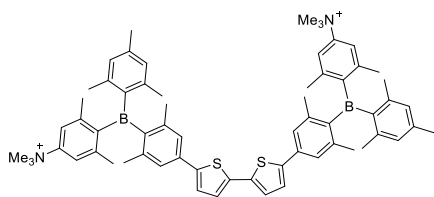
 Cat²⁺		Functional used: TD-DFT CAM-B3LYP 6-31G(d,p), gas phase		
Calculated Absorption Spectrum		Orbital	Energy [eV]	Symmetry
		L+4	-4.86	A
		L+3	-5.00	A
		L+2	-5.12	A
		L+1	-5.40	A
		LUMO	-6.33	A
		HOMO	-7.69	A
		H-1	-7.74	A
		H-2	-7.95	A
		H-3	-7.99	A
H-4	-8.05	A		
Orbitals Relevant for S ₁ ←S ₀ Transition		Other Relevant Orbitals		
 HOMO		 HOMO-1		
 LUMO		 LUMO+1		
		 HOMO-2		
		 HOMO-3		
		 LUMO+2		
		 LUMO+3		

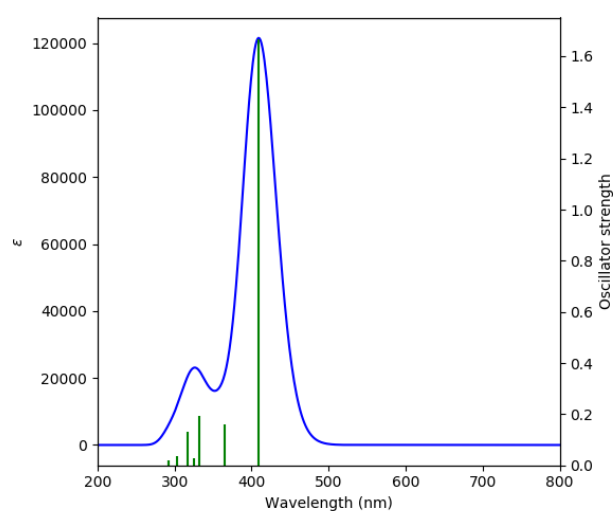
Table 11.14: Lowest energy singlet electronic transitions of **Cat²⁺** (TD-DFT CAM-B3LYP 6-31G(d,p), gas phase).

State	E [eV]	λ [nm]	f	Symmetry	Major Contributions	Λ
1	2.16	574	1.130	A	HOMO->LUMO (79%)	0.311
2	3.09	402	8E-4	A	H-1->LUMO (98%)	0.019
3	3.12	397	0.775	A	HOMO->LUMO (12%), HOMO->L+2 (51%), HOMO->L+4 (12%), HOMO->L+5 (12%)	0.436
4	3.24	383	0.046	A	H-6->LUMO (24%), H-3->LUMO (22%), H-2->LUMO (29%)	0.194
5	3.36	369	0	A	H-3->LUMO (53%), H-2->LUMO (45%)	0.076
6	3.45	360	0.032	A	H-6->LUMO (34%), H-3->LUMO (19%), H-2->LUMO (23%)	0.205
7	3.47	358	0.002	A	H-4->LUMO (92%)	0.0230
8	3.51	354	0.007	A	HOMO->L+1 (89%)	0.086
9	3.70	335	6E-4	A	H-5->LUMO (90%)	0.066
10	3.81	325	0.110	A	H-1->L+2 (10%), H-1->L+5 (19%), H-1->L+9 (48%)	0.304

Cat(i)²⁺

Functional used: TD-DFT CAM-B3LYP
6-31G(d,p), gas phase

Calculated Absorption Spectrum



Orbital

Energy
[eV]

Symmetry

L+4	-3.99	B
L+3	-4.06	A
L+2	-4.40	B
L+1	-5.05	A
LUMO	-5.15	B
HOMO	-7.77	A
H-1	-8.80	B
H-2	-8.96	A
H-3	-9.03	B
H-4	-9.07	A

Orbitals Relevant for $S_1 \leftarrow S_0$ Transition

Other Relevant Orbitals

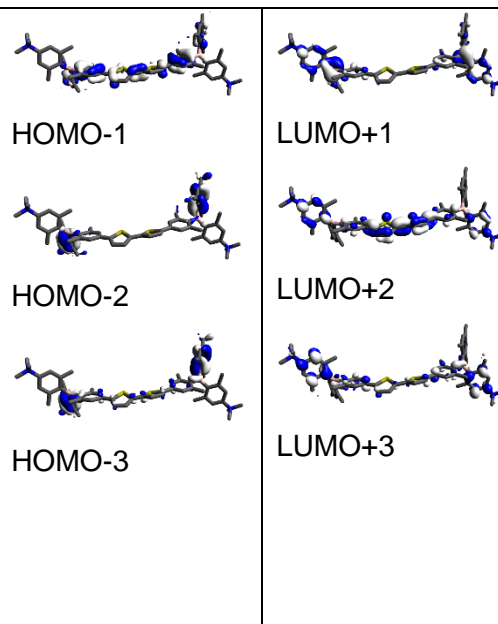
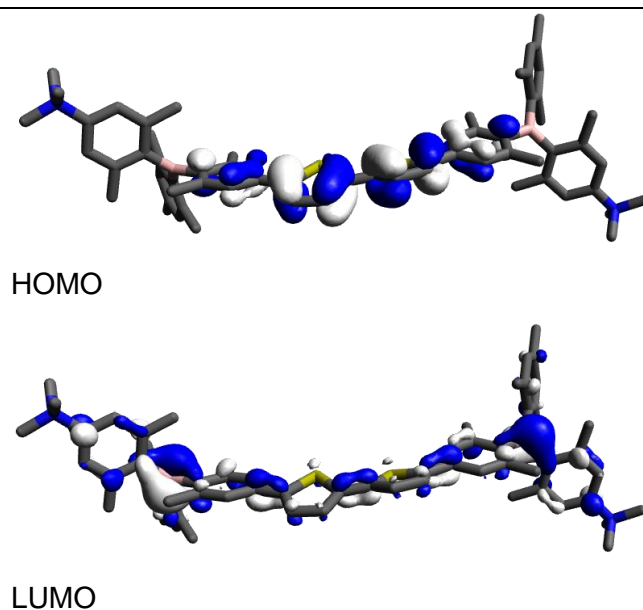
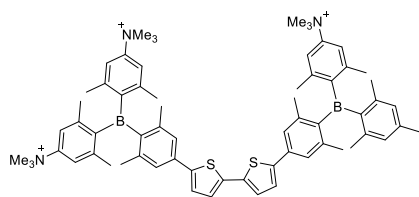


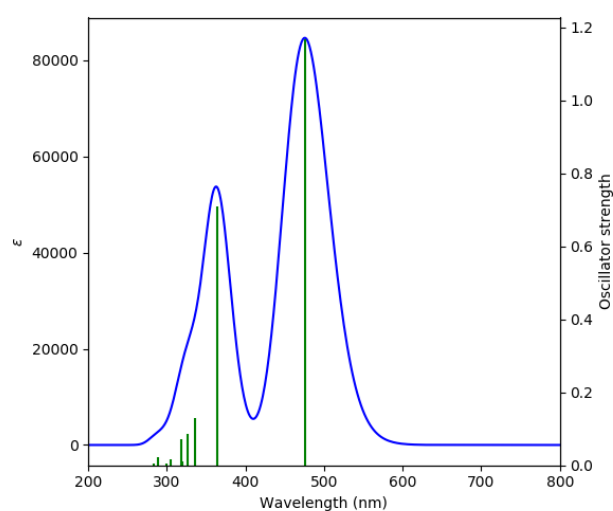
Table 11.15: Lowest energy singlet electronic transitions of **Cat(i)**²⁺ (TD-DFT CAM-B3LYP 6-31G(d,p), gas phase).

State	E [eV]	λ [nm]	f	Symmetry	Major Contributions	Λ
1	3.03	410	1.667	B	H-1->L+1 (10%), HOMO->LUMO (66%), HOMO->L+2 (16%)	0.519
2	3.40	364	0.160	A	H-1->LUMO (25%), HOMO->L+1 (56%)	0.428
3	3.73	332	0.195	B	H-3->L+1 (16%), H-2->LUMO (32%), H-1->L+1 (18%), HOMO->L+2 (19%)	0.510
4	3.82	325	0.026	A	H-3->LUMO (35%), H-2->L+1 (36%), HOMO->L+1 (11%)	0.485
5	3.92	317	0.129	B	H-3->L+1 (19%), H-2->LUMO (10%), HOMO->L+2 (36%)	0.568
6	4.09	303	0.038	A	H-5->LUMO (43%), H-4->L+1 (41%)	0.333
7	4.10	303	0.008	B	H-5->L+1 (40%), H-4->LUMO (42%)	0.333
8	4.23	293	0.020	A	H-7->LUMO (45%), H-6->L+1 (31%)	0.405
9	4.24	293	0.018	B	H-7->L+1 (34%), H-6->LUMO (43%)	0.416
10	4.40	282	2E-4	A	H-10->L+1 (17%), H-1->LUMO (27%), HOMO->L+1 (18%)	0.5256

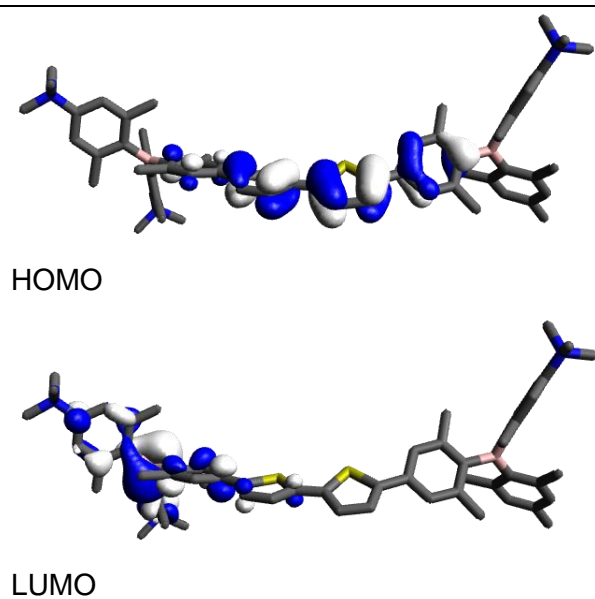
Cat³⁺

Functional used: TD-DFT CAM-B3LYP
6-31G(d,p), gas phase

Calculated Absorption Spectrum



Orbital	Energy [eV]	Symmetry
L+4	-5.92	A
L+3	-5.97	A
L+2	-6.16	A
L+1	-6.30	A
LUMO	-7.34	A
HOMO	-9.20	A
H-1	-9.86	A
H-2	-9.97	A
H-3	-10.28	A
H-4	-10.35	A

Orbitals Relevant for $S_1 \leftarrow S_0$ Transition

Other Relevant Orbitals

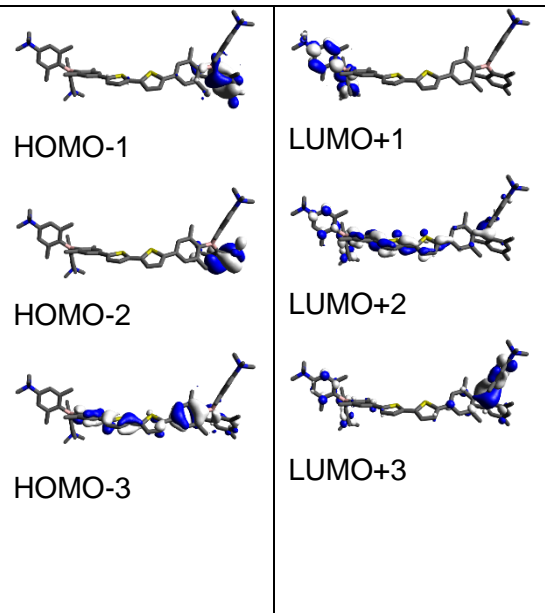
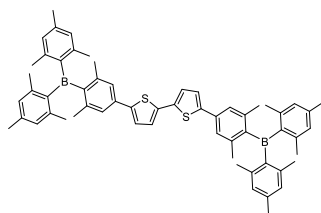


Table 11.16: Lowest energy singlet electronic transitions of **Cat**³⁺ (TD-DFT CAM-B3LYP 6-31G(d,p), gas phase).

State	E [eV]	λ [nm]	f	Symmetry	Major Contributions	Δ
1	2.61	475	1.169	A	HOMO->LUMO (74%)	0.333
2	3.40	364	0.711	A	HOMO->L+2 (53%)	0.526
3	3.70	335	0.129	A	H-1->L+2 (17%), H-1->L+3 (33%), HOMO->L+2 (10%), HOMO->L+3 (12%)	0.395
4	3.79	327	0.087	A	H-6->LUMO (12%), H-3->LUMO (41%), HOMO->LUMO (19%)	0.327
5	3.88	319	0.010	A	H-9->LUMO (68%), H-7->LUMO (18%)	0.358
6	3.90	318	0.071	A	H-3->L+2 (10%), H-3->L+3 (11%), H-1->L+3 (15%), HOMO->L+3 (27%)	0.421
7	4.07	305	0.015	A	H-2->L+2 (21%), H-2->L+3 (53%)	0.233
8	4.14	299	0.005	A	HOMO->L+1 (86%)	0.093
9	4.30	289	0.022	A	H-4->L+2 (32%), H-4->L+3 (41%)	0.259
10	4.38	283	0.004	A	H-1->LUMO (87%)	0.110

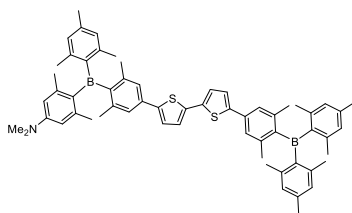
11.7.2.2 Sulfur Atoms of Bithiophene on Opposite Sides

**Neut0**
 Functional used: TD-DFT CAM-B3LYP
 6-31G(d,p), gas phase

Calculated Absorption Spectrum		Orbital	Energy [eV]	Symmetry
	L+4	-0.06	A	
	L+3	-0.49	B	
	L+2	-1.25	A	
	L+1	-1.69	B	
	LUMO	-1.96	A	
	HOMO	-4.97	B	
	H-1	-5.93	A	
	H-2	-5.97	A	
	H-3	-5.97	B	
	H-4	-6.16	B	
Orbitals Relevant for $S_1 \leftarrow S_0$ Transition		Other Relevant Orbitals		
 HOMO		 HOMO-1	 LUMO+1	
 LUMO		 HOMO-2	 LUMO+2	
		 HOMO-3	 LUMO+3	

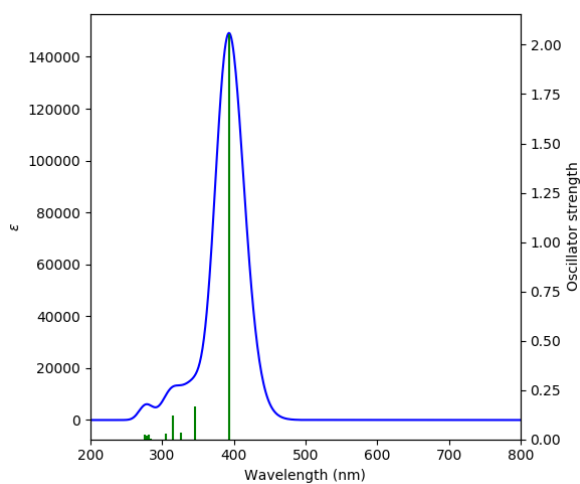
 Table 11.17: Lowest energy singlet electronic transitions of **Neut0** (TD-DFT CAM-B3LYP 6-31G(d,p), gas phase).

State	E [eV]	λ [nm]	f	Symmetry	Major Contributions	Λ
1	3.18	390	2.002	B	HOMO->LUMO (81%)	0.690
2	3.74	331	0.002	A	H-1->LUMO (26%), HOMO->L+1 (49%)	0.553
3	3.94	315	0.077	A	H-3->L+1 (44%), H-2->LUMO (34%), H-2->L+2 (15%)	0.485
4	3.94	315	0.165	B	H-3->LUMO (34%), H-3->L+2 (15%), H-2->L+1 (44%)	0.484
5	4.03	308	0.014	B	H-4->LUMO (13%), H-1->L+1 (27%), HOMO->L+2 (37%)	0.608
6	4.40	282	0.000	A	H-7->LUMO (19%), H-4->L+1 (32%), HOMO->L+1 (21%)	0.589
7	4.41	281	0.011	A	H-11->L+1 (17%), H-10->LUMO (28%), H-6->L+1 (16%), H-5->LUMO (16%)	0.452
8	4.41	281	0.036	B	H-11->LUMO (28%), H-10->L+1 (16%), H-6->LUMO (17%), H-5->L+1 (17%)	0.447
9	4.50	276	0.005	B	H-7->L+1 (21%), H-4->LUMO (16%), HOMO->L+2 (17%)	0.563
10	4.50	276	0.040	A	H-11->L+1 (14%), H-10->LUMO (18%), H-6->L+1 (24%), H-5->LUMO (15%), H-5->L+2 (12%)	0.444

**Neut1**

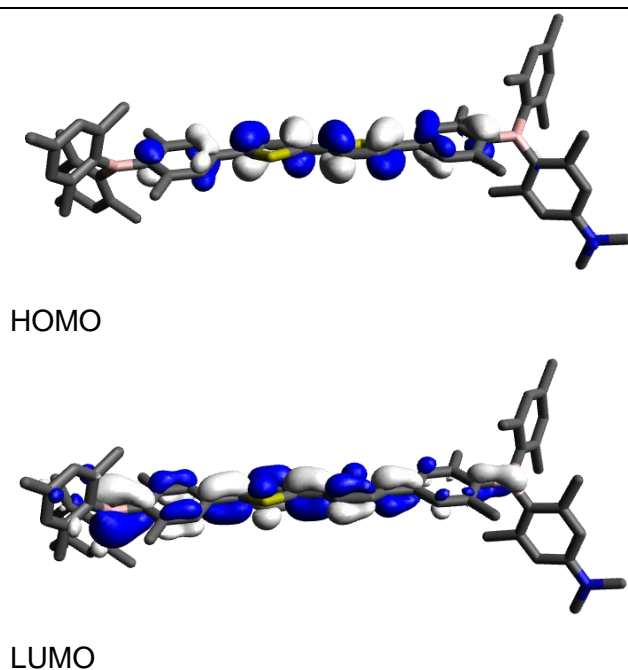
Functional used: TD-DFT CAM-B3LYP 6-31G(d,p), gas phase

Calculated Absorption Spectrum



Orbital	Energy [eV]	Symmetry
---------	-------------	----------

L+4	-0.03	A
L+3	-0.42	A
L+2	-1.16	A
L+1	-1.55	A
LUMO	-1.88	A
HOMO	-4.87	A
H-1	-5.07	A
H-2	-5.84	A
H-3	-5.94	A
H-4	-5.96	A

Orbitals Relevant for $S_1 \leftarrow S_0$ Transition

Other Relevant Orbitals

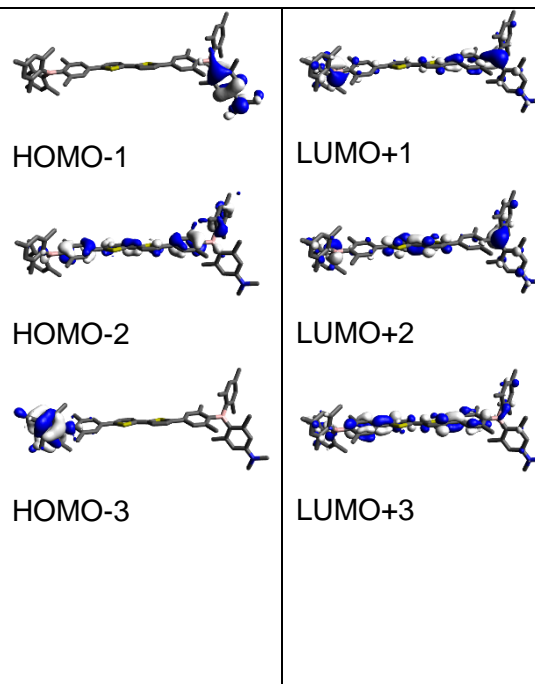
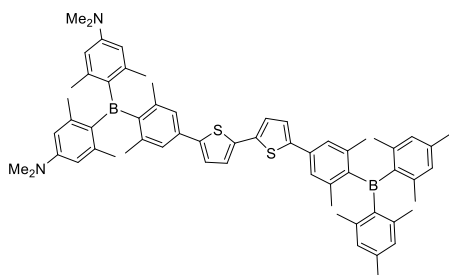


Table 11.18: Lowest energy singlet electronic transitions of **Neut1** (TD-DFT CAM-B3LYP 6-31G(d,p), gas phase).

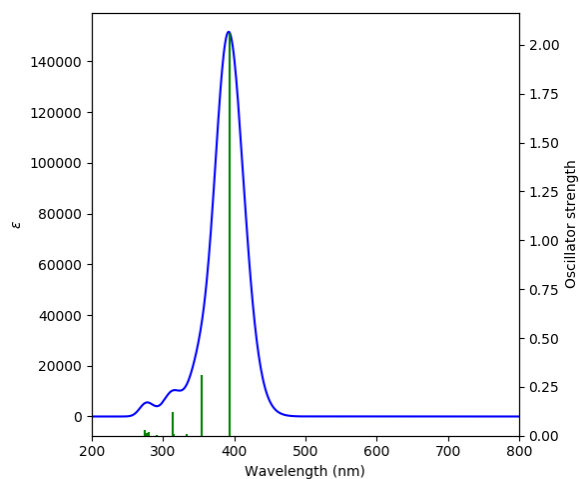
State	E [eV]	λ [nm]	f	Symmetry	Major Contributions	Δ
1	3.15	394	2.055	A	HOMO->LUMO (78%)	0.680
2	3.58	346	0.169	A	H-1->LUMO (20%), H-1->L+1 (34%), H-1->L+2 (17%), HOMO->L+1 (10%)	0.376
3	3.80	326	0.032	A	H-2->LUMO (22%), HOMO->L+1 (38%)	0.540
4	3.94	314	0.120	A	H-3->LUMO (46%), H-3->L+1 (35%), H-3->L+2 (11%)	0.357
5	4.05	306	0.027	A	H-2->L+1 (29%), HOMO->L+2 (32%)	0.592
6	4.36	284	0.002	A	H-6->LUMO (11%), H-4->L+1 (27%), HOMO->L+1 (16%)	0.530
7	4.41	281	0.023	A	H-11->LUMO (37%), H-11->L+1 (10%),H-7- >LUMO (21%), H-7->L+1 (12%)	0.365
8	4.46	278	0.019	A	H-6->L+1 (21%), HOMO->L+2 (14%)	0.522
9	4.48	277	0.014	A	H-10->LUMO (11%), H-10->L+1 (12%), H-8->L+1 (12%), H-5->L+1 (10%)	0.401
10	4.50	276	0.026	A	H-11->LUMO (22%), H-7->LUMO (22%), H-7->L+1 (21%)	0.350



Functional used: TD-DFT CAM-B3LYP 6-31G(d,p), gas phase

Neut2

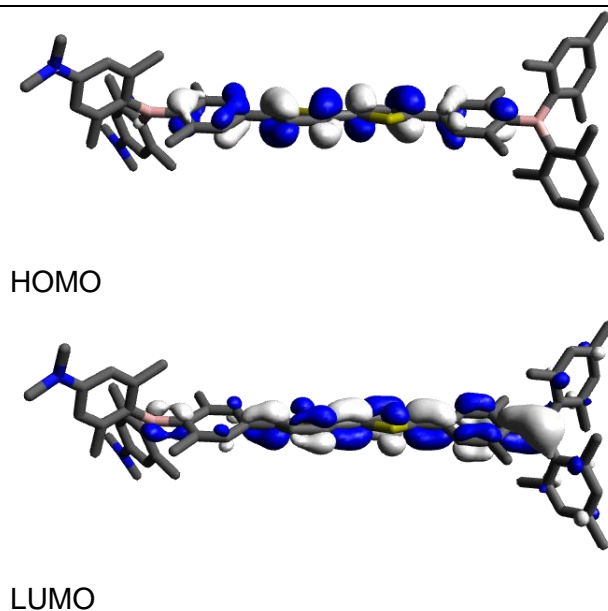
Calculated Absorption Spectrum



Orbital	Energy [eV]	Symmetry
---------	-------------	----------

L+4	-0.01	A
L+3	-0.35	A
L+2	-1.06	A
L+1	-1.46	A
LUMO	-1.83	A
HOMO	-4.82	A
H-1	-4.84	A
H-2	-5.05	A
H-3	-5.82	A
H-4	-5.93	A

Orbitals Relevant for $S_1 \leftarrow S_0$ Transition



Other Relevant Orbitals

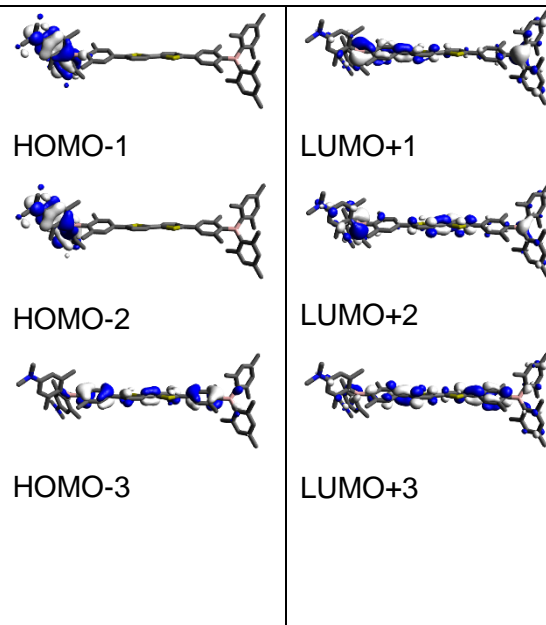
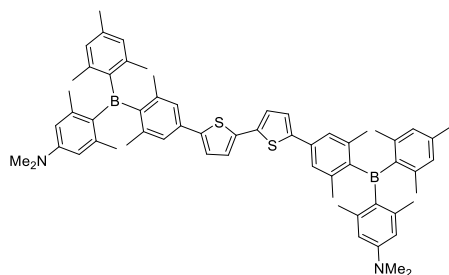


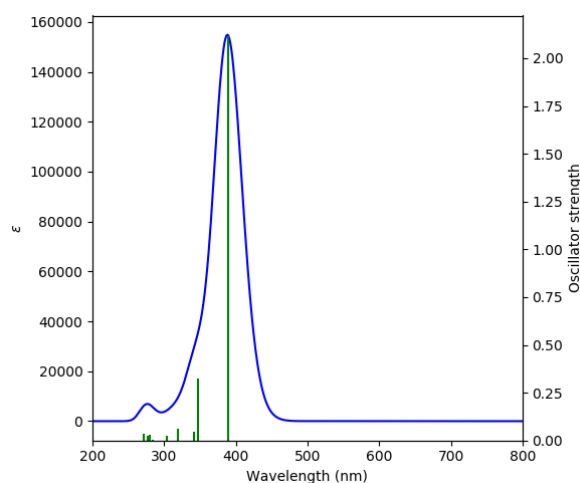
Table 11.19: Lowest energy singlet electronic transitions of **Neut2** (TD-DFT CAM-B3LYP 6-31G(d,p), gas phase).

State	E [eV]	λ [nm]	f	Symmetry	Major Contributions	Δ
1	3.16	393	2.062	A	HOMO->LUMO (76%)	0.664
2	3.50	354	0.309	A	H-1->LUMO (16%), H-1->L+1 (43%), H-1->L+2 (31%)	0.307
3	3.72	333	0.001	A	H-3->LUMO (16%), H-2->L+1 (10%), H-2->L+2 (10%), HOMO->L+1 (34%)	0.527
4	3.93	315	0.001	A	H-2->L+1 (23%), HOMO->L+1 (12%), HOMO->L+2 (15%)	0.510
5	3.95	314	0.123	A	H-4->LUMO (52%), H-4->L+1 (34%)	0.367
6	4.25	292	0.004	A	H-3->L+1 (16%), H-2->L+1 (11%), HOMO->L+2 (24%)	0.515
7	4.42	281	0.021	A	H-11->LUMO (37%), H-8->LUMO (25%), H-8->L+1 (11%)	0.382
8	4.45	279	0.015	A	H-7->LUMO (15%), H-7->L+1 (11%), H-6->L+1 (11%), HOMO->L+2 (13%)	0.544
9	4.49	276	0.014	A	H-9->LUMO (21%), H-9->L+1 (29%), H-5->L+1 (12%)	0.336
10	4.51	275	0.027	A	H-11->LUMO (25%), H-8->LUMO (23%), H-8->L+1 (20%)	0.363

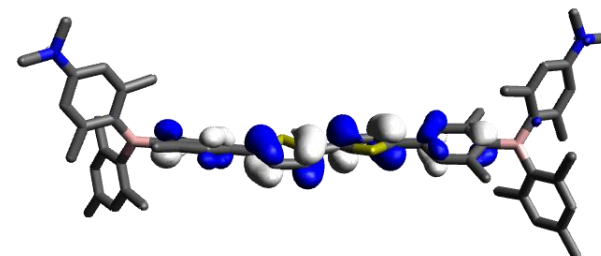
**Neut(i)2**

Functional used: TD-DFT CAM-B3LYP 6-31G(d,p), gas phase

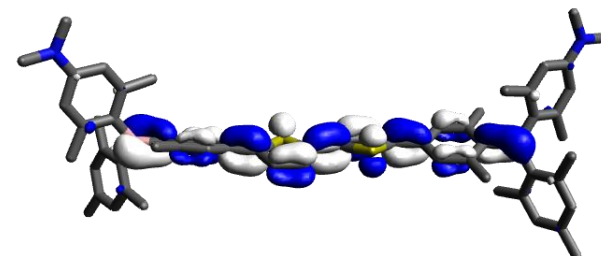
Calculated Absorption Spectrum



Orbital	Energy [eV]	Symmetry
L+4	0.16	A
L+3	-0.33	B
L+2	-1.06	A
L+1	-1.44	B
LUMO	-1.74	A
HOMO	-4.81	B
H-1	-5.04	A
H-2	-5.06	B
H-3	-5.78	A
H-4	-5.90	B

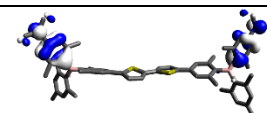
Orbitals Relevant for $S_1 \leftarrow S_0$ Transition

HOMO

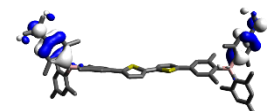


LUMO

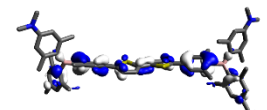
Other Relevant Orbitals



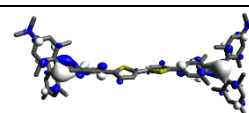
HOMO-1



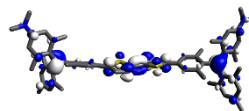
HOMO-2



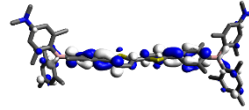
HOMO-3



LUMO+1



LUMO+2

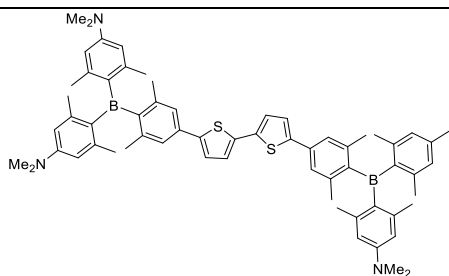


LUMO+3

Table 11.20: Lowest energy singlet electronic transitions of **Neut(i)2** (TD-DFT CAM-B3LYP 6-31G(d,p), gas phase).

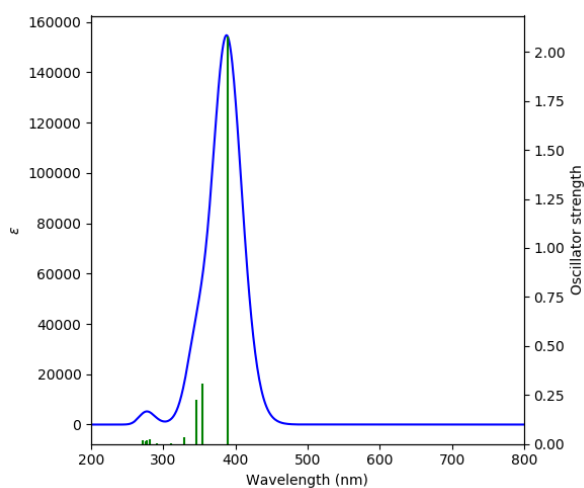
State	E [eV]	λ [nm]	f	Symmetry	Major Contributions	Δ
1	3.19	389	2.117	B	HOMO->LUMO (80%)	0.700
2	3.57	347	0.322	A	H-2->L+1 (30%), H-1->LUMO (30%), H-1->L+2 (14%), HOMO->L+1 (13%)	0.425
3	3.63	342	0.044	B	H-2->LUMO (32%), H-2->L+2 (12%), H-1->L+1 (37%)	0.459
4	3.88	320	0.064	A	H-4->L+1 (11%), H-3->LUMO (24%), HOMO->L+1 (34%)	0.553
5	4.08	304	0.024	B	H-4->LUMO (15%), H-3->L+1 (29%), HOMO->L+2 (30%)	0.570
6	4.36	284	0.006	A	H-5->LUMO (21%), H-5->L+2 (10%), H-4->L+1 (31%), HOMO->L+1 (16%)	0.530
7	4.43	280	0.030	B	H-5->L+1 (29%), H-4->LUMO (16%), HOMO->L+2 (21%)	0.545
8	4.47	277	0.003	A	H-11->L+1 (10%), H-10->LUMO (20%), H-9->LUMO (15%), H-8->L+1 (11%)	0.456
9	4.48	277	0.026	B	H-11->LUMO (19%), H-9->L+1 (10%), H-8->LUMO (12%), H-7->L+1 (10%)	0.452
10	4.56	272	0.037	A	H-11->L+1 (10%), H-10->LUMO (12%), H-7->LUMO (13%), H-7->L+2 (13%),	0.441

H-6→L+1 (24%)

**Neut3**

Functional used: TD-DFT CAM-B3LYP 6-31G(d,p), gas phase

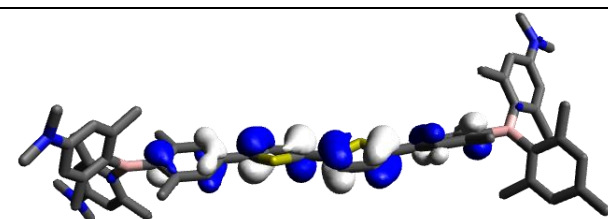
Calculated Absorption Spectrum



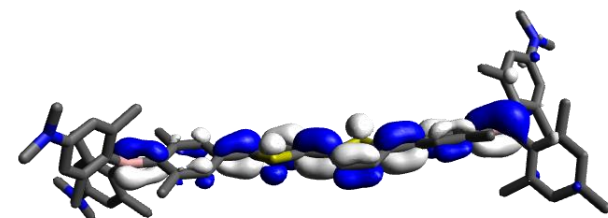
Orbital	Energy [eV]	Symmetry
L+4	0.18	A
L+3	-0.26	A
L+2	-0.97	A
L+1	-1.35	A
LUMO	-1.69	A
HOMO	-4.76	A
H-1	-4.82	A
H-2	-5.02	A
H-3	-5.04	A
H-4	-5.74	A

Orbitals Relevant for S₁←S₀ Transition

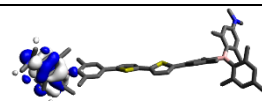
Other Relevant Orbitals



HOMO



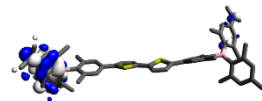
LUMO



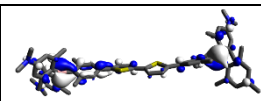
HOMO-1



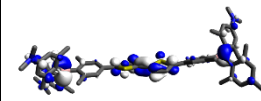
HOMO-2



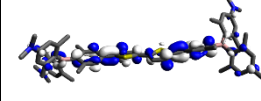
HOMO-3



LUMO+1



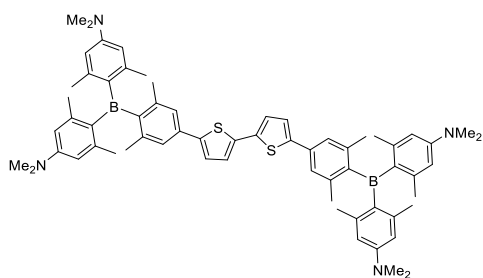
LUMO+2



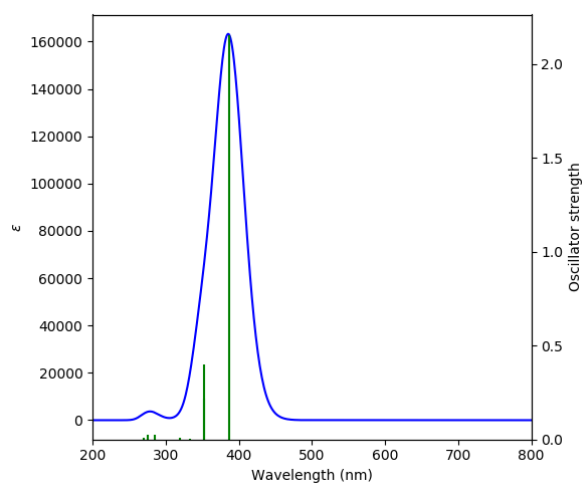
LUMO+3

Table 11.21: Lowest energy singlet electronic transitions of **Neut3** (TD-DFT CAM-B3LYP 6-31G(d,p), gas phase).

State	E [eV]	λ [nm]	f	Symmetry	Major Contributions	Δ
1	3.19	389	2.080	A	HOMO->LUMO (80%)	0.703
2	3.50	354	0.309	A	H-1->LUMO (23%), H-1->L+1 (43%), H-1->L+2 (24%)	0.295
3	3.58	346	0.226	A	H-2->LUMO (36%), H-2->L+1 (23%), H-2->L+2 (10%), HOMO->L+1 (10%)	0.403
4	3.77	328	0.034	A	H-4->LUMO (11%), H-3->LUMO (17%), H-2->L+1 (10%), HOMO->L+1 (21%)	0.501
5	3.99	311	0.004	A	H-4->LUMO (12%), H-3->L+1 (18%), HOMO->L+1 (15%), HOMO->L+2 (12%)	0.545
6	4.25	291	0.003	A	H-5->LUMO (11%), H-4->L+1 (16%), H-3->L+1 (11%), HOMO->L+1 (11%), HOMO->L+2 (18%)	0.515
7	4.41	281	0.026	A	H-5->LUMO (17%), H-5->L+1 (25%), HOMO->L+2 (19%)	0.507
8	4.46	278	0.018	A	H-11->LUMO (23%), H-9->LUMO (15%), H-7->LUMO (11%)	0.375
9	4.50	276	0.014	A	H-10->LUMO (27%), H-10->L+1 (22%), H-6->L+1 (12%)	0.364
10	4.58	271	0.019	A	H-6->L+1 (19%), H-6->L+2 (16%)	0.360

Neut4

Functional used: TD-DFT CAM-B3LYP 6-31G(d,p), gas phase

Calculated Absorption Spektrum

Orbital	Energy [eV]	Symmetry
L+4	0.34	A
L+3	-0.18	B
L+2	-0.89	A
L+1	-1.25	B
LUMO	-1.60	A
HOMO	-4.70	B
H-1	-4.80	A
H-2	-4.80	B
H-3	-4.99	A
H-4	-5.02	B

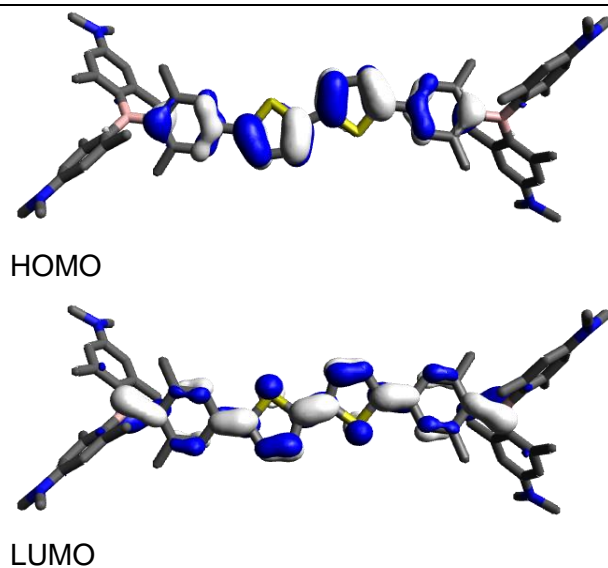
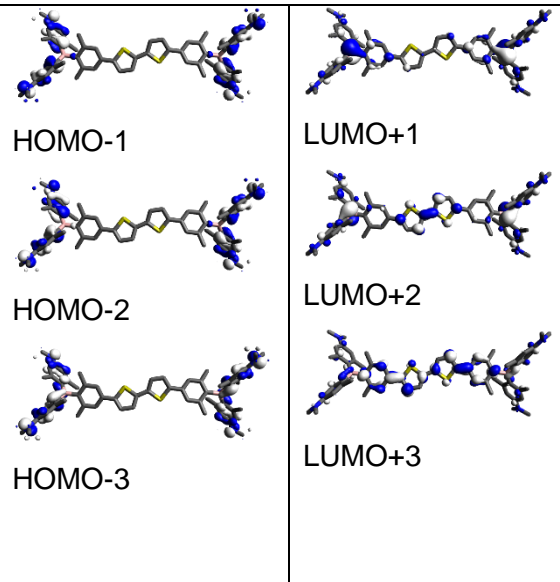
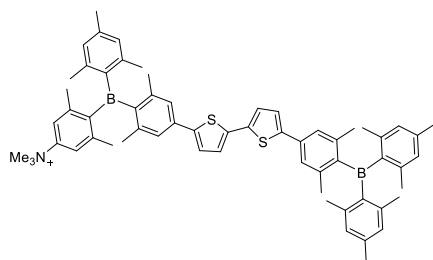
Orbitals Relevant for $S_1 \leftarrow S_0$ Transition**Other Relevant Orbitals**

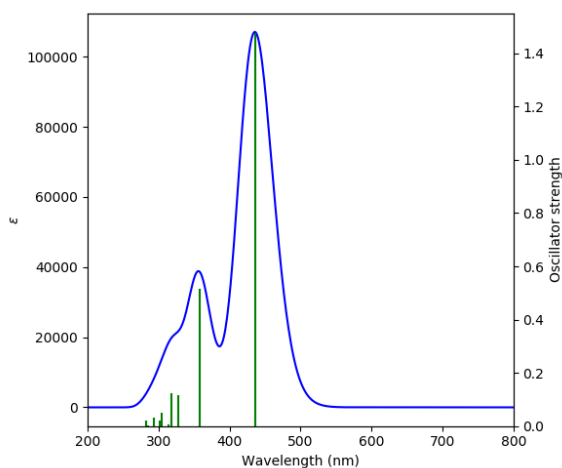
Table 11.22: Lowest energy singlet electronic transitions of **Neut4** (TD-DFT CAM-B3LYP 6-31G(d,p), gas phase).

State	E [eV]	λ [nm]	f	Symmetry	Major Contributions	Δ
1	3.2	387	2.156	A	HOMO->LUMO (82%)	0.717
2	3.51	353	0.219	B	H-2->L+1 (42%), H-1->LUMO (31%), H-1->L+2 (18%)	0.416
3	3.51	353	0.400	A	H-2->LUMO (31%), H-2->L+2 (18%), H-1->L+1 (42%)	0.416
4	3.72	334	0.003	B	H-4->L+1 (15%), H-3->LUMO (21%), H-3->L+2 (10%), HOMO->L+1 (31%)	0.509
5	3.88	319	0.009	A	H-4->LUMO (28%), H-3->L+1 (34%), HOMO->L+2 (15%)	0.528
6	4.17	298	0.000	B	H-5->LUMO (12%), H-4->L+1 (27%), H-3->LUMO (15%), HOMO->L+1 (29%)	0.533
7	4.34	286	0.024	A	H-5->L+1 (23%), H-4->LUMO (11%), HOMO->L+2 (39%)	0.581
8	4.50	276	0.001	B	H-11->L+1 (18%), H-10->LUMO (33%), H-7->L+1 (10%), H-6->LUMO (11%)	0.463
9	4.50	276	0.026	A	H-11->LUMO (33%), H-10->L+1 (17%), H-7->LUMO (11%), H-6->L+1 (11%)	0.462
10	4.58	271	0.008	B	H-10->LUMO (10%), H-7->L+1 (20%), H-6->LUMO (10%), H-6->L+2 (13%)	0.456



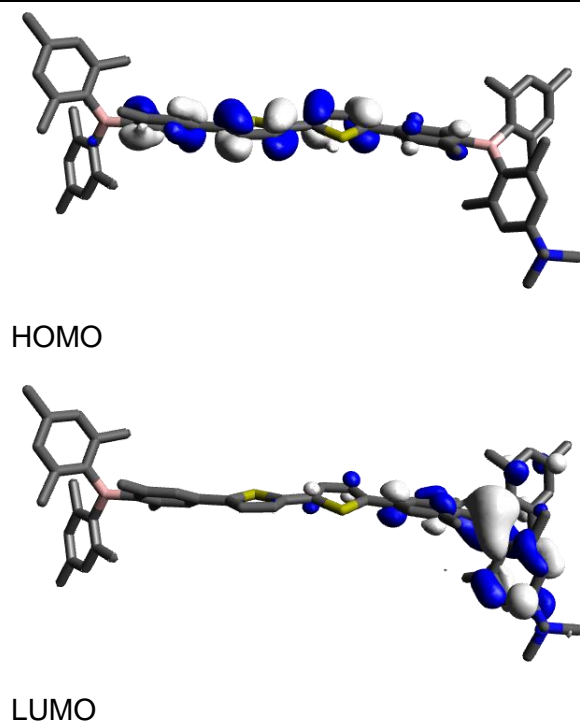
Functional used: TD-DFT CAM-B3LYP 6-31G(d,p), gas phase

Calculated Absorption Spectrum



Orbital	Energy [eV]	Symmetry
L+4	-2.49	A
L+3	-2.87	A
L+2	-3.22	A
L+1	-3.36	A
LUMO	-4.24	A
HOMO	-6.33	A
H-1	-6.78	A
H-2	-6.98	A
H-3	-7.02	A
H-4	-7.10	A

Orbitals Relevant for S₁←S₀ Transition



Other Relevant Orbitals

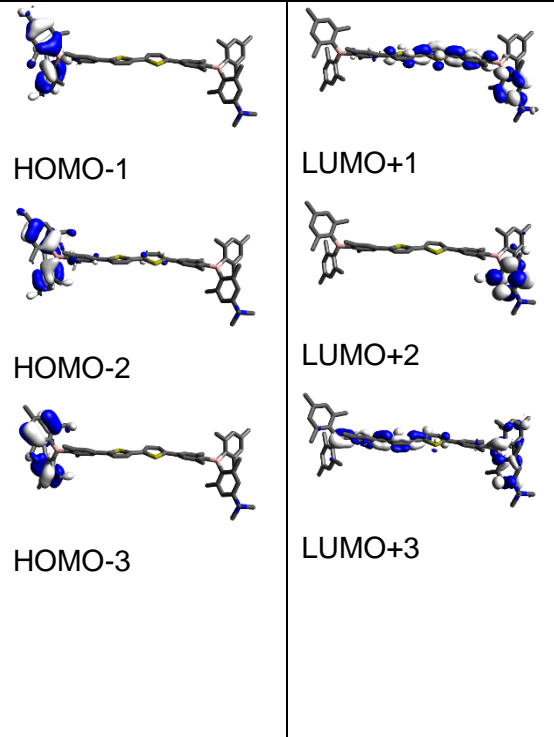
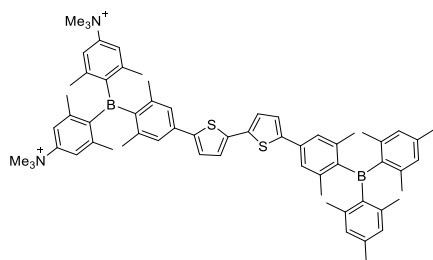


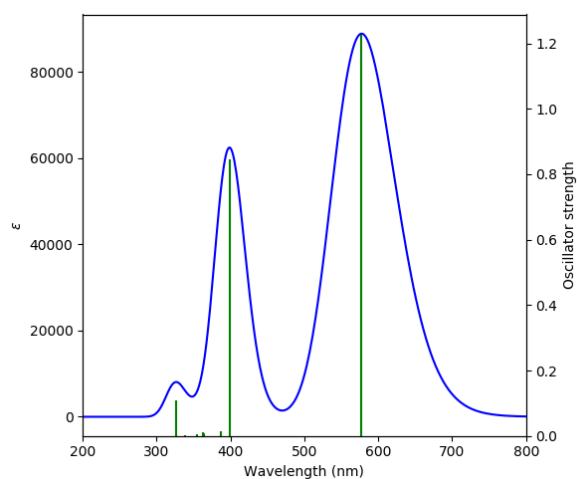
Table 11.23: Lowest energy singlet electronic transitions of **Cat**¹⁺ (TD-DFT CAM-B3LYP 6-31G(d,p), gas phase).

State	E [eV]	λ [nm]	f	Symmetry	Major Contributions	Δ
1	2.85	436	1.477	A	HOMO->LUMO (60%), HOMO->L+1 (18%)	0.355
2	3.47	358	0.515	A	HOMO->LUMO (10%), HOMO->L+1 (42%), HOMO->L+3 (22%)	0.518
3	3.78	328	0.115	A	H-7->LUMO (62%), HOMO->LUMO (10%)	0.425
4	3.89	319	0.123	A	H-1->L+3 (27%), H-1-> L+4 (49%)	0.345
5	3.95	314	0.005	A	H-2->L+3 (10%), H-2-> L+4 (15%), HOMO-> L+4 (27%)	0.499
6	4.07	305	0.051	A	H-10->LUMO (14%), H-9->LUMO (20%), H-5->LUMO (20%), HOMO->LUMO (14%)	0.377
7	4.11	302	0.023	A	H-9->LUMO (53%)	0.424
8	4.21	294	0.033	A	H-12->LUMO (16%), H-11->LUMO (45%)	0.423
9	4.36	285	0.003	A	H-2->L+3 (13%), H-2->L+4 (15%), HOMO->L+3 (29%)	0.541
10	4.39	283	0.021	A	H-6->L+3 (13%), H-3->L+3 (17%), H-3->L+4 (27%)	0.261

Cat²⁺

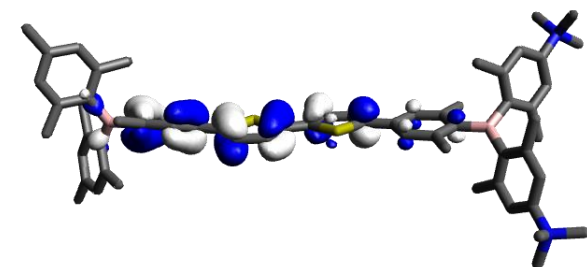
Functional used: TD-DFT CAM-B3LYP 6-31G(d,p), gas phase

Calculated Absorption Spectrum

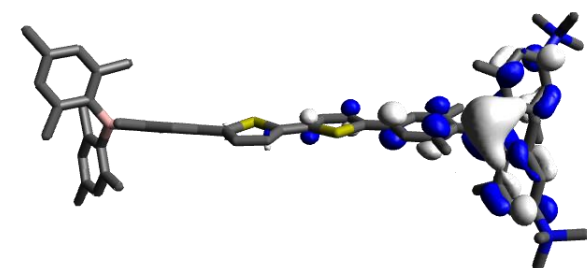


Orbital	Energy [eV]	Symmetry
---------	-------------	----------

L+4	-4.87	A
L+3	-5.00	A
L+2	-5.12	A
L+1	-5.40	A
LUMO	-6.34	A
HOMO	-7.66	A
H-1	-7.66	A
H-2	-7.88	A
H-3	-7.92	A
H-4	-7.97	A

Orbitals Relevant for S₁←S₀ Transition

HOMO



LUMO

Other Relevant Orbitals

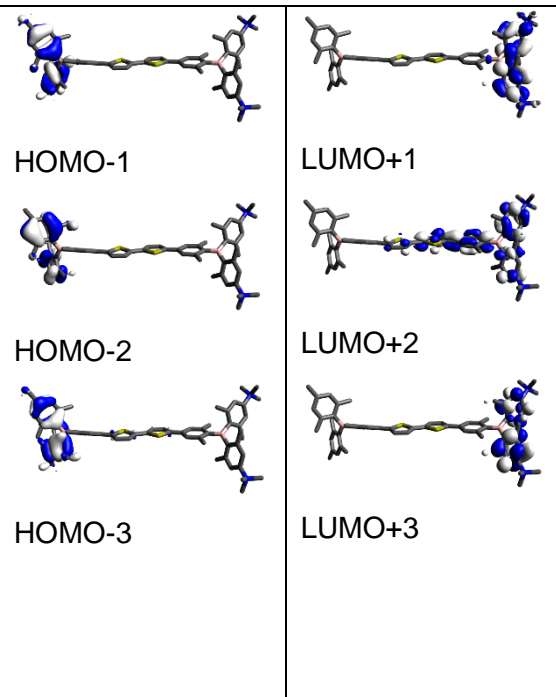
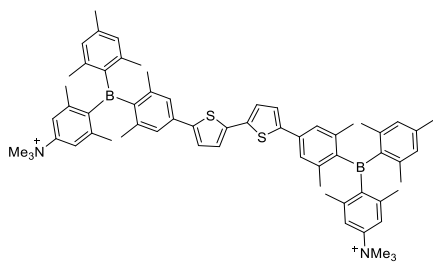


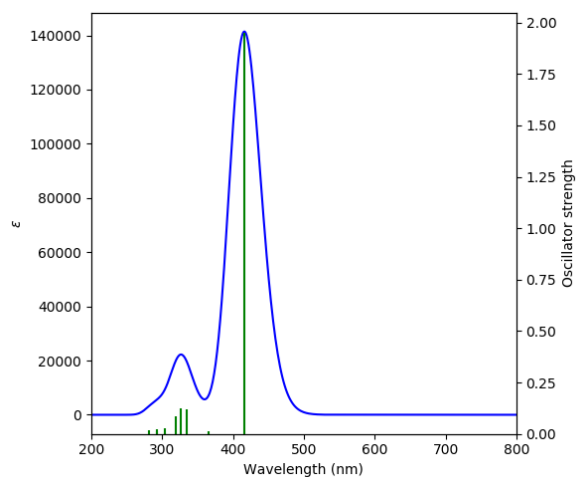
Table 11.24: Lowest energy singlet electronic transitions of **Cat**²⁺ (TD-DFT CAM-B3LYP 6-31G(d,p), gas phase).

State	E [eV]	λ [nm]	f	Symmetry	Major Contributions	Δ
1	2.15	577	1.227	A	HOMO->LUMO (78%)	0.297
2	3.03	409	5E-4	A	H-1->LUMO (98%)	0.017
3	3.11	399	0.845	A	HOMO->LUMO (13%), HOMO->L+2 (47%), HOMO->L+4 (12%), HOMO->L+5 (12%)	0.411
4	3.20	387	0.016	A	H-6->LUMO (21%), H-3->LUMO (48%)	0.208
5	3.30	375	1E-4	A	H-2->LUMO (90%)	0.044
6	3.41	364	0.007	A	H-6->LUMO (18%), H-4->LUMO (51%), H-3->LUMO (18%)	0.111
7	3.41	363	0.010	A	H-6->LUMO (21%), H-4->LUMO (48%), H-3->LUMO (18%)	0.121
8	3.49	355	0.005	A	HOMO->L+1 (88%)	0.081
9	3.67	338	9E-4	A	H-5->LUMO (90%)	0.064
10	3.80	326	0.109	A	H-1->L+2 (10%), H-1->L+5 (18%), H-1->L+9 (50%)	0.301

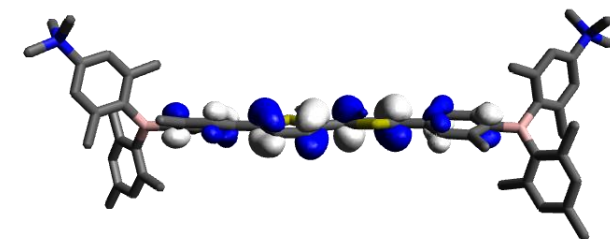
**Cat(i)²⁺**

Functional used: TD-DFT CAM-B3LYP 6-31G(d,p), gas phase

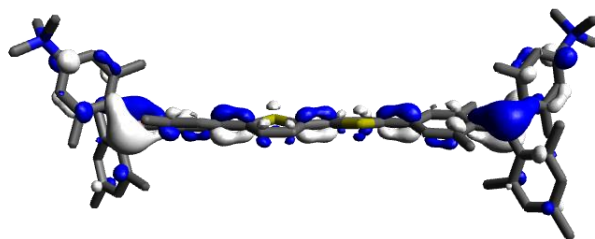
Calculated Absorption Spectrum



Orbital	Energy [eV]	Symmetry
L+4	-3.99	A
L+3	-4.05	B
L+2	-4.41	A
L+1	-5.04	B
LUMO	-5.14	A
HOMO	-7.72	B
H-1	-8.79	A
H-2	-8.93	B
H-3	-9.01	A
H-4	-9.04	B

Orbitals Relevant for $S_1 \leftarrow S_0$ Transition

HOMO



LUMO

Other Relevant Orbitals

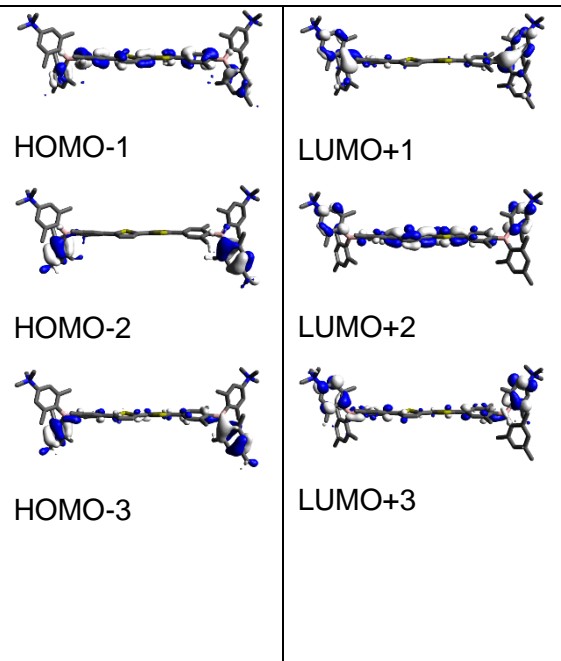
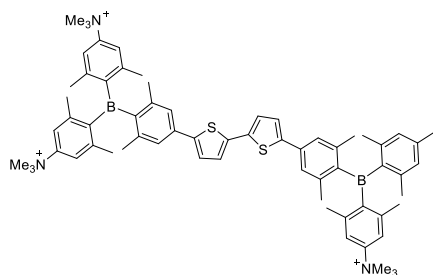


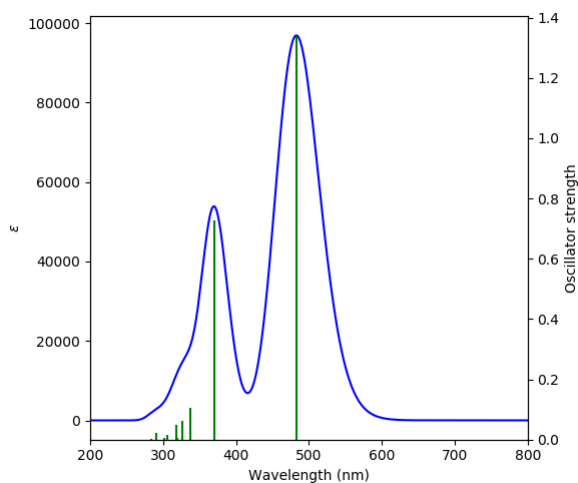
Table 11.25: Lowest energy singlet electronic transitions of **Cat(i)**²⁺ (TD-DFT CAM-B3LYP 6-31G(d,p), gas phase).

State	E [eV]	λ [nm]	f	Symmetry	Major Contributions	Δ
1	2.98	416	1.952	B	HOMO->LUMO (67%), HOMO->L+2 (17%)	0.530
2	3.39	366	0.011	A	H-1->LUMO (24%), HOMO->L+1 (57%)	0.423
3	3.71	335	0.121	B	H-3->L+1 (12%), H-2->LUMO (30%), H-1->L+1 (21%), HOMO->L+2 (22%)	0.516
4	3.80	326	0.126	A	H-3->LUMO (33%), H-2->L+1 (36%), HOMO->L+1 (11%)	0.489
5	3.89	319	0.084	B	H-3->L+1 (22%), H-2->LUMO (13%), HOMO->L+2 (33%)	0.564
6	4.08	304	0.002	A	H-5->L+1 (41%), H-4->LUMO (43%)	0.328
7	4.08	304	0.027	B	H-5->LUMO (42%), H-4->L+1 (40%)	0.326
8	4.23	293	0.014	A	H-7->L+1 (33%), H-6->LUMO (42%)	0.418
9	4.23	293	0.022	B	H-7->LUMO (46%), H-6->L+1 (31%)	0.405
10	4.39	282	0.020	A	H-10->L+1 (15%), H-3->LUMO (12%), H-1->LUMO (28%), HOMO->L+1 (21%)	0.517

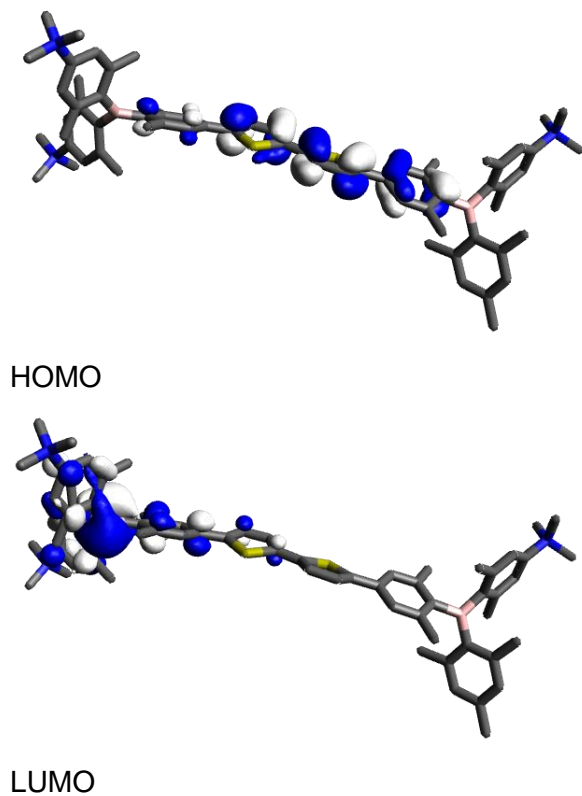
**Cat³⁺**

Functional used: TD-DFT CAM-B3LYP
6-31G(d,p), gas phase

Calculated Absorption Spectrum



Orbital	Energy [eV]	Symmetry
L+4	-5.89	A
L+3	-5.94	A
L+2	-6.16	A
L+1	-6.28	A
LUMO	-7.31	A
HOMO	-9.14	A
H-1	-9.80	A
H-2	-9.90	A
H-3	-10.28	A
H-4	-10.31	A

Orbitals Relevant for $S_1 \leftarrow S_0$ Transition

Other Relevant Orbitals

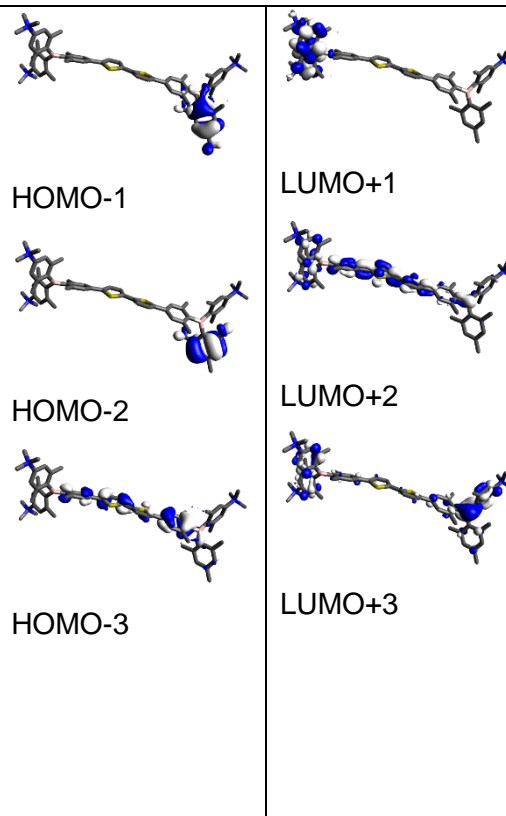


Table 11.26: Lowest energy singlet electronic transitions of **Cat**³⁺ (TD-DFT CAM-B3LYP 6-31G(d,p), gas phase).

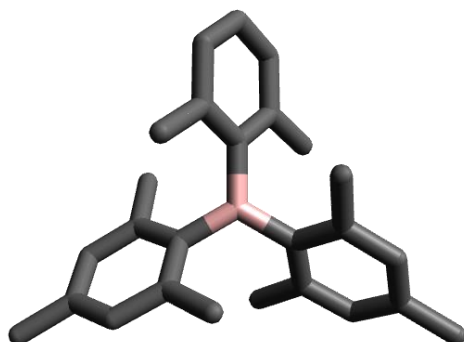
State	E [eV]	λ [nm]	f	Symmetry	Major Contributions	Δ
1	2.57	483	1.338	A	HOMO->LUMO (74%), HOMO->L+2 (10%)	0.345
2	3.35	371	0.729	A	HOMO->L+2 (57%)	0.547
3	3.67	338	0.107	A	H-1->L+2 (18%), H-1->L+3 (32%), HOMO->L+3 (11%)	0.385
4	3.80	327	0.063	A	H-6->LUMO (12%), H-3->LUMO (41%), HOMO->LUMO (16%)	0.336
5	3.88	319	0.007	A	H-10->LUMO (48%), H-7->LUMO (14%)	0.349
6	3.89	319	0.047	A	H-10->LUMO (12%), H-1->L+3 (12%), HOMO->L+3 (22%)	0.402
7	4.05	306	0.016	A	H-2->L+2 (22%), H-2->L+3 (50%)	0.211
8	4.11	302	0.004	A	HOMO->L+1 (87%)	0.087
9	4.27	291	0.023	A	H-4->L+2 (33%), H-4->L+3 (36%)	0.265
10	4.33	284	0.004	A	H-1->LUMO (82%)	0.121

11.8 XYZ Coordinates

11.8.1 Chapter 3

3.1a

TD-DFT CAM-B3LYP 6-31G(d,p), gas
phase, S₀



Point group: C₂

Total energy: -648639.32 kcal/mol

Dipole moment: 0.55 D

Imaginary frequencies: 0

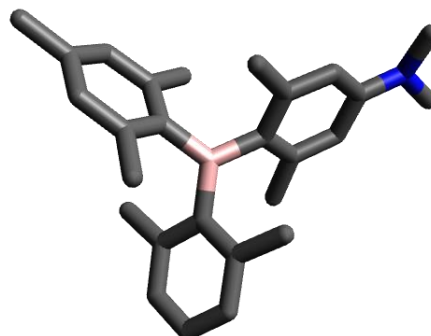
Optimized x, y, z coordinates

C	0.	0.	4.64884
C	-0.92274	0.77092	3.94848
C	-0.9257	0.79423	2.55046
C	0.	0.	1.82789
C	0.9257	-0.79423	2.55046
C	0.92274	-0.77092	3.94848
B	0.	0.	0.25435
C	-0.00469	-1.36079	-0.52917
C	0.00469	1.36079	-0.52917
C	-0.90551	1.58952	-1.59185
C	-0.90433	2.81482	-2.26233
C	0.	3.82913	-1.94322
C	0.9035	3.5958	-0.90492
C	0.91092	2.39671	-0.18901
C	0.90551	-1.58952	-1.59185
C	0.90433	-2.81482	-2.26233
C	0.	-3.82913	-1.94322
C	-0.9035	-3.5958	-0.90492
C	-0.91092	-2.39671	-0.18901
C	1.92213	2.24979	0.9286
C	-1.91939	0.55122	-2.02528
C	1.91939	-0.55122	-2.02528

C	-1.92213	-2.24979	0.9286
C	0.01916	5.12506	-2.71344
C	-1.94973	1.66915	1.85841
C	1.94973	-1.66915	1.85841
C	-0.01916	-5.12506	-2.71344
H	0.	0.	5.73497
H	-1.64982	1.36932	4.49081
H	1.64982	-1.36932	4.49081
H	-1.62666	2.98088	-3.05839
H	1.61801	4.37223	-0.64084
H	1.62666	-2.98088	-3.05839
H	-1.61801	-4.37223	-0.64084
H	2.66274	3.05267	0.88123
H	1.44383	2.28772	1.91137
H	2.46085	1.2991	0.88068
H	-2.45189	0.10841	-1.17878
H	-2.66454	0.99942	-2.68808
H	-1.44385	-0.27574	-2.56015
H	2.45189	-0.10841	-1.17878
H	2.66454	-0.99942	-2.68808
H	1.44385	0.27574	-2.56015
H	-2.66274	-3.05267	0.88123
H	-1.44383	-2.28772	1.91137
H	-2.46085	-1.2991	0.88068
H	-0.97249	5.37322	-3.10273
H	0.35973	5.95609	-2.08885
H	0.69976	5.06297	-3.57171
H	-2.70343	2.0121	2.57241
H	-1.48557	2.55018	1.40614
H	-2.4714	1.14428	1.05293
H	2.4714	-1.14428	1.05293
H	2.70343	-2.0121	2.57241
H	1.48557	-2.55018	1.40614
H	0.97249	-5.37322	-3.10273
H	-0.35973	-5.95609	-2.08885
H	-0.69976	-5.06297	-3.57171

3.2a

TD-DFT CAM-B3LYP 6-31G(d,p), gas
phase, S₀



Point group: C_1

Total energy: -708017.08 kcal/mol

Dipole moment: 2.73 D

Imaginary frequencies: 0

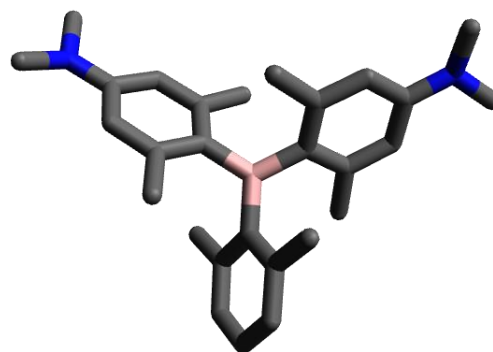
Optimized x, y, z coordinates

C	1.97458	4.47391	0.12215
C	2.46312	3.59744	-0.84191
C	2.02787	2.26941	-0.89143
C	1.05428	1.80799	0.02827
C	0.55188	2.71232	0.99726
C	1.02896	4.0262	1.03982
B	0.55137	0.31343	0.00103
C	-0.97347	-0.00834	-0.0186
C	1.61602	-0.84622	-0.00604
C	1.53668	-1.88591	-0.96622
C	2.50962	-2.88818	-0.99462
C	3.55867	-2.92406	-0.07443
C	3.62729	-1.90493	0.87694
C	2.69123	-0.86889	0.91603
C	-1.52425	-1.03316	0.79779
C	-2.89025	-1.30025	0.79243
C	-3.77907	-0.60477	-0.05134
C	-3.23385	0.40752	-0.86597
C	-1.87634	0.71368	-0.84542
C	2.85963	0.19701	1.97787
C	0.43034	-1.9494	-1.99914
C	-0.67354	-1.85798	1.74259
C	-1.41509	1.82475	-1.76688
C	4.56985	-4.04258	-0.09024
C	2.61154	1.3682	-1.95873
C	-0.49087	2.30315	2.01685
N	-5.12878	-0.90585	-0.0831
C	-6.03969	-0.02945	-0.79676
C	-5.67845	-1.83168	0.89
H	2.32903	5.50002	0.15854
H	3.19699	3.94305	-1.56518
H	0.64888	4.70462	1.79908
H	2.44494	-3.66464	-1.75377
H	4.43605	-1.91323	1.60443
H	-3.26511	-2.06385	1.46223
H	-3.87575	0.9713	-1.53118
H	3.18256	1.14802	1.5452
H	1.92744	0.39833	2.514
H	3.60564	-0.11101	2.71559
H	0.2545	-0.98467	-2.4832
H	0.6785	-2.67431	-2.77942
H	-0.52198	-2.24669	-1.55044
H	0.01764	-1.24229	2.32383
H	-1.30603	-2.40591	2.44644

H	-0.06127	-2.58444	1.20145
H	-1.1518	2.72735	-1.20891
H	-0.52815	1.5452	-2.34129
H	-2.20443	2.08418	-2.47764
H	4.70823	-4.44188	-1.09927
H	5.5427	-3.70709	0.28111
H	4.24785	-4.87512	0.5478
H	3.16768	1.95565	-2.69448
H	3.29248	0.62719	-1.53057
H	1.84016	0.80891	-2.49664
H	-0.25507	1.34824	2.49533
H	-0.57247	3.05866	2.80333
H	-1.4765	2.18264	1.55785
H	-7.05237	-0.42631	-0.71795
H	-6.03857	0.99689	-0.40022
H	-5.78519	0.02052	-1.86121
H	-6.74087	-1.97287	0.68823
H	-5.19369	-2.81106	0.81606
H	-5.5677	-1.47639	1.92581

3.3a

TD-DFT CAM-B3LYP 6-31G(d,p), gas
phase, S_0

Point group: C_1

Total energy: -767388.41 kcal/mol

Dipole moment: 2.65 D

Imaginary frequencies: 0

Optimized x, y, z coordinates

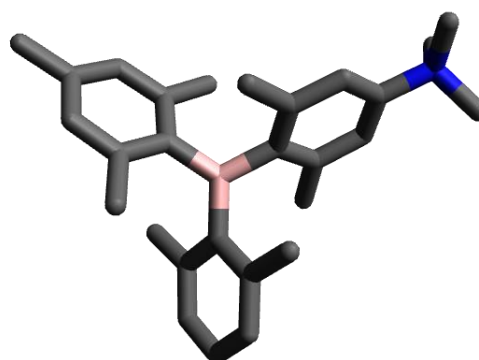
C	0.07324	5.06539	-0.04675
C	-0.67274	4.39003	0.91463
C	-0.717	2.99235	0.93791
C	0.02686	2.24408	-0.0071
C	0.79481	2.94071	-0.97226
C	0.79637	4.33915	-0.98835
B	0.00032	0.66532	0.01506

C	1.34712	-0.12862	0.03011
C	-1.37287	-0.08217	0.02094
C	-1.61425	-1.16465	0.90791
C	-2.84846	-1.8092	0.93599
C	-3.89934	-1.43898	0.07419
C	-3.65176	-0.38342	-0.82477
C	-2.43589	0.29551	-0.84024
C	1.55225	-1.23784	-0.8323
C	2.76528	-1.92209	-0.84757
C	3.82214	-1.5779	0.01772
C	3.61868	-0.47961	0.87567
C	2.42533	0.23809	0.87722
C	-2.29393	1.42263	-1.84263
C	-0.56514	-1.65899	1.88412
C	0.48912	-1.71326	-1.80264
C	2.32804	1.40266	1.84146
C	-1.56222	2.32376	2.00184
C	1.61815	2.21536	-2.01598
N	5.00984	-2.29258	0.02907
C	6.15138	-1.76017	0.75032
C	5.25357	-3.28204	-1.00399
H	0.09102	6.15141	-0.06206
H	-1.23433	4.95179	1.65655
H	1.37587	4.86114	-1.7454
H	-2.98867	-2.61471	1.64597
H	-4.41601	-0.08042	-1.52941
H	2.88431	-2.73644	-1.55121
H	4.40193	-0.17178	1.55708
H	-2.29313	2.39897	-1.35046
H	-1.36017	1.35824	-2.40784
H	-3.11927	1.40526	-2.55982
H	-0.06918	-0.83907	2.40991
H	-1.01947	-2.31251	2.63417
H	0.22425	-2.22142	1.37771
H	0.02541	-0.88715	-2.34793
H	0.9212	-2.39945	-2.53655
H	-0.32201	-2.23505	-1.28709
H	2.35868	2.36171	1.31728
H	1.39531	1.38951	2.41177
H	3.15546	1.3798	2.55603
H	-1.86463	3.04894	2.76269
H	-2.4667	1.87985	1.57594
H	-1.02906	1.51316	2.5075
H	1.05855	1.40979	-2.5006
H	1.94556	2.90911	-2.79557
H	2.50668	1.75298	-1.57636
H	6.98852	-2.45287	0.65498
H	6.47162	-0.77602	0.37542
H	5.92785	-1.657	1.81762
H	6.21511	-3.7625	-0.8184
H	4.48515	-4.06207	-0.98658
H	5.2729	-2.84873	-2.01606
C	-6.1086	-1.8056	-0.91676
H	-5.7586	-2.07881	-1.92437
H	-7.01775	-2.36988	-0.70489

H	-6.37407	-0.74331	-0.9293
C	-5.25908	-3.3109	0.87554
H	-5.0466	-3.14153	1.93666
H	-6.28642	-3.66924	0.79891
H	-4.58714	-4.10665	0.5192
N	-5.12701	-2.08131	0.11578

3.2c

TD-DFT CAM-B3LYP 6-31G(d,p), gas phase, S₀



Point group: C₁

Total energy: -732910.16 kcal/mol

Dipole moment: 17.30 D

Imaginary frequencies: 0

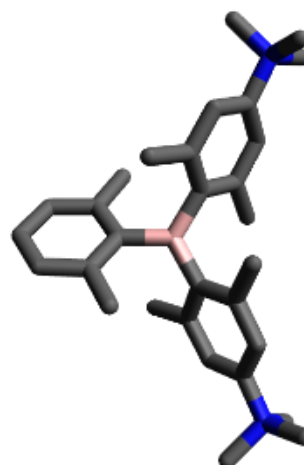
Optimized x, y, z coordinates

C	-2.21131	4.49974	0.03195
C	-2.74042	3.57547	0.92721
C	-2.33727	2.23695	0.90467
C	-1.34575	1.81668	-0.0219
C	-0.80232	2.77117	-0.92032
C	-1.2533	4.09299	-0.89217
B	-0.84906	0.33344	-0.00098
C	0.7183	0.05813	-0.00078
C	-1.83234	-0.87505	0.01969
C	-1.63509	-1.98472	0.88342
C	-2.52696	-3.05701	0.86122
C	-3.61164	-3.09526	-0.01847
C	-3.79225	-2.01157	-0.88071
C	-2.94454	-0.90274	-0.86546
C	1.29516	-0.8019	-0.96032
C	2.67985	-1.02315	-0.97548
C	3.48479	-0.41299	-0.02464
C	2.9366	0.42731	0.93927
C	1.56242	0.67784	0.9516

C	-3.24742	0.22055	-1.83524
C	-0.49381	-2.04625	1.8777
C	0.46424	-1.51521	-2.00255
C	1.02563	1.61626	2.00715
C	-4.57355	-4.25412	-0.01594
C	-2.97781	1.29315	1.90112
C	0.24264	2.40492	-1.95357
N	4.9793	-0.63597	-0.00175
C	5.44689	-1.56307	-1.09128
C	5.68917	0.68605	-0.18821
C	5.37827	-1.24694	1.32252
H	-2.54638	5.5321	0.05203
H	-3.48491	3.89229	1.65162
H	-0.84925	4.80917	-1.60187
H	-2.37448	-3.88643	1.54736
H	-4.62307	-2.02841	-1.58137
H	3.0807	-1.67918	-1.73578
H	3.55415	0.90883	1.68963
H	-3.65134	1.09713	-1.32109
H	-2.36196	0.56055	-2.37925
H	-3.98492	-0.10431	-2.57289
H	-0.36707	-1.10869	2.42638
H	-0.67281	-2.83301	2.61443
H	0.46116	-2.26336	1.38814
H	-0.24818	-0.84429	-2.48796
H	1.09849	-1.94917	-2.77962
H	-0.12377	-2.31784	-1.5496
H	0.70835	2.5629	1.5625
H	0.15121	1.20119	2.51429
H	1.78298	1.82778	2.76609
H	-4.08904	-5.17645	0.31562
H	-5.41046	-4.06142	0.66606
H	-4.99716	-4.42427	-1.00938
H	-3.51952	1.85768	2.66373
H	-3.68823	0.61836	1.41513
H	-2.24935	0.65851	2.41346
H	-0.00121	1.47992	-2.48407
H	0.33171	3.19517	-2.70288
H	1.23007	2.26524	-1.50149
H	6.52725	-1.66679	-1.00044
H	4.9683	-2.53234	-0.96629
H	5.1946	-1.13414	-2.05901
H	6.76516	0.50946	-0.18151
H	5.41374	1.3575	0.6208
H	5.37322	1.10787	-1.14116
H	4.84188	-2.18783	1.43603
H	6.45576	-1.41408	1.32007
H	5.10548	-0.56852	2.12654

3.3c

TD-DFT CAM-B3LYP 6-31G(d,p), gas
phase, S₀



Point group: C₁

Total energy: -817135.15 kcal/mol

Dipole moment: 12.83 D

Imaginary frequencies: 0

Optimized x, y, z coordinates

C	-0.0006	5.15561	-0.00051
C	0.85111	4.45681	-0.8509
C	0.87988	3.06062	-0.85172
C	-0.00007	2.33455	0.0001
C	-0.88022	3.06068	0.85172
C	-0.85199	4.45685	0.85027
B	0.00002	0.78	0.00015
C	-1.37342	-0.0113	-0.01976
C	1.37345	-0.0113	0.02001
C	1.66414	-1.01341	-0.93109
C	2.91796	-1.64156	-0.94464
C	3.87197	-1.29814	0.0029
C	3.59259	-0.34099	0.97327
C	2.35871	0.31478	0.98573
C	-1.6643	-1.01309	0.93156
C	-2.91812	-1.64128	0.94504
C	-3.87187	-1.29822	-0.00286
C	-3.59226	-0.34139	-0.97351
C	-2.35844	0.31444	-0.98588
C	2.1402	1.37045	2.04563
C	0.66298	-1.42616	-1.98585
C	-0.66328	-1.42547	1.98661
C	-2.13968	1.36973	-2.04611
C	1.84003	2.38753	-1.81115
C	-1.83972	2.38755	1.81176
N	-5.23935	-1.93781	-0.01026
C	-5.41674	-2.95279	1.0897
C	-5.46425	-2.64664	-1.329
C	-6.29607	-0.8687	0.17903
N	5.23947	-1.93767	0.01013

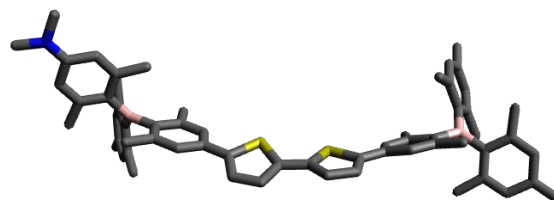
C	5.41655	-2.95316	-1.08942
C	5.46485	-2.6459	1.32911
C	6.29607	-0.8686	-0.17999
H	-0.00084	6.24079	-0.00077
H	1.50539	5.00259	-1.52371
H	-1.5064	5.00269	1.5229
H	3.10678	-2.38438	-1.70703
H	4.32383	-0.06981	1.72627
H	-3.10709	-2.38381	1.70767
H	-4.32334	-0.07055	-1.7268
H	2.87855	1.27879	2.84543
H	2.22313	2.37382	1.61915
H	1.14869	1.30541	2.49861
H	0.28112	-0.56552	-2.54215
H	1.11026	-2.11036	-2.70995
H	-0.19925	-1.926	-1.53647
H	-0.28142	-0.56463	2.54258
H	-1.11063	-2.10939	2.71092
H	0.19897	-1.92551	1.53747
H	-2.87797	1.27792	-2.84594
H	-2.22239	2.37326	-1.61997
H	-1.14813	1.30438	-2.49898
H	2.19706	3.10533	-2.55267
H	2.71729	1.98718	-1.29304
H	1.3831	1.55765	-2.35704
H	-1.38175	1.55886	2.35864
H	-2.19765	3.10573	2.55247
H	-2.71643	1.98543	1.29412
H	-5.29183	-2.46323	2.05361
H	-6.42421	-3.35803	1.00903
H	-4.68669	-3.75011	0.96396
H	-5.40782	-1.92514	-2.13995
H	-6.45041	-3.11063	-1.3098
H	-4.68739	-3.40071	-1.4466
H	-7.27556	-1.34698	0.1881
H	-6.10469	-0.36596	1.1259
H	-6.23623	-0.1552	-0.63877
H	5.29125	-2.46405	-2.05352
H	6.42409	-3.35826	-1.00893
H	4.68662	-3.75047	-0.96305
H	5.40873	-1.92403	2.13975
H	6.451	-3.1099	1.30977
H	4.68802	-3.39991	1.44735
H	7.27559	-1.34682	-0.18914
H	6.10437	-0.36632	-1.12705
H	6.23643	-0.15471	0.63749

11.8.2 Chapter 4

11.8.2.1 Sulfur Atoms of Bithiophene on Same Side

Neut1

TD-DFT CAM-B3LYP 6-31G(d,p), gas phase, S_0



Point group: C_1

Total energy: -2048455.90 kcal/mol

Dipole moment: 2.67 D

Imaginary frequencies: 0

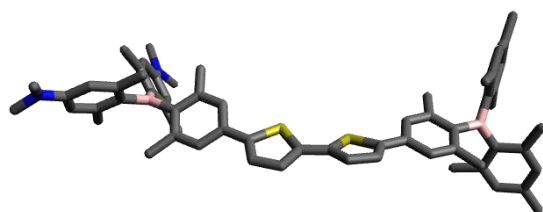
Optimized x, y, z coordinates

C	-2.73078	-2.22937	-0.75892
C	-2.46186	-3.50928	-1.19669
C	-1.0869	-3.84734	-1.17229
C	-0.2776	-2.83094	-0.7048
S	-1.24413	-1.43294	-0.27755
C	-4.01895	-1.54869	-0.66485
C	1.15711	-2.84827	-0.54271
S	2.09973	-1.37351	-0.45807
C	3.60262	-2.26311	-0.28937
C	3.35305	-3.61956	-0.30933
C	1.98335	-3.95052	-0.44617
C	4.88133	-1.57263	-0.15037
C	5.04679	-0.23962	-0.55141
C	6.26198	0.42676	-0.40385
C	7.38893	-0.25241	0.12469
C	7.23137	-1.60794	0.51362
C	5.99256	-2.23371	0.39424
C	-4.11566	-0.15065	-0.67318
C	-5.3469	0.49919	-0.60149
C	-6.5449	-0.24929	-0.49215
C	-6.45014	-1.66458	-0.46991
C	-5.20714	-2.28726	-0.56432
B	-7.95012	0.45955	-0.41864
B	8.77219	0.47697	0.27902
C	10.08218	-0.21101	-0.24669
C	8.84035	1.89074	0.95855
C	-8.9672	0.08046	0.69915

C	-8.30394	1.55458	-1.4924	H	10.39371	-0.01459	2.56172
C	-8.1175	1.31906	-2.87663	H	12.15674	-0.09449	2.50973
C	-8.42716	2.31509	-3.8057	H	11.30547	1.36094	1.97143
C	-8.89561	3.56957	-3.41162	H	9.9093	5.86802	3.50528
C	-9.05991	3.80544	-2.04551	H	9.13653	6.61015	2.10359
C	-8.79103	2.82311	-1.08925	H	8.15185	6.01203	3.45084
C	-10.34793	-0.10183	0.41436	H	14.36236	-1.36776	-2.19258
C	-11.24629	-0.46144	1.41456	H	14.29667	-2.55567	-0.88988
C	-10.8389	-0.63046	2.75303	H	13.50227	-2.88812	-2.43936
C	-9.47589	-0.41985	3.04259	H	6.45029	0.85541	2.419
C	-8.557	-0.09728	2.04834	H	7.94217	0.12169	2.97668
C	11.23747	-0.29407	0.57063	H	7.17797	1.38726	3.94115
C	12.38568	-0.93194	0.09565	H	9.66503	2.29166	-1.72265
C	12.45172	-1.46945	-1.19101	H	10.56628	3.76794	-1.36852
C	11.31679	-1.37347	-1.99823	H	11.18522	2.19092	-0.85595
C	10.1394	-0.77296	-1.54696	H	8.17453	-1.43111	-2.1922
C	9.55309	2.95527	0.35127	H	8.49623	0.2564	-2.54294
C	9.58137	4.21332	0.95729	H	9.27509	-0.99938	-3.50838
C	8.95228	4.45738	2.17933	H	-9.16614	4.2528	0.47958
C	8.26334	3.40312	2.7816	H	-9.90057	2.66804	0.76919
C	8.18424	2.14035	2.19036	H	-8.17879	2.88407	1.00314
C	11.2736	0.26773	1.97657	H	-8.11515	-0.85771	-2.94966
C	9.03755	5.80902	2.84175	H	-7.74477	-0.06834	-4.48469
C	13.71771	-2.10833	-1.70302	H	-6.53643	-0.13231	-3.19347
C	7.39935	1.06944	2.91875	H	-10.95817	1.10008	-1.28707
C	10.27859	2.79212	-0.96804	H	-10.3043	-0.4617	-1.73435
C	8.95987	-0.73304	-2.49593	H	-11.92333	-0.36167	-1.03485
C	-9.01893	3.17514	0.36636	H	-6.48632	-0.73902	2.16382
C	-7.60232	-0.00395	-3.40251	H	-6.67462	1.00072	2.07084
C	-10.9119	0.05059	-0.984	H	-7.05665	0.15958	3.57603
C	-7.11879	0.09264	2.48647	H	-4.33431	2.40015	-0.50214
C	-5.34824	2.01263	-0.63221	H	-5.74015	2.39367	-1.5792
C	-7.67247	-2.55043	-0.34655	H	-5.97129	2.44026	0.15875
C	8.37131	-2.41331	1.1009	H	-8.47423	-2.24769	-1.02586
C	6.32976	1.87068	-0.85454	H	-7.41637	-3.58906	-0.57309
N	-11.73813	-0.99277	3.73899	H	-8.0931	-2.5155	0.66235
C	-11.31617	-0.99461	5.12767	H	8.90488	-1.86794	1.8845
C	-13.15972	-0.99348	3.44537	H	7.99732	-3.34253	1.53897
C	-9.23912	4.62663	-4.43061	H	9.11317	-2.67051	0.33987
H	-3.23389	-4.17279	-1.56693	H	5.44215	2.13158	-1.43684
H	-0.69188	-4.79441	-1.51969	H	6.38924	2.55299	-0.00209
H	4.14088	-4.35972	-0.2403	H	7.20659	2.0714	-1.47647
H	1.60564	-4.96576	-0.45797	H	-10.4756	-1.67995	5.28095
H	4.21128	0.28837	-1.00234	H	-11.00943	0.00174	5.48028
H	5.88251	-3.25359	0.74887	H	-12.14168	-1.3393	5.75137
H	-3.21143	0.44482	-0.76472	H	-13.53036	-0.00248	3.14373
H	-5.15628	-3.37129	-0.53028	H	-13.396	-1.70026	2.64216
H	-8.29253	2.109	-4.86529	H	-13.7078	-1.30841	4.33395
H	-9.41055	4.78086	-1.71545	H	-9.09931	5.63294	-4.02506
H	-12.28316	-0.61228	1.14155	H	-10.28694	4.54546	-4.74581
H	-9.11927	-0.50488	4.06131	H	-8.62202	4.53121	-5.32888
H	13.25405	-1.00801	0.74619				
H	11.3474	-1.78364	-3.00518				
H	10.11202	5.02452	0.46396				
H	7.76775	3.57108	3.73515				

Neut2

TD-DFT CAM-B3LYP 6-31G(d,p), gas
phase, S₀



Point group: C₁

Total energy: -2107825.36 kcal/mol

Dipole moment: 2.19 D

Imaginary frequencies: 0

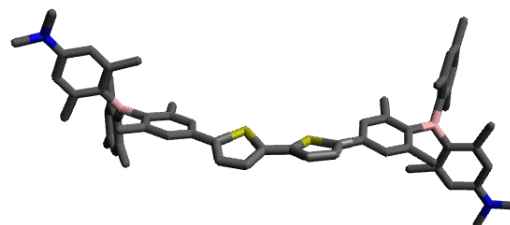
Optimized x, y, z coordinates

	C	13.1065	1.8939	2.04826
	C	12.2654	2.84051	1.593
	C	12.3111	5.77056	-0.57407
	C	12.6154	7.07973	-0.50883
	C	11.7852	8.02703	-0.02747
	C	10.5957	7.55445	0.39708
	C	10.2399	6.2573	0.35661
	C	-4.34322	-6.27077	-0.29075
	C	-4.81386	-7.3214	-0.98563
	C	-4.01852	-8.08178	-1.75257
	C	-2.7171	-7.76257	-1.81212
	C	-2.20813	-6.71902	-1.13321
	C	-2.62965	-5.59966	2.84077
	C	-2.92335	-5.43776	4.14292
	C	-3.36952	-4.27157	4.63264
	C	-3.51774	-3.24996	3.77617
	C	-3.23393	-3.37157	2.46708
	C	-5.32258	-5.46892	0.53977
	C	-3.68752	-4.13184	6.10257
	C	-4.58725	-9.25289	-2.51836
	C	-3.44047	-2.16388	1.57754
	C	-2.12296	-6.95227	2.38737
	C	-0.72464	-6.4431	-1.25852
	C	11.9555	4.0223	2.48945
	C	11.4805	1.39997	-1.76242
	C	13.3391	4.81853	-1.15141
	C	8.87137	5.86762	0.87787
	C	8.87972	1.92422	1.18313
	C	9.77087	4.80627	-2.83061
	C	-3.21564	-3.47757	-2.13574
	C	0.15854	-3.83954	1.56452
	N	12.0997	9.26995	0.0221
	C	11.13	10.2567	0.56742
	C	13.4318	9.71548	-0.4663
	N	14.257	-0.0974	1.81207
	C	14.8465	0.06778	3.16733
	C	14.5918	-1.28775	0.98605
	H	5.65771	3.33303	-4.35211
	H	3.4418	2.26552	-4.77234
	H	-0.27762	-0.44992	-4.03253
	H	1.58067	1.08936	-4.66778
	H	1.36096	-2.10607	0.10663
	H	-1.47272	-1.82269	-3.02929
	H	6.74494	1.41814	-0.14344
	H	7.47878	3.87922	-3.51232
	H	13.0874	-0.15129	-0.52493
	H	13.5107	2.0769	3.05489
	H	13.6161	7.34315	-0.88232
	H	9.83323	8.23247	0.80836
	H	-5.88447	-7.57841	-0.93063
	H	-2.05113	-8.37663	-2.43971
	H	-2.79977	-6.28225	4.84068
	H	-3.88131	-2.28456	4.16387
	H	-5.13552	-4.37656	0.47856
	H	-6.37412	-5.60596	0.20227
	C	5.7314	2.2123	-2.46813
	C	5.21609	2.62609	-3.63743
	C	4.02883	2.0584	-3.86726
	C	3.69591	1.23422	-2.86296
	S	4.77686	1.26744	-1.86304
	C	6.91273	2.58475	-1.9205
	C	2.55843	0.50687	-2.80266
	S	2.15575	-0.41512	-1.727
	C	0.85627	-0.91084	-2.21243
	C	0.60209	-0.31569	-3.3894
	C	1.59439	0.50931	-3.73506
	C	0.07612	-1.812	-1.56941
	C	0.41462	-2.37275	-0.39072
	C	-0.34819	-3.27519	0.25295
	C	-1.52285	-3.65298	-0.29035
	C	-1.90605	-3.11486	-1.46568
	C	-1.10571	-2.21872	-2.07131
	C	7.34929	2.12982	-0.72855
	C	8.51843	2.49645	-0.17246
	C	9.31785	3.36156	-0.82831
	C	8.92464	3.84117	-2.02546
	C	7.74313	3.44846	-2.5357
	B	10.7157	3.80583	-0.19925
	B	-2.44737	-4.72473	0.44698
	C	-3.02914	-5.96805	-0.36728
	C	-2.78651	-4.55636	1.99742
	C	11.1074	5.35154	-0.13648
	C	11.7226	2.7049	0.36698
	C	12.0375	1.62201	-0.37071
	C	12.8825	0.70484	0.13484
	C	13.4534	0.79151	1.35346

H	-5.27549	-5.78754	1.60549
H	-4.49883	-4.8389	6.38996
H	-2.78652	-4.35995	6.7165
H	-4.025	-3.10681	6.37414
H	-4.99894	-10.01	-1.81264
H	-5.40774	-8.91441	-3.19138
H	-3.82728	-9.76252	-3.15165
H	-2.47389	-1.63646	1.41294
H	-3.88006	-2.43191	0.59415
H	-4.14525	-1.42649	2.02244
H	-1.30078	-6.87028	1.64626
H	-1.70227	-7.54906	3.22717
H	-2.95388	-7.54724	1.94574
H	-0.54364	-5.64058	-2.00868
H	-0.26495	-6.14778	-0.29238
H	-0.15472	-7.33884	-1.59205
H	12.1425	3.80537	3.56466
H	12.593	4.89218	2.21289
H	10.8886	4.32417	2.43883
H	11.4012	2.34166	-2.34441
H	12.1243	0.73382	-2.37881
H	10.475	0.92552	-1.70215
H	13.9161	4.33326	-0.33208
H	12.8797	4.03216	-1.78577
H	14.0727	5.3303	-1.81323
H	8.14779	5.78852	0.03529
H	8.8858	4.90681	1.43326
H	8.46069	6.61024	1.59763
H	7.98774	1.581	1.75306
H	9.55279	1.04549	1.06299
H	9.37141	2.67063	1.84116
H	10.8523	4.56067	-2.78508
H	9.51815	4.79483	-3.9142
H	9.61783	5.84777	-2.46806
H	-4.04478	-3.59881	-1.40802
H	-3.56507	-2.6926	-2.84283
H	-3.10187	-4.41945	-2.71845
H	1.2623	-3.74781	1.67178
H	-0.30206	-3.29654	2.42046
H	-0.05133	-4.9244	1.66822
H	11.5542	11.2846	0.54267
H	10.2026	10.2997	-0.04811
H	10.8992	10.0531	1.63792
H	13.5463	10.8165	-0.35665
H	14.2568	9.26671	0.13265
H	13.5581	9.50769	-1.55332
H	15.5156	-0.78553	3.41522
H	15.4863	0.97774	3.22558
H	14.0603	0.07145	3.95646
H	15.2977	-1.95789	1.52447
H	13.6894	-1.90682	0.77845
H	15.1121	-0.99782	0.04483

Neut(i)2

TD-DFT CAM-B3LYP 6-31G(d,p), gas
phase, S₀



Point group: C₂

Total energy: -2107825.49 kcal/mol

Dipole moment: 1.45 D

Imaginary frequencies: 0

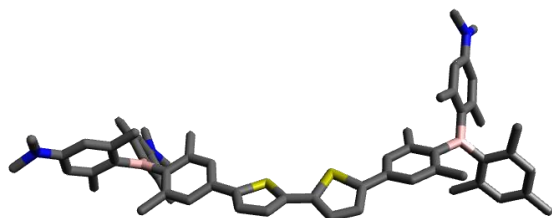
Optimized x, y, z coordinates

C	-0.85961	4.37527	-1.55815
C	-0.67947	4.5146	-0.17531
C	-0.95446	5.71245	0.48275
C	-1.45278	6.82594	-0.23774
C	-1.64915	6.68478	-1.63562
C	-1.34608	5.48181	-2.26994
B	-1.76189	8.19427	0.47895
C	-3.1327	8.90461	0.26772
C	-0.66264	8.82886	1.40976
C	-0.99063	9.24978	2.72289
C	0.	9.77209	3.55812
C	1.31918	9.92891	3.12918
C	1.63605	9.52409	1.83141
C	0.67947	8.96829	0.97865
C	-3.21402	10.30568	0.04328
C	-4.44005	10.92975	-0.1678
C	-5.65394	10.21533	-0.12206
C	-5.57566	8.82716	0.10763
C	-4.35577	8.18069	0.283
C	1.12534	8.54702	-0.40559
C	-2.39474	9.13677	3.27999
C	-1.982	11.18576	-0.02094
C	-4.40611	6.68477	0.52026
C	2.36253	10.54121	4.0293
C	-0.71415	5.76824	1.97626
C	-2.18521	7.81453	-2.49027
N	-6.87125	10.84963	-0.28997
C	-8.07592	10.05516	-0.44748
C	-6.9029	12.24469	-0.6886
H	-0.29066	3.6773	0.39773

H	-1.51822	5.39112	-3.33811	C	0.71415	-5.76824	1.97626
H	-0.26583	10.06784	4.57063	C	2.18521	-7.81453	-2.49027
H	2.65781	9.63784	1.47586	B	1.76189	-8.19427	0.47895
H	-4.44477	11.9926	-0.37422	H	0.54004	-4.76532	2.37499
H	-6.48045	8.23409	0.15208	H	-0.15369	-6.38738	2.21938
H	1.1651	7.45819	-0.50135	H	1.5646	-6.19681	2.51456
H	0.44769	8.90518	-1.18618	H	1.67927	-8.76291	-2.28851
H	2.12105	8.94222	-0.62461	H	2.05555	-7.58561	-3.55162
H	-2.84547	8.16026	3.08176	H	3.24933	-7.98704	-2.30619
H	-2.3887	9.28819	4.36299	C	3.1327	-8.90461	0.26772
H	-3.0639	9.88023	2.83717	C	0.66264	-8.82886	1.40976
H	-1.19243	10.75031	-0.63884	C	3.21402	-10.30568	0.04328
H	-2.23275	12.16429	-0.43957	C	4.35577	-8.18069	0.283
H	-1.54845	11.34281	0.97045	C	0.99063	-9.24978	2.72289
H	-4.05757	6.12593	-0.35262	C	-0.67947	-8.96829	0.97865
H	-3.77612	6.37658	1.35855	C	4.44005	-10.92975	-0.1678
H	-5.42924	6.36644	0.73771	C	1.982	-11.18576	-0.02094
H	2.14629	10.34402	5.08337	C	5.57566	-8.82716	0.10763
H	3.36049	10.15233	3.80643	C	4.40611	-6.68477	0.52026
H	2.40242	11.63046	3.90353	C	0.	-9.77209	3.55812
H	-0.54004	4.76532	2.37499	C	2.39474	-9.13677	3.27999
H	0.15369	6.38738	2.21938	C	-1.63605	-9.52409	1.83141
H	-1.5646	6.19681	2.51456	C	-1.12534	-8.54702	-0.40559
H	-1.67927	8.76291	-2.28851	C	5.65394	-10.21533	-0.12206
H	-2.05555	7.58561	-3.55162	H	4.44477	-11.9926	-0.37422
H	-3.24933	7.98704	-2.30619	H	1.19243	-10.75031	-0.63884
H	-8.9311	10.722	-0.56209	H	2.23275	-12.16429	-0.43957
H	-8.03439	9.39226	-1.32457	H	1.54845	-11.34281	0.97045
H	-8.25636	9.43333	0.43639	H	6.48045	-8.23409	0.15208
H	-7.93974	12.57952	-0.73512	H	4.05757	-6.12593	-0.35262
H	-6.38361	12.87321	0.04291	H	3.77612	-6.37658	1.35855
H	-6.43991	12.41683	-1.67211	H	5.42924	-6.36644	0.73771
C	-0.55475	3.12661	-2.25065	C	-1.31918	-9.92891	3.12918
C	-0.25767	2.93087	-3.58322	H	0.26583	-10.06784	4.57063
S	-0.53583	1.59365	-1.39833	H	2.84547	-8.16026	3.08176
C	0.0057	1.58092	-3.9207	H	2.3887	-9.28819	4.36299
H	-0.18887	3.74791	-4.29112	H	3.0639	-9.88023	2.83717
C	-0.09539	0.71563	-2.84965	H	-2.65781	-9.63784	1.47586
H	0.29763	1.25075	-4.91037	H	-1.1651	-7.45819	-0.50135
C	0.09539	-0.71563	-2.84965	H	-0.44769	-8.90518	-1.18618
C	-0.0057	-1.58092	-3.9207	H	-2.12105	-8.94222	-0.62461
S	0.53583	-1.59365	-1.39833	N	6.87125	-10.84963	-0.28997
C	0.25767	-2.93087	-3.58322	C	-2.36253	-10.54121	4.0293
H	-0.29763	-1.25075	-4.91037	C	8.07592	-10.05516	-0.44748
C	0.55475	-3.12661	-2.25065	C	6.9029	-12.24469	-0.6886
H	0.18887	-3.74791	-4.29112	H	-2.14629	-10.34402	5.08337
C	0.85961	-4.37527	-1.55815	H	-3.36049	-10.15233	3.80643
C	0.67947	-4.5146	-0.17531	H	-2.40242	-11.63046	3.90353
C	1.34608	-5.48181	-2.26994	H	8.9311	-10.722	-0.56209
C	0.95446	-5.71245	0.48275	H	8.03439	-9.39226	-1.32457
H	0.29066	-3.6773	0.39773	H	8.25636	-9.43333	0.43639
C	1.64915	-6.68478	-1.63562	H	7.93974	-12.57952	-0.73512
H	1.51822	-5.39112	-3.33811	H	6.38361	-12.87321	0.04291
C	1.45278	-6.82594	-0.23774	H	6.43991	-12.41683	-1.67211

Neut3

TD-DFT CAM-B3LYP 6-31G(d,p), gas
phase, S₀



Point group: C₁

Total energy: -2167195.35 kcal/mol

Dipole moment: 3.44 D

Imaginary frequencies: 0

Optimized x, y, z coordinates

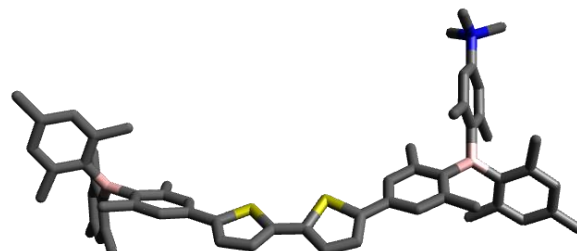
C	9.90704	3.42036	1.43045
C	9.71436	2.36777	0.54049
C	11.20562	-0.78372	-0.49921
C	12.20847	-1.25939	-1.34748
C	12.00024	-1.41959	-2.7186
C	10.74193	-1.0975	-3.22966
C	9.70528	-0.64934	-2.40743
C	-10.45974	-0.3902	0.14389
C	-11.51121	-0.96123	0.85663
C	-11.34389	-1.43751	2.1718
C	-10.05217	-1.35232	2.72707
C	-8.98202	-0.81782	2.01431
C	-8.74703	2.76466	-0.3102
C	-8.85356	3.97063	-0.9985
C	-8.39712	4.11156	-2.32377
C	-7.78664	2.98893	-2.91635
C	-7.63957	1.78679	-2.22937
C	-10.77026	0.09692	-1.25748
N	-8.54719	5.30155	-3.01781
N	-12.40563	-1.96224	2.89147
C	-6.96239	0.65306	-2.97239
C	-9.28617	2.73779	1.10621
C	-7.64006	-0.78403	2.71705
C	10.24529	2.55964	-0.86585
C	7.79726	-0.06047	2.81854
C	11.53999	-0.62875	0.97007
C	8.3729	-0.33708	-3.0553
C	6.20202	1.5856	-0.34134
C	8.46527	-2.9968	0.0777
C	-7.74864	-2.64141	-0.81988
C	-5.35492	1.68419	0.52713
C	13.09125	-1.95069	-3.61383
N	9.69765	4.38507	3.65702
C	-12.14365	-2.65832	4.13795
C	-13.66596	-2.21408	2.21769
C	-8.99831	6.48545	-2.31017
C	-7.85037	5.4808	-4.2786
C	10.25423	5.63525	3.1738
C	9.04526	4.37158	4.95381
H	4.03455	-4.6187	-1.10508
H	1.48145	-5.19822	-1.1254
H	-3.38099	-4.61113	0.0559
H	-0.84738	-5.26615	-0.04195
H	-3.25608	0.05906	0.42706
H	-5.24348	-3.53023	-0.82499
H	4.05815	0.03818	-0.54384
H	5.93433	-3.78919	-0.06529
H	8.4219	2.08487	4.17685
H	10.4087	4.30977	1.07053
H	13.18134	-1.50603	-0.92778
H	10.5613	-1.20175	-4.29728
H	-12.47654	-1.03621	0.37189
H	-9.87027	-1.7083	3.73342
H	-9.29861	4.81432	-0.48614
H	-7.41582	3.04671	-3.93206
C	3.53402	-2.62534	-0.42756
C	3.2603	-3.92376	-0.80329
C	1.87982	-4.23989	-0.81467
C	1.07045	-3.1873	-0.43648
S	2.04313	-1.78162	-0.04952
C	4.8294	-1.95983	-0.32416
C	-0.36931	-3.17416	-0.32865
S	-1.29496	-1.68947	-0.4338
C	-2.81353	-2.54189	-0.22333
C	-2.5832	-3.89661	-0.10667
C	-1.21349	-4.25331	-0.15981
C	-4.08656	-1.82693	-0.19672
C	-4.16272	-0.47014	0.14678
C	-5.37657	0.21576	0.1585
C	-6.58316	-0.4623	-0.14332
C	-6.51205	-1.83878	-0.47412
C	-5.28058	-2.48967	-0.51743
C	4.94856	-0.56457	-0.38806
C	6.18368	0.07259	-0.2779
C	7.37027	-0.69023	-0.13649
C	7.25511	-2.10243	-0.08784
C	6.00316	-2.70981	-0.15846
B	8.77416	0.02095	-0.06408
B	-7.96745	0.29454	-0.11556
C	-9.15652	-0.3068	0.70162
C	-8.1281	1.63344	-0.90533
C	9.92337	-0.4755	-1.01872
C	9.01731	1.19297	0.9332
C	8.54615	1.13888	2.27319
C	8.78082	2.18515	3.16026
C	9.46519	3.35254	2.76691

H	-10.02083	-0.22576	-1.98486
H	-11.74245	-0.2807	-1.58666
H	-10.79657	1.18909	-1.3073
H	-5.9534	0.46892	-2.59311
H	-7.50866	-0.28895	-2.87545
H	-6.88516	0.88478	-4.03823
H	-8.58826	2.27262	1.80724
H	-9.48801	3.75363	1.45749
H	-10.21564	2.16545	1.17233
H	-6.94972	-1.52369	2.30216
H	-7.14875	0.18804	2.62233
H	-7.75949	-0.994	3.78351
H	10.52289	3.60443	-1.03012
H	11.12858	1.94202	-1.0499
H	9.51119	2.28533	-1.6278
H	8.27588	-1.00548	2.5492
H	7.74294	-0.01338	3.90953
H	6.7756	-0.10797	2.43186
H	11.6416	0.42362	1.25092
H	10.76669	-1.04729	1.62035
H	12.48147	-1.13426	1.20239
H	7.61632	-1.08421	-2.7992
H	7.97479	0.63167	-2.73929
H	8.47147	-0.31506	-4.14404
H	5.23461	1.96578	-0.68048
H	6.41582	2.02398	0.63762
H	6.9686	1.96414	-1.02318
H	9.12772	-2.65164	0.87695
H	8.15825	-4.01812	0.31883
H	9.06688	-3.02816	-0.83486
H	-8.39355	-2.12048	-1.53359
H	-7.47159	-3.60338	-1.26007
H	-8.36013	-2.83412	0.06613
H	-4.38236	1.96134	0.94304
H	-5.54675	2.31704	-0.34396
H	-6.11983	1.93622	1.2674
H	14.08286	-1.68	-3.23918
H	13.05433	-3.0456	-3.67437
H	12.99417	-1.56606	-4.63331
H	-11.49147	-3.53538	4.00758
H	-11.67004	-1.9924	4.86733
H	-13.08949	-2.9943	4.56474
H	-14.07413	-1.29005	1.79486
H	-13.57618	-2.94853	1.40234
H	-14.38853	-2.5925	2.9419
H	-9.98477	6.32128	-1.86392
H	-8.31039	6.79236	-1.50715
H	-9.0897	7.31085	-3.01739
H	-6.75733	5.40207	-4.17627
H	-8.17383	4.73731	-5.01503
H	-8.08749	6.4667	-4.68035
H	9.60448	6.13456	2.4391
H	10.39973	6.3111	4.01723
H	11.23107	5.47407	2.70524
H	9.34164	3.49129	5.53489

H	9.34906	5.25547	5.5156
H	7.94785	4.37164	4.87589

Cat¹⁺

TD-DFT CAM-B3LYP 6-31G(d,p), gas
phase, S₀

Point group: C₁

Total energy: -2073358.59 kcal/mol

Dipole moment: 41.42 D

Imaginary frequencies: 0

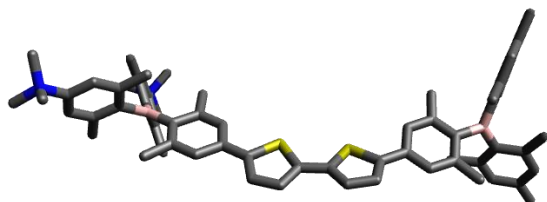
Optimized x, y, z coordinates

C	-2.61631	-2.45432	-1.22375
C	-2.31362	-3.6631	-1.81997
C	-0.93189	-3.87247	-2.02585
C	-0.14404	-2.81837	-1.59872
S	-1.1436	-1.5424	-0.93591
C	-3.91843	-1.92606	-0.85001
C	1.29093	-2.70074	-1.67331
S	2.18495	-1.5498	-0.69987
C	3.71762	-2.07182	-1.37194
C	3.51392	-3.0809	-2.29151
C	2.15505	-3.43283	-2.46478
C	4.97569	-1.46092	-0.95259
C	5.10063	-0.80425	0.27899
C	6.30707	-0.23803	0.68756
C	7.44278	-0.29376	-0.15847
C	7.31645	-0.94498	-1.41195
C	6.10348	-1.52135	-1.78377
C	-4.05041	-0.85532	0.04951
C	-5.2924	-0.33173	0.39199
C	-6.48486	-0.90063	-0.13317
C	-6.35775	-2.00531	-1.02393
C	-5.09791	-2.47492	-1.38125
B	-7.88959	-0.32013	0.198
B	8.80979	0.35412	0.28136
C	9.56043	1.32385	-0.69647
C	9.4077	0.02478	1.69324
C	-9.11428	-1.22448	0.5463

C	-8.0899	1.25926	0.18089	H	10.10282	-2.61197	3.75464
C	-7.71816	2.01669	-0.95088	H	11.27248	-0.9083	-0.34905
C	-7.90623	3.40621	-0.97005	H	12.73511	-0.02968	-0.80206
C	-8.4394	4.04352	0.14072	H	11.94937	0.27361	0.7539
C	-8.80524	3.3189	1.27089	H	12.15517	-1.02802	5.53585
C	-8.64686	1.93131	1.29514	H	10.91088	-0.05443	6.32057
C	-10.39295	-1.01415	-0.03101	H	10.64286	-1.78418	6.03835
C	-11.46816	-1.82688	0.33031	H	12.11161	4.83082	-2.84747
C	-11.33728	-2.8414	1.28138	H	12.46999	3.49202	-3.93791
C	-10.0821	-3.03326	1.86319	H	10.98725	4.44015	-4.15033
C	-8.97321	-2.26511	1.50364	H	7.93443	-2.54067	1.27673
C	10.94643	1.16231	-0.95201	H	9.38756	-2.43767	0.29834
C	11.59537	2.01501	-1.84739	H	9.38699	-3.42606	1.75978
C	10.92788	3.06248	-2.48521	H	8.85398	2.80384	1.71084
C	9.56697	3.22648	-2.22123	H	9.99634	3.16194	3.00882
C	8.87523	2.3736	-1.35848	H	10.57563	2.75753	1.38681
C	9.87074	1.0621	2.54244	H	6.78251	1.87287	-1.6457
C	10.37448	0.75574	3.80847	H	7.11698	2.61972	-0.0936
C	10.47529	-0.55999	4.26425	H	7.11922	3.60695	-1.55641
C	10.03049	-1.57953	3.42045	H	-9.29181	1.88718	3.35595
C	9.48933	-1.31123	2.16156	H	-9.97827	0.59924	2.34819
C	11.76666	0.06632	-0.30424	H	-8.31405	0.4932	2.88446
C	11.07201	-0.8725	5.61274	H	-7.64123	0.47596	-2.47905
C	11.66071	4.00256	-3.40793	H	-7.11429	2.07202	-3.02391
C	9.0258	-2.48843	1.32926	H	-6.07238	1.08029	-1.98845
C	9.81924	2.52153	2.14067	H	-10.67215	1.0574	-0.62745
C	7.39716	2.63042	-1.15085	H	-9.86944	0.07332	-1.84581
C	-9.08016	1.192	2.53957	H	-11.59986	-0.11053	-1.5713
C	-7.10673	1.3797	-2.17812	H	-6.96007	-3.07499	1.50968
C	-10.64246	0.05726	-1.07207	H	-7.14608	-1.67598	2.5463
C	-7.65712	-2.57353	2.18716	H	-7.81975	-3.22961	3.0456
C	-5.3091	0.82072	1.37528	H	-4.3378	0.91638	1.86635
C	-7.55453	-2.68564	-1.65583	H	-5.52434	1.77319	0.8805
C	8.47323	-1.04818	-2.38292	H	-6.06045	0.68828	2.15857
C	6.34793	0.4321	2.0443	H	-8.27549	-1.9736	-2.06656
C	-12.50462	-3.72068	1.6466	H	-7.23292	-3.34037	-2.46917
N	-8.64087	5.54123	0.1645	H	-8.10026	-3.29418	-0.92975
C	-8.20726	6.20761	-1.11325	H	9.39263	-1.38502	-1.89581
C	-10.10652	5.85033	0.36873	H	8.24175	-1.75766	-3.18166
C	-7.83102	6.14061	1.29175	H	8.69902	-0.08117	-2.84034
H	-3.06716	-4.40083	-2.0677	H	5.33686	0.55581	2.44139
H	-0.51541	-4.78002	-2.44468	H	6.92689	-0.15493	2.76233
H	4.32851	-3.56795	-2.81281	H	6.81299	1.42111	2.00354
H	1.81356	-4.19255	-3.15748	H	-13.45716	-3.20589	1.49478
H	4.24628	-0.75854	0.94889	H	-12.51912	-4.62469	1.02592
H	6.02479	-2.00257	-2.75362	H	-12.45007	-4.04466	2.68954
H	-3.15986	-0.43501	0.50726	H	-8.38575	7.277	-1.0094
H	-5.02715	-3.27995	-2.10481	H	-7.14708	6.0209	-1.2722
H	-7.61669	3.94545	-1.86144	H	-8.79301	5.81117	-1.94018
H	-9.22211	3.80497	2.14633	H	-10.23882	6.93269	0.37311
H	-12.43472	-1.66644	-0.14107	H	-10.43271	5.42818	1.31557
H	-9.96259	-3.80937	2.61495	H	-10.66467	5.39647	-0.44879
H	12.65263	1.86056	-2.04998	H	-6.78432	5.88981	1.12629
H	9.02839	4.03782	-2.70559	H	-7.97468	7.22152	1.28974
H	10.70255	1.566	4.45548	H	-8.16527	5.71893	2.23597

Cat²⁺

TD-DFT CAM-B3LYP 6-31G(d,p), gas
phase, S₀

Point group: C₁

Total energy: -2157601.66 kcal/mol

Dipole moment: 79.15 D

Imaginary frequencies: 0

Optimized x, y, z coordinates

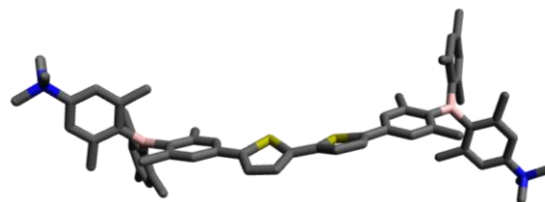
C	-2.07149	-2.08916	-1.41167	C	-7.99539	2.51562	1.04584
C	-1.80164	-3.19227	-2.21298	C	-9.74553	-0.59051	-0.32034
C	-0.43725	-3.48543	-2.34997	C	-10.80082	-1.44974	0.01835
C	0.3923	-2.61357	-1.64887	C	-10.62823	-2.38871	1.02551
S	-0.56271	-1.41474	-0.80559	C	-9.41883	-2.47982	1.7074
C	-3.347	-1.51286	-1.07333	C	-8.34991	-1.64712	1.36588
C	1.82279	-2.63568	-1.57688	C	11.73755	0.45956	-0.7752
S	2.75126	-1.33377	-0.85679	C	12.55213	0.96561	-1.78992
C	4.26657	-2.15371	-1.17102	C	12.06144	1.83093	-2.76995
C	4.03432	-3.35798	-1.81531	C	10.70673	2.16569	-2.72646
C	2.67155	-3.62986	-2.04157	C	9.85191	1.65311	-1.74885
C	5.53947	-1.56286	-0.78154	C	10.35309	1.40639	2.46331
C	5.62025	-0.58564	0.22086	C	10.69699	1.42296	3.8166
C	6.84004	-0.03166	0.60289	C	10.59781	0.28421	4.61842
C	8.0363	-0.43408	-0.04208	C	10.11271	-0.88686	4.03279
C	7.9579	-1.41308	-1.06487	C	9.72587	-0.93497	2.69228
C	6.72713	-1.96655	-1.41047	C	12.37731	-0.46007	0.24415
C	-3.45324	-0.3279	-0.31625	C	11.02882	0.31025	6.06229
C	-4.67395	0.24827	-0.00246	C	12.9722	2.40598	-3.82391
C	-5.90019	-0.37273	-0.40731	C	9.20667	-2.25308	2.15714
C	-5.79444	-1.59051	-1.15813	C	10.51645	2.6939	1.68241
C	-4.55518	-2.11485	-1.48599	C	8.39729	2.07187	-1.79867
B	-7.26342	0.2385	-0.05469	C	-8.38449	1.80028	2.31801
B	9.42628	0.19675	0.36686	C	-6.56039	1.9004	-2.46485
C	10.35768	0.79175	-0.7422	C	-9.98187	0.40435	-1.43277
C	9.84934	0.21741	1.87467	C	-7.05261	-1.83555	2.11866
C	-8.49785	-0.68575	0.33321	C	-4.6258	1.51244	0.83254
C	-7.47623	1.81419	-0.06878	C	-7.00311	-2.3361	-1.6882
C	-7.13186	2.55178	-1.22556	C	9.18462	-1.89162	-1.81026
C	-7.28992	3.94538	-1.25327	C	6.83573	0.99915	1.71051
C	-7.76758	4.61212	-0.13467	N	-11.73167	-3.34674	1.40668
C	-8.1248	3.90608	1.0106	C	-12.98588	-3.14481	0.5973
				C	-11.26393	-4.76876	1.17883
				C	-12.09123	-3.15775	2.86418
				N	-7.90409	6.11606	-0.11632
				C	-7.48694	6.75666	-1.41504
				C	-9.34599	6.49513	0.13866
				C	-7.02657	6.68691	0.97735
				H	-2.57586	-3.76713	-2.70604
				H	-0.0535	-4.29654	-2.9552
				H	4.83245	-4.03805	-2.08365
				H	2.3122	-4.53926	-2.50779
				H	4.71698	-0.27287	0.73791
				H	6.68695	-2.70236	-2.20731
				H	-2.54712	0.15445	0.03694
				H	-4.51696	-3.02006	-2.08149
				H	-7.01381	4.46752	-2.15887
				H	-8.50015	4.41186	1.89322
				H	-11.72913	-1.35637	-0.52804
				H	-9.27093	-3.20345	2.50127
				H	13.60115	0.68058	-1.81431
				H	10.30496	2.8411	-3.47816
				H	11.05958	2.34892	4.25659
				H	10.03166	-1.78646	4.6384
				H	11.78768	-1.36335	0.42365

H	13.36812	-0.77266	-0.09504
H	12.49287	0.03293	1.21352
H	12.09186	0.05744	6.15739
H	10.89053	1.30145	6.50328
H	10.46826	-0.41374	6.66049
H	13.46345	3.31726	-3.46148
H	13.7615	1.70027	-4.09808
H	12.41924	2.67152	-4.72919
H	8.12715	-2.22178	1.98208
H	9.67282	-2.52906	1.20694
H	9.40749	-3.05917	2.86745
H	9.6407	2.92875	1.07094
H	10.68173	3.53306	2.36307
H	11.36767	2.64268	0.99768
H	7.75262	1.25483	-2.13608
H	8.02109	2.38819	-0.82148
H	8.26531	2.90919	-2.4889
H	-8.64995	2.50735	3.1071
H	-9.23827	1.13788	2.15366
H	-7.5655	1.17973	2.69332
H	-7.05908	0.96029	-2.70689
H	-6.64642	2.56322	-3.32937
H	-5.50237	1.65951	-2.32565
H	-9.94473	1.4311	-1.05956
H	-9.22024	0.31992	-2.21332
H	-10.95479	0.24999	-1.90463
H	-6.31879	-2.36482	1.50427
H	-6.59206	-0.88481	2.39405
H	-7.21144	-2.41303	3.03258
H	-3.63066	1.64017	1.26377
H	-4.84249	2.40465	0.23746
H	-5.34221	1.49622	1.65763
H	-7.73945	-1.66839	-2.14278
H	-6.69696	-3.05513	-2.45107
H	-7.5198	-2.89324	-0.90088
H	10.00707	-2.13973	-1.13388
H	8.95515	-2.785	-2.39669
H	9.56152	-1.12323	-2.49044
H	5.81465	1.32007	1.93353
H	7.27742	0.59955	2.62719
H	7.41496	1.88875	1.448
H	-13.7223	-3.87174	0.93662
H	-13.3592	-2.13562	0.76021
H	-12.76341	-3.30753	-0.45545
H	-12.07477	-5.44835	1.44186
H	-10.39453	-4.96435	1.80114
H	-10.99867	-4.87385	0.1279
H	-12.41392	-2.12702	3.00328
H	-12.89456	-3.84986	3.1173
H	-11.2179	-3.35902	3.47905
H	-7.61655	7.83297	-1.31187
H	-6.44114	6.52665	-1.60887
H	-8.11825	6.3828	-2.21877
H	-9.42573	7.58237	0.13952
H	-9.65713	6.09746	1.10117

H	-9.95518	6.06617	-0.65558
H	-5.99859	6.38831	0.77745
H	-7.12125	7.77294	0.96858
H	-7.34673	6.29074	1.93754

Cat(i)²⁺

TD-DFT CAM-B3LYP 6-31G(d,p), gas
phase, S₀



Point group: C₂

Total energy: -2157604.10 kcal/mol

Dipole moment: 5.13 D

Imaginary frequencies: 0

Optimized x, y, z coordinates

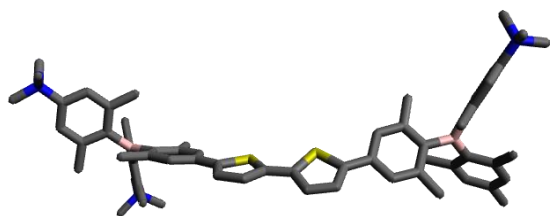
C	1.3291	2.8835	2.18084
C	0.97884	2.76766	3.5113
C	0.3817	1.52911	3.84089
C	0.27178	0.66876	2.76541
S	0.92976	1.40771	1.32093
H	1.10941	3.57189	4.22482
H	0.00804	1.28174	4.82683
C	-0.27178	-0.66876	2.76541
C	-0.3817	-1.52911	3.84089
S	-0.92976	-1.40771	1.32093
C	-0.97884	-2.76766	3.5113
H	-0.00804	-1.28174	4.82683
C	-1.3291	-2.8835	2.18084
H	-1.10941	-3.57189	4.22482
C	1.94026	4.01937	1.50077
C	1.87829	4.16791	0.10771
C	2.61426	5.00974	2.23317
C	2.43548	5.26611	-0.54379
H	1.35751	3.42051	-0.48372
C	3.20248	6.10667	1.61119
H	2.69597	4.91021	3.31057
C	3.11696	6.26678	0.2016
C	2.2902	5.32601	-2.05014
C	3.90012	7.11803	2.49685
B	3.75604	7.48877	-0.5302
H	1.97064	4.35643	-2.43945

H	1.54934	6.07123	-2.35243	H	-2.69597	-4.91021	3.31057
H	3.22327	5.59522	-2.55181	C	-3.11696	-6.26678	0.2016
H	3.60164	8.14488	2.26743	C	-2.2902	-5.32601	-2.05014
H	3.66197	6.9358	3.54738	C	-3.90012	-7.11803	2.49685
H	4.98811	7.06879	2.3897	B	-3.75604	-7.48877	-0.5302
C	5.23457	7.94022	-0.15402	H	-1.97064	-4.35643	-2.43945
C	2.98676	8.29172	-1.62449	H	-1.54934	-6.07123	-2.35243
C	5.51005	9.27953	0.19715	H	-3.22327	-5.59522	-2.55181
C	6.30251	7.01164	-0.18118	H	-3.60164	-8.14488	2.26743
C	3.59768	8.65741	-2.85249	H	-3.66197	-6.9358	3.54738
C	1.64707	8.70583	-1.3919	H	-4.98811	-7.06879	2.3897
C	6.81677	9.67669	0.51555	C	-5.23457	-7.94022	-0.15402
C	4.4293	10.33535	0.24647	C	-2.98676	-8.29172	-1.62449
C	7.60283	7.42805	0.11422	C	-5.51005	-9.27953	0.19715
C	6.0877	5.55713	-0.5303	C	-6.30251	-7.01164	-0.18118
C	2.88205	9.38915	-3.80059	C	-3.59768	-8.65741	-2.85249
C	5.01111	8.24508	-3.20877	C	-1.64707	-8.70583	-1.3919
C	0.97884	9.46738	-2.35202	C	-6.81677	-9.67669	0.51555
C	0.89725	8.37575	-0.11766	C	-4.4293	-10.33535	0.24647
C	7.84995	8.75256	0.46233	C	-7.60283	-7.42805	0.11422
H	6.98093	10.71015	0.78784	C	-6.0877	-5.55713	-0.5303
H	3.5356	9.98181	0.76581	C	-2.88205	-9.38915	-3.80059
H	4.78164	11.2334	0.75996	C	-5.01111	-8.24508	-3.20877
H	4.11306	10.61661	-0.76148	C	-0.97884	-9.46738	-2.35202
H	8.40102	6.69517	0.06946	C	-0.89725	-8.37575	-0.11766
H	5.54741	5.03995	0.26689	C	-7.84995	-8.75256	0.46233
H	5.49063	5.44003	-1.43811	H	-6.98093	-10.71015	0.78784
H	7.04054	5.04584	-0.68817	H	-3.5356	-9.98181	0.76581
C	1.57267	9.81643	-3.5671	H	-4.78164	-11.2334	0.75996
H	3.35565	9.63276	-4.74832	H	-4.11306	-10.61661	-0.76148
H	5.20932	7.19362	-2.98179	H	-8.40102	-6.69517	0.06946
H	5.19201	8.38725	-4.27685	H	-5.54741	-5.03995	0.26689
H	5.75572	8.83655	-2.66619	H	-5.49063	-5.44003	-1.43811
H	-0.03865	9.79259	-2.15045	H	-7.04054	-5.04584	-0.68817
H	0.58417	7.32793	-0.09406	C	-1.57267	-9.81643	-3.5671
H	1.4975	8.54051	0.78132	H	-3.35565	-9.63276	-4.74832
H	0.0004	8.99422	-0.0349	H	-5.20932	-7.19362	-2.98179
C	0.83272	10.64721	-4.58237	H	-5.19201	-8.38725	-4.27685
C	9.7788	8.33631	1.9474	H	-5.75572	-8.83655	-2.66619
C	9.40757	10.60403	1.1396	H	0.03865	-9.79259	-2.15045
H	1.18042	10.44111	-5.59807	H	-0.58417	-7.32793	-0.09406
H	-0.24391	10.46121	-4.54225	H	-1.4975	-8.54051	0.78132
H	0.98502	11.71713	-4.39537	H	-0.0004	-8.99422	-0.0349
H	10.80196	8.64095	2.16913	C	-0.83272	-10.64721	-4.58237
H	9.12663	8.52754	2.79829	C	-9.7788	-8.33631	1.9474
H	9.74917	7.28078	1.69016	C	-9.40757	-10.60403	1.1396
H	10.45822	10.80051	1.34851	H	-1.18042	-10.44111	-5.59807
H	9.07489	11.21414	0.30222	H	0.24391	-10.46121	-4.54225
H	8.8081	10.8089	2.02438	H	-0.98502	-11.71713	-4.39537
C	-1.94026	-4.01937	1.50077	H	-10.80196	-8.64095	2.16913
C	-1.87829	-4.16791	0.10771	H	-9.12663	-8.52754	2.79829
C	-2.61426	-5.00974	2.23317	H	-9.74917	-7.28078	1.69016
C	-2.43548	-5.26611	-0.54379	H	-10.45822	-10.80051	1.34851
H	-1.35751	-3.42051	-0.48372	H	-9.07489	-11.21414	0.30222
C	-3.20248	-6.10667	1.61119	H	-8.8081	-10.8089	2.02438

C	-10.1457	-8.89688	-0.4332
H	-10.11562	-7.83936	-0.68207
H	-9.75124	-9.4825	-1.26225
H	-11.16639	-9.19953	-0.19773
N	-9.27384	-9.14904	0.7766
C	10.1457	8.89688	-0.4332
H	10.11562	7.83936	-0.68207
H	9.75124	9.4825	-1.26225
H	11.16639	9.19953	-0.19773
N	9.27384	9.14904	0.7766

Cat³⁺

TD-DFT CAM-B3LYP 6-31G(d,p), gas
phase, S₀

Point group: C₁

Total energy: -2241823.38 kcal/mol

Dipole moment: 40.50 D

Imaginary frequencies: 0

Optimized x, y, z coordinates

C	3.66113	-0.39604	-2.25592
C	3.36874	-0.55302	-3.59553
C	1.99683	-0.76507	-3.85821
C	1.21319	-0.77367	-2.71933
S	2.20092	-0.51635	-1.29429
C	4.96861	-0.15183	-1.65011
C	-0.21627	-0.95873	-2.66673
S	-1.2019	-0.35506	-1.35311
C	-2.67825	-0.94517	-2.10438
C	-2.38031	-1.56229	-3.30777
C	-1.00788	-1.57447	-3.62283
C	-3.98247	-0.7422	-1.50442
C	-4.17979	0.12982	-0.41828
C	-5.4383	0.37046	0.11862
C	-6.58836	-0.30243	-0.39671
C	-6.38359	-1.22309	-1.47203
C	-5.11627	-1.40934	-2.0065
C	5.2864	-0.59094	-0.35759
C	6.54948	-0.37607	0.19261
C	7.53685	0.33388	-0.5365

C	7.21248	0.79398	-1.84057
C	5.95308	0.53318	-2.37658
B	8.96089	0.61862	0.05385
B	-8.00033	-0.0213	0.15872
C	-9.05497	-1.19376	0.35246
C	-8.44425	1.4578	0.53395
C	9.58222	2.04713	0.02491
C	9.80709	-0.56938	0.68748
C	10.05322	-1.75416	-0.03985
C	10.87973	-2.75576	0.49001
C	11.43576	-2.59502	1.75087
C	11.17488	-1.45308	2.50186
C	10.37467	-0.43481	1.97786
C	10.93413	2.26654	-0.35566
C	11.46093	3.55777	-0.35333
C	10.70575	4.66326	0.04697
C	9.38307	4.44277	0.43723
C	8.80499	3.1726	0.41401
C	-10.35057	-1.1346	-0.20492
C	-11.2484	-2.19995	-0.04328
C	-10.87236	-3.31389	0.69357
C	-9.61029	-3.38233	1.27606
C	-8.69451	-2.34096	1.10379
C	-8.99533	1.77732	1.79378
C	-9.36884	3.09411	2.09927
C	-9.2199	4.0919	1.14636
C	-8.69908	3.79686	-0.10964
C	-8.29861	2.49484	-0.4225
C	-10.81286	0.05046	-1.02122
N	-9.60763	5.52203	1.43681
N	-11.80627	-4.48555	0.88002
C	-7.70639	2.25984	-1.79381
C	-9.17718	0.7312	2.86925
C	-7.32672	-2.50206	1.72721
C	10.15954	0.79692	2.82698
C	9.46782	-1.98541	-1.41414
C	11.84635	1.14621	-0.81215
C	7.35792	3.06019	0.84812
C	6.81367	-0.89968	1.58767
C	8.18967	1.5712	-2.69695
C	-7.51365	-1.99704	-2.12054
C	-5.5086	1.33748	1.28312
C	11.29144	6.0502	0.02849
N	12.34684	-3.64258	2.34689
C	12.5499	-4.82534	1.43729
C	13.70582	-3.03284	2.61504
C	11.75486	-4.15518	3.64054
C	-13.13713	-4.28711	0.20093
C	-11.1754	-5.73164	0.29409
C	-12.07179	-4.69636	2.35533
C	-10.15716	5.70805	2.82771
C	-8.39018	6.41272	1.30285
C	-10.67387	5.96939	0.45949
H	4.13041	-0.53437	-4.36499
H	1.58548	-0.88561	-4.85283


```

H   -3.13551  -1.98648  -3.95763
H   -0.59645  -2.03391  -4.51251
H   -3.3257   0.64883   0.00621
H   -4.99923  -2.10041  -2.83359
H    4.54414  -1.13686   0.2179
H    5.7168   0.90244  -3.36928
H   11.06109  -3.63566  -0.11144
H   11.59444  -1.31849   3.49277
H   12.48911   3.70963  -0.67185
H    8.78324   5.28794   0.76465
H  -12.22135  -2.12037  -0.50789
H   -9.30355  -4.24332   1.85924
H   -9.76753   3.29488   3.08397
H   -8.58031   4.56451  -0.86597
H  -10.09474   0.30526  -1.80545
H  -11.76989  -0.15192  -1.50685
H  -10.93279   0.93843  -0.39477
H   -6.62008   2.1472   -1.73585
H   -8.08592   1.34831  -2.25981
H   -7.92598   3.09579  -2.462
H   -8.25773   0.16397   3.03896
H   -9.46208   1.18539   3.82073
H   -9.95221   0.01139   2.59267
H   -6.5754   -2.72786   0.96537
H   -6.99157  -1.59307   2.2313
H   -7.32347  -3.31291   2.45933
H   10.43976   0.60921   3.86649
H   10.75657   1.63442   2.45624
H    9.11847   1.12668   2.81438
H    9.66652  -1.14687  -2.08683
H    9.8851   -2.88455  -1.87354
H    8.38188  -2.09727  -1.36422
H   12.20825   0.54737   0.02995
H   11.35277   0.45977  -1.50542
H   12.72039   1.55423  -1.32493
H    6.69483   2.87602  -0.00201
H    7.19111   2.24511   1.55775
H    7.03497   3.98666   1.3287
H    5.89303  -1.27249   2.04254
H    7.53818  -1.71946   1.57904
H    7.21454  -0.12511   2.24884
H    9.18893   1.12793  -2.70257
H    7.84044   1.61496  -3.73118
H    8.30745   2.59659  -2.33615
H   -8.37486  -1.36542  -2.35343
H   -7.17519  -2.44576  -3.0567
H   -7.87467  -2.80647  -1.47926
H   -4.51301   1.49697   1.7027
H   -5.89638   2.31397   0.97724
H   -6.15074   0.97589   2.09011
H   12.36416   6.03465   0.23922
H   11.16083   6.51194  -0.95756
H   10.80496   6.70023   0.76023
H   13.21541  -5.52398   1.94227
H   11.58924  -5.29957   1.24624

```

```

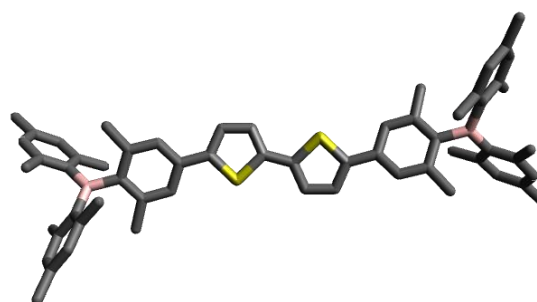
H    13.003   -4.48832   0.50708
H    14.3575  -3.80191   3.03042
H    13.59769  -2.21213   3.31933
H    14.10177  -2.66043   1.67144
H    10.77453  -4.57567   3.4213
H    12.41847  -4.917     4.0503
H    11.65495  -3.33031   4.34112
H   -13.74126  -5.17377   0.38701
H   -13.62745  -3.41102   0.621
H   -12.97974  -4.16547  -0.869
H   -11.86733  -6.56421   0.42197
H   -10.24189  -5.93862   0.81097
H   -10.9832   -5.55011  -0.76233
H   -12.51584  -3.78554   2.75429
H   -12.7549   -5.53824   2.4687
H   -11.13408  -4.90603   2.86338
H   -10.4088   6.76063   2.94833
H   -11.05116   5.09861   2.94499
H   -9.39855   5.42388   3.55441
H   -8.68311   7.43785   1.53005
H   -8.00885   6.34952   0.28696
H   -7.63525   6.06359   2.00577
H   -11.53278   5.30875   0.56774
H   -10.94881   6.99826   0.69204
H   -10.28295   5.90763  -0.5528

```

11.8.2.2 Sulfur Atoms of Bithiophene on Opposite Sides

Neut0

TD-DFT CAM-B3LYP 6-31G(d,p), gas phase, S_0



Point group: C_2

Total energy: -1989087.35 kcal/mol

Dipole moment: 0.15 D

Imaginary frequencies: 0

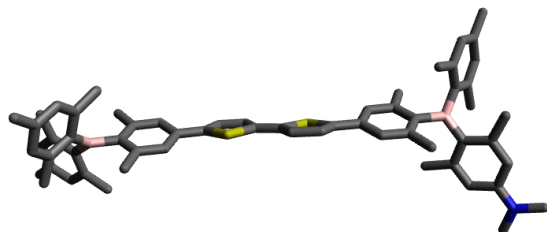
Optimized x, y, z coordinates

C	0.18473	0.69669	-0.31627	H	-5.41898	11.24177	0.48076
C	1.43729	1.26254	-0.44564	H	-3.09041	10.01711	-1.87341
C	1.42634	2.67795	-0.40302	H	-4.29621	11.24864	-1.49053
C	0.16965	3.22238	-0.24378	H	-2.57919	11.54228	-1.17734
S	-1.02967	1.94681	-0.12052	H	-4.17099	8.89946	3.83715
H	2.33355	0.67133	-0.59358	H	-2.15693	7.851	3.9149
H	2.31483	3.28563	-0.5233	H	-1.96142	6.90209	2.43485
C	-0.18473	-0.69669	-0.31627	H	-0.86565	8.22893	2.77229
C	-1.43729	-1.26254	-0.44564	C	2.05681	12.9657	-2.63447
S	1.02967	-1.94681	-0.12052	C	-6.1615	10.56655	3.01392
C	-1.42634	-2.67795	-0.40302	H	2.698	13.49504	-1.92373
H	-2.33355	-0.67133	-0.59358	H	2.69341	12.52201	-3.40553
C	-0.16965	-3.22238	-0.24378	H	1.42599	13.71684	-3.12595
H	-2.31483	-3.28563	-0.5233	H	-6.99493	10.78688	2.34064
C	-0.21129	4.62953	-0.17033	H	-6.48761	9.80045	3.72344
C	-1.51208	5.05767	-0.46943	H	-5.95832	11.47799	3.58984
C	0.72784	5.60163	0.20549	C	0.21129	-4.62953	-0.17033
C	-1.88093	6.3992	-0.38525	C	1.51208	-5.05767	-0.46943
H	-2.25069	4.329	-0.79132	C	-0.72784	-5.60163	0.20549
C	0.40001	6.95461	0.25679	C	1.88093	-6.3992	-0.38525
H	1.73072	5.2914	0.48147	H	2.25069	-4.329	-0.79132
C	-0.9225	7.38177	-0.02955	C	-0.40001	-6.95461	0.25679
C	-3.3149	6.75519	-0.71626	H	-1.73072	-5.2914	0.48147
C	1.48873	7.92665	0.66009	C	0.9225	-7.38177	-0.02955
B	-1.31485	8.90194	0.04653	C	3.3149	-6.75519	-0.71626
H	-3.82204	5.90595	-1.1817	C	-1.48873	-7.92665	0.66009
H	-3.87445	7.03516	0.18054	B	1.31485	-8.90194	0.04653
H	-3.38469	7.60224	-1.40444	H	3.82204	-5.90595	-1.1817
H	1.15477	8.62857	1.42948	H	3.87445	-7.03516	0.18054
H	2.35489	7.38883	1.05465	H	3.38469	-7.60224	-1.40444
H	1.82091	8.52999	-0.18922	H	-1.15477	-8.62857	1.42948
C	-0.41888	9.9773	-0.66495	H	-2.35489	-7.38883	1.05465
C	-2.60099	9.33999	0.83309	H	-1.82091	-8.52999	-0.18922
C	-0.00591	11.14735	0.02097	C	0.41888	-9.9773	-0.66495
C	0.00591	9.80175	-2.00612	C	2.60099	-9.33999	0.83309
C	-3.5439	10.22328	0.24938	C	0.00591	-11.14735	0.02097
C	-2.8555	8.85757	2.14172	C	-0.00591	-9.80175	-2.00612
C	0.812	12.08118	-0.61917	C	3.5439	-10.22328	0.24938
C	-0.39985	11.42307	1.45702	C	2.8555	-8.85757	2.14172
C	0.79624	10.77429	-2.62254	C	-0.812	-12.08118	-0.61917
C	-0.38393	8.58839	-2.82423	C	0.39985	-11.42307	1.45702
C	-4.69462	10.58305	0.95446	C	-0.79624	-10.77429	-2.62254
C	-3.36785	10.78524	-1.14589	C	0.38393	-8.58839	-2.82423
C	-4.00137	9.26644	2.82739	C	4.69462	-10.58305	0.95446
C	-1.90941	7.91194	2.85175	C	3.36785	-10.78524	-1.14589
C	1.21642	11.92063	-1.9456	C	4.00137	-9.26644	2.82739
H	1.13934	12.96039	-0.06887	C	1.90941	-7.91194	2.85175
H	-0.25659	10.55293	2.10395	C	-1.21642	-11.92063	-1.9456
H	0.19738	12.24251	1.86593	H	-1.13934	-12.96039	-0.06887
H	-1.4549	11.69963	1.53747	H	0.25659	-10.55293	2.10395
H	1.09793	10.63057	-3.65763	H	-0.19738	-12.24251	1.86593
H	-0.16201	8.75374	-3.88194	H	1.4549	-11.69963	1.53747
H	0.15706	7.69417	-2.50167	H	-1.09793	-10.63057	-3.65763
H	-1.44927	8.35502	-2.74191	H	0.16201	-8.75374	-3.88194
C	-4.93863	10.12531	2.2505	H	-0.15706	-7.69417	-2.50167

H	1.44927	-8.35502	-2.74191
C	4.93863	-10.12531	2.2505
H	5.41898	-11.24177	0.48076
H	3.09041	-10.01711	-1.87341
H	4.29621	-11.24864	-1.49053
H	2.57919	-11.54228	-1.17734
H	4.17099	-8.89946	3.83715
H	2.15693	-7.851	3.9149
H	1.96142	-6.90209	2.43485
H	0.86565	-8.22893	2.77229
C	-2.05681	-12.9657	-2.63447
C	6.1615	-10.56655	3.01392
H	-2.698	-13.49504	-1.92373
H	-2.69341	-12.52201	-3.40553
H	-1.42599	-13.71684	-3.12595
H	6.99493	-10.78688	2.34064
H	6.48761	-9.80045	3.72344
H	5.95832	-11.47799	3.58984

Neut1

TD-DFT CAM-B3LYP 6-31G(d,p), gas
phase, S₀



Point group: C₁

Total energy: -2048457.89 kcal/mol

Dipole moment: 2.68 D

Imaginary frequencies: 0

Optimized x, y, z coordinates

C	-2.74756	-0.3049	0.56457
C	-2.02546	-0.35756	1.73777
C	-0.62241	-0.32098	1.55019
C	-0.24306	-0.23868	0.2253
S	-1.65998	-0.19544	-0.80887
C	-4.19602	-0.32397	0.38359
C	1.08345	-0.18656	-0.33597
S	2.4982	-0.15499	0.70117
C	3.58755	-0.09367	-0.67449
C	2.86673	-0.10423	-1.84965
C	1.46423	-0.15632	-1.66284

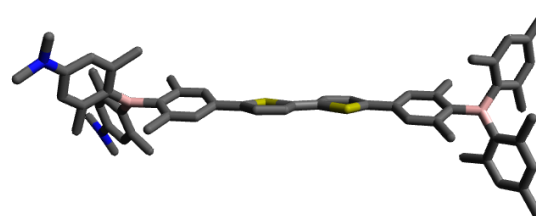
C	5.03482	-0.04466	-0.49274
C	5.61322	0.3887	0.70849
C	6.99486	0.42118	0.88889
C	7.86195	0.05057	-0.17014
C	7.28094	-0.37038	-1.39447
C	5.89601	-0.43361	-1.52991
C	-4.78374	-0.73052	-0.82201
C	-6.16748	-0.76591	-0.98762
C	-7.02417	-0.36217	0.06616
C	-6.43286	0.06273	1.28369
C	-5.04697	0.06761	1.42774
B	-8.59154	-0.4015	-0.09059
B	9.42237	0.10088	0.0084
C	10.31335	0.79884	-1.08004
C	10.0865	-0.54724	1.27494
C	-9.45196	0.84494	0.27447
C	-9.26733	-1.72008	-0.6215
C	-8.95176	-2.98581	-0.06957
C	-9.55659	-4.14053	-0.57153
C	-10.45687	-4.09631	-1.63738
C	-10.75127	-2.84942	-2.19193
C	-10.19045	-1.66998	-1.69591
C	-10.66261	0.72058	1.00896
C	-11.41331	1.84129	1.35131
C	-11.02845	3.14013	0.96264
C	-9.84471	3.262	0.20768
C	-9.06188	2.15625	-0.11074
C	11.4628	0.1533	-1.60146
C	12.23052	0.77983	-2.58579
C	11.92336	2.05675	-3.05896
C	10.79858	2.69516	-2.53346
C	9.9873	2.08764	-1.5726
C	11.04519	0.16592	2.03795
C	11.60789	-0.41732	3.17547
C	11.28237	-1.7141	3.57693
C	10.34837	-2.41871	2.81535
C	9.73922	-1.85733	1.69095
C	11.88975	-1.22688	-1.14713
C	11.93946	-2.34432	4.77861
C	12.79456	2.73657	-4.08456
C	8.72832	-2.70083	0.94255
C	11.47632	1.57316	1.68109
C	8.78192	2.85955	-1.07798
C	-10.58878	-0.36702	-2.35803
C	-7.97807	-3.13914	1.07968
C	-11.1843	-0.61977	1.48654
C	-7.80651	2.42045	-0.9174
C	-6.70648	-1.23431	-2.32231
C	-7.26372	0.52086	2.46429
C	8.12266	-0.79807	-2.57829
C	7.51656	0.89187	2.23015
N	-11.77833	4.24788	1.3122
C	-11.44017	5.54602	0.75824
C	-13.09136	4.0655	1.90361
C	-11.11133	-5.35222	-2.15514

H	-2.4958	-0.45143	2.70885
H	0.09334	-0.3672	2.36289
H	3.33657	-0.04978	-2.82401
H	0.74977	-0.16623	-2.47782
H	4.97064	0.72313	1.51805
H	5.47452	-0.81062	-2.45634
H	-4.14806	-1.05292	-1.64211
H	-4.6156	0.4109	2.36304
H	-9.3134	-5.10141	-0.12331
H	-11.43961	-2.79342	-3.0324
H	-12.31486	1.6956	1.93301
H	-9.52408	4.23469	-0.14345
H	13.09457	0.2587	-2.99184
H	10.54231	3.69149	-2.88663
H	12.32294	0.15462	3.7625
H	10.08189	-3.43148	3.10922
H	11.05601	-1.93429	-1.12077
H	12.64816	-1.63303	-1.82185
H	12.31068	-1.20509	-0.13792
H	12.8563	-2.87488	4.49292
H	12.21803	-1.59194	5.52212
H	11.27944	-3.07258	5.25888
H	13.58791	3.32094	-3.60206
H	13.28074	2.00917	-4.7411
H	12.21611	3.42616	-4.70629
H	7.70713	-2.34415	1.10458
H	8.8949	-2.68949	-0.13833
H	8.77877	-3.74129	1.2745
H	10.62748	2.22656	1.46024
H	12.03461	2.02223	2.50694
H	12.11594	1.58413	0.79402
H	7.84844	2.43835	-1.46205
H	8.7015	2.85261	0.01277
H	8.83864	3.90307	-1.39918
H	-11.11551	-0.56149	-3.29644
H	-11.24705	0.22543	-1.71589
H	-9.72704	0.26735	-2.58402
H	-8.1712	-2.42356	1.88439
H	-8.04399	-4.14343	1.50701
H	-6.94579	-2.9761	0.75698
H	-11.58986	-1.21151	0.66142
H	-10.40259	-1.22804	1.94876
H	-11.97846	-0.47924	2.22486
H	-6.90549	2.3092	-0.30786
H	-7.70055	1.73031	-1.75835
H	-7.81725	3.43709	-1.31966
H	-5.90293	-1.29516	-3.0611
H	-7.17178	-2.2205	-2.24227
H	-7.47094	-0.55911	-2.71776
H	-8.09209	-0.1605	2.6775
H	-6.64561	0.58778	3.36378
H	-7.71023	1.50276	2.28389
H	8.91877	-1.49169	-2.29329
H	7.50247	-1.29473	-3.3292
H	8.61037	0.0582	-3.05226

H	6.71186	1.34356	2.81622
H	7.93495	0.06394	2.80911
H	8.3122	1.63533	2.12924
H	-10.417	5.83167	1.0253
H	-11.52463	5.57543	-0.33863
H	-12.11229	6.29772	1.17353
H	-13.77946	3.51494	1.24498
H	-13.02458	3.52066	2.85191
H	-13.52709	5.04267	2.11428
H	-11.35424	-5.267	-3.21836
H	-12.04848	-5.55736	-1.62268
H	-10.46459	-6.2243	-2.02098

Neut2

TD-DFT CAM-B3LYP 6-31G(d,p), gas
phase, S₀



Point group: C₁

Total energy: -2107827.53 kcal/mol

Dipole moment: 2.36 D

Imaginary frequencies: 0

Optimized x, y, z coordinates

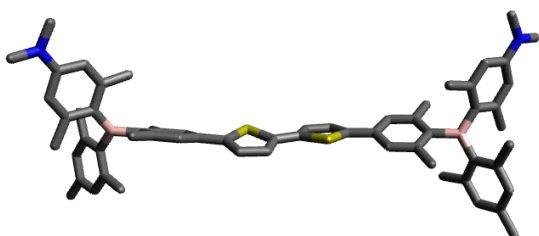
C	2.39264	-0.56318	0.36365
C	1.66064	-1.51957	1.03444
C	0.25884	-1.36155	0.91012
C	-0.10986	-0.27732	0.13932
S	1.31566	0.57023	-0.43452
C	3.84301	-0.42044	0.27389
C	-1.43174	0.18319	-0.204
S	-2.85713	-0.62997	0.41693
C	-3.93426	0.48154	-0.41228
C	-3.20188	1.40899	-1.12224
C	-1.80032	1.2441	-1.00727
C	-5.38391	0.35377	-0.30389
C	-5.98709	-0.3228	0.76544
C	-7.372	-0.42994	0.87957
C	-8.21587	0.13014	-0.113
C	-7.60886	0.80363	-1.20481
C	-6.22232	0.91366	-1.27959
C	4.45154	0.28029	-0.77657

C	5.83583	0.42772	-0.85423	H	-5.78011	1.42201	-2.13072
C	6.67331	-0.16868	0.12014	H	3.83218	0.70703	-1.56072
C	6.06246	-0.8929	1.17444	H	4.22615	-1.50474	2.09406
C	4.6744	-0.99065	1.24944	H	8.65461	4.57326	1.09382
B	8.24301	-0.02677	0.03708	H	11.2033	3.03205	-2.01628
B	-9.77829	0.00314	-0.00912	H	11.90398	-2.48312	1.74043
C	-10.60908	-0.48363	-1.24961	H	9.36427	-4.48695	-1.10191
C	-10.50574	0.36235	1.33532	H	-13.34229	0.35857	-3.12108
C	9.13674	-1.3061	0.12151	H	-10.68022	-2.95576	-3.60901
C	8.87839	1.39138	-0.12762	H	-12.79589	-0.89039	3.54165
C	8.43747	2.50465	0.635	H	-10.66231	2.81479	3.7111
C	9.01204	3.76235	0.47159	H	-11.44176	2.18056	-0.7687
C	10.03132	3.99475	-0.47253	H	-12.99913	1.98531	-1.57727
C	10.44736	2.89803	-1.25274	H	-12.70245	1.23436	-0.00221
C	9.90867	1.62595	-1.07651	H	-13.46083	1.91026	4.84487
C	10.28578	-1.34233	0.95539	H	-12.80779	0.46654	5.62056
C	11.06068	-2.49462	1.06139	H	-11.91735	1.99756	5.69485
C	10.77051	-3.65516	0.31735	H	-13.70987	-2.53066	-4.35439
C	9.63267	-3.61927	-0.51231	H	-13.41291	-1.00637	-5.19161
C	8.82649	-2.48755	-0.60173	H	-12.30045	-2.37026	-5.40318
C	-11.76181	0.22343	-1.67513	H	-8.18606	2.22123	1.62606
C	-12.47503	-0.21098	-2.7947	H	-9.3415	2.77582	0.42931
C	-12.10939	-1.35713	-3.50277	H	-9.31191	3.52551	2.02729
C	-10.9817	-2.05875	-3.07277	H	-10.95261	-2.40817	0.94369
C	-10.2236	-1.63707	-1.97825	H	-12.40453	-2.45506	1.94708
C	-11.46296	-0.51701	1.90133	H	-12.43619	-1.68482	0.35376
C	-12.08269	-0.19177	3.10999	H	-8.07887	-1.94708	-1.86139
C	-11.8164	1.00562	3.77643	H	-8.96275	-2.66916	-0.53026
C	-10.8834	1.87544	3.20926	H	-9.02189	-3.42008	-2.12678
C	-10.2185	1.57017	2.01961	H	11.0387	0.95347	-2.78605
C	-12.24981	1.47126	-0.96923	H	11.08965	-0.16432	-1.41467
C	-12.53422	1.36115	5.05368	H	9.65334	-0.07868	-2.4109
C	-12.92264	-1.8382	-4.6776	H	7.49176	1.51245	2.32737
C	-9.21306	2.57472	1.49665	H	7.32364	3.2702	2.31675
C	-11.83146	-1.8349	1.25254	H	6.36082	2.26846	1.22174
C	-9.00938	-2.46057	-1.60285	H	11.15583	0.63321	1.1867
C	10.44917	0.52691	-1.96963	H	9.86712	0.30214	2.32342
C	7.3472	2.38154	1.68006	H	11.4457	-0.46211	2.54648
C	10.70923	-0.15581	1.79823	H	6.69128	-2.63438	-0.96309
C	7.6277	-2.57279	-1.5245	H	7.54398	-1.69821	-2.1751
C	6.39874	1.21618	-2.0178	H	7.69712	-3.45739	-2.16351
C	6.87825	-1.55498	2.26477	H	5.62564	1.39568	-2.77001
C	-8.42384	1.43199	-2.31575	H	6.78963	2.18413	-1.69171
C	-7.92167	-1.16938	2.08123	H	7.2276	0.69646	-2.50716
N	11.57266	-4.7823	0.39343	H	7.64541	-0.88845	2.66966
C	11.10947	-6.02524	-0.19604	H	6.23408	-1.86483	3.09235
C	12.61542	-4.84712	1.40053	H	7.40266	-2.43841	1.88995
N	10.6037	5.24755	-0.62255	H	-9.24841	2.03937	-1.9318
C	11.50614	5.48927	-1.73296	H	-7.79442	2.07872	-2.9328
C	9.98648	6.39248	0.02187	H	-8.87091	0.67354	-2.96412
H	2.12393	-2.3331	1.57903	H	-7.12182	-1.70585	2.59839
H	-0.46322	-2.03146	1.36274	H	-8.38852	-0.48467	2.79456
H	-3.66357	2.20662	-1.69124	H	-8.68668	-1.90005	1.80388
H	-1.07777	1.88856	-1.49443	H	11.86691	-6.79553	-0.046
H	-5.36212	-0.75498	1.54196	H	10.16421	-6.37881	0.24319

H	10.95867	-5.91571	-1.27544
H	13.16185	-5.78449	1.28884
H	13.33226	-4.02899	1.27375
H	12.22206	-4.79627	2.42761
H	11.88255	6.51114	-1.67114
H	12.36848	4.81569	-1.6891
H	11.02308	5.35725	-2.71348
H	10.57161	7.28564	-0.20058
H	8.9522	6.56361	-0.31331
H	9.97152	6.26969	1.11023

Neut(i)2

TD-DFT CAM-B3LYP 6-31G(d,p), gas
phase, S₀



Point group: C₂

Total energy: -2107827.20 kcal/mol

Dipole moment: 3.83 D

Imaginary frequencies: 0

Optimized x, y, z coordinates

C	0.47212	4.61157	-0.45084
C	1.79357	4.96514	-0.75561
C	2.22704	6.28937	-0.71158
C	1.33503	7.3213	-0.32878
C	0.00052	6.96565	-0.00417
C	-0.41012	5.6362	-0.07692
B	1.79357	8.82787	-0.28892
C	1.52334	9.70597	0.96953
C	2.52951	9.42846	-1.54411
C	3.75535	10.12356	-1.39199
C	4.42428	10.61637	-2.51512
C	3.90484	10.47658	-3.80331
C	2.69171	9.80143	-3.94819
C	2.01015	9.26735	-2.8521
C	1.04708	11.04013	0.85375
C	0.78998	11.812	1.98299
C	1.03242	11.32758	3.28397
C	1.51058	10.00708	3.40047
C	1.73729	9.20825	2.28368

C	0.70849	8.53983	-3.11449
C	4.39695	10.34214	-0.03725
C	0.75439	11.67956	-0.48866
C	2.24919	7.80564	2.54296
C	4.61757	11.05975	-4.99731
C	3.66968	6.57178	-1.0728
C	-1.02357	7.99558	0.4254
N	0.8153	12.11555	4.39939
C	0.87153	11.51619	5.72034
C	0.16804	13.40585	4.2498
H	2.49409	4.19284	-1.06122
H	-1.43216	5.3848	0.18947
H	5.37565	11.12645	-2.38074
H	2.26803	9.68133	-4.94288
H	0.39026	12.80829	1.84196
H	1.71192	9.58879	4.37865
H	0.81683	7.45984	-2.97962
H	-0.08936	8.86113	-2.43841
H	0.36784	8.72021	-4.13772
H	4.40879	9.43329	0.57093
H	5.43071	10.67893	-0.1547
H	3.85891	11.09537	0.54562
H	0.19247	11.01606	-1.15093
H	0.16956	12.59403	-0.3567
H	1.67451	11.94009	-1.01881
H	1.478	7.05368	2.35461
H	3.09693	7.54861	1.90271
H	2.5732	7.70304	3.58214
H	5.69966	11.09221	-4.84012
H	4.42089	10.47868	-5.90313
H	4.28602	12.08741	-5.19188
H	4.24172	5.64155	-1.12473
H	3.74913	7.07551	-2.04001
H	4.15794	7.22166	-0.34072
H	-1.03411	8.86889	-0.23295
H	-2.02722	7.56167	0.42134
H	-0.81809	8.3704	1.43199
H	0.68161	12.28517	6.46984
H	0.13086	10.71357	5.85305
H	1.86331	11.09576	5.92049
H	0.11672	13.89475	5.22328
H	0.74165	14.05681	3.58123
H	-0.85394	13.32537	3.84938
C	0.01207	3.22781	-0.51878
C	-1.27265	2.75442	-0.68048
S	1.13687	1.88652	-0.38723
C	-1.3634	1.34146	-0.71912
H	-2.12462	3.41114	-0.80716
C	-0.14546	0.70597	-0.5846
H	-2.29091	0.80128	-0.86976
C	0.14546	-0.70597	-0.5846
C	1.3634	-1.34146	-0.71912
S	-1.13687	-1.88652	-0.38723
C	1.27265	-2.75442	-0.68048
H	2.29091	-0.80128	-0.86976

```

C   -0.01207  -3.22781  -0.51878
H    2.12462  -3.41114  -0.80716
C   -0.47212  -4.61157  -0.45084
C   -1.79357  -4.96514  -0.75561
C    0.41012  -5.6362   -0.07692
C   -2.22704  -6.28937  -0.71158
H   -2.49409  -4.19284  -1.06122
C   -0.00052  -6.96565  -0.00417
H    1.43216  -5.3848   0.18947
C   -1.33503  -7.3213   -0.32878
C   -3.66968  -6.57178  -1.0728
C    1.02357  -7.99558   0.4254
B   -1.79357  -8.82787  -0.28892
H   -4.24172  -5.64155  -1.12473
H   -3.74913  -7.07551  -2.04001
H   -4.15794  -7.22166  -0.34072
H    1.03411  -8.86889  -0.23295
H    2.02722  -7.56167   0.42134
H    0.81809  -8.3704    1.43199
C   -1.52334  -9.70597   0.96953
C   -2.52951  -9.42846  -1.54411
C   -1.04708  -11.04013  0.85375
C   -1.73729  -9.20825  2.28368
C   -3.75535  -10.12356  -1.39199
C   -2.01015  -9.26735  -2.8521
C   -0.78998  -11.812    1.98299
C   -0.75439  -11.67956  -0.48866
C   -1.51058  -10.00708  3.40047
C   -2.24919  -7.80564  2.54296
C   -4.42428  -10.61637  -2.51512
C   -4.39695  -10.34214  -0.03725
C   -2.69171  -9.80143  -3.94819
C   -0.70849  -8.53983  -3.11449
C   -1.03242  -11.32758  3.28397
H   -0.39026  -12.80829  1.84196
H   -0.19247  -11.01606  -1.15093
H   -0.16956  -12.59403  -0.3567
H   -1.67451  -11.94009  -1.01881
H   -1.71192  -9.58879  4.37865
H   -1.478    -7.05368  2.35461
H   -3.09693  -7.54861  1.90271
H   -2.5732   -7.70304  3.58214
C   -3.90484  -10.47658  -3.80331
H   -5.37565  -11.12645  -2.38074
H   -4.40879  -9.43329  0.57093
H   -5.43071  -10.67893  -0.1547
H   -3.85891  -11.09537  0.54562
H   -2.26803  -9.68133  -4.94288
H   -0.81683  -7.45984  -2.97962
H    0.08936  -8.86113  -2.43841
H   -0.36784  -8.72021  -4.13772
N   -0.8153   -12.11555  4.39939
C   -4.61757  -11.05975  -4.99731
C   -0.87153  -11.51619  5.72034
C   -0.16804  -13.40585  4.2498

```

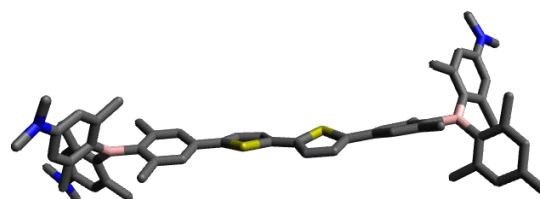
```

H   -5.69966  -11.09221  -4.84012
H   -4.42089  -10.47868  -5.90313
H   -4.28602  -12.08741  -5.19188
H   -0.68161  -12.28517  6.46984
H   -0.13086  -10.71357  5.85305
H   -1.86331  -11.09576  5.92049
H   -0.11672  -13.89475  5.22328
H   -0.74165  -14.05681  3.58123
H    0.85394  -13.32537  3.84938

```

Neut3

TD-DFT CAM-B3LYP 6-31G(d,p), gas phase, S₀



Point group: C₁

Total energy: -2167196.94 kcal/mol

Dipole moment: 2.47 D

Imaginary frequencies: 0

Optimized x, y, z coordinates

```

C   -3.52784  0.77948  -0.57225
C   -2.77529  1.87572  -0.9361
C   -1.37775  1.64539  -0.91665
C   -1.03448  0.36449  -0.53367
S   -2.47571  -0.56785  -0.17216
C   -4.98015  0.65564  -0.49106
C    0.27533  -0.22375  -0.40443
S    1.71128  0.78294  -0.35719
C    2.76605  -0.61338  -0.21757
C    2.01764  -1.77079  -0.18787
C    0.62166  -1.55518  -0.29369
C    4.21654  -0.46299  -0.1434
C    4.86657  0.67492  -0.64081
C    6.25058  0.82302  -0.55889
C    7.04702  -0.20539  0.00193
C    6.39465  -1.36462  0.49177
C    5.00627  -1.46863  0.43379
C   -5.61867  -0.59046  -0.55896
C   -7.00427  -0.71117  -0.46446
C   -7.81487  0.44413  -0.33565
C   -7.17382  1.70785  -0.28691

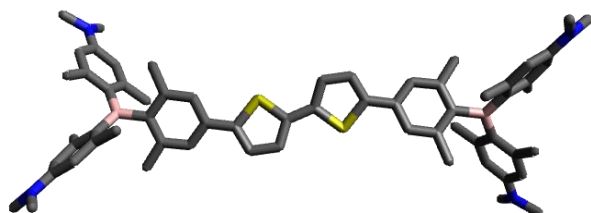
```

C	-5.78432	1.79531	-0.34152	H	-5.02144	-1.48628	-0.70445
B	-9.38373	0.31724	-0.2691	H	-5.31284	2.76856	-0.24706
B	8.61683	-0.06481	0.07863	H	-9.85115	-1.70846	3.97959
C	9.51836	-1.21588	-0.47404	H	-12.51375	-3.03897	0.86724
C	9.24543	1.22144	0.70493	H	-12.89605	3.38128	-1.14982
C	-10.25968	1.2069	-1.22765	H	-10.57394	2.10625	-4.51033
C	-10.05333	-0.67323	0.73022	H	12.21008	-3.11512	0.42639
C	-9.60233	-0.79383	2.07276	H	9.83753	-3.29761	-3.16285
C	-10.21674	-1.67139	2.9611	H	11.64139	3.56661	0.05442
C	-11.28765	-2.4981	2.56674	H	8.93261	3.30636	3.39206
C	-11.71644	-2.40135	1.22782	H	10.12058	-1.00713	2.2768
C	-11.13866	-1.50211	0.33638	H	11.69587	-1.7982	2.14219
C	-11.33445	1.97442	-0.71291	H	11.45773	-0.1503	1.54157
C	-12.08521	2.78714	-1.56574	H	6.65808	1.30913	2.19482
C	-11.82992	2.85226	-2.93672	H	7.74218	0.07063	2.79793
C	-10.78228	2.08122	-3.44297	H	7.55602	1.58041	3.69478
C	-9.98981	1.28127	-2.61618	H	10.14173	1.13937	-1.9707
C	10.62369	-1.70225	0.27311	H	11.53193	2.19548	-1.69241
C	11.40266	-2.75574	-0.19917	H	11.53161	0.52724	-1.10102
C	11.16128	-3.35375	-1.4516	H	7.1443	-1.73535	-2.20935
C	10.06745	-2.86932	-2.19526	H	8.0517	-0.32306	-2.71383
C	9.25665	-1.8414	-1.72106	H	8.2179	-1.8342	-3.61223
C	10.31738	1.89833	0.06502	H	-12.34368	-2.35282	-1.23661
C	10.85144	3.06737	0.60136	H	-12.28501	-0.58459	-1.26225
C	10.38816	3.60463	1.81844	H	-10.9102	-1.50881	-1.83109
C	9.32744	2.93176	2.45595	H	-8.54745	1.09335	2.34402
C	8.75784	1.78247	1.91436	H	-8.43365	-0.01877	3.71104
C	10.99228	-1.13593	1.62992	H	-7.49374	-0.30275	2.23995
N	10.95488	4.74311	2.36874	H	-12.19298	1.02438	1.03911
N	11.96853	-4.37124	-1.9349	H	-10.83214	2.06277	1.40694
C	7.61982	1.15176	2.69087	H	-12.38936	2.78319	0.9839
C	10.91003	1.41562	-1.24394	H	-7.88893	0.89857	-2.99802
C	8.1082	-1.40999	-2.61038	H	-8.86663	-0.55658	-2.94228
C	-11.69682	-1.48663	-1.07251	H	-8.96422	0.50703	-4.34786
C	-8.46048	0.03922	2.61955	H	-6.84032	-2.82339	-0.86535
C	-11.70489	1.96141	0.75575	H	-7.96029	-2.4299	0.44875
C	-8.86969	0.49073	-3.25867	H	-8.44372	-2.16643	-1.21391
C	-7.59336	-2.10542	-0.5292	H	-8.706	2.9328	0.6572
C	-7.95681	2.99482	-0.13758	H	-7.28796	3.82624	0.10073
C	7.16391	-2.50917	1.11721	H	-8.49581	3.24318	-1.05597
C	6.85914	2.0953	-1.10987	H	7.9055	-2.16166	1.84239
C	-12.64189	3.7489	-3.837	H	6.48393	-3.19124	1.63521
N	-11.89515	-3.36342	3.45821	H	7.71257	-3.08065	0.36322
C	11.5449	-5.11868	-3.10486	H	6.12176	2.65154	-1.69518
C	12.95578	-4.97294	-1.0579	H	7.21911	2.74536	-0.30742
C	11.90339	5.51445	1.58688	H	7.71882	1.89656	-1.75641
C	10.29561	5.39602	3.48508	H	-13.66331	3.87026	-3.46435
C	-12.87879	-4.31484	2.97504	H	-12.19809	4.75028	-3.90123
C	-11.29167	-3.58973	4.75894	H	-12.69418	3.35146	-4.85485
H	-3.22149	2.81298	-1.2455	H	10.58207	-5.63134	-2.95759
H	-0.64071	2.38719	-1.20167	H	11.4465	-4.46185	-3.97584
H	2.46731	-2.7544	-0.12866	H	12.30042	-5.86873	-3.34208
H	-0.11126	-2.3534	-0.3168	H	13.67159	-4.22376	-0.70358
H	4.28097	1.45588	-1.11803	H	12.50715	-5.45602	-0.17606
H	4.52364	-2.34154	0.86245	H	13.51531	-5.7263	-1.61393

H	12.76998	4.90427	1.31135
H	11.46597	5.9188	0.66092
H	12.26591	6.34942	2.18785
H	9.27751	5.73489	3.23992
H	10.22816	4.72488	4.34806
H	10.88262	6.26386	3.78825
H	-12.46113	-5.02552	2.24581
H	-13.27184	-4.88214	3.81944
H	-13.72102	-3.8004	2.49992
H	-11.23832	-2.65977	5.33579
H	-11.90797	-4.29199	5.32126
H	-10.27432	-4.00249	4.68785

Neut4

TD-DFT CAM-B3LYP 6-31G(d,p), gas
phase, S₀



Point group: C₂

Total energy: -2226566.36 kcal/mol

Dipole moment: 0.6266 D

Imaginary frequencies: 0

Optimized x, y, z coordinates

C	0.28414	0.66252	-0.47675
C	1.6026	1.04216	-0.62621
C	1.79771	2.44444	-0.5762
C	0.63687	3.16442	-0.39011
S	-0.73213	2.07423	-0.24997
H	2.40027	0.3281	-0.79544
H	2.76256	2.91815	-0.71006
C	-0.28414	-0.66252	-0.47675
C	-1.6026	-1.04216	-0.62621
S	0.73213	-2.07423	-0.24997
C	-1.79771	-2.44444	-0.5762
H	-2.40027	-0.3281	-0.79544
C	-0.63687	-3.16442	-0.39011
H	-2.76256	-2.91815	-0.71006
C	0.46442	4.61135	-0.29731
C	-0.76731	5.22553	-0.56273
C	1.54133	5.43412	0.0655
C	-0.93714	6.60517	-0.45482

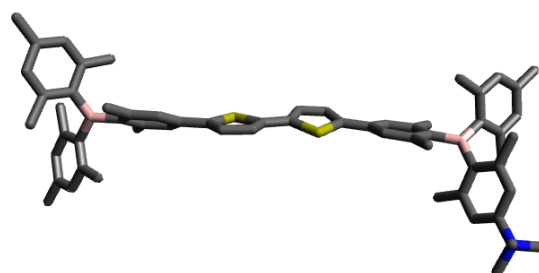
H	-1.60971	4.61455	-0.87521
C	1.41011	6.81941	0.14073
H	2.4959	4.98003	0.31296
C	0.1573	7.43468	-0.10739
C	-2.3106	7.17263	-0.74525
C	2.63348	7.62536	0.52391
B	-0.01639	8.99832	0.01149
H	-2.94503	6.41864	-1.21931
H	-2.80557	7.50835	0.17038
H	-2.26766	8.04006	-1.41025
H	2.41871	8.35556	1.3096
H	3.4283	6.96783	0.88693
H	3.02093	8.19229	-0.32732
C	0.97117	9.94494	-0.7445
C	-1.17529	9.57459	0.8878
C	1.55397	11.06504	-0.09472
C	1.34882	9.71212	-2.09282
C	-2.00316	10.62474	0.40962
C	-1.46163	9.06471	2.18108
C	2.46468	11.88565	-0.75567
C	1.25199	11.40647	1.35086
C	2.23304	10.56348	-2.75027
C	0.79411	8.55076	-2.89234
C	-3.05921	11.11235	1.17527
C	-1.80605	11.24978	-0.95722
C	-2.49906	9.58835	2.94837
C	-0.63687	7.95946	2.80877
C	2.81337	11.67226	-2.10379
H	2.91012	12.70382	-0.20376
H	1.2861	10.52815	2.00066
H	1.97508	12.13376	1.73076
H	0.25131	11.8331	1.46298
H	2.47134	10.35374	-3.78553
H	1.22709	7.59895	-2.5724
H	-0.28911	8.4529	-2.78141
H	1.00955	8.67933	-3.95665
C	-3.33782	10.60988	2.46153
H	-3.67466	11.89854	0.75609
H	-1.65541	10.49981	-1.73803
H	-2.67799	11.84992	-1.23211
H	-0.92639	11.89908	-0.98097
H	-2.65085	9.19003	3.9437
H	-0.8503	6.98942	2.35133
H	0.43716	8.12887	2.69422
H	-0.84938	7.88184	3.87861
N	3.68549	12.52001	-2.76821
N	-4.39684	11.09524	3.21193
C	4.20404	12.12953	-4.06654
C	4.41155	13.52566	-2.01499
C	-4.53045	10.69024	4.59899
C	-5.07984	12.30088	2.78017
H	4.86402	12.91445	-4.43802
H	4.7714	11.18691	-4.03312
H	3.3931	12.00856	-4.79278
H	5.01961	14.11605	-2.70165

H	3.72107	14.21069	-1.51185
H	5.07497	13.09203	-1.25069
H	-3.67319	10.996	5.21855
H	-5.43265	11.13899	5.01664
H	-4.63359	9.60306	4.68009
H	-5.53519	12.16251	1.79355
H	-5.88169	12.5283	3.48369
H	-4.41056	13.17296	2.72414
C	-0.46442	-4.61135	-0.29731
C	0.76731	-5.22553	-0.56273
C	-1.54133	-5.43412	0.0655
C	0.93714	-6.60517	-0.45482
H	1.60971	-4.61455	-0.87521
C	-1.41011	-6.81941	0.14073
H	-2.4959	-4.98003	0.31296
C	-0.1573	-7.43468	-0.10739
C	2.3106	-7.17263	-0.74525
C	-2.63348	-7.62536	0.52391
B	0.01639	-8.99832	0.01149
H	2.94503	-6.41864	-1.21931
H	2.80557	-7.50835	0.17038
H	2.26766	-8.04006	-1.41025
H	-2.41871	-8.35556	1.3096
H	-3.4283	-6.96783	0.88693
H	-3.02093	-8.19229	-0.32732
C	-0.97117	-9.94494	-0.7445
C	1.17529	-9.57459	0.8878
C	-1.55397	-11.06504	-0.09472
C	-1.34882	-9.71212	-2.09282
C	2.00316	-10.62474	0.40962
C	1.46163	-9.06471	2.18108
C	-2.46468	-11.88565	-0.75567
C	-1.25199	-11.40647	1.35086
C	-2.23304	-10.56348	-2.75027
C	-0.79411	-8.55076	-2.89234
C	3.05921	-11.11235	1.17527
C	1.80605	-11.24978	-0.95722
C	2.49906	-9.58835	2.94837
C	0.63687	-7.95946	2.80877
C	-2.81337	-11.67226	-2.10379
H	-2.91012	-12.70382	-0.20376
H	-1.2861	-10.52815	2.00066
H	-1.97508	-12.13376	1.73076
H	-0.25131	-11.8331	1.46298
H	-2.47134	-10.35374	-3.78553
H	-1.22709	-7.59895	-2.5724
H	0.28911	-8.4529	-2.78141
H	-1.00955	-8.67933	-3.95665
C	3.33782	-10.60988	2.46153
H	3.67466	-11.89854	0.75609
H	1.65541	-10.49981	-1.73803
H	2.67799	-11.84992	-1.23211
H	0.92639	-11.89908	-0.98097
H	2.65085	-9.19003	3.9437
H	0.8503	-6.98942	2.35133

H	-0.43716	-8.12887	2.69422
H	0.84938	-7.88184	3.87861
N	-3.68549	-12.52001	-2.76821
N	4.39684	-11.09524	3.21193
C	-4.20404	-12.12953	-4.06654
C	-4.41155	-13.52566	-2.01499
C	4.53045	-10.69024	4.59899
C	5.07984	-12.30088	2.78017
H	-4.86402	-12.91445	-4.43802
H	-4.7714	-11.18691	-4.03312
H	-3.3931	-12.00856	-4.79278
H	-5.01961	-14.11605	-2.70165
H	-3.72107	-14.21069	-1.51185
H	-5.07497	-13.09203	-1.25069
H	3.67319	-10.996	5.21855
H	5.43265	-11.13899	5.01664
H	4.63359	-9.60306	4.68009
H	5.53519	-12.16251	1.79355
H	5.88169	-12.5283	3.48369
H	4.41056	-13.17296	2.72414

Cat¹⁺

TD-DFT CAM-B3LYP 6-31G(d,p), gas
phase, S₀

Point group: C₁

Total energy: -2073359.69 kcal/mol

Dipole moment: 47.70 D

Imaginary frequencies: 0

Optimized x, y, z coordinates

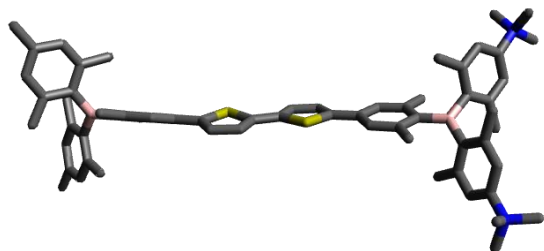
C	-2.54897	-3.58563	-1.71223
C	-2.38839	-2.33078	-1.15741
C	-1.04564	-1.89622	-1.09767
C	-0.14404	-2.81837	-1.59872
S	-0.98431	-4.25366	-2.14685
C	-3.77867	-4.32568	-1.94545
C	1.29093	-2.70074	-1.67331
S	2.18495	-1.5498	-0.69987

C	3.71762	-2.07182	-1.37194	N	-7.2982	-12.47904	-2.42177
C	3.51392	-3.0809	-2.29151	C	-6.63385	-13.0378	-1.19249
C	2.15505	-3.43283	-2.46478	C	-8.70687	-13.02552	-2.47058
C	4.97569	-1.46092	-0.95259	C	-6.5205	-12.96465	-3.62391
C	5.10063	-0.80425	0.27899	H	-3.22298	-1.71924	-0.83661
C	6.30707	-0.23803	0.68756	H	-0.74231	-0.92414	-0.72946
C	7.44278	-0.29376	-0.15847	H	4.32851	-3.56795	-2.81281
C	7.31645	-0.94498	-1.41195	H	1.81356	-4.19255	-3.15748
C	6.10348	-1.52135	-1.78377	H	4.24628	-0.75854	0.94889
C	-3.82514	-5.42352	-2.82046	H	6.02479	-2.00257	-2.75362
C	-4.99342	-6.14855	-3.02888	H	-2.92927	-5.70445	-3.36613
C	-6.20293	-5.76832	-2.38553	H	-4.95976	-3.14114	-0.58947
C	-6.16768	-4.63799	-1.51892	H	-6.34711	-10.69376	-0.52226
C	-4.97157	-3.963	-1.2973	H	-8.35365	-10.90436	-4.34179
B	-7.52048	-6.57556	-2.56544	H	-12.16586	-5.97457	-1.76233
B	8.80979	0.35412	0.28136	H	-10.37012	-3.52232	-4.77248
C	9.56043	1.32385	-0.69647	H	12.65263	1.86056	-2.04998
C	9.4077	0.02478	1.69324	H	9.02839	4.03782	-2.70559
C	-8.9053	-5.88913	-2.78928	H	10.70255	1.566	4.45548
C	-7.45768	-8.16577	-2.51891	H	10.10282	-2.61197	3.75464
C	-6.85405	-8.82764	-1.42786	H	11.27248	-0.9083	-0.34905
C	-6.81	-10.2285	-1.3816	H	12.73511	-0.02968	-0.80206
C	-7.34237	-10.9683	-2.4273	H	11.94937	0.27361	0.7539
C	-7.9347	-10.33783	-3.5172	H	12.15517	-1.02802	5.53585
C	-8.00809	-8.94378	-3.56541	H	10.91088	-0.05443	6.32057
C	-10.06701	-6.29046	-2.08082	H	10.64286	-1.78418	6.03835
C	-11.29152	-5.67055	-2.33267	H	12.11161	4.83082	-2.84747
C	-11.42544	-4.66974	-3.29774	H	12.46999	3.49202	-3.93791
C	-10.28424	-4.29053	-4.00813	H	10.98725	4.44015	-4.15033
C	-9.03412	-4.86106	-3.76179	H	7.93443	-2.54067	1.27673
C	10.94643	1.16231	-0.95201	H	9.38756	-2.43767	0.29834
C	11.59537	2.01501	-1.84739	H	9.38699	-3.42606	1.75978
C	10.92788	3.06248	-2.48521	H	8.85398	2.80384	1.71084
C	9.56697	3.22648	-2.22123	H	9.99634	3.16194	3.00882
C	8.87523	2.3736	-1.35848	H	10.57563	2.75753	1.38681
C	9.87074	1.0621	2.54244	H	6.78251	1.87287	-1.6457
C	10.37448	0.75574	3.80847	H	7.11698	2.61972	-0.0936
C	10.47529	-0.55999	4.26425	H	7.11922	3.60695	-1.55641
C	10.03049	-1.57953	3.42045	H	-8.85808	-9.0506	-5.54807
C	9.48933	-1.31123	2.16156	H	-9.63919	-7.86838	-4.48138
C	11.76666	0.06632	-0.30424	H	-8.07795	-7.50669	-5.18861
C	11.07201	-0.8725	5.61274	H	-6.87426	-7.26095	0.07552
C	11.66071	4.00256	-3.40793	H	-6.0413	-8.73823	0.57129
C	9.0258	-2.48843	1.32926	H	-5.28607	-7.6145	-0.57245
C	9.81924	2.52153	2.14067	H	-9.94233	-8.36603	-1.4472
C	7.39716	2.63042	-1.15085	H	-9.19104	-7.23812	-0.32446
C	-8.68064	-8.31228	-4.76199	H	-10.94711	-7.34265	-0.4183
C	-6.23296	-8.07289	-0.27447	H	-7.19128	-3.7367	-3.98186
C	-10.03106	-7.36456	-1.01358	H	-7.25118	-5.1702	-4.98579
C	-7.86252	-4.35928	-4.58031	H	-8.21657	-3.75749	-5.42074
C	-4.92196	-7.31024	-3.99875	H	-4.00319	-7.25856	-4.58775
C	-7.38875	-4.14614	-0.76957	H	-4.92742	-8.27367	-3.47903
C	8.47323	-1.04818	-2.38292	H	-5.76066	-7.31856	-4.70026
C	6.34793	0.4321	2.0443	H	-7.93826	-4.95601	-0.28211
C	-12.75161	-3.99915	-3.54424	H	-7.09711	-3.43	0.00226

H -8.0975 -3.65023 -1.4382
 H 9.39263 -1.38502 -1.89581
 H 8.24175 -1.75766 -3.18166
 H 8.69902 -0.08117 -2.84034
 H 5.33686 0.55581 2.44139
 H 6.92689 -0.15493 2.76233
 H 6.81299 1.42111 2.00354
 H -13.58694 -4.65765 -3.29124
 H -12.8501 -3.09573 -2.93038
 H -12.85715 -3.69402 -4.58895
 H -6.64514 -14.12403 -1.27132
 H -5.60772 -12.67863 -1.14582
 H -7.18912 -12.72288 -0.31124
 H -8.66058 -14.11486 -2.45522
 H -9.19226 -12.68294 -3.38061
 H -9.24538 -12.6497 -1.60189
 H -5.51739 -12.54429 -3.56972
 H -6.48495 -14.05425 -3.60104
 H -7.01346 -12.62378 -4.53049

Cat²⁺

TD-DFT CAM-B3LYP 6-31G(d,p), gas
 phase, S₀



Point group: C₁

Total energy: -2157602.57 kcal/mol

Dipole moment: 85.40 D

Imaginary frequencies: 0

Optimized x, y, z coordinates

C 1.98343 -0.3578 0.56799
 C 1.23503 -1.05531 1.50745
 C -0.15307 -0.92284 1.35165
 C -0.51904 -0.11475 0.27948
 S 0.90691 0.48161 -0.54563
 C 3.41587 -0.2726 0.44423
 C -1.83304 0.2323 -0.16698
 S -3.25705 -0.4671 0.58546
 C -4.33025 0.43364 -0.4635
 C -3.59892 1.21069 -1.34784

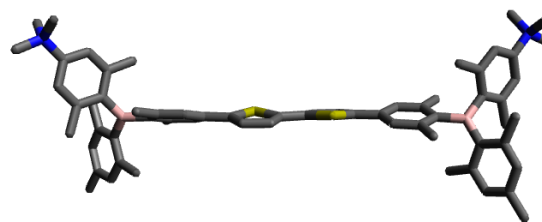
C -2.20503 1.09981 -1.1824
 C -5.77713 0.31053 -0.34824
 C -6.38459 -0.13345 0.83501
 C -7.76938 -0.23292 0.95085
 C -8.59939 0.09384 -0.15061
 C -7.98859 0.52763 -1.35439
 C -6.60243 0.64047 -1.43409
 C 4.03476 0.57324 -0.49904
 C 5.41199 0.6795 -0.6131
 C 6.27593 -0.11363 0.20974
 C 5.6478 -0.99111 1.15474
 C 4.26823 -1.04011 1.26683
 B 7.80366 -0.02904 0.08384
 B -10.17185 -0.02035 -0.0385
 C -10.96449 -0.8263 -1.12185
 C -10.90905 0.67614 1.15457
 C 8.70747 -1.3302 0.21989
 C 8.522 1.36352 -0.18578
 C 8.25238 2.46077 0.66521
 C 8.85918 3.70449 0.43536
 C 9.71416 3.87071 -0.64419
 C 10.00329 2.80234 -1.48849
 C 9.42551 1.55134 -1.2592
 C 9.78844 -1.40584 1.12476
 C 10.53888 -2.58391 1.24973
 C 10.23461 -3.68163 0.45705
 C 9.19558 -3.62063 -0.46629
 C 8.42314 -2.4624 -0.58625
 C -12.12405 -0.27116 -1.72384
 C -12.80232 -0.98174 -2.71601
 C -12.39859 -2.25601 -3.11999
 C -11.26513 -2.80396 -2.51645
 C -10.53928 -2.11111 -1.54574
 C -11.88135 -0.03156 1.90859
 C -12.50662 0.58562 2.9939
 C -12.23485 1.90817 3.3496
 C -11.28707 2.60521 2.59766
 C -10.61473 2.01265 1.52728
 C -12.6577 1.09672 -1.35209
 C -12.9626 2.57099 4.49072
 C -13.17883 -3.02585 -4.15423
 C -9.59948 2.85452 0.78296
 C -12.26354 -1.46469 1.60175
 C -9.3197 -2.79242 -0.96101
 C 9.76285 0.42975 -2.21301
 C 7.29545 2.36798 1.83237
 C 10.15374 -0.2445 2.01973
 C 7.28245 -2.48604 -1.57789
 C 5.92796 1.61961 -1.68436
 C 6.43381 -1.85865 2.11771
 C -8.80111 0.88265 -2.58047
 C -8.34001 -0.69637 2.27319
 N 11.00435 -4.97557 0.57454
 C 12.09962 -4.91186 1.60668
 C 10.05962 -6.0881 0.97784

C	11.64553	-5.31062	-0.75436
N	10.346	5.20882	-0.94599
C	9.95588	6.27601	0.04394
C	11.8528	5.08162	-0.9118
C	9.90527	5.67437	-2.31748
H	1.68164	-1.6389	2.30294
H	-0.88021	-1.39151	2.0033
H	-4.06688	1.86623	-2.07079
H	-1.48558	1.65283	-1.77582
H	-5.76762	-0.37507	1.69631
H	-6.15356	0.95932	-2.36953
H	3.41286	1.16624	-1.16236
H	3.83212	-1.6946	2.0131
H	8.6241	4.51442	1.11192
H	10.66924	2.91546	-2.33671
H	11.34043	-2.60278	1.97512
H	8.95047	-4.46731	-1.09781
H	-13.6743	-0.53091	-3.18371
H	-10.936	-3.79696	-2.81348
H	-13.23118	0.0205	3.57526
H	-11.06366	3.63789	2.85514
H	-11.87184	1.85567	-1.30377
H	-13.39574	1.42924	-2.08646
H	-13.13983	1.08649	-0.3705
H	-13.89215	3.03795	4.14292
H	-13.23311	1.84848	5.26585
H	-12.35598	3.35677	4.94969
H	-13.99344	-3.59286	-3.68736
H	-13.63129	-2.35768	-4.8925
H	-12.54418	-3.74265	-4.68273
H	-8.57476	2.53855	1.00009
H	-9.72514	2.7958	-0.30197
H	-9.69322	3.90557	1.06801
H	-11.39333	-2.10503	1.4329
H	-12.83442	-1.89154	2.4303
H	-12.87771	-1.53189	0.69932
H	-8.39142	-2.33593	-1.31734
H	-9.29789	-2.74145	0.13136
H	-9.30204	-3.84889	-1.24094
H	10.37719	0.78458	-3.04353
H	10.3071	-0.3706	-1.7051
H	8.85973	-0.01746	-2.63855
H	7.40693	1.43461	2.38697
H	7.44657	3.19685	2.52824
H	6.25746	2.39814	1.48836
H	10.53015	0.60044	1.43714
H	9.28733	0.11528	2.58203
H	10.9218	-0.52617	2.74347
H	6.32287	-2.59959	-1.06558
H	7.21476	-1.56041	-2.15268
H	7.39307	-3.31507	-2.28106
H	5.11947	1.89287	-2.36574
H	6.32605	2.54588	-1.25923
H	6.72595	1.17354	-2.28324
H	7.26065	-1.31885	2.58642

H	5.78258	-2.21952	2.91668
H	6.86357	-2.73525	1.62362
H	-9.63471	1.54943	-2.34335
H	-8.17657	1.38267	-3.32533
H	-9.23628	-0.00838	-3.04063
H	-7.55018	-1.0952	2.91513
H	-8.83095	0.12402	2.80335
H	-9.0925	-1.47941	2.14556
H	12.59839	-5.87974	1.62376
H	12.8089	-4.13447	1.32928
H	11.66232	-4.7038	2.58123
H	10.63068	-7.01166	1.07489
H	9.29216	-6.20059	0.21645
H	9.60211	-5.81633	1.92794
H	12.31103	-4.49255	-1.026
H	12.2035	-6.241	-0.64713
H	10.87126	-5.42471	-1.50854
H	10.45347	7.19933	-0.24888
H	8.87664	6.41277	0.01741
H	10.28156	5.97897	1.03894
H	12.29002	6.05778	-1.12248
H	12.1695	4.3613	-1.6616
H	12.14184	4.73748	0.08015
H	8.81853	5.74399	-2.31854
H	10.35412	6.64787	-2.51587
H	10.23041	4.95301	-3.0627

Cat(i)²⁺

TD-DFT CAM-B3LYP 6-31G(d,p), gas phase, S₀



Point group: C₂

Total energy: -2157605.56 kcal/mol

Dipole moment: 25.77 D

Imaginary frequencies: 0

Optimized x, y, z coordinates

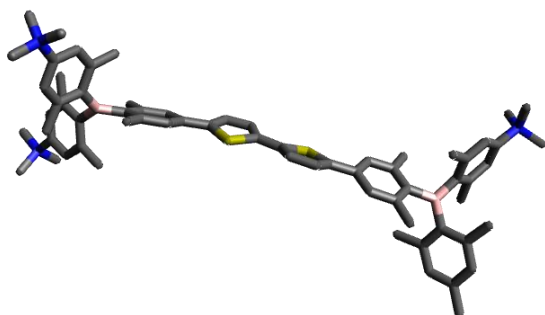
C	1.3291	2.8835	2.18084
C	0.97884	2.76766	3.5113
C	0.3817	1.52911	3.84089
C	0.27178	0.66876	2.76541

S	0.92976	1.40771	1.32093	H	-0.03865	9.79259	-2.15045
H	1.10941	3.57189	4.22482	H	0.58417	7.32793	-0.09406
H	0.00804	1.28174	4.82683	H	1.4975	8.54051	0.78132
C	-0.27178	-0.66876	2.76541	H	0.0004	8.99422	-0.0349
C	-0.3817	-1.52911	3.84089	C	0.83272	10.64721	-4.58237
S	-0.92976	-1.40771	1.32093	C	9.7788	8.33631	1.9474
C	-0.97884	-2.76766	3.5113	C	9.40757	10.60403	1.1396
H	-0.00804	-1.28174	4.82683	H	1.18042	10.44111	-5.59807
C	-1.3291	-2.8835	2.18084	H	-0.24391	10.46121	-4.54225
H	-1.10941	-3.57189	4.22482	H	0.98502	11.71713	-4.39537
C	1.94026	4.01937	1.50077	H	10.80196	8.64095	2.16913
C	1.87829	4.16791	0.10771	H	9.12663	8.52754	2.79829
C	2.61426	5.00974	2.23317	H	9.74917	7.28078	1.69016
C	2.43548	5.26611	-0.54379	H	10.45822	10.80051	1.34851
H	1.35751	3.42051	-0.48372	H	9.07489	11.21414	0.30222
C	3.20248	6.10667	1.61119	H	8.8081	10.8089	2.02438
H	2.69597	4.91021	3.31057	C	-1.94026	-4.01937	1.50077
C	3.11696	6.26678	0.2016	C	-1.87829	-4.16791	0.10771
C	2.2902	5.32601	-2.05014	C	-2.61426	-5.00974	2.23317
C	3.90012	7.11803	2.49685	C	-2.43548	-5.26611	-0.54379
B	3.75604	7.48877	-0.5302	H	-1.35751	-3.42051	-0.48372
H	1.97064	4.35643	-2.43945	C	-3.20248	-6.10667	1.61119
H	1.54934	6.07123	-2.35243	H	-2.69597	-4.91021	3.31057
H	3.22327	5.59522	-2.55181	C	-3.11696	-6.26678	0.2016
H	3.60164	8.14488	2.26743	C	-2.2902	-5.32601	-2.05014
H	3.66197	6.9358	3.54738	C	-3.90012	-7.11803	2.49685
H	4.98811	7.06879	2.3897	B	-3.75604	-7.48877	-0.5302
C	5.23457	7.94022	-0.15402	H	-1.97064	-4.35643	-2.43945
C	2.98676	8.29172	-1.62449	H	-1.54934	-6.07123	-2.35243
C	5.51005	9.27953	0.19715	H	-3.22327	-5.59522	-2.55181
C	6.30251	7.01164	-0.18118	H	-3.60164	-8.14488	2.26743
C	3.59768	8.65741	-2.85249	H	-3.66197	-6.9358	3.54738
C	1.64707	8.70583	-1.3919	H	-4.98811	-7.06879	2.3897
C	6.81677	9.67669	0.51555	C	-5.23457	-7.94022	-0.15402
C	4.4293	10.33535	0.24647	C	-2.98676	-8.29172	-1.62449
C	7.60283	7.42805	0.11422	C	-5.51005	-9.27953	0.19715
C	6.0877	5.55713	-0.5303	C	-6.30251	-7.01164	-0.18118
C	2.88205	9.38915	-3.80059	C	-3.59768	-8.65741	-2.85249
C	5.01111	8.24508	-3.20877	C	-1.64707	-8.70583	-1.3919
C	0.97884	9.46738	-2.35202	C	-6.81677	-9.67669	0.51555
C	0.89725	8.37575	-0.11766	C	-4.4293	-10.33535	0.24647
C	7.84995	8.75256	0.46233	C	-7.60283	-7.42805	0.11422
H	6.98093	10.71015	0.78784	C	-6.0877	-5.55713	-0.5303
H	3.5356	9.98181	0.76581	C	-2.88205	-9.38915	-3.80059
H	4.78164	11.2334	0.75996	C	-5.01111	-8.24508	-3.20877
H	4.11306	10.61661	-0.76148	C	-0.97884	-9.46738	-2.35202
H	8.40102	6.69517	0.06946	C	-0.89725	-8.37575	-0.11766
H	5.54741	5.03995	0.26689	C	-7.84995	-8.75256	0.46233
H	5.49063	5.44003	-1.43811	H	-6.98093	-10.71015	0.78784
H	7.04054	5.04584	-0.68817	H	-3.5356	-9.98181	0.76581
C	1.57267	9.81643	-3.5671	H	-4.78164	-11.2334	0.75996
H	3.35565	9.63276	-4.74832	H	-4.11306	-10.61661	-0.76148
H	5.20932	7.19362	-2.98179	H	-8.40102	-6.69517	0.06946
H	5.19201	8.38725	-4.27685	H	-5.54741	-5.03995	0.26689
H	5.75572	8.83655	-2.66619	H	-5.49063	-5.44003	-1.43811

H	-7.04054	-5.04584	-0.68817
C	-1.57267	-9.81643	-3.5671
H	-3.35565	-9.63276	-4.74832
H	-5.20932	-7.19362	-2.98179
H	-5.19201	-8.38725	-4.27685
H	-5.75572	-8.83655	-2.66619
H	0.03865	-9.79259	-2.15045
H	-0.58417	-7.32793	-0.09406
H	-1.4975	-8.54051	0.78132
H	-0.0004	-8.99422	-0.0349
C	-0.83272	-10.64721	-4.58237
C	-9.7788	-8.33631	1.9474
C	-9.40757	-10.60403	1.1396
H	-1.18042	-10.44111	-5.59807
H	0.24391	-10.46121	-4.54225
H	-0.98502	-11.71713	-4.39537
H	-10.80196	-8.64095	2.16913
H	-9.12663	-8.52754	2.79829
H	-9.74917	-7.28078	1.69016
H	-10.45822	-10.80051	1.34851
H	-9.07489	-11.21414	0.30222
H	-8.8081	-10.8089	2.02438
C	-10.1457	-8.89688	-0.4332
H	-10.11562	-7.83936	-0.68207
H	-9.75124	-9.4825	-1.26225
H	-11.16639	-9.19953	-0.19773
N	-9.27384	-9.14904	0.7766
C	10.1457	8.89688	-0.4332
H	10.11562	7.83936	-0.68207
H	9.75124	9.4825	-1.26225
H	11.16639	9.19953	-0.19773
N	9.27384	9.14904	0.7766

Cat³⁺

TD-DFT CAM-B3LYP 6-31G(d,p), gas
phase, S₀

Point group: C₁

Total energy: -2241826.32 kcal/mol

Dipole moment: 40.27 D

Imaginary frequencies: 0


Optimized x, y, z coordinates

C	-3.66446	0.45801	-0.66012
C	-2.92193	1.08263	-1.64318
C	-1.53109	1.07764	-1.39525
C	-1.1826	0.44466	-0.21636
S	-2.61324	-0.16385	0.59554
C	-5.11104	0.26399	-0.60439
C	0.12794	0.23935	0.34125
S	1.56535	0.50626	-0.62281
C	2.62022	0.05066	0.70773
C	1.86307	-0.2965	1.81368
C	0.47223	-0.19051	1.6129
C	4.0632	0.06024	0.57038
C	4.7045	0.69408	-0.50928
C	6.08731	0.7171	-0.64115
C	6.91678	0.05154	0.31317
C	6.26601	-0.60623	1.40377
C	4.88325	-0.57764	1.52076
C	-5.78722	0.0715	0.60855
C	-7.16669	-0.1234	0.65166
C	-7.92151	-0.1627	-0.54854
C	-7.24049	0.03796	-1.77931
C	-5.86475	0.25726	-1.78722
B	-9.46354	-0.44491	-0.54748
B	8.45289	0.03213	0.16552
C	9.28461	-1.28288	0.48847
C	9.24501	1.32295	-0.31478
C	-10.0915	-1.51089	-1.49484
C	-10.41998	0.36133	0.43365
C	-10.41753	1.77271	0.45314
C	-11.32172	2.47543	1.26269
C	-12.20611	1.7779	2.07303
C	-12.20248	0.38676	2.09599
C	-11.32585	-0.328	1.27596
C	-11.28177	-1.25028	-2.22634
C	-11.82547	-2.23415	-3.05167
C	-11.25185	-3.50339	-3.16464
C	-10.09277	-3.76311	-2.43012
C	-9.49443	-2.79523	-1.62174
C	10.38094	-1.27569	1.37782
C	11.08063	-2.4576	1.66152
C	10.71095	-3.64358	1.0432
C	9.65017	-3.66989	0.14305
C	8.92593	-2.50666	-0.13186
C	10.14978	1.28595	-1.39774
C	10.81956	2.44681	-1.81102
C	10.61295	3.64048	-1.13428
C	9.74465	3.69563	-0.04824
C	9.04986	2.55425	0.36095
C	10.82489	-0.01455	2.08263
N	11.31031	4.91283	-1.55213
N	11.43396	-4.93822	1.32775


C	8.09134	2.69897	1.52115	H	-8.4353	2.45456	-0.06526
C	10.41055	0.01481	-2.17261	H	-12.5554	0.22071	-1.25584
C	7.76004	-2.62106	-1.0877	H	-11.29518	0.93143	-2.25781
C	-11.39542	-1.83713	1.3202	H	-12.69321	0.17328	-3.01383
C	-9.46761	2.57991	-0.40171	H	-7.34464	-2.73065	-1.32336
C	-11.98857	0.08915	-2.18327	H	-8.24849	-2.89651	0.17064
C	-8.23305	-3.19166	-0.88207	H	-8.09881	-4.27524	-0.91838
C	-7.80929	-0.32134	2.00759	H	-7.04848	-0.41641	2.78571
C	-7.95233	0.0202	-3.11556	H	-8.4563	0.51981	2.27331
C	7.02633	-1.32287	2.50145	H	-8.42678	-1.22401	2.04281
C	6.64202	1.43242	-1.85637	H	-8.88881	0.58363	-3.09967
C	-11.84882	-4.54655	-4.07156	H	-7.31729	0.45319	-3.8921
N	-13.20421	2.49784	2.94943	H	-8.208	-0.99905	-3.41772
C	-13.11177	3.99588	2.82984	H	7.88554	-0.74971	2.85893
C	-14.60727	2.09273	2.55234	H	6.37336	-1.50194	3.35826
C	-12.9612	2.13717	4.39798	H	7.4049	-2.29386	2.16823
C	12.55883	-4.77491	2.31741	H	5.84275	1.63693	-2.57173
C	10.45974	-5.94421	1.90459	H	7.09924	2.39028	-1.59094
C	12.02701	-5.48316	0.0459	H	7.40469	0.84683	-2.37604
C	12.2185	4.71953	-2.73927	H	-12.93478	-4.44154	-4.14228
C	10.27752	5.95369	-1.93108	H	-11.4463	-4.45216	-5.08727
C	12.15588	5.42973	-0.40775	H	-11.62142	-5.55734	-3.72336
H	-3.3737	1.559	-2.50414	H	-13.86227	4.43009	3.48879
H	-0.8034	1.54322	-2.04987	H	-12.11838	4.31904	3.13477
H	2.30012	-0.59222	2.75942	H	-13.3101	4.28578	1.79987
H	-0.26432	-0.40244	2.37843	H	-15.31686	2.63073	3.18139
H	4.10252	1.19439	-1.26157	H	-14.72311	1.02073	2.68882
H	4.42227	-1.07952	2.36435	H	-14.74969	2.3495	1.50371
H	-5.22904	0.09344	1.54017	H	-11.94332	2.42809	4.65329
H	-5.36009	0.38644	-2.73917	H	-13.68206	2.67226	5.01663
H	-11.30045	3.55591	1.22943	H	-13.0819	1.06463	4.52569
H	-12.88178	-0.17112	2.73107	H	13.02027	-5.75074	2.46099
H	-12.72218	-2.00842	-3.62321	H	13.29037	-4.07555	1.91723
H	-9.63971	-4.74905	-2.49308	H	12.15655	-4.41406	3.26204
H	11.89908	-2.40793	2.36614	H	10.99945	-6.8667	2.11913
H	9.35275	-4.58739	-0.35211	H	9.66902	-6.13305	1.1831
H	11.48634	2.37519	-2.65906	H	10.03839	-5.52411	2.81667
H	9.57635	4.61945	0.49371	H	12.71498	-4.73938	-0.35336
H	9.98826	0.48735	2.57654	H	12.5532	-6.4104	0.27304
H	11.57452	-0.23028	2.84699	H	11.2293	-5.67235	-0.66773
H	11.25719	0.70036	1.37743	H	12.67535	5.68094	-2.96892
H	7.05484	2.70102	1.17236	H	12.99	3.99471	-2.48671
H	8.17513	1.87588	2.23385	H	11.63088	4.37737	-3.58896
H	8.27003	3.63129	2.06183	H	10.79632	6.85961	-2.24488
H	9.4793	-0.4611	-2.49195	H	9.64649	6.16326	-1.07125
H	11.00231	0.21108	-3.06929	H	9.6754	5.55357	-2.7455
H	10.95143	-0.7145	-1.56356	H	12.88247	4.66129	-0.14798
H	6.80939	-2.60093	-0.54736	H	12.65938	6.34076	-0.73145
H	7.72606	-1.79587	-1.80194	H	11.51643	5.64011	0.44563
H	7.80927	-3.55408	-1.65389				
H	-11.95205	-2.17755	2.19683				
H	-11.88743	-2.23045	0.42665				
H	-10.40336	-2.29259	1.35535				
H	-9.49676	2.26601	-1.44856				
H	-9.71343	3.64392	-0.36753				

11.9 Declaration of Authorship

11.9.1 Chapter 2



**Julius-Maximilians-
UNIVERSITÄT
WÜRZBURG**



**Fakultät für
CHEMIE UND
PHARMAZIE**

Erklärung zur Autorenschaft

Titel der Dissertation: Influence of Charge and Its Distribution on Biological Applications of Bis-Triarylboranes and Preliminary Investigations on H₂O₂-Cleavable Aryl Boronate Esters, Titel der Veröffentlichung: Synthetic Approaches to Triarylboranes from 1885 to 2020, Sarina M. Berger, Matthias Fergner, Todd B. Marder*, *Chem. Eur. J.*, **2021**, 27, 7043-7058.

Detaillierte Darstellung der Anteile an der Veröffentlichung (in %)
Angabe Autoren/innen (ggf. Haupt- / Ko- / korrespondierende/r Autor/in) mit Vorname Nachname (Initialen)

Sarina M. Berger (SMB), shared first authorship together with MF), **Matthias Fergner (MF)**, **Matthias Fergner (MF)**, shared first authorship together with SMB), **Todd B. Marder*** (TBM, corresponding author)

Autor	SMB	MF	TBM	Σ in Prozent
Literature research	20%	20%		40%
Structuring and organizing results	8%	8%		16%
Writing publication	20%	20%		40%
Correcting publication			3%	3%
Coordinating publication			1%	1%
Summe	48%	48%	4%	100%

Die Mitautoren der in dieser (teil-)kumulativen Dissertation verwendeten Manuskripte sind sowohl über die Nutzung als auch über die angegebenen Eigenanteile informiert und stimmen dem zu.

Angabe Autorenschaft: Anwählen Dropdownmenü / Autorenuunterschrift **oder** Angabe Verweis: Kontrollkästchen über Eigenschaften aktivieren !

Sarina Berger
Autor/in 1 (Sarina M. Berger)

Hauptautor/in

£ Verweis: E-Mail hinterlegt

M

Autor/in 2 (Matthias Feger)

Hauptautor/in

£ Verweis: E-Mail hinterlegt

T Marder

Autor/in 3 (Todd B. Marder)

Korrespondenzautor/in

£ Verweis: E-Mail hinterlegt

Würzburg, 14 June 2021
(Datum)

T Marder

Prof. Dr. Todd B. Marder (Betreuer/in)

11.9.2 Chapter 5



Erklärung zur Autorenschaft

Titel der Dissertation: Influence of Charge and Its Distribution on Biological Applications of Bis-Triarylboranes and Preliminary Investigations on H₂O₂-Cleavable Aryl Boronate Esters, Titel der Veröffentlichung: Applications of Triarylborane Materials in Cell Imaging and Sensing of Bio-relevant Molecules such as DNA, RNA, and Proteins, Sarina M. Berger, Todd B. Marder*, Mater. Horiz., 2021, DOI: 10.1039/d1mh00696g.

Detaillierte Darstellung der Anteile an der Veröffentlichung (in %) Angabe Autoren/innen (ggf. Haupt- / Ko- / korrespondierende/r Autor/in) mit Vorname Nachname (Initialen)

Sarina M. Berger (SMB, first author), Todd B. Marder* (TBM, corresponding author)

Autor	SMB	TBM	Σ in Prozent
Literature research	40%		40%
Structuring and organizing results	15%		15%
Writing publication	30%	2%	32%
Correcting publication	5%	5%	10%
Coordinating publication		3%	3%
Summe	90%	10%	100%

Die Mitautoren der in dieser (teil-)kumulativen Dissertation verwendeten Manuskripte sind sowohl über die Nutzung als auch über die angegebenen Eigenanteile informiert und stimmen dem zu.

Julius-Maximilians-UNIVERSITÄT WÜRZBURG
Angabe Autorenschaft: Anwählen Dropdownmenü / Autorenuunterschrift oder Angabe Verweis: Kontrollkästchen über Eigenschaften aktivieren!

Fakultät für CHEMIE UND PHARMAZIE

Sarina Berger
Autor/in 1 (Sarina M. Berger)
Hauptautor/in
 Verweis: E-Mail hinterlegt

Todd B. Marder
Autor/in 2 (Todd B. Marder)
Korrespondenzautor/in
 Verweis: E-Mail hinterlegt

Würzburg, 15 June 2021 (Datum)

T. Marder
Prof. Dr. Todd B. Marder (Betreuer/in)

11.10 Affidavit / Eidesstattliche Erklärung

11.10.1 Affidavit

I hereby state that the dissertation entitled *Influence of Charge and Its Distribution on Biological Applications of Bis-Triarylboranes and Preliminary Investigations on H₂O₂-Cleavable Aryl Boronate Esters* was done by myself, without the help of any commercial sources. I declare that citations were marked properly, and the rules for good scientific practice of the Julius-Maximilians-Universität Würzburg were obeyed. Furthermore, I declare that I have not tried to obtain any other academic degrees besides the degrees I provided for the registration of this dissertation. In addition, I confirm that this thesis was not submitted to any other examination committee before, neither in this nor in a modified version

Würzburg, 24.06.2021

Sarina Maria Berger

11.10.2 Eidesstattliche Erklärung

Hiermit erkläre ich an Eides statt, dass ich die Dissertation mit dem Titel *Influence of Charge and Its Distribution on Biological Applications of Bis-Triarylboranes and Preliminary Investigations on H₂O₂-Cleavable Aryl Boronate Esters* selbständig angefertigt, übernommene Inhalte eindeutig gekennzeichnet und die Regeln der Julius-Maximilians-Universität Würzburg über gute wissenschaftliche Praxis eingehalten habe.

Ich erkläre außerdem, dass ich die Gelegenheit zum Promotionsvorhaben nicht kommerziell vermittelt bekommen und insbesondere nicht eine Person oder Organisation eingeschaltet habe, die gegen Entgelt Betreuerinnen bzw. Betreuer für die Anfertigung von Dissertationen sucht.

Ich habe früher außer den mit dem Promotionsgesuch urkundlich vorgelegten Graden keine weiteren akademischen Grade erworben oder zu erwerben versucht.

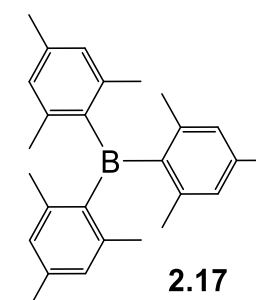
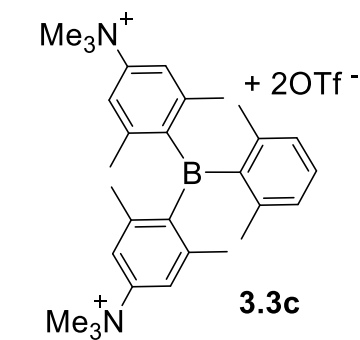
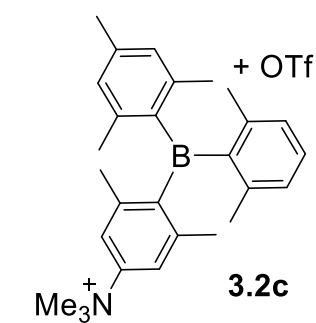
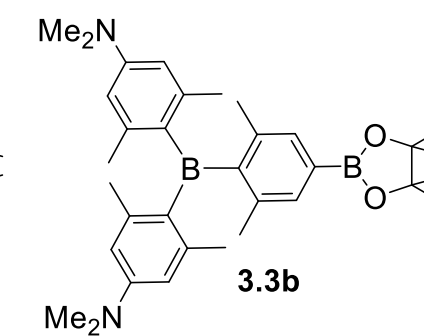
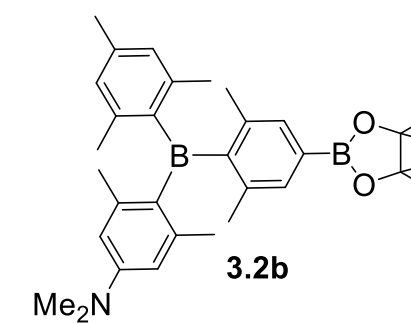
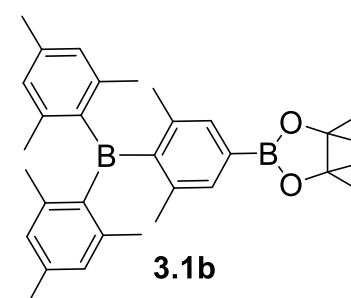
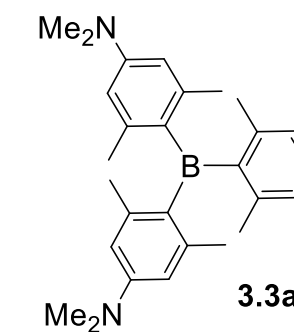
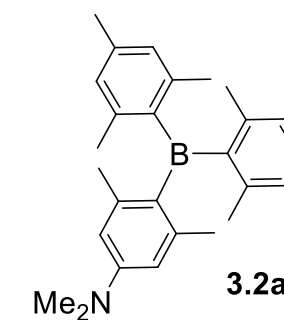
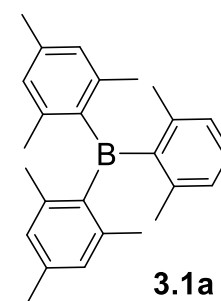
Die eingereichte und oben genannte Dissertation habe ich weder vollständig noch teilweise schon einmal einer anderen Fakultät mit dem Ziel einen akademischen Grad zu erwerben vorgelegt.

Würzburg, den 24.06.2021

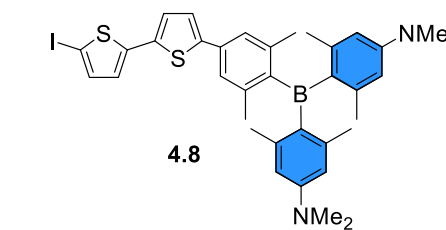
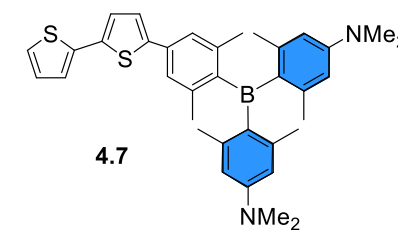
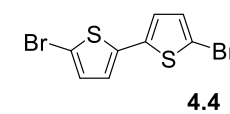
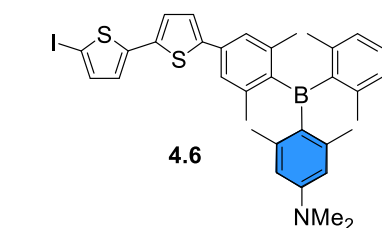
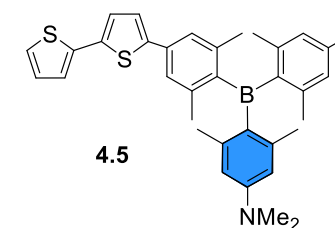
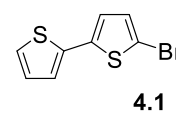
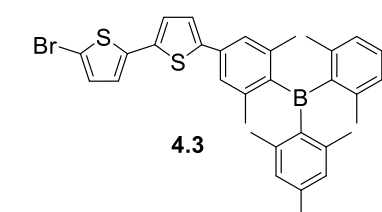
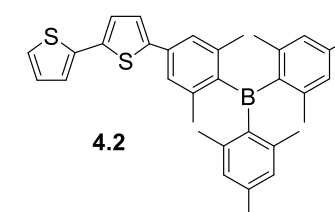
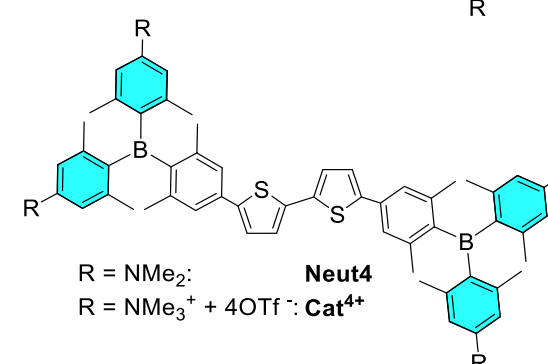
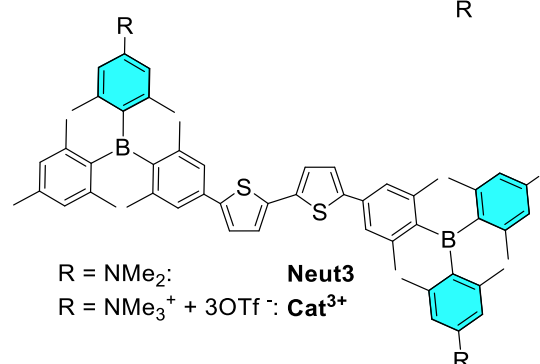
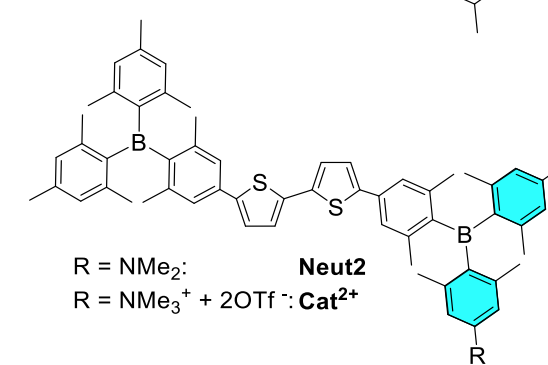
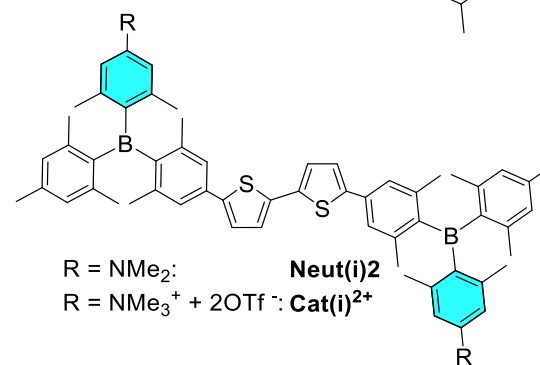
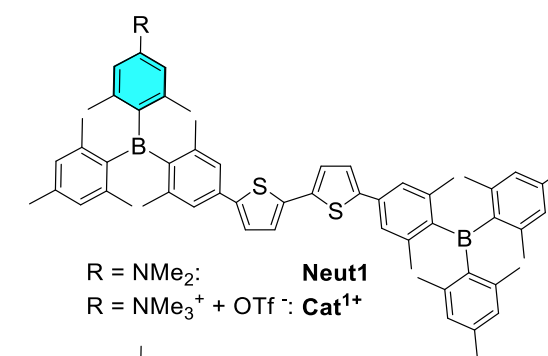
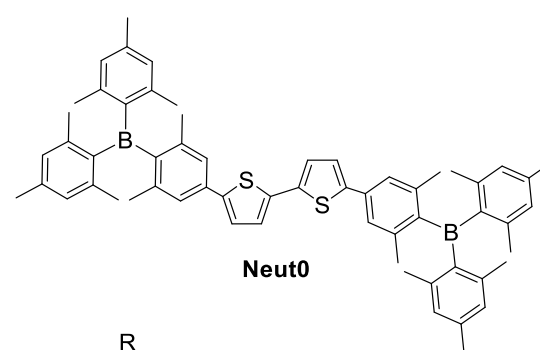
Sarina Maria Berger

11.11 List of Compounds

11.11.1 Chapter 3



11.11.2 Chapters 4 and 6



11.11.3 Chapter 7

